FACING MARINE DEOXYGENATION

EDITED BY: Arthur Capet, Perran Cook, Aurélien Paulmier, Christophe Rabouille, Raquel Vaquer-Sunyer, Babette Hoogakker and Emilio Garcia-Robledo

PUBLISHED IN: Frontiers in Marine Science and Frontiers in Earth Science

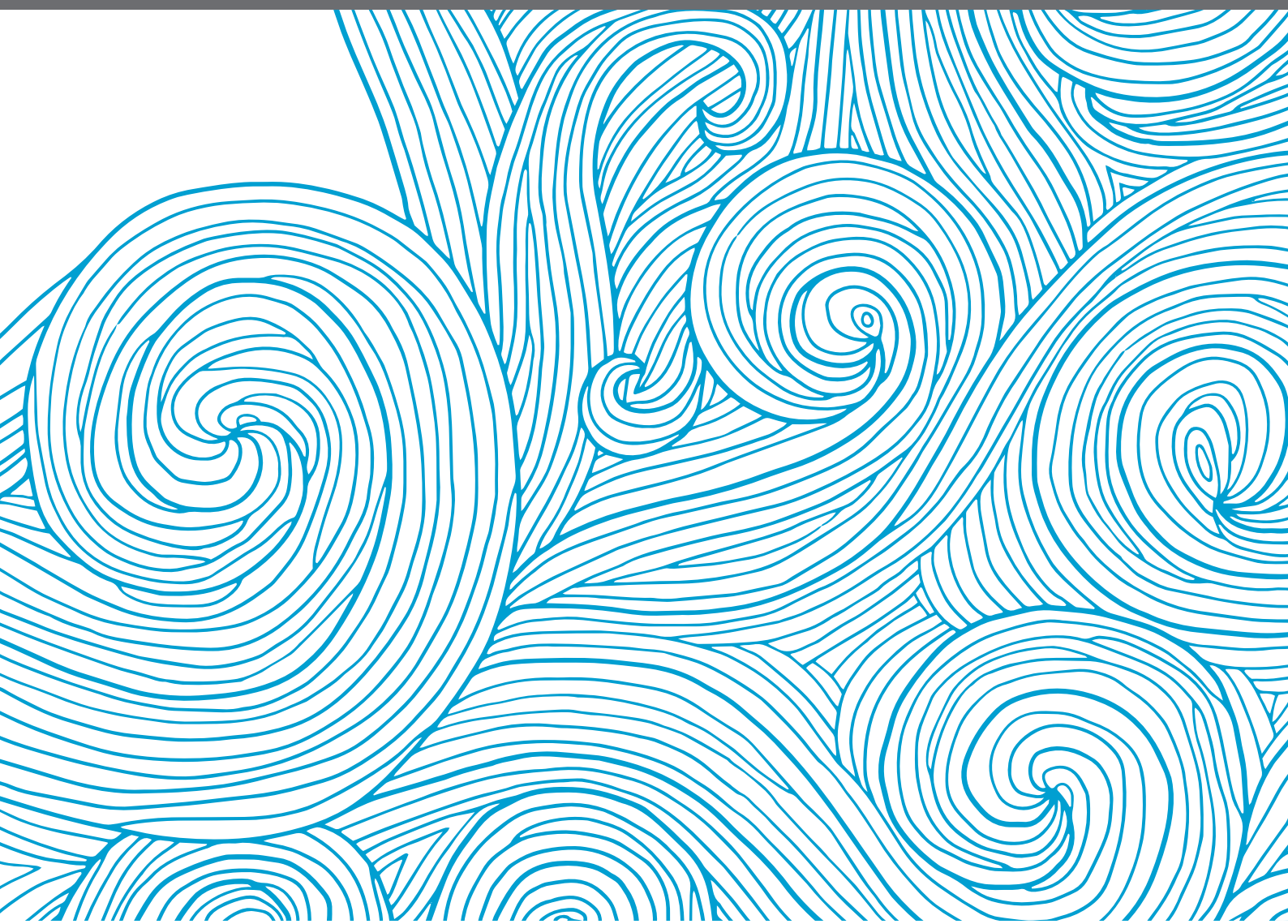

frontiers Research Topics

ISSN 1664-8714
ISBN 978-2-88963-586-3
DOI 10.3389/978-2-88963-586-3

About Frontiers

Frontiers is more than just an open-access publisher of scholarly articles: it is a pioneering approach to the world of academia, radically improving the way scholarly research is managed. The grand vision of Frontiers is a world where all people have an equal opportunity to seek, share and generate knowledge. Frontiers provides immediate and permanent online open access to all its publications, but this alone is not enough to realize our grand goals.

Frontiers Journal Series

The Frontiers Journal Series is a multi-tier and interdisciplinary set of open-access, online journals, promising a paradigm shift from the current review, selection and dissemination processes in academic publishing. All Frontiers journals are driven by researchers for researchers; therefore, they constitute a service to the scholarly community. At the same time, the Frontiers Journal Series operates on a revolutionary invention, the tiered publishing system, initially addressing specific communities of scholars, and gradually climbing up to broader public understanding, thus serving the interests of the lay society, too.

Dedication to Quality

Each Frontiers article is a landmark of the highest quality, thanks to genuinely collaborative interactions between authors and review editors, who include some of the world's best academicians. Research must be certified by peers before entering a stream of knowledge that may eventually reach the public - and shape society; therefore, Frontiers only applies the most rigorous and unbiased reviews.
Frontiers revolutionizes research publishing by freely delivering the most outstanding research, evaluated with no bias from both the academic and social point of view. By applying the most advanced information technologies, Frontiers is catapulting scholarly publishing into a new generation.

What are Frontiers Research Topics?

Frontiers Research Topics are very popular trademarks of the Frontiers Journals Series: they are collections of at least ten articles, all centered on a particular subject. With their unique mix of varied contributions from Original Research to Review Articles, Frontiers Research Topics unify the most influential researchers, the latest key findings and historical advances in a hot research area! Find out more on how to host your own Frontiers Research Topic or contribute to one as an author by contacting the Frontiers Editorial Office: researchtopics@frontiersin.org

FACING MARINE DEOXYGENATION

Topic Editors:
Arthur Capet, MAST - University of Liège, Belgium
Perran Cook, Monash University, Australia
Aurélien Paulmier, UMR5566 Laboratoire d'études en géophysique et océanographie spatiales (LEGOS), France
Christophe Rabouille, UMR8212 Laboratoire des Sciences du Climat et de l'Environnement (LSCE), France
Raquel Vaquer-Sunyer, Instituto Mediterráneo de Estudios Avanzados (IMEDEA), Spain
Babette Hoogakker, Heriot-Watt University, United Kingdom
Emilio Garcia-Robledo, University of Cádiz, Spain

Citation: Capet, A., Cook, P., Paulmier, A., Rabouille, C., Vaquer-Sunyer, R., Hoogakker, B., Garcia-Robledo, E., eds. (2020). Facing Marine Deoxygenation. Lausanne: Frontiers Media SA. doi: 10.3389/978-2-88963-586-3

Table of Contents

05 ***Editorial: Facing Marine Deoxygenation***
Arthur Capet, Perran Cook, Emilio Garcia-Robledo, Babette Hoogakker, Aurélien Paulmier, Christophe Rabouille and Raquel Vaquer-Sunyer

08 ***A Novel Modeling Approach to Quantify the Influence of Nitrogen Inputs on the Oxygen Dynamics of the North Sea***
Fabian Große, Markus Kreus, Hermann-Josef Lenhart, Johannes Pätsch and Thomas Pohlmann

29 ***Response of Sea Urchin Fitness Traits to Environmental Gradients Across the Southern California Oxygen Minimum Zone***
Kirk N. Sato, Andreas J. Andersson, James M. D. Day, Jennifer R. A. Taylor, Michael B. Frank, Jae-Young Jung, Joanna McKittrick and Lisa A. Levin

44 ***Predator Avoidance in the European Seabass After Recovery From Short-Term Hypoxia and Different CO_2 Conditions***
Alexandra Steckbauer, Carlos Díaz-Gil, Josep Alós, Ignacio A. Catalán and Carlos M. Duarte

53 ***Winning Ways With Hydrogen Sulphide on the Namibian Shelf***
Bronwen Currie, Anne Christine Utne-Palm and Anne Gro Vea Salvanes

62 ***Epifaunal Foraminifera in an Infaunal World: Insights Into the Influence of Heterogeneity on the Benthic Ecology of Oxygen-Poor, Deep-Sea Habitats***
Ryan A. Venturelli, Anthony E. Rathburn, Ashley M. Burkett and Wiebke Ziebis

75 ***Effect of Marine Hypoxia on Baltic Sea Cod* Gadus morhua*: Evidence From Otolith Chemical Proxies***
Karin E. Limburg and Michele Casini

87 ***Microbial Respiration, the Engine of Ocean Deoxygenation***
Carol Robinson

100 ***Rates and Pathways of N_2 Production in a Persistently Anoxic Fjord: Saanich Inlet, British Columbia***
Céline C. Michiels, Julia A. Huggins, Karina E. Giesbrecht, Jenifer S. Spence, Rachel L. Simister, Diana E. Varela, Steven J. Hallam and Sean A. Crowe

123 ***Interactive Effects of Hypoxia and Temperature on Coastal Pelagic Zooplankton and Fish***
Michael R. Roman, Stephen B. Brandt, Edward D. Houde and James J. Pierson

141 ***Sampling and Processing Methods Impact Microbial Community Structure and Potential Activity in a Seasonally Anoxic Fjord: Saanich Inlet, British Columbia***
Mónica Torres-Beltrán, Andreas Mueller, Melanie Scofield, Maria G. Pachiadaki, Craig Taylor, Kateryna Tyshchenko, Céline Michiels, Phyllis Lam, Osvaldo Ulloa, Klaus Jürgens, Jung-Ho Hyun, Virginia P. Edgcomb, Sean A. Crowe and Steven J. Hallam

157 ***Multidecadal Changes in Marine Subsurface Oxygenation Off Central Peru During the Last ca. 170 Years***
Jorge Cardich, Abdelfettah Sifeddine, Renato Salvatteci, Dennis Romero, Francisco Briceño-Zuluaga, Michelle Graco, Tony Anculle, Carine Almeida and Dimitri Gutiérrez

173 ***Ventilation of the Upper Oxygen Minimum Zone in the Coastal Region Off Mexico: Implications of El Niño 2015–2016***

Pablo N. Trucco-Pignata, José Martín Hernández-Ayón, Eduardo Santamaria-del-Angel, Emilio Beier, Laura Sánchez-Velasco, Victor M. Godínez and Orión Norzagaray

190 ***Scenarios of Deoxygenation of the Eastern Tropical North Pacific During the Past Millennium as a Window Into the Future of Oxygen Minimum Zones***

Konstantin Choumiline, Ligia Pérez-Cruz, Andrew B. Gray, Steven M. Bates and Timothy W. Lyons

213 ***Dynamics of the Carbonate System Across the Peruvian Oxygen Minimum Zone***

Jose M. Hernandez-Ayon, Aurélien Paulmier, Veronique Garcon, Joel Sudre, Ivonne Montes, Cecilia Chapa-Balcorta, Giovanni Durante, Boris Dewitte, Cristophe Maes and Marine Bretagnon

frontiers in Marine Science

EDITORIAL
published: 14 February 2020
doi: 10.3389/fmars.2020.00046

Editorial: Facing Marine Deoxygenation

Arthur Capet[1]*, *Perran Cook*[2], *Emilio Garcia-Robledo*[3], *Babette Hoogakker*[4], *Aurélien Paulmier*[5], *Christophe Rabouille*[6] and *Raquel Vaquer-Sunyer*[7]

[1] Department of Astrophysics, Oceanography, and Geophysics, MAST - University of Liège, Liège, Belgium, [2] Water Studies, School of Chemistry, Monash University, Melbourne, VIC, Australia, [3] Department of Biology, University of Cádiz, Cádiz, Spain, [4] The Lyell Centre, Heriot-Watt University, Edinburgh, United Kingdom, [5] Laboratoire d'Études en Géophysique et Océanographie Spatiales (LEGOS), CNRS/IRD/UPS/CNES UMR 5566, Université de Toulouse, Toulouse, France, [6] UMR8212 Laboratoire des Sciences du Climat et de l'Environnement (LSCE), Gif-sur-Yvette, France, [7] Department of Global Change Research, Instituto Mediterráneo de Estudios Avanzados, Esporles, Spain

Keywords: marine deoxygenation, multiple stressors, coastal deoxygenation, oxygen minimum zone (OMZ), ocean dead zones, hypoxia, acidification

Editorial on the Research Topic

Facing Marine Deoxygenation

INTRODUCTION

Marine deoxygenation is increasingly recognized as a major environmental threat (Breitburg et al., 2018).

Global warming drives a substantial part of this deoxygenation trend (Keeling et al., 2010), which is projected to continue during the next decades both in the open ocean and in the coastal waters. Future increasing anthropogenic pressures (e.g., eutrophication) are expected to further exacerbate this trend (Fennel and Testa, 2019).

Several main challenges need to be addressed by the scientific community:

1) To understand natural variability in marine oxygenation. As observations only cover the last ca. 60 years, we lack information about longer-term variability and trends in ocean oxygenation and associated drivers (Kamykowski and Zentara, 1990; Schmidtko et al., 2017; Oschlies et al., 2018).
2) To understand and predict the response of global biogeochemical cycles to deoxygenation. In particular, how lower oxygen conditions affect community respiration, the nitrogen (Zehr, 2009; Lam and Kuypers, 2011) and phosphorus cycles (Conley et al., 2002; Watson et al., 2017) across the estuarine-shelves-ocean continuum, including feed-backs on the climate system.
3) To evaluate and mitigate the threat posed by deoxygenation on valuable marine goods and services (Cooley, 2012) and on marine biodiversity (Vaquer-Sunyer and Duarte, 2008).

Open ocean (Paulmier and Ruiz-Pino, 2009) and coastal (Diaz and Rosenberg, 2008; Rabalais et al., 2009) deoxygenation differ in terms of temporal scale, morphology, driving processes, and implications. However, we gathered contributions related to both typologies in order to highlight interactions, differences and similarities, and to promote a common concern on marine deoxygenation so as to raise public awareness and facilitate mitigation strategies (Levin and Breitburg, 2015).

We provide below an overview of the contributions collected in this Research Topic, as well as emerging points of attention.

OPEN ACCESS

Edited and reviewed by:
Marta Marcos, University of the Balearic Islands, Spain

***Correspondence:**
Arthur Capet
acapet@uliege.be

Specialty section:
This article was submitted to Coastal Ocean Processes, a section of the journal Frontiers in Marine Science

Received: *09 January 2020*
Accepted: *24 January 2020*
Published: *14 February 2020*

Citation:
Capet A, Cook P, Garcia-Robledo E, Hoogakker B, Paulmier A, Rabouille C and Vaquer-Sunyer R (2020) Editorial: Facing Marine Deoxygenation. Front. Mar. Sci. 7:46. doi: 10.3389/fmars.2020.00046

CONTRIBUTIONS

Variability and Driving Processes

The variability in morphological expressions of low oxygen marine conditions is addressed at time scales from millenia to days, and described in relation with driving processes.

Long-term variability of Oxygen Minimum Zones (OMZ) in upwelling systems is addressed by Cardich et al. for the Peruvian system and by Choumiline et al. in the Californian system. Paleo-oceanographic and instrumental records indicate contraction and expansion periods for the Peruvian OMZ through the last 170 years, with a slight modern oxygenation trends (1960–2010) (Cardich et al.). The authors attribute centennial scales of variation to subsurface ventilation, and decadal scales to changes in local productivity. Using sediment core proxy records, Choumiline et al. highlight that expansions of the Californian OMZ during the last millennium coincide with increased productivity and upwelling during cold intervals. OMZ contractions are depicted between those intervals, pointing toward subsurface circulation and solar insolation as lead drivers of OMZ extent at a centennial scale. No evidence for recent warming effect on the OMZ extent could be depicted for the Californian area.

Long term redox history is crucial, as the closest analog for future climate and oceanographic change. However, methodological challenges remain regarding the processing of paleo proxies. Venturelli et al. question oxygenation proxies based on benthic foraminiferal assemblages, by collecting modern assemblages across spatial oxygenation gradients. A dominance of sediment-dwelling taxa over epifaunal taxa is generally considered to indicate low oxygen conditions. Here, the authors evidence that heterogeneous benthic habitat (e.g., grain size) also affects the distribution of benthic foraminifera, and thereby question the use of epifaunal foraminifera presence as an evidence for bottom oxygenated conditions.

On a closer time frame, Trucco-Pignata et al., detail the perturbation of an OMZ located in the tropical Pacific off central Mexico in response to 2015-2016 El-Nino, and describe associated changes in the carbonate system. The authors describe the role of mesoscale activity in driving the transitional regimes before and after the perturbation.

Terrestrial and atmospheric nutrient loads as drivers of coastal and shelves deoxygenation are addressed by Große et al.. As a tool to develop mitigation strategies, the authors propose a modeling approach to map the relative contributions of specific oxygen consumption terms. Targeting N-fueled oxygen consumption in the North Sea, they indicate an important contribution of Atlantic nitrogen inflow, and highlight the role of European rivers (∼30–40%) in fueling O_2 consumption in the southern North Sea. The authors conclude that reducing riverine N inputs would adequately mitigate low O_2 levels in the southern North Sea.

Two manuscripts address microbial respiration as a lead biogeochemical term of the oxygen budget. Robinson review those processes involving or involved in variations of microbial respiration rates, which are seldom accounted for within ocean models. Mechanisms contributing to deoxygenation are reviewed, as well as common techniques for measuring respiration rates and measured ranges in different parts of the ocean. The authors describe recent advances in the field and discuss the combined effect of decreasing oxygen and increasing carbon dioxide concentrations on respiration rates. Torres-Beltrán et al. report outcomes from the Scientific Committee on Oceanographic Research (SCOR) Working Group 144 "*Microbial Community Responses to Ocean Deoxygenation*" workshop (Vancouver, July 2014), aiming at standardizing process rate and multi-omic data collection in marine low-oxygen environment. In particular, large differences in recovered microbial groups were identified for identical samplings following different experimental protocols, to an extent that might alter inferred metabolic rates. The authors call for standardized techniques facilitating cross-scale comparisons and accurate assessment of *in situ* microbial activity.

Impacts

Further contributions aimed at characterizing the impacts of marine deoxygenation on biogeochemical and biological systems.

Impacts on the carbonate system were addressed by Hernandez-Ayon et al. and Trucco-Pignata et al. From a cruise across the Peruvian OMZ, Hernandez-Ayon et al. highlight that oxygenation conditions altered the carbonate system so as to affect air-sea CO_2 exchanges estimates, and that the variability and spatial heterogeneity in oxygen conditions hampered clear estimates of *in situ* based carbon budget for the area.

Michiels et al. address deoxygenation impacts on the nitrogen cycle. They quantify pelagic denitrification and anammox in a permanently anoxic fjord (British Columbia), during and before a water renewal cycle, and set those measurements in relation with microbial communities. Denitrification accounted for two thirds of nitrogen removal, and experienced peaks related with outbursts of an Arcobacter taxa.

Deoxygenation impacts on different life forms are discussed for pelagic (Roman et al.; Limburg and Casini; Steckbauer et al.), and benthic (Sato et al.) communities, as well as for the whole benthic-pelagic ecosystem in the Namibian coast (Currie et al.).

Roman et al. review the indices used to quantify hypoxic stress on zooplankton and fish populations, both from metabolic and ecological perspectives. The authors analyze a metric (Oxygen Stress Level) integrating oxygen demand in relation to oxygen availability for a coastal copepod and compare the prediction of oxygen stress to actual copepod distributions in low-oxygen areas.

Limburg and Casini use otolith proxies to reconstruct exposure of Baltic Cod to hypoxic conditions within different periods. The authors demonstrate how cod otolith can be used to inform retrospectively about exposure to hypoxia, growth and metabolic status, thereby reflecting the worsening situation for cod in the Baltic.

Steckbauer et al. investigate how co-occurence of short-term hypoxia and acidification affects European seabass juveniles, aiming at the synergistic stress that fish populations will have to face in tomorrow's ocean. Results suggest that recovery from

acidification takes longer than from short-term hypoxia, by affecting the sensorial and behavioral capacities of fish.

The combined impacts of low oxygen and low pH environment are also addressed by Sato et al. for the benthic fragile sea urchin. Although this urchin might be tolerant to foreseen evolution of oxygen and pH, differences measured across oxygen and pH gradients in critical morphological traits for reproduction and vulnerability indicate that the ecology and fitness of this dominant echinoid might be challenged on the California margin.

Finally, Currie et al. document the Namibian coastal waters as an ecosystem having evolutionarily adapted to cope with perennial anoxia and toxic hydrogen sulfide. This adaptation includes promoting sulfide-oxidizing bacteria as enablers of local detoxified habitat niches and food supply to a specific food-web.

PERSPECTIVES

This collection thus extends, non-exhaustively, on important aspects of the marine deoxygenation challenge: from coastal to open ocean frameworks, and from drivers to impacts. A number of overarching gaps emerge:

- Improvement of experimental design is required to isolate multi-stress impacts at different biological levels (i.e., individual metabolism, ecological functions, species interactions) while remaining consistent within realistic natural conditions.
- Driving mechanisms operating over a large range of temporal scales should be embedded within studies aiming at quantifying deoxygenation impacts on biogeochemical cycles, in particular for climatic assessment.
- Metabolic rates and microbial respiration require a strong focus in terms of sampling programs, standardized experimental protocols, and model formulation.

AUTHOR CONTRIBUTIONS

All authors summarized manuscripts submitted to the Research Topic to contribute to this overview. AC merged the contributions and wrote the present editorial. All authors then contributed to revision and editing.

FUNDING

AC was funded by a FRS-FNRS grant (Belgium). PC was supported by Australian Research Council grant DP150101281. EG-R was supported by the Poul Due Jensen Foundation (Denmark). CR was funded by INSU-EC2CO MissRhoDia project and PHC Cai Yuanpei (28001NF).

REFERENCES

Breitburg, D., Levin, L. A., Oschlies, A., Grégoire, M., Chavez, F. P., Conley, D. J., et al. (2018). Declining oxygen in the global ocean and coastal waters. *Science* 359:eaam7240. doi: 10.1126/science.aam7240

Conley, D. J., Humborg, C., Rahm, L., Savchuk, O. P., and Wulff, F. (2002). Hypoxia in the Baltic Sea and basin-scale changes in phosphorus biogeochemistry. *Environ. Sci. Technol.* 36, 5315–5320. doi: 10.1021/es025763w

Cooley, S. R. (2012). How human communities could "feel"changing ocean biogeochemistry. *Curr. Opin. Environ. Sustain.* 4, 258–263. doi: 10.1016/j.cosust.2012.04.002

Diaz, R. J., and Rosenberg, R. (2008). Spreading dead zones and consequences for marine ecosystems. *Science* 321,926–929. doi: 10.1126/science.1156401

Fennel, K., and Testa, J. M. (2019). Biogeochemical controls on coastal hypoxia. *Annu. Rev. Mar. Sci.* 11, 105–130. doi: 10.1146/annurev-marine-010318-095138

Kamykowski, D., and Zentara, S.-J. (1990). Hypoxia in the world ocean as recorded in the historical data set. *Deep Sea Res. Part A Oceanogr. Res. Pap.* 37,1861–1874. doi: 10.1016/0198-0149(90)90082-7

Keeling, R. E., Körtzinger, A., and Gruber, N. (2010). Ocean deoxygenation in a warming world. *Annu. Rev. Mar. Sci.* 2, 199–229. doi: 10.1146/annurev.marine.010908.163855

Lam, P., and Kuypers, M. M. M. (2011). Microbial nitrogen cycling processes in oxygen minimum zones. *Annu. Rev. Mar. Sci.* 3, 317–345. doi: 10.1146/annurev-marine-120709-142814

Levin, L. A., and Breitburg, D. L. (2015). Linking coasts and seas to address ocean deoxygenation. *Nat. Clim. Change* 5, 401–403. doi: 10.1038/nclimate2595

Oschlies, A., Brandt, P., Stramma, L., and Schmidtko, S. (2018). Drivers and mechanisms of ocean deoxygenation. *Nat. Geosci.* 11, 467–473. doi: 10.1038/s41561-018-0152-2

Paulmier, A., and Ruiz-Pino, D. (2009). Oxygen minimum zones (OMZs) in the modern ocean. *Prog. Oceanogr.* 80, 113–128. doi: 10.1016/j.pocean.2008.08.001

Rabalais, N. N., Díaz, R. J. and Levin, L. A. (2009). Dynamics and distribution of natural and human-caused coastal hypoxia. *Biogeosciences* 7, 585–619. doi: 10.5194/bg-7-585-2010

Schmidtko, S., Stramma, L., and Visbeck, M. (2017). Decline in global oceanic oxygen content during the past five decades. *Nature* 542, 335–339. doi: 10.1038/nature21399

Vaquer-Sunyer, R., and Duarte, C. M. (2008). Thresholds of hypoxia for marine biodiversity. *Proc. Natl. Acad. Sci. U.S.A.* 105, 15452–15457. doi: 10.1073/pnas.0803833105

Watson, A. J., Lenton, T. M., and Mills, B. J. W. (2017). Ocean deoxygenation, the global phosphorus cycle and the possibility of human-caused large-scale ocean anoxia. *Philos. Trans. Ser. A Math. Phys. Eng. Sci.* 375:20160318. doi: 10.1098/rsta.2016.0318

Zehr, J. P. (2009). New twist on nitrogen cycling in oceanic oxygen minimum. *Proc. Natl. Acad. Sci. U.S.A.* 106, 4575–4576. doi: 10.1073/pnas.0901266106

Conflict of Interest: The authors declare that the research was conducted in the absence of any commercial or financial relationships that could be construed as a potential conflict of interest.

frontiers in Marine Science

ORIGINAL RESEARCH
published: 29 November 2017
doi: 10.3389/fmars.2017.00383

A Novel Modeling Approach to Quantify the Influence of Nitrogen Inputs on the Oxygen Dynamics of the North Sea

Fabian Große[1,2]*, *Markus Kreus*[3,4], *Hermann-Josef Lenhart*[1], *Johannes Pätsch*[3] and *Thomas Pohlmann*[3]

[1] Scientific Computing Group, Department of Informatics, Universität Hamburg, Hamburg, Germany, [2] Marine Environmental Modelling Group, Department of Oceanography, Dalhousie University, Halifax, NS, Canada, [3] Institute of Oceanography, Universität Hamburg, Hamburg, Germany, [4] Federal Waterways Engineering and Research Institute, Hamburg, Germany

Oxygen (O_2) deficiency, i.e., dissolved O_2 concentrations below $6\,mg\,O_2\,L^{-1}$, is a common feature in the southern North Sea. Its evolution is governed mainly by the presence of seasonal stratification and production of organic matter, which is subsequently degraded under O_2 consumption. The latter is strongly influenced by riverine nutrient loads, i.e., nitrogen (N) and phosphorus (P). As riverine P loads have been reduced significantly over the past decades, this study aims for the quantification of the influence of riverine and non-riverine N inputs on the O_2 dynamics in the southern North Sea. For this purpose, we present an approach to expand a nutrient-tagging technique for physical-biogeochemical models — often referred to as 'trans-boundary nutrient transports' (TBNT) — by introducing a direct link to the O_2 dynamics. We apply the expanded TBNT to the physical-biogeochemical model system HAMSOM-ECOHAM and focus our analysis on N-related O_2 consumption in the southern North Sea during 2000–2014. The analysis reveals that near-bottom O_2 consumption in the southern North Sea is strongly influenced by the N supply from the North Atlantic across the northern shelf edge. However, riverine N sources — especially the Dutch, German and British rivers — as well as the atmosphere also play an important role. In the region with lowest simulated O_2 concentrations (around 56 °N, 6.5 °E), riverine N on average contributes 39% to overall near-bottom O_2 consumption during seasonal stratification. Here, the German and the large Dutch rivers constitute the highest riverine contributions (11% and 10%, respectively). At a site in the Oyster Grounds (around 54.5 °N, 4 °E), the average riverine contribution adds up to 41%, even exceeding that of the North Atlantic. Here, highest riverine contributions can be attributed to the Dutch and British rivers adding up to almost 28% on average. The atmospheric contribution results in 13%. Our results emphasize the importance of anthropogenic N inputs and seasonal stratification for the O_2 conditions in the southern North Sea. They further suggest that reductions in the riverine and atmospheric N inputs may have a relevant positive effect on the O_2 levels in this region.

Keywords: North Sea, eutrophication, nitrogen, oxygen deficiency, biogeochemical modeling, nutrient tagging, trans-boundary nutrient transports (TBNT)

OPEN ACCESS

Edited by:
Christophe Rabouille, UMR8212 Laboratoire des Sciences du Climat et de l'Environnement (LSCE), France

Reviewed by:
Perran Cook, Monash University, Australia
X. Antón Álvarez-Salgado, Consejo Superior de Investigaciones Científicas (CSIC), Spain
Martin Johnson, University of East Anglia, United Kingdom

***Correspondence:**
Fabian Große
fabian.grosse@dal.ca

Specialty section:
This article was submitted to Marine Biogeochemistry, a section of the journal Frontiers in Marine Science

Received: *05 September 2017*
Accepted: *14 November 2017*
Published: *29 November 2017*

Citation:
Große F, Kreus M, Lenhart H-J, Pätsch J and Pohlmann T (2017) A Novel Modeling Approach to Quantify the Influence of Nitrogen Inputs on the Oxygen Dynamics of the North Sea. Front. Mar. Sci. 4:383. doi: 10.3389/fmars.2017.00383

1. INTRODUCTION

The availability of dissolved oxygen (O_2) in marine waters is crucial for the metabolism of many marine species (e.g., Rosenberg et al., 1991; Díaz and Rosenberg, 1995). Hypoxic conditions, i.e., dissolved O_2 concentration $< 2\,mg\,O_2\,L^{-1}$ (e.g., Tyson and Pearson, 1991; Rabalais et al., 2002), constitute a major stressor to marine species and can have a severe impact on an ecosystem's biodiversity (Gray et al., 2002; Vaquer-Sunyer and Duarte, 2008; Topcu et al., 2009; Friedrich et al., 2014).

In the North Sea — a northwestern European shelf sea — hypoxic conditions occurred in the summers of the 1980s (Rachor and Albrecht, 1983; von Westernhagen and Dethlefsen, 1983; Brockmann and Eberlein, 1986; Peeters et al., 1995), causing death of benthic and demersal species (von Westernhagen and Dethlefsen, 1983). Different studies showed that these occurrences of low O_2 conditions evolved during seasonal stratification (von Westernhagen and Dethlefsen, 1983; Peeters et al., 1995), driven by eutrophication due to excess riverine nutrient loads (Brockmann and Eberlein, 1986; Brockmann et al., 1988; Peeters et al., 1995). In consequence, the 2nd International Conference on the Protection of the North Sea declared to "aim to achieve a substantial reduction (of the order of 50%) in inputs of phosphorus (P) and nitrogen (N) to these areas between 1985 and 1995" (ICNS-2, 1988), in order to mitigate the effects of eutrophication in the North Sea.

Despite significant reductions in riverine nutrients, especially for P but not for N (Artioli et al., 2008; Claussen et al., 2009; OSPAR, 2013), seasonal O_2 deficiency (i.e., dissolved O_2 concentration $< 6\,mg\,O_2\,L^{-1}$; OSPAR, 2003) still occurs regularly in the southeastern North Sea (Topcu and Brockmann, 2015). Ongoing O_2 monitoring even suggests recurrent (close-to-)hypoxic conditions (Weigelt-Krenz, pers. comm.), though, scientific publications on such events are sparse (Weston et al., 2008). Thus, O_2 deficiency remains a persistent problem in the North Sea and the investigation of its causes is essential for the ecological management.

Große et al. (2016) applied a physical-biogeochemical model to the North Sea analyzing the physico-biochemical interactions that make the southeastern North Sea most susceptible to O_2 deficiency. They found that the occurrence of distinct seasonal thermal stratification, resulting in a thin sub-thermocline layer in this region of intermediate depth, and high local near-surface net primary production (NPP) constitute the key factors. Consequently, near-bottom O_2 concentrations can become especially low during years of very high NPP. High NPP enhances (pelagic and benthic) bacterial re-mineralization of organic matter, consistently accounting for more than 80% of near-bottom O_2 consumption in the region of lowest bottom O_2 concentrations (about 55.5–56.0 °N, 6–7 °E).

In contrast to near-shore eutrophication problem areas affected by high river loads entering the coastal areas, the off-shore areas affected by O_2 deficiency are exposed to a wider variety of nutrient sources. Thus, the key question is which nutrient inputs drive NPP and O_2 consumption finally, resulting in O_2 deficiency in these North Sea regions?

Past studies suggested that nutrient inputs from adjacent North Sea regions may have contributed to the evolution of hypoxia in the 1980s (Brockmann and Eberlein, 1986; Brockmann et al., 1988). More recent publications also pointed on nutrient inputs from adjacent seas, especially the Northeast Atlantic (Artioli et al., 2008; Gröger et al., 2013). In addition, the model study by Troost et al. (2013) highlighted the influence of atmospheric N deposition on NPP in the southeastern North Sea and on near-bottom O_2 concentrations. Quantifying the contributions of these different nutrient sources in the regions susceptible to O_2 deficiency is vital for the development of potential management strategies for these regions. This demand is in line with the "integrated target-oriented and source-oriented" management approach by OSPAR (1999).

A nutrient tagging method applicable to biogeochemical models — often referred to as "trans-boundary nutrient transports" (TBNT; e.g., Blauw et al., 2006; OSPAR, 2010) — facilitates the tracing of elements (e.g., N) from individual sources throughout the entire biochemical cycle and the entire ecosystem (Ménesguen et al., 2006). By this, the TBNT method enables the quantification of the influence of these individual nutrient sources on biochemical quantities (e.g., total nitrogen; TN) and processes (e.g., NPP) in different regions of an ecosystem.

This method has been applied to various European marine ecosystems, including the Baltic Sea (e.g., Neumann, 2007; Radtke et al., 2012) and the North Sea (e.g., Blauw et al., 2006; Lacroix et al., 2007; Painting et al., 2013; Troost et al., 2013). Troost et al. (2013) demonstrated the importance of atmospheric N deposition for the off-shore regions of the southern North Sea, where it contributed 10–20% to overall TN and even 20–30% to NPP in 2002. Other studies (OSPAR, 2010; Painting et al., 2013) showed that N inputs from the large Dutch and German rivers are the major contributors to TN in the coastal southern and southeastern North Sea, respectively, while those from the rivers at the British North Sea coast extend far east into the off-shore southern North Sea. This, together with the findings by Große et al. (2016), suggests that these N sources have a strong influence on the O_2 dynamics in the southern and southeastern North Sea.

Up to now, the TBNT method was limited to the tracing of elements brought into the system by the selected sources, not allowing for the consideration of O_2. Thus, quantitative analyses of the influence of different nutrient sources on the O_2 dynamics required additional model scenarios within which individual nutrient sources were removed (e.g., Troost et al., 2013) or nutrient loads were reduced (e.g., Lenhart et al., 2010). This implies an individual scenario was required for each individual nutrient source in order to assess its impact on the O_2 conditions which is time-consuming and causes high computational costs.

Therefore, this study presents a new approach for expanding the TBNT method by a direct link of the O_2 dynamics to the nutrient inputs from individual sources. We focus on the relative importance of riverine vs. non-riverine sources of N, and their influence on the O_2 dynamics in the regions most susceptible to O_2 deficiency.

We first describe the applied HAMSOM-ECOHAM model and provide the relevant information on the theory and the implementation of TBNT. Große et al. (2016) showed that

the model system captures the main features of observed O_2 concentrations in the North Sea. Therefore, only the simulated volume transports are validated and spatial distributions of TN from selected sources are presented and compared to earlier TBNT studies. Finally, the results of the expanded TBNT method are presented with special focus on two regions regularly affected by O_2 deficiency — the southeastern North Sea (Topcu and Brockmann, 2015) and the Oyster Grounds (e.g., Greenwood et al., 2010).

2. MATERIALS AND METHODS

2.1. The HAMSOM-ECOHAM Model

We use a three-dimensional (3D) model consisting of the physical model HAMSOM (HAMburg Shelf Ocean Model; Backhaus, 1985; Pohlmann, 1991, 1996) and the biogeochemical model ECOHAM (ECOsystem model, HAMburg; Pätsch and Kühn, 2008; Kühn et al., 2010; Lorkowski et al., 2012; Große et al., 2016). HAMSOM is a baroclinic, primitive equation model using the hydrostatic and Boussinesq approximations (Pohlmann, 1991). The current velocities are calculated using the component-upstream scheme. The horizontal is discretized on a staggered Arakawa C-grid (Arakawa and Lamb, 1977) and z-coordinates are applied to the vertical. A detailed description of HAMSOM is provided by Pohlmann (1991, 1996, 2006). HAMSOM applications can be found, e.g., in Backhaus and Hainbucher (1987), Chen et al. (2013), Pohlmann (1996), and Mathis and Pohlmann (2014). The 3D fields of temperature (T), salinity (S), advective flow and vertical turbulent mixing coefficients calculated by HAMSOM are used as forcing for ECOHAM.

The ECOHAM model represents all parameter groups of a so-called NPZD-type model (nutrients-phytoplankton-zooplankton-detritus) to represent the lower trophic level dynamics. It describes two phytoplankton groups (diatoms, flagellates) and two zooplankton groups (micro- and mesozooplankton). In addition, the "microbial loop" (Azam et al., 1983) is represented. ECOHAM simulates the cycles of carbon (C), N, P, silicon (Si) and O_2 (Pätsch and Kühn, 2008; Lorkowski et al., 2012). The present version of ECOHAM is identical to that used by Große et al. (2016). Lorkowski et al. (2012) provide a full description of the ECOHAM model equations and parameter settings. Here, we will only summarize the relevant features of the O_2 cycle.

Figure 1 illustrates the O_2 cycle implemented to ECOHAM (Müller, 2008; Pätsch and Kühn, 2008), including the links to the cycles of C, N and P. The arrows indicate the loss or gain of a substance, e.g., NH_4^+ is released during benthic re-mineralization and utilized during pelagic nitrification. The air-sea flux of O_2 is parametrized according to Wanninkhof (1992). In the interior water column, NPP [according to Liebig (1841) and Steele (1962)] constitutes a source process for O_2 and links O_2 to the cycles of N, P, and C. All other biochemical processes, namely respiration by zooplankton (Sterner and Elser, 2002) and aerobic bacteria, and nitrification, represent O_2-consuming processes. While the former processes constitute links of O_2 to the cycles of C, N, and P, nitrification is only linked to N. Pelagic denitrification is implemented to ECOHAM, but is negligible as it only takes place under anaerobic conditions, not occurring in the North Sea. Pelagic anaerobic NH_4^+ oxidation (anammox) is not implemented for the same reason (Große et al., 2016). NPP is T-dependent and pelagic nitrification is light-limited in the applied model setup.

The sediment is described by a simple zero-dimensional module (Pätsch and Kühn, 2008). Benthic re-mineralization follows a first-order approach inhibiting year-to-year accumulation of matter (Große et al., 2016). Benthic

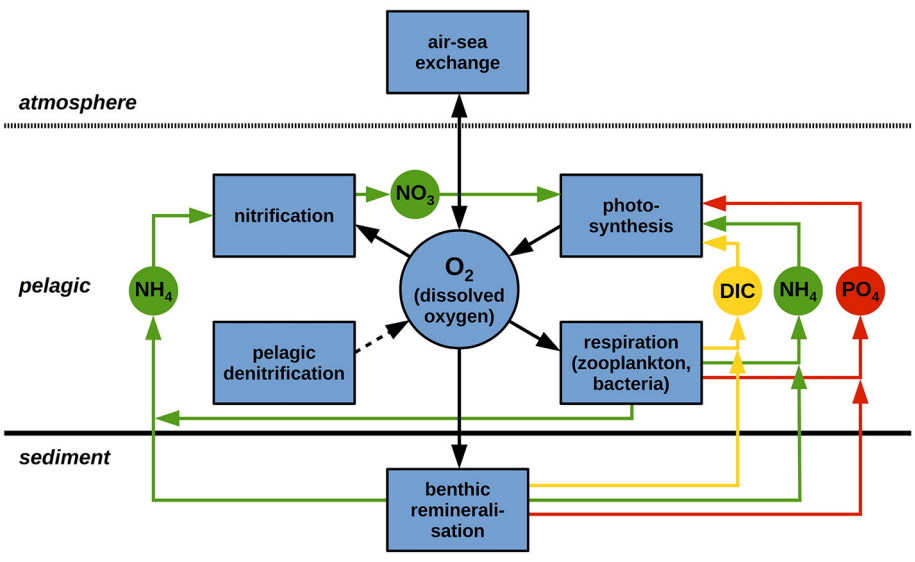

FIGURE 1 | Schematic view of the O_2 cycle as implemented to ECOHAM (black framed boxes and black arrows), including the links to the C, N, and P cycles (yellow, green and red, respectively). Linking state variables are: dissolved inorganic C (DIC), NH_4^+, NO_3^-, and PO_4^{3-}. Adapted from Müller (2008).

denitrification is linked to benthic O_2 consumption according to Seitzinger and Giblin (1996), reducing the O_2 concentration in the deepest pelagic layer (Fennel et al., 2006). Explicit benthic nitrification and benthic anammox are not implemented (Pätsch and Kühn, 2008).

In relation to the re-mineralization processes it has to be mentioned that the C:N:P ratios of particulate (POM) and dissolved organic matter (DOM) can evolve freely with time. POM is represented by two detritus species (small/large). Model DOM and POM only represent the reactive fractions (Kühn et al., 2010). Carbon oxidation occurs with a molar ratio of $C/O_2 = 1$ (Neumann, 2000; Paulmier et al., 2009). Therefore, the O_2 consumption due to respiratory processes can be described by the corresponding net C release, except for nitrification for which the molar ratio between NH_4^+ uptake and O_2 consumption is 2. The model equations and parameters of the biochemical processes affecting O_2 are given in Appendix A (Supplementary Material).

2.2. The TBNT Method

The basic concept of TBNT is that any property (e.g., input source) of an element (e.g., N) can be traced throughout the entire elemental cycle represented by a biogeochemical model. This is done by introducing additional model state variables and processes for each property. This concept dates back to the work by Ménesguen and Hoch (1997), who introduced the age as a property, and later on has been applied to various models and ecosystems (e.g., Wijsman et al., 2004; Blauw et al., 2006; Ménesguen et al., 2006; Lacroix et al., 2007; Neumann, 2007; Timmermann et al., 2010; Radtke et al., 2012; Painting et al., 2013; Troost et al., 2013; Perrot et al., 2014; Radtke and Maar, 2016).

According to Ménesguen and Hoch (1997), any property p (e.g., origin/source etc.) can be attached to any state variable X, and can be traced within a biogeochemical model by solving an additional differential equation for the product $X \cdot p$ instead of the bulk state variable X. The product $X \cdot p$ then represents that subset of the state variable X with the defined property p. Technically, the product $X \cdot p$ is introduced into the model as a new fraction state variable $X_p = X \cdot p$ and the related processes are introduced according to the differential equation describing the changes in the corresponding bulk state variable X. Each combination of state variables X and properties p_i (e.g., different input sources), $X_p^i = X \cdot p_i$, requires an additional differential equation to be solved by the model. For easier readability, X_p^i is hereafter denoted as X^i.

Compared to existing TBNT studies, we apply a slightly different approach which allows for the diagnostic calculation of the temporal evolution and spatial dispersal of X_i. In the following, the theory for this element tracing approach is briefly described. In this context, the terms "bulk" and "fraction" are used to refer to the overall state variables and processes, and their labeled counterparts, respectively. Thereafter, the approach for linking the biochemical processes affecting O_2 to the cycle of a traced element is presented.

2.2.1. Tracing Elements from Individual Sources

The convection-diffusion equation describes the change in concentration of a selected bulk state variable with time due to different physical and biochemical processes. This equation represents the differential equation solved by physical-biogeochemical models. A detailed derivation of the convection-diffusion equation for a fraction variable starting from that for a bulk state variable is provided by Radtke (2012). The source-specific convection-diffusion equation for a constant volume V as used in this study reads as follows:

$$\frac{dC_X^i}{dt} = \underbrace{\nabla \cdot \left(\overline{\overline{D}} \nabla C_X\right) \cdot \frac{C_X^i}{C_X}}_{diffusion} \quad \underbrace{- \nabla \cdot (\vec{v} C_X) \cdot \frac{C_X^i}{C_X}}_{convection/advection} \quad \underbrace{+ R_{C_X} \cdot \frac{C_{X_{\text{in}}}^i}{C_{X_{\text{in}}}}}_{sources/sinks}. \tag{1}$$

Here, C_X^i and C_X represent the concentrations of the fraction of state variable X originating from the i-th input source and that of the corresponding bulk state variable, respectively. The diffusive transport is calculated according to Fick's first law, with the second order diffusion tensor (or diffusivity) $\overline{\overline{D}}$. In the convective/advective transport term, $\vec{v}$ represents the three-dimensional velocity vector. R_{C_X} represents the change in concentration of X due to the sources and sinks (i.e., biochemical processes, input from external sources). The index X_{in} in the fraction of this term indicates that the relative contribution of the state variable, that is consumed by a biochemical process, is used.

For n individually labeled input sources (i.e., $i = 1, 2, ..., n-1, n$), the concentration of each bulk state variable X at a specific location and point in time equals the sum of its contributing fraction state variables:

$$C_X = \sum_{i=1}^{n} C_X^i. \tag{2}$$

According to Equation (1) all physical (diffusion and transport) and biochemical processes (sources/sinks) affecting C_X^i are calculated as the product of the process based on C_X and the relative contribution of the fraction variable, C_X^i/C_X. Thus, the major assumption of Equation (1) is that there is no preference for any fraction variable X^i by any (physical or biochemical) process, which relates to the fact that all fraction variables X^i are chemically and physically identical.

Compared to previous TBNT studies (e.g., Ménesguen et al., 2006; Radtke et al., 2012) this implies a different treatment of the diffusive transport. In our study its calculation bases on the spatial gradients of the bulk variable concentration. In earlier studies the concentration gradients of the fraction variable were used. In fact, it is difficult to state which approach is more correct than the other as the diffusive transport according to Fick's first law is a net transport, i.e., the actual gross transports are not known. However, it has to be noted that the diffusive transports of the individual fraction variables X^i according to Ménesguen et al. (2006) and Radtke et al. (2012) can be opposed, while those following Equation (1) are unidirectional. Despite this different treatment the resulting differences in the fraction variable distributions are expected to be generally small

and noticeable differences may only occur in the case of large differences between the spatial gradients of the fraction and bulk variables. The diffusive transport of the bulk variable will be the same in both cases.

The advantage of the calculation based on Equation (1) is that the element tracing can be conducted by means of a post-processing software utilizing the standard output of the applied model. It only requires the provision of the 3D output fields of all processes and state variables involved in the selected elemental cycle.

2.2.2. Linking Oxygen-Affecting Processes to Labeled Nutrients

In order to allow for the quantification of the influence of (organic and inorganic) nutrients from individual sources on the O_2 dynamics the establishment of a link between the two is required. This implies that only the local biochemical processes affecting O_2 can be linked to labeled nutrients, while physical processes (i.e., lateral effects) that only depend on O_2 itself cannot be considered explicitly.

According to Equation (1) biochemical processes on fraction variables (e.g., uptake of NO_3^- containing N from the Elbe by diatoms) can be calculated using the bulk process and the relative contribution of the fraction variable to the bulk variable:

$$R_{C_X^i} = R_{C_X} \cdot \frac{C_X^i}{C_X}. \tag{3}$$

Similarly, Equation (3) can be used for linking the O_2-affecting processes to labeled nutrients. In case of ECOHAM, the O_2 dynamics are linked to the cycles of C, N, and P by different processes (see **Figure 1**). In case of O_2-affecting processes whose formulation is based on a state variable containing the labeled element, this state variable can be used for the link to the O_2 cycle. For instance, O_2 consumption due to nitrification is based on NH_4^+ containing the labeled element in case of N labeling.

For processes whose formulation is based on a different element than the labeled one (e.g., NPP with 'currency' C instead of N), a different approach is required. In ECOHAM, the formulation of the change in O_2 due to these processes is based on quantities that contain the currency and the labeled element, e.g., diatoms containing C, N, and P. Assuming that the concentration of the currency of the process is proportional to the currency of the labeled element these model quantities can be described as "mediators," X_M. These mediators can be used for establishing the link between the labeled element and the O_2 cycle. For O_2-affecting processes linked to these labeled mediator variables Equation (3) then reads as:

$$R_{C_{O_2}^i} = R_{C_{O_2}} \cdot \frac{C_{X_M}^i}{C_{X_M}}, \tag{4}$$

with the O_2-affecting, biochemical bulk process $R_{C_{O_2}}$, and $C_{X_M}^i$ and C_{X_M} representing the concentrations of the mediator fraction and bulk variable, respectively.

Using Equation (4), the following mediator variables are used for the O_2-affecting processes shown in **Figure 1**: diatoms and flagellates for NPP, micro- and mesozooplankton for zooplankton respiration. For pelagic re-mineralization (i.e., bacterial respiration), the bacteria are used while for benthic re-mineralization the amount of detrital matter in the sediment is used. In case of N labeling in ECOHAM, the mediator state variables are: diatom-N and flagellate-N for NPP, micro- and mesozooplankton-N for zooplankton respiration, bacteria-N for pelagic re-mineralization and sediment-N for benthic re-mineralization. In case of P labeling, which is not part of this study, the corresponding model state variables can be used as mediator.

The use of the mediator implies that the concentration of the C-based mediator variable (e.g., diatom-C) is proportional to the corresponding concentration of the N-based mediator variable (e.g., diatom-N), according to the applied stoichiometry. Conceptually, their use can be interpreted such that the biomasses (containing C, N, and P) of the different organisms (phyto-/zooplankton, bacteria) and that of benthic detrital matter are controlled by N from the individual input sources.

Our study focuses on the influence of N on near-bottom O_2 in the off-shore regions of the North Sea, where NPP is negligible due to light limitation (Große et al., 2016). Therefore, we use gross O_2 consumption (GOC), i.e., the sum of all biochemical O_2-consuming processes as the key quantity in our analysis. In ECOHAM, these processes are: pelagic and benthic re-mineralization, zooplankton respiration and nitrification. The here used GOC is comparable to the often used "apparent oxygen utilization (AOU)".

2.3. Model Setup and TBNT Calculation

2.3.1. Model Setup

The model setup used for this study is identical to that described in Große et al. (2016). Both, HAMSOM and ECOHAM, are applied to the same model domain and grid, comprising the entire North Sea, large parts of the northwest European continental shelf and parts of the adjacent Northeast Atlantic Ocean (see **Figure 2**). The domain extends from 15.250 °W to 14.083 °E and from 47.583 °N to 63.983 °N. The horizontal resolution is 1/5 ° (1/3 °) with 82 (88) grid points in latitudinal (longitudinal) direction. The vertical dimension is resolved by 31 z-layers with a surface layer of 10 m average thickness. Below the surface layer, layer thicknesses increase from 5 m to 1,000 m in the deepest layers.

HAMSOM uses monthly, climatological distributions of T and S based on the World Ocean Atlas 2001 (Conkright et al., 2002) for initialization and open boundaries. The open boundary treatment for advective flow as well as T and S is described in Chen et al. (2013). The meteorological forcing is derived from NCEP/NCAR reanalysis data (Kalnay et al., 1996; Kistler et al., 2001) and provides 6-hourly information on air temperature, cloud coverage, relative humidity and wind velocity components.

For ECOHAM, short-wave radiation is calculated from astronomical radiation and cloud coverage applying a correction factor of 0.9 to account for underestimated cloud coverage in the NCEP data in temperate zones. For the biogeochemical state variables a climatology of depth-dependent monthly averages was prescribed at the boundaries and annually varying data was

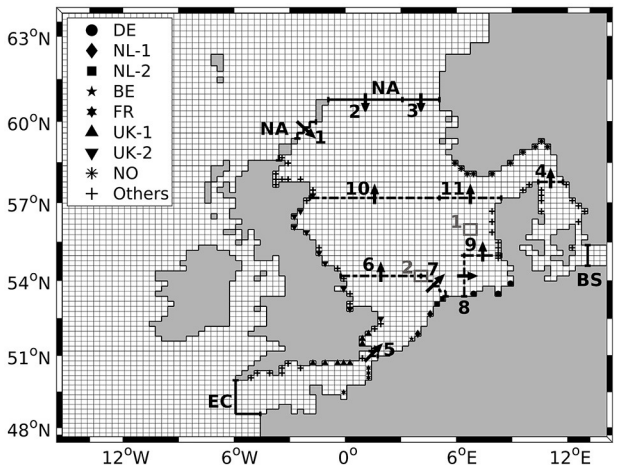

FIGURE 2 | Model domain with sub-domain used for TBNT analysis, defined by three boundaries (solid black): North Atlantic (NA), English Channel (EC) and Baltic Sea (BS). Different markers indicate river input locations for German (DE), Dutch (NL-1/NL-2), Belgian (BE), French (FR), British (UK-1/UK-2), Norwegian (NO) and other rivers (see **Table 1**). Dash-dotted lines mark sections 1 to 11 used for the validation of the volume transports simulated by HAMSOM, with arrows indicating the direction of positive net flow. Ticks mark start/end points of sections. Boxes 1 and 2 indicate regions used for time series analyses in Section 3.2.

provided for dissolved inorganic carbon (DIC; Lorkowski et al., 2012). A daily climatology of suspended particulate matter was derived from results of Pohlmann and Puls (1994) to include its effect on the light climate.

Daily freshwater run-off and nutrient load data for 254 rivers were provided by Sonja van Leeuwen (pers. comm.) and constitute an updated dataset of that used by Lenhart et al. (2010) covering the period 1977–2014. River inputs of particulate organic N (PON) were calculated as TN minus NO_3^- and NH_4^+, which are all available in the original data. Dissolved organic N is considered to be zero. The same approach was applied for organic P loads. Particulate organic C loads were derived from the PON loads using a C:N ratio of 106:16 (Redfield, 1934). A detailed description of the nutrient load calculation for the German and Dutch rivers is given in Pätsch et al. (2016).

The atmospheric N deposition was derived following Große et al. (2016), using annual data from the EMEP (Cooperative program for monitoring and evaluation of the long-range transmissions of air pollutants in Europe) model covering the period 1995–2012 and long-term trends (Schöpp et al., 2003). Atmospheric deposition is implemented as inputs of NO_3^- and NH_4^+.

Both model compartments ran over the period 1977–2014. A time step of 10 minutes was applied for the HAMSOM simulation and daily fields of *T*, *S*, advective flow and the vertical turbulent diffusion coefficient were stored as output. This daily output was used as physical forcing for ECOHAM, which ran off-line applying a time step of 30 minutes. Daily ECOHAM output was stored for the entire N cycle and the biochemical processes affecting O_2.

TABLE 1 | List of source groups defined for the TBNT analysis, including abbreviations (used in **Figure 2** and in-text) and list of individual group members.

Source group	Abbreviation	(Number of) contributing sources
North Atlantic	NA	Northern and northwestern North Sea boundary
English Channel	EC	Southwestern end of English Channel
Baltic Sea	BS	Baltic Sea boundary
Atmosphere	Atmosphere	Surface layer of entire North Sea domain
German rivers	DE	(3) Elbe, Weser, Ems
Dutch rivers (group 1)	NL-1	(3) Rhine, Meuse, North Sea Canal
Dutch rivers (group 2)	NL-2	(2) Lake Ijssel West, Lake Ijssel East
Belgian rivers	BE	(1) Scheldt
French rivers	FR	(4) Authie, Canche, Somme, Seine
British rivers (group 1)	UK-1	(22) Avon at Bournemouth, Frome, Itchen, Meon, Stour at Bournemouth, Test, Wallington, Yar, Adur, Arun, Cuckmere, Ouse at Newhaven, Waller's Haven, Thames, Chelmer, Colne, Darent, Deben, Frome, Gipping, Holland Brook, Medway, Stour at Harwich
British rivers (group 2)	UK-2	(27) Babingley, Ouse at King's Lynn, Nene, Welland, North Esk, South Esk, Almond, Blyth, Dighty Water, Earn, Eden in Scotland, Eye Water, Esk at Edinburgh, Firth of Forth, Humber, Leven in Scotland, Tay, Tees, Tweed, Tyne,Tyne in Scotland, Wansbeck, Water of Leith, Wear, Yare, Ythan
Norwegian rivers	NO	(12) Bjerkreim, Drammen, Glomma, Kvina, Lygna, Mandal, Nidelva, Numedal, Otra, Sira, Skien, Tovdal
Other rivers	Others	(68) remaining rivers: 6 Swedish, 25 Danish, 37 British

River groups defined in relation to regional OSPAR river groups (ICG-EMO, 2009; OSPAR, 2010; Los et al., 2014).

2.3.2. TBNT Setup

For the TBNT calculation, a sub-domain within the model domain was defined, comprising the North Sea, the English Channel and the Kattegat/Belts. The outer boundaries of this sub-domain (hereafter "North Sea domain") are: North Atlantic (NA) in the North, English Channel (EC) in the Southwest and Baltic Sea (BS) in the East (see **Figure 2**). An individual input source was defined for each of these outer boundaries and matter entering the North Sea across these boundaries is labeled accordingly. One atmospheric source for the entire North Sea domain was defined to include atmospheric N deposition. The individual rivers inside the North Sea domain were grouped to 8 river groups according to OSPAR (ICG-EMO, 2009; OSPAR, 2010; Los et al., 2014). One additional river group was defined collecting all rivers not attributed to one of the OSPAR groups (hereafter "*other* rivers/*others*"). The input locations of the rivers of the individual groups are indicated in **Figure 2** (see different markers). **Table 1** provides a complete list of all source groups.

The TBNT analysis was conducted for the period 2000–2014 using the daily ECOHAM output. A sensitivity study

with an ECOHAM output time step of two hours showed that the effect of the output time step on the TBNT results is negligible (not shown). All labeled variables (except for the *other* rivers) are initialized with a relative contribution of 0% to the corresponding model state variables. The *other* rivers are initialized with a relative contribution of 100% within the entire North Sea domain. This implies that the matter initially present inside the domain is fully attributed to the *other* rivers, while the matter originating from the specifically defined sources has to enter the system successively.

Starting from the initial distribution, the year 1999 was re-run seven times with the final distribution of the relative contributions of each labeled state variable used as initialization for the subsequent one. This implies a minor shift in the actual masses of individual labeled state variables between the end and the beginning of two subsequent spin-up years. After the seventh re-run a quasi-steady state was reached. This gives confidence (1) that realistic distributions of the fraction variables are reached and (2) that the matter attributed to the *other* rivers actually relates to these rivers and not to the initial mass. The advantage of this procedure is that the TBNT analysis can be applied to a comparably short model simulation requiring only one additional year prior to the analysis period. A comparison of a spin-up over a sequence of seven years showed negligible differences (not shown) justifying this procedure.

The TBNT calculation utilizes a base time step of one day (in relation to the daily model output) which is halved recursively during the calculation in case of fraction variables becoming negative.

2.3.3. Atmospheric and Riverine N Input

The applied atmospheric and riverine TN inputs are crucial for the results of the TBNT analysis. Therefore, **Figures 3A,B** show time series of the annual atmospheric and riverine TN input into the North Sea domain, respectively. In both panels, the left *y* axes refer to the absolute TN input (in kt N a^{-1}). The right *y* axis in **Figure 3A** refers to the contributions of the atmospheric input into different subregions of the North Sea domain, relative to the total input into the domain: southern North Sea (▲; area of $1.7 \cdot 10^5$ km^2), northern North Sea (▼; $3.8 \cdot 10^5$ km^2), English Channel (◀; $0.9 \cdot 10^5$ km^2) and Kattegat/Belts (▶; $0.5 \cdot 10^5$ km^2). The southern North Sea represents the North Sea region south of 56 °N until transport section 5 in the Strait of Dover (see **Figure 2**). The northern North Sea represents the part of the TBNT domain north of 56 °N, including the Skagerrak north of section 4. The English Channel is the region between the EC boundary and section 5, while the Kattegat/Belts region is limited by the BS boundary and section 4. The total area of the North Sea domain is $6.9 \cdot 10^5$ km^2.

Figure 3A shows that the atmospheric input (solid line) decreases slowly throughout 2000–2014, with a relative reduction of about 13% relating to the observed trend (Schöpp et al., 2003). The atmospheric deposition yields 490 kt N a^{-1} in 2000 and stays around 485 kt N a^{-1} during 2001–2004. From 2005 on, it shows a steady decrease reaching 430 kt N a^{-1} in 2014.

The relative contributions of the atmospheric TN input into the different subregions of the TBNT domain (dotted lines) are stable throughout 2000–2014. This relates to the fact that only the total, domain-wide N deposition decreases, while the spatial patterns do not change. The largest part of about 44.7% is deposited in the northern North Sea. About 31.6%

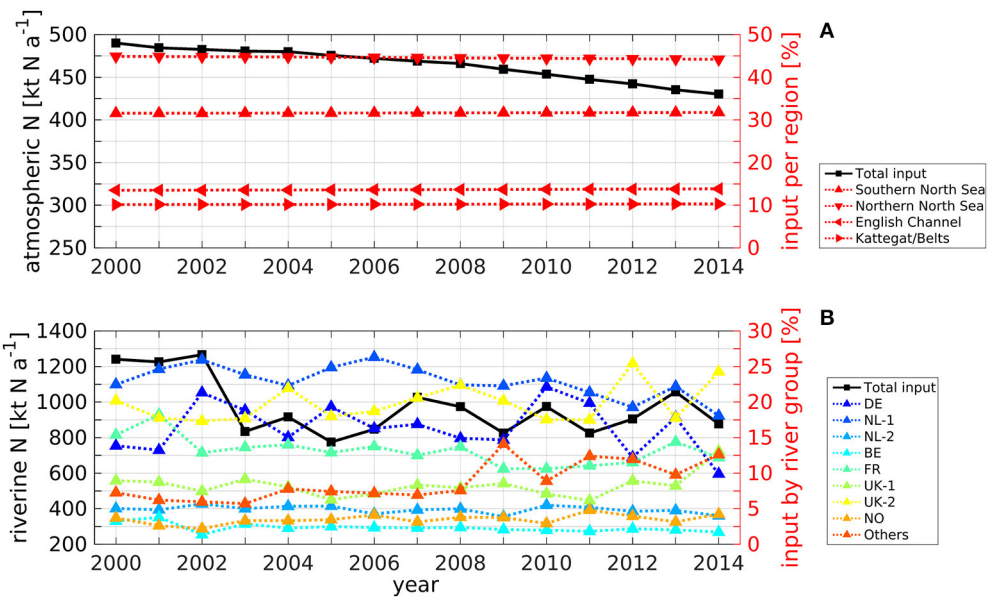

FIGURE 3 | Time series of annual **(A)** atmospheric and **(B)** riverine TN input (left *y* axes and solid lines) into the TBNT domain (see **Figure 2**). Relative contributions (right *y* axes and dotted lines) represent the contribution to the total input into the TBNT domain by different regions in case of atmospheric deposition and by different river groups (see **Table 1**) in case of riverine input.

enter the southern North Sea, whose area is less than half of that of the northern North Sea region, emphasizing the remarkable spatial differences in atmospheric N deposition. The relative contributions to the English Channel region and the Kattegat/Belts are about 13.6% and 10.1%, respectively.

The absolute annual riverine TN input into the TBNT domain (**Figure 3B**; solid line) ranges between 775 kt N a^{-1} in 2005 and 1266 kt N a^{-1} in 2002. An apparent step change is seen between 2002 and 2003. The relative contributions of the different river groups to riverine TN input (dotted lines) show that the NL-1 rivers (incl. Rhine and Meuse; see **Table 1**) are the largest TN source during most years with values between 18.1% and 26.3%. The UK-2 rivers, located at the British east coast, are of similar importance ranging between 17.3% and 25.4%. The DE rivers constitute the third largest source during most years with contributions of 9.9–22.1%. The FR rivers contribute 10.6–18.2%. The UK-1 and *other* rivers show values between 6.1–13.1% and 5.7–14.1%, respectively, with higher values in the period after 2008 compared to the earlier period. This indicates that the relative importance of the different rivers on the North Sea system changed during this period. The remaining rivers (NL-2, BE, and NO) are less important (<5%).

The relative contributions show that the drop in TN input from 2002 to 2003 mainly relates to decreasing inputs from the DE and NL-1 rivers. Interestingly, the DE rivers show particularly high relative contributions in 2002 and 2010 (21.3% and 22.1%, respectively). Both relate to Elbe flood events in August 2002 (e.g., Ulbrich et al., 2003) and late summer 2010 (e.g., Kienzler et al., 2015; Philipp et al., 2015), respectively.

It should be noted that average annual PON:TN ratios for most groups are in the range of 0.16–0.19. Only the UK rivers show lower ratios around 0.08 and the NL-2 and NO rivers show comparably high ratios of about 0.45 and 0.47, respectively, though corresponding to small overall N loads. The standard deviation of the annual ratios is <0.05 for all groups. Thus, inorganic N inputs dominate the ecosystem dynamics.

3. RESULTS

This section first provides a brief validation of simulated volume transports as well as spatial distributions of TN from different sources and minimum O_2 concentrations, simulated by the applied model and TBNT framework. By this, we demonstrate that the applied setup reproduces the main features of the North Sea ecosystem relevant to this study. This yields the basis for our analysis of the influence of N inputs on the O_2 dynamics.

3.1. Validation

3.1.1. Volume Transports

Table 2 presents volume transports across defined sections simulated by HAMSOM and corresponding transports from other modeling studies (Ozer, 2011; Winther and Johannessen, 2006) and observations (Winther and Johannessen, 2006). The 11 sections used for the comparison are indicated in **Figure 2** (arrows indicate direction of positive net flow/inflow). They were selected with respect to the North Sea general circulation and data availability. Ozer (2011) conducted a model intercomparison on the North Sea circulation in 2008. Thus, the corresponding HAMSOM transports across these sections are calculated for 2008 only. For the other sections, given values represent statistics over the 15-year period 2000–2014. The provided observation data were compiled by Winther and Johannessen (2006) and originate from Otto et al. (1990), Rodhe (1996), Rydberg et al. (1996), and Danielssen et al. (1997).

TABLE 2 | Volume transports across defined sections (see **Figure 2**) derived from HAMSOM over entire period 2000–2014 compared to values from Winther and Johannessen (2006) and values for 2008 compared to Ozer (2011).

Section	Analysis	This study		Winther and Johannessen (2006)			Ozer (2011)
Number	Period	HAMSOM		Model		Observation	Range of model averages
(Flow)		Mean	Min/max	Mean	Min/max	Literature	Three different models
1 (in)	2000–2014	0.57	$4 \cdot 10^{-5}$/2.76	0.49	0.01/2.36	0.30	–
2 (in)	2000–2014	1.26	0.21/3.94	0.50	0.02/2.04	0.60	–
3 (in)	2000–2014	0.42	$3 \cdot 10^{-4}$/3.03	1.23	0.18/2.91	0.70 – 1.11	–
3 (out)	2000–2014	2.19	0.10/7.01	2.33	0.67/5.73	1.80	–
4 (net)	2000–2014	0.017	−0.46/0.39	0.014	–/–	0.015	–
5 (in)	2000–2014	0.14	$2 \cdot 10^{-5}$/0.89	0.16	0.00/1.03	0.10 – 0.17	–
5 (net)	2008*	0.10	−0.35/0.72	–	–/–	–	0.080 – 0.121
6 (net)	2008*	−0.08	−1.64/0.76	–	–/–	–	−0.085 – −0.027
7 (net)	2008*	0.18	−0.37/1.28	–	–/–	–	0.163 – 0.207
8 (net)	2008*	0.09	−0.28/0.80	–	–/–	–	0.127 – 0.130
9 (net)	2008*	0.09	−0.21/0.78	–	–/–	–	0.105 – 0.122
10 (net)	2008*	−0.44	−4.50/1.41	–	–/–	–	−0.470 −0.337
11 (net)	2008*	0.55	−0.77/2.94	–	–/–	–	0.362 – 0.421

The asterisk (*) indicates identical analysis periods for this study and the values used for comparison. Observed literature values compiled by Winther and Johannessen (2006) originate from Otto et al. (1990), Rodhe (1996), Rydberg et al. (1996), and Danielssen et al. (1997). Parentheses in first column indicate type of transport: "in"/"out" , gross in-/outflow; "net" , net flow. All values in Sverdrup (1 Sv = 10^6 m^3 s^{-1}).

HAMSOM reproduces the gross inflow from the North Atlantic across the northern shelf edge (**Table 2**, sections 1 to 3). Average gross inflow through the three sections simulated by HAMSOM adds up to 2.25 Sv. This is comparable to the results of Winther and Johannessen (2006) yielding 2.22 Sv and close to the upper end of the observed range (1.60–2.01 Sv). The ratio between the inflows through sections 2 and 3 is opposite to that for the transports simulated by Winther and Johannessen (2006) and to the literature values. However, it should be noted that these transports are highly sensitive to the position of the separation between sections 2 and 3. The higher minimum–maximum range in the HAMSOM transports (compared to Winther and Johannessen, 2006) likely relates to the longer analysis period. Regarding the outflow in the Norwegian Trench area (section 3), HAMSOM shows good agreement with the other studies.

The net transport through section 4 (Kattegat) corresponds with the results of Winther and Johannessen (2006) and observations. The same applies to the gross inflow through the English Channel (section 5), for which the average net inflow in 2008 matches with Ozer (2011). The comparison of the transports across the northern shelf edge (sections 1–3) with those through sections 4 and 5 emphasizes that the Atlantic inflow from the North constitutes the dominant inflow into the North Sea.

For sections 6 and 7, the net transports are in the range reported by Ozer (2011). Though, transports for section 6 are rather at its upper end. The negative net transport through section 6 implies southward flow in the southwestern North Sea driven by the Atlantic inflow from the North and freshwater discharge from the rivers at the British east coast. In contrast, the northwestward flow in the eastern part (section 7) is governed by the continental coastal current driven by the English Channel inflow and riverine freshwater especially from the large Dutch rivers.

For the net flow into and out of the German Bight (sections 8 and 9, respectively), HAMSOM yields values of about 0.09 Sv, slightly below the range provided by Ozer (2011). This likely relates to the bathymetry in combination with the vertical resolution resulting in a distinct step in the model bathymetry causing a northward turn of parts of the coastal current before crossing section 8 (not shown).

The negative net flow across section 10 in the western central North Sea simulated by HAMSOM indicates the mainly southward flow in this region. The average value of −0.44 Sv is in the range found by Ozer (2011). In the eastern central North Sea (section 11), the positive net flow derived from HAMSOM represents the generally northward flow in this region relating to the cyclonic recirculation of most of the southward flowing water masses north of Dogger Bank (Lenhart and Pohlmann, 1997). The transport is slightly above the range reported by Ozer (2011), which may relate to a lower inflow from the Baltic Sea indicated by the differences in the transports across section 4.

In summary, the HAMSOM volume transports across the outer boundaries and in the interior of the North Sea show good agreement with other models and observations and represent well the general cyclonic circulation (e.g., Otto et al., 1990). Therefore, the current fields simulated by HAMSOM provide a reliable basis for the TBNT analysis.

3.1.2. Spatial Distributions of TN from Different Sources

In order to give insight in the dispersal of N from different input sources in the North Sea, **Figure 4** shows the mass-weighted average relative contributions of selected input sources to TN (i.e., the sum of all N-related model state variables incl. sediment-N) during 2000–2014: (**Figure 4A**) atmosphere, (**Figure 4B**) German rivers (DE), (**Figure 4C**) 1st group of Dutch rivers (NL-1), and (**Figure 4D**) 2nd group of British rivers (UK-2). By aggregating pelagic and benthic state variables the internal processes (e.g., uptake of NO_3^- by diatoms) cancel out and the spatial distributions of TN from the different sources basically reflect the effect of lateral exchange processes. Only the loss of molecular N_2 due to benthic denitrification, and atmospheric N deposition have an additional influence. The individual N sources were selected in relation to existing TBNT studies on TN (OSPAR, 2010; Painting et al., 2013; Troost et al., 2013).

The relative contributions show that the southeastern North Sea is strongly affected by atmospheric N deposition (**Figure 4A**) as well as the selected riverine N sources (**Figures 4B–D**). In contrast, these input sources are of minor importance ($< 2.5\%$) in the entire northern and large parts of the central North Sea. In these regions, TN is dominated by the NA influence (not shown) which decreases from 100% in the off-shore regions of the northern North Sea to about 50% along the 50-m-isobath.

In the coastal northwestern North Sea, the UK-2 (see **Figure 4D**) and *other* rivers (not shown) have an increased influence. In the northeastern North Sea, the atmosphere (see **Figure 4C**) and the Norwegian rivers (NO; not shown) constitute relevant contributions besides the NA contribution.

The atmospheric contribution (**Figure 4A**) plays a relevant role in the southern central and southern North Sea, ranging between 5% in the southwestern North Sea and 19% near the Danish west coast. Furthermore, the contributions of the DE, NL-1, and UK-2 rivers (**Figures 4B–D**, respectively) to TN are high in the southern central and southern North Sea. In the vicinity of the river mouths of Rhine/Meuse (NL-1), Humber and Wash (UK-2) as well as Elbe and Weser (DE), the contributions of the corresponding rivers can reach values of almost 100%. However, their contributions decrease to <40–60% within a distance of about 100 km from each river mouth.

Though, the contribution of the NL-1 and UK-2 rivers (**Figures 4C,D**, respectively) extends far into the off-shore regions of the southern North Sea. The former reaches values well above 10% in almost the entire southeastern North Sea, while the latter stays well above 10% in the entire southwestern part. The DE inputs (**Figure 4B**) extend northward along the German and Danish west coast. This illustrates the cyclonic general circulation of the North Sea.

The relevant contributions of the selected TN sources are accompanied by a steady decrease in the NA and EC contributions (not shown) from about 60% in the off-shore parts to 5–10% in the coastal regions between the mouths of Rhine/Meuse and the Danish northwest coast.

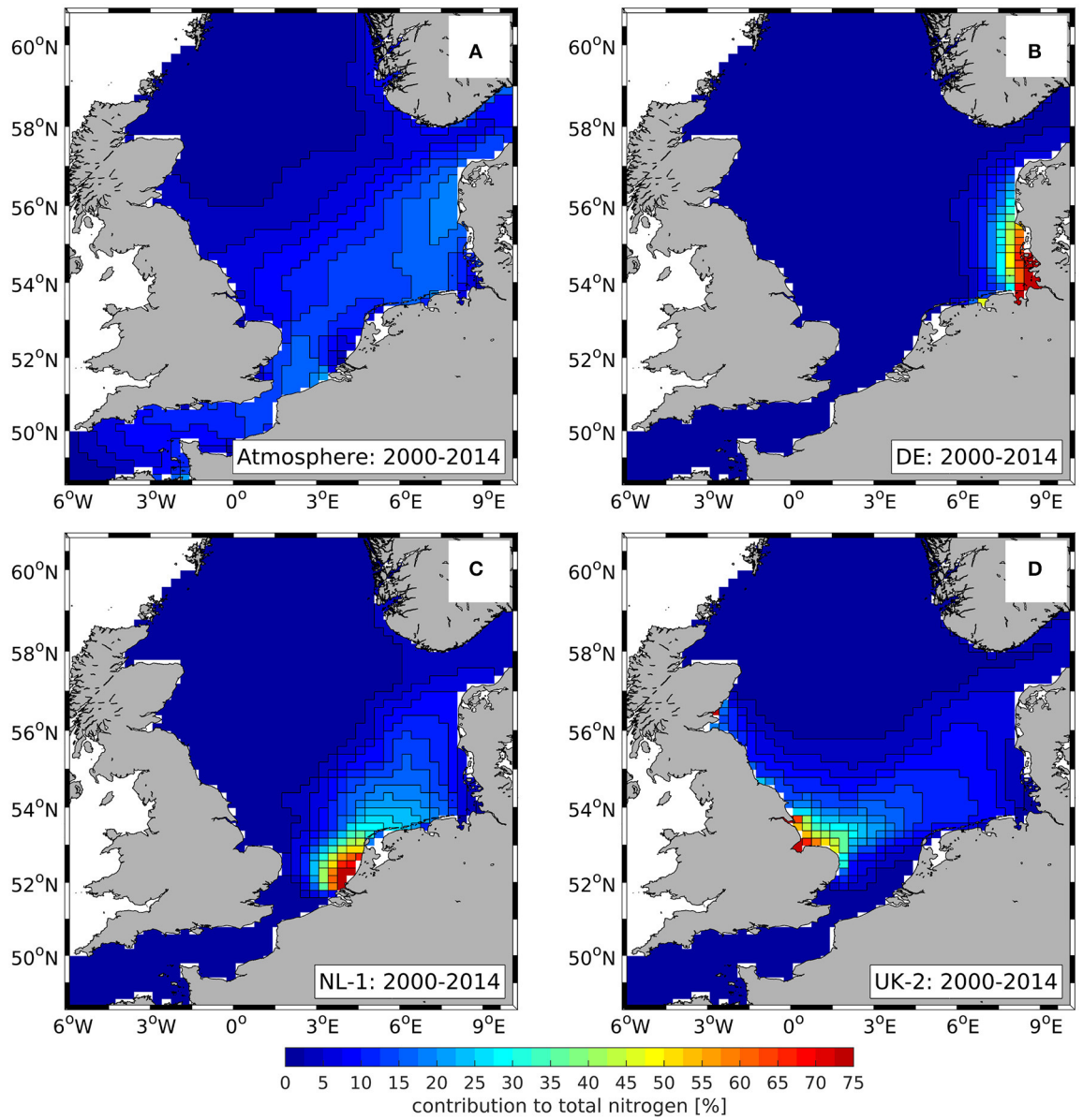

FIGURE 4 | Spatial distribution of 15-year, water column averaged relative contributions of TN from different sources during 2000–2014: **(A)** atmosphere, **(B)** German rivers (DE), **(C)** 1st group of Dutch rivers (NL-1), **(D)** 2nd group of British rivers (UK-2). Color scale cut at upper limit. Same color scale for all panels.

3.1.3. Minimum Bottom O_2 Concentrations

Große et al. (2016) showed that the applied model setup reproduces the main spatial and temporal features of North Sea O_2, only slightly overestimating near-bottom O_2 concentrations. Therefore, **Figure 5** only shows the spatial distribution of the overall minimum simulated bottom O_2 concentration during 2000–2014. By this, a first insight in the concurrence of N from individual input sources and low O_2 concentrations is provided.

Lowest simulated O_2 concentrations occur in the region between 54.5–56.5 °N and 4–7.5 °E. This is in good agreement with recurrent observations of O_2 deficiency in this region in recent years (Figure 14 in Topcu and Brockmann, 2015). Minimum O_2 concentrations of 5.2 mg O_2 L^{-1} are found in region 1 (see **Figure 5**) which, therefore, is used for a detailed analysis of the O_2 dynamics in relation to N inputs. Region 1 is hereafter referred to as "O_2 deficiency zone" (ODZ). The comparison with the spatial patterns of TN from individual sources (see **Figure 4**) indicates that this region is under strong influence of the DE rivers, but also the NL-1 and UK-2 rivers. The atmosphere and the NA also play a relevant role.

Low simulated O_2 concentrations also occur directly north of Dogger Bank which matches with observations (Weston et al., 2008; Greenwood et al., 2010; Queste et al., 2016). The same applies to the Oyster Grounds site (see **Figure 5**, region 2)

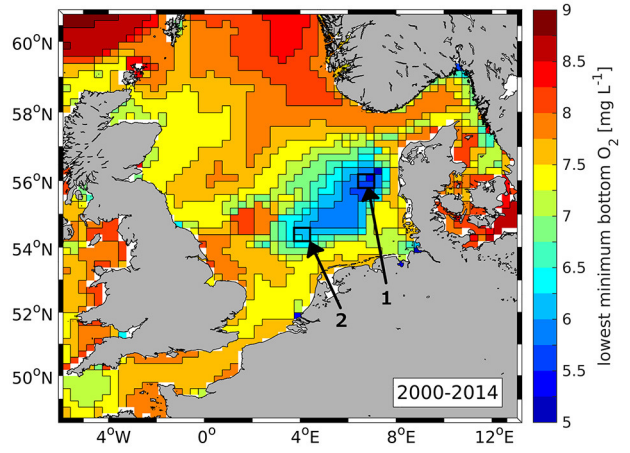

FIGURE 5 | Spatial distribution of lowest simulated bottom O_2 concentration during 2000–2014. Boxes 1 and 2 indicate regions used for the time series analyses in Section 3.2.

where simulated minimum near-bottom concentrations yield 6–6.5 mg O_2 L^{-1}. As the Oyster Grounds are well known being susceptible to low O_2 conditions (de Wilde et al., 1984; Peeters et al., 1995; Weston et al., 2008; Greenwood et al., 2010), this region is also used for a detailed analysis. At this site, the comparison with **Figure 4** indicates a strong influence of the NL-1 and UK-2 rivers, and the NA (not shown). The atmospheric contribution is lower than at the ODZ site. It should be noted that the term "Oyster Grounds" used in this study refers explicitly to the defined region 2 which was chosen in relation to the study site of Greenwood et al. (2010).

3.2. O_2 Consumption Related to N from Individual Sources

Based on the good agreement of the presented results with existing observations and modeling studies, the following analyses focus on the influence of N from selected input sources on near-bottom GOC.

3.2.1. Spatial Distributions

Figure 6A shows the spatial distributions of annual GOC in the model bottom layer averaged over 2000–2014. The corresponding average relative contributions related to selected N input sources are given in **Figures 6B–F**: (**Figure 6B**) boundaries (NA, EC, and BS), (**Figure 6C**) atmosphere, (**Figure 6D**) DE rivers, (**Figure 6E**) NL-1 rivers, and (**Figure 6F**) UK-2 rivers.

GOC shows a general South-North gradient with high values (>0.3 kg O_2 m^{-2} a^{-1}) in the coastal southern North Sea and low values (<0.1 kg O_2 m^{-2} a^{-1}) in the deep northern parts. The lower values in the deep North Sea regions relate to lower near-surface NPP and greater bottom depths, resulting in less organic matter reaching the bottom. Highest GOC occurs in the vicinity of large river mouths (e.g., Elbe) due to riverine input of organic matter additionally enhancing local GOC. Here, values of up to about 1.3 kg O_2 m^{-2} a^{-1} are simulated.

It can be seen that the coastal regions of highest GOC do not correspond to the regions of lowest bottom O_2 concentrations (see **Figure 5**). This relates to the strong tidal mixing inhibiting long-lasting seasonal stratification which constitutes the prerequisite for the evolution of low O_2 conditions (Greenwood et al., 2010; Große et al., 2016). In the off-shore regions of the southeastern North Sea average annual GOC ranges between 0.1 kg O_2 m^{-2} a^{-1} and 0.2 kg O_2 m^{-2} a^{-1}. Here, GOC increases with decreasing water depth due to higher organic matter availability near the seafloor (Große et al., 2016).

The spatial distributions of source-specific relative contributions to GOC (see **Figures 6B–F**) basically represent the patterns shown for TN (see **Figure 4**). Thus, the input of N from the boundaries (see **Figure 6B**), especially the NA, dominates most off-shore regions of the North Sea, while the atmosphere and the riverine contributions from NL-1 and UK-2 (see **Figures 6C,E,F**, respectively) play an important role for GOC in the southern North Sea. The DE rivers' influence on GOC is confined to the German Bight and Danish west coast (see **Figure 6D**).

Minor differences can be seen with respect to the relative importance of the atmosphere which shows a slightly higher contribution to GOC in most off-shore areas compared to its contribution to TN. This likely relates to the stronger influence of atmospheric N deposition on NPP as deposited inorganic N is immediately available to primary producers. At river mouth locations, the corresponding river groups show slightly higher contributions to GOC than to TN which underlines the relevance of riverine organic matter for local GOC.

3.2.2. Inter-Annual Variability in the ODZ

Figure 7 provides a more detailed insight in the influence of N from individual sources on GOC in the region most susceptible to O_2 deficiency. It shows the time series of average daily, near-bottom GOC at the ODZ site (see **Figure 5**, region 1) during the stratified period (t_{strat}) of the individual years 2000–2014, and average values over t_{strat} of the entire period. t_{strat} is derived from simulated T following Große et al. (2016). The entire period from the very first day of stratification until the very last day (incl. intermittences) is used for averaging. Consequently, average daily GOC provides a comparable measure for analyzing inter-annual variations in the influence of N from individual sources on the O_2 dynamics, independent of the duration of seasonal stratification. For a more quantitative description, **Table 3** (left-hand side) provides the corresponding average (and standard deviation) values for t_{strat}, average daily GOC and the relative contributions of individual N sources to average daily GOC for the entire period 2000–2014, and for the years 2002 and 2010. All values refer to a bottom layer of 6.5 m average thickness.

Figure 7 and **Table 3** show that 2002 represents an exceptional year with the highest daily GOC (0.61 g O_2 m^{-2} day^{-1}). This high GOC coincides with the longest t_{strat} of 186 days, resulting in the lowest bottom O_2 concentrations in the vicinity of the ODZ site in 2002 (Große et al., 2016). In contrast, 2010 constitutes the year of lowest GOC (0.31 g O_2 m^{-2} day^{-1}) resulting in higher bottom O_2 concentrations. Interestingly, 2011 also shows high daily GOC of 0.56 g O_2 m^{-2} day^{-1}, though, O_2 deficiency does not occur in

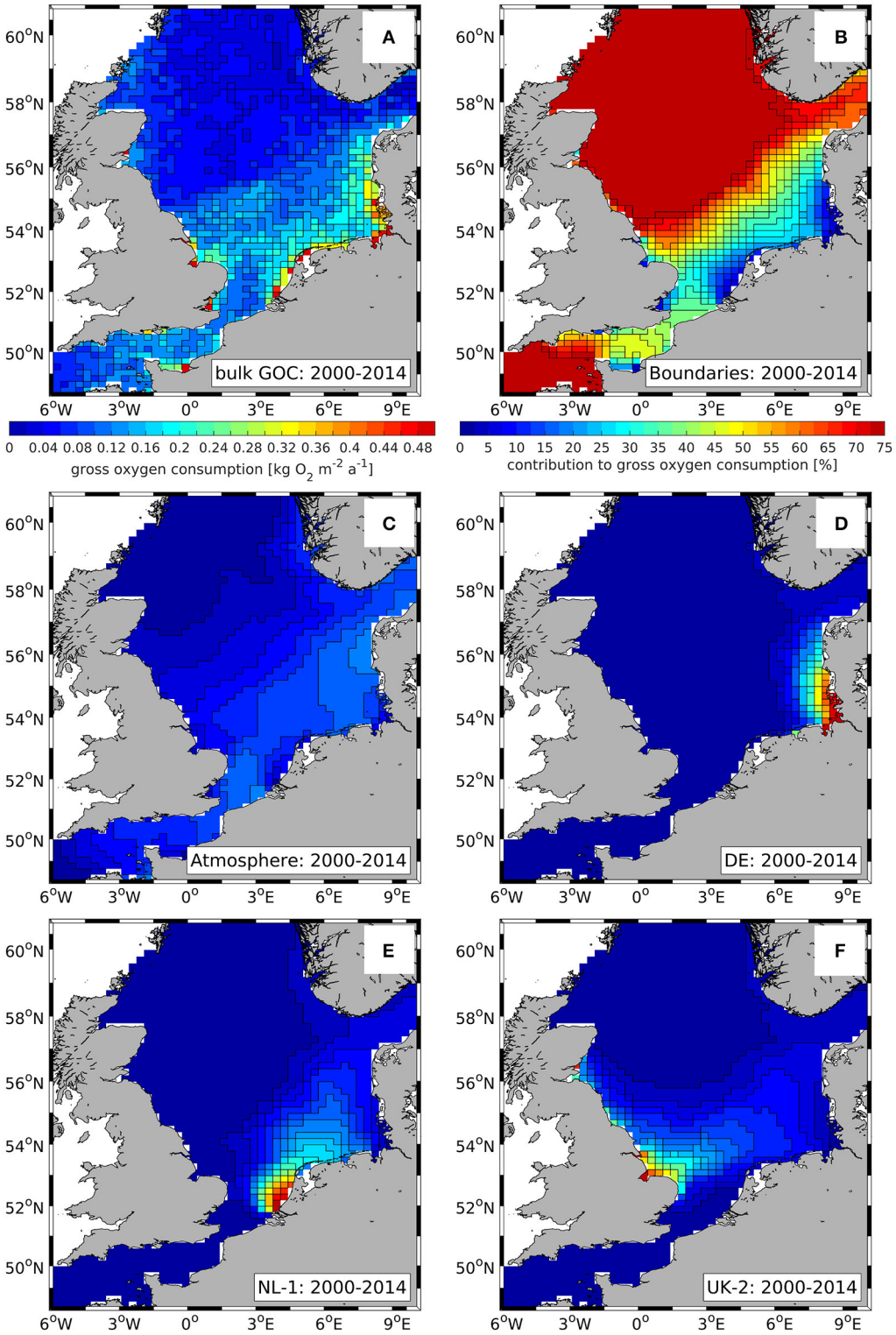

FIGURE 6 | Spatial distribution of **(A)** 15-year averaged, annual near-bottom gross O_2 consumption (GOC) and **(B–F)** average relative contributions due to N from different sources during 2000–2014: **(B)** boundaries (NA, EC, and BS), **(C)** atmosphere, **(D)** German rivers (DE), **(E)** 1st group of Dutch rivers (NL-1), **(F)** 2nd group of British rivers (UK-2). Both color scales cut at upper limits. Color scale of **(B)** also applies to **(C–F)**.

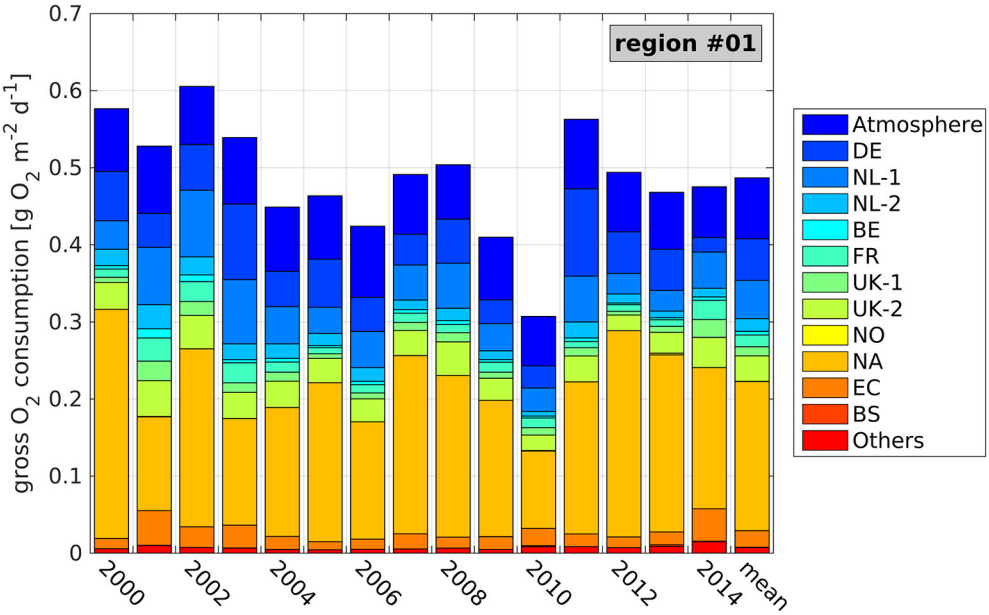

FIGURE 7 | Average daily, near-bottom gross O_2 consumption (GOC) during seasonal stratification and contributions of the different N sources (see **Table 1**) at the ODZ site (see **Figure 5**, region 1) during the individual years 2000–2014, and averaged over the entire period. Values refer to a bottom layer thickness of 6.5 m.

TABLE 3 | Averages and standard deviations (std) during 2000–2014 and values for 2002 and 2010 at ODZ site and at Oyster Grounds (see **Figure 5**, regions 1 and 2, respectively): stratification periods [t_{strat}; according to Equations (1, 2) in Große et al. (2016)], daily near-bottom GOC and relative contributions of different N sources.

	ODZ site (region 1)			Oyster Grounds (region 2)		
	Average ± std	2002	2010	Average ± std	2002	2010
t_{strat}	159 ± 17	186	161	162 ± 13	173	160
GOC	0.49 ± 0.07	0.61	0.31	0.34 ± 0.04	0.39	0.23
Atmosphere	16.6 ± 2.7	12.4	20.9	13.1 ± 1.6	11.1	15.5
DE	11.0 ± 4.0	9.9	9.4	0.2 ± 0.4	0.1	0.4
NL-1	10.0 ± 3.1	14.3	9.8	14.6 ± 3.5	15.9	11.6
NL-2	3.3 ± 1.1	3.8	2.0	1.6 ± 0.9	1.9	2.6
BE	0.9 ± 0.4	1.5	0.8	1.6 ± 0.4	1.4	1.0
FR	3.1 ± 1.4	4.2	4.1	4.0 ± 1.6	7.7	3.2
UK-1	2.4 ± 1.2	3.0	3.1	3.9 ± 1.4	4.6	2.6
UK-2	6.8 ± 1.2	7.1	6.6	12.9 ± 2.6	11.5	11.9
NO	0.1 ± 0.1	0.0	0.3	–	–	–
NA	39.8 ± 8.7	38.1	32.7	39.3 ± 7.1	35.6	41.3
EC	4.4 ± 2.1	4.4	7.2	6.7 ± 2.8	8.4	6.9
BS	0.1 ± 0.2	0.0	0.5	–	–	–
Others	1.5 ± 0.6	1.2	2.7	2.1 ± 0.9	1.8	3.0
All rivers	39.1 ± 7.5	45.0	38.7	40.9 ± 6.1	44.9	36.2
All boundaries	44.3 ± 7.7	42.6	40.4	46.0 ± 5.8	44.0	48.2

t_{strat} given in days, GOC in g O_2 m^{-2} d^{-1} and relative contributions in %.

2011 as a result of comparably short t_{strat} of only 135 days (not shown). This puts emphasis on the crucial role of stratification for the evolution of O_2 deficiency in the off-shore North Sea.

The NA contribution constitutes the major influence on N-related GOC at the ODZ site, with an average contribution of 39.8% to daily GOC and maximum contributions of up to 54.2%. This maximum is reached in 2000, when daily GOC reaches its second highest value of 0.58 g O_2 m^{-2} day^{-1}. However, it can be seen that years of high contributions by the NL-1 or DE rivers can also show very high GOC (2002 and 2011, respectively). The NL-1 contribution is highest in 2002 resulting in 15.4%, while the DE contribution is highest in 2011 (20.1%). This can be attributed to the Elbe flood in January 2011 (e.g., Kienzler et al., 2015; Mudersbach et al., 2017). Interestingly, the Elbe flood in August 2002 (Ulbrich et al., 2003; Kienzler et al., 2015; Mudersbach et al., 2017) is not reflected in a higher DE contribution in 2002, as the related loads reached the ODZ site after the growing season. However, it explains the large DE contribution of 18.2% in 2003 which is the second largest during the entire period.

The atmosphere constitutes the second largest contribution to GOC at the ODZ site, while the DE and NL-1 rivers constitute the major riverine sources yielding 11.0% and 10.0%, respectively (see **Table 3**). The British rivers (UK-1 and UK-2) also play a relevant role, adding up to 9.2%. The other sources are of minor importance with average contributions of <5%. However, they can show higher values during individual years (see maximum values in **Table 3**). The minimum–maximum ranges further indicate that especially the DE and NL-1 contributions as well as the NA contribution can show high variations between individual years. The average integrated riverine contribution to GOC of 39.1% is in the same order as the NA contribution and only about 5% less than the integrated contribution from the boundaries (NA, EC, and BS). This illustrates the great importance of riverine N inputs on O_2 deficiency at the

ODZ site, especially, from the German, Dutch, and British rivers.

3.2.3. Inter-Annual Variability in the Oyster Grounds

Figure 8 shows the time series of average daily, near-bottom GOC at the Oyster Grounds site (see **Figure 5**, region 2) analogous to **Figure 7**. The corresponding values are given in **Table 3** (right-hand side).

Average daily GOC is generally lower than at the ODZ site, which only partly relates to the smaller bottom layer thickness of 5.5 m. As for the ODZ site, minimum and maximum GOC rates occur in the years 2010 ($0.23\,g\,O_2\,m^{-2}\,day^{-1}$) and 2002 ($0.39\,g\,O_2\,m^{-2}\,day^{-1}$), respectively. However, some differences between the two sites can be seen for the other years, e.g., in 2011, which constitutes the year of only seventh strongest GOC in the Oyster Grounds.

The contributions of the individual N sources to GOC reveal the causes for these regional differences. First, the DE contribution is very small in most years as the DE rivers are downstream the Oyster Grounds relative to the general circulation. Consequently, the high N inputs from these rivers in 2011 do not affect GOC in the Oyster Grounds region. Second, the absolute NA contribution, which is the largest among all contributions, is clearly lower (average of $0.13\,g\,O_2\,m^{-2}\,day^{-1}$) than at the ODZ site (average of $0.19\,g\,O_2\,m^{-2}\,day^{-1}$). However, the relative NA contribution is about the same as at the ODZ site (39.3%) due to the lower overall GOC. In addition, the absolute atmospheric contribution is lower in the Oyster Grounds (average of $0.04\,g\,O_2\,m^{-2}\,day^{-1}$ compared to $0.06\,g\,O_2\,m^{-2}\,day^{-1}$ at the ODZ site), which also results in a slightly lower relative contribution of 13.1%.

Table 3 reveals further differences for the remaining N sources compared to the ODZ site. The influence of the NL-1 and UK-2 rivers is visibly higher, yielding average relative contributions of 14.6% and 12.9%, respectively. These values correspond to a similar average absolute NL-1 contribution ($0.05\,g\,O_2\,m^{-2}\,day^{-1}$) as for the ODZ site and an increased average absolute contribution of the UK-2 rivers ($0.04\,g\,O_2\,m^{-2}\,day^{-1}$ compared to $0.03\,g\,O_2\,m^{-2}\,day^{-1}$). Consequently, years of high contributions of either of the two N sources result in high GOC in the Oyster Grounds (see **Figure 8**; e.g., 2002, 2003, 2013). The remaining contributions are less important for GOC in the Oyster Grounds. Though, minor increases in the relative contributions can be seen in basically all contributions, except for the NL-2 and NO rivers, and the BS. This relates to the downstream locations of these sources relative to the Oyster Grounds.

The average integrated riverine contribution to N-related GOC in the Oyster Grounds adds up to 40.9%, with 30% attributed to the Dutch and British rivers. This is even higher than the NA contribution and only about 5% less than the integrated contribution from the boundaries, putting emphasis on the importance of riverine N on the O_2 dynamics in the Oyster Grounds.

4. DISCUSSION

This study, for the first time, presents a detailed quantitative analysis of the O_2 dynamics of the North Sea in relation to N inputs from various external sources, including rivers, the atmosphere and adjacent seas. By this, the presented approach

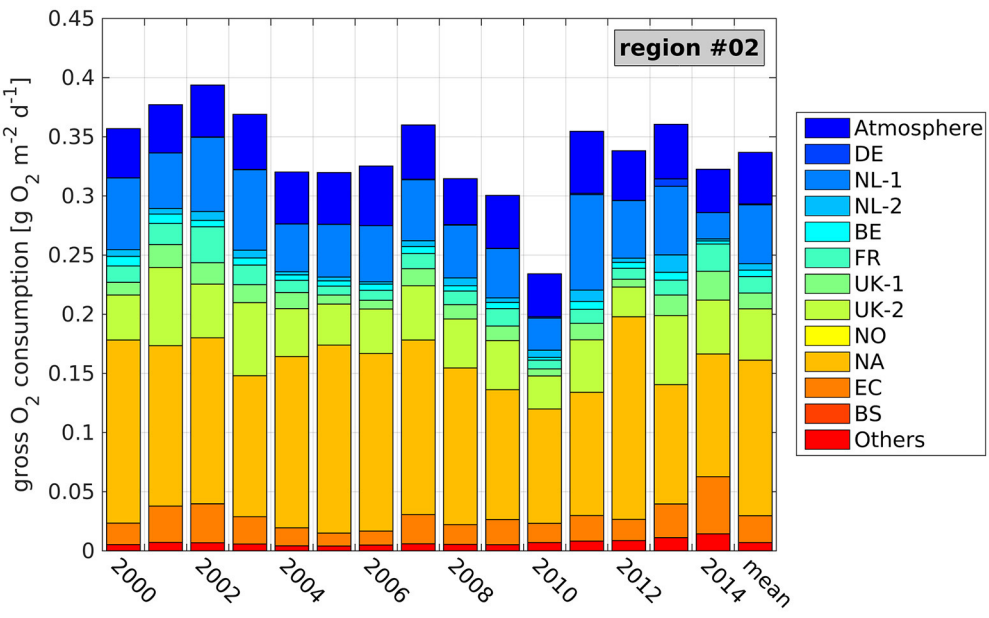

FIGURE 8 | Average daily, near-bottom gross O_2 consumption (GOC) during seasonal stratification and contributions of the different N sources (see **Table 1**) at the Oyster Grounds site (see **Figure 5**, region 2) during the individual years 2000–2014, and averaged over the entire period. Values refer to a bottom layer thickness of 5.5 m. Note different *y* axis compared to **Figure 7**.

constitutes a valuable tool for the source-oriented approach advocated by OSPAR (1999).

There have been earlier studies on the relationship between river nutrient loads and O_2 deficiency (e.g., Brockmann et al., 1988; Topcu and Brockmann, 2015). However, these studies rely on statistical analyses and the qualitative description of the interactions controlling the evolution of O_2 deficiency. Other studies investigated the effect of river nutrients on the North Sea biochemistry based on nutrient reduction scenarios (e.g., Skogen et al., 2004; Lenhart et al., 2010). Though, only Lenhart et al. (2010) considered implications for the O_2 conditions in the North Sea based on a model comparison.

However, these scenario-based approaches do not allow for the analysis of the current state of the ecosystem, that is represented by a reference scenario with realistic forcing data, with respect to the influence of nutrients from individual sources on the O_2 dynamics. Furthermore, the assessment of the influence of individual sources would require an individual scenario for each source, which is time-consuming and costly. In contrast, the present method requires only one model simulation and one TBNT analysis dealing with all selected N input sources at once.

The source-specific information on GOC obtained from the expanded TBNT method can be used for speeding up the iterative process of finding optimal N reduction targets using the linear optimization method described by Los et al. (2014). Nevertheless, actual N reduction scenarios will still be necessary in order to assess the actual impact of the derived reductions targets, due to the non-linear ecosystem interactions.

With respect to the presented results, the simulated volume transports show good agreement with other models and literature values. The same applies to the spatial distributions of TN from individual sources which correspond to results of other North Sea TBNT studies (OSPAR, 2010; Painting et al., 2013; Troost et al., 2013), giving confidence for the applicability of a TBNT post-processing software. Consequently, the analysis of GOC related to N from these sources can be assumed to yield valid information. However, the applied model setup has some limitations which require discussion.

4.1. Limitations of the Model Forcing and Setup

The forcing provided for the different N input sources (rivers and atmosphere) has a strong influence on the results of the TBNT analysis. Although the river data is compiled to the best knowledge and represents the state of the art of North Sea river data, it is based on assumptions as a result of limited data availability. An upscaling based on the distance between gauge station and river mouth and catchment area size is applied to the British rivers (van Leeuwen, pers. comm.). Here, the uncertainty can become high in case of a large distance. In addition, for some rivers only monthly data exist which have to be interpolated to daily time series, partly with support of climatologies which may not fully represent the recent state. Furthermore, estuarine retention of N and P is not considered, although they were found to be non-negligible, e.g., in the Elbe estuary (Behrendt, 1996; Dähnke et al., 2008).

Furthermore, point sources (e.g., sewage treatment plants) in the estuaries — downstream the nutrient monitoring locations used for the load calculation (Pätsch et al., 2016) — are not considered in the river data, except for the British rivers. For the major Dutch rivers (excl. the smaller North Sea Canal) nutrient concentrations are measured right at the floodgates, i.e., point sources are implicitly considered. For the German rivers, which together with the former two are the most important riverine N sources, only limited information on point sources are available. However, Dähnke et al. (2008) found no evidence of a significant influence of point sources on NO_3^- concentrations in the Elbe estuary, based on stable isotope analyses. A catchment modeling study for the Weser shows that only about $0.1\,kt\,N\,a^{-1}$ enter the surface waters along the Weser estuary (Heidecke et al., 2015). Hence, it can be assumed that neglecting point sources in the estuaries is a reasonable constraint.

For the atmospheric N deposition the data availability also constitutes a relevant constraint. In order to run a realistic simulation, the data needs to be provided for the entire simulation period and model domain. This can be obtained by temporal extrapolation and spatial interpolation to the model grid, based on the original N deposition data from EMEP. However, this original data as well as the spatio-temporal processing are subject to uncertainties. In this study, annual EMEP data was used, though, also monthly data are available (Desmit et al., 2015). As atmospheric N deposition in the North Sea region experiences a distinct annual cycle with higher summer and lower winter values (e.g., Neumann et al., 2016), the use of these monthly data could be worthwhile for future analyses. Differences in the applied atmospheric deposition data may also partly explain the minor differences between the results for the atmospheric contribution to TN of this study and those of Troost et al. (2013), who found a higher atmospheric contribution in the southern North Sea.

Another N-related aspect not considered in ECOHAM is the exchange between the North Sea and the Wadden Sea. Postma (1981) describe the Wadden Sea as a relevant sink for organic and source of inorganic matter. Other studies reported the Wadden Sea constitutes an important sink of N due to benthic denitrification (e.g., Kieskamp et al., 1991; van Beusekom and de Jonge, 1998; van Beusekom et al., 1999). Both would affect N availability in the open North Sea, especially, upstream of the ODZ site. Therefore, the Wadden Sea should be included in future studies.

With respect to the TBNT results, we consider the NA contribution to TN (and GOC) in the southeastern North Sea to be slightly overestimated. We conclude this from a comparison of the source-specific TN contributions of the other most relevant sources (atmosphere, DE, NL-1, and UK-2) to a box in the inner German Bight (not shown) calculated in our study with other TBNT studies on TN (e.g., OSPAR, 2010; Painting et al., 2013; Troost et al., 2013). This may relate to the limited spatial resolution of about 20 km that does not allow for the representation of sub-mesoscale features such as eddies (e.g.,

Johannessen et al., 1989; Røed and Fossum, 2004; Albretsen, 2007).

4.2. Limitations of the Model Intrinsics and the TBNT Method

With respect to the hydrodynamics, the component-upstream advection scheme applied by HAMSOM could be an additional cause for the overestimation of the NA contribution as it results in high numerical diffusion (Lenhart and Pohlmann, 1997). However, the identification of the actual cause goes beyond the scope of this study.

Regarding the model biogeochemistry, it should be noted that the benthic re-mineralization tends to be slightly underestimated by ECOHAM (Große et al., 2016). On the one hand, this can affect the overall GOC. On the other hand, the contributions of individual N sources to GOC may be affected as the influence of sources with high contributions to benthic re-mineralization would be amplified relative to sources with only low contributions. In addition, the rather simple sediment module does not allow for long-term storage or burial of organic matter in the sediment. However, this matches with observational studies that found burial of N and C in the North Sea sediment being only small relative to annual cycles of NPP and respiration (Wirth and Wiesner, 1988; de Haas et al., 1997; Brion et al., 2004).

In relation to the benthic processes, it should also be noted that simulated daily benthic denitrification rates in the inner German Bight are up to 4 times higher than those recently reported by Marchant et al. (2016). However, this only applies to few very near-shore areas in the model. In the off-shore regions nitrification rates range between 0.4 and 2 mmol N m^{-2} day^{-1}, which is in the range they found. Hence, we rate the additional N loss in our simulation as acceptable as it only occurs in a very small region. In addition, the here applied simple benthic module only includes the effect of O_2 availability in the pelagic bottom layer on benthic processes. As anoxic conditions do not occur in the pelagic North Sea, this has no effect on the benthic processes. Thus, the incorporation of a more complex benthic module, that resolves vertical O_2 gradients within the sediment, would be worthwhile.

Furthermore, ECOHAM applies constant C:N:P ratios to phytoplankton, zooplankton and bacteria (Lorkowski et al., 2012; Große et al., 2016). Though, it is known that elemental ratios vary between different phytoplankton species (e.g., Geider and La Roche, 2002; Quigg et al., 2003; Malzahn et al., 2010) as well as under varying environmental conditions (e.g., Rhee, 1978; Goldman et al., 1979). In fact, different elemental ratios, e.g., in phytoplankton, would impact on the entire ecosystem including organic matter production and, thus, on the O_2 dynamics. For instance, unpublished sensitivity studies showed that organic matter export below 30 m varies by up to 13% with varying stoichiometry (Redfield $\pm$ 50%). Consequently, this may slightly change the relative contributions of the different N sources to GOC in relation to temporal variability in these contributions combined with temporal variability in the elemental ratios. However, in order to assess the impact of different stoichiometry a comprehensive sensitivity analysis would be required which is beyond the scope of this study.

With respect to the expansion of TBNT by the link to the O_2 cycle, the use of the mediators in case of C-based O_2-affecting processes (e.g., NPP) constitutes a key element. Therefore, discussion of the constraints of this approach is required. The actual values of the C-based O_2-affecting processes are proportional to the concentration of the C-based mediator state variable (see Appendix A.1–A.4). The use of the mediator implies that the concentration of the C-based mediator variable is proportional to the corresponding N-based mediator variable. This evidently can be applied in the case of a fixed C:N ratio as used for phytoplankton, zooplankton and bacteria in the present study.

Conceptually, this also holds for a varying stoichiometry as used for benthic detrital matter (i.e., sediment-N/-C) in ECOHAM. Higher concentrations of sediment-N allow for higher concentrations of sediment-C and, thus, benthic O_2 consumption. However, temporal variations in the C:N ratio in benthic detrital matter in combination with temporal variations in the contributions of individual N sources to sediment-N can affect the contributions of these sources to benthic O_2 consumption and, thus, to near-bottom GOC.

A quantitative analysis of this effect would require a comprehensive sensitivity study on the effect of different C:N ratios on the TBNT results. Here, we will only discuss effects of the mediator use in relation to potential event-driven changes in the C:N ratio in benthic detrital matter.

In the off-shore regions of the southern and southeastern North Sea — which are in the focus of this study — benthic organic matter originates mainly from local NPP (Große et al., 2016). Thus, organic matter input from rivers especially during the summer period does not need to be considered. Davies and Payne (1984) observed C:N ratios of 9–18 in particulate organic matter 2 m above the sea floor in the northern North Sea during the spring bloom 1976. For the southern North Sea off Belgium, Tungaraza et al. (2003) report C:N ratios of 5.7–11.2 in particulate organic matter, depending on the phytoplankton species composition. This indicates that even over short periods of time (days to weeks) C:N ratios in organic matter may vary by a factor of 2. If such short-term variations coincide with strong variations in the contributions by individual N sources to detrital matter, this may result in an under-/overestimation of the influence of individual N sources on GOC. Analogously, such effects may occur, e.g., during events of strong rainfall over sea during the growing season, which enhance wet N deposition and thereby enable new production due to increased NO_3^- availability (e.g., Dugdale and Goering, 1967).

Regarding the here presented analysis of source-specific GOC at the ODZ and the Oyster Grounds sites it should be noted that the C:N ratios in benthic detrital matter show only very minor variations, ranging from 7.5 to 7.9, during the growing season. As this period basically corresponds to the summer stratified period, which is in the focus of this study, the effect of changing C:N ratios on the source-specific contributions to GOC is considered to be small. However, considering model applications using variable phytoplankton stoichiometry additional efforts would

be required for further improving the mediator approach. Here, it may be feasible to use the actual C:N ratios and relative contributions by the individual N sources in both, detrital matter that was previously sedimented and newly sedimented matter, as a weighing factor. By this potential errors in the current approach could be minimized.

Besides the effects of varying C:N ratios, differences in the re-mineralization rates of C (0.028 day^{-1}) and N (0.0333 day^{-1}) may affect the results of the expanded TBNT due to a temporal delay between C and N re-mineralization (and benthic denitrification). However, in the present study the time series of sediment-N and -C (not shown) reveal maximum temporal delays of only 2–3 days. Therefore, we consider this to have only a minor impact on the results.

In relation to the mediators, it has to be stated clearly that the results of this study can only be interpreted with respect to N, i.e., they do not reflect the overall influence of the selected input sources on the O_2 dynamics. Labeling C or P from individual input sources will likely result in different relative contributions. On the one hand, this may relate to changes in the inputs by the different sources relative to each other (e.g., different ratios between P loads of individual rivers compared to N loads). On the other hand, selected processes (e.g., nitrification) cannot be considered in case of P labeling, while other processes such as P release from the sediment under anoxic conditions would play an additional role when considering P (e.g., Hupfer and Lewandowski, 2008). However, this process is not included in ECOHAM as it is designed primarily to represent the O_2 cycle in relation to N and C. As N constitutes the limiting nutrient among these two with respect to organic matter production, we focused our analysis on N. In order to assess the overall impact of nutrients (i.e., N and P) from individual sources on the North Sea O_2 dynamics, an analogous analysis for P would be required. However, this is beyond the scope of this study. In relation to that, it also has to be noted that the TBNT analysis does not replace actual nutrient reduction scenarios, but rather constitutes a useful tool for speeding up the iterative process of finding an optimal nutrient reduction setup (Los et al., 2014).

Furthermore, the presented method cannot be applied to formulations of benthic O_2 consumption only based on the O_2 concentration itself, e.g., that by Hetland and DiMarco (2008), as those cannot be linked to external nutrients.

Due to these uncertainties and constraints, we highly recommend applying the presented method to different models and model setups. This would provide a range of the contributions of the individual N sources on the O_2 dynamics of the North Sea, giving a more reliable estimate of their actual influence. The only requirement for such approach is the process-based parametrization of the O_2-affecting processes in that model, such that a mediator substance provides a link between the labeled element and the O_2 cycle.

5. CONCLUSIONS

The here presented expansion of the TBNT method and the corresponding analysis of source-specific GOC represent the first approach for quantifying the influence of N inputs from different sources on the O_2 dynamics of a marine ecosystem. Our study focused on the North Sea and our analysis constitutes a major advancement toward the source-oriented approach for the ecological management of O_2 deficiency in the North Sea (OSPAR, 1999). Besides this, the described method can be applied analogously to different elements (e.g., P or C), ecosystems and models. Therefore, it could be used for the investigation of other ecosystems affected by eutrophication-related O_2 deficiency, e.g., the Baltic Sea (e.g., Rosenberg, 1985) or the northern Gulf of Mexico (e.g., Rabalais and Turner, 2001).

The present analysis focused on the general spatial patterns and inter-annual variability in the regions most susceptible to O_2 deficiency. Though, the applied method can also be used for analyzing the influences of individual sources of N (and other nutrients) on different time scales (days to decades).

While GOC in the northern and northern central North Sea is dominated by the N inputs from the North Atlantic, GOC in the southern central and southern North Sea is under the combined influence of the North Atlantic (NA), the English Channel (EC), the atmosphere and the large riverine N sources. Among the riverine N sources, especially, the large Dutch rivers (NL-1; incl. Rhine and Meuse) and the rivers at the British east coast (UK-2) have a relevant influence on GOC in the off-shore regions of the southern North Sea, while the German rivers dominate the southeastern coastal North Sea.

The analysis of GOC at the two study sites confirmed that seasonal stratification constitutes the prerequisite for the evolution of O_2 deficiency in the off-shore regions of the southern North Sea (Große et al., 2016). It further revealed that riverine N inputs play a major role for the bottom O_2 dynamics, with average relative contributions of about 40% during 2000–2014. Depending on their timing, flood events in the German or Dutch rivers can increase the riverine contribution to even more than 50%. In addition, atmospheric N contributes about 15% to the overall GOC at both sites. As riverine and atmospheric inputs are strongly anthropogenically affected (Paerl, 1997; Schöpp et al., 2003) this emphasizes the large human impact on the O_2 conditions in the North Sea regions most susceptible to O_2 deficiency.

Consequently, thoroughly defined riverine N reductions, e.g., under the European Union's Water Framework Directive (EU, 2000) likely constitute a potent means for improving the O_2 conditions in the southern North Sea. In combination with potential future reductions in atmospheric N deposition — as adopted within the Gothenburg Protocol (UNESC, 1999) — such reductions may improve the North Sea O_2 conditions or mitigate potential negative effects of climate change.

In this context it is important to note that also future changes in the physical environment, e.g., in stratification or seawater *T*, will have a relevant impact on the O_2 conditions of the North Sea as they play a key role in the O_2 dynamics (Greenwood et al., 2010; Große et al., 2016). However, our results emphasize that future scenarios for the North Sea require realistic estimates for both, the climatic conditions and the riverine and atmospheric N loads in order to provide a likely picture of the future North Sea O_2 conditions.

AUTHOR CONTRIBUTIONS

The original manuscript was conceptualized and set up by FG and H-JL. The simulations were set up and conducted jointly by FG, MK, and JP. All analyses were conducted by FG. All authors contributed equally to the reworking of the original manuscript toward the submitted version.

FUNDING

This study received funding from the German Environmental Protection Agency (UBA), in the frame of the project "Implementation of Descriptor 5 Eutrophication to the "MSFD", SN: 3713225221, and the Cluster of Excellence "CliSAP" (EXC177), Universität Hamburg, funded by the German Science Foundation (DFG).

ACKNOWLEDGMENTS

We thank the three reviewers for their helpful comments and constructive criticism on the original manuscript. We would like to thank Sonja van Leeuwen from Cefas for providing freshwater discharge and nutrient load data for the major rivers across Europe. We further thank Jerzy Bartnicki from EMEP for providing atmospheric N deposition data. The model simulations were conducted on "Mistral," the Atos bullx DLC B700 mainframe at the German Climate Computing Center (DKRZ) in Hamburg. The methods used in this study were published as part of the dissertation by Große (2017).

SUPPLEMENTARY MATERIAL

The Supplementary Material for this article can be found online at: https://www.frontiersin.org/articles/10.3389/fmars.2017.00383/full#supplementary-material

REFERENCES

Albretsen, J. (2007). The impact of freshwater discharges on the ocean circulation in the Skagerrak/northern North Sea area. Part II: energy analysis. *Ocean Dynam.* 57, 287–304. doi: 10.1007/s10236-007-0121-6

Arakawa, A., and Lamb, V. (1977). "Computational design of the basic dynamical processes of the {UCLA} general circulation model," in *General Circulation Models of the Atmosphere, Vol. 17, Methods in Computational Physics: Advances in Research and Applications*, ed J. Chang (London: Elsevier), 173–265.

Artioli, Y., Friedrich, J., Gilbert, A., McQuatters-Gollop, A., Mee, L., Vermaat, J., et al. (2008). Nutrient budgets for European seas: a measure of the effectiveness of nutrient reduction policies. *Mar. Pollut. Bull.* 56, 1609–1617. doi: 10.1016/j.marpolbul.2008.05.027

Azam, F., Fenchel, T., Field, J., Gray, J., Meyer-Reil, L., and Thingstad, F. (1983). The ecological role of water-column microbes in the sea. *Mar. Ecol. Prog. Ser.* 10, 257–263. doi: 10.3354/meps010257

Backhaus, J. (1985). A three-dimensional model for the simulation of shelf sea dynamics. *Ocean Dynam.* 38, 165–187. doi: 10.1007/BF02328975

Backhaus, J., and Hainbucher, D. (1987). A finite difference general circulation model for shelf seas and its application to low frequency variability on the North European Shelf. *Elsev. Oceanogr. Ser.* 45, 221–244. doi: 10.1016/S0422-9894(08)70450-1

Behrendt, H. (1996). Inventories of point and diffuse sources and estimated nutrient loads – a comparison for different river basins in Central Europe. *Water Sci. Technol.* 33, 99–107.

Blauw, A., van de Wolfshaar, K., and Meuwese, H. (2006). Transboundary nutrient transports in the North Sea. *WL|Delft Hydraulics Reports*, Z4188 (Accessed Sep 16, 2016).

Brion, N., Baeyens, W., de Galan, S., Elskens, M., and Laane, R. (2004). The North Sea: source or sink for nitrogen and phosphorus to the Atlantic Ocean? *Biogeochemistry* 68, 277–296. doi: 10.1023/B:BIOG.0000031041.38663.aa

Brockmann, U., Billen, G., and Gieskes, W. (1988). "North Sea Nutrients and Eutrophication," in *Pollution of the North Sea: An Assessment*, eds W. Salomons, B. Bayne, E. Duursma, and U. Förstner (Berlin; Heidelberg: Springer), 348–389.

Brockmann, U., and Eberlein, K. (1986). "River input of nutrients into the German Bight," in *The Role of Freshwater Outflow in Coastal Marine Ecosystems*, ed S. Stig (Berlin; Heidelberg: Springer), 231–240.

Chen, X., Liu, C., O'Driscoll, K., Mayer, B., Su, J., and Pohlmann, T. (2013). On the nudging terms at open boundaries in regional ocean models. *Ocean Model.* 66, 14–25. doi: 10.1016/j.ocemod.2013.02.006

Claussen, U., Zevenboom, W., Brockmann, U., Topcu, D., and Bot, P. (2009). Assessment of the eutrophication status of transitional, coastal and marine waters within OSPAR. *Hydrobiologia* 629, 49–58. doi: 10.1007/s10750-009-9763-3

Conkright, M. E., Locarnini, R. A., Garcia, H. E., O'Brien, T. D., Boyer, T. P., and Stephens, C. (2002). *World Ocean Atlas 2001: Objective Analyses, Data Statistics, and Figures: CD-ROM Documentation*. (Accessed on November 16, 2016)

Dähnke, K., Bahlmann, E., and Emeis, K. (2008). A nitrate sink in estuaries? An assessment by means of stable nitrate isotopes in the Elbe estuary. *Limnol. Oceanogr.* 53, 1504–1511. doi: 10.4319/lo.2008.53.4.1504

Danielssen, D., Edler, L., Fonselius, S., Hernroth, L., Ostrowski, M., Svendsen, E., and Talpsepp, L. (1997). Oceanographic variability in the Skagerrak and northern Kattegat, May–June, 1990. *ICES J. Mar. Sci.* 54, 753–773. doi: 10.1006/jmsc.1996.0210

Davies, J., and Payne, R. (1984). Supply of organic matter to the sediment in the northern North Sea during a spring phytoplankton bloom. *Mar. Biol.* 78, 315–324. doi: 10.1007/BF00393017

de Haas, H., Boer, W., and van Weering, T. (1997). Recent sedimentation and organic carbon burial in a shelf sea: the North Sea. *Mar. Geol.* 144, 131–146. doi: 10.1016/S0025-3227(97)00082-0

de Wilde, P., Berghuis, E., and Kok, A. (1984). Structure and energy demand of the benthic community of the oyster ground, central north sea. *Neth. J. Sea Res.* 18, 143–159. doi: 10.1016/0077-7579(84)90029-2

Desmit, X., Lacroix, G., Dulière, V., Lancelot, C., Gypens, N., Ménesguen, A., et al. (2015). *Ecosystem models as support to eutrophication management in the North Atlantic OCean.* (EMoSEM) Final report. (Accessed on January 11, 2017).

Díaz, R., and Rosenberg, R. (1995). Marine benthic hypoxia: a review of its ecological effects and the behavioural responses of benthic macrofauna. *Oceanogr. Mar. Biol.* 33, 245–03.

Dugdale, R., and Goering, J. (1967). Uptake of new and regenerated forms of nitrogen in primary productivity. *Limnol. Oceanogr.* 12, 196–206. doi: 10.4319/lo.1967.12.2.0196

EU (2000). *Directive 2000/60/EC of the European Parliament and of the Council of 23 October 2000 Establishing a Framework for Community Action in the Field of Water Policy*, Vol. 43. Brussels. (Accessed on January 04, 2017).

Fennel, K., Wilkin, J., Levin, J., Moisan, J., O'Reilly, J., and Haidvogel, D. (2006). Nitrogen cycling in the Middle Atlantic bight: results from a three-dimensional model and implications for the North Atlantic nitrogen budget. *Glob. Biogeochem. Cycles* 20:GB3007. doi: 10.1029/2005GB002456

Friedrich, J., Janssen, F., Aleynik, D., Bange, H., Boltacheva, N., Çagatay, M., et al. (2014). Investigating hypoxia in aquatic environments: diverse approaches to addressing a complex phenomenon. *Biogeosciences* 11, 1215–1259. doi: 10.5194/bg-11-1215-2014

Geider, R., and La Roche, J. (2002). Redfield revisited: variability of C:N:P in marine microalgae and its biochemical basis. *Eur. J. Phycol.* 37, 1–17. doi: 10.1017/S0967026201003456

Goldman, J., McCarthy, J., and Peavey, D. (1979). Growth rate influence on the chemical composition of phytoplankton in oceanic waters. *Nature* 279:1. doi: 10.1038/279210a0

Gray, J., Wu, R., and Or, Y. (2002). Effects of hypoxia and organic enrichment on the coastal marine environment. *Mar. Ecol. Prog. Ser.* 238, 249–279. doi: 10.3354/meps238249

Greenwood, N., Parker, E., Fernand, L., Sivyer, D., Weston, K., Painting, S., et al. (2010). Detection of low bottom water oxygen concentrations in the North Sea; implications for monitoring and assessment of ecosystem health. *Biogeosciences* 7, 1357–1373. doi: 10.5194/bg-7-1357-2010

Gröger, M., Maier-Reimer, E., Mikolajewicz, U., Moll, A., and Sein, D. (2013). NW European shelf under climate warming: implications for open ocean-shelf exchange, primary production, and carbon absorption. *Biogeosciences* 10, 3767–3792. doi: 10.5194/bg-10-3767-2013

Große, F. (2017). *The Influence of Nitrogen Inputs on the Oxygen Dynamics of the North Sea*. Ph.D. thesis, Universität Hamburg, Hamburg. Available online at: http://ediss.sub.uni-hamburg.de/volltexte/2017/8524

Große, F., Greenwood, N., Kreus, M., Lenhart, H.-J., Machoczek, D., Pätsch, J., et al. (2016). Looking beyond stratification: a model-based analysis of the biological drivers of oxygen deficiency in the North Sea. *Biogeosciences* 13, 2511–2535. doi: 10.5194/bg-13-2511-2016

Heidecke, C., Hirt, U., Kreins, P., Kuhr, P., Kunkel, R., Mahnkopf, J., et al. (2015). *Endbericht zum Forschungsprojekt "Entwicklung eines Instrumentes für ein flussgebietsweites Nährstoffmanagement in der Flussgebietseinheit Weser" AGRUM^{+}-Weser*. Thünen Report 21, Johann Heinrich von Thünen-Institut, Braunschweig.

Hetland, R., and DiMarco, S. (2008). How does the character of oxygen demand control the structure of hypoxia on the Texas–Louisiana continental shelf? *J. Mar. Syst.* 70, 49–62. doi: 10.1016/j.jmarsys.2007.03.002

Hupfer, M., and Lewandowski, J. (2008). Oxygen Controls the phosphorus release from lake sediments – a long-lasting paradigm in limnology. *Int. Rev. Hydrobiol.* 93, 415–432. doi: 10.1002/iroh.200711054

ICG-EMO (2009). *ICG-EMO 3rd OSPAR Workshop User Guide*. Brussels: Intersessional Correspondence Group on Eutrophication Modelling.

ICNS-2 (1988). Second international conference on the protection of the North Sea: ministerial declaration calling for reduction of pollution. *Int. Legal Mater.* 27, 835–848.

Johannessen, J., Sandven, S., Lygre, K., Svendsen, E., and Johannessen, O. (1989). Three-dimensional structure of mesoscale eddies in the Norwegian Coastal Current. *J. Phys. Oceanogr.* 19, 3–19. doi: 10.1175/1520-0485(1989)019<0003:TDSOME>2.0.CO;2

Kalnay, E., Kanamitsu, M., Kistler, R., Collins, W., Deaven, D., Gandin, L., et al. (1996). The NCEP/NCAR 40-year reanalysis project. *B. Am. Meteorol. Soc.* 77, 437–471. doi: 10.1175/1520-0477(1996)077<0437:TNYRP>2.0.CO;2

Kienzler, S., Pech, I., Kreibich, H., Müller, M., and Thieken, A. (2015). After the extreme flood in 2002: changes in preparedness, response and recovery of flood-affected residents in Germany between 2005 and 2011. *Nat. Hazard. Earth Sys.* 15, 505–526. doi: 10.5194/nhess-15-505-2015

Kieskamp, W., Lohse, L., Epping, E., and Helder, W. (1991). Seasonal variation in denitrification rates and nitrous oxide fluxes in intertidal sediments of the western Wadden Sea. *Mar. Ecol. Prog. Ser.* 72, 145–151. doi: 10.3354/meps072145

Kistler, R., Collins, W., Saha, S., White, G., Woollen, J., Kalnay, E., et al. (2001). The NCEP-NCAR 50-year reanalysis: monthly means CD-ROM and documentation. *Am. Meteorol. Soc.* 82, 247–267. doi: 10.1175/1520-0477(2001)082<0247:TNNYRM>2.3.CO;2

Kühn, W., Pätsch, J., Thomas, H., Borges, A., Schiettecatte, L.-S., Bozec, Y., et al. (2010). Nitrogen and carbon cycling in the North Sea and exchange with the North Atlantic–A model study, Part II: carbon budget and fluxes. *Cont. Shelf Res.* 30, 1701–1716. doi: 10.1016/j.csr.2010.07.001

Lacroix, G., Ruddick, K., Gypens, N., and Lancelot, C. (2007). Modelling the relative impact of rivers (Scheldt/Rhine/Seine) and Western Channel waters on the nutrient and diatoms/Phaeocystis distributions in Belgian waters (Southern North Sea). *Cont. Shelf Res.* 27, 1422–1446. doi: 10.1016/j.csr.2007.01.013

Lenhart, H.-J., Mills, D., Baretta-Bekker, H., van Leeuwen, S., van der Molen, J., Baretta, J., et al. (2010). Predicting the consequences of nutrient reduction on the eutrophication status of the North Sea. *J. Mar. Syst.* 81, 148–170. doi: 10.1016/j.jmarsys.2009.12.014

Lenhart, H.-J., and Pohlmann, T. (1997). The ICES-boxes approach in relation to results of a North Sea circulation model. *Tellus A* 49, 139–160. doi: 10.3402/tellusa.v49i1.12217

Liebig, J. (1841). *Die Organische Chemie in ihrer Anwendung auf Agricultur und Physiologie*. F. Vieweg und Sohn. Braunschweig. (Accessed on January 17, 2017).

Lorkowski, I., Pätsch, J., Moll, A., and Kühn, W. (2012). Interannual variability of carbon fluxes in the North Sea from 1970 to 2006 – Competing effects of abiotic and biotic drivers on the gas-exchange of CO_2. *Estuar. Coast. Shelf Sci.* 100, 38–57. doi: 10.1016/j.ecss.2011.11.037

Los, F., Troost, T., and van Beek, J. (2014). Finding the optimal reduction to meet all targets – applying Linear Programming with a nutrient tracer model of the North Sea. *J. Mar. Syst.* 131, 91–101. doi: 10.1016/j.jmarsys.2013.12.001

Malzahn, A., Hantzsche, F., Schoo, K. L., Boersma, M., and Aberle, N. (2010). Differential effects of nutrient-limited primary production on primary, secondary or tertiary consumers. *Oecologia* 162, 35–48. doi: 10.1007/s00442-009-1458-y

Marchant, H., Holtappels, M., Lavik, G., Ahmerkamp, S., Winter, C., and Kuypers, M. (2016). Coupled nitrification–denitrification leads to extensive N loss in subtidal permeable sediments. *Limnol. Oceanogr.* 61, 1033–1048. doi: 10.1002/lno.10271

Mathis, M., and Pohlmann, T. (2014). Projection of physical conditions in the North Sea for the 21st century. *Clim. Res.* 61, 1–17. doi: 10.3354/cr01232

Ménesguen, A., Cugier, P., and Leblond, I. (2006). A new numerical technique for tracking chemical species in a multi-source, coastal ecosystem, applied to nitrogen causing Ulva blooms in the Bay of Brest (France). *Limnol. Oceanogr.* 51, 591–601. doi: 10.4319/lo.2006.51.1_part_2.0591

Ménesguen, A., and Hoch, T. (1997). Modelling the biogeochemical cycles of elements limiting primary production in the English Channel. I. Role of thermohaline stratification. *Mar. Ecol. Prog. Ser.* 146, 173–188. doi: 10.3354/meps146173

Mudersbach, C., Bender, J., and Netzel, F. (2017). An analysis of changes in flood quantiles at the gauge Neu Darchau (Elbe River) from 1875 to 2013. *Stoch. Env. Res. Risk Assess.* 31, 145–157. doi: 10.1007/s00477-015-1173-7

Müller, L. (2008). *Sauerstoffdynamik der Nordsee — Untersuchungen mit einem drei-dimensionalen Ökosystemmodell*. Ph.D. thesis, Universität Hamburg. Available online at: http://ediss.sub.uni-hamburg.de/volltexte/2008/3663/pdf/LM-Doktorarbeit_19.03.08.pdf (Accessed on November 20, 2017).

Neumann, D., Matthias, V., Bieser, J., Aulinger, A., and Quante, M. (2016). Sensitivity of modeled atmospheric nitrogen species and nitrogen deposition to variations in sea salt emissions in the North Sea and Baltic Sea regions. *Atmos. Chem. Phys.* 16, 2921–2942. doi: 10.5194/acp-16-2921-2016

Neumann, T. (2000). Towards a 3D-ecosystem model of the Baltic Sea. *J. Mar. Syst.* 25, 405–419. doi: 10.1016/S0924-7963(00)00030-0

Neumann, T. (2007). The fate of river-borne nitrogen in the Baltic Sea–An example for the River Oder. *Estuar. Coast. Shelf Sci.* 73, 1–7. doi: 10.1016/j.ecss.2006.12.005

OSPAR (1999). *Strategy to Combat Eutrophication, Reference number: 1998–18*. London: OSPAR Commission, (Accessed on January 23, 2017).

OSPAR (2003). *OSPAR Integrated Report 2003 on the Eutrophication Status of the OSPAR Maritime Area Based Upon the First Application of the Comprehensive Procedure*. London: OSPAR Commission. (Accessed on January 05, 2017).

OSPAR (2010). *Results of the 2009 ICG-EMO Workshop on transboundary nutrient transport, vol. 540/2011*. London: OSPAR Commission.

OSPAR (2013). *Riverine Inputs and Direct Discharges to Convention Waters – Contracting Parties' RID 2011 Data Report, vol. 598/2013*. London: OSPAR Commission. (Accessed on January 04, 2017).

Otto, L., Zimmerman, J., Furnes, G., Mork, M., Saetre, R., and Becker, G. (1990). Review of the physical oceanography of the North Sea. *Neth. J. Sea Res.* 26, 161–238. doi: 10.1016/0077-7579(90)90091-T

Ozer, J. (2011). *Model to Model Comparison of Transports Through North Sea Transects*. Brussels: North West Shelf Operational Oceanographic System (NOOS). (Accessed on November 04, 2016).

Paerl, H. (1997). Coastal eutrophication and harmful algal blooms: Importance of atmospheric deposition and groundwater as "new" nitrogen and other nutrient sources. *Limnol. Oceanogr.* 42, 1154–1165. doi: 10.4319/lo.1997.42.5_part_2.1154

Painting, S., Foden, J., Forster, R., van der Molen, J., Aldridge, J., Best, M., et al. (2013). Impacts of climate change on nutrient enrichment. *Mar. Clim. Change Impacts Partnership*. 219–235. doi: 10.14465/2013.arc23.219-235

Pätsch, J., and Kühn, W. (2008). Nitrogen and carbon cycling in the North Sea and exchange with the North Atlantic–A model study. Part I. Nitrogen budget and fluxes. *Cont. Shelf Res.* 28, 767–787. doi: 10.1016/j.csr.2007.12.013

Pätsch, J., Lenhart, H.-J., and Schütt, M. (2016). *Daily Loads of Nutrients, Total Alkalinity, Dissolved Inorganic Carbon and Dissolved Organic Carbon of the European Continental Rivers for the Years 1977–2014*. Technical Report, Institut fü| Meereskunde, Universität. Hamburg.

Paulmier, A., Kriest, I., and Oschlies, A. (2009). Stoichiometries of remineralisation and denitrification in global biogeochemical ocean models. *Biogeosciences* 6, 923–935. doi: 10.5194/bg-6-923-2009

Peeters, J., Los, F., Jansen, R., Haas, H., Peperzak, L., and de Vries, I. (1995). The oxygen dynamics of the Oyster Ground, North Sea. Impact of eutrophication and environmental conditions. *Ophelia* 42, 257–288. doi: 10.1080/00785326.1995.10431508

Perrot, T., Rossi, N., Ménesguen, A., and Dumas, F. (2014). Modelling green macroalgal blooms on the coasts of Brittany, France to enhance water quality management. *J. Mar. Syst.* 132, 38–53. doi: 10.1016/j.jmarsys.2013.12.010

Philipp, A., Kerl, F., and Müller, U. (2015). Ansprüche potenzieller Nutzer an ein Hochwasser-Frühwarnsystem für Sachsen. *Hydrol. Wasserbewirts.* 1, 4–22. doi: 10.5675/HyWa_2015.1_1

Pohlmann, T. (1991). *Untersuchung hydro- und Thermodynamischer Prozesse in der Nordsee mit einem Dreidimensionalen Numerischem Modell*. *Berichte aus dem Zentrum für Meeres- und Klimaforschung*, Ph.D. Thesis. Reihe B(Nr. 23).

Pohlmann, T. (1996). Predicting the thermocline in a circulation model of the North Sea - Part I: model description, calibration and verification. *Cont. Shelf Res.* 16, 131–146. doi: 10.1016/0278-4343(95)90885-S

Pohlmann, T. (2006). A meso-scale model of the central and southern North Sea: consequences of an improved resolution. *Cont. Shelf Res.* 26, 2367–2385. doi: 10.1016/j.csr.2006.06.011

Pohlmann, T., and Puls, W. (1994). "Currents and Transport in Water," in *Circulation and Contaminant Fluxes in the North Sea*, ed J. Sündermann (Berlin; Heidelberg: Springer), 345–402.

Postma, H. (1981). Exchange of materials between the North Sea and the Wadden Sea. *Mar. Geol.* 40, 199–213. doi: 10.1016/0025-3227(81)90050-5

Queste, B., Fernand, L., Jickells, T., Heywood, K., and Hind, A. (2016). Drivers of summer oxygen depletion in the central North Sea. *Biogeosciences* 13, 1209–1222. doi: 10.5194/bg-13-1209-2016

Quigg, A., Finkel, Z., Irwin, A., Rosenthal, Y., Ho, T.-Y., Reinfelder, J., et al. (2003). The evolutionary inheritance of elemental stoichiometry in marine phytoplankton. *Nature* 425, 291–294. doi: 10.1038/nature01953

Rabalais, N., and Turner, R. (2001). *Hypoxia in the Northern Gulf of Mexico: Description, Causes and Change*, Washington, DC: Coastal and Estuarine Studies. American Geophysical Union, 1–36

Rabalais, N., Turner, R., and Scavia, D. (2002). Beyond Science into Policy: gulf of Mexico Hypoxia and the Mississippi River. *BioScience* 52, 129–142. doi: 10.1641/0006-3568(2002)052[0129:BSIPGO]2.0.CO;2

Rachor, E., and Albrecht, H. (1983). *Sauerstoffmangel im Bodenwasser der Deutschen Bucht*, *Vol. 19*. Bremerhaven: Veröfflichungen des Instituts für Meeresforschung.

Radtke, H. (2012). *Einfluss biologischer Prozesse auf die Ausbreitungswege von Nährstoffen in der Ostsee*. Ph.D. thesis, Universität Rostock. (Accessed on September 16, 2017).

Radtke, H. and Maar, M. (2016). Estimating the effective nitrogen import: an example for the North Sea-Baltic Sea boundary. *J. Geophys. Res. Biogeo.* 121, 2562–2575. doi: 10.1002/2016JG003516

Radtke, H., Neumann, T., Voss, M., and Fennel, W. (2012). Modeling pathways of riverine nitrogen and phosphorus in the Baltic Sea. *J. Geophys. Res. Oceans* 117, 1–15. doi: 10.1029/2012JC008119

Redfield, A. (1934). *On the Proportions of Organic Derivatives in Sea Water and Their Relation to the Composition of Plankton*. University Press of Liverpool. (Accessed on October 16, 2017).

Rhee, G.-Y. (1978). Effects of N:P atomic ratios and nitrate limitation on algal growth, cell composition, and nitrate uptake. *Limnol. Oceanogr.* 23, 10–25. doi: 10.4319/lo.1978.23.1.0010

Rodhe, J. (1996). On the dynamics of the large-scale circulation of the Skagerrak. *J. Sea Res.* 35, 9–21. doi: 10.1016/S1385-1101(96)90731-5

Røed, L., and Fossum, I. (2004). Mean and eddy motion in the Skagerrak/northern North Sea: insight from a numerical model. *Ocean Dynam.* 54, 197–220. doi: 10.1007/s10236-003-0076-1

Rosenberg, R. (1985). Eutrophication – the future marine coastal nuisance? *Mar. Pollut. Bull.* 16, 227–231. doi: 10.1016/0025-326X(85)90505-3

Rosenberg, R., Hellman, B., and Johansson, B. (1991). Hypoxic tolerance of marine benthic fauna. *Mar. Ecol. Prog. Ser.* 79, 127–131. doi: 10.3354/meps079127

Rydberg, L., Haamer, J., and Liungman, O. (1996). Fluxes of water and nutrients within and into the Skagerrak. *J. Sea Res.* 35, 23–38. doi: 10.1016/S1385-1101(96)90732-7

Schöpp, W., Posch, M., Mylona, S., and Johansson, M. (2003). Long-term development of acid deposition (1880–2030) in sensitive freshwater regions in Europe. *Hydrol. Earth Syst. Sci.* 7, 436–446. doi: 10.5194/hess-7-436-2003

Seitzinger, S., and Giblin, A. (1996). Estimating denitrification in North Atlantic continental shelf sediments. *Biogeochemistry* 35, 235–260. doi: 10.1007/BF02179829

Skogen, M., Søiland, H., and Svendsen, E. (2004). Effects of changing nutrient loads to the North Sea. *J. Marine Syst.* 46, 23–38. doi: 10.1016/j.jmarsys.2003.11.013

Steele, J. (1962). Environmental control of photosynthesis in the sea. *Limnol. Oceanogr.* 7, 137–150. doi: 10.4319/lo.1962.7.2.0137

Sterner, R., and Elser, J. (2002). *Ecological Stoichiometry: The Biology of Elements from Molecules to the Biosphere*. Princeton University Press.

Timmermann, K., Markager, S., and Gustafsson, K. (2010). Streams or open sea? Tracing sources and effects of nutrient loadings in a shallow estuary with a 3D hydrodynamic–ecological model. *J. Mar. Syst.* 82, 111–121. doi: 10.1016/j.jmarsys.2010.04.008

Topcu, D., Brockmann, U., and Claussen, U. (2009). Relationship between eutrophication reference conditions and boundary settings considering OSPAR recommendations and the Water Framework Directive – examples from the German Bight. *Hydrobiologia* 629, 91–106. doi: 10.1007/s10750-009-9778-9

Topcu, H., and Brockmann, U. (2015). Seasonal oxygen depletion in the north sea, a review. *Mar. Pollut. Bull.* 99, 5–27. doi: 10.1016/j.marpolbul.2015.06.021

Troost, T., Blaas, M., and Los, F. (2013). The role of atmospheric deposition in the eutrophication of the North Sea: a model analysis. *J. Marine Syst.* 125, 101–112. doi: 10.1016/j.jmarsys.2012.10.005

Tungaraza, C., Rousseau, V., Brion, N., Lancelot, C., Gichuki, J., Baeyens, W., et al. (2003). Contrasting nitrogen uptake by diatom and Phaeocystis-dominated phytoplankton assemblages in the North Sea. *J. Exp. Mar. Biol. Ecol.* 292, 19–41. doi: 10.1016/S0022-0981(03)00145-X

Tyson, R., and Pearson, T. (1991). Modern and ancient continental shelf anoxia: an overview. *Geol. Soc. Lond. Spec. Publ.* 58, 1–24. doi: 10.1144/GSL.SP.1991.058.01.01

Ulbrich, U., Brücher, T., Fink, A., Leckebusch, G., Krüger, A., and Pinto, J. (2003). The central European floods of August 2002: Part 1 – Rainfall periods and flood development. *Weather* 58, 371–377. doi: 10.1256/wea.61.03A

UNESC (1999). *Protocol to the 1979 Convention on Long-range Transboundary Air Pollution to Abate Acidification, Eutrophication and Ground-level Ozone*. Gothenburg: United Nations (Accessed on January 09, 2017).

van Beusekom, J., Brockmann, U., Hesse, K.-J., Hickel, W., Poremba, K., and Tillmann, U. (1999). The importance of sediments in the transformation and turnover of nutrients and organic matter in the Wadden Sea and German Bight. *Deutsch. Hydrografische Z.* 51, 245–266. doi: 10.1007/BF02764176

van Beusekom, J., and de Jonge, V. (1998). Retention of phosphorus and nitrogen in the Ems estuary. *Estuaries* 21, 527–539. doi: 10.2307/1353292

Vaquer-Sunyer, R., and Duarte, C. (2008). Thresholds of hypoxia for marine biodiversity. *Proc. Natl. Acad. Sci. U.S.A.* 105, 15452–15457. doi: 10.1073/pnas.0803833105

von Westernhagen, H., and Dethlefsen, V. (1983). North Sea Oxygen Deficiency 1982 and its Effects on the Bottom Fauna. *Ambio* 12, 264–266.

Wanninkhof, R. (1992). Relationship between wind speed and gas exchange over the ocean. *J. Geophys. Res. Oceans* 97, 7373–7382. doi: 10.1029/92JC00188

Weston, K., Fernand, L., Nicholls, J., Marca-Bell, A., Mills, D., Sivyer, D., et al. (2008). Sedimentary and water column processes in the Oyster Grounds: a potentially hypoxic region of the North Sea. *Mar. Environ. Res.* 65, 235–249. doi: 10.1016/j.marenvres.2007.11.002

Wijsman, J., Los, H., and van Beek, J. (2004). *The Filtering Capacity of an Estuary for Nutrients*. WL|Delft Hydraulics Reports, Z2836:51.

Winther, N., and Johannessen, J. (2006). North Sea circulation: atlantic inflow and its destination. *J. Geophys. Res. Oceans* 111, 1–12. doi: 10.1029/2005JC003310

Wirth, H., and Wiesner, M. (1988). *Sedimentary facies in the North Sea*. Mitteilungen aus dem Geologisch-Paläontologischen Institut der Universität (Hamburg).

Conflict of Interest Statement: The authors declare that the research was conducted in the absence of any commercial or financial relationships that could be construed as a potential conflict of interest.

frontiers in Marine Science

ORIGINAL RESEARCH
published: 22 August 2018
doi: 10.3389/fmars.2018.00258

Response of Sea Urchin Fitness Traits to Environmental Gradients Across the Southern California Oxygen Minimum Zone

Kirk N. Sato[1], Andreas J. Andersson[1], James M. D. Day[1], Jennifer R. A. Taylor[1], Michael B. Frank[2], Jae-Young Jung[2], Joanna McKittrick[2,3] and Lisa A. Levin[1]*

[1] Scripps Institution of Oceanography, University of California, San Diego, La Jolla, CA, United States, [2] Materials Science and Engineering Program, University of California, San Diego, La Jolla, CA, United States, [3] Department of Mechanical and Aerospace Engineering, University of California, San Diego, La Jolla, CA, United States

OPEN ACCESS

Edited by:
Aurélien Paulmier, UMR5566 Laboratoire d'études en géophysique et océanographie spatiales (LEGOS), France

Reviewed by:
Jacqueline L. Padilla-Gamino, University of Washington, United States
Laura Ramajo, Adolfo Ibáñez University, Chile

***Correspondence:**
Kirk N. Sato
kirk.sato@oist.jp

Specialty section:
This article was submitted to Global Change and the Future Ocean, a section of the journal Frontiers in Marine Science

Received: *16 April 2018*
Accepted: *11 July 2018*
Published: *22 August 2018*

Citation:
Sato KN, Andersson AJ, Day JMD, Taylor JRA, Frank MB, Jung J-Y, McKittrick J and Levin LA (2018) Response of Sea Urchin Fitness Traits to Environmental Gradients Across the Southern California Oxygen Minimum Zone. Front. Mar. Sci. 5:258. doi: 10.3389/fmars.2018.00258

Marine calcifiers are considered to be among the most vulnerable taxa to climate-forced environmental changes occurring on continental margins with effects hypothesized to occur on microstructural, biomechanical, and geochemical properties of carbonate structures. Natural gradients in temperature, salinity, oxygen, and pH on an upwelling margin combined with the broad depth distribution (100–1,100 m) of the pink fragile sea urchin, *Strongylocentrotus* (formerly *Allocentrotus*) *fragilis*, along the southern California shelf and slope provide an ideal system to evaluate potential effects of multiple climate variables on carbonate structures *in situ*. We measured, for the first time, trait variability across four distinct depth zones using natural gradients as analogues for species-specific implications of oxygen minimum zone (OMZ) expansion, deoxygenation and ocean acidification. Although *S. fragilis* may likely be tolerant of future oxygen and pH decreases predicted during the twenty-first century, we determine from adults collected across multiple depth zones that urchin size and potential reproductive fitness (gonad index) are drastically reduced in the OMZ core (450–900 m) compared to adjacent zones. Increases in porosity and mean pore size coupled with decreases in mechanical nanohardness and stiffness of the calcitic endoskeleton in individuals collected from lower pH_{Total} (7.57–7.59) and lower dissolved oxygen (13–42 μmol kg^{-1}) environments suggest that *S. fragilis* may be potentially vulnerable to crushing predators if these conditions become more widespread in the future. In addition, elemental composition indicates that *S. fragilis* has a skeleton composed of the low Mg-calcite mineral phase of calcium carbonate (mean Mg/Ca = 0.02 mol mol^{-1}), with Mg/Ca values measured in the lower end of values reported for sea urchins known to date. Together these findings suggest that ongoing declines in oxygen and pH will likely affect the ecology and fitness of a dominant echinoid on the California margin.

Keywords: ocean deoxygenation, ocean acidification, echinoid, sea urchin, *Strongylocentrotus fragilis*, oxygen minimum zone, carbonate geochemistry, biomechanics

INTRODUCTION

Continental margin ecosystems along eastern boundary upwelling systems experience sharp natural gradients in temperature, salinity, dissolved oxygen (DO), and pH over short vertical distances (Feely et al., 2008; Levin and Sibuet, 2012; Sperling et al., 2016; **Figure 1**). In the eastern Pacific these gradients are associated with oxygen minimum zones (OMZs) that originate from combined respiration of abundant sinking organic matter and reduced exposure to more oxygenated water masses (Gilly et al., 2013). In contrast to regions affected by coastal hypoxia, which are primarily caused by eutrophication (Diaz and Rosenberg, 2008), OMZs are formed *via* natural processes (Helly and Levin, 2004; Breitburg et al., 2018). In the Southern California Bight (SCB) OMZ, two distinct intermediate water masses converge and contribute to upwelled source water: the relatively cool, less saline, high-DO, high pH Pacific Subarctic Upper Water (PSUW) advected from the north and the relatively warm, salty, low-DO, low-pH Pacific Equatorial Water (PEW) advected from the south (Nam et al., 2015). OMZs are defined as midwater areas where DO levels are <22 μmol kg^{-1} (<0.5 ml l^{-1}), and OMZ properties (e.g., thickness, boundary depths, seasonality, oxygen minima values) vary geographically (Helly and Levin, 2004; Gallo and Levin, 2016) and over multiple time-scales (Moffitt et al., 2015). In recent decades, OMZs have appeared to expand in tropical and subtropical regions (Stramma et al., 2010; Schmidtko et al., 2017; Levin, 2018) with major ecological implications for marine populations and communities (Gilly et al., 2013; Gallo and Levin, 2016; Sato et al., 2017).

According to life-history theory, the variability of key life-history traits for organisms, including body size, gonad index, and properties of structural elements confer species variable fitness (Lack, 1947; Smith and Fretwell, 1974; Denny et al., 1985; Fabian and Flatt, 2012; MacLean and Beissinger, 2017). Continental margin communities and species that are exposed to concomitant drivers associated with anthropogenic climate change such as warming, ocean acidification (OA) and deoxygenation are excellent candidates to investigate trait variability patterns (Gruber, 2011; Kroeker et al., 2016). To better understand the evolutionary and ecological consequences of multiple climate change drivers in the ocean such as OA and deoxygenation, it is critical to characterize environmental effects on the variability of traits linked to fitness *in situ* within key species (i.e., phenotypic buffering) (Reusch, 2014; Sunday et al., 2014; Swezey et al., 2017a; Des Roches et al., 2018). The upper and lower boundaries of severe OMZs on upwelling margins exhibit strong vertical zonation of benthic invertebrate communities, with rapid shifts from dense benthic megafauna and calcareous invertebrates outside the OMZ to communities dominated by annelids and calcareous foraminifera within the OMZ (Levin, 2003; Gooday et al., 2010). Only recently has there been investigation of the interplay of temperature, oxygen and pH effects on extant benthos in these areas (Sperling et al., 2016; Sato et al., 2018).

Echinoid sea urchins are important benthic grazers (Pearse, 2006), algal detritivores (Barry et al., 2014; Sato et al., 2018) and deposit feeders (Lohrer et al., 2005). The pink urchin, *Strongylocentrotus fragilis*, is a dominant megafaunal species on the outer shelf (120–200 m) and upper slope (200–500 m) in southern California (Thompson et al., 1993; Sato et al., 2017; Walther et al., 2017). *S. fragilis* also occurs, although infrequently, in the OMZ core (500–900 m) and below the OMZ core, in the Lower OMZ (LOMZ; 900–1,200 m) where DO and pH are higher than in the OMZ core (Sumich and McCauley, 1973; Barry et al., 2014; Taylor et al., 2014; **Figure 1**). Sato et al. (2018) previously described natural history traits of *S. fragilis* in the SCB including spatial variability in density, distribution, feeding behavior, and relative growth rates, as well as seasonal patterns in reproductive potential. *S. fragilis* thus serves as a model species to evaluate how multiple parameters that are likely to be modified under climate change (e.g., temperature, DO, and pH) may potentially influence sublethal fitness traits on both macro- and microscale levels (Byrne et al., 2014; Taylor et al., 2014; Carrington et al., 2015; Swezey et al., 2017b).

There is compelling evidence that projected future changes in ocean temperature, carbonate chemistry, and DO will affect morphological function of calcified hard parts and fitness success. For example, weaker structures in intertidal mussels (Gaylord et al., 2011; Carrington et al., 2015), crustaceans (Taylor et al., 2015; deVries et al., 2016; Lowder et al., 2017), coccolithophorids (Ziveri et al., 2014), and sea urchins (Presser et al., 2010; Collard et al., 2016) could increase vulnerability to predation. Sea urchins produce ellipsoid-shaped, calcitic skeletal structures called tests, as well as calcitic spines, both of which provide the organism with a variety of critical functions such as protection against predators, sensing, locomotion, and feeding (Pearse, 2006). An improved understanding of the relationship between material properties (e.g., hardness, stiffness) of *S. fragilis* skeletal tests and the environmental gradients they experience on the continental margin can provide valuable information regarding *S. fragilis*' potential survival under climate change and its vulnerability to crushing predators (e.g., crabs and fish).

Calcified sea urchin tests are typically composed primarily of calcite ($CaCO_3$) with various amounts of magnesium incorporated in their calcareous structures (i.e., $MgCO_3$ or Mg calcite). Organisms that produce Mg calcite containing significant amounts of Mg are potentially highly vulnerable to future changes in the seawater carbonate system linked to anthropogenic increases in atmospheric pCO_2 as Mg calcite phases with 8–12 mol% $MgCO_3$ are more soluble than aragonite (Walter and Morse, 1984; Morse et al., 2006; Andersson et al., 2008). While several datasets quantify % $MgCO_3$ in field-collected sea urchins (e.g., Clarke and Wheeler, 1917; Chave, 1954; Kuklinski and Taylor, 2009) and in controlled laboratory experiments (e.g., Hermans et al., 2010; Lavigne et al., 2013), the biomineral Mg composition of *S. fragilis*, a potential climate change-tolerant species, has yet to be reported. In addition, few studies attempt to link spatial patterns of Mg content with material properties of calcified hard parts in the context of physicochemical variables affected by climate change (Byrne et al., 2014). Notably, some deep-water echinoderms distributed

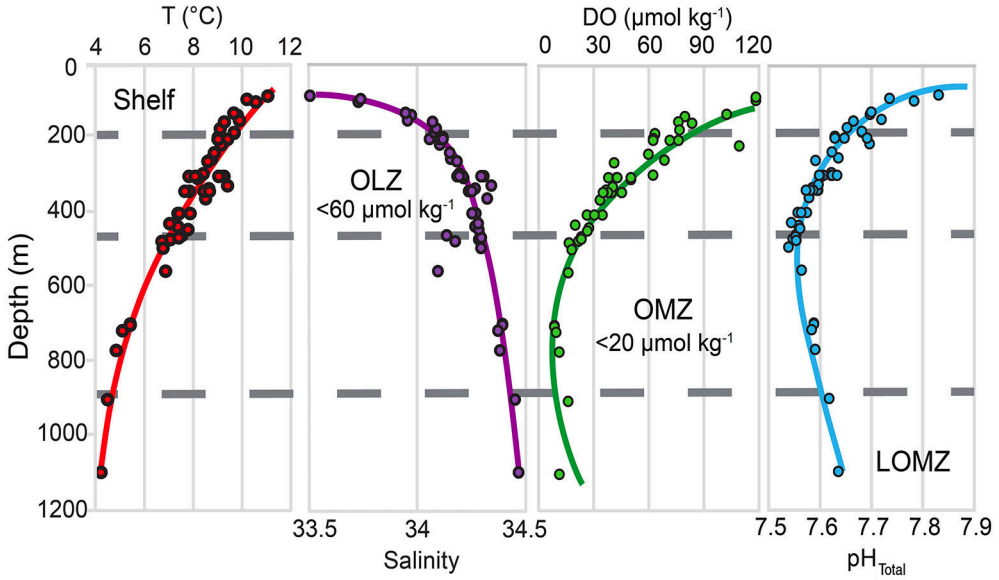

FIGURE 1 | Depth profiles for temperature (T), salinity, dissolved oxygen (DO), and *in situ* pH_{Total} in southern California, indicating the vertical structure of key variables likely to be modified under climate change. Horizontal gray dashed lines separate the continental margin into four depth zones: Shelf, Oxygen Limited Zone (OLZ), Oxygen Minimum Zone (OMZ), and Lower Oxygen Minimum Zone (LOMZ). Points indicate trawl depths of urchin collection sites throughout southern California.

across the globe have been found to be tolerant of waters undersaturated with respect to the polymorph of their species-specific calcareous structure (Ω_i <1) (Lebrato et al., 2016).

In some biogenic structures, metal enrichment can form significantly tougher composite structures (Naleway et al., 2016). For example, the protodolomite stone part of each tooth of the urchin feeding apparatus (Aristotle's lantern) can exceed 40–45% $MgCO_3$ (Wang et al., 1997), which may have led to the taxon's evolutionary success (Candia Carnevali et al., 1993; Ma et al., 2009; Reich and Smith, 2009; Frank et al., 2015). Further evidence suggests that temperature, but not pH, may be positively related to both Mg content and hardness of some urchin's calcitic structures (Byrne et al., 2014), while another study suggested Mg was not related to hardness (Moureaux et al., 2010). In addition to Mg, numerous other co-precipitated elements are differentially incorporated into biotic calcitic structures such as phosphorus (P; e.g., calcium phosphate) and strontium (Sr; e.g., strontium calcite) (Mackenzie et al., 1983). Some trace metals, such as iron (Fe) and zinc (Zn), have been found to enhance mechanical properties of biomineralized structures (e.g., iron oxides, zinc oxides), and inspire the development of anthropogenic biomaterials (Meyers et al., 2008; Agaogullari et al., 2012; Naleway et al., 2016).

To better understand the link between environmental change and fitness, we set out to elucidate the relationships among physicochemical variables (temperature, salinity, DO, and pH) and skeletal traits (morphological, biomineral element composition, material properties and microstructure) of *S. fragilis* across the southern California OMZ. Our main objective was to measure variability of *S. fragilis* across four depth zones (Shelf, OLZ, OMZ, and Lower OMZ) with associated differences in temperature, salinity, DO, and pH. We compared the following five potential fitness traits: (i) size (test diameter), (ii) gonad index, (iii) biomineral element composition, (iv) material properties (hardness and stiffness), and (v) test microstructure (porosity). We hypothesized that *S. fragilis* in the Shelf zone would exhibit the highest mean size and gonad index, strongest skeletal tests, and lowest porosity compared to conspecifics in OLZ, OMZ, and LOMZ depth bins because the unfavorable environmental conditions in these zones (lower T, O_2, pH, and food availability) should limit calcification, growth, and gonadal production.

MATERIALS AND METHODS

Field Sampling

To better understand the relationships of urchin body size, reproductive potential, and various biogeochemical, biomechanical, and material properties across multiple environmental gradients, *Strongylocentrotus fragilis* individuals were collected from various depths between 77 and 1,116 m throughout the SCB using depth-stratified otter trawls over a period of four years between July 2012 and July 2016 (see Sato et al., 2017). Urchins were collected year-round in collaboration with the Southern California Coastal Water Research Project's Bight'13 Trawl Survey (2013), the National Oceanic and Atmospheric Administration (NOAA) West Coast Groundfish Bottom Trawl Survey (2014), as well as Scripps Institution of Oceanography (SIO) course cruises and SIO student cruises in 2014–2016 on the R/V *Robert Gordon Sproul*, the R/V *New Horizon*, and the R/V *Melville*. During each trawl, the GPS coordinates and bottom depth of the trawl start location were recorded (Supplementary Material, **Table S1**). Upon retrieval, ~25 *S. fragilis* urchins were haphazardly selected, frozen at

−20°C on board and transported back to the laboratory at SIO where they were maintained in a −20°C freezer until analysis.

For elemental, biomechanical, and porosity analyses, a subset of urchins were selected from the following four depth zones, corresponding to the concomitant environmental variables (**Figure 1** and **Table 1**): continental shelf (Shelf; 80–200 m), oxygen limited zone (OLZ; 201–450 m), oxygen minimum zone (OMZ; 451–900 m), and lower oxygen minimum zone (LOMZ; 901–1,116 m).

Hydrographic Data

Each SCB trawl was assigned a single value for temperature, salinity, DO, and pH near (<10 m from seafloor) or on the seafloor (**Figure 1**). Hydrographic data were obtained in one of three ways: (1) During the 2014 NOAA survey cruise, conductivity, temperature, depth, and dissolved oxygen sensors (CTD-O_2) (Sea-Bird Scientific, Bellevue, WA, USA, SBE 19plus) were directly attached to the trawl net. These recorded *in situ* temperature (°C), salinity (PSU), and DO (μmol kg^{-1}). (2) During the SIO cruises, CTD-O_2 casts (Sea-Bird Scientific, Bellevue, WA, USA) were conducted immediately before the trawls were deployed. (3) Historical CTD-O_2 data from quarterly hydrographic cruises conducted by the California Cooperative Oceanic Fisheries Investigations (CalCOFI) were obtained from the CalCOFI station, sampling date and depth nearest in space and time to the trawl providing urchins. Although direct comparison of hydrographic data across methods was not possible because data were collected at different locations and times, each instrument was pre-calibrated according to manufacturer specifications or by applying a linear correction based on discrete samples (Nam et al., 2015).

Data for pH_{Total} were obtained in two ways: (1) In San Diego, discrete water samples were taken at depths by CTD rosette corresponding to urchin trawls aboard the R/V *Melville* during the student-led San Diego Coastal Expedition cruises in June/July and December 2012. Briefly, water samples were collected in Pyrex serum bottles following standard procedures (Dickson et al., 2007). Within 4 h of collection, pH was analyzed spectrophotometrically onboard at 20°C using unpurified *m*-cresol purple as indicator dye. The pH data accuracy and precision were ± 0.02 (1 s.d.) and ± 0.0015, respectively, when compared to certified reference materials (Takeshita et al., 2015). For further discussion, see Nam et al. (2015) and Takeshita et al. (2015). (2) For urchin collection sites in Santa Barbara (<500 m), $pH_{Seawater}$ was calculated using a robust empirical relationship with temperature and dissolved oxygen concentration ($r^2 = 0.98$, root mean square error = 0.024) determined by Alin et al. (2012). $pH_{Seawater}$ values were converted to the pH_{Total} scale using the "pHconv" function in the R package *seacarb*. All pH_{Total} values were corrected to reflect *in situ* conditions using the "pHinsi" function with dissociation constants from Lueker et al. (2000) and Dickson (1990).

Data in the upper 500 m are comparable to mean results of Nam et al. (2015), which described the seasonal variability of multiple underreported hydrographic variables at a relatively high spatial sampling resolution. Our results below 500 m to basin depths (>1,000 m), are also consistent with a persistent, well defined OMZ documented in previous published datasets (Nam et al., 2015).

Laboratory Analyses

Urchin Size and Gonad Index

Urchin size and reproductive potential were compared across depth zones to assess relative habitat quality. Frozen urchins were thawed and rinsed clean in the laboratory prior to dissection. Spines were removed prior to measurement of the individual urchin test length diameter (TLD) *via* calibrated dial calipers to the nearest 0.1 mm. Wet weights of gonads (five lobes) were measured along with the weight of each individual drained of its internal fluids to the nearest 0.001 gram. Gonad Index was calculated as the ratio of gonad wet weight to body weight.

Biomineral Element Composition of Tests

Multiple elements were measured in the calcified material to better understand the relationships among environmental conditions and mechanical and structural properties. Up to 10 interambulacral ossicle plates from each urchin, located 3–4 ossicles from the apex (dorsal surface), were dissected and air-dried in glass vials. Ossicles were transferred to a trace element clean room and placed in 5 mL plastic vials that had been pre-washed with 10% nitric acid. The ossicles were then soaked in a clean solution of 15% Optima grade hydrogen peroxide (Fisher Chemical) buffered with 0.05 M Suprapur sodium hydroxide (EMD Chemicals) for approximately 24 h to remove organic tissue, rinsed in ultrapure water three times, and set to dry under a Class-100 laminar flow hood for approximately 48 h. A total of one to five ossicles from each individual were weighed together (4–15 mg total weight) and placed in pre-cleaned Teflon vials

TABLE 1 | Mean values (± 1 SE) of hydrographic variables (Depth, Temperature, Salinity, Oxygen, and *in situ* pH_{Total}), gonad index (% weight) and total length of the test diameter of urchins separated by depth zone bin.

Zone	n	Depth (m)	Temp (°C)	Salinity	Oxygen (μmol kg^{-1})	pH_{Total}	TLD (mm)	Gonad Index
Shelf	134	155.36 ± 3.43	9.64 ± 0.05	33.98 ± 0.01	85.05 ± 1.93	7.69 ± 0.01	60.46 ± 1.17	6.57 ± 0.38
OLZ	403	328.30 ± 2.33	8.43 ± 0.03	34.25 ± 0.01	41.88 ± 0.60	7.59 ± 0.01	48.26 ± 0.40	4.79 ± 0.19
OMZ	95	590.20 ± 13.33	6.22 ± 0.11	34.29 ± 0.01	15.83 ± 0.56	7.57 ± 0.01	45.49 ± 0.82	1.85 ± 0.18
LOMZ	24	1014.33 ± 20.15	4.33 ± 0.03	34.46 ± 0.01	13.32 ± 0.49	7.63 ± 0.01	51.08 ± 2.88	4.15 ± 1.01

Shelf, <200 m; OLZ, Oxygen Limited Zone (22–60 μmol oxygen kg^{-1}); OMZ, Oxygen Minimum Zone core (<22 μmol oxygen kg^{-1}); LOMZ, Lower Oxygen Minimum Zone (>750 m where dissolved oxygen begins to increase).

for digestion with 1 ml of concentrated Teflon-distilled (TD) nitric acid (14.7 M HNO_3) on a hotplate at 100°C for >24 h. Digested samples were dried down, re-acidified with 0.5 mL TD HNO_3, doped with a 1 ppm indium solution (to monitor instrumental drift), and diluted with 3 mL of ultrapure water to achieve a dilution factor of 250 ×. Samples were further diluted to achieve a final dilution factor of 8,000 × prior to solution-based analysis using a *ThermoScientific iCAPq* inductively coupled plasma-mass spectrometer (ICP-MS; Thermo Fisher Scientific GmbH, Bremen, Germany), mass calibrated on the day of analysis. Atomic masses of the elements of interest (^{10}B, ^{11}B, ^{25}Mg, ^{26}Mg, ^{31}P, ^{42}Ca, ^{44}Ca, ^{55}Mn, ^{57}Fe, ^{60}Ni, ^{66}Zn, ^{68}Zn, ^{86}Sr, ^{87}Sr, ^{110}Cd, ^{111}Cd, ^{137}Ba, ^{238}U) were measured for 30 ratios, resulting in internal precision of better than 2% (2 s.d.). Elements were corrected for total mole fraction. Total procedural blanks run with samples represented <3% of the measurement for all elements. Raw data were corrected off line for instrument background, drift and blank. Samples were bracketed by internal standards of *Cancer productus* crab carapace ($n = 4$), which allowed for calculation of absolute values, although we report ratios relative to mol Ca^{-1}. The crab standards yielded external precision of better than 2% for each element, including Ca (2 s.d.) and were calibrated relative to solution and powder standards by bracketing and standard addition procedures. The elements B, P, Ba, and Mn were not included in the NMDS analysis if data were flagged with greater than 2% internal precision.

Seawater Element/Ca ratios (E_{SW}/Ca_{SW}) from published datasets collected from sites in the California Current (Biller and Bruland, 2013) and the north Pacific Ocean (Supplementary Material, **Figure S1**) were used to compare with ICP-MS results. Due to low sample sizes of urchins in LOMZ, these urchins were grouped with OMZ urchins (**Table 2**). Partition coefficients for each element (D_E) in urchin tests were calculated using the equation,

$$D_E = (E_{urchin}/Ca_{urchin})/(E_{SW}/Ca_{SW}), \quad (1)$$

where E represented the element concentration and Ca was the calcium concentration (in the urchin ossicles as measured by ICP-MS and in seawater as estimated from published datasets).

Test Biomechanical Properties

To evaluate potential susceptibility to predation by crushing across depth zones, hardness (i.e., resistance to permanent indentation) and stiffness (i.e., elastic modulus, or resistance to elastic deformation) of each ossicle were measured using a nanoindentation materials testing machine (Nano Hardness Tester, Nanovea, Irvine, CA, USA) equipped with a 200–μm diameter spherical tip. Ossicle surfaces were smoothed using ultra fine sandpaper (P6000) and then rinsed with MilliQ water and dried under a hood. Sanded ossicles were mounted with super glue onto a steel block (Supplementary Material, **Figure S2**). Indentations were performed by penetrating into each ossicle with a maximum load of 30 mN and loading and unloading rates of 60 mN min^{-1}. A total of three to five indents were made on each ossicle (1–2 ossicles from each individual, $n = 8$–15 indiv. depth $zone^{-1}$). All indents were spaced sufficiently apart (a minimum of 10 times the penetration depth) to avoid influence from adjacent indents.

Test Porosity

To better understand the structural implications of variable environmental conditions and drivers of biomechanical properties, test porosity was also determined across depth zones. Replicate ossicles (also located 3–4 interambulacral plates away from the apex) were bisected using a razor blade, carefully cleaned using a paintbrush under a stereomicroscope, secured to a double 90° SEM mount revealing the cross-section (Supplementary Material, **Figure S3**), and sputter coated with iridium (Emitech sputter coater K575X) for image analysis using scanning electron microscopy (SEM). Images of urchin plate cross-sections (three per plate) were obtained at 300–400 × magnification using an ultra-high-resolution SEM (FEI XL-30 SFEG Scanning Electron Microscope) set to an acceleration voltage of 5 kV to achieve a resolution of 2.5 nm. SEM micrographs were analyzed for porosity (%) by calculating the ratio of pore area to total area of the micrograph using *ImageJ* (Supplementary Material, **Figure S3**; Schneider et al., 2012). The color threshold for each 2-D SEM micrograph was adjusted using either a mixed or traditional segmentation algorithm in the DiameterJ Segmentation plugin (Hotaling et al., 2015). For each micrograph, the output result that best fit the original was manually determined from 16 possible black and white images. The outlines of segments or pores (pore size area: 0-infinity μm^2) were determined automatically, and the area (μm^2) of each pore was calculated (Supplementary Material, **Figure S3**). Outlined areas were visually inspected for detection errors and manually traced using the polygon tool if needed. The mean 2-D porosity for each ossicle (i.e., individual urchin), and the mean porosity and variance for each depth zone ($n = 5$ individual urchins per depth zone) were calculated.

High-resolution micro-computed tomography (HR-μCT) was used to explore the spatial variability of porosity within individual ossicles and to obtain more accurate estimations of three-dimensional porosity. Single ossicles from 333 m and 1,116 m were selected to represent a broad range in physicochemical environments. Each ossicle was embedded in epoxy and scanned with an isotropic voxel size of 400 nm at a 40 kV acceleration voltage. The rotation angle and tilt increment were set at 360° and 0.2°, respectively, using a MicroXCT-200 scanner (Xradia, Pleasanton, CA) at the National Center for Microscopy and Imaging Research facility (University of California, San Diego). Each scan was selected for visualization using Amira software (FEI Visualization Sciences Group, Burlington, MA). Distribution of surface porosity was visualized by creating volume renderings of each ossicle and adjusting the threshold range limits (i.e., average range threshold limits and upper range (low porosity) threshold limits). To quantify 3-D porosity for each sample, a 200–μm sided box was haphazardly placed inside the initial scan file, additional volume renderings were created, and the percent porosity was calculated from Material Statistics outputs.

TABLE 2 | Mean values (± 1 SE) of hydrographic variables (Depth, Temperature, Salinity, Oxygen, and pH_{Total}) and [E/Ca_{urchin}] ratios of *Strongylocentrotus fragilis* urchin tests separated by depth zone bin.

Zone	n	Depth (m)	Temp (°C)	Salinity	Oxygen (μmol kg^{-1})	pH_{Total}
Shelf	24	174.2 ± 10.5	9.44 ± 0.17	33.98 ± 0.05	90.39 ± 8.53	7.69 ± 0.02
OLZ	20	362.5 ± 8.01	8.05 ± 0.10	34.29 ± 0.08	33.08 ± 0.77	7.57 ± 0.01
OMZ/LOMZ	26	681.8 ± 32.4	5.55 ± 0.19	34.36 ± 0.01	14.61 ± 0.71	7.57 ± 0.06
URCHIN (μmol mol Ca^{-1})						
Zone	**n**	**Zn**	**Ni**	**Cd**	**U**	**P**
Shelf	24	12.66 ± 1.89	10.566 ± 0.07	0.98 ± 0.09	0.22 ± 0.02	9.46 ± 1.41
OLZ	20	8.62 ± 0.87	10.506 ± 0.04	0.74 ± 0.04	0.13 ± 0.01	1.33 ± 0.19
OMZ/LOMZ	26	9.69 ± 1.48	10.528 ± 0.09	0.61 ± 0.07	0.12 ± 0.01	4.47 ± 0.64
URCHIN (mmol mol Ca^{-1})						
Zone	**n**	**Mg**	**Sr**	**Fe**		
Shelf	24	19.86 ± 0.22	5.90 ± 0.04	6.93 ± 0.12		
OLZ	20	19.88 ± 0.18	5.93 ± 0.03	7.28 ± 0.12		
OMZ/LOMZ	26	18.49 ± 0.13	5.79 ± 0.03	6.94 ± 0.16		

Shelf = <200 m; OLZ, Oxygen Limited Zone (22–60 μmol oxygen kg^{-1}); OMZ, Oxygen Minimum Zone core (<22 μmol oxygen kg^{-1}); LOMZ, Lower Oxygen Minimum Zone (>750 m where dissolved oxygen begins to increase).

Statistical Analyses

To examine the environmental (e.g., depth, temperature, salinity, DO, pH_{Total}) and zonal effects (e.g., Shelf, OLZ, OMZ, and LOMZ) on urchin test size, gonad index, single element concentrations, hardness, stiffness, and porosity, the data were tested for normality using the Shapiro-Wilk test and homogeneity of variances using the Breusch–Pagan test. In each univariate analysis, where assumptions of normality and homoscedasticity were met, parametric tests such as linear regression with hydrographic variables as explanatory factors or one-factor analysis of variance (ANOVA) with depth zone as a factor were employed. If the data violated these assumptions, the Box-Cox power transformation in R was used to transform the data. If the transformation did not improve normality or homoscedasticity of the data, then non-parametric tests were used. Specifically, Kruskal-Wallis tests were used to compare TLD and gonad index across zones, followed by *post hoc* Dunn's tests to analyze differences between zones. One-way ANOVAs were employed to compare mechanical properties of ossicles (i.e., hardness, stiffness) and ossicle 2-D porosity across zones, followed by Tukey HSD tests to analyze differences between zones.

Non-metric multidimensional scaling (NMDS) ordinations were employed to evaluate the multi-elemental biomineral composition patterns among urchins collected from different depth zones. Urchin samples were organized and analyzed based on their origin of collection at four depth-, temperature-, salinity-, pH-, and oxygen-related zones (e.g., Shelf, OLZ, OMZ, and LOMZ). Mole fraction ratios of element to calcium were converted to mmol mol^{-1} or μmol mol^{-1} (for standardization purposes) and square-root transformed prior to Bray-Curtis distance similarity matrix calculation using the *vegan* package (v. 2.4-2) in R (Oksanen et al., 2017). Elements and hydrographic variables were tested for ordination significance based on a permutation test with 999 iterations using the function "envfit" (*vegan* package) with equally weighted "sites" (i.e., indiv. urchins). Vectors of variables with a significance of $p < 0.05$ were scaled relative to their correlation coefficient and plotted onto the 2-D ordination space.

RESULTS

Multiple fitness-related traits were compared across multiple concomitant environmental gradients to better understand the potential implications of future climate change in a region characterized by expanding low-oxygen, low-pH zones. Large differences were seen across depth zones, with all trait patterns pointing to the model urchin species, *Strongylocentrotus fragilis*, having the highest fitness in the Shelf zone and lowest in the OMZ. Biomineral elemental composition of calcified test ossicles revealed significant linear relationships of only Mg and Sr with some environmental variables (i.e., temperature, oxygen, and salinity).

Urchin Size and Gonad Index

Urchin test length diameter (TLD) ranged from 22.3–88.1 mm (**Table 1**; n = 656 indiv.; 53 sites). Mean TLD was significantly different between Shelf, OLZ, and OMZ (**Figure 2A**; Kruskal-Wallis: $\chi^2 = 111.11$, $p < 0.001$), but not OLZ and LOMZ. The mean TLD of *S. fragilis* in the Shelf zone was ∼25% greater than in the OLZ, ∼30% greater than in the OMZ, and ∼15% greater than in the LOMZ (Dunn's test: $p \leq 0.001$). On average, *S. fragilis* TLD in the OMZ (core region) were ∼5% smaller than in the OLZ and ∼10% smaller than in the LOMZ ($p < 0.05$).

Mean gonad index (GI) of *S. fragilis* was significantly different among depth zones (**Figure 2B**; Kruskal-Wallis: $\chi^2 = 107.35$, $p < 0.001$). Mean GI in the Shelf zone was ∼40% greater than in the OLZ, ∼250% greater than in the OMZ, and ∼60% greater than in the LOMZ (Dunn's test: $p \leq 0.001$). Mean GI in the OMZ was ∼60% lower than in the OLZ and ∼55% lower than in the LOMZ

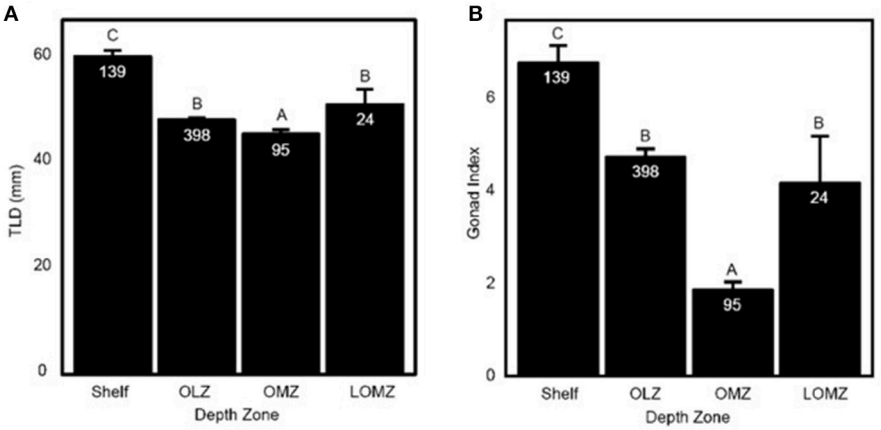

FIGURE 2 | Representation of *Strongylocentrotus fragilis* traits across depth zones. **(A)** Total length of diameter (TLD; mm) of tests collected throughout the SCB. **(B)** Mean Gonad Index (GI). Error bars are standard errors and numbers in barplots are numbers of dissected urchins (*N*). Shelf = <200 m; OLZ = Oxygen Limited Zone (22–60 μmol oxygen kg^{-1}); OMZ = Oxygen Minimum Zone core (<22 μmol oxygen kg^{-1}); LOMZ = Lower Oxygen Minimum Zone (>900 m where dissolved oxygen begins to increase).

(Dunn's test: $p \leq 0.006$). There was no significant difference in mean GI between the OLZ and the LOMZ (Dunn's test: $p = 0.12$). Urchins were collected primarily during summer months (Supplementary Material, **Table S1**), which minimized the effect of seasonal variability on these results; see Sato et al. (2018) for seasonal changes in *S. fragilis* reproductive cycle.

Biomineral Element Composition

For a total of 70 out of 103 samples used in subsequent analyses, each element was detected without being flagged for having greater than 2% internal precision. The Sr/Ca ratio in the calcified test ossicles was positively related to temperature (**Figure 3A**; Linear Regression: $r^2 = 0.34$, $p = 0.028$) and DO (**Figure 3B**; Linear Regression: $r^2 = 0.41$, $p = 0.014$), but not salinity, pH or depth. Mg/Ca ratios of all ossicles were <0.025 (**Table 2**). Mg/Ca ratios were positively related to temperature (**Figure 3C**; Linear Regression: $r^2 = 0.39$, $p = 0.018$) and negatively related to salinity (**Figure 3D**; Linear Regression: $r^2 = 0.46$, $p = 0.018$), but there was no relationship with DO, pH, or depth. There were no significant relationships of the remaining element to Ca ratios (Fe/Ca, Zn/Ca, Ni/Ca, Cd/Ca, U/Ca, and P/Ca) with any environmental variables. Mean molar ratios (± 1 s.e.) of all elements to Ca are shown in **Table 2**.

There were significant relationships between the ratios of Fe/Ca and Cd/Ca in tests and in seawater (**Figure 4**). We found greater Fe concentration in tests in response to greater Fe concentrations in seawater (**Figure 4A**; Linear Regression: $r^2 = 0.99$; $p < 0.001$), and lower Cd concentration in tests in response to greater Cd concentrations in seawater (**Figure 4B**; Linear Regression: $r^2 = 0.99$; $p < 0.001$). Although similar positive (Mg, U, Ni) and negative (Sr, P, Zn) trends were observed for other elements, these relationships were not significant (Linear Regression: $p > 0.05$; Supplemental Material, **Figure S4**). The partition coefficient (D_E) was >1 for Ni, Zn, Cd and Fe, and <1 for Mg, Sr, P, and U (**Figure 4C**). For elements with $D_E > 1$, D_E was highest in urchins from the Shelf and lowest in urchins from the OMZ.

Test Mechanical Properties

Mean hardness of skeletal test ossicles ranged from 0.06 to 0.18 GPa (**Figure 5A**). Ossicles from the Shelf zone were approximately 188% harder than those in the OMZ and 110% harder than those collected from the OLZ and the LOMZ (**Figure 5A**; 1-way ANOVA: $F_{(3,42)} = 11.22$, $p < 0.001$; Tukey HSD: $p \leq 0.005$). Mean hardness of OMZ urchin ossicles was 32% lower than those from the LOMZ, but this was not statistically significant (**Figure 5A**; Tukey HSD: $p > 0.05$).

Mean stiffness (i.e., elastic modulus) of test ossicles ranged from 2.69 to 10.10 GPa (**Figure 5B**). Stiffness values were square-root transformed, and significant differences were found among depth zones (**Figure 5B**; 1-way ANOVA: $F_{(3,42)} = 17.78$, $p < 0.001$). Mean stiffness of the ossicles from Shelf zone was between 140–280% greater than that of ossicles from the other three depth zones (**Figure 5B**; Tukey HSD: $p < 0.001$).

Porosity

Two-dimensional porosity (% pore area) of cross sections of test ossicles ranged from 35% in samples collected from the Shelf to >45% in LOMZ samples and differed significantly across depth zones (**Figure 5C**; 1-way ANOVA: $F_{(3,15)} = 9.143$, $p = 0.001$). Mean 2-D porosity of Shelf urchin ossicles was 19% lower than OMZ urchin ossicles (Tukey HSD: $p = 0.004$) and 22% lower than LOMZ urchin ossicles ($p = 0.001$). Consistent with the change in porosity, the mean pore size was significantly different across depth zones (**Figure 5D**; 1-way ANOVA: $F_{(3,15)} = 9.542$, $p < 0.001$). Mean pore size in the LOMZ was almost double that of the Shelf urchins (Tukey HSD: $p < 0.001$).

Analysis of HR-μCT scans for 3-D assessment revealed significant variability in porosity across the outer surface and within the sponge-like stereom of the ossicle (Supplementary Material, **Figure S5**). 3-D porosity analysis from 200-μm-sided

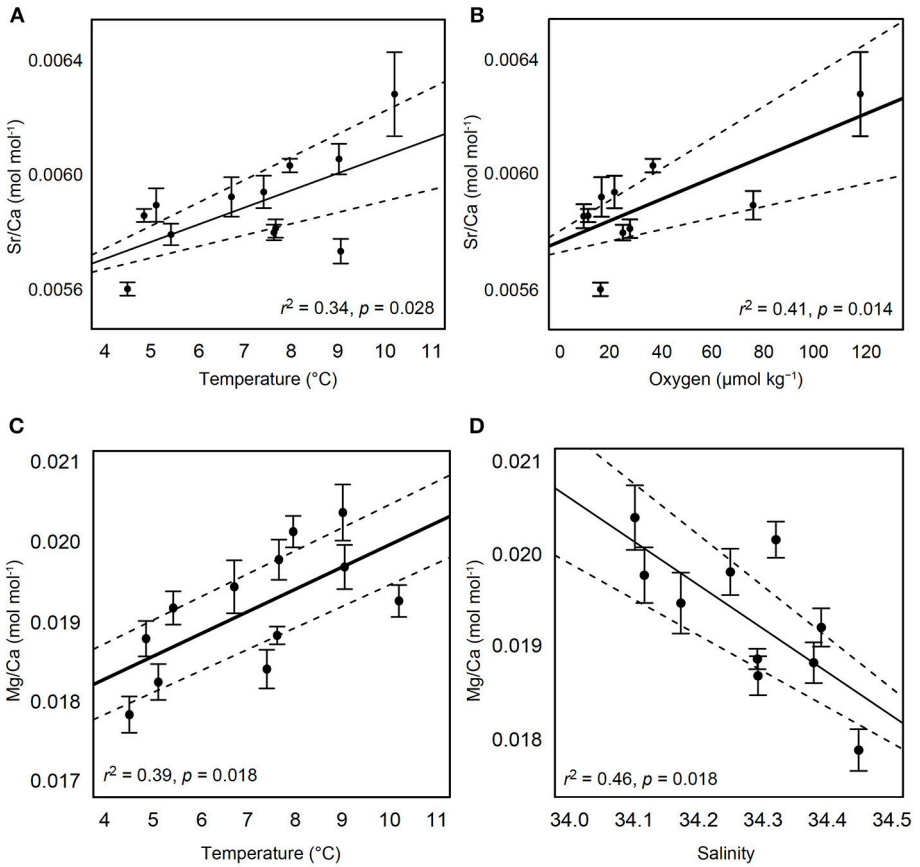

FIGURE 3 | Relationships of test ossicle elemental concentrations and hydrographic variables. Ratios of Sr/Ca (mol mol^{-1}) with **(A)** temperature and **(B)** dissolved oxygen. Ratios of Mg/Ca (mol mol^{-1}) with **(C)** temperature and **(D)** salinity. Black solid lines indicate the best fit line result of linear regression. Dashed lines indicate 95% confidence intervals. Error bars are ± 1 standard error.

volume renderings of urchins from both 333 m and 1116 m exhibited ∼80% pore space compared to the 2-D porosity estimates of 35–45% (**Figure 5D**).

Multivariate Test Properties

NMDS ordination analysis resulted in significant correlations of multiple elements and mechanical response variables within the 2-D ordination space (Supplementary Material, **Figure S6**; 2-D stress = 0.08). Magnesium was not correlated with nanohardness as originally hypothesized. Instead, Sr/Ca, Ni/Ca, and the lack of Cd/Ca appeared positively correlated with *S. fragilis* test hardness and stiffness. U/Ca appeared to be positively correlated with pore size and total porosity within the test structure.

DISCUSSION

Results offer new insights into the evolutionary and ecological consequences of multiple climate change parameters on fitness traits of a model species including its structural properties and potential vulnerability to crushing predators. Sea urchins are generally thought to be vulnerable to the chemical changes in marine systems associated with acidification, and presumed deoxygenation (Dupont et al., 2010; Kroeker et al., 2010; Kurihara et al., 2013), but previous studies have not considered urchins exposed to deeper intermediate waters. In southern California, for example, the upper boundary (60 µmol kg^{-1}) of the OLZ has shoaled by as much at 100 m over the past 25 years (Bograd et al., 2008, 2015). This change coincides with an upslope expansion of deep-water sea urchin species, including the pink sea urchin, *Strongylocentrotus fragilis*, and an apparent habitat compression for a shallower urchin species, *Lytechinus pictus* (Sato et al., 2017). The observed shoaling of low oxygen zones coupled with predicted acidification and undersaturation of subsurface waters with respect to calcium carbonate mineral phases (Alin et al., 2012; Gruber et al., 2012; Bograd et al., 2015) present the impetus to better understand the functional implications of multiple climate change drivers on key taxa like *S. fragilis* in southern California. We compared urchin size (test diameter), gonad index, biomineral element composition, material properties (hardness and stiffness), and test microstructure (porosity) of *S. fragilis* across four depth zones (Shelf, OLZ, OMZ, and Lower OMZ). Our results support our hypothesis that *S. fragilis* in the Shelf zone exhibited higher fitness properties compared to those in OLZ, OMZ, and LOMZ depth bins.

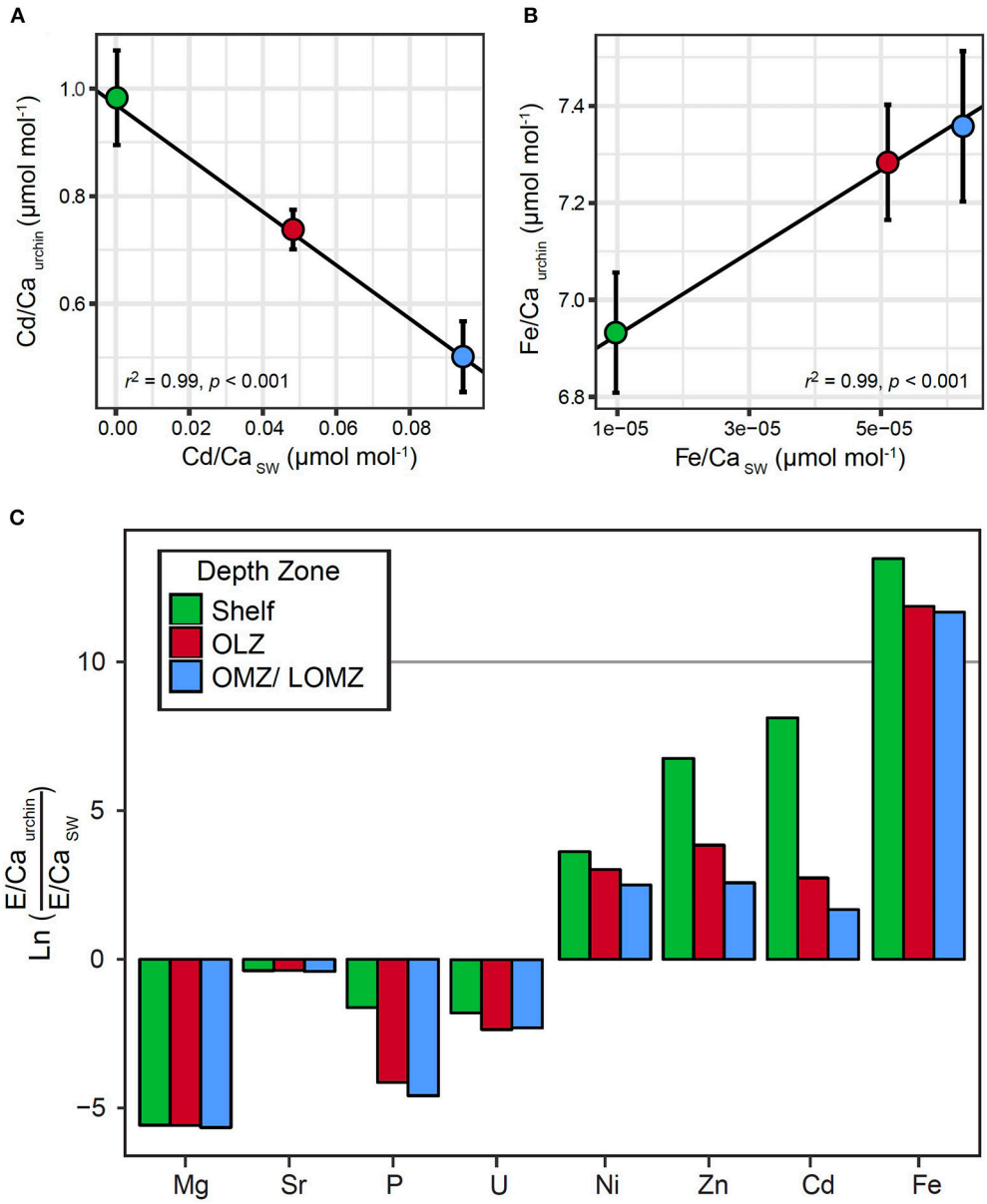

FIGURE 4 | Relationships between element to calcium ratios in *Strongylocentrotus fragilis* test plates (E/Ca_{urchin}) and element to calcium ratios in seawater (E/Ca_{SW}) within different depth zones. E/Ca_{urchin} were averaged across depth bins, Shelf (green), Oxygen Limited Zone (red), and Oxygen Minimum Zone / LOMZ (blue). Black lines indicate significant linear regression relationships which yielded empirical partition coefficients (D_{metal}) for **(A)** Cd and **(B)** Fe. Error bars indicate ± 1 standard error. **(C)** Natural log-transformed ratios of elemental incorporation in *Strongylocentrotus fragilis* E/Ca_{Urchin} versus element concentration ratios in seawater E/Ca_{SW}. Ln values >0 indicate $E/Ca_{Urchin} > E/Ca_{SW}$. Values <0 indicate $E/Ca_{Urchin} < E/Ca_{SW}$. Elemental concentrations of various elements in seawater (Mg, Sr, P, U, Ni, Zn, Cd, Fe, and Ca) in the upper 1,000 m of the water column were extracted from Biller and Bruland (2013) and Dr. Kenneth Johnson's Periodic Table of Elements in the Ocean. Available online at: http://www.mbari.org/science/upper-ocean-systems/chemical-sensor-group.

Size and Reproductive Potential

S. fragilis may respond to unfavorable future acidification and deoxygenation by either shrinking in size (**Figure 2A**), as seen in other animals (Piersma and Drent, 2003), including *S. purpuratus* (Ebert, 1967, 1968), by limiting gonad production (**Figure 2B**), or by growing slower (Sato et al., 2018). Availability of the preferred food, sunken kelp detritus, likely plays an important role in the trait differences seen in *S. fragilis* from the Shelf compared to other zones (**Figures 2**, **4**). Using remotely operated vehicles (ROVs), Sato et al. (2018) observed aggregations of *S. fragilis* feeding on giant kelp detritus at depths shallower than 500 m, but no aggregations were seen on sunken detritus deeper than 500 m. Smaller urchins with significantly reduced GI in the OMZ support previous findings of reduced relative

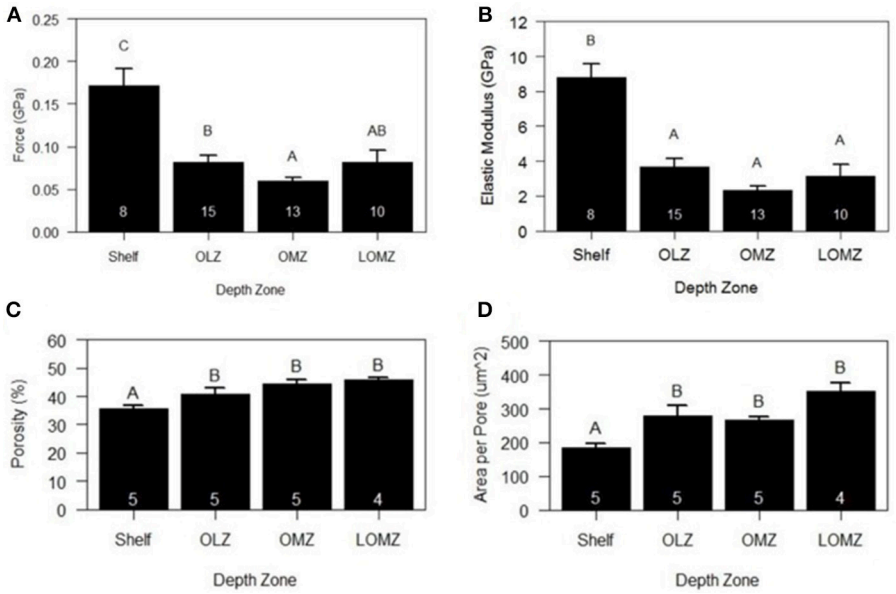

FIGURE 5 | Mean biomechanical and material properties of *Strongylocentrotus fragilis* across depth zones. **(A)** Hardness (GPa). **(B)** Stiffness (i.e., Elastic Modulus). **(C)** % Porosity. **(D)** Area per pore (μm^2). White numbers inside bars indicate number of individual urchin replicates. Errors bars indicate +1 standard error. Shelf = <200 m; OLZ = Oxygen Limited Zone (22–60 μmol oxygen kg^{-1}); OMZ = Oxygen Minimum Zone core (<22 μmol oxygen kg^{-1}); LOMZ = Lower Oxygen Minimum Zone (>900 m where dissolved oxygen begins to increase).

growth rates (Sato et al., 2018), which is consistent with the theory that increased food availability may mitigate negative impacts on growth and gonad production (Ebert, 1968; Dupont et al., 2013). However, deep-sea urchin food availability remains underrecorded in this region indicating that more data are required to better understand how *S. fragilis* will be impacted by future OA and deoxygenation.

A subtropical urchin species, *Hemicentrotus pulcherrimus*, exposed to elevated pCO_2 (1,000 μatm) for 16 days exhibited an initial suppression of food intake and a subsequent delay in gonad production and reproductive phenology after longer-term exposure to elevated CO_2 conditions (Kurihara et al., 2013). Since no effect was found on growth rate or respiration rate, the authors suggested that the reduced feeding could negatively affect the quality of *H. pulcherrimus* eggs (size and nutrient content). Although we did not investigate the quality of *S. fragilis* eggs, it is quite likely that OMZ urchins received less food input in the form of allochthonous kelp than those in the Shelf zone, as reflected by their smaller size and lower gonad index. Furthermore, the gonad index of *S. fragilis* from the OMZ in this study was lower than previously reported GIs measured in urchins from a repeat OLZ station (~350 m) over 4 years (Sato et al., 2018). Here we found significantly larger individuals with higher gonad indices in the LOMZ compared to the OMZ core, which suggests that physicochemical factors like pH and oxygen are likely key drivers in gonad production and growth processes.

Microstructure and Biomechanics

The observed increases in 2-D porosity and mean pore size of tests seen at OLZ, OMZ, and LOMZ depths relative to conspecifics from Shelf depths (**Figures 5C,D**) are consistent with the hypothesis that sublethal effects on form and function may occur under energetically stressful conditions (Todgham and Hofmann, 2009; Byrne et al., 2014). Although recent evidence suggests some urchin species including the congener, *S. purpuratus*, may have the evolutionary capacity to adapt or acclimatize to OA levels expected under "business-as-usual" CO_2 emission scenarios (Kelly et al., 2013; Hofmann et al., 2014), fitness trait responses to OA and other potential climate change parameters are context-dependent (e.g., species, life-history stage; Dupont et al., 2010; Padilla-Gamiño et al., 2013; Dubois, 2014). Compared to shallow-water urchin species, *S. fragilis* appears to have a more limited ability to regulate acid-base balance of its extracellular fluids in response to month-long exposure to decreased pH_{Total} (~7.2) levels, which were predicted to simulate year 2300 conditions in the OMZ (Taylor et al., 2014). In contrast, a temperate shallow urchin species (*Paracentrotus lividus*) was shown to regulate extracellular pH by compensating coelomic fluid acidosis with both bicarbonate and non-bicarbonate buffers (Collard et al., 2013, 2014); and *P. lividus* exhibited no significant differences in the mechanical properties of its skeletal test after long-term exposure (12 months) to future pCO_2 scenarios (Collard et al., 2016).

Regulation of internal pH for calcification is thought to be energy intensive (McCulloch et al., 2012), and if food availability is limited, energy allocation also might shift away from calcification and growth to other physiological functions (e.g., see Hennige et al. (2015) for cold water corals). Higher 2-D porosity and larger pore sizes of *S. fragilis* in the OLZ, OMZ, and LOMZ compared to those at Shelf depths are consistent

with previous findings that pH and DO are strongly related to growth rate (Sato et al., 2018). Alternatively, the critical proteins, glycoproteins, and polysaccharides responsible for biomineral crystal nucleation may be in higher demand within the organic matrix during *S. fragilis* skeletogenesis in these zones (Hermans et al., 2010; Addadi and Weiner, 2014). Comparative analysis between proteomes of *S. fragilis* and the shallow-water congener, *S. purpuratus* by Oliver et al. (2010) concluded that genes responsible for skeletal development and sulfur metabolism (e.g., carbohydrate sulfotransferases) were expressed more in *S. fragilis* relative to *S. purpuratus*. These results provide further evidence that *S. fragilis* is better adapted to potentially grow at deeper, energetically costly depths despite the greater demand to produce precursor macromolecules for skeletogenesis (Mann et al., 2008) and maintain extracellular acid-base regulation of internal fluids (Taylor et al., 2014).

Test Minerology

Biocalcification rates by echinoderms (e.g., sea urchins, sea stars, brittle stars, crinoids) contribute significantly to calcium carbonate production on a global scale (Lebrato et al., 2010). Some sea urchins, but not all (Presser et al., 2010), produce skeletal tests containing ∼12–18% mol% $MgCO_3$ (Chave, 1954; Andersson et al., 2008; Lavigne et al., 2013; Lebrato et al., 2016), which are more soluble than tests with lower $MgCO_3$. *S. fragilis* skeletal test ossicles collected across all SCB sites spanning multiple environmental conditions, revealed low mean (±1 s.e.) concentrations of Mg (0.019 ± 0.001 mol mol Ca^{-1}, i.e., 1.9% $MgCO_3$), which suggests that the Mg content of their skeletal tests falls in the lower end of values documented for sea urchin species (range: ∼0.042–0.19 mol Mg mol Ca^{-1}) collected from natural environments (see Supplementary Table in Lebrato et al., 2016). Calcite with lower amounts of Mg is less soluble than other common biogenic mineral phases of calcium carbonate such as aragonite, which is deposited by corals (Andersson and Mackenzie, 2012) and pteropods (Bednaršek et al., 2016, 2017). The low $MgCO_3$ content found in *S. fragilis* tests provides additional support to previous conclusions about their high tolerance to low pH, low oxygen waters in the southern CA OMZ (Sato et al., 2017). The low-Mg calcite may provide *S. fragilis* potentially higher mineral stability and tolerance to low-pH and low seawater carbonate saturation state conditions (e.g., ocean acidification). Although our findings support this hypothesis, further analyses are required on other species, whole individuals, spines, and early life-history stages to fully characterize the variability of Mg incorporation (Lavigne et al., 2013; Byrne et al., 2014).

Dissolved metals have been used as paleoceanographic environmental proxies to help reconstruct past seawater conditions (Hönisch and Allen, 2013; Janssen et al., 2014) and in ecology as environmental markers to model dispersal and population connectivity (Levin, 2006; Fodrie et al., 2011). Elements such as Sr, cadmium (Cd), and manganese (Mn), have been used as environmental proxies for seawater temperature, dissolved oxygen, and pH (Marchitto et al., 2000; Russell et al., 2004; Tribovillard et al., 2006; Walther and Limburg, 2012; Limburg et al., 2015; Supplementary Material, **Table S2**), but the underlying mechanisms for linking the environmental exposure history of the organism to the boron (B) and uranium (U) content of their carbonate are poorly known (Frieder et al., 2014; Levin et al., 2015). At the same time, some heavy metals (e.g., Zn, Cd, and nickel (Ni)) are considered to be toxic to marine organisms in low concentrations (Fairbairn et al., 2011; Chiarelli and Roccheri, 2014; Kanold et al., 2016). Calcification mechanisms in adult echinoids and other calcifiers are poorly understood (see Politi et al., 2004 and Von Euw et al., 2017), and any future attempts at proxy development using calcitic *S. fragilis* tests will depend on the extent to which *S. fragilis* controls calcification biologically.

Despite such small variation in Mg/Ca (s.d. = 0.5%), we detected positive relationships of Mg in *S. fragilis* with temperature and salinity (**Figures 3C, D**) and of Sr content with temperature and oxygen (**Figures 3A,B**). Although we used mean environmental values in our analyses, these relationships are consistent with results of previous studies on echinoid urchins and other calcifying taxa (Chave, 1954; Moberly, 1968; Mackenzie et al., 1983; Levin et al., 2015; Williams et al., 2017). The positive linear relationship between Sr content and mean dissolved oxygen (**Figure 3A**) is also consistent with the linear relationship between relative growth rate and dissolved oxygen content across the depth range described for *S. fragilis* in Sato et al. (2018). The important influences of growth rates and other biologically mediated vital effects on Mg and Sr incorporation during skeletogenesis confound the development of trace elements as environmental proxies in *S. fragilis* (Chave, 1954; Weiner and Dove, 2003). However, our ability to detect linear trends of small variations in Mg/Ca and Sr/Ca over a broad spatial range and environmental conditions combined with trace metal incorporation warrants further hypothesis testing under controlled laboratory conditions.

Partition coefficients (D_E) greater than 1 (Ni/Ca, Zn/Ca, Cd/Ca, and Fe/Ca) could suggest that *S. fragilis* may actively control the incorporation of these trace metals into the test (**Figure 4C**). Alternatively, *S. fragilis* may actively remove these elements from the test organic matrix to avoid the potential lethal effects of toxic dissolved metal ions or molecules (e.g., Zn^{2+} and $CdCl^{+}$), which has been demonstrated in other urchin species albeit at likely different environmental concentrations (Fairbairn et al., 2011; Chiarelli and Roccheri, 2014). For these trace metals, higher partition coefficients in urchins from the Shelf relative to those in deeper depth bins may also suggest a decrease in the efficiency of elemental uptake during calcification in unfavorable conditions (**Figure 4C**). However, the lower partition coefficients in OLZ and OMZ depth bins may support an alternative non-biological uptake hypothesis, i.e., that foreign ions precipitate inorganically from the calcification fluid as a result of variable growth rates and by extension, calcification rates (Lavigne et al., 2013). Notably, these passive "kinetic effects" of trace elemental incorporation in biogenic calcareous structures are not well understood.

Although the D_{Metal} in *S. fragilis* appears to be exceptionally high for several elements (**Table 2**), it is possible that these could

be overestimations given chemical observations of significantly higher concentrations of these elements (Fe, Mn, Co, Cu) in the benthic boundary layer where urchins live relative to the adjacent water column (Biller and Bruland, 2013). Low-pH environments can limit the bioavailability of other elements (e.g., Zn, Cd), but the majority of trace metal and acidification studies focus on phytoplankton (Kim et al., 2016). However, the mechanisms of trace metal incorporation during calcification in urchins is largely unexplored. Gaps in knowledge concerning the microenvironments in which soft-sediment urchins grow limit our ability to fully understand how vital effects control incorporation of trace metals into *S. fragilis* tests and by extension, mechanical properties (Naleway et al., 2016) and fitness (Byrne et al., 2014).

The opposing directions of the relationships between $E/Ca_{calcite}$ and E/Ca_{SW} in Cd and Fe (**Figures 4A,B**) raises questions about why *S. fragilis* differentially incorporates these trace metals into the skeletal test (Milton and Chenery, 2001). The strong negative relationship between hardness and $Cd/Ca_{calcite}$ (Supplementary Material, **Figure S6**) suggests that Cd could have a direct or indirect negative effect on the hardness of the calcitic test. The tight coupling between dissolved Cd and phosphate, PO_4^{3-}, is well known in oxygenated waters (>75 μmol kg^{-1}), but this coupling breaks down in oxygen-deprived zones (<75 μmol kg^{-1}) because Cd sulfide (CdS) precipitates where sulfide is present, especially in OLZ and OMZ sediments (Janssen et al., 2014). *S. fragilis* calcite from Shelf urchins contains approximately two times more Cd than OMZ urchins and approximately 30% more Cd than OLZ urchins (**Table 2**). Although sulfur was not measured in the urchin calcite, *S. fragilis* is capable of metabolizing sulfur as demonstrated by positive selection for carbohydrate sulfotransferase genes (Oliver et al., 2010), suggesting low oxygen environments may be indirectly linked to multiple fitness trait responses. However, *S. fragilis* larval ecology, dispersal distances, and gene flow across populations require further investigation to better understand its capacity to adapt to rising acidity and declining oxygen throughout its biogeographic range.

CONCLUSIONS

The relatively low solubility of calcite with low Mg content compared to other mineral phases of $CaCO_3$ (e.g., aragonite, high-Mg calcite, amorphous $CaCO_3$) may suggest a potential evolutionary strategy selected for in *S. fragilis* to tolerate unfavorable carbonate chemistry conditions (Lebrato et al., 2016). It is possible however, that maintenance of low Mg-calcite (0.02 mol mol^{-1}) and calcification in the Oxygen Limited Zone and Oxygen Minimum Zone, occurs at the expense of other fitness-related traits such as size, reproductive potential, and growth (Sato et al., 2018). Although *S. fragilis* may be more tolerant of future climatic changes than other species, our results suggest that *S. fragilis* is more vulnerable to the future upslope expansion of OMZs and calcium carbonate undersaturated waters than previously thought (Taylor et al., 2014; Sato et al., 2017). Higher porosity, larger pore sizes, and softer, more pliant/flexible skeletal tests found in persistently low pH (7.57–7.59) and low dissolved oxygen (13–42 μmol kg^{-1}) zones could reduce *S. fragilis* fitness by making them more vulnerable to crushing predators on the slope such as lithodid crabs or predatory fish, which may currently avoid low pH, low oxygen zones. On the other hand, *S. fragilis*' ability to tolerate these low pH, low oxygen conditions may provide protection from some predators if they do not have the same tolerance.

AUTHOR CONTRIBUTIONS

KS and LL designed the study, carried out the field work, analyzed the results, and wrote the initial draft of the manuscript. KS, JD, and AA conducted geochemical analyses. KS and JT carried out biomechanics work. KS, MF, J-YJ, and JM conducted microscopy and tomography work. All authors edited manuscript drafts.

ACKNOWLEDGMENTS

We thank the National Oceanic and Atmospheric Administration (NOAA), SCCWRP, UC Ship Funds, and the California Current Ecosystem Long Term Ecological Research program for the ship time necessary to conduct field work, and the various crew and volunteers who helped KS collect urchins, especially Michael Navarro, Natalya Gallo, and Phil Zerofski. Daniel Jio, Katy Kelsoe, Stephanie Luong, Marissa Mangelli, Jackson Powell, and Ximena Trujillo assisted in the laboratory. We are grateful to Andrew Mehring and Martin Tresguerres for constructive comments on earlier manuscript drafts. Funding was provided by the Tegner Fellowship, Sussman Fellowship, and SIO Education office to KNS. Funding to LAL and KNS was provided by NOAA Grant No. NA14OAR4170075, California Sea Grant College Program Project No. R/SSFS-02 through NOAA's National Sea Grant College Program, U.S. Department of Commerce. JM, MBF and J-YJ acknowledge support from a Multi-University Research Initiative (MURI) through the Air Force Office of Scientific Research of the United States (AFOSR-FA9550-15-1-0009) and a National Science Foundation Biomaterials Program Grant 1507978. This work was performed in part at the San Diego Nanotechnology Infrastructure (SDNI) of UCSD, a member of the National Nanotechnology Coordinated Infrastructure, which is supported by the National Science Foundation (Grant ECCS-1542148). The statements, findings, conclusions and recommendations are those of the authors and do not necessarily reflect the views of California Sea Grant or NOAA.

SUPPLEMENTARY MATERIAL

The Supplementary Material for this article can be found online at: https://www.frontiersin.org/articles/10.3389/fmars.2018.00258/full#supplementary-material

REFERENCES

Addadi, L., and Weiner, S. (2014). Biomineralization: mineral formation by organisms. *Phys. Scr.* 89:098003. doi: 10.1088/0031-8949/89/9/098003

Agaogullari, D., Kel, D., Gökçe, H., Duman, I., Öveçoglu, M. L., Akarsubaşi, A. T., et al. (2012). Bioceramic production from sea urchins. *Acta Phys. Pol. A* 121, 23–26. doi: 10.12693/APhysPolA.121.23

Alin, S. R., Feely, R. A., Dickson, A. G., Hernández-Ayón, J. M., Juranek, L. W., Ohman, M. D., et al. (2012). Robust empirical relationships for estimating the carbonate system in the southern California current system and application to CalCOFI hydrographic cruise data (2005-2011). *J. Geophys. Res.* 117:C05033. doi: 10.1029/2011JC007511

Andersson, A. J., and Mackenzie, F. T. (2012). Revisiting four scientific debates in ocean acidification research. *Biogeosciences* 9, 893–905. doi: 10.5194/bg-9-893-2012

Andersson, A. J., Mackenzie, F. T., and Bates, N. R. (2008). Life on the margin: implications of ocean acidification on Mg-calcite, high latitude and cold-water marine calcifiers. *Mar. Ecol. Prog. Ser.* 373, 265–273. doi: 10.3354/meps07639

Barry, J. P., Lovera, C., Buck, K. R., Peltzer, E. T., Taylor, J. R., Walz, P., et al. (2014). Use of a free ocean CO2 enrichment (FOCE) system to evaluate the effects of ocean acidification on the foraging behavior of a deep-sea urchin. *Environ. Sci. Technol.* 48, 9890–9897. doi: 10.1021/es501603r

Bednaršek, N., Feely, R. A., Tolimieri, N., Hermann, A. J., Siedlecki, S. A., Waldbusser, G. G., et al. (2017). Exposure history determines pteropod vulnerability to ocean acidification along the US West Coast. *Sci. Rep.* 7, 1–12. doi: 10.1038/s41598-017-03934-z

Bednaršek, N., Harvey, C. J., Kaplan, I. C., Feely, R. A., and MoŽina, J. (2016). Pteropods on the edge: cumulative effects of ocean acidification, warming, and deoxygenation. *Prog. Oceanogr.* 145, 1–24. doi: 10.1016/j.pocean.2016.04.002

Biller, D. V., and Bruland, K. W. (2013). Sources and distributions of Mn, Fe, Co, Ni, Cu, Zn, and Cd relative to macronutrients along the central California coast during the spring and summer upwelling season. *Mar. Chem.* 155, 50–70. doi: 10.1016/j.marchem.2013.06.003

Bograd, S. J., Buil, M. P., Di Lorenzo, E., Castro, C. G., Schroeder, I. D., Anderson, C. R., et al. (2015). Changes in source waters to the Southern California Bight. *Deep Sea Res. II Top. Stud. Oceanogr.* 112, 42–52. doi: 10.1016/j.dsr2.2014.04.009

Bograd, S. J., Castro, C. G., Di Lorenzo, E., Palacios, D. M., Bailey, H., Gilly, W., et al. (2008). Oxygen declines and the shoaling of the hypoxic boundary in the California Current. *Geophys. Res. Lett.* 35:L12607. doi: 10.1029/2008GL034185

Breitburg, D., Levin, L. A., Oschlies, A., Grégoire, M., Chavez, F. P., Conley, D. J., et al. (2018). Declining oxygen in the global ocean and coastal waters. *Science* 359:eaam7240. doi: 10.1126/science.aam7240

Byrne, M., Smith, A. M., West, S., Collard, M., Dubois, P., Graba-Landry, A., et al. (2014). Warming influences Mg^{2+} content, while warming and acidification influence calcification and test strength of a sea urchin. *Environ. Sci. Technol.* 48, 12620–12627. doi: 10.1021/es5017526

Candia Carnevali, M. D., Wilkie, I. C., Lucca, E., Andrietti, F., and Melone, G. (1993). The Aristotle's lantern of the sea-urchin *Stylocidaris affinis* (Echinoida, Cidaridae): functional morphology of the musculo-skeletal system. *Zoomorphology* 113, 173–189.

Carrington, E., Waite, J. H., Sarà, G., and Sebens, K. P. (2015). Mussels as a model system for integrative ecomechanics. *Ann. Rev. Mar. Sci.* 7, 443–469. doi: 10.1146/annurev-marine-010213-135049

Chave, K. E. (1954). Aspects of the Biogeochemistry of magnesium, 1. Calcareous marine organisms. *J. Geol.* 62, 266–283.

Chiarelli, R., and Roccheri, M. C. (2014). Marine invertebrates as bioindicators of heavy metal pollution. *Open J. Met.* 4, 93–106. doi: 10.4236/ojmetal.2014.44011

Clarke, F. W., and Wheeler, W. D. (1917). The inorganic constituents of marine constituents of marine invertebrates. *U.S. Geol. Surv.* 102:56.

Collard, M., Dery, A., Dehairs, F., and Dubois, P. (2014). Euechinoidea and Cidaroidea respond differently to ocean acidification. *Comp. Biochem. Physiol. Part A Mol. Integr. Physiol.* 174, 45–55. doi: 10.1016/j.cbpa.2014.04.011

Collard, M., Laitat, K., Moulin, L., Catarino, A. I., Grosjean, P., and Dubois, P. (2013). Buffer capacity of the coelomic fluid in echinoderms. *Comp. Biochem. Physiol. A Mol. Integr. Physiol.* 166, 199–206. doi: 10.1016/j.cbpa.2013.06.002

Collard, M., Rastrick, S. P. S., Calosi, P., Demolder, Y., Dille, J., Findlay, H. S., et al. (2016). The impact of ocean acidification and warming on the skeletal mechanical properties of the sea urchin *Paracentrotus lividus* from laboratory and field observations. *ICES J. Mar. Sci.* 73, 727–738. doi: 10.1093/icesjms/fst176

Denny, M., Daniel, T., and Koehl, M. (1985). Mechanical limits to size in wave-swept organisms. *Ecol. Monogr.* 55, 69–102.

Des Roches, S., Post, D. M., Turley, N. E., Bailey, J. K., Hendry, A. P., Kinnison, M. T., et al. (2018). The ecological importance of intraspecific variation. *Nat. Ecol. Evol.* 2, 57–64. doi: 10.1038/s41559-017-0402-5

deVries, M. S., Webb, S. J., Tu, J., Cory, E., Morgan, V., Sah, R. L., et al. (2016). Stress physiology and weapon integrity of intertidal mantis shrimp under future ocean conditions. *Sci. Rep.* 6, 1–15. doi: 10.1038/srep38637

Diaz, R. J., and Rosenberg, R. (2008). Spreading dead zones and consequences for marine ecosystems. *Science* 321, 926–929. doi: 10.1126/science.1156401

Dickson, A. G. (1990). Standard potential of the reaction: $AgCl_{(s)} + 1/2\ H_{2(g)} = Ag_{(s)} + HCl_{(aq)}$, and the standard acidity constant of the ion HSO_4^- in synthetic sea water from 273.15 to 318.15 K. *J. Chem. Thermodyn.* 22, 113–127. doi: 10.1016/0021-9614(90)90074-Z

Dickson, A. G., Sabine, C. L., and Christian, J. R., (eds.). (2007). *Guide to Best Practices for Ocean CO_2 Measurements*. 3rd Edn. Sidney, BC: PICES Special Edition.

Dubois, P. (2014). The skeleton of postmetamorphic echinoderms in a changing world. *Biol. Bull.* 226, 223–236. doi: 10.1086/BBLv226n3p223

Dupont, S., Dorey, N., Stumpp, M., Melzner, F., and Thorndyke, M. (2013). Long-term and trans-life-cycle effects of exposure to ocean acidification in the green sea urchin *Strongylocentrotus droebachiensis*. *Mar. Biol.* 160, 1835–1843. doi: 10.1007/s00227-012-1921-x

Dupont, S., Ortega-Martínez, O., and Thorndyke, M. (2010). Impact of near-future ocean acidification on echinoderms. *Ecotoxicology* 19, 449–462. doi: 10.1007/s10646-010-0463-6

Ebert, T. A. (1967). Negative growth and longevity in the purple sea urchin *Strongylocentrotus purpuratus* (Stimpson). *Science* 157, 557–558.

Ebert, T. A. (1968). Growth rates of the sea urchin *Strongylocentrotus purpuratus* related to food availability and spine abrasion. *Ecology* 49, 1075–1091. doi: 10.2307/1934491

Fabian, D., and Flatt, T. (2012). Life history evolution. *Nat. Educ. Knowl.* 3:24.

Fairbairn, E. A., Keller, A. A., Mädler, L., Zhou, D., Pokhrel, S., and Cherr, G. N. (2011). Metal oxide nanomaterials in seawater: linking physicochemical characteristics with biological response in sea urchin development. *J. Hazard. Mater.* 192, 1565–1571. doi: 10.1016/j.jhazmat.2011.06.080

Feely, R. A., Sabine, C. L., Hernandez-Ayon, J. M., Ianson, D., and Hales, B. (2008). Evidence for upwelling of corrosive "acidified" water onto the continental shelf. *Science* 320, 1490–1492. doi: 10.1126/science.1155676

Fodrie, F. J., Becker, B. J., Levin, L. A., Gruenthal, K., and McMillan, P. (2011). Connectivity clues from short-term variability in settlement and geochemical tags of mytilid mussels. *J. Sea Res.* 65, 141–150. doi: 10.1016/j.seares.2010.09.001

Frank, M., Naleway, S., Jung, J.-Y., Wirth, T., Cheung, C., Loera, F., et al. (2015). A protocol for bioinspired design: a ground sampler based on sea urchin jaws. *J. Vis. Exp.* 110:e53554. doi: 10.3791/53554

Frieder, C. A., Gonzalez, J. P., and Levin, L. A. (2014). Uranium in larval shells as a barometer of molluscan ocean acidification exposure. *Environ. Sci. Technol.* 48, 6401–6408. doi: 10.1021/es500514j

Gallo, N. D., and Levin, L. A. (2016). Fish ecology and evolution in the world's oxygen minimum zones and implications of ocean deoxygenation. *Adv. Mar. Biol.* 74, 117–198. doi: 10.1016/bs.amb.2016.04.001

Gaylord, B., Hill, T. M., Sanford, E., Lenz, E. A., Jacobs, L. A., Sato, K. N., et al. (2011). Functional impacts of ocean acidification in an ecologically critical foundation species. *J. Exp. Biol.* 214, 2586–2594. doi: 10.1242/jeb.055939

Gilly, W. F., Beman, J. M., Litvin, S. Y., and Robison, B. H. (2013). Oceanographic and biological effects of shoaling of the oxygen minimum zone. *Ann. Rev. Mar. Sci.* 5, 393–420. doi: 10.1146/annurev-marine-120710-100849

Gooday, A. J., Bett, B. J., Escobar, E., Ingole, B., Levin, L. A., Neira, C., et al. (2010). Habitat heterogeneity and its influence on benthic biodiversity in oxygen minimum zones. *Mar. Ecol.* 31, 125–147. doi: 10.1111/j.1439-0485.2009.00348.x

Gruber, N. (2011). Warming up, turning sour, losing breath: ocean biogeochemistry under global change. *Philos. Trans. R. Soc. London A Math. Phys. Eng. Sci.* 369, 1980–1996. doi: 10.1098/rsta.2011.0003

Gruber, N., Hauri, C., Lachkar, Z., Loher, D., Frolicher, T. L., and Plattner, G. K. (2012). Rapid progression of ocean acidification in the California Current System. *Science* 337, 220–223. doi: 10.1126/science.1216773

Helly, J. J., and Levin, L. A. (2004). Global distribution of naturally occurring marine hypoxia on continental margins. *Deep. Res. Part I Oceanogr. Res. Pap.* 51, 1159–1168. doi: 10.1016/j.dsr.2004.03.009

Hennige, S. J., Wicks, L. C., Kamenos, N. A., Perna, G., Findlay, H. S., and Roberts, J. M. (2015). Hidden impacts of ocean acidification to live and dead coral framework. *Proc. R. Soc. B Biol. Sci.* 282:20150990. doi: 10.1098/rspb.2015.0990

Hermans, J., Borremans, C., Willenz, P., Andre, L., and Dubois, P. (2010). Temperature, salinity and growth rate dependences of Mg/Ca and Sr/Ca ratios of the skeleton of the sea urchin *Paracentrotus lividus* (Lamarck): an experimental approach. *Mar. Biol.* 157, 1293–1300. doi: 10.1007/s00227-010-1409-5

Hofmann, G. E., Evans, T. G., Kelly, M. W., Padilla-Gamiño, J. L., Blanchette, C. A., Washburn, L., et al. (2014). Exploring local adaptation and the ocean acidification seascape – studies in the California Current Large Marine Ecosystem. *Biogeosciences* 11, 1053–1064. doi: 10.5194/bg-11-1053-2014

Hönisch, B., and Allen, K. A. (2013). "Paleoceanography, physical and chemical proxies: Carbon Cycle Proxies ($\delta_{11}B$, $\delta_{13}C_{calcite}$, $\delta_{13}C_{organic}$, Shell Weights, B/Ca, U/Ca, Zn/Ca, Ba/Ca)," in Encyclopedia of Quaternary *Science* 849–858. doi: 10.1016/B978-0-444-53643-3.00288-0

Hotaling, N. A., Bharti, K., Kriel, H., and Simon, C. G. (2015). DiameterJ: a validated open source nanofiber diameter measurement tool. *Biomaterials* 61, 327–338. doi: 10.1016/j.biomaterials.2015.05.015

Janssen, D. J., Conway, T. M., John, S. G., Christian, J. R., Kramer, D. I., Pedersen, T. F., et al. (2014). Undocumented water column sink for cadmium in open ocean oxygen-deficient zones. *Proc. Natl. Acad. Sci. U S A.* 111, 6888–6893. doi: 10.1073/pnas.1402388111

Kanold, J. M., Wang, J., Brümmer, F., and Siller, L. (2016). Metallic nickel nanoparticles and their effect on the embryonic development of the sea urchin *Paracentrotus lividus*. *Environ. Pollut.* 212, 224–229. doi: 10.1016/j.envpol.2016.01.050

Kelly, M. W., Padilla-Gamiño, J. L., and Hofmann, G. E. (2013). Natural variation and the capacity to adapt to ocean acidification in the keystone sea urchin *Strongylocentrotus purpuratus*. *Glob. Chang. Biol.* 19, 2536–2546. doi: 10.1111/gcb.12251

Kim, J.-M., Baars, O., and Morel, F. M. M. (2016). The effect of acidifcation on the bioavailability and electrochemical lability of zinc in seawater. *Philos. Trans. R. Soc. A Math. Phys. Eng. Sci.* 374:20150296. doi: 10.1098/rsta.2015.0296

Kroeker, K. J., Kordas, R. L., Crim, R. N., and Singh, G. G. (2010). Meta-analysis reveals negative yet variable effects of ocean acidification on marine organisms. *Ecol. Lett.* 13, 1419–1434. doi: 10.1111/j.1461-0248.2010.01518.x

Kroeker, K. J., Sanford, E., Rose, J. M., Blanchette, C. A., Chan, F., Chavez, F. P., et al. (2016). Interacting environmental mosaics drive geographic variation in mussel performance and predation vulnerability. *Ecol. Lett.*, 771–779. doi: 10.1111/ele.12613

Kuklinski, P., and Taylor, P. D. (2009). Mineralogy of Arctic bryozoan skeletons in a global context. *Facies* 55, 489–500. doi: 10.1007/s10347-009-0179-3

Kurihara, H., Yin, R., Nishihara, G. N., Soyano, K., and Ishimatsu, A. (2013). Effect of ocean acidification on growth, gonad development and physiology of the sea urchin *Hemicentrotus pulcherrimus*. *Aquat. Biol.* 18, 281–292. doi: 10.3354/ab00510

Lack, D. (1947). The significance of clutch size. *Ibis* 89, 302–352.

Lavigne, M., Hill, T. M., Sanford, E., Gaylord, B., Russell, A. D., Lenz, E. A., et al. (2013). The elemental composition of purple sea urchin (*Strongylocentrotus purpuratus*) calcite and potential effects of pCO_2 during early life stages. *Biogeosciences* 10, 3465–3477. doi: 10.5194/bg-10-3465-2013

Lebrato, M., Andersson, A. J., Ries, J. B., Aronson, R. B., Lamare, M. D., Koeve, W., et al. (2016). Benthic marine calcifiers coexist with $CaCO_3$-undersaturated seawater worldwide. *Global Biogeochem. Cycles* 30, 1038–1053. doi: 10.1002/2015GB005260

Lebrato, M., Iglesias-Rodriguez, D., Feely, R. A., Greeley, D., Jones, D. O. B., Suarez-Bosche, N., et al. (2010). Global contribution of echinoderms to the marine carbon cycle: $CaCO_3$ budget and benthic compartments. *Ecol. Monogr.* 80, 441–467. doi: 10.1890/09-0553.1

Levin, L. A. (2003). "Oxygen minimum zone benthos: adaptation and community response to hypoxia," in *Oceanogr. Mar. Biol. Ann. Rev.* Vol. 41, (London: Aberdeen University Press/Allen & Unwin), 1–45.

Levin, L. A. (2006). Recent progress in understanding larval dispersal: new directions and digressions. *Integr. Comp. Biol.* 46, 282–297. doi: 10.1093/icb/icj024

Levin, L. A. (2018). Manifestation, drivers, and emergence of open ocean deoxygenation. *Ann. Rev. Mar. Sci.* 10, 17.1-17.32. doi: 10.1146/annurev-marine-121916-063359

Levin, L. A., Hönisch, B., and Frieder, C. A. (2015). Geochemical proxies for estimating faunal exposure to ocean acidification. *Oceanography* 28, 62–73. doi: 10.5670/oceanog.2015.32

Levin, L. A., and Sibuet, M. (2012). Understanding continental margin biodiversity: a new imperative. *Ann. Rev. Mar. Sci.* 4, 79–112. doi: 10.1146/annurev-marine-120709-142714

Limburg, K. E., Walther, B. D., Lu, Z., Jackman, G., Mohan, J., Walther, Y., et al. (2015). In search of the dead zone: use of otoliths for tracking fish exposure to hypoxia. *J. Mar. Syst.* 141, 167–178. doi: 10.1016/j.jmarsys.2014.02.014

Lohrer, A. M., Thrush, S. F., Hunt, L., Hancock, N., and Lundquist, C. (2005). Rapid reworking of subtidal sediments by burrowing spatangoid urchins. *J. Exp. Mar. Bio. Ecol.* 321, 155–169. doi: 10.1016/j.jembe.2005.02.002

Lowder, K. B., Allen, M. C., Day, J. M. D., Deheyn, D. D., and Taylor, J. R. A. (2017). Assessment of ocean acidification and warming on the growth, calcification, and biophotonics of a California grass shrimp. *ICES J. Mar. Sci.* 74, 1150–1158. doi: 10.1093/icesjms/fsw246

Lueker, T. J., Dickson, A. G., and Keeling, C. D. (2000). Ocean pCO_2 calculated from dissolved inorganic carbon, alkalinity, and equations for K_1 and K_2 : validation based on laboratory measurements of CO_2 in gas and seawater at equilibrium. *Mar. Chem.* 70, 105–119. doi: 10.1016/S0304-4203(00)00022-0

Ma, Y., Aichmayer, B., Paris, O., Fratzl, P., Meibom, A., Metzler, R. A., et al. (2009). The grinding tip of the sea urchin tooth exhibits exquisite control over calcite crystal orientation and Mg distribution. *Proc. Natl. Acad. Sci. U S A.* 106, 6048–6053. doi: 10.1073/pnas.0810300106

Mackenzie, F. T., Bischoff, W. D., Bishop, F. C., Loijens, M., Schoonmaker, J., and Wollast, R. (1983). "Mg-calcites: low temperature occurrence, solubility and solid-solution behavior," in *Reviews in Mineralogy, Carbonates: Mineralogy and Chemistry*, ed. R. J. Reeder (Washington, DC: Mineralogical Society of America), 97–143.

MacLean, S. A., and Beissinger, S. R. (2017). Species' traits as predictors of range shifts under contemporary climate change: a review and meta-analysis. *Glob. Chang. Biol.* 23, 4094–4105. doi: 10.1111/gcb.13736

Mann, K., Poustka, A., and Mann, M. (2008). The sea urchin (*Strongylocentrotus purpuratus*) test and spine proteomes. *Proteome Sci.* 6:22. doi: 10.1016/j.ydbio.2006.07.044

Marchitto, T. M., Curry, W. B., and Oppo, D. W. (2000). Zinc concentrations in benthic foraminfera reflect seawater chemistry. *Paleoceanography* 15, 299–306. doi: 10.1029/1999PA000420

McCulloch, M., Trotter, J., Montagna, P., Falter, J., Dunbar, R., Freiwald, A., et al. (2012). Resilience of cold-water scleractinian corals to ocean acidification: boron isotopic systematics of pH and saturation state up-regulation. *Geochim. Cosmochim. Acta* 87, 21–34. doi: 10.1016/j.gca.2012.03.027

Meyers, M. A., Chen, P.-Y., Lin, A. Y.-M., and Seki, Y. (2008). Biological materials: structure and mechanical properties. *Prog. Mater. Sci.* 53, 1–206. doi: 10.1016/j.pmatsci.2007.05.002

Milton, D. A., and Chenery, S. R. (2001). Sources and uptake of trace metals in otoliths of juvenile barramundi (*Lates calcarifer*). *J. Exp. Mar. Bio. Ecol.* 264, 47–65. doi: 10.1016/S0022-0981(01)00301-X

Moberly, R. (1968). Composition of magnesian calcites of algae and pelecypods by electron microprobe analysis. *Sedimentology* 11, 61–82.

Moffitt, S. E., Moffitt, R. A., Sauthoff, W., Davis, C. V., Hewett, K., and Hill, T. M. (2015). Paleoceanographic insights on recent oxygen minimum zone expansion: lessons for modern oceanography. *PLoS ONE* 10:e0115246. doi: 10.1371/journal.pone.0115246

Morse, J. W., Andersson, A. J., and Mackenzie, F. T. (2006). Initial responses of carbonate-rich shelf sediments to rising atmospheric pCO_2 and "ocean

acidification": role of high Mg-calcites. *Geochim. Cosmochim. Acta* 70, 5814–5830. doi: 10.1016/j.gca.2006.08.017

Moureaux, C., Pérez-Huerta, A., Compère, P., Zhu, W., Leloup, T., Cusack, M., et al. (2010). Structure, composition and mechanical relations to function in sea urchin spine. *J. Struct. Biol.* 170, 41–49. doi: 10.1016/j.jsb.2010.01.003

Naleway, S. E., Taylor, J. R. A., Porter, M. M., Meyers, M. A., and McKittrick, J. (2016). Structure and mechanical properties of selected protective systems in marine organisms. *Mater. Sci. Eng. C Mater. Biol. Appl.* 59, 1143–1167. doi: 10.1016/j.msec.2015.10.033

Nam, S., Takeshita, Y., Frieder, C. A., Martz, T., and Ballard, J. (2015). Seasonal advection of pacific equatorial water alters oxygen and pH in the Southern California Bight. *J. Geophys. Res. Ocean.* 120, 5387–5399. doi: 10.1002/2015JC010859

Oksanen, J., Blanchet, F. G., Friendly, M., Kindt, R., Legendre, P., McGlinn, D., et al. (2017). *vegan: Community Ecology Package.* R Package Version 2.4-2. Available online at: https://cran.r-project.org/package=vegan.

Oliver, T. A., Garfield, D. A., Manier, M. K., Haygood, R., Wray, G. A., and Palumbi, S. R. (2010). Whole-genome positive selection and habitat-driven evolution in a shallow and a deep-sea urchin. *Genome Biol. Evol.* 2, 800–814. doi: 10.1093/gbe/evq063

Padilla-Gamiño, J. L., Kelly, M. W., Evans, T. G., and Hofmann, G. E. (2013). Temperature and CO_2 additively regulate physiology, morphology and genomic responses of larval sea urchins, *Strongylocentrotus purpuratus*. *Proc. R. Soc. B* 280:20130155. doi: 10.1098/rspb.2013.0155

Pearse, J. S. (2006). Ecological role of purple sea urchins. *Science* 314, 940–941. doi: 10.1126/science.1131888

Piersma, T., and Drent, J. (2003). Phenotypic flexibility and the evolution of organismal design. *Trends Ecol. Evol.* 18, 228–233. doi: 10.1016/S0169-5347(03)00036-3

Politi, Y., Arad, T., Klein, E., Weiner, S., and Addadi, L. (2004). Sea urchin spine calcite forms via a transient amorphous calcium carbonate phase. *Science* 306, 1161–1164. doi: 10.1126/science.1102289

Presser, V., Gerlach, K., Vohrer, A., Nickel, K. G., and Dreher, W. F. (2010). Determination of the elastic modulus of highly porous samples by nanoindentation: a case study on sea urchin spines. *J. Mater. Sci.* 45, 2408–2418. doi: 10.1007/s10853-010-4208-y

Reich, M., and Smith, A. B. (2009). Origins and biomechanical evolution of teeth in echinoids and their relatives. *Palaeontology* 52, 1149–1168. doi: 10.1111/j.1475-4983.2009.00900.x

Reusch, T. B. (2014). Climate change in the oceans: evolutionary versus phenotypically plastic responses of marine animals and plants. *Evol. Appl.* 7, 104–122. doi: 10.1111/eva.12109

Russell, A. D., Hönisch, B., Spero, H. J., and Lea, D. W. (2004). Effects of seawater carbonate ion concentration and temperature on shell U, Mg, and Sr in cultured planktonic foraminifera. *Geochim. Cosmochim. Acta* 68, 4347–4361. doi: 10.1016/j.gca.2004.03.013

Sato, K. N., Levin, L. A., and Schiff, K. (2017). Habitat compression and expansion of sea urchins in response to changing climate conditions on the California continental shelf and slope (1994–2013). *Deep Sea Res. II Top. Stud. Oceanogr.* 137, 377–389. doi: 10.1016/j.dsr2.2016.08.012

Sato, K. N., Powell, J., Rudie, D., and Levin, L. A. (2018). Evaluating the promise and pitfalls of a potential climate change–tolerant sea urchin fishery in southern California. *ICES J. Mar. Sci.* 75, 1029–1041. doi: 10.1093/icesjms/fsx225

Schmidtko, S., Stramma, L., and Visbeck, M. (2017). Decline in global oceanic oxygen content during the past five decades. *Nature* 542, 335–339. doi: 10.1038/nature21399

Schneider, C. A., Rasband, W. S., and Eliceiri, K. W. (2012). NIH Image to ImageJ: 25 years of image analysis. *Nat. Methods* 9, 671–675. doi: 10.1038/nmeth.2089

Smith, C. C., and Fretwell, S. D. (1974). The optimal balance between size and number of offspring. *Am. Nat.* 108, 499–506.

Sperling, E. A., Frieder, C. A., and Levin, L. A. (2016). Biodiversity response to natural gradients of multiple stressors on continental margins. *Proc. R. Soc. Lond. B Biol. Sci.* 283:20160637. doi: 10.1098/rspb.2016.0637

Stramma, L., Schmidtko, S., Levin, L. A., and Johnson, G. C. (2010). Ocean oxygen minima expansions and their biological impacts. *Deep Sea Res. I Oceanogr. Res. Pap.* 57, 587–595. doi: 10.1016/j.dsr.2010.01.005

Sumich, J. L., and McCauley, J. E. (1973). Growth of a sea urchin, *Allocentrotus fragilis*, off the Oregon coast. *Coast. Pacific Sci.* 27, 156–167.

Sunday, J. M., Calosi, P., Dupont, S., Munday, P. L., Stillman, J. H., and Reusch, T. B. (2014). Evolution in an acidifying ocean. *Trends Ecol. Evol.* 29, 117–125. doi: 10.1016/j.tree.2013.11.001

Swezey, D. S., Bean, J. R., Hill, T. M., Gaylord, B., Ninokawa, A. T., and Sanford, E. (2017a). Plastic responses of bryozoans to ocean acidification. *J. Exp. Biol.* 220, 4399–4409. doi: 10.1242/jeb.163436

Swezey, D. S., Bean, J. R., Ninokawa, A. T., Hill, T. M., Gaylord, B., and Sanford, E. (2017b). Interactive effects of temperature, food and skeletal mineralogy mediate biological responses to ocean acidification in a widely distributed bryozoan. *Proc. R. Soc. B* 284, 20162349. doi: 10.1098/rspb.2016.2349

Takeshita, Y., Frieder, C. A., Martz, T. R., Ballard, J. R., Feely, R. A., Kram, S., et al. (2015). Including high-frequency variability in coastal ocean acidification projections. *Biogeosciences* 12, 5853–5870. doi: 10.5194/bg-12-5853-2015

Taylor, J. R., Gilleard, J. M., Allen, M. C., and Deheyn, D. D. (2015). Effects of CO_2-induced pH reduction on the exoskeleton structure and biophotonic properties of the shrimp *Lysmata californica*. *Sci. Rep.* 5:10608. doi: 10.1038/srep10608

Taylor, J. R., Lovera, C., Whaling, P. J., Buck, K. R., Pane, E. F., and Barry, J. P. (2014). Physiological effects of environmental acidification in the deep-sea urchin *Strongylocentrotus fragilis*. *Biogeosciences* 11, 1413–1423. doi: 10.5194/bg-11-1413-2014

Thompson, B., Tsukada, D., and Laughlin, J. (1993). Megabenthic assemblages of coastal shelves, slopes, and basins off southern California. *Bull. South. Calif. Acad. Sci.* 92, 25–42.

Todgham, A. E., and Hofmann, G. E. (2009). Transcriptomic response of sea urchin larvae *Strongylocentrotus purpuratus* to CO_2-driven seawater acidification. *J. Exp. Biol.* 212, 2579–2594. doi: 10.1242/jeb.032540

Tribovillard, N., Algeo, T. J., Lyons, T., and Riboulleau, A. (2006). Trace metals as paleoredox and paleoproductivity proxies: an update. *Chem. Geol.* 232, 12–32. doi: 10.1016/j.chemgeo.2006.02.012

Von Euw, S., Zhang, Q., Manichev, V., Murali, N., Gross, J., Feldman, L. C., et al. (2017). Biological control of aragonite formation in stony corals. *Science* 356, 933–938. doi: 10.1126/science.aam6371

Walter, L. M., and Morse, J. W. (1984). Reactive surface area of skeletal carbonates during dissolution: effect of grain size. *J. Sediment. Res.* 54, 1081–1090.

Walther, B. D., and Limburg, K. E. (2012). The use of otolith chemistry to characterize diadromous migrations. *J. Fish Biol.* 81, 796–825. doi: 10.1111/j.1095-8649.2012.03371.x

Walther, S. M., Williams, J. P., Latker, A., Cadien, D. B., Diehl, D. W., Miller, E., et al. (2017). *Southern California Bight 2013 Regional Monitoring* Program: Volume VIII. Demersal Fishes and Megabenthic Invertebrates. South. Calif. Coast. Water Res. Proj. Costa Mesa, CA.

Wang, R. Z., Addadi, L., and Weiner, S. (1997). Design strategies of sea urchin teeth: structure, composition, and micromechanical relations to function. *Philos. Trans. R. Soc. B* 352, 469–480.

Weiner, S., and Dove, P. M. (2003). An overview of biomineralization processes and the problem of the vital effect. *Rev. Mineral. Geochemistry* 54, 1–29. doi: 10.2113/0540001

Williams, B., Halfar, J., Delong, K. L., Smith, E., Steneck, R., Lebednik, P. A., et al. (2017). North Pacific twentieth century decadal-scale variability is unique for the past 342 years. *Geophys. Res. Lett.* 44, 3761–3769. doi: 10.1002/2017GL073138

Ziveri, P., Passaro, M., Incarbona, A., Milazzo, M., Rodolfo-Metalpa, R., and Hall-Spencer, J. M. (2014). Decline in coccolithophore diversity and impact on coccolith morphogenesis along a natural CO_2 gradient. *Biol. Bull.* 226, 282–290. doi: 10.1086/BBLv226n3p282

Conflict of Interest Statement: The authors declare that the research was conducted in the absence of any commercial or financial relationships that could be construed as a potential conflict of interest.

frontiers in Marine Science

ORIGINAL RESEARCH
published: 09 October 2018
doi: 10.3389/fmars.2018.00350

Predator Avoidance in the European Seabass After Recovery From Short-Term Hypoxia and Different CO_2 Conditions

Alexandra Steckbauer[1,2]*, *Carlos Díaz-Gil*[1,3], *Josep Alós*[1], *Ignacio A. Catalán*[1] and *Carlos M. Duarte*[2]

[1] Instituto Mediterráneo de Estudios Avanzados, (CSIC-UIB), Esporles, Spain, [2] Red Sea Research Center, King Abdullah University of Science and Technology, Thuwal, Saudi Arabia, [3] Laboratori d'Investigacions Marines i Aqüicultura (Balearic Government), Illes Balears, Spain

Short-term hypoxia that lasts just a few days or even hours is a major threat for the marine ecosystems. The single effect of the human-induced levels of hypoxia and other anthropogenic impacts such as elevated pCO_2 can reduce the ability of preys to detect their predators across taxa. Moreover, both processes, hypoxia and elevated pCO_2, are expected to co-occur in certain habitats, but the synergic consequences of both processes and the ability of fish to recover remain unknown. To provide empirical evidence to this synergy, we experimentally evaluated the risk-taking behavior in juveniles of the European seabass (*Dicentrachus labrax*), an important commercial fisheries species after recovering from short-term hypoxia and different pH scenarios. The behavior of seabass juveniles was monitored in an experimental arena before and after the exposure to a simulated predator and contrasted to control fish (BACI design) (current levels of hypoxia and elevated pCO_2) using a mechanistic function-valued modeling trait approach. Results revealed that fish recovering from elevated pCO_2, alone or combined with hypoxia, presented less avoidance behavior in failing to seek refuge when a simulated predator was present in the arena compared to those exposed to control pCO_2 levels. Our results show that recovery from short-term exposure to acidification and hypoxia was not synergistic and suggest that recovery from acidification takes longer than from short-term hypoxia treatment through a potential effect on the sensorial and hence behavioral capacities of fish.

Keywords: recovery, behavior, hypoxia, elevated pCO_2, acidification, biased random walk, predator-prey interactions

OPEN ACCESS

Edited by:
Aurélien Paulmier, UMR5566 Laboratoire d'études en Géophysique et Océanographie Spatiales (LEGOS), France

Reviewed by:
Shiguo Li, Research Center for Eco-Environmental Sciences (CAS), China
Yuanyuan Feng, Tianjin University of Science and Technology, China

***Correspondence:**
Alexandra Steckbauer
alexandra.steckbauer@ kaust.edu.sa
steckbauer.ocean@gmail.com

Specialty section:
This article was submitted to Global Change and the Future Ocean, a section of the journal Frontiers in Marine Science

Received: *29 March 2018*
Accepted: *11 September 2018*
Published: *09 October 2018*

Citation:
Steckbauer A, Díaz-Gil C, Alós J, Catalán IA and Duarte CM (2018) Predator Avoidance in the European Seabass After Recovery From Short-Term Hypoxia and Different CO_2 Conditions. Front. Mar. Sci. 5:350. doi: 10.3389/fmars.2018.00350

INTRODUCTION

Worldwide marine costal ecosystems are decreasing their dissolved oxygen (DO) by 5.5 ± 0.2% $year^{-1}$ (Vaquer-Sunyer and Duarte, 2008) and expected to decrease even faster in the future (Conley et al., 2009). Especially in a 30 km band along the coastline the decline in oxygen concentrations is more prevalent and acute (Gilbert et al., 2009). Furthermore shallow and enclosed bays with soft substrate, receiving riverine inputs, and showing high stratification are most likely to experience hypoxia (Stachowitsch and Avcin, 1988). In coastal ecosystems, short-term hypoxia can

only last a few days or even hours and has been observed in various sites (Breitburg, 1990; Levin et al., 2009; Rabalais et al., 2010; Vaquer-Sunyer et al., 2012; Benito et al., 2015). In Chesapeake Bay, for example, 40% of the days DO values are below 2 mg L^{-1} and 10% below 1 mg L^{-1} (Breitburg, 1990; also see review Steckbauer et al., 2011), and in the Mediterranean Sea DO can reach up to 14.8 mg L^{-1} in March but decline below 2 mg L^{-1} during summer months and is directly correlated with high water temperatures (Benito et al., 2015). Ecosystems with sea grasses or macroalgae might experience hypoxia on a daily basis as a result of the DO fluctuations due to production during the day and respiration during the night (Tyler and Targett, 2007; Rabalais et al., 2010; Hendriks et al., 2014), which increases in the summer months due to higher temperatures (Vaquer-Sunyer et al., 2012; Melzner et al., 2013).

Although mobile species are more likely to escape hypoxic areas, it is known that they can be trapped or affected by it, as hypoxia leads to habitat loss, increased energetic costs, altered ecological performances, or even worse, result in direct mortality (Craig et al., 2001). Many examples across taxa demonstrate how increased severity of hypoxia induces behavioral changes in preys that make them more vulnerable to predators (Taylor and Eggleston, 2000; Mistri, 2004; Riedel et al., 2007). Fish are particularly vulnerable to coastal hypoxia, which often results in fish kills and "dead-zones" to fisheries (Vaquer-Sunyer and Duarte, 2008), with sublethal levels of hypoxia affecting predator-prey interactions through behavioral changes in prey that make them more vulnerable to predators (Taylor and Eggleston, 2000; Mistri, 2004; Riedel et al., 2007). Several fish species have shown a reduced swimming performance under hypoxia caused either directly or as a result of saving oxygen consumption for other activities such as digestion (Chabot and Claireaux, 2008), also affecting their vulnerability to predators (Domenici et al., 2007). Moreover, an increased severity of hypoxia not only affects individual organisms but the social structure of fish schools, making them more vulnerable to disruption and consequently decreasing their anti-predator abilities (Whoriskey et al., 1985; Domenici et al., 2007). Diel-cycling hypoxia might be less effectively avoided by fish and could provide chronic exposure that affects reproduction (Levin et al., 2009) and lowers the avoidance threshold for further hypoxic events (Brady and Targett, 2013). Some fish species have been shown to quickly recover their swimming ability and ventilating capacities after hypoxia (Farrell et al., 1998), and this rapid recovery can even confer them competitive benefits (Wu, 2001). Although anti-predator response has previously been evaluated under treatment conditions, no data exists of effects after short-term exposure.

Increasing anthropogenic CO_2 emissions and decreasing seawater pH, a process termed Ocean Acidification (OA) in the open ocean (Orr et al., 2005), represents an emerging pressure in the ocean ecosystem (Doney et al., 2009; Kroeker et al., 2013). In eutrophied coastal areas, the trend toward increased CO_2 is amplified by respiratory CO_2 release associated with a decline in O_2 concentrations in hypoxic areas (Cai et al., 2011; Duarte et al., 2013), which are proliferating worldwide (Diaz and Rosenberg, 2008; Vaquer-Sunyer and Duarte, 2008). Hence, increasing CO_2 and declining O_2 concentrations are often co-occurring stressors (Brewer and Peltzer, 2009; Mayol et al., 2012), which may amplify the responses of organisms to each individual stressor (Burgents et al., 2005; Kim et al., 2013; Rosa et al., 2013; Gobler et al., 2014). Yet, whereas the experimental assessment of the responses of marine organisms to elevated pCO_2 has increased rapidly (Hendriks et al., 2010; Kroeker et al., 2013), assessments of the responses to the combined levels of increasing CO_2 and declining O_2 concentrations are scarce (Burgents et al., 2005; Kim et al., 2013; Rosa et al., 2013; Gobler et al., 2014). In parallel, evidence that elevated pCO_2 induces changes in the behavior of prey affecting its interactions with the predators has been reported (Dixson et al., 2010). Those authors observed altered behavior of larval fish at 700 ppm CO_2, with many individuals becoming attracted to the smell of predators and completely impaired ability to sense predators at 850 ppm CO_2. Fish are especially vulnerable to elevated pCO_2 because it reduces their ability to detect their predators with consequences for recruitment and settlement processes, population dynamics, and ecosystem (Munday et al., 2010; Cripps et al., 2011; Allan et al., 2013). Therefore, there is growing evidence for disrupted predator-prey interactions induced by elevated pCO_2.

The prevalence of the co-occurrence of these two stressors is predicted to increase as hypoxia continues to spread across the coastal ocean and pCO_2 increases due to eutrophication and respiration (Mayol et al., 2012; Melzner et al., 2013). Available evidence suggests that synergies between hypoxia and elevated pCO_2 affect the physiology, condition, metabolism and life history of invertebrates, such as marine bivalves, sipunculid worms, and shrimps (Reipschläger et al., 1997; Burgents et al., 2005; Pörtner et al., 2005; Kim et al., 2013; Gobler et al., 2014). Moreover, a recent study (DePasquale et al., 2015) showed the negative effects of the combined conditions of hypoxia and elevated pCO_2 on hatching and survival of three estuarine fish species *Menidia beryllina*, *Menidia menidia*, and *Cyprinodon variegatus*. Anti-predator behavior in fish has been shown to be influenced by both hypoxia (Kramer, 1987; Poulin et al., 1987; Domenici et al., 2007) and elevated pCO_2 (Ferrari et al., 2012b; Allan et al., 2013), but the possible synergistic effect on anti-predator behavior of fish has not been tested to date.

Here we test the predator-avoidance behavior of fish after recovering from a short-term event of hypoxia and elevated pCO_2, either in isolation or in combination. Specifically, we predict that hypoxia and elevated pCO_2 together should exert synergistic effects disrupting the behavior of juvenile fish to a greater extent than observed under the individual stressors.

MATERIALS AND METHODS

The experiment was conducted during end of September and beginning of October 2012 at the regional government aquaculture laboratory (LIMIA), Mallorca, Spain. The experiment was performed with naïve 5-month old juvenile European seabass (9.0 ± 0.63 (SD) cm total length, n = 24), reared from wild parents of Mediterranean origin by a commercial aquaculture producer (CULMAREX; Mallorca, Spain). In the aquaculture station, the juvenile production

cycle is set at 20°C, oxygen levels over 8 mg L^{-1} and pH = 7.9 (CULMAREX pers. comm.). Prior to the experiment, individuals were acclimated for 48 h in a 100-liter tank, aerated and with open water circulation. Fish were fed *ad libitum* twice daily with food pellets (CV4 Skretting pellets). A random subsample of fish ($n = 6$ per treatment) from this tank was moved to each one of four treatment tanks (25 l) and exposed to one of the four experimental treatments.

The four treatments involved two different levels of CO_2 (and pH) and oxygen, as follows: (a) Control—involving pCO_2 corresponding to atmospheric equilibrium (380 ppm) and saturated oxygen (6–8 mg L^{-1}); (b) Hypoxia *alone* - pCO_2 corresponding to atmospheric equilibrium (380 ppm) and low oxygen (2.0–3.5 mg L^{-1}, after Vaquer-Sunyer and Duarte, 2008); (c) Acidification *alone*—a treatment with elevated pCO_2, corresponding to atmospheric levels expected by the end of the century (1000 ppm, Orr et al., 2005) and saturated oxygen; and (d) Combined Hypoxia and Acidification *together*—treatment with low O_2 (2.0–3.5 mg L^{-1}) and elevated pCO_2 (1000 ppm) (**Table 1**). The four treatment tanks were filled with 20 μm-filtered water, which was prepared following the protocol explained above, and placed in temperature-controlled chambers at 24°C. Dissolved oxygen (DO) levels between 2.0 and 3.5 mg L^{-1}, were chosen to represent sublethal O_2 concentrations (Vaquer-Sunyer and Duarte, 2008). For further details of gas mixing and measurements of water conditions see **Supporting Material 1**.

After remaining for short time exposure (4 days) in the treatment tanks, 3 fish per treatment (12 individuals, repeated next day to a total of 24 individuals) were transferred for acclimation into individual rectangular observing arenas (6 L; 25 × 14 × 17 cm) under control conditions, the night (12 h) before the behavioral assay. Individual arenas were visually isolated from each other to avoid disturbance from the other fish and contained a refuge (a piece of artificial seagrass) on one side of the arena. We based our behavioral assay in the replicated-BACI design, which was adapted from (Ferrari et al., 2012a) and followed three observational periods based on video-recording: I) a 5-min recording before-stimulus (simulated predator) period, II) a 1-min stimulus period, and III) a 5-min after-stimulus period. The stimulus consisted of the introduction of a dead individual of the predator species *Scorpaena porcus* inside a watertight (to avoid odor cues) clear plastic bag filled in with water. The bag was placed at the opposite side of the refuge and contained a thin layer of gravel to ensure it would sink and settle properly on the bottom of the tank. The bag occupied less than 5% of the bottom surface of the arena. To stimulate prey fish activity, 4–5 food pellets were added on the opposite side of the shelter before the three periods. The experiment was monitored through video recording using a video camera (Go Pro Model Hero2, © Woodman Labs, Inc.) located above the experimental arenas. Videos were reduced to one frame *per second* sequences (300 frames per period, i.e., 600 frames for each fish trial). These frame sequences were obtained and analyzed using ImageJ (Schneider et al., 2012). The position of the fish was followed using a tracking plug-in (MTrack) within the same software (Meijering et al., 2012), which allowed recording the coordinates of the fish for each frame. In addition, the coordinates of the borders of the aquarium, the refuge and the predator were obtained. The order of fish from the different treatments was randomized and the video observer was blind with respect to the CO_2 and O_2 treatment groups. The behavioral assays were simultaneously performed in three fish per treatment (as in Rosa et al., 2013) distributed randomly in 12 arenas. After the 5 min of the above detailed protocol, the behavioral assay finished and arenas were cleaned and prepared for the next day assay.

Data obtained from each of the 24 fish was composed of a number of coordinates, which were spatially and temporally correlated over time named as discrete-time Markov chain. Therefore, we adopted a function-valued approach where the parameters of a behavioral movement model were compared, rather than comparing direct observations (e.g., distances covered and speeds of fish in the arena) to correct for temporal and spatial autocorrelation (Stinchcombe and Kirkpatrick, 2012). We modeled the movement of the fish as a Biased Random Walk model (BRW), being representative of the risk-taking behavior adopted by a prey-fish in the field. This approach models fish movement within the arena as a random process, but with a tendency (see parameter k below) to remain close to a specific point (the refuge). The tendency to remain close to the refuge is expected to increase in the presence of a predator, and the model tests if the treatments affect their tendency to remain close to the refuge in the presence of those predators. This modeling approach has been widely used to describe the home range behavior of marine coastal fish, where the spatial coverage used by the fish reaches an asymptote because the random movement has an extra pattern that links the fish to a specific point or center of the home range (Börger et al., 2008; Palmer et al., 2009; Alós et al., 2012).

The model describes the trajectory of a given fish in the behavioral arena as

$$\vec{r}_{n+1} = \vec{r}_{SC} + e^{-k_n \Delta t}\left(\vec{r}_n - \vec{r}_{SC}\right) + \vec{R}_{n+1} \qquad (1)$$

where $\vec{r}_n$ and $\vec{r}_{n+1}$ denote the position of the center of the activity area at the instant n and n+1, respectively, $\vec{r}_{SC}$is the position of the refuge, k min^{-1} describes the tendency to move to the refuge and $\vec{R}_{n+1}$ describes the stochastic component of the movement process, through a normally distributed term with zero mean and standard deviation (τ) approximated by:

$$\tau = \sqrt{\varepsilon\left(1 - e^{-2k\Delta t}\right)/2k} \qquad (2)$$

where ε defines the scale of the random walk and k defines the tendency to remain near the refuge. For a given activity area size, k increases with the tendency to move to and remain close to the refuge. As k asymptotically approaches zero, the movement pattern approaches a standard (i.e., unbiased) random walk. When k is negative, fish tend to avoid the shelter. The movement parameter k of the i fish was hierarchically estimated from the two time-series (before and after stimulus) for each treatment where fish were considered a random level using a Bayesian approach. The difference $k_{after,i}$. and

TABLE 1 | Measured conditions (mean ± SE) of the seawater of each treatment: Control (ambient pCO_2 and ambient O_2), Hypoxia (ambient pCO_2 and reduced O_2), Acidification (elevated pCO_2 and ambient O_2) and Combined (reduced O_2 and elevated pCO_2).

	Control		Hypoxia		Acidification		Combined	
	Mean	SE	Mean	SE	Mean	SE	Mean	SE
Temperature (°C)	23.8	0.01	23.8	0.01	23.8	0.01	23.8	0.01
Oxygen (mg L^{-1})	5.99	0.22	3.22	0.21	6.37	0.6	3.21	0.07
pH_{NBS} (24°C; average of 5 days)	7.87	0.07	7.72	0.08	7.64	0.10	7.60	0.08
pCO_2 (μatm)	1226.3	237.9	1832.5	351.8	2345.5	560.8	2599.2	472.3
Total Alkalinity	2922.3	64.9	2960.0	25.3	3037.0	39.8	3132.8	74.8

$k_{before,i}$ (or δk_i) gives an estimate of how much the movement characteristics of the fish i changed between the "before" and "after" it experienced the stimulus. The model was hierarchical in the sense that the data of all fish were analyzed together and all δk_i of the fish submitted to the same treatment are assumed to be normally distributed around $\delta k_{treatment}$. Note that the top level of the model was a crossed two (fixed) factors design (Control, Hypoxia, Acidification, Combination). To provide a measure of significance of a change in the $\delta k_{treatment}$ we assumed the effect to be relevant when the Bayesian Credibility Intervals (BCI) of the posterior distribution of the $\delta k_{treatment}$ did not involve zero (pure absence of change in the behavior).

The Bayesian approach has several advantages for deriving inferences in such complex hierarchical models with temporal and spatial autocorrelation (Lunn et al., 2000), being thus suitable to test our hypothesis. Inter-treatment comparisons were conducted by comparing the Bayesian treatment means of each parameter using intervals (2.5 and 97.5%). Unlike the p-value, the Bayesian posterior distributions are interpreted correctly as a belief that there is a given probability that the parameter of interest lies within the interval (Ellison, 2004). The model was implemented and run using the *R2jags* library (Horne et al., 2007; available at: http://cran.r-project.org/web/packages/R2jags/index.html) of the R package (at http://www.r-project.org/), which uses Just another Gibbs sampler (JAGS http://mcmc-jags.sourceforge.net/) to perform Markov Chain Monte Carlo (MCMC) sampling of probability distribution of models parameters. We assumed that the priors for δk_i were normally distributed with mean $\delta k_{treatment}$ and the same tolerance (1/variance) for all four groups of fish. A uniform uninformative flat prior was assumed for this common tolerance. Similarly, uninformative priors were assumed for between-fish variability (within treatment) and for SD_i (Equation 2). Finally, normal uninformative priors were assumed for $\delta k_{treatment}$. Three MCMC were run using randomly chosen initial values for all the estimated parameters (within reasonable intervals). The chains were iterated until convergence was reached. Then 1,000 valid iterations were obtained for estimating posteriors. Intuitive interpretation of the movement parameters is not straightforward. Therefore, just for graphically interpretation the estimated values of $k_{treatment}$ and SD_i were used to simulate 1,000 consecutive fish positions that were visualized by 2D kernel density plots completed using *adehabitatHR* package in R (Calenge, 2006).

All procedures were carried out in strict accordance with the recommendations from Directive 2010/175 63/UE, adhering to Spanish law (RD53/ 2013, BOE n. 34 February 8th 2013).

RESULTS

The treatment conditions of temperature and oxygen matched the target concentrations and were held to a stable level. Unfortunately, the pCO_2 in the water was higher than target values (380 and 1000 ppm) due to the respiration of the fish and thus the pH lower than intended (**Table 1**). Temperature was 23.8°C (±0.01 SE) throughout the experiment. Oxygen was held to a value of 5.99 ± 0.022 mg L^{-1} and 6.37 ± 0.60 mg L^{-1} for the Control and Acidification treatment, and 3.22 ± 0.21 mg L^{-1} and 3.21 ± 0.07 mg L^{-1} for the Hypoxia and Combined treatment, respectively. pH_{NBS} was 7.87 ± 0.07 SE and 7.72 ± 0.08 for the Control and Hypoxia treatment, and 7.64 ± 0.10 and 7.60 ± 0.08 for the Acidification and Combined treatment, respectively. No significant difference in size between treatments was observed (p = 0.89, one-way ANOVA).

There was a significant change (larger k, i.e., greater tendency to swim near the refuge after the presence of the predator) for the fish in the Control ($\delta k_{treatment}$= 0.1238 ± 0.0575 min^{-1}) and Hypoxia ($\delta k_{treatment}$= 0.2222 ± 0.1019 min^{-1}) treatments (**Table 2**). Conversely, fish submitted to Acidification ($\delta k_{treatment}$= 0.0298 ± 0.0647 min^{-1}) and the Combined treatments ($\delta k_{treatment}$= 0.0031 ± 0.0616 min^{-1}) did not change their behavior in the presence of the predator (**Figure 1**). The absence of a change in trend toward remaining near the refuge in the presence of the predator was evident when the fish were concurrently exposed to elevated pCO_2 with or without the combination of reduced O_2 values (**Figure 2**; **Table 2**).

As shown in the 2-dimensional kernel density plot (**Figure 1**), fish in the Control and Hypoxia treatments were attracted by the food (released to the left of each tank, in **Figure 1**) and left the refuge, but as soon as the stimulus (simulated predator) was added to the experimental arena, fish enhanced their tendency to move around the refuge. Fish that were exposed to elevated pCO_2 only and to the combined treatment moved randomly in the middle of the arena and showed no attraction toward the refuge in the absence or in the presence of the virtual predator (**Figure 1**). Fish in the Acidification treatment showed a slightly

stronger, although non-significant, average effect to be attracted by the shelter than fish in the Combined treatment (**Figure 2**).

DISCUSSION

Whereas hypoxia and elevated pCO_2 are concurrent stressors that are increasing in coastal areas, experimental assessments of the responses of organisms have focused on individual stressors, with only a few experiments (e.g., Burgents et al., 2005; Kim et al., 2013; Gobler et al., 2014; DePasquale et al., 2015; Steckbauer et al., 2015; Klein et al., 2017) examining the potential synergy between these concurrent stressors. Although little is known about the concurrent effects of hypoxia and elevated pCO_2 on teleost fish, a recent study showed the negative effects of the combined stressors on hatching and survival on the three estuarine fish species *Menidia beryllina*, *Menidia menidia*, and *Cyprinodon variegates* (DePasquale et al., 2015). The present results support previous results (Ferrari et al., 2012b), in that elevated pCO_2, even after a time of recovery (and despite our differences in pH were not very high) leads to a disruption of the capacity of the fish to avoid predation risk, and shows that this shift in behavior is, however, not associated with hypoxia. Therefore, the hypothesis of significant synergy between these two stressors was rejected. Nevertheless, as physiological recovery from hypoxia is often a matter of hours (Farrell et al., 1998), the results might have been different had the animals been tested immediately, without the over-night recovery or if tests had been conducted under treatment conditions.

Hypoxia can constrain fish movement, which is energy demanding, affecting the capacity of fish to move toward refuge in the presence of a predator (Kramer, 1987). Although, fish are able to escape hypoxic areas (Tyler and Targett, 2007), previous diel-cycle hypoxia lowers the avoidance threshold from <2.8 mg O_2 L^{-1} (in saturation-acclimated fish) to $\sim$ 1.4 mg O_2 L^{-1} (in diel-cycling hypoxia acclimated fish) in the juvenile weakfish *Cynoscion regalis* (Brady and Targett, 2013). Moreover, fish can be trapped when a flooding tide appears, but are able to recover from short-term hypoxia very quickly (Rabalais et al., 2001). After recovering for 45 min the swimming performance and ventilation rate in the wild sockeye salmon (*Oncorhynchus nerka*) returned to those of the control values (Farrell et al., 1998). However, as shown on the juvenile summer flounder *Paralichthys dentatus* (Brady and Targett, 2010), diel-cycling hypoxia-acclimated individual did not recover as well from low DO exposure as did saturation-acclimated fish. This indicates that the oxygen value of the water prior to a hypoxic event influences the capability of species to cope with their escaping capabilities and recovery after the event.

Predator-prey interactions play a major role in structuring food webs and are a main driver of behavioral responses, including avoidance responses of fish to predators (Turner and Mittelbach, 1990). In general, prey fish randomly forage in their home range, with a general tendency to remain near

TABLE 2 | Bayesian Confidence Intervals indicating the tendency of the fish to remain close to their refuge after introduction of a predator: a $\delta k > 0$ indicates the tendency to move to and remain close to the refuge; a δk around 0 means the movement pattern approaches a (i.e., unbiased) random walk, and a negative δk shows that the fish tend to avoid the shelter.

Treatment	$\delta k \pm SD$	Bayesian Credibility Intervals		
		2.5%	50%	97.5%
Control	0.1238 ± 0.0575	−0.0086	0.1234	0.2379
Hypoxia	0.2222 ± 0.1019	−0.0257	0.2191	0.4270
Acidification	0.0298 ± 0.0647	−0.0966	0.0288	0.1618
Combined	0.0031 ± 0.0616	−0.1204	0.0022	0.1247

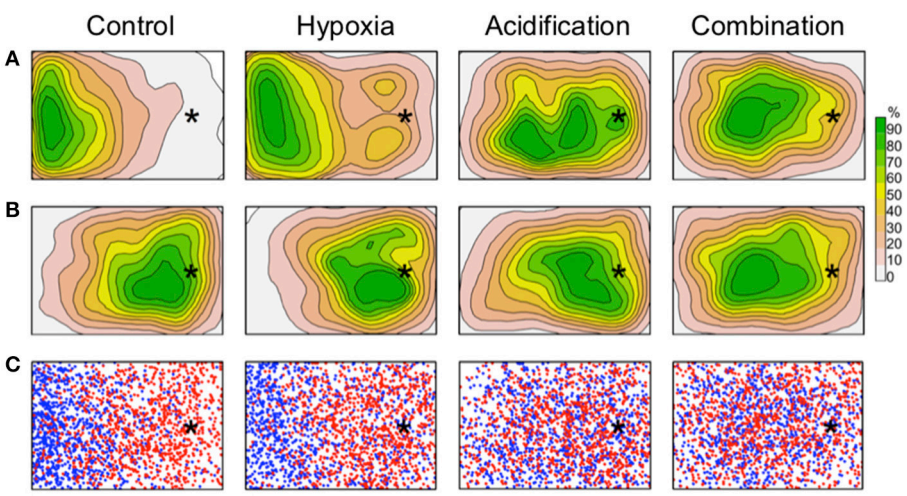

FIGURE 1 | Behavioral response shown as 2-dimensional kernel density plot. The model shows behavioral response to the 4 treatments before **(A)** and after introduction of the simulated predator **(B)** Lower graphs **(C)** show a simulated distribution before (blue) and after (red) the predator was introduced to the arenas (after the model developed by Palmer et al. (2009). The stars mark the position of the shelter. Simulated predator, food, and aeration were positioned at the left side of the arenas (not visible in the square).

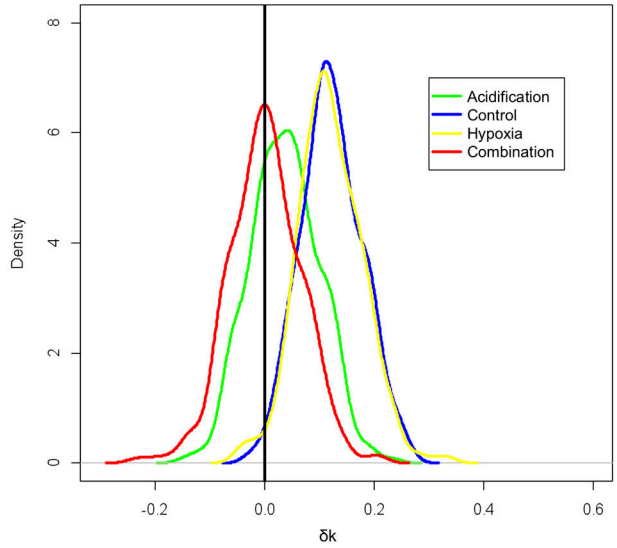

FIGURE 2 | Tendency of the fish to remain close to the refuge: increase in *k* indicates the tendency to move to and remain close to the refuge; a decrease toward zero means the movement pattern approaches a (i.e., unbiased) random walk, and a negative *k* shows that the fish tend to avoid the shelter.

refuges, particularly so in the presence of predators (Krause et al., 1998). We examined this behavior using a function-valued approach, where we compared the parameters of the behavioral model rather than inferring statistics on the fish positions *per se*, avoiding the problems derived from spatial and temporal autocorrelation of the observations on position. Using this approximation, we obtained more accurate information of how the two stressors tested (Hypoxia and Acidification) affect each individuals capacity to hide from predators. The novel approach used here provides a pathway for further studies testing similar hypothesis across taxa under laboratory conditions.

As the results of this study correlated to elevated pCO_2 and not hypoxia, the question remains, why there is a bigger impact of that stressor. The elevated pCO_2 values are leading to a lower pH in the blood (hypercapnia), and thereby are a substantial threat to some species as elevated pCO_2 lowers the pH of animal tissues, affecting its performance (Pörtner et al., 2004). It is known that elevated pCO_2 values readily cross biological membranes, enter the blood and intracellular spaces. Active animals with locomotory muscles, such as epipelagic fish, use passive buffering of short-term pH changes in the body associated with elevated pCO_2 in ambient waters. They have high activities of anaerobic metabolic enzymes and have high capacity for buffering pH changes (Castellini and Somero, 1981; Seibel et al., 1997), whereas organisms with low buffering capacity will experience greater fluctuations in intracellular pH during hypercapnia. Although shallow-water fish are capable to compensate for acid–base disturbances within several days when exposed to mild hypercapnia (Michaelidis et al., 2007; Ishimatsu et al., 2008), other experiments show that a similar increase in seawater pCO_2 lowers the intracellular pH of a sluggish benthic fish by 0.2, whereas in an active epipelagic fish such as tuna, it only causes a 0.02 pH unit drop (Seibel and Walsh, 2003; Fabry et al., 2008). As we did not measure pH or PCO_2 in the blood of the test species, it is uncertain how the blood pH was affected by the different treatments and to what extent they suffered from hypercapnia and how far they normalized after recovering overnight.

The lack of predator avoidance under elevated pCO_2 is most likely related to interference with neurotransmitter function (Nilsson et al., 2012). Those authors reversed abnormal olfactory preferences and loss of behavioral lateralization by treating the fish with an antagonist of the GABA-A receptor, indicating that elevated pCO_2 interferes with neurotransmitter function. Elevated pCO_2 decreases the cognitive abilities in juvenile coral reef fish to detect predator odor (Ferrari et al., 2012a). As a consequence of a much-reduced ability to assess predation risk, even when recovering for 12 h, they will have a much lower survival. Elevated pCO_2 levels also have a negative impact on the ability of larval clownfish to detect olfactory cues that help them locate reef habitat and suitable settlement sites (Munday et al., 2010). Moreover, elevated pCO_2 might also cause a shift in predator behavior as shown for the common coral reef meso-predator, the brown dottyback (*Pseudochromis fuscus*), by shifting from preference to avoidance of the smell of injured prey (Cripps et al., 2011). Although the different oxygen and CO_2 levels might be influencing both, prey and predator, it is yet unclear if the altered behavior of predators is sufficient to fully compensate for the effects of ocean acidification on prey mortality.

Despite a clear interpretation of some of the results can be made, there are some limitations to this study. The total number of fish per treatment, six, was not large, but uncertainty was dealt with optimally through a probabilistic approach. This, however, suggests that small non-significant differences observed could change if sample size was enlarged. Also, it is clear that known physiological explanations match our behavioral results, but both plastic and genetic adaptations may be more important at population level in future scenarios. Furthermore, although the arenas were bubbled with 380 ppm CO_2 (Control and Hypoxia) and 1000 ppm CO_2 (Acidification and Combined), the calculated pCO_2 of the water was higher than expected due to the respiration of the individuals. This however, still enabled the observation of the typical negative effects of elevated pCO_2 on behavior, especially as elevated pCO_2 in coastal ecosystems nowadays can already be as high or higher than the predictions for the open ocean for the end of the century.

CONCLUSIONS

With this study we show that fish recovering from single or combined effects of CO_2 and hypoxia only show behavioral alterations due to prior elevated pCO_2 history. This effect is evident even after one night of recovery. The lack of effect of hypoxia, combined or not with CO_2, should be further tested using shorter recovery times, or during the treatment. The consequences of the present findings must be understood in a

frame of slow but needed progress toward the combined effects of changing levels of these stressors in the frame of warmer and more acidic oceans.

AUTHOR CONTRIBUTIONS

AS, JA, IC, and CD designed the research. AS, JA, and IC executed the research. AS, CD-G, JA, and IC analyzed the data. All authors contributed to writing and improving the manuscript.

ACKNOWLEDGMENTS

This is a contribution to the projects MedSeA of the FP7 of the EU (contract no. FP7-ENV-2010-265103) and ESTRESX (ref. CTM2012-32603), funded by the Spanish ministry of economy and competitivity. AS was funded by a Ph.D. fellowship from the Government of the Balearic Islands (Department on Education, Culture, and Universities) and the EU (European Social Fund) as well as King Abdullah University of Science and Technology. CD-G was funded by a fellowship from the National Institute for Agricultural and Food Research and Technology (INIA). JA was supported by a JdC post-doc grant funded by the Spanish Ministry of Economy, Industry and Competitiveness (ref. IJCI-2016-27681). IC thanks the funding of CERES H2020 project (BG-02-2015, 678193). We thank I.E. Hendriks and Miquel Palmer for advice, and Culmarex Group for providing European Sea Bass specimens.

SUPPLEMENTARY MATERIAL

The Supplementary Material for this article can be found online at: https://www.frontiersin.org/articles/10.3389/fmars.2018.00350/full#supplementary-material

REFERENCES

Allan, B. J. M., Domenici, P., Mccormick, M. I., Watson, S., and Munday, P. L. (2013). Elevated CO_2 affects predator-prey interactions through altered performance. *PLoS ONE* 8:e58520. doi: 10.1371/journal.pone.0058520

Alós, J., Palmer, M., and Arlinghaus, R. (2012). Consistent selection towards low activity phenotypes when catchability depends on encounters among human predators and fish. *PLoS ONE* 7:e48030. doi: 10.1371/journal.pone.0048030

Benito, J., Benejam, L., Zamora, L., and García-Berthou, E. (2015). Diel cycle and effects of water flow on activity and use of depth by common carp. *Trans. Am. Fish. Soc.* 144, 491–501. doi: 10.1080/00028487.2015.1017656

Börger, L., Dalziel, B. D., and Fryxell, J. M. (2008). Are there general mechanisms of animal home range behaviour? A review and prospects for future research. *Ecol. lett.* 11, 637–650. doi: 10.1111/j.1461-0248.2008.01182.x

Brady, D., and Targett, T. (2013). Movement of juvenile weakfish *Cynoscion regalis* and spot *Leiostomus xanthurus* in relation to diel-cycling hypoxia in an estuarine tidal tributary. *Mar. Ecol. Prog. Ser.* 491, 199–219. doi: 10.3354/meps10466

Brady, D. C., and Targett, T. E. (2010). Characterizing the escape response of juvenile summer flounder *Paralichthys dentatus* to diel-cycling hypoxia. *J. Fish Biol.* 77, 137–152. doi: 10.1111/j.1095-8649.2010.02663.x

Breitburg, D. L. (1990). Near-shore hypoxia in the chesapeake bay - patterns and relationships among physical factors. *Estuar. Coast. Shelf Sci.* 30, 593–609. doi: 10.1016/0272-7714(90)90095-9

Brewer, P. G., and Peltzer, E. T. (2009). Limits to marine life. *Science* 324, 347–348. doi: 10.1126/science.1170756

Burgents, J. E., Burnett, K. G., and Burnett, L. E. (2005). Effects of hypoxia and hypercapnic hypoxia on the localization and the elimination of *Vibrio campbellii* in *Litopenaeus vannamei*, the Pacific white shrimp. *Biol. Bull.* 208, 159–168. doi: 10.2307/3593148

Cai, W. J., Hu, X., Huang, W. J., Murrell, M. C., Lehrter, J. C., Lohrenz, S. E., et al. (2011). Acidification of subsurface coastal waters enhanced by eutrophication. *Nat. Geosci.* 4, 766–770. doi: 10.1038/ngeo1297

Calenge, C. (2006). The package "adehabitat" for the R software: a tool for the analysis of space and habitat use by animals. *Ecol. Modell.* 197, 516–519. doi: 10.1016/j.ecolmodel.2006.03.017

Castellini, M., and Somero, G. (1981). Buffering capacity of vertebrate muscle: correlations with potentials for anaerobic function. *J. Comp. Physiol.* 143, 191–198.

Chabot, D., and Claireaux, G. (2008). Environmental hypoxia as a metabolic constraint on fish: the case of Atlantic cod, *Gadus morhua*. *Mar. Pollut. Bull.* 57, 287–294. doi: 10.1016/j.marpolbul.2008.04.001

Conley, D. J., Carstensen, J., Vaquer-Sunyer, R., and Duarte, C. M. (2009). Ecosystem thresholds with hypoxia. *Hydrobiologia* 629, 21–29. doi: 10.1007/s10750-009-9764-2

Craig, J. K., Crowder, L. B., Gray, C. D., McDaniel, C. J., Kenwood, T. A., and Hanifen, J. G. (2001). "Ecological effects of hypoxia on fish, sea turtles, and marine mammals in the northwestern Gulf of Mexico," in *Coastal Hypoxia: Consequences for Living Resources: Ecosystems,* eds N. N. Rabalais and R. E. Turner (Washington, DC: American Geophysical Union), 269–291.

Cripps, I. L., Munday, P. L., and McCormick, M. I. (2011). Ocean acidification affects prey detection by a predatory reef fish. *PLoS ONE* 6:e22736. doi: 10.1371/journal.pone.0022736

DePasquale, E., Baumann, H., and Gobler, C. (2015). Vulnerability of early life stage Northwest Atlantic forage fish to ocean acidification and low oxygen. *Mar. Ecol. Prog. Ser.* 523, 145–156. doi: 10.3354/meps11142

Diaz, R. J., and Rosenberg, R. (2008). Spreading dead zones and consequences for marine ecosystems. *Science* 321, 926–929. doi: 10.1126/science.1156401

Dixson, D. L., Munday, P. L., and Jones, G. P. (2010). Ocean acidification disrupts the innate ability of fish to detect predator olfactory cues. *Ecol. Lett.* 13, 68–75. doi: 10.1111/j.1461-0248.2009.01400.x

Domenici, P., Lefrançois, C., and Shingles, A. (2007). Hypoxia and the antipredator behaviours of fishes. *Philos. Transac. R. Soc. Lond. Ser. B Biol. Sci.* 362, 2105–2121. doi: 10.1098/rstb.2007.2103

Doney, S. C., Fabry, V. J., Feely, R. A., and Kleypas, J. A. (2009). Ocean acidification: the other CO_2 problem. *Ann. Rev. Mar. Sci.* 1, 169–192. doi: 10.1146/annurev.marine.010908.163834

Duarte, C. M., Hendriks, I. E., Moore, T. S., Olsen, Y. S., Steckbauer, A., Ramajo, L., et al. (2013). Is ocean acidification an open-ocean syndrome? understanding anthropogenic impacts on seawater pH. *Estuar. Coast.* 36, 221–236. doi: 10.1007/s12237-013-9594-3

Ellison, A. M. (2004). Bayesian inference in ecology. *Ecol. Lett.* 7, 509–520. doi: 10.1111/j.1461-0248.2004.00603.x

Fabry, V. J., Seibel, B. A., Feely, R. A., and Orr, J. C. (2008). Impacts of ocean acidification on marine fauna and ecosystem processes. *J. Mar. Sci.* 65, 414–432. doi: 10.1093/icesjms/fsn048

Farrell, A. P., Gamperl, A. K., and Birtwell, I. K. (1998). Prolonged swimming, recovery and repeat swimming performance of mature sockeye salmon *Oncorhynchus nerka* exposed to moderate hypoxia and pentachlorophenol. *J. Exp. Biol.* 201, 2183–2193.

Ferrari, M. C. O., Manassa, R. P., Dixson, D. L., Munday, P. L., McCormick, M. I., Meekan, M. G., et al. (2012a). Effects of ocean acidification on learning in coral reef fishes. *PLoS ONE* 7:e31478. doi: 10.1371/journal.pone.0031478

Ferrari, M. C. O., McCormick, M. I., Munday, P. L., Meekan, M. G., Dixson, D. L., Lönnstedt, O., et al. (2012b). Effects of ocean acidification

on visual risk assessment in coral reef fishes. *Funct. Ecol.* 26, 553–558. doi: 10.1111/j.1365-2435.2011.01951.x

Gilbert, D., Rabalais, N. N., Diaz, R. J., Zhang, J., Version, P., Discussion, I., et al. (2009). Evidence for greater oxygen decline rates in the coastal ocean than in the open ocean. *Biogeosci. Discuss.* 6, 9127–9160. doi: 10.5194/bgd-6-9127-2009

Gobler, C. J., DePasquale, E. L., Griffith, A. W., and Baumann, H. (2014). Hypoxia and acidification have additive and synergistic negative effects on the growth, survival, and metamorphosis of early life stage bivalves. *PLoS ONE* 9:e83648. doi: 10.1371/journal.pone.0083648

Hendriks, I. E., Duarte, C. M., and Álvarez, M. (2010). Vulnerability of marine biodiversity to ocean acidification: a meta-analysis. *Estuar. Coast. Shelf Sci.* 86, 157–164. doi: 10.1016/j.ecss.2009.11.022

Hendriks, I. E., Olsen, Y. S., Ramajo, L., Basso, L., Steckbauer, A., Moore, T. S., et al. (2014). Photosynthetic activity buffers ocean acidification in seagrass meadows. *Biogeosciences* 11, 333–346. doi: 10.5194/bg-11-333-2014

Horne, J., Garton, E., Krone, S., and Lewis, J. (2007). Analyzing animal movements using Brownian bridges. *Ecology* 88, 2354–2363. doi: 10.1890/06-0957.1

Ishimatsu, A., Hayashi, M., and Kikkawa, T. (2008). Fishes in high-CO_2, acidified oceans. *Mar. Ecol. Prog. Ser.* 373, 295–302. doi: 10.3354/meps07823

Kim, T. W., Barry, J. P., and Micheli, F. (2013). The effects of intermittent exposure to low pH and oxygen conditions on survival and growth of juvenile red abalone. *Biogeosciences* 10, 7255–7262. doi: 10.5194/bg-10-7255-2013

Klein, S. G., Pitt, K. A., Nitschke, M. R., Goyen, S., Welsh, D. T., Suggett, D. J., et al. (2017). *Symbiodinium mitigate* the combined effects of hypoxia and acidification on a non-calcifying cnidarian. *Glob. Chang. Biol.* 23, 3690–3703. doi: 10.1111/gcb.13718

Kramer, D. L. (1987). Dissolved oxygen and fish behavior. *Environ. Biol. Fishes* 18, 81–92. doi: 10.1007/BF00002597

Krause, J., Loader, S. P., McDermott, J., and Ruxton, G. D. (1998). Refuge use by fish as a function of body length-related metabolic expenditure and predation risks. *Proc. R. Soc. Lond. B* 265, 2373–2379. doi: 10.1098/rspb.1998.0586

Kroeker, K. J., Kordas, R. L., Crim, R., Hendriks, I. E., Ramajo, L., Singh, G. S., et al. (2013). Impacts of ocean acidification on marine organisms: quantifying sensitivities and interaction with warming. *Glob. Chang. Biol.* 19, 1884–1896. doi: 10.1111/gcb.12179

Levin, L. A., Ekau, W., Gooday, A. J., Jorissen, F., Middelburg, J. J., Naqvi, S. W. A., et al. (2009). Effects of natural and human-induced hypoxia on coastal benthos. *Biogeosciences* 6, 2063–2098. doi: 10.5194/bg-6-2063-2009

Lunn, D. J., Thomas, A., Best, N., and Spiegelhalter, D. (2000). WinBUGS–a Bayesian modelling framework: concepts, structure, and extensibility. *Stat. Comput.* 10, 325–337. doi: 10.1023/A:1008929526011

Mayol, E., Ruiz-Halpern, S., Duarte, C. M., Castilla, J. C., and Pelegri, J. L. (2012). Coupled CO_2 and O_2-driven compromises to marine life in summer along the Chilean sector of the Humboldt current system. *Biogeosciences* 9, 1183–1194. doi: 10.5194/bg-9-1183-2012

Meijering, E., Dzyubachyk, O., and Smal, I. (2012). Methods for cell and particle tracking. *Meth. Enzymol.* 504, 183–200. doi: 10.1016/B978-0-12-391857-4.00009-4

Melzner, F., Thomsen, J., Koeve, W., Oschlies, A., Gutowska, M. A., Bange, H. W., et al. (2013). Future ocean acidification will be amplified by hypoxia in coastal habitats. *Mar. Biol.* 160, 1875–1888. doi: 10.1007/s00227-012-1954-1

Michaelidis, B., Spring, A., and Pörtner, H. O. (2007). Effects of long-term acclimation to environmental hypercapnia on extracellular acid–base status and metabolic capacity in Mediterranean fish *Sparus aurata*. *Mar. Biol.* 150, 1417–1429. doi: 10.1007/s00227-006-0436-8

Mistri, M. (2004). Effects of hypoxia on predator-prey interactions between juvenile *Carcinus aestuarii* and *Musculista senhousia*. *MEPS* 275, 211–217. doi: 10.3354/meps275211

Munday, P. L., Dixson, D. L., Mccormick, M. I., Meekan, M., Ferrari, M. C. O., and Chivers, D. P. (2010). Replenishment of fish populations is threatened by ocean acidification. *Proc. Natl. Acad. Sci. U.S.A.* 107, 12930–12934. doi: 10.1073/pnas.1004519107

Nilsson, G. E., Dixson, D. L., Domenici, P., Mccormick, M. I., Sørensen, C., Watson, S., et al. (2012). Near-future carbon dioxide levels alter fish behaviour by interfering with neurotransmitter function. *Nat. Climate Change* 2, 201–204. doi: 10.1038/nclimate1352

Orr, J. C., Fabry, V. J., Aumont, O., Bopp, L., Doney, S. C., Feely, R. A., et al. (2005). Anthropogenic ocean acidification over the twenty-first century and its impact on calcifying organisms. *Nature* 437, 681–686. doi: 10.1038/nature04095

Palmer, H., Beutel, M., and Gebremariam, S. (2009). High rates of ammonia removal in experimental oxygen-activated nitrification wetland mesocosms. *J. Environ. Eng. ASCE* 135, 972–979. doi: 10.1061/(ASCE)EE.1943-7870.0000053

Pörtner, H. O., Langenbuch, M., and Michaelidis, B. (2005). Synergistic effects of temperature extremes, hypoxia, and increases in CO_2 on marine animals: from Earth history to global change. *J. Geophys. Res.* 110:C09S10. doi: 10.1029/2004JC002561

Pörtner, H. O., Langenbuch, M., and Reipschläger, A. (2004). Biological impact of elevated ocean CO_2 concentrations : lessons from animal physiology and earth history. *J. Oceanogr.* 60, 705–718. doi: 10.1007/s10872-004-5763-0

Poulin, R., Wolp, N. G., and Kramer, D. L. (1987). The effect of hypoxia on the vulnerability of guppies (*Poecilia reticulata*, *Poeciliidae*) to an aquatic predator (*Astronotus ocektus*, *Cichlidae*). *Environ. Biol. Fishes* 20, 285–292.

Rabalais, N. N., Diaz, R. J., Levin, L. A., Turner, R. E., Gilbert, D., and Zhang, J. (2010). Dynamics and distribution of natural and human-caused hypoxia. *Biogeosciences* 7, 585–619. doi: 10.5194/bg-7-585-2010

Rabalais, N. N., Turner, R. E., and Wiseman, W. J. J. (2001). Hypoxia in the Gulf of Mexico. *JEQ* 30, 320–329. doi: 10.2134/jeq2001.302320x

Reipschläger, A., Nilsson, G. E., and Pörtner, H. O. (1997). A role for adenosine in metabolic depressionin themarine invertebrate *Sipunculus nudus*. *Am. J. Physiol.* 272, R350–R356.

Riedel, B., Stachowitsch, M., and Zuschin, M. (2007). Sea anemones and brittle stars: unexpected predatory interactions during induced *in situ* oxygen crises. *Mar. Biol.* 153, 1075–1085. doi: 10.1007/s00227-007-0880-0

Rosa, R., Trübenbach, K., Repolho, T., Pimentel, M., Faleiro, F., Boavida-Portugal, J., et al. (2013). Lower hypoxia thresholds of cuttlefish early life stages living in a warm acidified ocean. *Proc. R. Soc. B.* 280:20131695. doi: 10.1098/rspb.2013.1695

Schneider, C. A., Rasband, W. S., and Eliceiri, Z. (2012). NIH Image to ImageJ: 25 years of image analysis. *Nat. Methods* 9, 671–675. doi: 10.1038/nmeth.2089

Seibel, A., Thuesen, E. V., Childress, J. J., and Gorodezky, L. A. (1997). Decline in pelagic Cephalopod metabolism habitat depth reflects differences in locomotory efficiency. *Biol. Bull.* 192, 262–278. doi: 10.2307/1542720

Seibel, B. A., and Walsh, P. J. (2003). Biological impacts of deep-sea carbon dioxide injection inferred from indices of physiological performance. *J. Exp. Biol.* 206, 641–650. doi: 10.1242/jeb.00141

Stachowitsch, M., and Avcin, A. (1988). *Eutrophication-Induced Modifications of Benthic Communities. Eutrophication in the Mediterranean Sea: Receiving Capacity and Monitoring of Long-Term Effects*. Regione Emilia Romagna and University of Bologna, Bologna. 49, 67–80.

Steckbauer, A., Duarte, C. M., Carstensen, J., Vaquer-Sunyer, R., and Conley, D. J. (2011). Ecosystem impacts of hypoxia: thresholds of hypoxia and pathways to recovery. *Environ. Res. Lett.* 6. doi: 10.1088/1748-9326/6/2/025003

Steckbauer, A., Ramajo, L., Hendriks, I. E., Fernandez, M., Lagos, N. A., Prado, L., et al. (2015). Synergistic effects of hypoxia and increasing CO_2 on benthic invertebrates of the central Chilean coast. *Front. Mar. Sci.* 2:49. doi: 10.3389/fmars.2015.00049

Stinchcombe, J. R., and Kirkpatrick, M. (2012). Genetics and evolution of function-valued traits: understanding environmentally responsive phenotypes. *Trends Ecol. Evol.* 27, 637–647. doi: 10.1016/j.tree.2012.07.002

Taylor, D. L., and Eggleston, D. B. (2000). Effects of hypoxia on an estuarine predator-prey interaction: foraging behavior and mutual interference in the blue crab *Callinectes sapidus* and the infaunal clam prey *Mya arenaria*. *Mar. Ecol. Prog. Ser.* 196, 221–237. doi: 10.3354/meps196221

Turner, A. M., and Mittelbach, G. G. (1990). Predator avoidance and community structure: interactions among piscivores, planktivores, and plankton. *Ecology* 71, 2214–2254. doi: 10.2307/1938636

Tyler, R. M., and Targett, T. E. (2007). Juvenile weakfish *Cynoscion regalis* distribution in relation to diel-cycling dissolved oxygen in an estuarine tributary. *Mar. Ecol. Prog. Ser.* 333, 257–269. doi: 10.3354/meps333257

Vaquer-Sunyer, R., and Duarte, C. M. (2008). Thresholds of hypoxia for marine biodiversity. *Proc. Natl. Acad. Sci. U.S.A.* 105, 15452–15457. doi: 10.1073/pnas.0803833105

Vaquer-Sunyer, R., Duarte, C. M., Jordà, G., and Ruiz-Halpern, S. (2012). Temperature dependence of oxygen dynamics and community metabolism in a shallow mediterranean macroalgal meadow (*Caulerpa prolifera*). *Estuar. Coast.* 35, 1182–1192. doi: 10.1007/s12237-012-9514-y

Whoriskey, F. G., Gaudreault, A., Martel, N., Campeau, S., and FitzGerald, G. J. (1985). The activity budget and behavior patterns of female threespine sticklebacks *Gasterosteus aculeatus* (L.). *Nat. Canad.* 112, 113–118.

Wu, R. S. S. (2001). *Responses of Benthic Communities to Hypoxia in a Sub-Tropical Environment: Problems and Hypotheses*. Ecosystems Research Division Athens, Georgia.

Conflict of Interest Statement: The authors declare that the research was conducted in the absence of any commercial or financial relationships that could be construed as a potential conflict of interest.

frontiers in Marine Science

MINI REVIEW
published: 11 October 2018
doi: 10.3389/fmars.2018.00341

Winning Ways With Hydrogen Sulphide on the Namibian Shelf

Bronwen Currie[1]*, *Anne Christine Utne-Palm*[2] *and Anne Gro Vea Salvanes*[3]

[1] Retired, Swakopmund, Namibia, [2] Institute of Marine Research, Bergen, Norway, [3] Department of Biological Sciences, University of Bergen, Bergen, Norway

The shelf sediments off Namibia are some of the most unusual and extreme marine habitats because of their extremely high hydrogen sulphide concentrations. High surface productivity of the northern Benguela upwelling system provides benthic life with so much carbon that biotic processes must rely on innovative mechanisms to cope with perennial anoxia and toxic hydrogen sulphide. Bottom dwelling communities are forced to adapt lifestyles to deal physiologically and behaviourally with these stressful conditions. The upside of hydrogen sulphide is that it fuels extensive mats of large sulphide-oxidizing bacteria on the seabed, which create detoxified habitat niches and food for the animals living there. The threat of hypoxic stress exacerbated by hydrogen sulphide is largely overcome in the water column by microbes that detoxify sulphide, allowing animals in the upper water layers to thrive in this productive upwelling area. The bearded goby *Sufflogobius bibarbatus* is a cornerstone species that successfully couples the inhospitable benthic environment with the pelagic. Benthic studies have as yet not characterized the sulphidic shelf communities, which have the potential to uncover biotic adaptations to toxic sulphide. This ancient shelf upwelling system has long operated under hypoxic pressure, balancing always the abundance of particulate food against oxygen limitation and hydrogen sulphide toxicity. Challenges faced by this unique system could include environmental changes related to climate change, or man-made physical disturbances of the anoxic, sulphide-rich seabed sediments.

Keywords: hydrogen sulphide, Namibia, benthic-pelagic coupling, Northern Benguela, shelf ecosystem

OPEN ACCESS

Edited by:
Arthur Capet,
MAST-University of Liège, Belgium

Reviewed by:
Dirk De Beer,
Max-Planck-Gesellschaft (MPG), Germany
Perran Cook,
Monash University, Australia
Anita Flohr,
University of Southampton, United Kingdom

***Correspondence:**
Bronwen Currie
currie32@gmail.com

Specialty section:
This article was submitted to Marine Biogeochemistry, a section of the journal Frontiers in Marine Science

Received: *01 June 2018*
Accepted: *05 September 2018*
Published: *11 October 2018*

Citation:
Currie B, Utne-Palm AC and Salvanes AGV (2018) Winning Ways With Hydrogen Sulphide on the Namibian Shelf. Front. Mar. Sci. 5:341. doi: 10.3389/fmars.2018.00341

INTRODUCTION

The highly productive Benguela Upwelling Ecosystem plays a major role in the circulation and fisheries production of the South Atlantic Ocean (Currie, 1953; Shannon, 1985; Shannon and Nelson, 1996). The upwelling regime has persisted for millenia (Diester-Haass et al., 2002). Despite the Namibian shelf being considered one of the most inhospitable, oxygen depleted, and sulphidic open shelf environments on earth (Baturin, 2002), it has sustained one of the world's most spectacular concentrations of marine life (Howarth et al., 2014). Palaeo-construction from inner shelf sediment cores reveals abundant fish populations over the last 3,200 years (Struck et al., 2002).

Much has been learned of how this ancient system successfully couples biological abundance with severe oxygen limitation, exacerbated by hydrogen sulphide. In this synthesis we review relevant knowledge regarding the biological integration of naturally occurring hydrogen sulphide into the system.

BACKGROUND AND SETTING

The broad continental shelf off central Namibia slopes gently to a shelf break at 300–350 m (Shannon, 1985). Intense euphotic productivity has long been observed (summarised in (Shannon and Pillar, 1986)), with primary production for the Benguela estimated at 0.37 Gt C yr^{-1} (Carr, 2002). A near-constant supply of organic material sinks towards the ocean floor adding to a diatomaceous, sulphidic mud belt that spans the inner Namibian shelf for >700 km in waters <200 m water depth (Bremner, 1983; Emeis et al., 2004). Extraordinarily high organic carbon accumulation [up to 23% dry weight (Bremner, 1978; Inthorn et al., 2006; Mollenhauer et al., 2007 and references therein] promotes bacterial production of hydrogen sulphide (H_2S). Compared to other Eastern Boundary Upwelling Systems, these features combined with a lack of reactive iron in the sediments to precipitate sulphide, concurrent build-up of methane, and low-oxygen upwelling source water, promote regular and frequent occurrences of H_2S in the water column so characteristic of Namibian waters. Extensive mats of Large Sulphide-oxidizing Bacteria (LSB) cover the mud, fueled by a continual, plentiful supply of H_2S from the sediment. Although not initially identified for their key role in the ecosystem when recorded as "slimy grass" from historical grab samples (von Bonde, 1928), these were almost certainly the Sulphide-oxidizing Bacteria described over 70 years later (Schulz et al., 1999). Historical records designated these areas to an "azoic zone" and also describe "sulphur eruptions" along the central coast (Gilchrist, 1914; Marchand, 1928; von Bonde, 1928; Copenhagen, 1934, 1953; Hart and Currie, 1960).

Upwelling

Most of Namibia's coast experiences perennial coastal upwelling (Shannon and Nelson, 1996). Oxygen-poor water from the Angola gyre (Hart and Currie, 1960; Stander, 1964; Bubnov, 1972) is entrained into South Atlantic Central Water, which dominates the mix of upwelling source water onto the shelf, particularly during late summer to autumn (Chapman and Shannon, 1987; Mohrholz et al., 2008). Although low in oxygen, this remotely-formed source water is neither sulphidic nor anoxic, varying intra- and inter-annually in oxygen content (Mohrholz et al., 2008). It intercepts the upper slope and shelf of the central coast to contribute to a permanent Oxygen Minimum Zone (OMZ: <0.5 ml O_2 L^{-1}; Helly and Levin, 2004). Microbial break-down from high organic loading over the shelf increases oxygen demand (Hart and Currie, 1960; Calvert and Price, 1971; Chapman and Shannon, 1987; Bailey, 1991). Direct contact of bottom water with the seabed influences dissolved components of the OMZ further (van der Plas et al., 2007). When H_2S diffuses into bottom water it becomes totally anoxic (Brüchert et al., 2003).

Shelf Sediments

High concentrations of H_2S characterize the inner shelf surface sediments between 19°S and 27°S (Brüchert et al., 2006). Here bacterial sulphate reduction rates in water depths 28–200 m vary between 3.1 and 62.7 mmol m^{-2} day^{-1}. Dissolved H_2S in porewaters can reach 22 mM just 10 cm below the sediment surface, consistently exceeding 2 mM at 6 cm sediment-depth. Limited oxidative precipitation of H_2S occurs, mainly due to low reactive iron in the diatomaceous mud (Brüchert et al., 2003, 2006; Borchers et al., 2005). The sulphide-rich muds favour trace metal enrichment, with some precipitation of the metals by H_2S (Borchers et al., 2005).

Intense microbial decay succession in the sediments leads to biogenic production of free methane gas within 100 cm of the sediment surface. These gas accumulations are patchy within the sediment, but significantly cover at least 1,350 km^2 of the mud belt (Emeis et al., 2004).

H_2S in the Water Column

Occasional occurrences of H_2S in bottom water are accompanied by extreme oxygen depletion. H_2S concentrations can reach >100 μM total H_2S (e.g., Copenhagen, 1934; Brüchert et al., 2003, 2006, 2009; Emeis et al., 2004; Lavik et al., 2009). Compared to sedimentary input, *in situ* generation of H_2S in the water column likely contributes minimally to these events, as measurements of sulphate reduction rates in bottom water showed no correlation to observed amounts of H_2S (Brüchert et al., 2006).

Various mechanisms responsible for transport of H_2S from the sediment into the overlying water have been suggested, mainly by diffusion and ebullition (Emeis et al., 2004; Weeks et al., 2004; Brüchert et al., 2006, 2009; van der Plas et al., 2007). The temporal and spatial variability of water column H_2S suggests that multiple mechanisms are active on the shelf, with gas ebullition closer inshore and diffusive supply in deeper waters (Brüchert et al., 2006, 2009). Whatever transport mechanism(s) are involved (discussed in Weeks et al., 2002, 2004; Emeis et al., 2004; Brüchert et al., 2006, 2009; Altenbach and Struck, 2006; van der Plas et al., 2007; Ohde and Dadou, 2018), the reality is that relatively high concentrations of H_2S do regularly occur in the water column, which pelagic organisms have to contend with.

During episodic, ephemeral "sulphur eruptions" described since the late nineteenth century (summarised in Hart and Currie, 1960) large amounts of H_2S rapidly pervade the whole water column. The H_2S oxidizes to colloidal sulphur that is clearly visible as milky turquoise surface water, which can be photographed and identified from space (Weeks et al., 2002, 2004; Ohde et al., 2007; Ohde and Dadou, 2018). Severe episodes have co-occurred with mass mortalities of marine life (Gilchrist, 1914; Copenhagen, 1953; Currie, 1953). Their true impact to the ecosystem (apart from obvious onshore wash-ups of dead littoral animals and fish) has not been quantified.

Methane in the water column is common (Scranton and Farrington, 1977; Monteiro et al., 2006). Ebullition of a mixture of H_2S and methane can explain sudden high concentrations of sulphide in the water (Emeis et al., 2004; Brüchert et al., 2006, 2009). Occasionally sedimentary methane dislodges whole chunks of mud, as evidenced by floating islands (Waldron, 1900; summary in Rogers and Bremner, 1991), and craters on the seabed (Brüchert et al., 2006).

FAUNA

Bacteria

Large Sulphide-oxidizing Bacteria (LSB) belonging to the Beggiatoceae fuel their metabolism with H_2S (Schulz and Jorgensen, 2001), converting H_2S into non-toxic sulphur that accumulates as distinctive shiny white micro-granules in their cytoplasm. During anoxic conditions, nitrate stored in large vacuoles is used as the electron acceptor for anaerobic oxidation of sulphide.

Discovery of extensive mats of active LSB covering the Namibian inner shelf were reported in 1999 (Schulz et al., 1999). Dominated by *Thiomargarita namibiensis,* nicknamed the "sulphur pearl of Namibia," these enormous, spherical bacteria reach a biomass of 47 g m^{-2} wet weight. As described in Salman et al. (2011, 2013) several members of the *Beggiatoacea* are abundant on the Namibian shelf. They flexibly use oxygen or nitrate as electron acceptors (Schulz et al., 1999; Schulz and De Beer, 2002; Brock and Schulz-Vogt, 2011; Salman et al., 2013), so are ideally suited to thrive on the plentiful sedimentary H_2S supply coupled with fluctuating bottom-water oxygen conditions. The bacterial mats are considered effective to stop most of the upward-diffusing hydrogen sulphide from entering the water column (Brüchert et al., 2006), and provide a detoxified microhabitat for eukaryotic benthic communities (Levin, 2003; Levin et al., 2009; **Figure 1**). These bacteria produce polyphosphates, resulting in high concentrations of inorganic phosphate in sediment pore waters during anoxic periods (Schulz and Schulz, 2005; van der Plas et al., 2007; Goldhammer et al., 2010; Brock and Schulz-Vogt, 2011). This sedimentary phosphate has the potential to enrich the upwelling water that passes over the shelf (Currie, 1953; van der Plas et al., 2007).

Despite the bacterial barrier, H_2S can comprise up to 25% of the total oxygen consumption in water on the shelf (Brüchert et al., 2006). When H_2S does diffuse into the water column, a consortium of anaerobic chemolithotrophic bacteria take on the detoxifying role. They metabolize H_2S using nitrate in the anaerobic waters to catalyze the conversion of H_2S to harmless sulphur (Lavik et al., 2009; **Figure 1**). Such events of H_2S in the lower water column may go unnoticed in surface water, because bacteria consume sulphide before it reaches the air–sea interface (Vaquer-Sunyer and Duarte, 2010).

Benthic Invertebrates

Contrary to the historical misnomer of "azoic," the diatomaceous mud belt is not barren of metazoan life (Edelman-Furstenberg and Kidwell, 2015). H_2S imposes severe respiratory stress on benthic animals that differ in tolerance at both species and population levels (Jahn and Theede, 1997; Vaquer-Sunyer and Duarte, 2010). The benthic invertebrate fauna of the Namibian sulphidic muds have not yet been characterized; critically this should include the small-sized (<300 μm) component. A pioneer study of macrofaunal diversity on a transect through the sulphidic mud from Walvis Bay (23°S) showed a 10-fold increase in diversity from 100 to 200–300 m water depths, as oxygen shifted from just under 2% saturation to 11–15% saturation (Sanders, 1969). Leiter and Altenbach (2010) found the heterotrophic foraminiferan *Virgulinella fragilis* largely restricted to the sulphidic shelf environment, co-occurring with less numerous *Nonionella stella* and *Discammina compressa.* Suggested possible survival strategies for *V. fragilis* included symbiotic sulphide-oxidizing bacteria, functional kleptoplasts, and peroxisome proliferation.

Macrofaunal components include annelids, molluscs and crustaceans (Copenhagen, 1953; Levin, 2003; Zettler et al., 2009, 2013; Eisenbarth and Zettler, 2016). LSB mats offer a potential abundant food supply for species that can tolerate the sulphur (Levin, 2003, 2005), but diets have not yet been examined. Polychaetes associated with the Namibian microbial mats have elaborate appendages to maximize oxygen uptake: *Diopatra* sp. has long spiral branchiae, nereids have posterior branchial proliferations and a tube-dwelling pectinariid has anterior gill filaments (Levin et al., 2009). Mollusc deposits at 133 m water depth on the shelf at 20°S reveal chemoautotrophic bivalves *Lucinoma capensis*, found also in recent samples (Edelman-Furstenberg, 2014). Lucinids are characteristic of upwelling systems with high, steady organic supply to H_2S-rich sediments, as discussed in Edelman-Furstenberg and Kidwell (2015). Other large-sized (>1 mm) taxa recorded from sulphidic muds are widely distributed over the Namibian shelf e.g., the gastropod *Nassarius vinctus* that extends its siphon to oxic waters (**Figure 1**); the polychaete *Paraprionospia pinnata* and the cumacean *Iphinoe africana* (Zettler et al., 2009, 2013; Edelman-Furstenberg, 2014; Steffani et al., 2015; Eisenbarth and Zettler, 2016). With the broad distribution of these species, their presence in sulphidic areas is considered not directly related to H_2S, but possibly due to a detoxified habitat niche provided by the bacteria.

Fish

Even in low concentrations, H_2S is usually toxic to vertebrates by inhibiting cytochrome c oxidase in the mitochondria (Bagarinao, 1992; Jahn and Theede, 1997). To survive fluctuating sulphidic environments, vertebrates require behavioural and physiological flexibility (Childress, 1995; Hagerman, 1998; Vaquer-Sunyer and Duarte, 2010). Namibian shelf fish distributions have not been attributed directly to H_2S, but given that dissolved H_2S reduces oxygen, tolerances of fish to gradients of oxygen-depletion are important (Gallo and Levin, 2016). The low diversity of the central shelf demersal fish assemblage between 19 and 27°S is ascribed to very low oxygen conditions (Hamukuaya et al., 1998). It is dominated by a few species, namely Cape hake (*Merluccius capensis)*, horse mackerel (*Trachurus capensis)*, and bearded goby (*Sufflogobius bibarbatus)*. For adult and juvenile horse mackerel, critical oxygen levels are reported as 10% and 11.2–13.2% air saturation, respectively (Ekau et al., 2010; Geist et al., 2013). Hake tolerate oxygen concentrations as low as 10.9 μmol kg^{-1} (0.2 ml L^{-1}; Woodhead et al., 1998). The bearded goby has a critical oxygen level of 5.3% air saturation (Utne-Palm et al., 2010) and tolerates oxygen levels as low as 0.3 μmol kg^{-1} or <0.12% air saturation (Salvanes et al., 2011). The goby's oxygen consumption is unaffected by 100–200 μM total sulphide (corresponding to 6–12 μM H_2S), dropping to a few percent at 11 to 14 μM H_2S, but shuts off at 500 μM total sulphide (30 μM H_2S; Utne-Palm et al., 2010). Gobies surviving high H_2S levels appear to rely on deep metabolic depression with extreme

1) Thick bacterial mats in 47 m water depth at 24º 01.62'S. "Holes" from methane bubbling are apparent.

2) The gastropod *Nassarius vinctus* commonly lives on bacterial mats; photographed from multicore from 65 m water depth at 24º01.62' S

3) 158 m water depth 23º17.42'S: juvenile hake swimming approximately 1 m above seabed over bacterial mats. Hake are approximately 35 cm total length

Ecological benefits of large sulphide-oxidizing bacteria:

- Bacterial mats of Beggiatoceae: *Thiomargarita namibiensis* and *Beggiatoa*-like spp. (1) metabolize H_2S to sulphur using either nitrate during anoxic conditions, or oxygen during oxic conditions.
- Bacterial mats provide a detoxified microhabitat for benthic organisms (2)
- Polyphosphates produced by large sulphide-oxidizing bacteria enriches pore water phosphate, enhancing nutrient input to upwelling water
- The bacteria are potential food for benthos
- In pelagic waters chemolithotrophic sulphide-oxidizing bacteria detoxify H_2S in anoxic waters in the water column, using nitrate
- A secondary consequence of bacterial sulphide oxidation is partitioning of predators and prey according to narrow differences in their tolerances to low oxygen - an example being between hake and goby shown in (3).

Photo credits: B.Currie. Images (1) and (3) captured from ROV footage by ROV operator Rainer Bahlo (with permission); image (2) from multicore (Cruise report: Leipe T., 2004)

FIGURE 1 | Processing of H2S by sulphide-oxidizing bacteria on the Namibian shelf.

anoxia tolerance facilitated by anaerobic respiration, to cope with sulphide induced respiratory stress, rather than H_2S tolerant cytochrome c or other respiratory strategies such as fermentation or specialized blood pigment (but see discussion in Utne-Palm et al., 2010).

High-resolution acoustic surveys of animal activity over the shelf OMZ visualize an empty area (no back scattering) directly over the sulphidic mud where severely hypoxic conditions prevail (0–0.2 ml L^1, 8.6 μmol kg $^{-1}$, 3.4% of surface air saturation; (Utne-Palm et al., 2010); **Figure 2**). During daytime

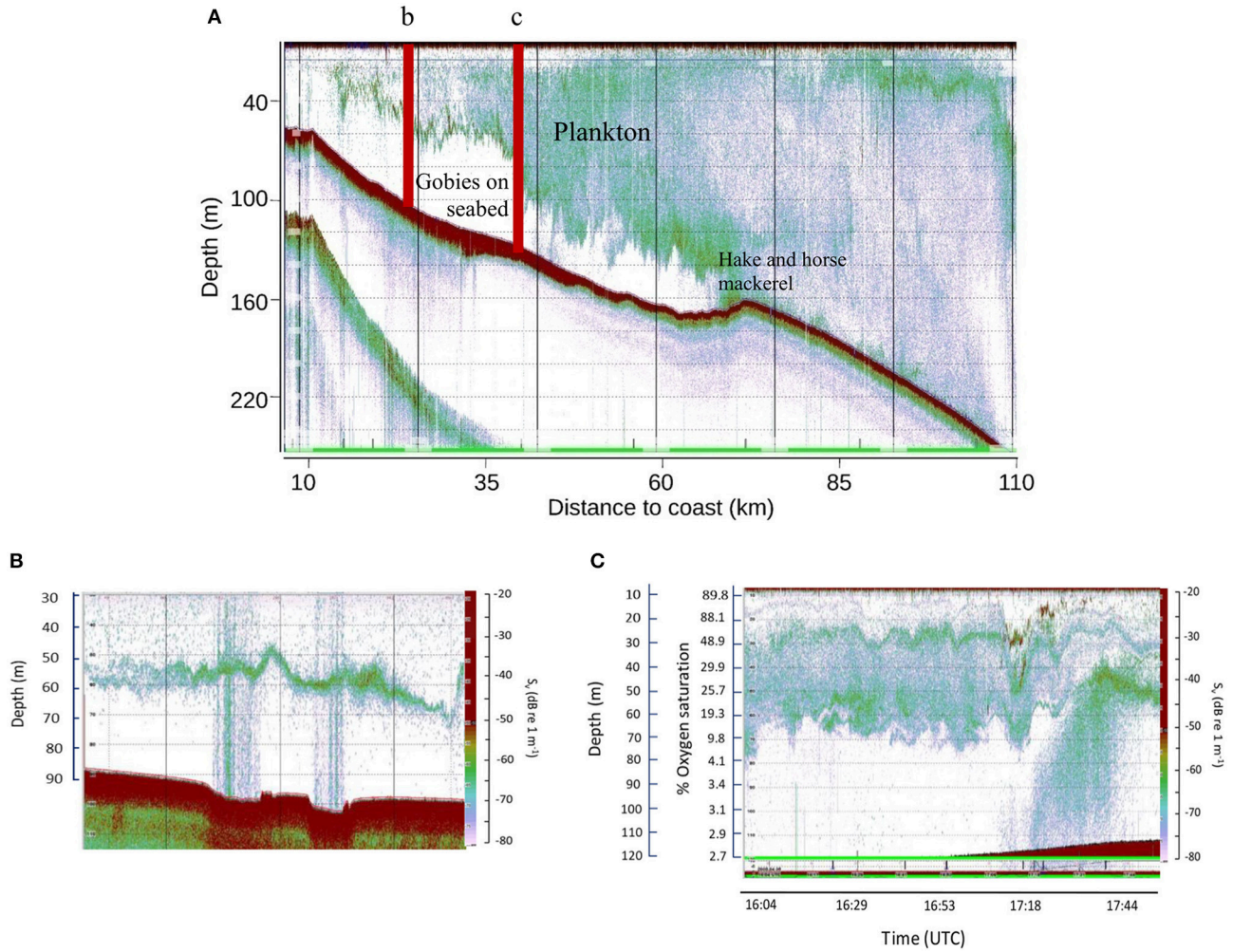

FIGURE 2 | Linking of respiratory niches on the Namibian shelf. **(A)** Composite 10-day high resolution acoustic image across the Namibian shelf, 23°20′S to 23°40′S showing lack of pelagic animals in the severely oxygen depleted bottom waters over the sulphidic mud (dissolved oxygen 0.1–0.2 ml L^{-1}, or 4.3–8.6 μmol kg $^{-1}$; 1.7–3.4% air saturation). As bottom water oxygen increases to >0.3 ml L^{-1} (13 μmol kg $^{-1}$; >5% air saturation) on the outer shelf in depths >160 m, plankton and fish (hake and horse mackerel) appear in bottom waters. The position of images (b) and (c) are indicated. **(B)** Methane bubbling from sediment. **(C)** Goby migration at sunset from sulphidic mud to oxygenated layers to replenish oxygen and enter the food web. Image credits: Images from (Utne-Palm, 2008), and Utne-Palm et al. (2010) Supplementary Information with permission.

large densities of gobies only, were present on the seabed, whilst predator species hake and horse mackerel were trawled deeper on the outer shelf where bottom water oxygen levels increased to >0.3 ml L^{-1}, 13.02 μmol kg $^{-1}$, >5% air saturation (Utne-Palm et al., 2010; **Figure 2A**). During hours of anaerobic exposure, gobies generate a lactate buildup or "oxygen debt" (Utne-Palm et al., 2010), likely explaining their migration into oxygen-sufficient (>20% air saturation) pelagic environments at night to replenish oxygen and feed in dense pelagic plankton layers from 60 m and higher above the sediment (**Figure 2C**). They return to the seabed at dawn to avoid visual predation by burying in the sulphidic mud (Salvanes et al., 2011). Gobies feed opportunistically on both pelagic and benthic organisms (Cedras et al., 2011; Hundt et al., 2011). Fatty acid and stable isotope signatures indicate that the diatom- and bacteria-rich sulphidic sediments contribute to approximately 15% of the gobies' diet (Van der Bank et al., 2011).

Whilst in the water column, gobies themselves are eaten, comprising >50% prey of commercially important hake and horse mackerel, and top predators (Crawford et al., 1985; David, 1987; Salvanes and Gibbons, 2018). This is especially relevant following the regime shift associated with the collapse of the sardine population (Cury and Shannon, 2004; van der Lingen et al., 2006).

BIOLOGICAL BENTHIC-PELAGIC COUPLING

Benthic-pelagic coupling includes inorganic and biological pathways, though the biological links are more difficult to

quantify (Marcus and Boero, 1998; Griffiths et al., 2017). In boundary upwelling OMZs, where steep vertical oxygen gradients segregate species (Levin, 2003), biological coupling is essential to overcome and fully exploit the different respiratory niches. The Namibian shelf offers an example of a mature ecosystem that exploits H_2S and integrates it into biological food webs (**Figures 1**, **2**).

- Methane coupled to microbial H_2S production in the sediments plays a key role in release of H_2S into the water column.
- Bacterial decay accumulates H_2S in the pore water. Some H_2S promotes metal burial within the sediment, beneficially keeping high metal concentrations unavailable for bio-uptake by animals in oxic waters.
- LSB on surface sediments (i) consume H_2S, lessening its toxic and deoxygenating effects on pelagic organisms (ii) establish a detoxified niche/habitat for benthos (iii) enrich overlying upwelling water with phosphate.
- Nutrient-rich upwelled water supports abundant phytoplankton diatom-dominated blooms. Sinking diatoms form biogenic mud where bacterial degradation accumulates H_2S in pore water. Escape of H_2S into the water column is detoxified by chemolithotrophic bacteria that mitigate sulphidic damage to pelagic life.
- Metazoan specialists equipped to cope with severely hypoxic to anoxic and sulphidic conditions integrate carbon from the sulphidic environment into the shelf food web. Key players are bacteria, benthic invertebrates and the remarkable bearded goby, which as both predator and prey, constitutes a cornerstone species in this ecosystem.

Reproductive stages of metazoan organisms are usually more vulnerable than adults to oxygen stress (Levin et al., 2009). Nursery grounds of commercially important pelagic and demersal fish species coincide spatially with the highest occurrences of sulphide eruptions on the Namibian shelf (Emeis et al., 2004), making young stages particularly vulnerable to sulphide outbreaks. An example is the catastrophic loss of juvenile hake in 1994, when they fled anoxic conditions on the shelf and were heavily cannibalized by adult hake in deeper waters (Hamukuaya et al., 1998). Extended batch spawning, high tolerances of key species to low oxygen, and horizontal transport of larvae and young across the shelf from better oxygenated areas, may be key to surviving sporadic sulphide events (Sundby et al., 2001; Hutchings et al., 2002; Utne-Palm et al., 2010; Geist et al., 2013). Gobies attach their eggs demersally (Skrypzeck et al., 2014) but the tolerance of eggs and larvae to H_2S remains unstudied.

GAPS IN KNOWLEDGE AND FUTURE OUTLOOK

Much remains to be understood of the responses of Namibian shelf biota to hydrogen sulphide. The timing, triggering, intensity and recovery of severe H_2S events and episodic "eruptions" remain elusive and inconclusive, despite various theories (Weeks et al., 2002, 2004; Emeis et al., 2004; Altenbach and Struck, 2006; Brüchert et al., 2006, 2009; van der Plas et al., 2007; Ohde and Dadou, 2018). To be genuinely useful to an ecosystem approach by ocean managers, the triggering of severe sulphidic episodes needs to be known. Whilst the oceanographical studies contribute to understanding, atmospheric pressure studies possibly affecting methane ebullition, merit further investigation.

The benthic invertebrate communities of the sulphidic inner shelf are not characterized. Scanty and inadequate sampling of the sulphidic mud fringes only, is documented. Dedicated qualitative, quantitative and experimental benthic studies will be required to understand how the animals living in this risky environment survive and contribute to the ecological functioning of the Namibian shelf system. Key knowledge gaps are how resilient the species are to H_2S exposure and sulphide-exacerbated hypoxic stress. What are critical levels, and sub-lethal effects from these stressors? Do the mats of LSB indeed protect benthic fauna from severe sulphide exposure in a narrow niche on the sediment? The nutritional role of LSB in the diet of the benthic animals is unknown, but are likely food (e.g., Levin, 2005) given the extensive bacterial coverage and its biomass estimates (e.g., Schulz et al., 1999). In the interest of both biogeochemistry and biology, it would be interesting to estimate how much carbon is fixed by the LSB mats. Also of interest will be investigations to examine whether the small benthic invertebrates living in the sulphidic environment are equipped with symbioses or metabolic mechanisms that allow them to survive intermittent, and sometimes high concentrations of H_2S. Metabolic responses to sulphide and anoxic stress (e.g., Larade and Storey, 2002; Menon et al., 2005) are largely unexplored.

At community level, it is not known whether extinction-recolonisation by the shelf fauna occurs after intense sulphidic "eruption" events. Life history strategies must have developed to deal with this risky environment: are life histories boom-and-bust, with short, highly fecund life cycles, serial spawning and efficient larval dispersal to promote species survival through extreme events, and/or are vulnerable early life stages replenished from better oxygenated areas on the shelf, following extinctions from episodes of sulphide? Reproductive strategies of benthic and pelagic species are key to understanding how this shallow system carries on despite the stress from H_2S.

FUTURE OUTLOOK

As summarized by Tobler et al. (2016), organisms living in H_2S-rich habitats provide unique examples that answer fundamental biological questions, such as how some organisms cope with environmental stressors considered lethal for most others; how biological processes—from cellular to ecosystem level—respond to H_2S; and how H_2S can shape the evolution of ecosystems. Ecological opportunities offered by sulphidic environments include resource availability, reduced competition, and reduced exposure to natural predators. Future studies could

contribute to understanding human-induced environmental change and develop potential biomedical applications (Tobler et al., 2016; Breiland et al., 2018). With increased deoxygenation predicted on a global scale (Deutsch et al., 2011) and emerging as a major threat to coastal ecosystems globally (Vaquer-Sunyer and Duarte, 2010) it is relevant to examine systems that have long adjusted to extreme oxygen stress and H_2S.

Eastern boundary upwelling areas, such as the northern Benguela off Namibia, serve as primary centres for fishery production. Taking modern cumulative pressures on the ocean into account as fisheries management moves towards an ecosystem-based approach in Namibia, and internationally, a better understanding of trophic interactions that couple anoxic benthic environments with productive fishing zones is important.

AUTHOR CONTRIBUTIONS

BC proposed the synthesis and all authors contributed to writing the manuscript. BC led manuscript production with contributions and comments from all authors.

ACKNOWLEDGMENTS

The authors acknowledge support from their parent organizations, though no funding was specifically allocated to this project. AGVS was funded by the University of Bergen and the Fullbright Foundation. Jock Currie is thanked for technical and editorial comments to the final manuscript. The authors acknowledge the multiple research cruises in Namibian waters, tainted with a strong odour of hydrogen sulphide that was well worth the exciting research findings!

REFERENCES

Altenbach, A., and Struck, U. (2006). "Some remarks on Namibia's shelf environments, and a possible teleconnection to the hinterland," in *The Changing Culture and Nature of Namibia: Case Studies*, ed H. Leser (Basel: The Sixth Namibia Workshop; Basler Afrika Bibliographien), 109–124.

Bagarinao, T. (1992). Sulfide as an environmental factor and toxicant: tolerance and adaptations in aquatic organisms. *Aquat. Toxicol.* 24, 21–62. doi: 10.1016/0166-445X(92)90015-F

Bailey, G. W. (1991). "Organic carbon flux and development of oxygen deficiency on the modern Benguela continental shelf south of 22°S: spatial and temporal variability," in *Modern and Ancient Continental Shelf Anoxia*, eds R. D. Tyson and T. H. Pearson (London: Geological Society, Special Publications), 171–183.

Baturin, G. N. (2002). Nodular fraction of phosphatic sand from the Namibia Shelf. *Lithol. Mineral Resour.* 37, 1–17. doi: 10.1023/A:1013628020381

Borchers, S. L., Schnetger, B., Böning, P., and Brumsack, H. J. (2005). Geochemical signatures of the Namibian diatom belt: perennial upwelling and intermittent anoxia. *Geochem. Geophys. Geosyst.* 6:20. doi: 10.1029/2004GC000886

Breiland, A. A., Flood, B. E., Nikrad, J., , Bakarich, J., Husman, M., Rhee, T., et al. (2018). Polyphosphate-accumulating bacteria: potential contributors to mineral dissolution in the oral cavity. *Appl. Environ. Microbiol.* 84, e02440–e02417. doi: 10.1128/AEM.02440-17

Bremner, J. M. (1978). *Sediments on the Continental Margin off South West Africa Between Latitudes 17^0 and 25^0 S*, PhD thesis, University of Cape Town, 300.

Bremner, J. M. (1983). "Biogenic sediments on the SW African (Namibian) continental margin," in *Coastal Upwelling: its Sediment Record. Part B: Sedimentary Records of Ancient Coastal Upwelling*, eds E. Suess and J. Thiede (New York, NY: Plenum Press), 610.

Brock, J., and Schulz-Vogt, H. N. (2011). Sulfide induces phosphate release from polyphosphate in cultures of a marine Beggiatoa strain. *ISME J.* 5, 497–506. doi: 10.1038/ismej.2010.135

Brüchert, V., Currie, B., and Peard, K. R. (2009). Hydrogen sulphide and methane emissions on the central Namibian shelf. *Prog. Oceanogr.* 83, 169–179. doi: 10.1016/j.pocean.2009.07.017

Brüchert, V., Currie, B., Peard, K. R., Lass, U., Endler, R., Dübecke, A., et al. (2006). "Biogeochemical and physical control on shelf anoxia and water column hydrogen sulphide in the Benguel a coastal upwelling system off Namibia," in *Past and Present Water Column Anoxia* (Dordrecht: Springer), 161–193.

Brüchert, V., Jorgensen, B. B., Neumann, K., Riechmann, D., Schlösser, M., and Schulz, H. (2003). Regulation of bacterial sulfate reduction and hydrogen sulfide fluxes in the central Namibian coastal upwelling zone. *Geochim. Cosmochim. Acta* 67, 4505–4518. doi: 10.1016/S0016-7037(03)00275-8

Bubnov, V. A. (1972). Structure and characteristics of the oxygen minimum layer in the southeastern Atlantic. *Oceanology* 12, 193–201.

Calvert, S. E., and Price, N. B. (1971). Upwelling and nutrient regeneration in the Benguela Current, October, 1968. *Deep-Sea Res. Oceanogr. Abstr.* 18, 505–523. doi: 10.1016/0011-7471(71)90074-X

Carr, M.-E. (2002). Estimation of potential productivity in Eastern Boundary Currents using remote sensing. *Deep Sea Res Part II Topical Studies Oceanogr.* 49, 59–80. doi: 10.1016/S0967-0645(01)00094-7

Cedras, R. B., Salvanes, A.-G., and Gibbons, M. J. (2011). Investigations into the diet and feeding ecology of the bearded goby Sufflogobius bibarbatus off Namibia. *Afr. J. Mar. Sci.* 33, 313–320. doi: 10.2989/1814232X.2011.600431

Chapman, P., and Shannon, L. V. (1987). Seasonality in the oxygen minimum layers at the extremities of the Benguela system. *South Afr. J. Mar. Sci.* 5, 85–94. doi: 10.2989/025776187784522162

Childress, J. J. (1995). Life in sulfidic environments: historical perspective and current research trends. *Integr. Comp. Biol.* 35, 83–90. doi: 10.1093/icb/35.2.83

Copenhagen, W. J. (1934). *Occurrence of Sulphides in Certain Areas of the Sea Bottom on the South African Coast. Investigational Report No 3*, Fisheries and Marine Biological Survey Division, Department of Commerce and Industries, Union of South Africa.

Copenhagen, W. J. (1953). The periodic mortality of fish in the Walvis region. *S. Afr. J. Sci.* 49:330.

Crawford, R. J. M., Cruickshank, R. A., Shelton, P. A., and Kruger, I. (1985). Partitioning of a goby resource amongst four avian predators and evidence for altered trophic flow in the pelagic community of an intense, perennial upwelling system. *South Afr. J. Mar. Sci.* 3, 215–228. doi: 10.2989/025776185784461252

Currie, R. (1953). Upwelling in the Benguela current. *Nature* 171, 497–500. doi: 10.1038/171497a0

Cury, P., and Shannon, L. (2004). Regime shifts in upwelling ecosystems: observed changes and possible mechanisms in the northern and southern Benguela. *Prog. Oceanogr.* 60, 223–243. doi: 10.1016/j.pocean.2004.02.007

David, J. H. M. (1987). Diet of the South African fur seal (1974–1985) and an assessment of competition with fisheries in southern Africa. *South Afr. J. Mar. Sci.* 5, 693–713. doi: 10.2989/025776187784522568

Deutsch, C., Brix, H., Ito, T., Frenzel, H., and Thompson, L. (2011). Climate-forced variability of ocean hypoxia. *Science* 333, 336–339. doi: 10.1126/science.1202422

Diester-Haass, L., Meyers, P. A., and Vidal, L. (2002). The late Miocene onset of high productivity in the Benguela Current upwelling system as part of a global pattern. *Mar. Geol.* 180, 87–103. doi: 10.1016/S0025-3227(01)00207-9

Edelman-Furstenberg, Y. (2014). Distribution and paleoecology of molluscan skeletal remains along an upwelling tract: Benguela system, Namibian shelf. *Mar. Geol.* 353, 153–162. doi: 10.1016/j.margeo.2014.04.011

Edelman-Furstenberg, Y., and Kidwell, S. M. (2015). Chemosymbiont-dominated seafloor communities in modern and Cretaceous upwelling systems support

a new, high-productivity variant of standard low-oxygen models. *Geology* 43, 975–978. doi: 10.1130/G37017.1

Eisenbarth, S., and Zettler, M. L. (2016). Diversity of the benthic macrofauna off northern Namibia from the shelf to the deep sea. *J. Mar. Syst.* 155, 1–10. doi: 10.1016/j.jmarsys.2015.10.017

Ekau, W., Auel, H., Pörtner, H.-O., and Gilbert, D. (2010). Impacts of hypoxia on the structure and processes in pelagic communities (zooplankton, macro-invertebrates and fish). *Biogeosciences* 7, 1669–1699. doi: 10.5194/bg-7-1669-2010

Emeis, K. C., Brüchert, V., Currie, B., Endler, R., Ferdelman, T., Kiessling, A., et al. (2004). Shallow gas in shelf sediments of the Namibian coastal upwelling ecosystem. *Cont. Shelf Res.* 24, 627–642. doi: 10.1016/j.csr.2004.01.007

Gallo, N. D., and Levin, L. A. (2016). "Fish ecology and evolution in the world's oxygen minimum zones and implications of ocean deoxygenation," in *Advances in Marine Biology* (London: Elsevier), 117–198.

Geist, S. J., Ekau, W., and Kunzmann, A. (2013). Energy demand of larval and juvenile Cape horse mackerels, *Trachurus capensis*, and indications of hypoxia tolerance as benefit in a changing environment. *Mar. Biol.* 160, 3221–3232. doi: 10.1007/s00227-013-2309-2

Gilchrist, J. D. F. (1914). *Marine Biological Report for the Year ending 30th June, 1914*. Cape Town: Union of South Africa. Available online at: http://archive.org/details/marinebiological21914cape (Accessed March 31, 2017).

Goldhammer, T., Brüchert, V., Ferdelman, T. G., and Zabel, M. (2010). Microbial sequestration of phosphorus in anoxic upwelling sediments. *Nat. Geosci.* 3:557. doi: 10.1038/ngeo913

Griffiths, J. R., Kadin, M., Nascimento, F. J. A., Tamelander, T., Törnroos, A., Bonaglia, S., et al. (2017). The importance of benthic–pelagic coupling for marine ecosystem functioning in a changing world. *Glob. Chang. Biol.* 23, 2179–2196. doi: 10.1111/gcb.13642

Hagerman, L. (1998). Physiological flexibility; a necessity for life in anoxic and sulphidic habitats. *Hydrobiologia* 375–376, 241–254. doi: 10.1023/A:1017033711985

Hamukuaya, H., O'Toole, M. J., and Woodhead, P. M. J. (1998). Observations of severe hypoxia and offshore displacement of Cape hake over the Namibian shelf in 1994. *South Afr. J. Mar. Sci.* 19, 57–59.

Hart, T. J., and Currie, R. I. (1960). *The Benguela Current*. Discovery Reports, University Press.

Helly, J. J., and Levin, L. A. (2004). Global distribution of naturally occurring marine hypoxia on continental margins. *Deep Sea Res. Part I Oceanogr. Res. Papers* 51, 1159–1168. doi: 10.1016/j.dsr.2004.03.009

Howarth, L. M., Roberts, C. M., Thurstan, R. H., and Stewart, B. D. (2014). The unintended consequences of simplifying the sea: making the case for complexity. *Fish Fish.* 15, 690–711. doi: 10.1111/faf.12041

Hundt, M., Utne-Palm, A. C., and Gibbons, M. J. (2011). Cross-shelf observations of diet and diel feeding behaviour of the bearded goby *Sufflogobius bibarbatus* off Namibia. *Afr. J. Mar. Sci.* 33, 119–126. doi: 10.2989/1814232X.2011.572365

Hutchings, L., Beckley, L. E., Griffiths, M. H., Roberts, M. J., Sundby, S., Lingen, C., et al. (2002). Spawning on the edge: spawning grounds and nursery areas around the southern African coastline. *Mar. Freshwater Res.* 53, 307–318. doi: 10.1071/MF01147

Inthorn, M., Wagner, T., Scheeder, G., and Zabel, M. (2006). Lateral transport controls distribution, quality, and burial of organic matter along continental slopes in high-productivity areas. *Geology* 34, 205–208. doi: 10.1130/G22153.1

Jahn, A., and Theede, H. (1997). Different degrees of tolerance to hydrogen sulphide in populations of *Macoma balthica* (Bivalvia, Tellinidae). *Mar. Ecol. Prog. Ser.* 154, 185–196. doi: 10.3354/meps154185

Larade, K., and Storey, K. B. (2002). A profile of the metabolic responses to anoxia in marine. *Sens. Signal. Cell Adaptation* 3, 27–46. doi: 10.1016/S1568-1254(02)80005-5

Lavik, G., Stührmann, T., Brüchert, V., Van der Plas, A., Mohrholz, V., Lam, P., et al. (2009). Detoxification of sulphidic African shelf waters by blooming chemolithotrophs. *Nature* 457, 581–584. doi: 10.1038/nature07588

Leipe, T. (2004). *Cruise report: R/V A.v.Humboldt, cruise No. 44/04/03, leg 3*. Warnemuende: Baltic Sea Research Institute.

Leiter, C., and Altenbach, A. V. (2010). Benthic foraminifera from the diatomaceous mud belt off Namibia: characteristic species for severe anoxia. *Palaeontologia Electronica* 13:19.

Levin, L. A. (2003). Oxygen minimum zone benthos: adaptation and community response to hypoxia. *Oceanogr. Mar. Biol.* 41, 1–45.

Levin, L. A. (2005). Ecology of cold seep sediments: interactions of fauna with flow, chemistry and microbes. *Oceanogr. Mar. Biol.* 43, 1–46. doi: 10.1201/9781420037449.ch1

Levin, L. A., Ekau, W., Gooday, A. J., Jorissen, F., Middelburg, J. J., Naqvi, S. W. A., et al. (2009). Effects of natural and human-induced hypoxia on coastal benthos. *Biogeosciences* 6, 2063–2098, doi: 10.5194/bg-6-2063-2009

Marchand, J. M. (1928). "Special reports: the nature of the sea-floor deposits in certain regions on the west coast," in *Fisheries and Marine Biological Survey. Report No. 6 for the Year Ending June, 1928*, ed C. von Bonde (Pretoria: Union of South Africa), 11.

Marcus, N. H., and Boero, F. (1998). Minireview: the importance of benthic-pelagic coupling and the forgotten role of life cycles in coastal aquatic systems. *Limnol. Oceanogr.* 43, 763–768. doi: 10.4319/lo.1998.43.5.0763

Menon, J., Willsie, J. K., Tauscher, A., and Arp, A. J. (2005). Epidermal ultrastructure and implications for sulfide tolerance in six species of deep-sea polychaetes. *Invertebrate Biol.* 122, 334–346. doi: 10.1111/j.1744-7410.2003.tb00098.x

Mohrholz, V., Bartholomae, C. H., Van der Plas, A. K., and Lass, H. U. (2008). The seasonal variability of the northern Benguela undercurrent and its relation to the oxygen budget on the shelf. *Continental Shelf Res.* 28, 424–441. doi: 10.1016/j.csr.2007.10.001

Mollenhauer, G., Inthorn, M., Vogt, T., Zabel, M., Sinninghe Damsté, J. S., and Eglinton, T. I. (2007). Aging of marine organic matter during cross-shelf lateral transport in the Benguela upwelling system revealed by compound-specific radiocarbon dating. *Geochem. Geophys. Geosyst.* 8:Q09004. doi: 10.1029/2007GC001603

Monteiro, P. M., van der Plas, A. K. A., Mohrholz, V., Mabille, E., Pascal, A., and Joubert, W. (2006). Variability of natural hypoxia and methane in a coastal upwelling system: ocean physics or shelf biology? *Geophys. Res. Lett.* 33:L16614. doi: 10.1029/2006GL026234

Ohde, T., and Dadou, I. (2018). Seasonal and annual variability of coastal sulphur plumes in the northern Benguela upwelling system. *PLoS ONE* 13:e0192140. doi: 10.1371/journal.pone.0192140

Ohde, T., Siegel, H., Rei\s smann, J., and Gerth, M. (2007). Identification and investigation of sulphur plumes along the Namibian coast using the MERIS sensor. *Continental Shelf Res.* 27, 744–756. doi: 10.1016/j.csr.2006.11.016

Rogers, J., and Bremner, J. M. (1991). The Benguela ecosystem. Part VII. Marine-geological aspects. *Oceanogr. Mar. Biol.* 29, 1–85.

Salman, V., Amann, R., Girnth, A. C., Polerecky, L., Bailey, J. V., Høgsland, S., et al. (2011). A single-cell sequencing approach to the classification of large, vacuolated sulfur bacteria. *Syst. Appl. Microbiol.* 34, 243–259. doi: 10.1016/j.syapm.2011.02.001

Salman, V., Bailey, J. V., and Teske, A. (2013). Phylogenetic and morphologic complexity of giant Sulphur bacteria. *Antonie van Leeuwenhoek*, 104, 169–186. doi: 10.1007/s10482-013-9952-y

Salvanes, A. G., Utne-Palm, A. C., Currie, B., and Braithwaite, V. A. (2011). Behavioural and physiological adaptations of the bearded goby, a key fish species of the extreme environment of the northern Benguela upwelling. *Mar. Ecol. Prog. Ser.* 425, 193–202. doi: 10.3354/meps08998

Salvanes, A. G. V., and Gibbons, M. J. (2018). Adaptation to hypoxic environments; bearded gobies *Sufflogobius bibarbatus* in the Benguela upwelling ecosystem. *J. Fish Biol.* 92, 752–772. doi: 10.1111/jfb.13547

Sanders, H. L. (1969). "Benthic marine diversity and the stability-time hypothesis," in *Brookhaven Symposia in Biology* (Upton, NY: Brookhaven National Laboratory), 71–81.

Schulz, H. N., Brinkhoff, T., Ferdelman, T. G., Mariné, M. H., Teske, A., and Jørgensen, B. B. (1999). Dense populations of a giant sulfur bacterium in Namibian shelf sediments. *Science* 284, 493–495. doi: 10.1126/science.284.5413.493

Schulz, H. N., and De Beer, D. (2002). Uptake rates of oxygen and sulfide measured with individual *Thiomargarita namibiensis* cells by using microelectrodes. *Appl. Environ. Microbiol.* 68, 5746–5749. doi: 10.1128/AEM.68.11.5746-5749.2002

Schulz, H. N., and Jorgensen, B. B. (2001). Big bacteria. *Annu. Rev. Microbiol.* 55, 105–137. doi: 10.1146/annurev.micro.55.1.105

Schulz, H. N., and Schulz, H. D. (2005). Large sulfur bacteria and the formation of phosphorite. *Science* 307, 416–418. doi: 10.1126/science.1103096

Scranton, M. I., and Farrington, J. W. (1977). Methane production in the waters off Walvis Bay. *J. Geophys. Res.* 82, 4947–4953. doi: 10.1029/JC082i031p04947

Shannon, L. V. (1985). The Benguela ecosystem. Part I. Evolution of the Benguela, physical features and processes. *Oceanogr. Mar. Biol.* 23, 105–182.

Shannon, L. V., and Nelson, G. (1996). "The Benguela: large scale features and processes and system variability," in *The South Atlantic: Present and Past Circulation,* eds G. Wefer, W. H. Berger, G. Siedler, and D. J. Webb (Berlin: Springer-Verlag), 163–210.

Shannon, L. V., and Pillar, S. C. (1986). The Benguela ecosystem. Part III. Plankton. *Oceanogr. Mar. Biol.* 24, 65–170.

Skrypzeck, H., Salvanes, A. G., Currie, B., and Kotze, A. (2014). First records of reproductive behaviour and early development of the bearded goby *Sufflogobius bibarbatus*. *J. Fish Biol.* 84, 1256–1261. doi: 10.1111/jfb.12347

Stander, G. H. (1964). *The Benguela Current off South West Africa. Investigational Report 2*. Marine Research Laboratory, South West Africa.

Steffani, N., Sedick, S., Rogers, J., and Gibbons, M. J. (2015). Infaunal benthic communities from the inner shelf off Southwestern Africa are characterised by generalist species. *PLoS ONE* 10:e0143637. doi: 10.1371/journal.pone.0143637

Struck, U., Altenbach, A. V., Emeis, K.-C., Alheit, J., Eichner, C., and Schneider, R. (2002). Changes of the upwelling rates of nitrate preserved in the δ15N-signature of sediments and fish scales from the diatomaceous mud belt of Namibia. *Geobios* 35, 3–11. doi: 10.1016/S0016-6995(02)00004-9

Sundby, S., Boyd, A. J., Hutchings, L., O'Toole, M. J., Thorisson, K., and Thorsen, A. (2001). Interaction between Cape hake spawning and the circulation in the Northern Benguela upwelling ecosystem. *South Afr. J. Mar. Sci.* 23, 317–336. doi: 10.2989/025776101784528971

Tobler, M., Passow, C. N., Greenway, R., Kelley, J. L., and Shaw, J. H. (2016). The evolutionary ecology of animals inhabiting hydrogen sulfide–rich environments. *Ann. Rev. Ecol. Evol. System.* 47, 239–262. doi: 10.1146/annurev-ecolsys-121415-032418

Utne-Palm, A. C. (2008). *Cruise Report: Gobies and Hake in the Hypoxic Waters of the Benguela Upwelling Current*. Cruise reports, R/V. G.O. Sars.

Utne-Palm, A. C., Salvanes, A. G., Currie, B., Kaartvedt, S., Nilsson, G. E., Braithwaite, V. A., et al. (2010). Trophic structure and community stability in an overfished ecosystem. *Science* 329, 333–336. doi: 10.1126/science.1190708

Van der Bank, M. G., Utne-Palm, A. C., Pittman, K., Sweetman, A. K., Richoux, N. B., Brüchert, V., et al. (2011). Dietary success of a 'new'key fish in an overfished ecosystem: evidence from fatty acid and stable isotope signatures. *Mar. Ecol. Prog. Ser.* 428, 219–233. doi: 10.3354/meps09078

van der Lingen, C. D., Shannon, L. J., Cury, P., Kreiner, A., Moloney, C. L., Roux, J.-P., et al. (2006). "Resource and ecosystem variability, including regime shifts, in the Benguela Current System," in *Large Marine Ecosystems Benguela - Predicting a Large Marine Ecosystem*, eds V. Shannon, G. Hempel, P. Malanotte-Rizzoli, C. Moloney, and J. Woods (Elsevier), 147–184.

van der Plas, A. K., Monteiro, P. M. S., and Pascall, A. (2007). Cross-shelf biogeochemical characteristics of sediments in the central Benguela and their relationship to overlying water column hypoxia. *Afr. J. Mar. Sci.* 29, 37–47. doi: 10.2989/AJMS.2007.29.1.3.68

Vaquer-Sunyer, R., and Duarte, C. M. (2010). Sulfide exposure accelerates hypoxia-driven mortalit. *Limnol. Oceanogr.* 55, 1075–1082. doi: 10.4319/lo.2010.55.3.1075

von Bonde, C. (1928). *Fisheries and Marine Biological Survey. Report No. 5 for the Years 1925-1927*. Pretoria: Union of South Africa.

Waldron, F. W. (1900). On the appearance and disappearance of a mud island at Walfish Bay. *Trans. South Afr. Philos. Soc.* 11, 185–188. doi: 10.1080/21560382.1900.9525965

Weeks, S. J., Currie, B., and Bakun, A. (2002). Satellite imaging: massive emissions of toxic gas in the Atlantic. *Nature* 415:493. doi: 10.1038/415493b

Weeks, S. J., Currie, B., Bakun, A., and Peard, K. R. (2004). Hydrogen sulphide eruptions in the Atlantic Ocean off southern Africa: implications of a new view based on SeaWiFS satellite imagery. *Deep Sea Res. Part I Oceanogr. Res. Papers* 51, 153–172. doi: 10.1016/j.dsr.2003.10.004

Woodhead, P. M., Hamukuaya, H., O'Toole, M. J., and McEnroe, M. (1998). "Effects of oxygen depletion in shelf waters on hake populations off central and northern Namibia," in *International Symposium, Environmental Variability in the South East Atlantic*, eds L. V. Shannon and M. J. O'Toole (Swakopmund: NATMIRC), 10.

Zettler, M. L., Bochert, R., and Pollehne, F. (2009). Macrozoobenthos diversity in an oxygen minimum zone off northern Namibia. *Mar. Biol.* 156, 1949–1961. doi: 10.1007/s00227-009-1227-9

Zettler, M. L., Bochert, R., and Pollehne, F. (2013). Macrozoobenthic biodiversity patterns in the northern province of the Benguela upwelling system. *Afr. J. Mar. Sci.* 35, 283–290. doi: 10.2989/1814232X.2013.798592

Conflict of Interest Statement: The authors declare that the research was conducted in the absence of any commercial or financial relationships that could be construed as a potential conflict of interest.

frontiers in Marine Science

ORIGINAL RESEARCH
published: 17 October 2018
doi: 10.3389/fmars.2018.00344

Epifaunal Foraminifera in an Infaunal World: Insights Into the Influence of Heterogeneity on the Benthic Ecology of Oxygen-Poor, Deep-Sea Habitats

Ryan A. Venturelli[1]†, Anthony E. Rathburn[1,2†], Ashley M. Burkett[1†] and Wiebke Ziebis[3]*

[1] Department of Earth and Environmental Systems, 159 Science Bldg, Indiana State University, Terre Haute, IN, United States, [2] Integrative Oceanography Division, Scripps Institution of Oceanography, San Diego, CA, United States, [3] Marine Environmental Biology, Department of Biological Sciences, University of Southern California, Los Angeles, CA, United States

OPEN ACCESS

Edited by:
Arthur Capet,
MAST – University of Liège, Belgium

Reviewed by:
Gerhard Schmiedl,
Universität Hamburg, Germany
Ursula Felicitas Marianne Witte,
University of Aberdeen,
United Kingdom

***Correspondence:**
Ryan A. Venturelli
raventurelli@mail.usf.edu

†Present address:
Ryan A. Venturelli,
College of Marine Science, University of South Florida, St. Petersburg, FL, United States
Anthony E. Rathburn,
Department of Geological Sciences, California State University, Bakersfield, CA, United States
Ashley M. Burkett,
Boone Pickens School of Geology, Oklahoma State University, Stillwater, OK, United States

Specialty section:
This article was submitted to Coastal Ocean Processes, a section of the journal Frontiers in Marine Science

Received: *27 May 2018*
Accepted: *06 September 2018*
Published: *17 October 2018*

Citation:
Venturelli RA, Rathburn AE, Burkett AM and Ziebis W (2018) Epifaunal Foraminifera in an Infaunal World: Insights Into the Influence of Heterogeneity on the Benthic Ecology of Oxygen-Poor, Deep-Sea Habitats. Front. Mar. Sci. 5:344. doi: 10.3389/fmars.2018.00344

A reduction in dissolved oxygen availability in marine habitats is among the predicted consequences of increasing global temperatures. An understanding of past oxygenation is critical for predictions of future changes in the extent and distribution of oxygen minimum zones (OMZs). Benthic foraminifera have been used to assess changes in paleo-oxygenation, and according to prevailing thought, oxygen-poor marine benthic habitats are dominated by sediment-dwelling infaunal foraminifera, while more oxygenated environments are populated with more epifaunal taxa. However, in this study we found elevated densities of epifaunal taxa in oxygen-poor habitats. A series of 16 multicores were taken on depth transects (360–3000 m) across an OMZ in the Southern California Bight to investigate the ecology of living (rose bengal stained) benthic foraminifera. Dissolved oxygen concentrations in bottom water at sampling sites varied from 21 to 162 μmol/l. Sampling focused on bathymetric highs in an effort to collect seafloor surface materials with coarse sediments in areas not typically targeted for sampling. Mean grain size varied from about 131 (gravelly sand) to about 830 μm (coarse sand with fine gravel). Vertical distribution patterns (0–2 cm) were consistent with those of conspecifics reported elsewhere, and reconfirm that *Cibicidoides wuellerstorfi* and *Hanzawaia nipponica* have a living preference at or near the sediment-water interface. As expected, assemblages were dominated by infaunal taxa, such as *Uvigerina* and *Bolivina*, traditionally associated with the supersaturated, unconsolidated mud, characteristic of OMZ habitats, suggesting that these taxa are not sensitive to substrate type. However, despite dysoxic conditions (21–28 μmol/l), epifaunal taxa comprised as much as 36% of the stained population at the five sites with the coarsest mean grain size, while other measured environmental parameters remained relatively constant. We suggest that these epifaunal taxa, including *C. wuellerstorfi*, prefer habitats with coarse grains that allow them to remain at or above the sediment-water interface.

These results suggest that seafloor habitat heterogeneity contributes to the distribution of benthic foraminifera, including in low-oxygen environments. We submit that paleo-oxygenation methods that use epifaunal indicator taxa need to reconsider the dissolved oxygen requirements of epifaunal taxa.

Keywords: benthic foraminifera, epifauna, infauna, oxygen, Southern California Bight

INTRODUCTION

Geographic and bathymetric variability in deep ocean oxygen concentrations has a profound impact on marine benthic ecosystem distribution patterns in modern and ancient oceans. As global temperatures rise, areas of oxygen-poor environments, including oxygen minimum zones (OMZs) are predicted to increase, changing seafloor habitats and species distributions (Levin, 2003). Understanding the responses of benthic organisms to changes in oxygen variability is the key to both predicting changes in benthic ecosystem distribution patterns of a deoxygenated future and interpreting the fossil record of dissolved oxygen changes of the geologic past.

As a result of their ecological and biogeochemical sensitivity to changes in their habitat in modern environments, benthic foraminifera preserved in the fossil record are often used as indicators of paleoenvironmental changes (e.g., Murray and Bowser, 2000). The utility of fossil benthic foraminifera in assessments of ancient changes in ocean conditions relies upon an understanding of the factors that influence modern foraminifera. As new information from living populations becomes available, methods using benthic foraminiferal proxies are modified to improve interpretations of the fossil record. For example, the realization that different benthic foraminifera have different microhabitat preferences (Corliss, 1985), in which some species live at or above the sediment-water interface (epifauna) while others live within the sediments (infaunal), dramatically changed the way that fossil foraminifera were used to evaluate paleoceanographic conditions (e.g., McCorkle et al., 1990; Jorissen et al., 2007).

One of the methods used to assess ecological and physiological limitations of deep-sea benthic foraminifera has been to examine species distributions from available core-tops and compare these with environmental parameters (reviewed in Murray and Bowser, 2000). Through this method and other techniques, the ecology of many benthic foraminiferal species has been characterized and applied in paleoenvironmental proxy analyses. Calcareous benthic foraminifera are often abundant in organic-rich, oxygen-poor environments in the modern ocean (reviewed in Sen Gupta and Machain-Castillo, 1993; and Bernhard and Sen Gupta, 1999). Foraminiferal studies of organic-rich, oxygen-poor environments have been typically based on samples from centers of oxygen-stressed basins, with characteristically thixotropic sediments resulting from organic flux generated by high surface productivity. Based largely on the abundance and rarity of different foraminiferal species in these organic-rich, oxygen-poor settings compared with other regions, ecological preferences and environmental limitations have been inferred and applied in proxy methods to reconstruct changes in both productivity (e.g., Loubere and Fariduddin, 1999) and paleoxygenation (Kaiho, 1991, 1994, 1999; Jannink et al., 2001; Schmiedl et al., 2003; reviewed in Jorissen et al., 2007). Many studies that use foraminifera to evaluate bottom water oxygen (BWO) concentrations consider epifaunal species as indicators of well-oxygenated environments (reviewed in Jorissen et al., 2007). For example, Kaiho (1991) proposed, and later modified (Kaiho, 1994, 1999), the Benthic Foraminiferal Oxygen Index (BFOI), where benthic foraminiferal species are grouped into oxygenic indicator categories (i.e., oxic, suboxic, and dysoxic). Species of *Cibicidoides*, in particular, along with several other epifaunal taxa, are regarded in BFOI analyses as "oxic indicator species," occurring in abundance where BWO values are >67 μmol/l (Kaiho, 1991, 1994, 1999). Likewise, deep infaunal taxa which typically dominate organic-rich, oxygen-poor environments, are regarded as indicators of oxygen-poor environments (Bernhard, 1986; Sen Gupta and Machain-Castillo, 1993; Bernhard and Sen Gupta, 1999, reviewed in Jorissen et al., 2007). BWO concentrations and organic input (food availability) are considered primary factors influencing benthic foraminiferal distribution and abundance (e.g., Perez-Cruz and Machain-Castillo, 1990; Rathburn and Corliss, 1994; Jorissen et al., 1995, 2007; Koho et al., 2008). However, relatively few studies have evaluated protoplasm-containing foraminifera from coarse-grained habitats in oxygen-poor settings. Substrate and attachment surfaces are known to be important for epifaunal foraminifera (e.g., Lutze and Thiel, 1989; Burkett et al., 2016), and increased abundances of epifaunal taxa in coarser-grained sediments has been noted in deep-water environments (Schönfeld, 2002). An understanding of the factors that influence benthic foraminifera in oxygen-poor environments is needed for high-resolution paleoceanographic studies (e.g., Stott et al., 1996; Hendy and Kennett, 2000), and to predict the responses of benthic species to deoxygenation in a globally warmer future.

Here we present results of living (rose bengal stained) benthic foraminifera from a depth transect, targeting coarse-grain sediment habitats, across a range of dissolved BWO concentrations in the Southern California Bight (SCB). Specific objectives of this research were to:

1. Examine living (rose bengal stained) benthic foraminiferal distribution patterns in the SCB.
2. Assess the ecology of foraminiferal species living in oxygen-deficient habitats of the SCB.
3. Evaluate paleoceanographic implications of the study's major findings.

Results from this study provide information relevant to both the ecology of modern oxygen-deficient seafloor habitats and fossil based assessments of paleoceanographic changes.

MATERIALS AND METHODS

Regional Setting

The Southern California Bight (**Figure 1**) extends from Point Conception to just south of San Diego. Oceanographically the region is dominated by the California Countercurrent, formed by a large-scale eddy in the California Current, along with seasonal upwelling resulting from strong offshore winds (Nelson et al., 1987). Most of the seafloor in this region is characterized by deep basins, separated by ridges, sills, and islands that run parallel to the shore. Together, these features have been referred to as "The Southern California Borderland" (Emery, 1960). California Borderland basin sediments are typically comprised of thixotropic, organic-rich, mud to silt-sized material on the basin floor, with coarse sediments dominating the bathymetric highs surrounding each basin (Gorsline et al., 1984). This region has been monitored by the California Cooperative Oceanic Fisheries Investigations (CalCOFI), collecting biologic and hydrographic data from a consistent array of stations since 1950. Typical data collected down to 500 m depth include temperature, salinity, oxygen, phosphate, silicate, nitrate and nitrite, chlorophyll, ^{14}C, primary productivity, phytoplankton biodiversity, zooplankton biomass, and zooplankton biodiversity (Bograd and Lynn, 2003). Seafloor samples for our study were collected from the SCB in July, 2011. CalCOFI reports indicate that upwelling off of central and southern California resumed earlier and stronger in the spring of 2010 after recovery from El Niño, which was in turn responsible for regional variability that persisted through the 2010–2011 winter. As a result of strong upwelling, robust sea surface productivity was evident within the SCB during the Summer of 2011 (BjorkstEdt et al., 2011). The OMZ of this region typically resides between 100 and 900 m water depth, with minimum oxygen values occurring from 300 to 500 m (Karstensen et al., 2008), though we found our lowest oxygen concentrations at our 1000 m site.

Sample Collection

Samples were collected with an Ocean Instruments multicorer during an *R/V New Horizon* cruise (NH1108 July 15–21, 2011). Within the study area, edges of basins and bathymetric highs were targeted in an effort to examine the distribution of living foraminiferal assemblages in oxygen-poor habitats with coarse-grained sediments. Sites were sampled from water depths of 360–2969 m, with BWO values ranging from 21 to 162 μmol/l (**Table 1**). The top 0–1 cm interval was sampled, then cores were sectioned into half-centimeter intervals (i.e., 0–1, 1–1.5, 1.5–2, etc.) and preserved in a 4% buffered formaldehyde solution (37% formaldehyde buffered with Mule Team Borax©), following methods outlined in Rathburn and Corliss (1994).

Surface sediments (0–1 cm) were also collected from twelve core locations and preserved by freezing (−80°C) for total organic carbon (TOC) and particle size analysis. Upon recovery on the ship, cores selected for microprofiling of dissolved oxygen were immediately moved to a controlled temperature environment (4°C) onboard the ship. The cores were subsequently sectioned into 0.5 and 1 cm intervals under a nitrogen atmosphere for pore water analyses.

Oxygen Microprofiles

Microprofiles of oxygen concentration were measured in vertical intervals of 250 mm using Clark-type amperometric oxygen sensors (Unisense, Aarhus Denmark) using methods outlined in

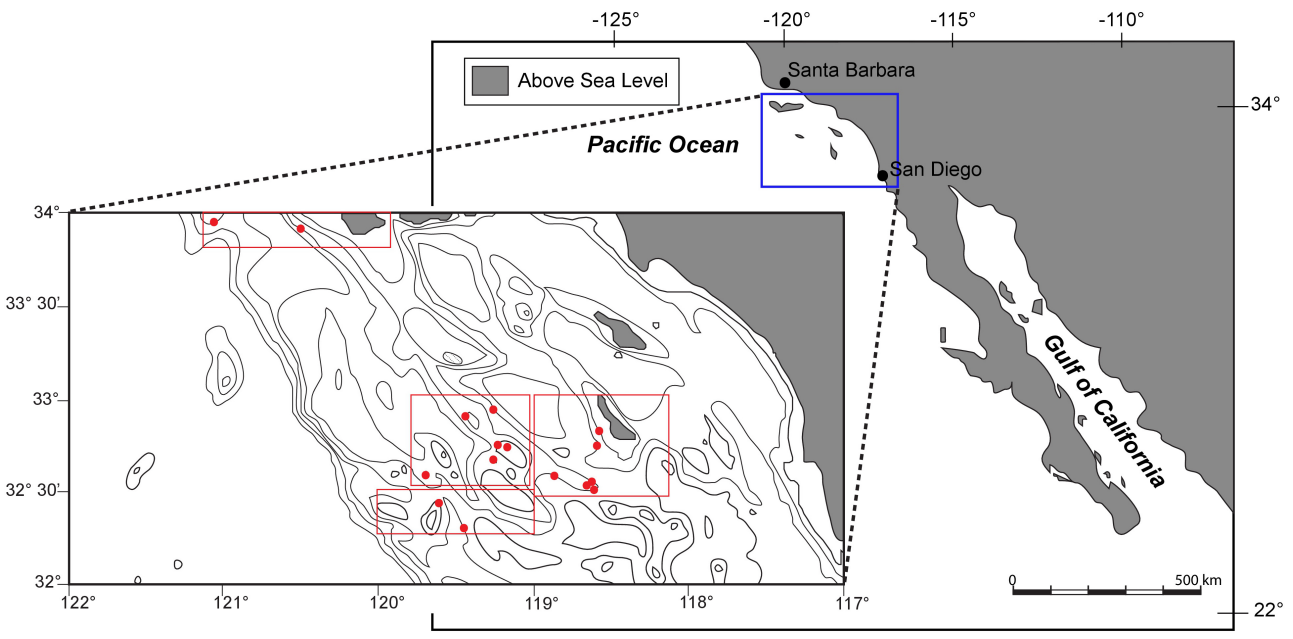

FIGURE 1 | Map and bathymetric chart of the study area within the Southern California Bight. Multicore locations, labeled with red filled circles, are described in detail with depth and environmental parameters in table one.

TABLE 1 | Core locations, depths, environmental parameters (oxygen, temperature), habitat parameters, (substrate mean grain size and total organic carbon), and live foraminiferal abundances.

Site Name	Depth	Oxygen (μmol/l)	Latitude (N)	Longitude (W)	Temperature (°C)	Mean Grain Size (μm)	Total Organic Carbon (%)	Standing Stock (#/cm^3)
CB	360	28.4	32-57.522	119-29.432	7.1	618.5	2.2	200.3
Z	430	27.2	32-45.238	118-31.378	6.7	–	1.3	93.5
G	600	25.8	32-39.200	119-22.317	6.1	131.1	2.2	98.8
BB	665	30.8	32-43.667	118-32.117	5.7	–	2.2	148.6
O	700	32.2	32-42.610	119-22.758	5.8	147.5	3.2	470.5
B	825	25.3	32-33.988	118-43.303	4.9	287.9	1.8	82.4
Y	910	26.2	32-33.055	118-39.445	3.4	271	2.1	86.2
J	1000	27.1	33-42.961	120-18.754	4.2	504.4	4.2	149.9
A	1050	21.0	32-33.730	118-37.129	4.0	238.9	1.7	191.0
E	1340	31.1	32-25.920	119-43.081	3.3	336.1	3.4	275.9
F	1380	31.8	32-39.255	119-44.700	3.1	153.1	2.0	125.3
D	1510	76.8	32-17.718	119-30.764	2.9	551.8	3.4	63.7
M	2970	161.7	33-45.591	121-0.560	–	829.7	2.1	146.6

Revsbech and Jørgensen (1986) and Revsbech et al. (1989). BWO for five of the 13 core sites were obtained from microprofiles (sites at 665, 700, 1000, 1510, and 2970 m). Sensors were attached to computer controlled motorized micromanipulators and driven vertically into the sediments on μm to mm intervals. Signals were amplified and transformed to millivolt (mV) by a 2-channel picoammeter (PA 2000; Unisense, Aarhus Denmark) and directly recorded on a computer using the software Profix (PyroScience, Aachen Germany). A linear calibration was performed on board immediately prior to measurements at 0% and 100% oxygen saturation. Calibration chambers filled with filtered seawater were kept at *in situ* temperature and purged by nitrogen or bubbled with air to create the respective standards.

Bottom Water Properties

Bottom water dissolved oxygen, temperature, and salinity values were obtained from CTD casts (rosette-equipped with an oxygen sensor) at eight of the 13 core sites. The remaining five core site BWO values were determined by oxygen microprofiling as mentioned above.

Sediment Properties: Particle Size and Total Organic Carbon

Both laser diffraction particle-size analysis and conventional dry sieving were used to determine grain size distribution for the surface sediments (0–1 cm) at the locations where surface sediments were available. Coarse-grained substrates led to difficulties in collecting multicores, and in a few locations the only cores available were used for foraminiferal analyses, with no sample remaining for particle size. Samples were analyzed at the National Lacustrine Core Facility (LacCore) on a *Partica* LA-950 Laser Diffraction Particle Size Distribution Analyzer to capture high-resolution data on the mud to sand size fraction (0.022–2000 μm). To analyze the sand and gravel portion, sediment samples were dry sieved on a ¼ phi interval from 5 (31 μm) to −2 (4 μm). Sediments were removed from sieves and weighed. All data (weight %) were entered into GRADISTAT (Blott and Pye, 2001) to generate statistical and graphical outputs including the mean and sorting of each sample. Surficial sediment samples for each of the multicores were sent to the University of Florida for analyses of organic carbon using a Carlo Erba NA1500 CNHS elemental analyzer.

Sample Processing

Rose bengal (65 mL) was added to each sample and allowed to stain for a minimum of 7 days. The limitations of rose bengal stain are well-known (Bernhard et al., 2006), and using a conservative approach, considering only those individuals with multiple, brightly stained chambers of protoplasm as alive at the time of collection, rose bengal staining provides a reliable assessment of living assemblages (Altenbach and Sarnthein, 1989; Murray and Bowser, 2000).

In order to determine original sediment volumes for each sample and to standardize for comparison between samples, volumetric procedures were followed as outlined in Rathburn and Corliss (1994). Cores were wet sieved from 0 to 2 cm (0–1, 1–1.5, and 1.5–2 cm), over a 63 and 150 μm mesh sieve. Using a modified Otto microsplitter (Otto, 1933), both the >150 μm and 63–150 μm portions were wet split to feasible working sizes, with a minimum target of 300 specimens in the >150 μm portion and 100 specimens in the 63–150 μm portion, and picked for living (stained) benthic foraminifera. Picked specimens were placed on microslides, identified to species, and counted.

Faunal distribution of the >150 μm fraction were analyzed in the surface sediments for each sampling location across the depth/oxygen transect. In a low oxygen environment, the majority (∼90%) of living benthic foraminifera typically inhabit the top 1 cm of sediment (Bernhard and Sen Gupta, 1999). Standing stocks of calcareous and agglutinated taxa were calculated for each site, and presented as number of individual foraminifera per area (#foraminifera/50 cm^2).

Diversity indices, including species richness (S), Shannon–Wiener diversity index (H), and evenness (J) were calculated using the free statistical software PAST (PAleontological STatistics; Version 3.05; Hammer et al., 2001).

For these analyses:

$$\text{Richness (S)} = \text{count of number of taxa per site}$$

$$\text{Diversity (H)} = -\sum_{i=1}^{s} p_i \ln p_i$$

$$\text{Evenness (J)} = \text{H/H}_{\max} = \text{H/lnS}$$

With p_i representing the proportion of the individual taxon to the population.

RESULTS

Bottom Water Properties

Bottom water oxygen values examined in this study ranged from 21 to 161 μmol/l (**Figure 2**). The terminology of Bernhard and Sen Gupta (1999) will be used, where "anoxic" refers to those regions where BWO equals 0 μmol/l, "dysoxic" refers to BWO between 4.5 and 45 μmol/l, and "oxic" represents BWO greater than 45 μmol/l. Site A (1000 m) is the only core site along the transect where dissolved BWO of 21 μmol/l was below 22.3 μmol/l and within the OMZ as defined by Helly and Levin (2004). The majority of core sites along the transect had dysoxic BWO values that ranged from 22 to 45 μmol/l. Core sites in the dysoxic zone included those at 360, 429, 600, 665, 700, 826, 910, 994, 1339, and 1378 m. Two sites, at 1510 and 2969 m, occur in water depths below the OMZ where BWO values were 77 and 162 μmol/l, respectively (**Table 1**; **Figure 2**). In addition to BWO measurements, pore water oxygen values were determined at six sites (**Figure 3**). Oxygen microprofiles reveal that oxygenated pore waters were present in sediment depths up to 5 mm.

Sediment Properties

Preferential sampling of bathymetric highs and basin edges yielded coarser grained sediments than in basin centers. The cause of the presence of coarse grains in these areas is unknown, but it is likely that bottom currents play a role. Particle size analyses revealed that substrates examined in this study were comprised primarily (41–97% of total sample) of sand-sized, siliciclastic sediments (>63 μm). Appreciable percentages of gravel-sized particles (>2 mm) were also found in several of the samples along the depth transect, namely at 360 (42%) and 2969 m (50.5%). Particle size distribution varied from site to site in this region (**Figure 2**), with mean grain sizes ranging from 131 μm at 600 m to 829 μm at 2969 m (**Figure 2**). TOC for the 13 sites along the transect ranged from 1.25 to 4.24% (**Table 1**; **Figure 2** and **Supplementary Data Sheet 1**).

Surface Sediment Standing Stock

>150 μm

Standing stocks of rose bengal stained specimens from the 0–1 cm interval were determined for all 13 locations (**Table 1** and **Supplementary Data**). On average, surface sediments across the transect contained 164 individuals/50 cm^2. Calcareous taxa were more prevalent than agglutinated taxa at the majority of sites across the transect, comprising anywhere from 53 to 98% of the total population. The deepest site on the transect, at 2969 m, had the greatest proportion of agglutinated taxa comprising 47% of the total population.

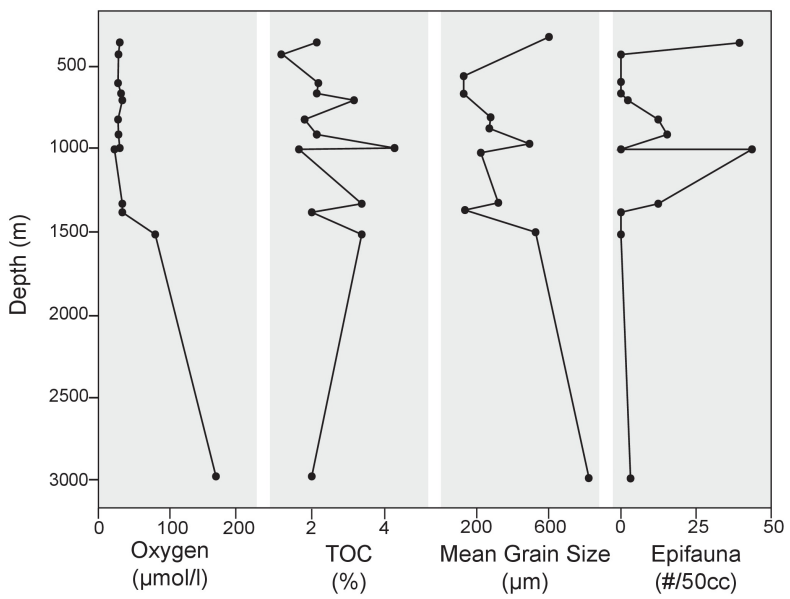

FIGURE 2 | Environmental and substrate parameters plotted along the depth transect along with standing stock of epifaunal foraminifera at each site. Mean grain size from particle size analysis lends insight to the heterogeneity of substrates sampled in this study. No apparent relationship between substrate and depth exists in this area.

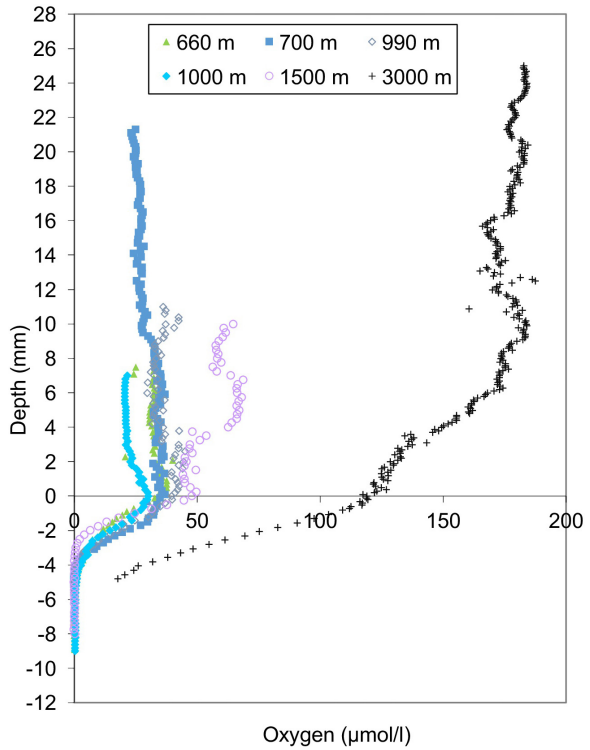

FIGURE 3 | Oxygen microprofiles for the six sites observed. Bottom water oxygen measurements from oxygen microprofiles were consistent with CTD casts. Oxygen microprofiles reveal that oxygenated pore waters were present in sediment depths up to 5 mm.

Maximum abundance of stained foraminifera in the 0–1 cm interval was observed at 700 m (470 individuals/50 cm^2). This site was overwhelmingly dominated by *Uvigerina peregrina* (80% of total population). *Uvigerina peregrina* was among the most abundant taxon at 10 of the 13 sites across the depth transect, with a maximum at 700 m at 375 individuals/50 cm^2. *Cassidulina laevigata*, *Bolivina spissa*, *Hoeglundina elegans*, *Uvigerina auberiana*, and *Cibicidoides wuellerstorfi*, were also among the most abundant taxa in the >150 µm size fraction of cores examined in this study (**Figure 4**).

63–150 µm

Standing stock abundances of the 0–1 cm interval were determined for six locations, 360, 600, 700, 826, 910, and 1000 m to compare the smaller size fraction with the >150 µm fraction. Since foraminiferal populations tend to be smaller in size in organic-rich, oxygen-poor environments (e.g., Perez-Cruz and Machain-Castillo, 1990), examination of this size fraction (despite the time-consuming nature of this effort) provides information for a larger, and more representative percentage of the population. On average, surface sediments across the transect contained 148 individuals/50 cm^2 (SD:111). Similar to the >150 µm size fraction, calcareous taxa comprise the majority of the population (87–100%). Stained agglutinated taxa are only present in this size fraction at 826, 910, and 1000 m. Dominant taxa in the 63–150 µm portion were not necessarily the same as those in the >150 µm size fraction. Among the most common taxa of the 63–150 µm fraction were *Bolivina spissa, Cassidulina carinata, Buliminella tenuata, Cibicidoides bradyi, Uvigerina proboscidea*, and *Uvigerina peregrina*. *Bolivina spissa*, the most abundant taxon in the 63–150 µm assemblage, had a peak abundance at 700 m with 128 individuals/50 cm^2. While most abundant in the larger size fraction, *Uvigerina peregrina* was only present at the 910 and 1000 m site in the 63–150 µm size fraction. In order to best understand the community over a range of sizes, the 63–150 µm was combined with the >150 µm portion and will be referred to henceforth as the "> 63 µm population" (**Figure 5**).

Epifauna

Epifaunal taxa present in cores from the SCB include *C. wuellerstorfi* and *Hanzawaia nipponica*. Contrary to expectations based on previous studies (i.e., BFOI-Kaiho, 1994), epifaunal taxa had a marked presence at 12 of the 13 sites analyzed, comprising as much as 35.7% of the total population despite oxygen-poor conditions. The presence and abundance of both taxa do not appear to be associated with changes in any of the measured environmental parameters (i.e., oxygen, TOC, grain size, and temperature; **Figure 2**). *C. wuellerstorfi* was present in the >150 µm portion of seven of the 13 sites, comprising 0.28–14.5% of the total population in the surface sediments. *H. nipponica* was present in abundance at four of the shallowest sites along the transect (360, 429, 600, and 700 m), with maximum abundances at 600 m, dominating the total population at that site and comprising 47% of the total benthic foraminiferal population.

Diversity and Dominance

>150 µm

A total of 60 taxa were identified in this region with 51 calcareous and 9 agglutinated in the >150 µm size fraction. Species richness was variable both across the transect and within different sections of the OMZ (**Figure 6**). Interestingly, the highest species richness value (27) was found at 1000 m, where BWO values were the lowest. In the dysoxic zone, richness varied from 7 to 23; while the two deepest stations had richness values of 13 and 18. Species were distributed relatively evenly (0.62–0.88), with the exception of the site at 700 m with an evenness value of 0.34.

Shannon diversity (H) of stained foraminifera varied across the transect. Maximum diversity (2.5) was observed at 1378 m. At 700 m depth, with a value of 1.05, we found the lowest diversity value of the sites examined in this study. Despite having the lowest BWO in the study area, the 1000 m had a diversity near the high end of the study area range (2.22). The two deepest sites, had similar diversities (2.25–2.37).

63–150 µm

The >63 µm fraction was analyzed for faunal distribution in the surface sediments at six locations (**Figure 7**) where 60 calcareous and 10 agglutinated taxa were found in the >63 µm fraction. Species richness was variable, ranging from 10 to 27, with the lowest and highest values being found at 600 and

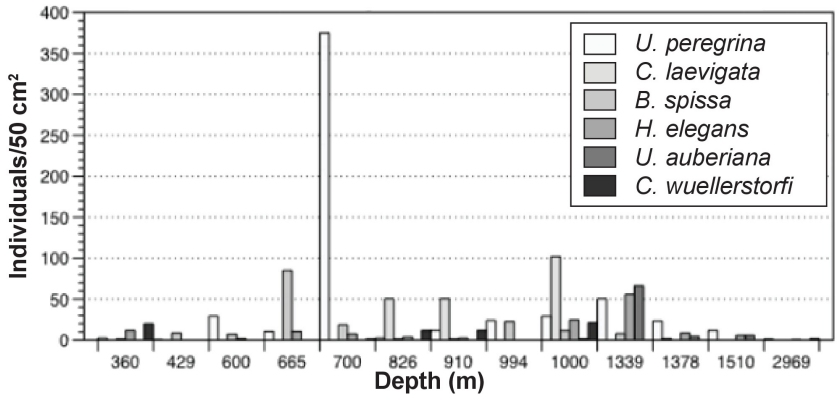

FIGURE 4 | Distribution of the six most abundant >150 micron taxa along the transect.

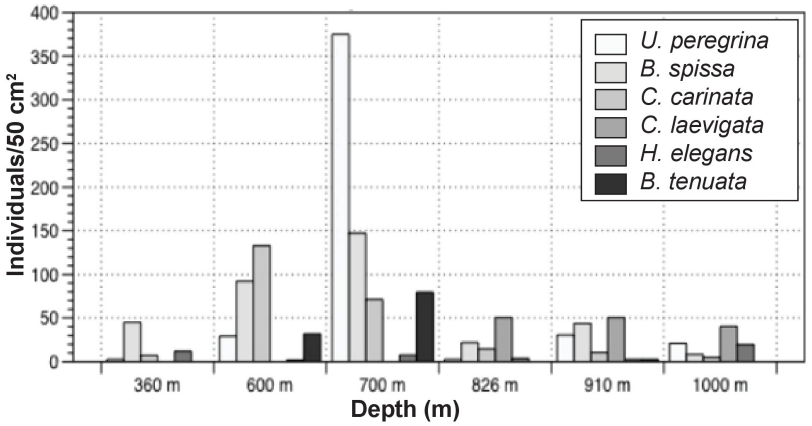

FIGURE 5 | Distribution of the six most abundant >63 micron taxa along the transect.

700 m, respectively. At 1000 m, where oxygen values were the lowest along the transect, richness was among the highest of sites examined for this size fraction (26). Evenness was similar for five of the six sites, with values ranging from 0.70–0.85. Minimum diversity values of 1.62 and 1.82 were found at 600 and 700 m, respectively. Sites exposed to dysoxic BWO had similar trends in richness, standing stock, and BWO. At 1000 m, where BWO values were the lowest of those examined in this study, richness and diversity values were among the highest (26 and 2.5, respectively).

DISCUSSION

Projected increases in size and location of OMZs and other dissolved oxygen-depleted marine habitats associated with climate change highlight the importance of understanding the responses of benthic ecosystems to deoxygenation (e.g., Kamykowski and Zentara, 1990; Sarmiento et al., 1998; Keeling and Garcia, 2002; Helly and Levin, 2004; Stramma et al., 2008; Meier et al., 2011). Benthic environments with limited oxygen availability are typically characterized by high organic carbon contents (high primary productivity), high sediment accumulation rates, fine grain size, low bioturbation, and generally homogeneous habitats (e.g., Reichart et al., 1998; Levin, 2003). As a result of their densities in oxygen-poor environments, and their fossil presence in high-resolution geologic records from OMZs, benthic foraminifera living in oxygen-poor habitats have been the focus of a number of studies (e.g., Sen Gupta and Machain-Castillo, 1993; Bernhard and Alve, 1996; Bernhard and Sen Gupta, 1999; Bernhard et al., 2000). It is well documented that foraminiferal assemblages collected from the soupy, organic-rich sediments of oxygen-poor shelf/slope habitats, including those of the California Borderlands Basins, are overwhelmingly dominated by infaunal taxa (e.g., Bernhard and Reimers, 1991; Silva et al., 1996; Gooday et al., 2009; Gooday and Jorissen, 2012). Enhanced foraminiferal diversity has been reported along OMZ boundaries (e.g., Phleger and Soutar, 1973), and since foraminifera are the predominate fauna persisting through an OMZ, there may be an enhanced regional diversity resulting from boundary effects and habitat heterogeneity (Mullins et al., 1985; Gooday et al., 2009; Gooday et al., 2010). In this study, there do not seem to be any boundary effects that could be related to changes in water

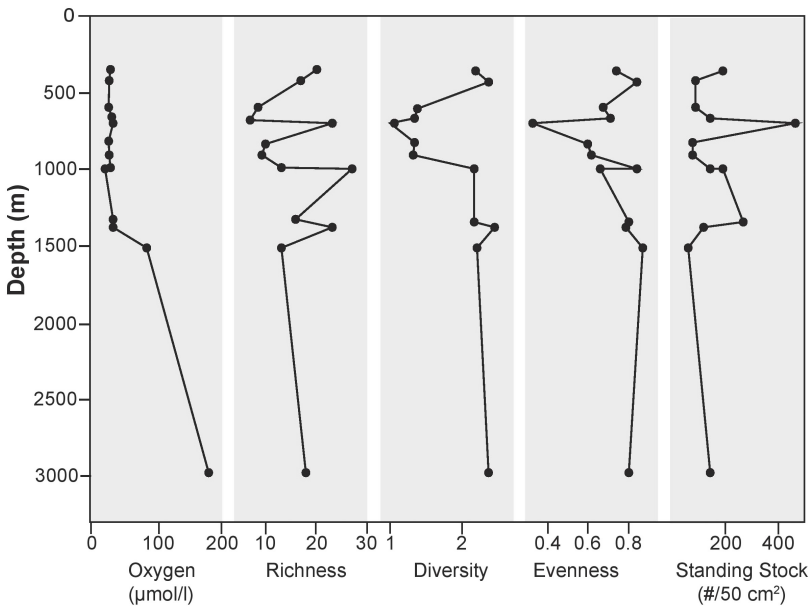

FIGURE 6 | Shannon Diversity indices in >150 micron size fraction.

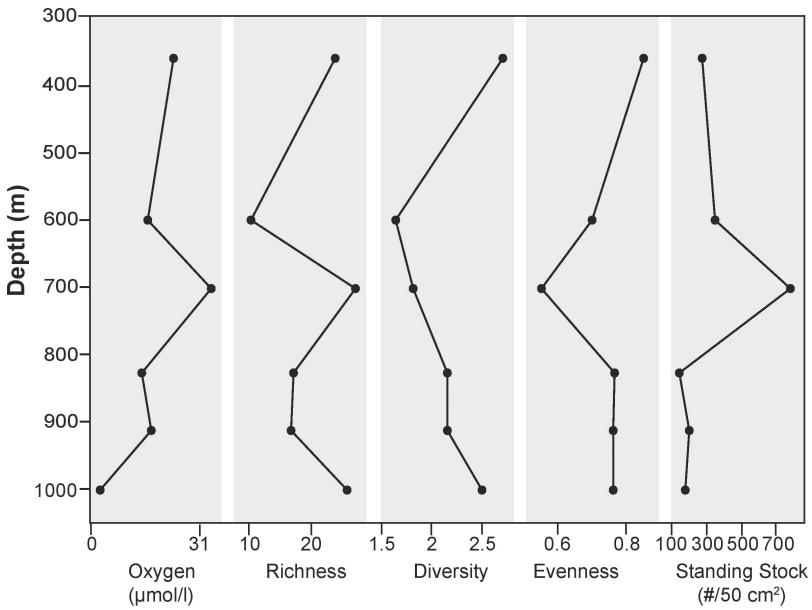

FIGURE 7 | Shannon Diversity indices in >63 micron size fraction.

properties, including dissolved oxygen. Differences in surficial sediment characteristics of the sampling sites in the present study likely create habitat heterogeneity, enhancing diversity, but infaunal taxa remain dominant in coarser-grained sites as they are in the fine-grained muds typical of organic-rich basins. Results from our study also show that epifauna can comprise an appreciable percentage (up to 35.7%) of assemblages in coarse-grained habitats with dissolved BWO values as low as 23 µmol/l.

Previous studies of living foraminifera in the region primarily sampled fine-grained sediments that typify high productivity environments (e.g., Phleger and Soutar, 1973; Bernhard and Reimers, 1991; Silva et al., 1996). Studies of living foraminifera off California reported that nearby study sites had a complete absence of epifaunal taxa in the Santa Barbara Basin with BWO values of 4.5 µmol/l (Bernhard and Reimers, 1991) and in the San Pedro Basin 2.3–18 µmol/l (Silva et al., 1996). Our results from the SCB show that, in many cases, foraminiferal

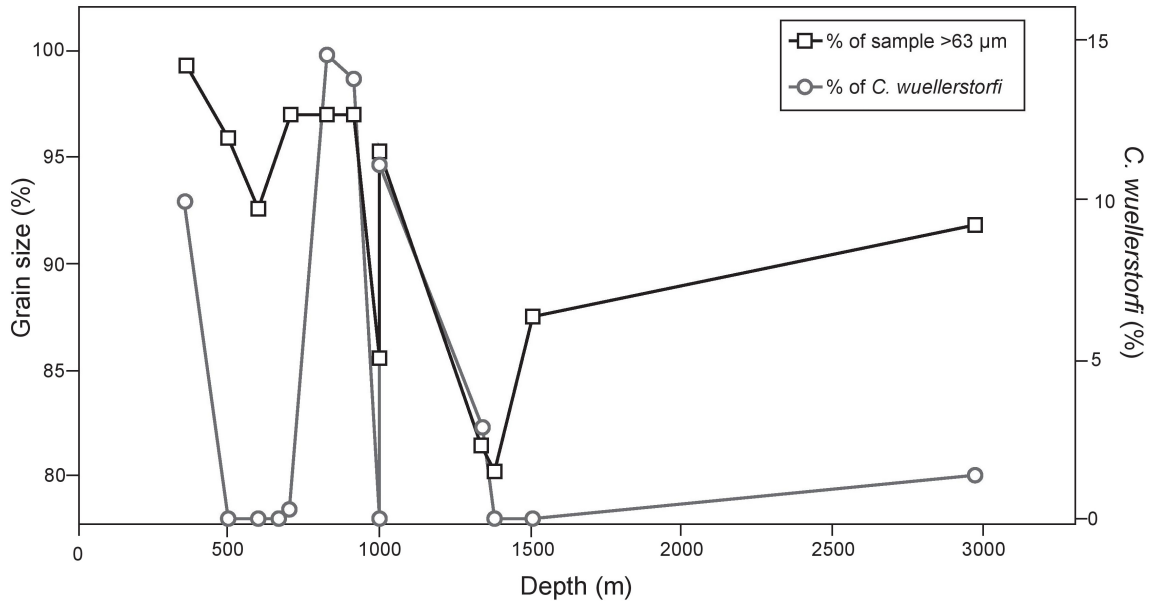

FIGURE 8 | Abundance of sand-sized particles or greater characterizing the substrate along with presence of *C. wuellerstorfi* at each depth. We demonstrate that substrates with greater concentrations of sand-sized particles may provide habitat stability for *C. wuellerstorfi* to persist, despite low bottom water oxygen concentrations.

assemblages collected from the edges of basins and on the ridges between basins have marked differences in assemblages when compared those found in nearby basin-focused studies of Phleger and Soutar (1973), Bernhard and Reimers (1991), and Silva et al. (1996). Basin ridges are characterized by coarser sediments (80–99% of the surface sediments are comprised of sand and gravel sized particles) (>63 μm), probably due to removal of fine-grained sediment by winnowing currents. In the Gulf of Cadiz, appreciable densities of epifauna, including several species of *Cibicidoides* and *Planulina*, were present on hard or gravel-laden substrates (Schönfeld, 2002). Schönfeld (2002) noted a relationship between coarse sediments and epifauna in the northeastern Atlantic, and suggested that at least some epifaunal foraminifera were likely to need currents for food acquisition. Schönfeld (2002) proposed that paleo-current velocities could be assessed by examining percentages of epifauna. Although we cannot evaluate the influence of currents on the foraminifera in our study area, at the micron scale, it would not require much energy to create flow around an epifaunal foraminiferan. We suggest the presence of attachment surfaces is the primary influence enhancing epifaunal percentages in our study area. Elevated epibenthic taxa (those that live attached above the average sediment-water interface) prefer a hard substrate for attachment. *C. wuellerstorfi* is commonly found attached to hard surfaces at or above the sediment-water interface (e.g., Lutze and Thiel, 1989; Burkett et al., 2016). Other unattached epifauna may also prefer access to bottom water than to be surrounded by sediment and pore water. Grain size analyses, in this study, were based on sediment samples from surface materials, and we cannot know how many of the coarse grains were at the sediment-water interface and available for attachment. As a result, a strong correlation between grain size results and all epifaunal taxa may not be expected. Nevertheless, at sites in this study where peak percentages of *C. wuellerstorfi* were present (>9% of population; 360, 826, 910, and 1000 m), the surface sediments were comprised primarily of sand and gravel-sized particles (95.4–99.7%; **Figure 8**).

Other epifauna (*H. nipponica*) did not show any apparent relationship with sedimentary characteristics. The sites in which the lowest BWO concentrations and TOC were found had some of the highest concentrations of *C. wuellerstorfi*. However, BWO and TOC, did not appear to influence the distribution of epifauna as a whole in our study (**Figure 2**). Typical organic-rich, oxygen-poor seafloor environments are characterized by fine-grained, soupy sediments that have few, if any hard substrates at the sediment-water interface. These environments are dominated by infaunal foraminifera that are adapted for reduced oxygen availability in pore waters (e.g., Bernhard, 1986; Sen Gupta and Machain-Castillo, 1993; Bernhard and Sen Gupta, 1999; Jorissen et al., 2007). Although oxygen and food availability are important limiting variables, we argue that, for at least some epifaunal taxa, the availability of hard substrate is a primary factor that limits their distribution.

Physiological limitations of deep-sea foraminifera have commonly been inferred from specimen distribution patterns collected from available core tops (Kaiho, 1991, 1994, 1999; Jannink et al., 2001; Schmiedl et al., 2003). These inferences have led to commonly held ideas about the oxygen requirements of some foraminiferal taxa. Although the lower limitations of BWO concentrations for epifauna are not yet well understood (Jorissen et al., 2007), several methods use deep-sea foraminiferal species or groups of taxa to assess BWO concentrations. Most of

these methods regard epifauna as indicators of well-oxygenated environments. Species of epifaunal *Cibicidoides*, in particular, are deemed "oxic indicator species" (reviewed in Jorissen et al., 2007).

Despite oxygen-poor conditions in the SCB, epifaunal "oxic indicator" taxa were present at most (12) of the sites observed. Previous studies found *C. wuellerstorfi* in BWO concentrations as low as 71.5 μmol/l in the SCB (Bernhard and Reimers, 1991), and a recent global study that included specimens from the SCB, found living *C. wuellerstorfi* in habitats ranging from ∼2 to 277 μmol/l with abundant specimens below 45 μmol/l (Rathburn et al., 2018). A year-long study off the coast of Oregon found that over one-thousand *C. wuellerstorfi* had colonized hard, artificial substrates in BWO concentrations of ∼11 μmol/l (Burkett et al., 2016). In a colonization study at 4000 m off the coast of California, the epifaunal species *Cibicides lobatulus*, was the most abundant organism attached to glass rods after a year on the seafloor well below the lysocline (Beaulieu, 2001). Results from our study are consistent with these findings, and support the idea that hard substrates that enable epifaunal species to maintain their position at or above the sediment-water interface are an important factor in the distribution of *C. wuellerstorfi*, and probably other epifaunal species. Heterogeneity of habitat plays a critical role in the diversity of benthic fauna, including those within oxygen-poor environments, and we suggest that the availability of surfaces for epifaunal attachment influences habitat heterogeneity and the presence of epifaunal foraminifera in oxygen-stressed conditions.

Vertical distribution patterns observed here are consistent with those reported in previous studies of rose bengal stained foraminifera. As expected, *C. wuellerstorfi* have epifaunal microhabitat preferences with population maxima in the top 1 cm of sediment (Corliss, 1985; Rathburn and Corliss, 1994; Rathburn et al., 1996; **Figure 9**). *H. nipponica* also has population maxima in the top 1 cm of sediment in this study, and together with its planoconvex morphology, indicate that this species is epifaunal (**Figure 9**). Other dominant species, typically classified as infaunal based on their vertical distribution patterns below 1 cm in sediment depth in other regions (*U. peregrina* and *C. laevigata*) also show population maxima in the upper 1 cm, with few or no individuals persisting to the lower sections of the sediment column. *Hoeglundina elegans* had density maxima in the top 1-cm of sediments in this study. It is noteworthy that *Hoeglundina elegans* is typically found in the top 1-cm of sediments and has been characterized as an epifaunal species by some workers (e.g., Corliss, 1985; Rathburn and Corliss, 1994; Rathburn et al., 1996), but has been considered as an infaunal species by others (e.g., Fontanier et al., 2006). Regardless of the microhabitat preference of *H. elegans*, it has previously been associated with high oxygen concentrations and relatively low food availability (Schmiedl et al., 1997; Lutze and Coulbourn, 1984; Koho et al., 2008), therefore it is worth mentioning that this species can adapt to a wide range of environmental conditions. The infaunal designation may have resulted from the common association of this species with oxygen-poor habitats. Nevertheless, to be conservative, we refrained from including this species as an epifaunal taxon. In our study, *H. elegans* was present at all but two sites along the transect, with maximum abundance at site E (1339 m), where it comprised 20% of the total benthic foraminiferal population. *Bolivina spissa*, however, is also regarded as an infaunal taxon and had a population that persisted lower in the sediment column, with population maxima in the 1–1.5 mm section of our cores.

As predicted by the TROX model (Jorissen et al., 1995), infaunal taxa dominate assemblages living at the sites examined, comprising 51–100% of the populations in the >150 μm fraction (**Figure 4**). Thus, despite the heterogeneity of substrates along the transect, infaunal taxa thrive in both the fine- and coarse-grained habitats. Infaunal populations are dominated by *Uvigerina peregrina*, *Cassidulina laevigata*, and *Bolivina spissa*, with varying abundances across the depth transect. Sites with high mean grain size (>500 μm) were dominated by *Cassidulina*

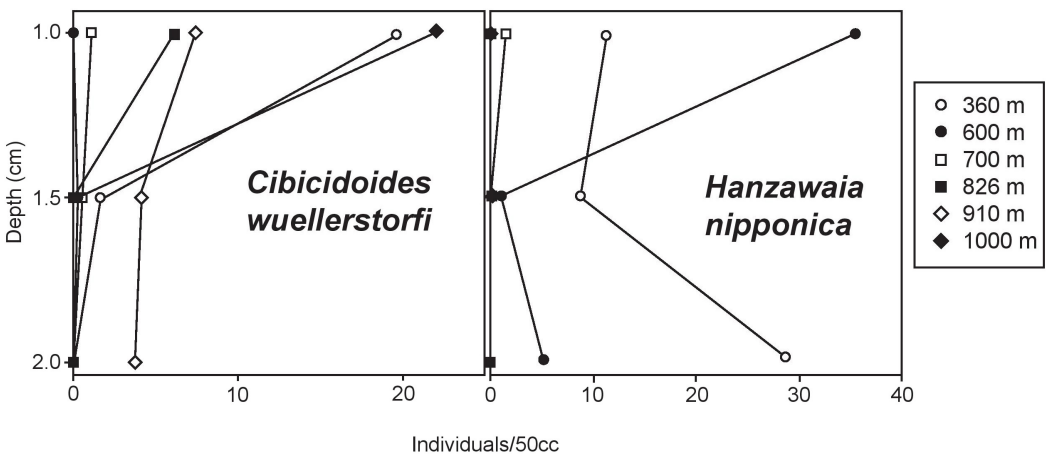

FIGURE 9 | Epifaunal foraminiferal verticle distribution within the top 2 cm of sediments analyzed from multicores at six sites along our transect. Epifaunal microhabitat preferences of *C. wuellerstorfi* are consistent with previous studies. Maximum abundances of *H. nipponica* in the top cm of sediment were observed at most sites, with the exception of 360 m, suggesting that this taxon can also be described as epifaunal.

laevigata and *Uvigerina peregrina*. This differed from the three sites with the lowest mean grain size (<150 μm) which showed an increased presence of less common taxa such as *Nonionella stella*, *Chilostomella oolina*, and *Globobulimina hoeglundi*, which were not observed at other sites with coarser grained substrates. It is possible that in the same way that these coarse grained habitats show an increased abundance of epifaunal taxa, there may be an influence as well on infaunal assemblages.

Results from this study indicate that the epifaunal taxa, *C. wuellerstorfi* and *H. nipponica*, can be abundant in habitats where BWO values fall well below the upper threshold of dysoxia. Epifauna such as these are clearly not restricted to well-oxygenated environments, and our results along with those of other recent studies (Burkett et al., 2016; Rathburn et al., 2018), indicate that the physiological limitations of *C. wuellerstorfi*, and probably other epifauna, should be expanded to include oxygen-poor environments. These results have appreciable consequences for methods that use epifauna for paleo-oxygenation indicators, and provide a greater understanding of the responses of benthic foraminiferal populations to deoxygenation.

CONCLUSION

Our examination of benthic foraminifera living in coarse-grained sediment environments in the SCB revealed elevated densities of epifaunal taxa in oxygen-poor habitats. In dysoxic conditions (21–28 μmol/l), epifaunal taxa comprised as much as 36% of the living (stained) population at the sites with the coarsest mean grain size. Infaunal assemblages varied between sites with different grain size characteristics, suggesting that substrate may also influence some infaunal taxa. Nevertheless, foraminiferal assemblages in our study were dominated by infaunal taxa, such as *Uvigerina* and *Bolivina*, traditionally associated with the supersaturated, unconsolidated mud, characteristic of oxygen-poor habitats, indicating that these taxa are not especially sensitive to substrate type. We suggest that at least some, perhaps many, epifaunal taxa, including *C. wuellerstorfi*, prefer habitats with coarse grains that allow them to remain at or above the sediment-water interface. It is clear that seafloor habitat heterogeneity influences the distribution of deep-sea benthic foraminifera, including in oxygen-poor environments. These results enhance our ability to predict changes in foraminiferal distribution patterns in deoxygenated seafloor habitats of the future, and also point to the need for consideration of substrate characteristics in assessments of ecological tolerances of foraminiferal species.

DATA AVAILABILITY STATEMENT

The datasets generated for this study can be found in the PANGAEA Data Publisher https://doi.pangaea.de/10.1594/PANGAEA.893323.

AUTHOR CONTRIBUTIONS

RV processed samples and specimens and performed the analyses. AR, AB, and RV analyzed the data. WZ measured oxygen microprofiles and calibrated California Borderland oxygen measurements. AR and AB collected the samples, and all of the authors contributed to the writing of the paper.

FUNDING

This material was based in part upon work supported by the National Science Foundation under grant OCE 10-60992 awarded to AR.

ACKNOWLEDGMENTS

The authors extend sincere gratitude to the captain and crew of the *R/V New Horizon* and the scientific party aboard NH1108. They also sincerely appreciate help from Jessica Heck for conducting grain size analyses at LacCore (National Lacustrine Core Facility), Department of Earth Sciences, University of Minnesota-Twin Cities.

SUPPLEMENTARY MATERIAL

The Supplementary Material for this article can be found online at: https://www.frontiersin.org/articles/10.3389/fmars.2018.00344/full#supplementary-material

REFERENCES

Altenbach, A., and Sarnthein, M. (1989). "Productivity record in benthic foraminifera," in *Productivity of the Ocean: Present and Past* eds W. H. Berger, V.S. Smetacek and G. Wefer (New York: John Wiley), 255–269.

Beaulieu, S. (2001). Life on glass houses: sponge stalk communities in the deep sea. *Mar. Biol.* 138, 803–817. doi: 10.1007/s002270000500

Bernhard, J. M. (1986). Characteristic assemblages and morphologies of benthic foraminifera from anoxic, organic-rich deposits; Jurassic through Holocene. *J. Foramin. Res.* 16, 207–215. doi: 10.2113/gsjfr.16.3.207

Bernhard, J. M., and Alve, E. (1996). Survival, ATP pool, and ultrastructural characterization of benthic foraminifera from Drammensfjord (Norway): response to anoxia. *Mar. Micropaleontol.* 28, 5–17. doi: 10.1016/0377-8398(95)00036-4

Bernhard, J. M., Buck, K. R., Farmer, M. A., and Bowser, S. S. (2000). The santa barbara basin is a symbiosis oasis. *Nature* 403:77. doi: 10.1038/47476

Bernhard, J. M., Ostermann, D. R., Williams, D. S., and Blanks, J. K. (2006). Comparison of two methods to identify live benthic foraminifera: a test between Rose bengal and celltracker green with implications for stable isotope paleoreconstructions. *Paleoceanography* 21:PA4210. doi: 10.1029/2006PA001290

Bernhard, J. M., and Reimers, C. E. (1991). Benthic foraminiferal population fluctuations related to anoxia: santa Barbara Basin. *Biogeochemistry* 15, 127–149. doi: 10.1007/BF00003221

Bernhard, J. M., and Sen Gupta, B. K. S. (1999). *Foraminifera of Oxygen-Depleted Environments Modern Foraminifera*. New York, NY: Springer, 201–216.

BjorkstEdt, E. P., Goericke, R., McClatchie, S., Weber, E., Watson, W., Lo, N., et al. (2011). State of the California Current 2010-2011: regionally variable responses

to a strong (but fleeting) La Niña. *California Cooper. Oceanic Fish. Invest. Rep.* 52, 36–68

Blott, S. J., and Pye, K. (2001). GRADISTAT: a grain size distribution and statistics package for the analysis of unconsolidated sediments. *Earth Surf. Process. Landf.* 26, 1237–1248. doi: 10.1002/esp.261

Bograd, S. J., and Lynn, R. J. (2003). Long-term variability in the southern California current system. *Deep Sea Res. Part II Top. Stud. Oceanogr.* 50, 2355–2370. doi: 10.1016/S0967-0645(03)00131-0

Burkett, A. M., Rathburn, A. E., Pérez, M. E., Levin, L. A., and Martin, J. B. (2016). Colonization of over a thousand *Cibicidoides wuellerstorfi* (foraminifera: schwager, 1866) on artificial substrates in seep and adjacent off-seep locations in dysoxic, deep-sea environments. *Deep Sea Res. Part I Oceanogr. Res. Papers* 117, 39–50. doi: 10.1016/j.dsr.2016.08.011

Corliss, B. H. (1985). Microhabitats of benthic foraminifera within deep-sea sediments. *Nature* 314:435. doi: 10.1038/314435a0

Emery, K. O. (1960). *The Sea off Southern California, a Modern Habitat of Petroleum*. 1 Oakland, CA: University of California.

Fontanier, C., Mackensen, A., Jorissen, F. J., Anschutz, P., Licari, L., and Griveaud, C. (2006). Stable oxygen and carbon isotopes of live benthic foraminifera from the bay of biscay: microhabitat impact and seasonal variability. *Mar. Micropaleontol.* 58, 159–183. doi: 10.1016/j.marmicro.2005.09.004

Gooday, A., Levin, L., da Silva, A. A., Bett, B., Cowie, G., Dissard, D., et al. (2009). Faunal responses to oxygen gradients on the Pakistan margin: a comparison of foraminiferans, macrofauna and megafauna. *Deep Sea Res. Part II Top. Stud. Oceanogr.* 56, 488–502. doi: 10.1016/j.dsr2.2008.10.003

Gooday, A. J., Bett, B. J., Escobar, E., Ingole, B., Levin, L. A., Neira, C., et al. (2010). Habitat heterogeneity and its influence on benthic biodiversity in oxygen minimum zones. *Mar. Ecol.* 31, 125–147. doi: 10.1111/j.1439-0485.2009.00348.x

Gooday, A. J., and Jorissen, F. J. (2012). Benthic foraminiferal biogeography: controls on global distribution patterns in deep-water settings. *Annu. Rev. Mar. Sci.* 4, 237–262. doi: 10.1146/annurev-marine-120709-142737

Gorsline, D., Kolpack, R., Karl, H., Drake, D., Thornton, S., Schwalbach, J., et al. (1984). Studies of fine-grained sediment transport processes and products in the California Continental Borderland. *Geological Soc. Lond. Special Public.* 15, 395–415. doi: 10.1144/GSL.SP.1984.015.01.26

Hammer, Ø., Harper, D., and Ryan, P. (2001). *PAST-Palaeontological Statistics*. Available at: www.uv.es/∼pardomv/pe/2001_1/past/pastprog/past.pdf, acessado em.

Helly, J. J., and Levin, L. A. (2004). Global distribution of naturally occurring marine hypoxia on continental margins. *Deep Sea Res. Part I Oceanogr. Res. Papers* 51, 1159–1168. doi: 10.1016/j.dsr.2004.03.009

Hendy, I. L., and Kennett, J. P. (2000). Dansgaard-oeschger cycles and the california current system: planktonic foraminiferal response to rapid climate change in Santa Barbara Basin, ocean drilling program hole 893A. *Paleoceanography* 15, 30–42. doi: 10.1029/1999PA000413

Jannink, N. T., Duijnstee, I., and van der Zwaan, B. (2001). *Foraminiferal Patterns in Two Trophically Different Regions: The Northern Adriatic Sea and The Southern Levantine Basin*. Available at: http://dspace.library.uu.nl/handle/1874/329017

Jorissen, F. J., de Stigter, H. C., and Widmark, J. G. (1995). A conceptual model explaining benthic foraminiferal microhabitats. *Mar. Micropaleontol.* 26, 3–15. doi: 10.1016/0377-8398(95)00047-X

Jorissen, F. J., Fontanier, C., and Thomas, E. (2007). Chapter seven paleoceanographical proxies based on deep-sea benthic foraminiferal assemblage characteristics. *Dev. Mar. Geology* 1, 263–325. doi: 10.1016/S1572-5480(07)01012-3

Kaiho, K. (1991). Global changes of Paleogene aerobic/anaerobic benthic foraminifera and deep-sea circulation. *Palaeogeogr. Palaeoclimatol. Palaeoecol.* 83, 65–85. doi: 10.1016/0031-0182(91)90076-4

Kaiho, K. (1994). Benthic foraminiferal dissolved-oxygen index and dissolved-oxygen levels in the modern ocean. *Geology* 22, 719–722. doi: 10.1130/0091-7613(1994)022<0719:BFDOIA>2.3.CO;2

Kaiho, K. (1999). Evolution in the test size of deep-sea benthic foraminifera during the past 120 my. *Mar. Micropaleontol.* 37, 53–65. doi: 10.1016/S0377-8398(99)00011-0

Kamykowski, D., and Zentara, S. -J. (1990). Hypoxia in the world ocean as recorded in the historical data set. *Deep Sea Res. Part A. Oceanogr. Res. Papers* 37, 1861–1874. doi: 10.1016/0198-0149(90)90082-7

Karstensen, J., Stramma, L., and Visbeck, M. (2008). Oxygen minimum zones in the eastern tropical Atlantic and Pacific oceans. *Prog. Oceanogr.* 77, 331–350. doi: 10.1016/j.pocean.2007.05.009

Keeling, R. F., and Garcia, H. E. (2002). The change in oceanic O2 inventory associated with recent global warming. *Proc. Natl. Acad. Sci. U.S.A.* 99, 7848–7853. doi: 10.1073/pnas.122154899

Koho, K., Langezaal, A., Van Lith, Y., Duijnstee, I., and Van der Zwaan, G. (2008). The influence of a simulated diatom bloom on deep-sea benthic foraminifera and the activity of bacteria: a mesocosm study. *Deep Sea Res. Part I Oceanogr. Res. Papers* 55, 696–719. doi: 10.1016/j.dsr.2008.02.003

Levin, L. (2003). Oxygen minimum zone benthos: adaptation and community response to hypoxia. *Oceanogr. Mar. Biol. Annu. Rev.* 41, 1–45

Loubere, P., and Fariduddin, M. (1999). Benthic foraminifera and the flux of organic carbon to the seabed Modern foraminifera. New York, NY: Springer, 181–199.

Lutze, G. F., and Coulbourn, W. T. (1984). Recent benthic foraminifera from the continental margin of northwest Africa: community structure and distribution. *Mar. Micropaleontol.* 8, 361–401. doi: 10.1016/0377-8398(84)90002-1

Lutze, G., and Thiel, H. (1989). Epibenthic foraminifera from elevated microhabitats; *Cibicidoides wuellerstorfi* and *Planulina ariminensis*. *J. Foraminiferal Res.* 19, 153–158. doi: 10.2113/gsjfr.19.2.153

McCorkle, D. C., Keigwin, L. D., Corliss, B. H., and Emerson, S. R. (1990). The influence of microhabitats on the carbon isotopic composition of deep-sea benthic foraminifera. *Paleoceanography* 5, 161–185. doi: 10.1029/PA005i002p00161

Meier, H. M., Andersson, H. C., Eilola, K., Gustafsson, B. G., Kuznetsov, I., Müller-Karulis, B., et al. (2011). Hypoxia in future climates: a model ensemble study for the Baltic Sea. *Geophys. Res. Lett.* 38:L24608. doi: 10.1007/s13280-013-0475-6

Mullins, H. T., Thompson, J. B., McDougall, K., and Vercoutere, T. L. (1985). Oxygen-minimum zone edge effects: evidence from the central California coastal upwelling system. *Geology* 13, 491–494. doi: 10.1130/0091-7613(1985)13<491:OZEEEF>2.0.CO;2

Murray, J. W., and Bowser, S. S. (2000). Mortality, protoplasm decay rate, and reliability of staining techniques to recognize 'living'foraminifera: a review. *J. Foraminiferal Res.* 30, 66–70. doi: 10.2113/0300066

Nelson, J. R., Beers, J. R., Eppley, R. W., Jackson, G. A., McCarthy, J. J., and Soutar, A. (1987). A particle flux study in the Santa Monica-San Pedro Basin off Los Angeles: particle flux, primary production, and transmissometer survey. *Cont. Shelf. Res.* 7, 307–328. doi: 10.1016/0278-4343(87)90071-9

Otto, G. H. (1933). Comparative tests of several methods of sampling heavy mineral concentrates. *J. Sediment. Res.* 3, 30–39. doi: 10.1306/D4268E3C-2B26-11D7-8648000102C1865D

Perez-Cruz, L. L., and Machain-Castillo, M. L. (1990). Benthic foraminifera of the oxygen minimum zone, continental shelf of the Gulf of Tehuantepec, Mexico. *J. Foraminiferal Res.* 20, 312–325. doi: 10.2113/gsjfr.20.4.312

Phleger, F. B., and Soutar, A. (1973). Production of benthic foraminifera in three east Pacific oxygen minima. *Micropaleontology* 19, 110–115. doi: 10.2307/1484973

Rathburn, A. E., and Corliss, B. H. (1994). The ecology of living (stained) deep-sea benthic foraminifera from the Sulu Sea. *Paleoceanography* 9, 87–150. doi: 10.1029/93PA02327

Rathburn, A. E., Corliss, B. H., Tappa, K. D., and Lohmann, K. C. (1996). Comparisons of the ecology and stable isotopic compositions of living (stained) benthic foraminifera from the Sulu and South China Seas. *Deep Sea Res. Part I Oceanogr. Res. Pap.* 43, 1617–1646. doi: 10.1016/S0967-0637(96)00071-4

Rathburn, A.E., Willingham, J., Ziebis, W., Burkett, A. M., Corliss, B. H. (2018). A New biological proxy for deep-sea paleo-oxygen: pores of epifaunal benthic foraminifera. *Sci. Rep.* 8:9456 doi: 10.1038/s41598-018-27793-4

Reichart, G. -J., Lourens, L., and Zachariasse, W. (1998). Temporal variability in the northern arabian sea oxygen minimum zone (OMZ) during the last 225,000 years. *Paleoceanography* 13, 607–621. doi: 10.1029/98PA02203

Revsbech, N. P., Christensen, P. B., Nielsen, L. P., and Sørensen, J. (1989). Denitrification in a trickling filter biofilm studied by a microsensor for oxygen and nitrous oxide. *Water Res.* 23, 867–871. doi: 10.1016/0043-1354(89)90011-0

Revsbech, N. P., and Jørgensen, B. B. (1986). "Microelectrodes: their use in microbial ecology," in *Advances in Microbial Ecology*. K. C. Marshall (New York, NY: Springer), 293–352.

Sarmiento, J. L., Hughes, T. M., Stouffer, R. J., and Manabe, S. (1998). Simulated response of the ocean carbon cycle to anthropogenic climate warming. *Nature* 393:245. doi: 10.1038/30455

Schmiedl, G., Mackensen, A., and Müller, P. J. (1997). Recent benthic foraminifera from the eastern South Atlantic Ocean: dependence on food supply and water masses. *Mar. Micropaleontol.* 32, 249–287. doi: 10.1016/S0377-8398(97)00023-6

Schmiedl, G., Mitschele, A., Beck, S., Emeis, K. -C., Hemleben, C., Schulz, H., et al. (2003). Benthic foraminiferal record of ecosystem variability in the eastern Mediterranean Sea during times of sapropel S 5 and S 6 deposition. *Palaeogeogr. Palaeoclimatol. Palaeoecol.* 190, 139–164. doi: 10.1016/S0031-0182(02)00603-X

Schönfeld, J. (2002). A new benthic foraminiferal proxy for near-bottom current velocities in the Gulf of Cadiz, northeastern Atlantic Ocean. *Deep Sea Res. Part I Oceanogr. Res. Papers* 49, 1853–1875. doi: 10.1016/S0967-0637(02)00088-2

Sen Gupta, B. K. S., and Machain-Castillo, M. L. (1993). Benthic foraminifera in oxygen-poor habitats. *Mar. Micropaleontol.* 20, 183–201. doi: 10.1016/0377-8398(93)90032-S

Silva, K. A., Corliss, B. H., Rathburn, A. E., and Thunell, R. C. (1996). Seasonality of living benthic foraminifera from the san pedro basin, California Borderland. *Oceanogr. Literat. Rev.* 9:916.

Stott, L.D., Hayden, T.P., and Griffith, J. (1996). Benthic foraminifera at the Los Angeles county whites point outfall revisited. *J. Foraminiferal Res.* 26, 357–368. doi: 10.2113/gsjfr.26.4.357

Stramma, L., Johnson, G. C., Sprintall, J., and Mohrholz, V. (2008). Expanding oxygen-minimum zones in the tropical oceans. *science* 320, 655–658. doi: 10.1126/science.1153847

Conflict of Interest Statement: The authors declare that the research was conducted in the absence of any commercial or financial relationships that could be construed as a potential conflict of interest.

frontiers in Marine Science

ORIGINAL RESEARCH
published: 18 December 2018
doi: 10.3389/fmars.2018.00482

Effect of Marine Hypoxia on Baltic Sea Cod *Gadus morhua*: Evidence From Otolith Chemical Proxies

Karin E. Limburg[1,2]* *and Michele Casini*[2]

[1] Department of Environmental and Forest Biology, State University of New York College of Environmental Science and Forestry, Syracuse, NY, United States, [2] Institute of Marine Research, Department of Aquatic Resources, Swedish University of Agricultural Sciences, Lysekil, Sweden

The Baltic Sea contains the world's largest anthropogenic deoxygenated zone, with increasing episodes and areal extent of hypoxia/anoxia. Atlantic cod in the Baltic has suffered a loss in condition which has been attributed mainly to hypoxia. Otoliths, the aragonitic structures that form part of the hearing/balance system in fishes, accumulate Mn in the presence of hypoxia and other reducing environments. Otoliths grow over the lifetime of fishes, and thus life-long records of hypoxia exposure exist for each individual fish. However, otolith Mn/Ca ratios are also sensitive to growth effects. We tested a new proxy to at least partially account for growth: Mn/Mg, since Mg levels reflect metabolic activity but not hypoxia. This and other elemental proxies were parsed annually from the otoliths to reconstruct lifetime histories of mean, maximum, and cumulative values of this proxy as well as others (Sr/Ca) that inform us about salinity conditions. We analyzed cod from five different time periods: Neolithic (4500 YBP, a normoxic baseline), 1980s, 1990s, 2000s, and 2010s – under different hypoxia intensities, assessing fish growth and condition in relation to hypoxia experience recorded by otolith proxies. Fish growth decreased with increasing hypoxia exposure; condition at capture (measured by Fulton's K index) showed a strongly positive relation to growth indexed by magnesium (Mg/Ca). We conclude that cod otolith chemistry proxies not only inform about the hypoxia, growth, and metabolic status of cod, retrospectively throughout life, but also reflect the worsening situation for cod in the Baltic.

Keywords: Baltic cod, hypoxia, otolith microchemistry, manganese, magnesium, growth effects

OPEN ACCESS

Edited by:
Arthur Capet,
MAST - University of Liège, Belgium

Reviewed by:
William Gerald Ambrose Jr.,
Coastal Carolina University,
United States
Ewan Hunter,
Centre for Environment, Fisheries and Aquaculture Science (CEFAS),
United Kingdom

***Correspondence:**
Karin E. Limburg
klimburg@esf.edu

Specialty section:
This article was submitted to Global Change and the Future Ocean, a section of the journal Frontiers in Marine Science

Received: *26 July 2018*
Accepted: *29 November 2018*
Published: *18 December 2018*

Citation:
Limburg KE and Casini M (2018) Effect of Marine Hypoxia on Baltic Sea Cod Gadus morhua: Evidence From Otolith Chemical Proxies. Front. Mar. Sci. 5:482. doi: 10.3389/fmars.2018.00482

INTRODUCTION

Hypoxia, or the occurrence of low oxygen levels in water, is spreading rapidly worldwide (Breitburg et al., 2018). Long recognized as a result of biochemical oxygen demand from organic pollution, hypoxia and the larger phenomenon of deoxygenation (loss of oxygen) are strongly affected by warming waters due to climate change. Although responses to hypoxia by fish and fisheries in many systems have been complex and thus difficult to interpret (Breitburg et al., 2009), there is increasing evidence that fishes exposed to hypoxia experience loss of habitat (a.k.a. habitat compression, Eby and Crowder, 2002; Diaz and Rosenberg, 2008; Stramma et al., 2012; Casini et al., 2016b) at times with concomitant declines in physical condition (e.g., Casini et al., 2016b).

The Baltic Sea ranks among the largest marine areas to have increased in hypoxic intensity and extent, from 5,000 to >60,000 km^2 in its major basins over the past century (Carstensen et al., 2014). Freshwater inflows from the drainage basin contain nutrients that stimulate production (Hong et al., 2017), eventually resulting in microbial respiration that depletes oxygen (Conley et al., 2009). Major inflows of oxygenated seawater through the Danish Straits provide temporary relief, but reoxygenated episodes have in the past two decades been rare or of shorter duration than anticipated, due to complex mixing and stagnation (Conley et al., 2009; Schmale et al., 2016). Consequently, as warming continues, Baltic hypoxia is likely to continue and intensify, with increased areas of hypoxic, anoxic, and sulfidic waters.

Of the fish species present in the Baltic Sea, the Eastern Baltic cod (*Gadus morhua*) (hereafter referred to as Baltic cod) is arguably the most affected by this situation. A demersal (near-bottom dwelling) apex fish predator, Baltic cod require salinities ≥11 for successful spawning (Nissling and Westin, 1997), typically at depths >80 m in the brackish Baltic proper. Increasingly, these depths are subject to seasonal hypoxia, and the volume available to successful reproduction has diminished (cf. Köster et al., 2005; Plikshs et al., 2015). Additionally, suitable nursery and adult habitats have declined by 30% (Casini et al., 2016b; Hinrichsen et al., 2017). Beyond hypoxia *per se*, cod have undergone other ecological changes over the past ca. 40 years, such that diet shifted from one dominated by benthos in the 1970s and 1980s to one dominated by pelagic species, most recently sprat (*Sprattus sprattus*; cf. Pachur and Horbowy, 2013). Today it appears that a combination of reduced prey availability, increased parasite burdens, and hypoxia have contributed to a worsening Baltic cod population status (Eero et al., 2015; Casini et al., 2016b). Indeed, Baltic cod may represent one of the most severely impacted fish populations documented to date (cf. Breitburg et al., 2009; Altenritter et al., 2018).

Exploited fish populations (stocks) are subject to regular status assessments, so that appropriate fishing exploitation levels can be set. Stock assessments are usually based on age-based demographic characteristics. Fish age is normally determined by counting pairs of opaque and translucent rings in otoliths, which are aragonitic ($CaCO_3$), incrementing structures inside fish heads. Part of the hearing and balance system in modern fishes, otoliths grow as the fish grows, providing a unique history for each individual (Campana and Neilson, 1985); and over 8×10^5 otoliths are aged annually for stock assessments by major fisheries labs around the world (Campana and Thorrold, 2001). Baltic cod otoliths, always somewhat difficult to age (Hüssy, 2010), became increasingly unreadable through the 2000s (Hüssy et al., 2016). In 2014, the stock assessment failed, due in great part to large uncertainties and inconsistencies in age determination (International Council for the Exploration of the Seas [ICES], 2014; Eero et al., 2015; Hüssy et al., 2016).

Besides tracking age and thus growth rates, otoliths also take up minor and trace elements as well as isotopes that can be interpreted in the context of experienced environment, fish physiology, or a combination thereof (Campana, 1999; Campana and Thorrold, 2001). Within the field of otolith research, questions of the relative influence of internal vs. external controls on otolith chemistry are topics of current interest (e.g., Sturrock et al., 2015; Grammer et al., 2017; Izzo et al., 2018). Increasingly, investigations of lifetime variations in otolith chemistry, either through taking transects of points along an otolith growth axis, or 2-D mapping of elemental concentrations (Limburg and Elfman, 2017), open up new and powerful insights into the complexities of fish life history (e.g., Campana and Thorrold, 2001; Elsdon et al., 2008; Pracheil et al., 2014).

Limburg et al. (2011, 2015) identified the trace element manganese, in ratio to calcium (Mn/Ca), as a potentially reliable proxy for hypoxia, regardless of salinity. Trace elements typically enter otoliths in dissolved form after uptake via the gills (Campana, 1999); and the dissolved forms of manganese are reduced (Trouwborst et al., 2006; Reddy and DeLaune, 2008). Nevertheless, incorporation of Mn into otoliths is also sensitive to growth (Limburg et al., 2011, 2015). In the present paper, we develop a new proxy that partially corrects for growth, based on evidence that another trace element, magnesium, reflects metabolic activity (Limburg et al., 2018). Here, we test the efficacy of different proxies (annual Mn/Ca, annual Mn/Mg, and lifetime-cumulative versions of same), as well as Mg/Ca, to document (1) exposure to hypoxia, (2) correlations to fish condition, a measure that is made only once – at the time of fish capture, and (3) possible effects of hypoxia on growth. We also develop a heuristic model as a dynamic hypothesis, that manganese uptake (and hence, the proxies) is a function of both exogenous (biogeochemical) and endogenous (physiological) controls.

MATERIALS AND METHODS

Baltic Sea cod otoliths were collated from several sources (**Table 1**). A majority came from the archives of the Department of Aquatic Resources, Swedish University of Agricultural Sciences (SLU, previously the research division of the Swedish Board of Fisheries until 2011). Of this collection, most ($N = 214$) were chosen originally to follow particular year-classes (1985, 1988, 1991, and 2005) as they aged; another 108 were selected to contrast condition factor (high or low); 11 collected in the Åland Sea in the northern Baltic proper in 2013; and four were collected in 2017, thus extending the time span of observation. Otoliths were aged using a combination of visual and chemical markers of seasonality (Heimbrand et al., unpublished), identifying contrasting "peaks" and "valleys" demarcating seasons; for an example, see Mg/Ca seasonal variations in Limburg et al. (2018). Finally, 10 well-preserved otoliths from a previous study of Neolithic cod (Limburg et al., 2008) were also analyzed, to examine otolith chemistry during a previous, hypoxia-free baseline period (Limburg et al., 2011). Although most of the modern material came from the southern Baltic proper (subdivision 25; **Figure 1**), some samples also came from the central and northern parts of the Baltic proper (subdivisions 26–29). The Neolithic otoliths came from subdivision 27 (**Figure 1**).

TABLE 1 | Otolith samples used in this study.

Location of collection	Year of collection	Quarter	ICES SD Area	SLU est. age	*SD*	*SE*	Est. age (this study)	*SD*	*SE*	*N*	Remarks
Selected by putative year class											
Southern Baltic proper	1991	4	25, 26	6	–	–	4.17	0.41	0.17	6	Putative year class 1985
Central Baltic proper	1991	4	27, 28	6	–	–	5	1.27	0.52	6	Putative year class 1985
Southern Baltic proper	1988	4	25	0	–	–	0	–	–	3	Year class 1988
Southern Baltic proper	1989	4	25	1	–	–	1	–	–	30	Year class 1988
Southern Baltic proper	1990	4	25	2	–	–	2.25	0.44	0.09	24	Putative year class 1988
Southern Baltic proper	1995	1, 4	25	7	–	–	6.57	0.53	0.20	7	Putative year class 1988
Central Baltic proper	1995	1	27	7	–	–	6.15	0.69	0.17	17	Putative year class 1988
(unknown)	1993	3		2	–	–	1.95	0.22	0.05	20	Putative year class 1991
Southern Baltic proper	1996	3,4	25	5	–	–	4.39	1.04	0.24	18	Putative year class 1991
(Southern Baltic proper)	2005	4	(25?)	0	–	–	0.2	0.35	0.07	22	Putative year class 2005
Southern Baltic proper	2006	4	25	1.20	0.48	0.10	1.73	0.83	0.18	22	Putative year class 2005
Southern Baltic proper	2007	4	25	2	–	–	3	0.89	0.19	21	Putative year class 2005
Southern Baltic proper	2010	1, 2, 3	25	5	–	–	5	0.69	0.16	18	Putative year class 2005
Selected to contrast condition											
Southern Baltic proper	1990–93	1	25	4	–	–	4.33	0.50	0.17	9	
Southern Baltic proper	1994–95	1	25	4	–	–	4.45	0.99	0.18	30	
Southern Baltic proper	2000–05	1	25	4	–	–	3	–		3	
Southern Baltic proper	2010–13	1	25	4	–	–	4.97	1.36	0.26	28	
Southern Baltic proper	2014–15	1	25	4	–	–	4.89	1.43	0.23	38	
Miscellaneous											
Northern Baltic proper	2013	3	29	4.18	1.33	0.40	4	1.10	0.33	11	Åland Sea
Southern Baltic proper	2017	1	25	3.5	2.12	1.50	5	1.41	1.00	2	
Central Baltic proper	2017	1	27	3	1.41	1.00	2.5	0.71	0.50	2	
Neolithic	4500 YBP	–	27	–	–	–	3.80	0.79	0.25	10	Archaeological site "Ajvide" on Gotland
Total										347	

Note: ICES SD Area = ICES Subdivision Area, see also ***Figure 1A****.*

Fish total length (L, mm) and fresh total weight (W, g) data accompanied the modern otoliths, so a measure of condition (Fulton's K) could be calculated as:

$K = W/(L^3) \times 10^6$.

In some cases, fish samples were obtained from commercial fisheries that gutted fish prior to landing. For those, correction factors (Casini et al., 2016a) were applied. For purposes of this analysis, K was grouped into two categories: low ($K < 9$) and high ($K \geq 9$).

Otolith Preparation and Chemical Analysis

Otoliths were cleaned prior to archiving. The experimental otoliths were first marked to identify the core region (seen on the otolith surface as a "V" notch), then embedded in a clean epoxy resin (EpoFix,®Struers) (**Supplementary Figure S-1**). Transverse sections were prepared by cutting the shortest axis approximately 0.5–1 mm on each side of the core (**Supplementary Figure S-1**), which was subsequently thinned and polished down with a series of grinding papers (60, 30, 15, 12, 9, 3, and 1 micron), creating a section 0.2–0.5 mm thick and exposing the core region. The core (primordium) in cod is very small, <100 microns, so care must be taken to locate it. Once prepared, otolith sections were cleaned with 95% ethanol and rinsed in deionized water, then mounted on petrographic slides with double-stick tape.

Otolith chemistry was analyzed by laser ablation inductively coupled plasma mass spectrometry (LA-ICPMS), mainly at the Analytical and Technical Services laboratory at SUNY-ESF, United States; five otoliths were analyzed at Lund University, Sweden (described in Limburg et al., 2018). A 198-nm laser system (ESI) ablated material from the exposed otolith surface along a prescribed transect along the ventro-dorsal axis. That material was transported via a carrier gas (ultra high purity He, 800 mL/min) into a PerkinElmer Elan DRc quadrupole mass spectrometer. Continuous transects were taken, mostly from ca. 300 microns from the core on the ventral side, through the core, and out along the dorsal axis (**Supplementary Figure S-1**), or else complete "palindromic transects" running from the ventral edge, over the core, and out the dorsal axis. The track width (spot size) was 100 μm, and travel speed was 5 μm/s (10 Hz, 90% power). This spot size and ablation speed did some averaging across growth zones, but was deemed acceptable as it captured the dynamics of the hypoxia proxies and other elements.

Isotopes monitored included ^{24}Mg, ^{26}Mg, ^{31}P, ^{43}Ca and ^{44}Ca (44 was a check on 43), ^{55}Mn, ^{63}Cu, ^{64}Zn, ^{88}Sr, ^{127}I, and ^{138}Ba. Briefly, Sr and Ba provide information on salinity and onshore–offshore habitat use, albeit with some confounding with temperature (Sr) and upwelling (Ba) influences; Mn and I are proxies for hypoxia (Lu et al., 2010; Limburg et al., 2015), Mg and P are under physiological control and help to identify seasonality of otolith growth; and Cu and Zn, typically elevated in the cores of cod and flounder otoliths (KL, unpublished observation), help to check accurate identification of the core. Pelletized carbonate standards [MACS-3, Wilson et al., 2008; MAPS-4 (USGS Geochemical Reference Materials), and an in-house standard made of crushed otoliths (Limburg et al., 2011)] were used for calibration and instrument drift corrections. Precision typically ranged from 5 to 15% on the standards, but re-running ablation tracks on otoliths produced nearly identical results.

Data Processing

Elemental concentrations (ppm) were expressed as ratios to Ca to correct for variations in the matrix. Mg/Ca ratios were calculated with ^{24}Mg; $^{26/24}$Mg ratios were calculated with background-subtracted, drift-corrected data for both isotopes, calibrated to reported average percentages of each isotope (Catanzaro et al., 1966).

We used the otolith chemistry to aid in identifying the locations of annuli (seasonal growth checks due to winters; Heimbrand et al., unpublished) on the otoliths. We then used Campana's "biological intercept" method (Campana, 1990) to back-calculate lengths-at-age for each fish, setting hatching length L_0 = 2.5 mm and otolith diameter at hatch O_0 = 50 microns. Otolith chemical data were parsed both annually (i.e., concentrations and ratios were calculated within annual growth zones) and averaged over the entire "life history transect" of the individual, using data collected on the dorsal axis, which provides the most detail. In addition, data from the otolith core region (inner 50 μm) and outer edge (200 μm) were collected.

A variety of potential hypoxia proxies were tested on the annual data. Mean Mn/Ca within annual growth zones, and means × growth zone widths, served as point and cumulative measures of hypoxia exposure within any given year. Cumulative Mn/Ca, summed over years of life, quantified the lifetime exposure up to any given age. To assess duration of exposure to hypoxia, all the annual means were subjected to statistical analysis (**Supplementary Table S-1**); we defined hypoxia exposure as exceeding the median value (across all fish) within a given age-class. Within any given year of otolith growth, the distance along the analysis transect corresponding to exceedance of the threshold, divided by that year's otolith growth increment, was used as a measure of the duration of exposure.

However, Mn/Ca is also sensitive to growth rate (Limburg et al., 2011, 2015). To explore this, we developed a simple, conceptual model (**Figure 2A**) using the platform STELLA®(model details are in the **Supplementary Information**). A bioenergetics module keeps track of the consumption and assimilation of food, respiration, and net growth, all of which are temperature-dependent. A biogeochemistry module simulates organic matter decomposition and the sequential reduction of oxygen, nitrate, and manganese; manganese oxidation produces dissolved Mn^{2+}, which can be taken up in otoliths. Otolith growth was modeled as a function of net metabolic activity, and Mn uptake/incorporation as the product of otolith growth and environmentally available Mn. The model uses realistic values, but is not calibrated with actual data on Baltic cod or on Baltic Sea biogeochemistry. The point of the model is

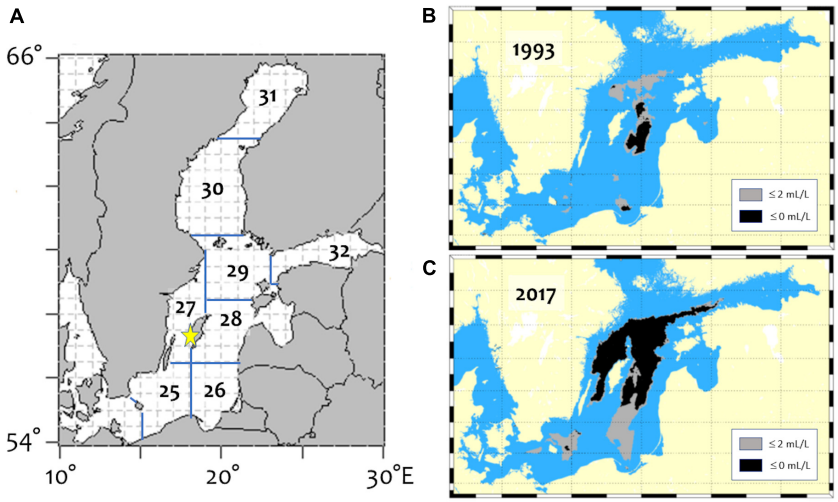

FIGURE 1 | Maps of the Baltic Sea, showing **(A)** ICES subdivisions; **(B)** lowest areal extent of hypoxia/anoxia on record since 1960, in 1993; and **(C)** areal extent of hypoxia/anoxia in 2017, typical of the worsening conditions. Star on **(A)** shows the location of Neolithic cod otolith remains.

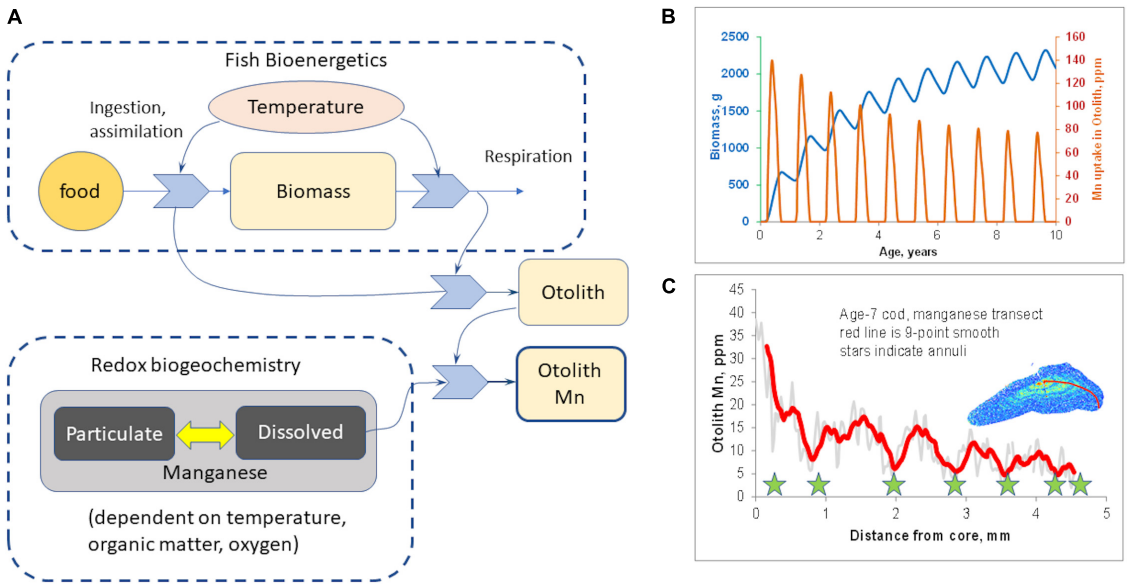

FIGURE 2 | Hypothesized mechanism of otolith manganese incorporation. **(A)** Schematic of conceptual model postulating mechanism of manganese incorporation into otoliths (see **Supplementary Information** for model details). Otolith Mn is a function both of fish growth and of availability of dissolved Mn (i.e., reduced Mn^{2+}). **(B)** Model output, simulating 10 years of growth where seasonal biogeochemistry is identical every year, but otolith Mn declines due to decrease in fish growth. **(C)** Otolith Mn in a 7-year-old Baltic cod, showing similar seasonal increases in summer, but overall decline due to natural decrease in growth with age.

simply to illustrate that both internal and external factors are involved.

We further note that magnesium uptake is growth-rate sensitive (Grammer et al., 2017; Limburg et al., 2018) but is independent of hypoxia. Therefore, we use Mn in ratio to Mg (Mn/Mg) as a new proxy to correct, at least in part, for growth effects on Mn uptake. We compiled similar statistics on annual and cumulative Mn/Mg to test for duration of exposure both annually and for lifetime, accumulative effects of hypoxia exposure.

Data were inspected for normality and analyzed, as appropriate, with continuous methods (regression, multiple regression), repeated measures ANOVA to account for possible within-subject autocorrelation, and two-way ANOVA to test for effects of age and other categorical variables (decade, categorized hypoxia exposure) on various proxies.

Hypotheses Tested

We use the otolith chemical data to address the following questions:

- Do hypoxia proxies track independent indices of hypoxia (e.g., areal or volumetric extent) over the past four decades?
- Does otolith Mg/Ca, our proxy for metabolic activity, correlate with condition factor?
- Do cod exposed to greater hypoxia show evidence of reduced growth?

RESULTS

Conceptual Model

The conceptual model (**Figure 2A**) was run to simulate 10 years of growth, but with the same pattern of seasonal hypoxia in every year. The model output (**Figure 2B**) shows that even with constant annual patterns of hypoxia, seasonal Mn incorporation declines as fish grow larger and their growth rate slows down asymptotically. This provides a conceptual null model if the environmental dynamics were identical year by year, and is qualitatively similar to what we have often observed in otolith Mn/Ca transects (for example, **Figure 2C**).

Annual Otolith Chemistry

Continuous "life history transects" along the major growth axes (ventro-dorsal) revealed great individual variability (cf. **Supplementary Figure S-2**). Nevertheless, some patterns in Mn/Ca were recognizable as associated with particular conditions. For example, we often observed a sudden drop in otolith Mn/Ca in the early 1990s (**Figure 3**), when major inflows of oxygenated North Sea water produced several years of low hypoxia. When hypoxia was moderately low, cod otolith Mg/Ca would often track Mn/Ca (**Figure 4**, top panel), but during episodes of apparently intense, summertime hypoxia as "recorded" in Mn/Ca ratios, the Mg/Ca de-coupled from the ordinary seasonal tracking with Mn/Ca, and instead declined (**Figure 4**, bottom panel). High episodes of hypoxia exposure as recorded in otoliths were more frequent after 2010 (**Figure 4**).

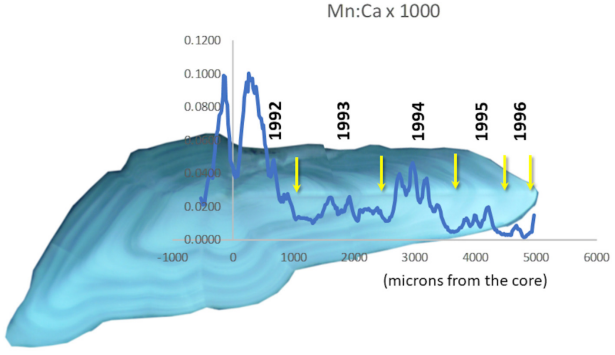

FIGURE 3 | Transect of Mn/Ca overlaid on an otolith from a cod that lived through a period of very low hypoxia in the Baltic. Annuli are marked with yellow arrows. Hypoxia reached a minimum in 1993 (**Figure 1B**).

Do Hypoxia Proxies Track Independent Indices of Hypoxia Over the Past Four Decades?

Our collection of modern cod data spans 30 years, from 1986 to 2016. Comparing hypoxia proxies in otoliths to indices of hypoxia intensity (i.e., hypoxic volume or bottom area in the Baltic), the proxy that best matches hypoxic intensity is the within-year Mn/Mg duration above the thresholds (**Figure 5**). The proxy drops in the early 1990s, and rises from 2003, worsening steadily into the 2010s (**Figure 5A**), and captures much of the dynamic of the volume of hypoxic water (**Figure 5B**), particularly when the otolith proxy data are lagged 1 year back as shown here. When this lagged proxy is plotted as a function of hypoxia volume, it may be visualized in two periods (**Figure 5C**): a period encompassing 1986–1995 when hypoxia was moderate to declining, and the 2000s–2010s, when hypoxia increased continuously. Our otolith data from 2003 to 2016 show a rise in hypoxia proxy that appears to be steeper than the corresponding increasing hypoxia volume. Our data appear to capture responses to major inflows (2003 and 2014) that brought in oxygenated water. Finally, we note that our hypoxia proxy does not track hypoxic bottom areal extent as well as it does hypoxic volume (areal extent-otolith proxy R^2 = 0.81 for period 1985–1994 and R^2 = 0.003 for period 2003–2016; volume-otolith proxy R^2 = 0.86 for period 1985–1994 and R^2 = 0.45 for period 2003–2016; **Figure 5C**).

Does Otolith Mg/Ca, Our Proxy for Metabolic Activity, Correlate With Condition Factor?

Factorial analysis of variance (ANOVA) of Mg/Ca by age and Fulton condition group (low < 9, vs. high ≥ 9) produced striking results (**Figure 6**). Low condition fish had less otolith Mg/Ca than high condition fish, and the gap between low and high tended to increase with fish age (**Figure 6A**). Repeated measures ANOVA yielded similar results (p = 0.011). As a result, the difference in lifetime cumulative Mg/Ca was also significant between Fulton groups and increased with age (**Figure 6B**). By contrast, a similar ANOVA performed with Mn/Ca as the dependent variable showed a significant decline with age, but not significant difference between Fulton groups.

Do Cod Exposed to Greater Hypoxia Show Evidence of Reduced Growth?

Back-calculated lengths at age (**Figure 7**) confirmed that growth was highest during the early 1990s, when hypoxia extent was lowest. Conversely, growth was poorest during the current decade of the 2010s, when hypoxia extent has been large and, in particular, anoxia has been increasing (Hansson et al., 2017).

We also tested directly whether growth (length at age) correlated to hypoxia exposure within a year. We grouped the hypoxia duration (fraction of an annual growth zone above the Mn/Mg thresholds) into four categories: $\leq$25%, $\leq$50%, $\leq$75%, and $\leq$100%. With the exception of the Age-0 (young-of-year) group, length at age declined with increasing annual hypoxia

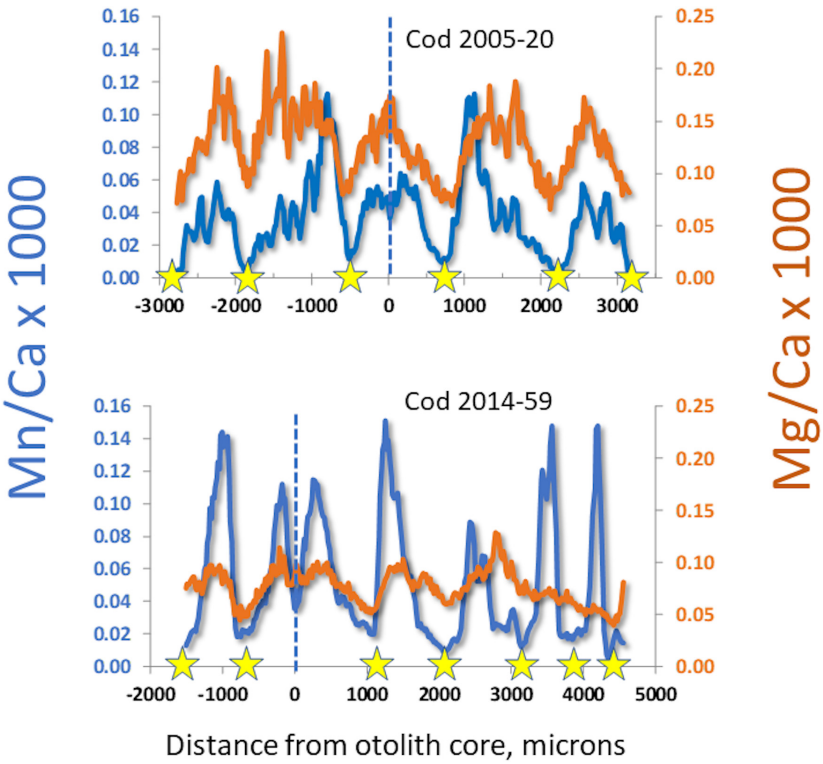

FIGURE 4 | Comparison of manganese and magnesium dynamics in otoliths from cod having experienced different lifetime hypoxia levels. Stars mark winters, dashed lines mark the otolith cores. Top: edge-to-edge otolith transect in a period with good oxygen conditions, with seasonal variations of Mn/Ca and Mg/Ca in synchrony. Bottom: partial otolith transect in a cod having experienced chronic seasonal hypoxia; note that Mn/Ca is higher and Mg/Ca lower than in top panel, and that magnesium begins to de-couple from seasonal patterns in third year.

exposure (**Figure 8**). In Age-0 fish, length was highest (117.7 mm) in the ≤50% group, and second highest (112.2 mm) in the ≤25% group. By Age-3, the size disparity between the least and most hypoxia-exposed fish was 38.6% (547.9 vs. 395.3 mm, respectively; **Figure 8**). The implication here is that, across all samples, growth was reduced as hypoxia exposure increased.

We examined Sr/Ca values as a proxy for salinity (but see caveats in the section "Discussion"). First-year Sr/Ca (×1000) values are lowest and are likely indicative of nearshore nursery habitats (Limburg et al., 2011), and increase as the fish begin to move into deeper, saltier water. ANOVA of Sr/Ca as a function of age and within-year hypoxia exposure revealed a complex response, but from Age-3 onward, Sr/Ca was highest in the 75–100% duration of hypoxia exposure category. Comparing just the lowest and highest exposure quantiles, Sr/Ca first increased, then decreased, for the 0–25% group, but increased linearly for the 75–100% group (**Figure 9**).

Lifetime, Core, and Outer Edge Otolith Data Analysis

Lifetime data, averaged over the entire otolith transects, did not reveal as many insights, and generally produced noisy relationships. For example, we tested whether an inverse relationship existed between lifetime mean Mn/Ca (our original hypoxia proxy) or the newer proxy (Mn/Mg) and I/Ca; neither of them produced significant results. Nevertheless, some variations are apparent when grouping element/Ca ratios by time period: Neolithic times vs. the decades of 1980s, 1990s, 2000s, and 2010s (**Supplementary Figure S-2**). We note that the Neolithic otolith chemistry shows much lower Mn/Ca and Mn/Mg, so much lower than today's cod otoliths that we could not use them as a hypoxia baseline – if we had, then all of the modern cod would exceed the threshold most of the time. Additionally, Mg/Ca was on par with modern fish, Sr/Ca was elevated as expected due to the saltier conditions of the past, and I/Ca was elevated (**Supplementary Figure S-2**).

Analyses of hypoxia proxies on the outermost 200 microns did not correlate with either growth rate or Fulton condition factor. Regression analysis of core chemistry produced a significant ($p < 10^{-4}$), if highly noisy ($R^2 = 0.014$), inverse relationship between I/Ca and Mn/Ca (I/Ca = 0.0023 – 0.0099 × Mn/Ca). Additionally, a positive relationship existed between core Cu/Ca and Zn/Ca (Zn/Ca = 0.0046 + 0.74 × Cu/Ca, $R^2 = 0.19$, $p < 10^{-6}$).

DISCUSSION

Analysis of annual data, parsed on laser transects along the dorsal axis of Baltic cod otoliths, demonstrated complex, individualistic

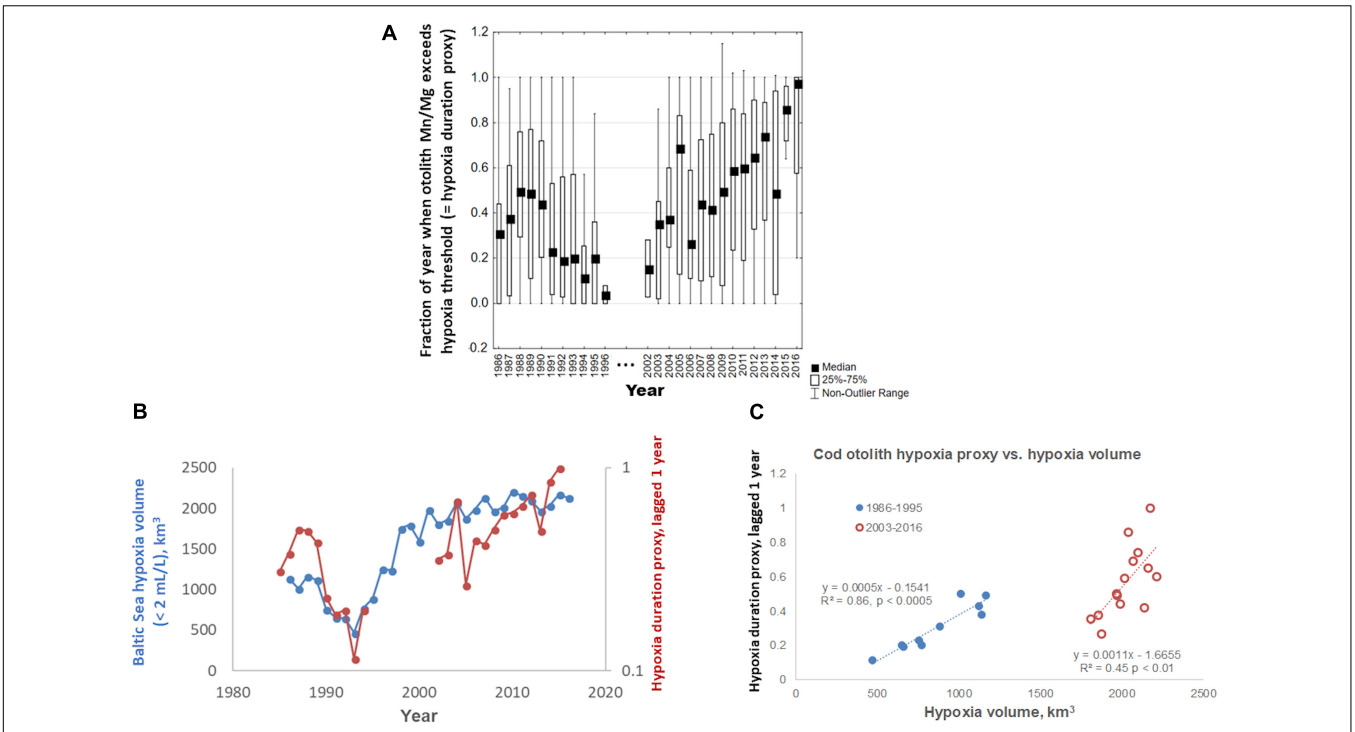

FIGURE 5 | (A) Within-year otolith Mn/Mg exceeding median threshold, a proxy for within-year duration of hypoxia exposure in Baltic cod otoliths, 1986–2016. **(B)** Concordance of Baltic Sea hypoxic water volume over the same time period, defined as water holding <2 mL/L dissolved oxygen (data courtesy O. Savchuk, Baltic Sea Centre, Stockholm University), and median otolith proxy values (from **A**) lagged 1 year back; note different axis scales; observations of $N \leq 2$ were deleted. **(C)** Median lagged otolith proxy values (from **B**), plotted vs. Baltic Sea hypoxia volume.

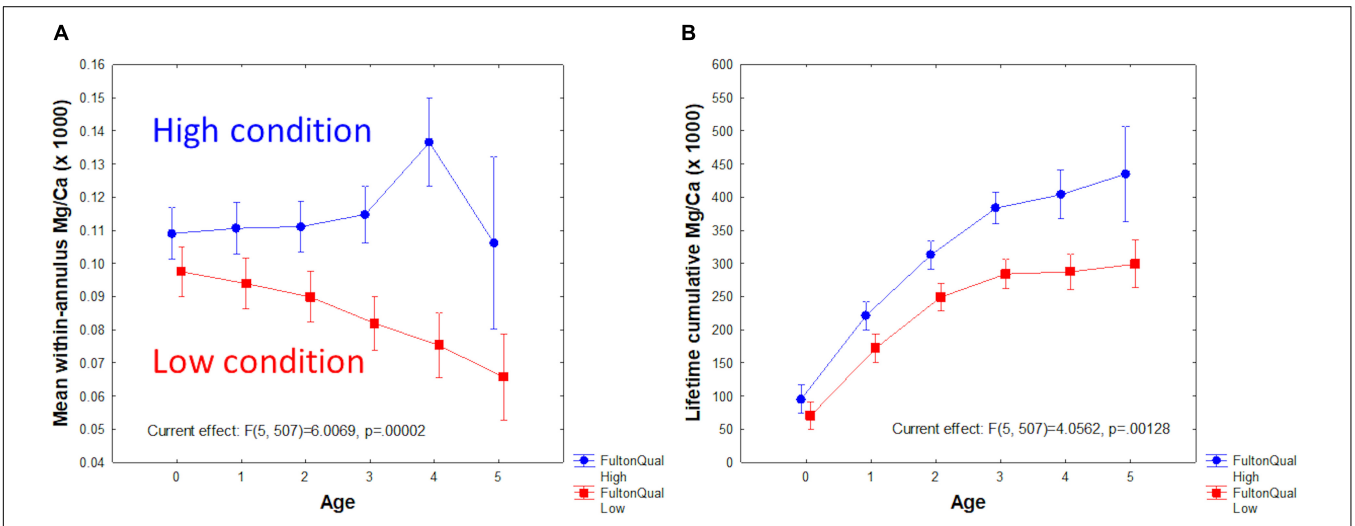

FIGURE 6 | Mg/Ca as a function of Fulton condition group (low < 9; high ≥ 9) and age. **(A)** Mean within-year Mg/Ca. **(B)** Lifetime accumulative Mg/Ca.

patterns of life histories. Despite the fact that the Baltic Sea is a very large system, and our collections constituted but a small sampling, some striking patterns emerged that reflect the changing circumstances of cod confronting hypoxia.

A variety of proxies for hypoxia, including Mn/Ca, Mn/Mg, and variants of these, were tested. We conclude that Mn/Mg, in which the growth- and hypoxia-sensitive element manganese is normalized to the (only) growth-sensitive trace element magnesium (Limburg et al., 2018), is a more robust metric for hypoxia than Mn/Ca, at least for cod. We tested the use of age-specific thresholds on these metrics, setting our thresholds for "exposure" at the median values across all modern fish that were analyzed. These thresholds appeared to work well, but they could be the subject of future refinement. Duration of Mn/Mg

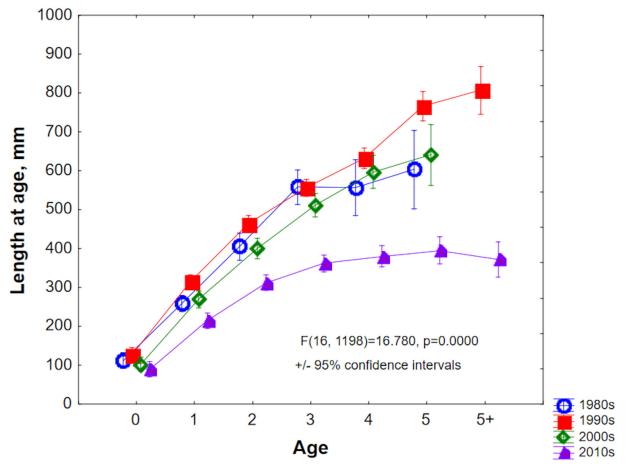

FIGURE 7 | Back-calculated lengths-at-age of Baltic cod, grouped by decade of capture.

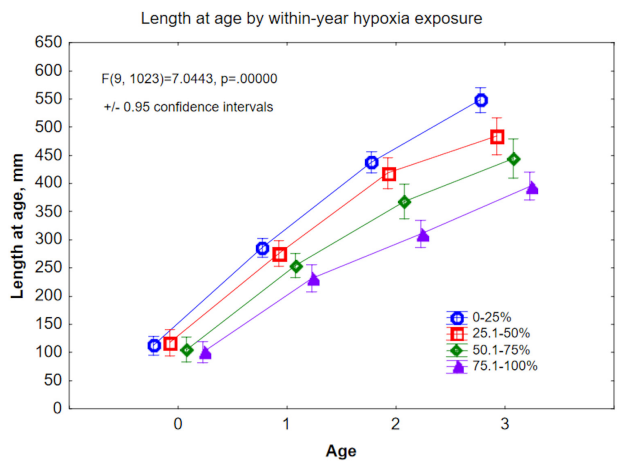

FIGURE 8 | Back-calculated length at age for Ages 0–3, plotted by within-year hypoxia exposure level. Hypoxia exposure is proxied here by Mn/Mg above the age-specific thresholds, expressed as fraction of the otolith annulus.

above age-specific thresholds generally agrees with the temporal patterns of hypoxia (**Figure 5**). Lagging the otolith proxy data by 1 year back significantly improved the correlations with hypoxic volume (**Figures 5B,C**). We do not know the reason for this, but speculate that it could be a slight temporal mis-match in when most of the samples were collected (winter–spring) vs. when hypoxia volume as used here is estimated (late summer–early autumn). Lagged correlations are not uncommon in the sclerochronology literature (e.g., Carré et al., 2005; Velarde et al., 2015; Judd et al., 2018). Hypoxia volume correlated better with our proxy than did hypoxia seafloor areal extent, perhaps because of the way that cod use the three-dimensional space. Finally, calculating the cumulative values of Mn/Mg across the otolith (as a substitute for time) provides a metric of the cumulative effect of exposure.

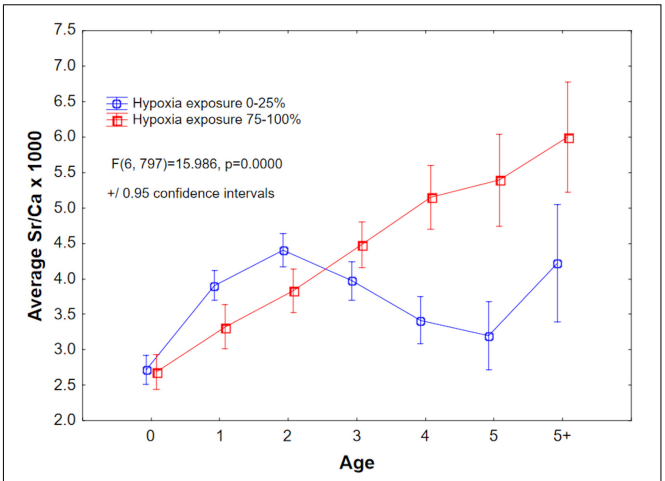

FIGURE 9 | Mean Sr/Ca × 1000, a proxy for salinity, plotted by age for the least and most hypoxia-exposed groups. See **Figure 8** for explanation of hypoxia exposure proxy.

We found strong, inverse relationships of hypoxia exposure to back-calculated growth (**Figures 7**, **8**), in agreement with laboratory experiments on Atlantic cod (Chabot and Dutil, 1999). Analyzed by decade, size at age was highest in the early 1990s when oxygen levels were highest, lowest in the most recent decade, and intermediate in the 1980s and 2000s, when hypoxia was present but not as severe as in recent years. We note that the 39% difference in length at Age-3 between least and most hypoxia-exposed fish (**Figure 8**) implies an even greater difference in weight, since the latter increases as roughly the cube of length[1]. Such differences have consequences for stock spawning biomass, reproductive potential (Mion et al., 2018) and the fisheries industry including economic losses (Svedäng and Hornborg, 2014). To illustrate the potential consequences in terms of economic value, assuming that prices were indifferent to quality of the fish, the weight differences alone imply a 64% loss in value (if value = price × quantity). A more complete assessment of the impact of hypoxia on this provisioning ecosystem service would require information on age-specific biomasses and quality, to which the hypoxia exposure categories could be parsed.

In addition, our results suggest a differentiation in habitat use and hypoxia exposure (**Figure 9**); fish that manifested the greatest exposure to hypoxia showed elevated Sr/Ca (a salinity proxy, but see discussion below) from Age-3 onward. Assuming that these fish remained in the Baltic and did not migrate out into the North Sea, our results suggest that fish that migrated into deeper, saltier Baltic water had a higher probability of encountering hypoxia, while those that remained in less saline (lower Sr/Ca) habitats were less exposed. This is consistent with tagging studies (e.g., Neuenfeldt et al., 2009).

We also explored otolith microchemistry relationships to fish condition as indexed by Fulton's K. The strongest relationship –

[1]From the length–weight relationship in the dataset: Weight = 4.45×10^{-6} $(\text{Length})^{3.11227783}$, $R^2 = 0.89$.

a separation of high from low condition groups by Mg/Ca – was an unanticipated result. However, in light of the growing evidence for Mg incorporation as a function of metabolic activity (Limburg et al., 2018), the extent to which condition reflects metabolism could explain this finding. The impact of hypoxia on metabolic activity is well documented for fishes in general (Fry, 1971; Claireaux and Chabot, 2016), and for cod in particular (Chabot and Claireaux, 2008). We find it remarkable that the separation of groups across all age classes is so strong (**Figure 6**), suggesting that condition factor, measured only at capture, may reflect long-term metabolic status of Baltic cod. In fish classified as high condition, Mg/Ca was nearly constant or increased moderately with age (up to Age-5, a group with only five observations and thus high variance); whereas fish classified as low condition showed a monotonic decline in Mg/Ca with age.

Current methodologies for collecting microchemical data allow for sampling trace elements and isotopes at varying levels of resolution and accuracy. With quadrupole LA-ICPMS methods, despite being the lowest resolution in the family of high-Z optimized mass spectrometers, low ppm levels of certain isotopes (e.g., ^{26}Mg, ^{63}Cu) are possible to quantify, and sensitivity to some isotopes (e.g., ^{55}Mn, ^{138}Ba) permits accuracy at high spatial resolution. The data collected for this study provide detail at sub-annual levels that we are currently unable to analyze statistically (e.g., the temporal dynamics seen in **Figures 2–4**) except on an annual or seasonal level. Techniques such as dynamic factor analysis (Zuur et al., 2003), which test for similarities across complex time series, are currently inadequate to handle the large data streams generated by otolith transect analysis – in our case, typically 200–400 replicates per chemical analyte × 10 analytes per fish, but some LA-ICPMS setups generate 10X the number of replicates. At this point, the recourse is to collect data at annual, or at best, coarsely monthly (e.g., Grammer et al., 2017) resolved data. There is a clear need to develop statistical methods to capture the rich detail of short-term dynamics, for example seen when summertime episodes of hypoxia are encountered.

Iodine, which is redox sensitive in carbonates (Lu et al., 2010), could be measured in Baltic cod otoliths, despite high background levels. Iodine appears to be bound in the organic matrix in otoliths (Z. Lu, Syracuse University, personal communication). I/Ca ratios were regularly elevated in the otolith cores, which are protein-dense. We also noted that Mn/Ca was almost always lower in the same otolith region, rising outside of the cores. It is possible that, as survivors, the individuals we measured were born in oxygenated water. However, the relationship of I/Ca to Mn/Ca in cod otoliths is complex, and incorporation of iodine appears to differ from manganese. Further research is needed to elucidate the uptake mechanism.

Strontium concentrations in the Baltic Sea vary with salinity due to large inputs of low-Sr fresh water (Andersson et al., 1992). Otolith uptake of Sr is also affected to some degree by temperature (Izzo et al., 2018), and Townsend et al. (1995) observed an inverse exponential relationship between Sr/Ca and water temperature in larval cod otoliths. In Baltic cod, it is likely that otolith Sr/Ca reflects a combination of temperature and salinity, thus higher levels of Sr/Ca reflect increased salinity and decreased temperature.

Compared to paleo conditions in the Baltic Sea as reflected in Neolithic cod otoliths, the Baltic today is less saline and more hypoxic (**Supplementary Figure S-2**). Even though manganese is partly affected (positively) by growth rate, the roughly 2.9-fold lower Mn/Ca in Neolithic cod is not explained by slower growth rates, because Neolithic cod grew faster and larger than modern Baltic cod (Limburg et al., 2008). It is impracticable to use the Neolithic otoliths to define thresholds for hypoxia exposure (cf. Altenritter et al., 2018), since so much of the data fall above the mean value [$Mn/Ca_{Neolithic}$ ($\times 10^3$) = 0.015]. The same holds true for the new proxy Mn/Mg ($Mn/Mg_{Neolithic}$ = 0.148, Mn/Mg_{Modern} = 0.412). Thus, we chose to use a population-level set of thresholds that defined hypoxia exposure as above the age-specific median values of Mn/Ca and Mn/Mg in modern cod.

Finally, we note that neither lifetime mean values, nor data collected on the outermost edges of otoliths, provided much insight into hypoxia exposure and growth. Lifetime mean values masked the details of year-specific conditions and averaged out differences. Edge analyses proved to be too variable to tease out signals, and suggest that edge chemistry does not necessarily shed insight on hypoxia impacts on growth.

We recommend parsing otolith transect data annually (or even seasonally, if possible) to capture the detail needed to examine hypoxia exposure and its consequences. This requires an understanding of how to determine what constitutes an annual growth zone on the otolith. For Baltic cod, this is a non-trivial problem and methods involving the use of otolith chemistry are in development (Heimbrand et al., unpublished) and used here. Although tedious and time-consuming to produce, the data sets generated provide invaluable information and insights. Going forward, these methods can be applied to study the further fluctuations in the status of Baltic cod as climate change and other drivers shape their environment.

CONCLUSION AND PERSPECTIVE

This study has further advanced our understanding of the utility of otolith chemical proxies to study hypoxia exposure and impact on individual fish within populations. Perhaps for the first time, proxies were used to quantify both lifetime exposure (through Mn proxies) and metabolic and growth responses – key information needed to understand population dynamics and thus to help manage the stocks.

The Baltic Sea is unusual in that it is so well studied, so hypoxic, and possesses the biogeochemistry amenable to use manganese as a hypoxia proxy. While this last is the case in some other hypoxic basins [e.g., the Black Sea (Lewis and Landing, 1991), the Gulf of Mexico (Mohan and Walther, 2016; Altenritter et al., 2018), and Chesapeake Bay, United States (Limburg, unpublished data)], many open marine systems with oxygen minimum zones (e.g., the California Current) may lack high enough concentrations of manganese to serve as such a proxy. The search for alternative proxies should continue for those systems, and may require further study of redox biogeochemistry likely to produce divalent cations that can substitute for otolith calcium (Campana and Thorrold, 2001), or other metals that

can be incorporated into otolith proteins (Thomas et al., 2017). These may include iron (indicative of anoxia, and detected on rare occasion by KL), zinc, and potentially bromine (Leri et al., 2010). Careful study and testing will be required, but benefits as demonstrated here, in terms of understanding hypoxia exposure, will be substantial.

AUTHOR CONTRIBUTIONS

KL conducted the research and analysis. Both authors conceived of and designed the study, and wrote the manuscript.

ACKNOWLEDGMENTS

We thank Y. Walther for providing otoliths from archival collections, and C. Olson for providing Neolithic samples. M. Leiditz and Y. Heimbrand prepared some of the otoliths used in this study. We also thank D. Driscoll, Y. Heimbrand, and T. Næraa for help conducting lab analyses; D. Swaney, B. Walther, and the reviewers provided helpful comments on earlier drafts. We also thank Associate Editor A. Capet. Financial support is acknowledged from the U.S. National Science Foundation (project award #1433759), the Swedish Research Council Formas (project dnr. 2015-865) and the Swedish Agency for Marine and Water Management.

SUPPLEMENTARY MATERIAL

The Supplementary Material for this article can be found online at: https://www.frontiersin.org/articles/10.3389/fmars.2018.00482/full#supplementary-material

REFERENCES

Altenritter, M. E., Cohuo, A., and Walther, B. D. (2018). Proportions of demersal fish exposed to sublethal hypoxia revealed by otolith chemistry. *Mar. Ecol. Prog. Ser.* 589, 193–208. doi: 10.3354/meps12469

Andersson, P. S., Wasserburg, G. J., and Ingri, J. (1992). The sources and transport of Sr and Nd isotopes in the Baltic Sea. *Earth Planet. Sci. Lett.* 113, 459–472. doi: 10.1016/0012-821X(92)90124-E

Breitburg, D., Levin, L. A., Oschlies, A., Grégoire, M., Chavez, F. P., Conley, D. J., et al. (2018). Declining oxygen in the global ocean and coastal waters. *Science* 359:eaam7240. doi: 10.1126/science.aam7240

Breitburg, D. L., Hondorp, D. W., Davias, L. A., and Diaz, R. J. (2009). Hypoxia, nitrogen, and fisheries: integrating effects across local and global landscapes. *Annu. Rev. Mar. Sci.* 1, 329–349. doi: 10.1146/annurev.marine.010908.163754

Campana, S., and Neilson, J. (1985). Microstructure of fish otoliths. *Can. J. Fish. Aquat. Sci.* 42, 1014–1032. doi: 10.1139/f85-127

Campana, S. E. (1990). How reliable are growth back-calculations based on otoliths? *Can. J. Fish. Aquat. Sci.* 47, 2219–2227. doi: 10.1139/f90-246

Campana, S. E. (1999). Chemistry and composition of fish otoliths: pathways, mechanisms and applications. *Mar. Ecol. Prog. Ser.* 188, 263–297. doi: 10.3354/meps188263

Campana, S. E., and Thorrold, S. R. (2001). Otoliths, increments, and elements: keys to a comprehensive understanding of fish populations? *Can. J. Fish. Aquat. Sci.* 58, 30–38. doi: 10.1139/f00-177

Carré, M., Bentaleb, I., Blamart, D., Ogle, N., Cardenas, F., Zevallos, S., et al. (2005). Stable isotopes and sclerochronology of the bivalve mesodesma donacium: potential application to peruvian paleoceanographic reconstructions. *Palaeogeo. Palaeoclim. Palaeoecol.* 228, 4–25. doi: 10.1016/j.palaeo.2005.03.045

Carstensen, J., Andersen, J. H., Gustafsson, B. G., and Conley, D. J. (2014). Deoxygenation of the baltic sea during the last century. *Proc. Nat. Acad. Sci. U.S.A.* 111, 5628–5633. doi: 10.1073/pnas.1323156111

Casini, M., Eero, M., Carlshamre, S., and Lövgren, J. (2016a). Using alternative biological information in stock assessment: condition-corrected natural mortality of Eastern Baltic cod. *ICES J. Mar. Sci.* 73, 2625–2631. doi: 10.1093/icesjms/fsw117

Casini, M., Käll, F., Hansson, M., Plikshs, M., Baranova, T., Karlsson, O., et al. (2016b). Hypoxic areas, density-dependence and food limitation drive the body condition of a heavily exploited marine fish predator. *R. Soc. Open Sci.* 3:160416.

Catanzaro, E. J., Murphy, T. J., Garner, E. L., and Shields, W. R. (1966). Absolute isotopic abundance ratios and atomic weight of magnesium. *J. Res. Nat. Bur. Stand. A* 70, 453–458. doi: 10.6028/jres.070A.037

Chabot, D., and Claireaux, G. (2008). Environmental hypoxia as a metabolic constraint on fish: the case of Atlantic cod, *Gadus morhua*. *Mar. Pollut. Bull.* 57, 287–294. doi: 10.1016/j.marpolbul.2008.04.001

Chabot, D., and Dutil, J.-D. (1999). Reduced growth of atlantic cod in nonlethal hypoxic conditions. *J. Fish Biol.* 55, 472–491. doi: 10.1111/j.1095-8649.1999.tb00693.x

Claireaux, G., and Chabot, D. (2016). Responses by fishes to environmental hypoxia: integration through Fry's concept of aerobic metabolic scope. *J. Fish Biol.* 88, 232–251. doi: 10.1111/jfb.12833

Conley, D. J., Björck, S., Bonsdorff, E., Carstensen, J., Destouni, G., Gustafsson, B. G., et al. (2009). Hypoxia-related processes in the Baltic Sea. *Environ. Sci. Technol.* 43, 3412–3420. doi: 10.1021/es802762a

Diaz, R. J., and Rosenberg, R. (2008). Spreading dead zones and consequences for marine ecosystems. *Science* 321, 926–929. doi: 10.1126/science.1156401

Eby, L. A., and Crowder, L. B. (2002). Hypoxia-based habitat compression in the neuse river estuary: context-dependent shifts in behavioral avoidance thresholds. *Can. J. Fish. Aquat. Sci.* 59, 952–965. doi: 10.1139/f02-067

Eero, M., Hjelm, J., Behrens, J., Buchmann, K., Cardinale, M., Casini, M., et al. (2015). Eastern baltic cod in distress: biological changes and challenges for stock assessment. *ICES J. Mar. Sci.* 72, 2180–2186. doi: 10.1093/icesjms/fsv109

Elsdon, T. S., Wells, B. K., Campana, S. E., Gillanders, B. M., Jones, C. M., Limburg, K. E., et al. (2008). Otolith chemistry to describe movements and life-history parameters of fishes: hypotheses, assumptions, limitations, and inferences. *OMBAR* 46, 297–330. doi: 10.1201/9781420065756.ch7

Fry, F. E. J. (1971). "The effect of environmental factors on the physiology of fish," in *Fish Physiology 6*, eds W. S. Hoar and D. J. Randall (Cambridge: Academic Press), 1–98.

Grammer, G. L., Morrongiello, J. R., Izzo, C., Hawthorne, P. J., Middleton, J. F., and Gillanders, B. M. (2017). Coupling biogeochemical tracers with fish growth reveals physiological and environmental controls on otolith chemistry. *Ecol. Monogr.* 87, 487–507. doi: 10.1002/ecm.1264

Hansson, M., Viktorsson, L., and Andersson, L. (2017). *Oxygen Survey in the Baltic Sea 2017 - Extent of Anoxia and Hypoxia, 1960-2017*. Report Oceanography No 63. Göteborg: Swedish Meteorological and Hydrological Institute.

Hinrichsen, H. H., von Dewitz, B., Lehmann, A., Bergström, U., and Hüssy, K. (2017). Spatio-temporal dynamics of cod nursery areas in the Baltic Sea. *Prog. Oceanogr.* 155, 28–40. doi: 10.1016/j.pocean.2017.05.007

Hong, B., Swaney, D. P., McCrackin, M., Svanback, A., Humborg, C., Gustafsson, B., et al. (2017). Advances in NANI and NAPI accounting for the baltic drainage basin: spatial and temporal trends and relationships to watershed TN and TP fluxes. *Biogeochemistry* 133, 245–261. doi: 10.1007/s10533-017-0330-0

Hüssy, K. (2010). Why is age determination of baltic cod (*Gadus morhua*) so difficult? *ICES J. Mar. Sci.* 67, 1198–1205.

Hüssy, K., Radtke, K., Plikshs, M., Oeberst, R., Baranova, T., Krumme, U., et al. (2016). Challenging ICES age estimation protocols: lessons learned from the eastern baltic cod stock. *ICES J. Mar. Sci.* 73, 2138–2149. doi: 10.1093/icesjms/fsw107

International Council for the Exploration of the Seas [ICES]. (2014). *Report of the Baltic Fisheries Assessment Working Group (WGBFAS), 3–10 April 2014 ICES HQ. ICES Document CM*2014/ACOM: 10. Denmark: ICES.

Izzo, C., Reis-Santos, P., and Gillanders, B. M. (2018). Otolith chemistry does not just reflect environmental conditions: a meta-analytic evaluation. *Fish Fish.* 19, 441–454. doi: 10.1111/faf.12264

Judd, E. J., Wilkinson, B. H., and Ivany, L. C. (2018). The life and time of clams: derivation of intra-annual growth rates from high-resolution oxygen isotope profiles. *Palaeogeo. Palaeoclim. Palaeoecol.* 490, 70–83. doi: 10.1016/j.palaeo.2017.09.034

Köster, F. W., Möllmann, C., Hinrichsen, H.-H., Tomkiewicz, J., Wieland, K., Kraus, G., et al. (2005). Baltic cod recruitment – the impact of climate and species interaction. *ICES J. Mar. Sci.* 62, 1408–1425. doi: 10.1016/j.icesjms.2005.05.004

Leri, A. C., Hakala, A., Marcus, M. A., Lanzirotti, A., Reddy, C. M., and Myneni, S. C. B. (2010). Natural organobromine in marine sediments: new evidence of biogeochemical Br cycling. *Glob. Biogeochem Cyc* 24:GB4017, doi: 10.1029/2010GB003794

Lewis, B. L., and Landing, W. (1991). The biogeochemistry of manganese and iron in the Black Sea. *Deep Sea Res. Part A Oceanogr. Res. Pap.* 38, S773–S803. doi: 10.1016/S0198-0149(10)80009-3

Limburg, K. E., and Elfman, M. (2017). Insights from two-dimensional mapping of otolith chemistry. *J. Fish Biol.* 90, 480–491. doi: 10.1111/jfb.13048

Limburg, K. E., Olson, C., Walther, Y., Dale, D., Slomp, C. P., and Høie, H. (2011). Tracking baltic hypoxia and cod migration over millennia with natural tags. *Proc. Nat. Acad. Sci. U.S.A.* 108, E177–E182. doi: 10.1073/pnas.1100684108

Limburg, K. E., Walther, B. D., Lu, Z., Jackman, G., Mohan, J., Walther, Y., et al. (2015). In search of the dead zone: use of otoliths for tracking fish exposure to hypoxia. *J. Mar. Sys.* 141, 167–178. doi: 10.1016/j.jmarsys.2014.02.014

Limburg, K. E., Walther, Y., Hong, B., Olson, C., and Storå, J. (2008). Prehistoric vs. modern baltic sea cod fisheries: selectivity across the millennia. *Proc. R. Soc. B* 275, 2659–2665. doi: 10.1098/rspb.2008.0711

Limburg, K. E., Wuenschel, M. J., Hüssy, K., Heimbrand, Y., and Samson, M. (2018). Making the otolith magnesium chemical calendar-clock tick: plausible mechanism and supporting evidence. *Rev. Fish. Sci. Aquacult.* 26, 479–493. doi: 10.1080/23308249.2018.1458817

Lu, Z., Jenkyns, H. C., and Rickaby, R. E. M. (2010). Iodine to calcium ratios inmarine carbonate as a paleo-redox proxy during oceanic anoxic events. *Geology* 38, 1107–1110. doi: 10.1130/G31145.1

Mion, M., Thorsen, A., Dierking, J., Herrmann, J.-P., Huwer, B., Vitale, F., et al. (2018). Effect of fish length and nutritional condition on the fecundity of distressed atlantic cod *Gadus morhua* from the Baltic Sea. *J. Fish Biol.* 92, 1016–1034. doi: 10.1111/jfb.13563

Mohan, J., and Walther, B. (2016). Out of breath and hungry: natural tags reveal trophic resilience of Atlantic croaker to hypoxia exposure. *Mar. Ecol. Prog. Ser.* 560, 207–221. doi: 10.3354/meps11934

Neuenfeldt, S., Andersen, K. H., and Hinrichsen, H.-H. (2009). Some atlantic cod *Gadus morhua* in the baltic sea visit hypoxic water briefly but often. *J. Fish Biol.* 75, 290–294. doi: 10.1111/j.1095-8649.2009.02281.x

Nissling, A., and Westin, L. (1997). Salinity requirements for successful spawning of baltic and belt sea cod and the potential for cod stock interactions in the Baltic Sea. *Mar. Ecol. Prog. Ser.* 152, 261–271. doi: 10.3354/meps152261

Pachur, M. E., and Horbowy, J. (2013). Food composition and prey selection of cod, *Gadus morhua* (Actinopterygii: Gadiformes: Gadidae), in the southern Baltic Sea. *Acta Ichthyol. Piscat.* 43, 109–118. doi: 10.3750/AIP2013.43.2.03

Plikshs, M., Hinrichsen, H.-H., Elferts, D., Sics, I., Kornilovs, G., and Köster, F. W. (2015). Reproduction of baltic cod, *Gadus morhua* (Actinopterygii: Gadiformes: Gadidae), in the Gotland Basin: causes of annual variability. *Acta Ichthyol. Piscat.* 45, 247–258. doi: 10.3750/AIP2015.45.3.04

Pracheil, B. M., Hogan, J. D., Lyons, J., and McIntyre, P. B. (2014). Using hard-part microchemistry to advance conservation and management of North American freshwater fishes. *Fisheries* 39, 451–465. doi: 10.1080/03632415.2014.937858

Reddy, K. R., and DeLaune, R. D. (2008). *Biogeochemistry of Wetlands: Science and Applications*. Boca Raton, FL: CRC Press, 800. doi: 10.1201/9780203491454

Schmale, O., Krause, S., Holtermann, P., Power Guerra, N. C., and Umlauf, L. (2016). Dense bottom gravity currents and their impact on pelagic methanotrophy at oxic/anoxic transition zones. *Geophys. Res. Lett.* 43, 5225–5232. doi: 10.1002/2016GL069032

Stramma, L., Prince, E. D., Schmidtko, S., Luo, J., Hoolihan, J. P., Visbeck, M., et al. (2012). Expansion of oxygen minimum zones may reduce available habitat for tropical pelagic fishes. *Nat. Clim. Change* 2:33. doi: 10.1038/nclimate1304

Sturrock, A. M., Hunter, E., Milton, J. A., Johnson, R. C., Waring, C. P., and Trueman, C. N. (2015). Quantifying physiological influences on otolith microchemistry. *Meth. Ecol. Evol.* 6, 806–816. doi: 10.1111/2041-210X.12381

Svedäng, H., and Hornborg, S. (2014). Selective fishing induces density-dependent growth. *Nat. Commun.* 5:4152. doi: 10.1038/ncomms5152

Thomas, O. R., Ganio, K., Roberts, B. R., and Swearer, S. E. (2017). Trace element–protein interactions in endolymph from the inner ear of fish: implications for environmental reconstructions using fish otolith chemistry. *Metallomics* 9, 239–249. doi: 10.1039/c6mt00189k

Townsend, D. W., Radtke, R. L., Malone, D. P., and Wallinga, J. P. (1995). Use of otolith strontium:calcium ratios for hindcastng larval cod *Gadus morhua* distributions relative to water masses on georges bank. *Mar. Ecol. Prog. Ser.* 119, 37–44. doi: 10.3354/meps119037

Trouwborst, R. E., Clement, B. G., Tebo, B. M., Glazer, B. T., and Luther, G. W. III (2006). Soluble Mn(III) in suboxic zones. *Science* 313, 1955–1957. doi: 10.1126/science.1132876

Velarde, A. A., Flye-Sainte-Marie, J., Mendo, J., and Jean, F. (2015). Sclerochronological records and daily microgrowth of the peruvian scallop (*Argopecten purpuratus*, Lamarck, 1819) related to environmental conditions in Paracas Bay, Pisco, Peru. *J. Sea Res.* 99, 1–8. doi: 10.1016/j.seares.2015.01.002

Wilson, S., Koenig, A., and Orklid, R. (2008). Development of microanalytical reference material (MACS-3) for LA-ICP-MS analysis of carbonate samples. *Geochim. Cosmochim. Acta Suppl.* 72:A1025.

Zuur, A. F., Tuck, I. D., and Bailey, N. (2003). Dynamic factor analysis to estimate common trends in fisheries time series. *Can. J. Fish. Aquat. Sci.* 60, 542–552. doi: 10.1139/f03-030

Conflict of Interest Statement: The authors declare that the research was conducted in the absence of any commercial or financial relationships that could be construed as a potential conflict of interest.

frontiers in Marine Science

REVIEW
published: 17 January 2019
doi: 10.3389/fmars.2018.00533

Microbial Respiration, the Engine of Ocean Deoxygenation

*Carol Robinson**

Centre for Ocean and Atmospheric Sciences, School of Environmental Sciences, University of East Anglia, Norwich, United Kingdom

Microbial plankton respiration is the key determinant in the balance between the storage of organic carbon in the oceans or its conversion to carbon dioxide with accompanying consumption of dissolved oxygen. Over the past 50 years, dissolved oxygen concentrations have decreased in many parts of the world's oceans, and this trend of ocean deoxygenation is predicted to continue. Yet despite its pivotal role in ocean deoxygenation, microbial respiration remains one of the least constrained microbial metabolic processes. Improved understanding of the magnitude and variability of respiration, including attribution to component plankton groups, and quantification of the respiratory quotient, would enable better predictions, and projections of the intensity and extent of ocean deoxygenation and of the integrative impact of ocean deoxygenation, ocean acidification, warming, and changes in nutrient concentration and stoichiometry on marine carbon storage. This study will synthesize current knowledge of respiration in relation to deoxygenation, including the drivers of its variability, identify key unknowns in our ability to project future scenarios and suggest an approach to move the field forward.

Keywords: microbial respiration, respiratory quotient, ocean deoxygenation, ocean acidification, multiple stressors

OPEN ACCESS

Edited by:
Emilio Garcia-Robledo, University of Cádiz, Spain

Reviewed by:
Carolin Regina Löscher, University of Southern Denmark, Denmark
Thomas Smith Weber, University of Rochester, United States
Helmut Maske, Ensenada Center for Scientific Research and Higher Education (CICESE), Mexico

***Correspondence:**
Carol Robinson
carol.robinson@uea.ac.uk

Specialty section:
This article was submitted to Marine Biogeochemistry, a section of the journal Frontiers in Marine Science

Received: *10 August 2018*
Accepted: *31 December 2018*
Published: *17 January 2019*

Citation:
Robinson C (2019) Microbial Respiration, the Engine of Ocean Deoxygenation. Front. Mar. Sci. 5:533. doi: 10.3389/fmars.2018.00533

INTRODUCTION

Dissolved oxygen (O_2) is fundamental to all aerobic life and thus plays a major role in marine microbial ecology and the biogeochemical cycling of elements such as carbon, nitrogen, phosphorus and sulfur. The measurement of seawater O_2 began during the 1873–1876 *HMS Challenger* expedition, and O_2 continues to be the most commonly measured indicator of marine biogeochemistry, with the current global database amounting to millions of measurements (Keeling et al., 2010; Schmidtko et al., 2017). Time series data over the past 50 years show declining O_2 in many regions of the world's oceans, and a significant increase in the aerial extent of oxygen minimum zones (OMZs) in the eastern tropical North Atlantic (ETNA) and equatorial Pacific. Stramma et al. (2008) determined the decrease in O_2 for the region of the ETNA between 10–14°N and 20–30°W in the depth range 300–700 m to be 0.09–0.34 μmol kg^{-1} year^{-1} between 1960 and 2008, while later studies revealed variations in this long term decline at interannual to multidecadal timescales consistent with natural climate variability (Brandt et al., 2015). The latest collation of global ocean dissolved oxygen data shows a decrease of more than 2% (4.8 $\pm$ 2.1 pmol), in the global oceanic oxygen content since 1960 (Schmidtko et al., 2017), however, at regional scales the changes are more complex. Deutsch et al. (2014) showed evidence for a decrease in the extent of oxygen minimum zones in the tropical Pacific Ocean over most of the 20th century. This was

related to weakening easterly trade winds in a warming climate which decrease the intensity of upwelling and therefore the magnitude of biological production, export of organic carbon and respiratory oxygen demand. In the coastal zone, low or zero oxygen conditions are induced by anthropogenic nutrient enrichment and eutrophication, with the number of these coastal zone hypoxic sites having increased by an order of magnitude since the 1960s (Diaz and Rosenberg, 2008). This "deoxygenation" of the open and coastal ocean is predicted to continue. Coupled climate – marine biogeochemical models all project a continued long term decrease in the global ocean O_2 inventory of between 1 and 7% by 2100 (Bopp et al., 2002; Keeling and Garcia, 2002; Keeling et al., 2010). Henson et al. (2017) investigated the trend in a multi-model mean ensemble of the Coupled Model Inter-comparison Project Phase 5 (CMIP5) output, run under a "business-as-usual" scenario (RCP8.5). This suggested that most of the world's oceans will experience a 1–2% decrease in the oxygen inventory per decade with respect to the mean of 1986–2005. However, the regions where temperature and O_2 changes are likely to have the greatest impact on marine ecosystems and biogeochemistry, the poles and the tropics, including the major eastern boundary upwelling systems where oxygen minimum zones occur (Gruber, 2011), are also the regions where inter-model agreement is low (Henson et al., 2017).

A number of physical, ecological, and biogeochemical mechanisms could contribute to the process of deoxygenation (**Figure 1**) including:

(1) The direct effect of increasing temperature reducing the solubility of oxygen in seawater. This physical chemical process is well constrained, with estimates of a decrease in O_2 of ca. 5 mmol m^{-3} for each 1°C increase in water temperature (Deutsch et al., 2011). Within the upper 1000 m, 50% of the observed O_2 loss is attributed to changes in solubility. This percentage decreases to 25% of the O_2 loss in the upper 2000 m and 15% of the O_2 loss over the full oceanic depth (Schmidtko et al., 2017).

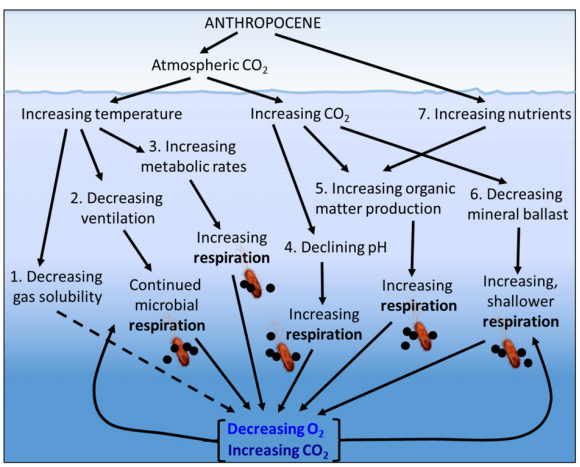

FIGURE 1 | Potential physical, ecological and biogeochemical mechanisms contributing to ocean deoxygenation in the Anthropocene.

(2) The indirect effect of increasing sea surface temperatures causing increased surface ocean stratification and reduced ventilation of the deep ocean, therefore increasing the length of time that deep water is separated from contact with the atmosphere. This delays the re-equilibration of dissolved oxygen to atmospheric concentrations while microbial degradation of organic matter associated with aerobic respiration consuming oxygen and producing carbon dioxide (CO_2) continues.

(3) The direct effect of increasing temperature on the metabolic rates of the plankton, with the expectation that for the same increase in temperature, heterotrophic processes such as microbial respiration which consume oxygen will increase more than autotrophic processes such as photosynthesis which produce oxygen (López-Urrutia et al., 2006; Wohlers et al., 2009), and that bacterioplankton growth efficiencies (the proportion of the carbon assimilated by bacterioplankton that is converted to biomass rather than being respired to CO_2) decrease with increasing temperature (Rivkin and Legendre, 2001). A warming ocean is therefore expected to change the depth distribution of oxygen consumption, with an increase in shallower warmer waters and a decrease at depth due to the reduced supply of organic matter. Whether this redistribution of oxygen consumption will lead to a decrease or increase in average oxygen concentrations remains uncertain.

(4) The direct effect of increasing CO_2 leading to increased bacterioplankton cell-specific respiration. The anthropogenically derived CO_2 in the atmosphere which is causing global warming is also dissolving in seawater, leading to increasing pCO_2 and decreasing seawater pH and carbonate ion concentration (ocean acidification). Elevated pCO_2 has been shown to increase the activity of bacterioplankton extracellular enzymes such as α and β–glucosidase (Piontek et al., 2010, 2013) and enhance bacterioplankton respiration (James et al., 2017).

(5) The indirect effect of increased photosynthesis caused by increasing concentrations of seawater CO_2. Increased CO_2 can enhance photosynthesis, producing an increased amount of particulate organic material (Riebesell and Tortell, 2011), a greater proportion of exudation of dissolved organic material (DOM; Engel et al., 2004) and increased carbon:nitrogen and carbon:phosphorus ratios of the DOM (Riebesell et al., 2007), leading to increased microbial respiration.

(6) The indirect effect of reduced calcium carbonate ballast due to decreasing seawater pH and carbonate ion concentration. The reduction in plankton extra-cellular calcium carbonate reduces the sinking rate of the plankton cells allowing respiration to occur at a shallower depth (Barker et al., 2003), and potentially allows a greater proportion of the exposed organic material to be respired in a given time.

(7) The indirect effect of increased coastal discharge of inorganic nutrients leading to increased primary production and thus increased phytoplankton derived particulate and dissolved organic carbon (or

eutrophication), which when degraded by heterotrophic bacteria supports increased microbial respiration. The indirect effect of increased discharge of inorganic nutrients and/or increased phytoplankton production of labile dissolved organic carbon "priming" the degradation of previously recalcitrant dissolved organic carbon (Jiao et al., 2011). The indirect effect of increased pollution-derived atmospheric deposition of soluble iron and fixed nitrogen leading to increased primary production and then increased respiration (Ito et al., 2016).

The inter-dependencies and feedbacks between these mechanisms mean that their individual effects on deoxygenation can be counteracted or exacerbated. For example, increased stratification due to increased surface temperature will reduce nutrient supply to the surface ocean, reducing primary production by an estimated 24% by the year 2300 when RCP8.5 predicts a fivefold increase in atmospheric CO_2 (Moore et al., 2018) which will offset the 27% increase in primary production due to carbon fertilization, estimated for a doubling of atmospheric CO_2 (Riebesell et al., 2007).

Apart from the temperature related decrease in oxygen solubility and ocean ventilation, all of these potential mechanisms causing deoxygenation depend on microbial aerobic respiration, the metabolic process driven by the degradation of dissolved and particulate organic carbon, which consumes oxygen, produces carbon dioxide and generates energy in the form of adenosine triphosphate (ATP). Midwater microbial communities – predominantly bacterioplankton, archaeoplankton and zooplankton – are therefore central to the challenge that is ocean deoxygenation because they both influence and are influenced by decreasing oxygen concentrations. Since the depletion of oxygen caused by microbial respiration is always accompanied by an increase in CO_2, ocean deoxygenation is always a dual stressor problem – both oxygen and CO_2 change (Brewer and Peltzer, 2009). Due to this complexity of feedbacks and interdependency, ocean deoxygenation is therefore a "wicked" problem contributing to the "super wicked" problem of climate change (Levin et al., 2012).

The aim of this paper is to explore this wicked problem from the perspective of microbial respiration, focusing on the key role that microbial respiration plays in enabling ocean deoxygenation and on how microbial respiration, and therefore the storage of carbon in the ocean, might be affected by ocean deoxygenation. I will build on previous reviews of microbial respiration (e.g., del Giorgio and Duarte, 2002; Robinson and Williams, 2005; Robinson, 2008; Arístegui et al., 2009; Regaudie-de-Gioux and Duarte, 2012, 2013) synthesizing what we know about midwater microbial respiration that could help us predict how microbial respiration might change in waters with reduced oxygen and increased carbon dioxide concentrations, and then identify areas of research that still need to be addressed and some emerging approaches that could be used.

MICROBIAL RESPIRATION

The magnitude and variability of marine microbial aerobic respiration is fundamental to deoxygenation, the formation of oxygen minimum zones and the efficiency of the biological carbon pump. Yet due to methodological limitations, the number of direct measurements and therefore our understanding of respiration, especially below the euphotic zone, is only loosely constrained.

Measurement Methods

The magnitude of midwater (i.e., between 100 and 1000 m depth range) respiration can be determined either from the oxygen consumption of an incubated water sample (Arístegui et al., 2005; Reinthaler et al., 2006; Baltar et al., 2010; Holtappels et al., 2014), from plankton electron transport system (ETS) activity (e.g., Packard et al., 2015; Osma et al., 2016; Martínez-García, 2017), from $^{14}CO_2$ production during incubations with ^{14}C labeled compounds (Hill et al., 2013), from measurements of bacterioplankton production and bacterioplankton growth efficiency (BGE = proportion of assimilated carbon used to produce bacterioplankton biomass) or from a time resolved estimate of the amount of oxygen consumed since a given water body left the sea surface where the dissolved oxygen concentration was in equilibrium with that in the atmosphere – the apparent (AOU; Sarmiento and Gruber, 2006), true (TOU) or evaluated (EOU; Duteil et al., 2013) oxygen utilization. Combining the estimate of oxygen utilization with an estimate of ventilation age from the distribution of tritium, radiocarbon or chlorofluorocarbons (CFCs), gives an average oxygen utilization rate (OUR; Jenkins, 1987). The efficiency of mesopelagic remineralization can also be inferred from the vertical profile of particle flux derived from underwater imaging, sediment trap data or thorium isotope disequilibria (Guidi et al., 2015) or reconstructed from large-scale ocean nutrient distributions (Weber et al., 2016).

Midwater respiration rates (60–300 $\mu mol\ O_2\ m^{-3}\ day^{-1}$) have been derived from direct measurements of oxygen consumption during incubations of 2–4 days. To minimize any potential artifacts due to such long incubations, data are only used when linearity in oxygen consumption and cell abundance are confirmed, or when significant relationships between oxygen consumption and bacterioplankton production during the incubations can be used with *in situ* bacterioplankton production measurements to "back-correct" the respiration to *in situ* values (Arístegui et al., 2005; Reinthaler et al., 2006; Mazuecos et al., 2015). The ETS method estimates the maximum activity (V_{max}) of the enzymes associated with the respiratory electron transport system of both eukaryotes and prokaryotes under substrate (NADH, NADPH) saturation, and is therefore a maximum "potential" respiration rate rather than the actual respiration rate. V_{max} is converted into rates of oxygen consumption using either an empirical relationship determined from bacterial cultures or application of an enzyme kinetic model (EKM). It therefore assumes an average relationship between enzyme mass and respiratory activity, and due to this assumption it has an estimated error of 31–38% (Packard et al.,

1988). A recent development of the ETS technique uses pyridine nucleotide concentrations and an EKM (Aguiar-González et al., 2012) to derive the actual respiration rate. This method has been used with cultured bacteria and zooplankton (Osma et al., 2016), but has not yet been tested in open waters.

A further modification of the ETS method derives respiration from the relationship between dissolved oxygen consumption and the *in vivo* reduction of 2-(p-iodophenyl)-3-(p-nitrophenyl)-5-phenyltetrazolium chloride (INT) to INT-formazan (Martínez-García et al., 2009). Martínez-García (2017) presents the first size-fractionated mesopelagic respiration data from station ALOHA in the North Pacific Subtropical Gyre using the INT technique, to show vertical and seasonal variability in respiration ranging from 56 to 107 μmol O_2 m^{-3} day^{-1} in the 100–1000 m depth horizon. These data are around an order of magnitude higher than earlier ETS estimates (1–7 mol O_2 m^{-2} y^{-1}; 3–25 μmol O_2 m^{-3} day^{-1}; Arístegui et al., 2003), which were calculated using a conversion factor derived from a senescent bacterial culture, suggesting that microbial communities in the mesopelagic ocean are much more active that previously assumed (Arístegui et al., 2009). Respiration can also be derived from the respiration of ^{14}C-leucine by bacterioplankton cells. Hill et al. (2013) determined respiration in the range 0.07–1.9 pmol leu L^{-1} h^{-1} between 20 and 160 m in the Atlantic Ocean after additions of ^{14}C-leucine at close to ambient (0.4 nmol L^{-1}) concentrations. Using ^{3}H-leucine bioassay isotope dilution to determine prokaryote production, and published estimates of prokaryote growth efficiencies, Giering et al. (2014) calculated depth integrated (50–1000 m) North Atlantic prokaryote respiration to be 71 mg C m^{-2} day^{-1}. Oxygen utilization rates including recent ones derived for the Pacific (Sonnerup et al., 2013, 2015) and Atlantic Oceans (Stanley et al., 2012) using transit time distributions, range from 0.3 to 50 μmol O_2 m^{-3} day^{-1} (0.03–18.2 mol O_2 m^{-2} y^{-1}; **Table 1**).

In the oxygen minimum zones (OMZ) where oxygen concentrations fall below 40 μmol L^{-1} or, in the most intense OMZs below 20 μmol L^{-1} (Paulmier and Ruiz-Pino, 2009), it is only relatively recently that techniques to accurately measure extremely low *in situ* oxygen concentrations and rates of oxygen consumption have become available. While Winkler titrations, electrochemical or optode sensors and oxygen isotope methods have detection limits around 0.1–1 μmol L^{-1}, the switchable trace oxygen (STOX) microsensor has a detection limit in the range 1–10 nmol L^{-1} (Revsbech et al., 2009, 2011), and in water bodies containing concentrations of O_2 less than 1 nmol L^{-1}, the ultra-sensitive Luminescence Measuring Oxygen Sensor (LUMOS) has a sensitivity of 7 pmol L^{-1} (Lehner et al., 2014, 2015). Good agreement was found between measurements of oxygen concentration and oxygen consumption made by STOX sensors, optode spots and membrane inlet mass spectrometric analysis of $^{18-18}O_2$ (Holtappels et al., 2014). Using these new nanomolar techniques, *in situ* oxygen and respiration measurements derived from consumption of oxygen, showed that aerobic respiration occurs efficiently at extremely low oxygen concentrations (Tiano et al., 2014; Kalvelage et al., 2015; Garcia-Robledo et al., 2016). As well as the difficulty in measuring very low oxygen concentrations and rates of oxygen consumption, the imperative to maintain *in situ* oxygen concentrations during shipboard sample collection, manipulation and analysis remains a significant challenge (Garcia-Robledo et al., 2016).

TABLE 1 | Recent midwater (100–1000 m) respiration estimates derived from dissolved oxygen consumption during a bottle incubation (ΔO_2), activity of the electron transport system (ETS), the reduction of the tetrazolium salt (INT), or the time resolved estimate of the amount of dissolved oxygen consumed since a water parcel was last in contact with the atmosphere, the oxygen utilization rate (OUR).

Region	Method	Respiration (μmol O_2 m^{-3} day^{-1})	Reference
NE Atlantic	ΔO_2	80–350	Arístegui et al., 2005
N Atlantic	ΔO_2	50–200	Reinthaler et al., 2006
Mediterranean Sea	ΔO_2	230–1650	Weinbauer et al., 2013
S Atlantic and Indian	ΔO_2	87–238	Mazuecos et al., 2015
NE Atlantic	ETS	120 ±14	Arístegui et al., 2005
N Atlantic	ETS	20–50	Reinthaler et al., 2006
Atlantic	ETS	66–88	Baltar et al., 2009a,b
N Atlantic	ETS	7–16	Fernández-Castro et al., 2016
Pacific coastal upwelling	ETS	3–750	Packard et al., 2015
N Pacific	INT	56–107	Martínez-García, 2017
Pacific	OUR	0.05–27	Feely et al., 2004
SE Pacific	OUR	5–55	Sonnerup et al., 2015
NE Pacific	OUR	0.3–30	Sonnerup et al., 2013
Atlantic	OUR	17 ± 3	Stanley et al., 2012

Apportionment to Microbial Group

In addition to bulk measurements of respiration, an appreciation of the proportion of respiration attributable to bacterioplankton or zooplankton and between particle-attached or free-living bacterioplankton is important for accurate predictions and projections of carbon remineralization and thus deoxygenation and marine carbon storage in a changing environment. Unfortunately, such apportionment of respiration to constituent plankton functional groups is hampered by the lack of a direct method able to differentiate the respiration of any component group from that of the rest of the plankton community. The post-incubation separation by filtration of a size class of the plankton community, coupled with the identification and enumeration of plankton within that size class, has become the pragmatic although imperfect field approach to infer the respiration of a particular group which dominates a particular size class. This is obviously problematic in environments where cells of the same size represent very different functional groups, for example, heterotrophic and autotrophic prokaryotes in the surface waters of oligotrophic gyres, but perhaps is less of a problem in coastal regions or in the mesopelagic.

The relative proportion of mesopelagic bacterioplankton and zooplankton respiration varies with euphotic zone productivity. Bacterioplankton respiration was 2- to 10-fold higher than zooplankton respiration at the oligotrophic ALOHA station in the North Pacific Subtropical Gyre, and up to fivefold higher at

the mesotrophic station K2 in the subarctic Pacific (Steinberg et al., 2008). Giering et al. (2014) found bacterioplankton respiration to dominate (70–92%) community respiration in the North Atlantic mesopelagic zone, while McDonnell et al. (2015) showed that the respiration rates of particle-associated microbes contributed 32–98% of the total respiration measured *in situ* at the Bermuda Atlantic Time-series Study site (BATS). Direct measurements of the oxygen consumption of microbes associated with phytodetrital aggregates collected using marine snow catchers in the northeast Atlantic, showed that the relative importance of particle-associated microbial respiration to the attenuation of particulate organic carbon (POC) increases from ∼8% in the upper mesopelagic (36–128 m) to ∼33% in the mid mesopelagic (129–500 m) as the rate of POC attenuation decreases (Belcher et al., 2016).

Influence of Environmental Conditions

Respiration rates vary in space and time depending on temperature, the quality and quantity of the organic substrate, availability of inorganic nutrients, and microbial community structure. Just like any other chemical reaction or metabolic rate, plankton respiration is related to temperature through an Arrhenius relationship. Mazuecos et al. (2015) derived mesopelagic respiration from oxygen consumption measurements and calculated a Q_{10} of 3.65 and an activation energy E_a of 0.90 eV for water temperatures between 8.7 and 14.9°C. This compared well with the temperature relationship of previously published mesopelagic respiration data (average Q_{10} of 4.07 and E_a of 0.98 eV), but is higher than the "optimal" Q_{10} values of between 1.5 and 2.6 of mesopelagic remineralization of particulate organic carbon derived from data-constrained modeling studies (DeVries and Weber, 2017; Laufkötter et al., 2017; Cram et al., 2018), and of activation energies determined for microbial respiration in surface waters (∼0.58 eV López-Urrutia and Móran, 2007; Yvon-Durocher et al., 2012).

Cell specific mesopelagic bacterioplankton respiration rates (**Table 2**) tend not to be correlated with temperature due to the ∼50-fold variability in cell specific respiration rates (0.1 to 5 fmol C cell^{-1} day^{-1}; Baltar et al., 2009a,b) related to the lack of a strong relationship between cell abundance and cell activity (del Giorgio and Gasol, 2008). For example, Reinthaler et al. (2006) found a threefold difference in bacterioplankton cell specific respiration rates in deep water masses of the east and west N Atlantic, with a general increase with depth, and with rates in the oxygen minimum zones intermediate between those in the more oxygenated water masses above and below.

Experiments which mimic the increase in pressure experienced by surface dwelling bacterioplankton as they descend to the mesopelagic zone associated with particles, show that rates of organic matter degradation decrease with increasing pressure (Tamburini et al., 2013). However, bacterioplankton which are endemic to the mesopelagic, adapt to conditions of high pressure, low temperature and low substrate availability, such that measurements of bacterioplankton production made at atmospheric pressure on decompressed samples underestimate *in situ* mesopelagic activity (Tamburini et al., 2013). As far as I am aware, measurements of mesopelagic bacterioplankton respiration have not yet been made at *in situ* pressures.

Nutrient addition experiments with oligotrophic and mesotrophic surface water plankton populations show increased plankton community and bacterioplankton respiration after addition of a mixture of glucose and amino acids (Martínez-García et al., 2013), and time series studies and data syntheses show significant correlations between bacterioplankton respiration and concentrations of dissolved organic carbon (Alonso-Sáez et al., 2008; Robinson, 2008). Bioavailability experiments with natural bacterioplankton communities and

TABLE 2 | Mesopelagic cell specific respiration (fmol C cell^{-1} day^{-1}) derived from measurements of electron transport system activity (ETS) or dissolved oxygen consumption (ΔO_2).

Region	Sample type	Cell specific respiration (fmol C cell^{-1} day^{-1})	Reference
Louisiana Shelf, United States	<1 μm, ΔO_2	2.4–8.7	Biddanda et al., 1994
Menai Strait, United Kingdom	<0.8 μm, ΔO_2	0.4–6.8	Blight et al., 1995
Gulf of Mexico, United States	<0.8 μm, ΔO_2	0.39	Jørgensen et al., 1999
Cardigan Bay, United Kingdom	0.2–12 μm, ΔO_2	4.28 ± 1.12	Mukhanov et al., 2003
North Sea	<0.8 μm, ΔO_2	0.3–3.6	Reinthaler et al., 2005
NW African coast	Whole sample, ΔO_2	0.2–2.0	Gasol et al., 2009
Temperate North Atlantic			Reinthaler et al., 2006
100–135 m	<0.6 μm, ΔO_2	Average 0.85	
402–725 m (O_2 minimum)	<0.6 μm, ΔO_2	Average 1.67	
1800–3000 m	<0.6 μm, ΔO_2	Average 2.74	
Southern Ocean			Obernoster et al., 2008
0–100 m	<0.8 μm, ΔO_2	0.5–1.9	
1000–4500 m	Whole sample, ΔO_2	0.23–6.9	
Subtropical North Atlantic			Baltar et al., 2009a
100 m	Whole sample, ETS	0.04–3.82	
200–1000 m	Whole sample, ETS	0.12–5.23	
1000–5000 m	Whole sample, ETS	0.43–7.66	
Subtropical North Atlantic			Baltar et al., 2009b
100 m	Whole sample, ETS	0.17–1.18	
200–1000 m	Whole sample, ETS	0.14–2.88	
1800–4500 m	Whole sample, ETS	0.23–6.90	

Adapted from Baltar et al. (2009b).

dissolved organic material harvested from cultures of four coastal diatoms under silicate and/or nitrate stress suggest that DOM remineralization and bacterioplankton growth efficiencies are influenced on time scales of a week by the nutrient stress under which the DOM is produced. However, on seasonal time scales, the diatom source species is more influential (Wear et al., 2015).

The interacting effect of increasing temperature and organic carbon supply on coastal bacterioplankton respiration and growth efficiencies has been studied recently in chemostats and turbidostats. In substrate limited conditions, growth efficiencies showed no trend with temperature, whereas under temperature limited, substrate replete conditions, bacterioplankton growth efficiencies increased with temperature (Maske et al., 2017). This contrasts with the meta-analysis of Rivkin and Legendre (2001) which showed a decrease in bacterioplankton growth efficiencies with increasing temperature.

In addition to the influence of nutrient availability and DOM composition, the bioavailability of DOM (and hence respiration rate) is also controlled by microbial community composition. Mesopelagic microbial communities in the eastern tropical South Pacific were able to utilize surface layer dissolved organic carbon which was recalcitrant to remineralization by surface microbial communities over time scales of 9–14 days (Letscher et al., 2015). Likewise, incubations of ambient seawater amended with DO^{13}C substrates including defined monosaccharides and exudates and lysates from ^{13}C-labeled *Synechococcus* cultures showed that each DOC substrate stimulated a different community growth response and a different rate of DOC removal (Nelson and Carlson, 2012). While *Synechococcus* exudates are incorporated by a wide diversity of bacterial taxa, defined monosaccharides and *Synechococcus* lysates were less bioavailable to ambient bacterioplankton.

RESPIRATORY QUOTIENTS

The relationship between the production of CO_2 and the consumption of O_2 during respiration is the respiratory quotient ($RQ = \Delta CO_2/-\Delta O_2$) and this varies depending on the stoichiometry of the organic substrate and the degree of oxidation or metabolic pathway used. Assuming complete oxidation, the RQ could range from 0.13 for lipid ($C_{40}H_{74}O_5$), 0.50 for methane (CH_4), 0.67 for saturated fatty acid (-CH_2-), 1.00 for glucose ($C_6H_{12}O_6$), 1.24 for nucleic acid ($C_1H_{1.3}O_{0.7}N_{0.4}P_{0.11}$), 1.33 for glycolic acid ($C_2H_4O_3$) and 4.00 for oxalic acid ($C_2H_2O_4$) (Rodrigues and Williams, 2001; Williams and del Giorgio, 2005; Berggren et al., 2011). Assuming the substrate is similar to the average composition of planktonic material, e.g., 65% protein, 19% lipid, 16% carbohydrate, or the typical composition of a phytoplankton cell, e.g., 40% protein, 40% carbohydrate, 15% lipid, 5% nucleic acid gives an RQ of 0.89 (Williams and del Giorgio, 2005). Quantifying the variability in RQ allows not only the production of CO_2 to be calculated from dissolved oxygen consumption, but also reveals shifts in plankton physiology that are not evident from any other measurement. Culture studies with marine bacteria (*Vibrio natriegens* and *Pseudomonas nautica*) show that the respiratory quotient varies with physiological state, metabolic pathway and carbon source (acetate or pyruvate) (Berdalet et al., 1995; Roy et al., 1999; Romero-Kutzner et al., 2015).

A systematic field study of the RQs of freshwater bacterioplankton showed large variability (1.2 ±0.45) with a significant negative correlation between RQ and *in situ* O_2 concentration and pH and a significant positive correlation between RQ and *in situ* pCO_2 (Berggren et al., 2011). Bacterioplankton RQs were low (average 0.81) in net autotrophic freshwater systems where reduced substrates derived from phytoplankton excretion are likely to dominate and higher (average 1.35) in net heterotrophic freshwater systems where oxidized substrates such as organic acids formed by photochemical processes could occur (Allesson et al., 2016). However, due to the low rates of oxygen consumption and CO_2 production by marine plankton, and the precision of methods to measure changes in dissolved inorganic carbon (DIC; ∼1–2 mmol m^{-3}), there has not been a systematic field study of the magnitude and variability of marine plankton RQs. Most studies of marine plankton respiration rely on measurements of dissolved oxygen consumption and assume a constant RQ of either 0.8 or 1.0 (e.g., Reinthaler et al., 2006; Nguyen et al., 2012; Teira et al., 2013), accepting that this introduces an error into the calculation of CO_2 production, since the RQ is likely to vary with environmental conditions and substrate availability.

Field measurements of the concurrent consumption of oxygen ($-\Delta O_2$) and production of DIC (ΔCO_2) of seawater samples incubated in the dark for 24h, can be used to derive an apparent respiratory quotient (ARQ; Angert et al., 2015). This is the integrative effect of not only the aerobic respiration of bacterio-, archaeo-, phyto-, and microzooplankton in the sample, but also all the other microbial metabolic processes which use or produce O_2 or CO_2, including nitrification (uptake of O_2 without production of CO_2), production of methane from acetate or methylamines (production of CO_2 without utilization of O_2), and production and dissolution of calcium carbonate (production or uptake of CO_2 without affecting O_2, respectively). The range of ARQs obtained from multiple field studies (Robertson, 1989; Wood, 1992; Robinson et al., 1999, 2002a,b; Sondergaard et al., 2000; Lefèvre et al., 2008 in **Figure 2**) spans the range of RQs calculated from the stoichiometry of potential substrates for microbial aerobic respiration with a median of 0.88 and an average of 1.11 ±0.76 (n = 149). There is some indication that higher ARQs occur in waters above the oxygen minimum zone in the Arabian Sea (Robinson and Williams, 1999) and lower ARQs occur during blooms of the coccolithophore *Emiliania huxleyi* (Holligan et al., 1993; Robertson et al., 1994). Until a more sensitive method is developed to measure CO_2 or DIC and a systematic study undertaken, derivation of CO_2 production from O_2 consumption will depend on using a constant $\Delta CO_2/-\Delta O_2$ ratio, accepting the potential 20–40% error (Reinthaler et al., 2006).

An apparent respiratory quotient integrated over longer time and larger space scales can also be derived from the relationship between DIC and AOU within a particular water mass. Measurements and models of the DIC:AOU ratio suggest a range between 0.51 and 0.85 depending on the composition

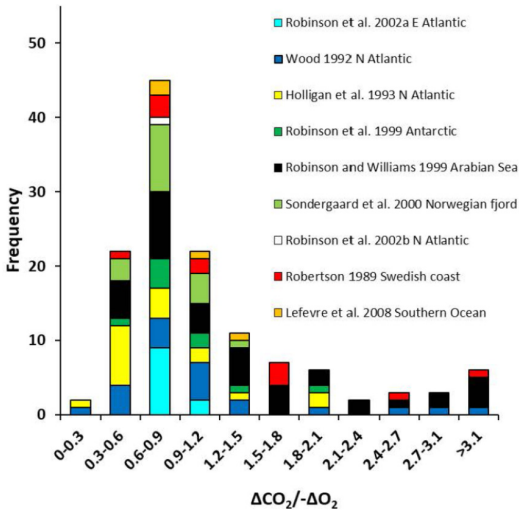

FIGURE 2 | Frequency histogram of apparent respiratory quotients (the ratio of oxygen consumption to production of dissolved inorganic carbon).

of the organic material being degraded – lower ratios are associated with the remineralization of labile and nitrogen-rich organic matter, higher ratios with remineralization of more recalcitrant organic matter (Thomas, 2002; Paulmier et al., 2009) – the combination of biogeochemical processes (e.g., respiration, nitrification, denitrification, anammox) occurring, and the history of the source water in terms of the different sensitivities of O_2 and DIC to changes in temperature and the different time scales of O_2 and CO_2 air-sea exchange (Anderson and Sarmiento, 1994; Thomas, 2002; Loucaides et al., 2012).

The ARQs of waters within oxygen minimum zones (and corresponding carbon maximum zones; Paulmier et al., 2011) vary between 0.6 and 1.5. Paulmier et al. (2011) determined the ARQ of waters in the shallow, very intense oxycline of Chilean coastal waters to be 1.1 ±0.3, potentially due to relatively higher rates of DIC production from more complete degradation of highly carbonated organic matter (Van Mooy et al., 2002; Paulmier et al., 2011).

SENSITIVITY TO DECREASING OXYGEN AND INCREASING CARBON DIOXIDE

Since the enzymes used during aerobic respiration require oxygen, at some level the rate of respiration will be directly sensitive to the ambient concentration of dissolved oxygen. In addition, dissolved oxygen concentration is a major determinant of microbial abundance and diversity (Wright et al., 2012) and will therefore indirectly affect the rate of respiration and other biogeochemical processes.

Hartnett et al. (1998), originally noted the strong negative relationship between sedimentary organic carbon preservation and length of exposure to oxygen, while Devol and Hartnett (2001) showed the influence of dissolved oxygen on midwater remineralisation. Calculated attenuation rates of particulate organic carbon flux for the oxic water column of the continental margin off Washington State were significantly higher than the attenuation rates calculated for the oxygen-deficient continental margin off northwest Mexico. A synthesis of attenuation length scale estimated from export flux and deep sediment trap data (Henson et al., 2012) shows clearly that mesopelagic remineralization is much reduced at low concentrations of dissolved oxygen (Sanders et al., 2016). Laufkötter et al. (2017) compiled particulate organic carbon flux measurements from 19 globally distributed sites and found that the attenuation of the flux of particulate organic matter depends on oxygen described by a half-saturation constant between 4 and 12 μmol L^{-1}. However, as well as any direct effect of reduced dissolved oxygen on aerobic microbial respiration, these attenuation rates will also include the indirect effect of reduced dissolved oxygen decreasing the depth of zooplankton diel vertical migration and so fragmentation, repackaging and respiration of organic carbon mediated by zooplankton (Cavan et al., 2016).

Due to the technical challenges of both measuring and maintaining extremely low oxygen concentrations, there are relatively few determinations of the oxygen sensitivity of aerobic respiration in low oxygen waters. Garcia-Robledo et al. (2016), using LUMOS optodes, found no apparent change in oxygen consumption rates at oxygen concentrations between ∼1.0 and 10 μmol L^{-1} in waters collected from the oxygen minimum zones of the eastern tropical Pacific Ocean and derived an apparent half saturation constant of 391 nmol O_2 L^{-1}. This agrees with a previous study using STOX microsensors which on average showed little oxygen dependence above oxygen concentrations of 500 nmol L^{-1} (Tiano et al., 2014). However, Kalvelage et al. (2015) showed an increase in aerobic respiration (from ∼0.1 to 8.0 μmol $L^{-1}d^{-1}$) with increasing ambient O_2 concentrations (from ∼1 to 20 μmol L^{-1}). This change in aerobic respiration is likely associated with changing community structure. Beman and Carolan (2013) sampled across oxygen gradients in the OMZ of the Gulf of California using pyrosequencing of 16S rRNA to show maximum values of bacterial richness on the edge of the OMZ where availability of oxidants and reductants contribute to functional and taxonomic diversity. Predicting the biochemical response of the microbial community to fluctuations in oxygen concentrations is extremely difficult, as both aerobic and anaerobic processes occur simultaneously, even in waters with undetectable oxygen concentrations (Bertagnolli and Stewart, 2018).

Since decreasing O_2 due to respiration will always be coupled with increasing CO_2, which leads to ocean acidification through decreasing pH and carbonate ion concentration, it is relevant to assess the positive or negative feedbacks associated with the direct and indirect effects of increasing CO_2 on plankton respiration. Many bacterial enzymatic processes involved in the utilization of organic compounds increase with increasing CO_2, or decreasing pH (e.g., Grossart et al., 2006; Piontek et al., 2010; Mass et al., 2013). Bunse et al. (2016) demonstrated upregulation of respiratory proton pumps at elevated CO_2 concentrations, presumably in order to export protons that invade the bacterioplankton cell as a result of low pH. Such proton exporting mechanisms are inherently energy demanding,

so that bacterioplankton would need to allocate more energy to cell maintenance instead of growth, implying a decrease in bacterial growth efficiency with increasing CO_2 (Bunse et al., 2016). This is consistent with measurements of the direct effect of increased CO_2 on bacterioplankton metabolism, revealing systematically greater cell-specific respiration in elevated CO_2 (James et al., 2017). This latter study also suggested that high CO_2 conditions may increase the ability of bacterioplankton to consume DOC, but with reduced growth efficiencies, leading to decreased storage of DOC.

Indirect effects of increased CO_2 on bacterioplankton respiration include increased respiration due to (1) the increased quantity and quality of phytoplankton derived particulate and dissolved organic carbon and/or (2) reduced calcium carbonate ballast enabling greater bacterial access to associated organic material. Mesocosm experiments in a range of nutrient regimes and plankton communities show equivocal results. Some show that bacteria benefitted both directly through enhanced enzymatic hydrolysis of organic matter and indirectly through increased availability of phytoplankton derived organic substrate (Grossart et al., 2006; Piontek et al., 2010), and that copepods increased their respiration rate at elevated CO_2 concentrations (Li and Gao, 2012). However, recent mesocosm and microcosm studies in an Arctic fjord, the Mediterranean Sea and the subtropical North Atlantic Ocean found no significant relationship between bacterioplankton or plankton community respiration and CO_2 concentrations (Motegi et al., 2013; Tanaka et al., 2013; Mercado et al., 2014; Maugendre et al., 2017; Filella et al., 2018), and Spilling et al. (2016) found a decrease in plankton community respiration at elevated CO_2 levels during a mesocosm experiment in the Baltic Sea.

As far as I am aware there have been no CO_2 manipulation studies of mesopelagic microbial communities or studies of the cumulative (additive, synergistic or antagonistic) effect of the combination of decreasing dissolved oxygen and increasing CO_2 on environmental genomics and plankton respiration, as have been undertaken for metabolic rates of invertebrate and vertebrate marine organisms (Gobler and Baumann, 2016).

KNOWN UNKNOWNS AND RECOMMENDATIONS FOR FUTURE RESEARCH

Current models do not reproduce the observed patterns of changes in dissolved oxygen, they underestimate the interannual to decadal variability in dissolved oxygen and they simulate only half of the oceanic oxygen loss inferred from observations (Oschlies et al., 2018). Increased *in situ* observations and quantitative mechanistic understanding of the influence of both physical and biological processes on dissolved oxygen changes are therefore required to develop and verify these numerical models. In particular, since these models account for the major physical and chemical processes involved in deoxygenation, but do not include some of the microbial processes and feedbacks discussed here, it is relevant to investigate whether including these microbiological processes would account for the additional decrease in oxygen needed to match the model outputs with the observations.

The major biological process influencing a decline in dissolved oxygen concentration is plankton respiration. Hence improved mechanistic understanding of the drivers influencing the variability of respiration, particularly those that are climate sensitive, or currently not represented in numerical models, is required. Examples would include the influence of changing inorganic nutrient concentrations and stoichiometry on plankton community structure including the proportion of respiration attributable to bacterioplankton or vertically migrating zooplankton and the size distribution and composition of exported particles, changes in the respiratory quotient, the interacting effects of increasing CO_2 and decreasing O_2 on bacterioplankton respiration, and the influence of warming and nutrient stoichiometry on the bacterial utilization of previously recalcitrant dissolved organic carbon (Jiao et al., 2010, 2014; Zhang et al., 2018). On a broader scale, this complex wicked problem also requires an appreciation of the potential feedbacks between primary production, nitrogen cycling, organic matter flux and oxygen consumption (Canfield, 2006; Boyle et al., 2013; Bristow et al., 2016). At the microbial scale, representation of symbiotic metabolic interactions (Wright et al., 2012), including the potential for cryptic oxygen cycling to occur within otherwise anoxic zones (Garcia-Robledo et al., 2017) is required.

A dedicated longtime and large spatial scale observational program is required, linked to a numerical modeling framework (Oschlies et al., 2018), and within which targeted manipulation experiments could take place. The observational program would include a range of methods for determining plankton respiration from the individual organism to the oceanographic region, including those already established (e.g., *in vitro* O_2 consumption, electron transport system activity, $^{14}CO_2$ production, AOU) and those currently in development (e.g., fluorescence, *in situ* respirometry, and derivation from optode measurements on moorings, gliders and biogeochemical Argo floats[1]), measured alongside the plankton community structure and organic/inorganic nutrient regime (e.g., Honjo et al., 2014; Collins et al., 2018). Metagenomic analysis coupled with trace chemical assays and isotope tracer experiments should be incorporated into the observational program to reveal the detail of low oxygen metabolic pathways (Bertagnolli and Stewart, 2018). In addition, established multidisciplinary time series and global surveys (e.g., OceanSITES[2] and GO-SHIP[3]) should begin to place as much emphasis on determining the plankton respiratory processes which utilize dissolved oxygen and convert organic carbon to CO_2, as they currently do on the autotrophic processes which produce dissolved oxygen and convert CO_2 to particulate and dissolved organic carbon. An implementation plan to specifically quantify the capacity for marine carbon storage through recalcitrant dissolved organic carbon (the microbial carbon pump), and the potential reduction in this capacity due to global change, leading to a positive

[1]http://www.argo.ucsd.edu/

[2]http://www.oceansites.org/index.html

[3]http://www.go-ship.org/index.html

feedback of increased oxygen consumption and CO_2 production, has recently been proposed (Robinson et al., 2018).

Isolation and cultivation of a greater number of microbes from low oxygen waters will help quantify the oxygen thresholds constraining chemical fluxes and identify the enzymes responsible (Bertagnolli and Stewart, 2018). A suite of single species and natural plankton community micro-, meso- and macro-cosm manipulation experiments should be embedded within the observational and modeling framework, specifically to confirm or refute proposed biological mechanisms of increasing ocean deoxygenation and the interacting effects of increasing CO_2 and decreasing O_2 on plankton metabolism (**Figure 1**). Since ocean deoxygenation is linked mechanistically to other ocean stressors (or drivers) including warming, acidification and nutrient availability and stoichiometry, these manipulation experiments will need to be multiple stressor experiments and follow appropriate best practice in design, implementation and statistical analysis (Riebesell and Gattuso, 2014; Boyd et al., 2016, 2018). The Scientific Committee on Oceanic Research (SCOR) working group 149 has recently released an open access decision support tool https://scor149-ocean.com/decision-support-tool/ to aid in design and interpretation of multiple stressor experiments, and a *Multiple Driver Best Practice Guide* will be launched in 2019.

The predictions and projections of the distribution and extent of ocean deoxygenation and the cumulative effects of other drivers of global change afforded by the observational verification of numerical models, need to also extend to predictions of the consequences of ocean deoxygenation on the ecosystem services and human livelihoods and welfare provided by the ocean (Breitburg et al., 2018). This aligns with the scientific objectives of the Integrated Marine Biosphere Research project (IMBeR) to *incorporate understanding of the drivers and consequences of global change on marine ecosystems and human societies at multiple scales into models to project and predict future states* (Hofmann and The IMBeR Scientific Steering Committee, 2016), and the Intergovernmental Oceanographic Commission (IOC) of UNESCO sponsored expert group, the Global Ocean Oxygen Network GO_2NE[4] which aims to improve ocean oxygen observation systems, identify and fill knowledge gaps, build capacity, and provide scientific advice to policy makers. GO_2NE also maintains the news site www.ocean-oxygen.org for scientists, stakeholders and the interested public.

Only through international co-ordination and collaboration will we be able to quantify the environmental, physiological and ecological drivers of variability in plankton respiration contributing to ocean deoxygenation, and hence predict and project the cumulative effect of ocean deoxygenation and other global change drivers on marine ecosystems and human societies.

[4] http://www.unesco.org/new/en/natural-sciences/ioc-oceans/sections-and-programmes/ocean-sciences/global-ocean-oxygen-network/

AUTHOR CONTRIBUTIONS

CR conceived and wrote the article.

FUNDING

This study was supported by funds from The Leverhulme Trust (Grant RPG-2017-089 awarded to CR) and the Natural Environment Research Council (NERC) of the United Kingdom (Grants NE/R000956/1 and NE/K00168X/1 awarded to CR). I gratefully acknowledge financial support from The Royal Society (United Kingdom), EurOceans and the Integrated Marine Biogeochemistry and Ecosystem Research (IMBER; http://www.imber.info/) project sponsored workshops on "Ocean ventilation and deoxygenation in a warming world" in September 2016 and on "Ocean deoxygenation and implications for marine biogeochemical cycles and ecosystems" in October 2011 which provided financial support for me to attend.

ACKNOWLEDGMENTS

This study arose from invitations to present at the two workshops described above. The manuscript benefits from discussions with Dr. Elena García-Martin (University of East Anglia, United Kingdom), the OCEANic release of Greenhouse gASes under pressure from multiple stressors (OCEAN-GASP) team led by Dr. Andrew Rees (Plymouth Marine Laboratory, United Kingdom), and the editorial and reviewing team at Frontiers.

REFERENCES

Aguiar-González, B., Packard, T. T., Berdalet, E., Roy, S., and Gómez, M. (2012). Respiration predicted from an Enzyme Kinetic Model and the Metabolic Theory of Ecology in two species of marine bacteria. *J. Exp. Mar. Biol. Ecol.* 412, 1–12. doi: 10.1016/j.jembe.2011.09.018

Allesson, L., Ström, L., and Berggren, M. (2016). Impact of photochemical processing of DOC on the bacterioplankton respiratory quotient in aquatic ecosystems. *Geophys. Res. Lett.* 43, 7538–7545. doi: 10.1002/2016GL069621

Alonso-Sáez, L., Vázquez-Domínguez, E., Cardelús, C., Pinhassi, J., Montserrat Sala, M., Lekunberri, I., et al. (2008). Factors controlling the year-round variability in carbon flux through bacteria in a coastal marine system. *Ecosystems* 11, 397–409. doi: 10.1007/s10021-008-9129-0

Anderson, L. A., and Sarmiento, J. L. (1994). Redfield ratios of remineralization determined by nutrient data analysis. *Glob. Biogeochem. Cycles* 8, 65–80. doi: 10.1029/93GB03318

Angert, A., Yakir, D., Rodeghiero, M., Preisler, Y., Davidson, E. A., and Weiner, T. (2015). Using O_2 to study the relationships between soil CO_2 efflux and soil respiration. *Biogeosciences* 12, 2089–2099. doi: 10.5194/bg-12-2089-2015

Arístegui, J., Duarte, C. M., Gasol, J. M., and Alonso-Sáez, L. (2005). Active mesopelagic prokaryotes support high respiration in the subtropical northeast Atlantic Ocean. *Geophys. Res. Lett.* 32:L03608. doi: 10.1029/2004GL021863

Arístegui, J., Gasol, J. M., Duarte, C. M., and Herndl, G. J. (2009). Microbial oceanography of the dark ocean's pelagic realm. *Limnol. Oceanogr.* 54, 1501–1529. doi: 10.4319/lo.2009.54.5.1501

Arístegui, J., Agustí, S., and Duarte, C. M. (2003). Respiration in the dark ocean. *Geophys. Res. Lett.* 30:1041. doi: 10.1029/2002GL016227

Baltar, F., Arístegui, J., Gasol, J. M., and Herndl, G. J. (2010). Prokaryotic carbon utilization in the dark ocean: growth efficiency, leucine-to-carbon conversion factors, and their relation. *Aquat. Microb. Ecol.* 60, 227–232. doi: 10.3354/ame01422

Baltar, F., Arístegui, J., Gasol, J. M., Sintes, E., and Herndl, G. J. (2009a). Evidence of prokaryotic metabolism on suspended particulate organic matter in the dark waters of the subtropical North Atlantic. *Limnol. Oceanogr.* 54, 182–193. doi: 10.4319/lo.2009.54.1.0182

Baltar, F., Arístegui, J., Sintes, E., van Aken, H. M., Gasol, J. M., and Herndl, G. J. (2009b). Prokaryotic extracellular enzymatic activity in relation to biomass production and respiration in the meso-and bathypelagic waters of the (sub)tropical Atlantic. *Environ. Microbiol.* 11, 1998–2014. doi: 10.1111/j.1462-2920.2009.01922.x

Barker, S., Higgins, J. A., and Elderfield, H. (2003). The future of the carbon cycle: review, calcification response, ballast and feedback on atmospheric CO_2. *Philos. Trans. R. Soc. A Math. Phys. Eng. Sci.* 361, 1977–1998; discussion 1998–1999. doi: 10.1098/rsta.2003.1238

Belcher, A., Iversen, M., Giering, S., Riou, V., Henson, S. A., Berline, L., et al. (2016). Depth-resolved particle-associated microbial respiration in the northeast Atlantic. *Biogeosciences* 13, 4927–4943. doi: 10.5194/bg-13-4927-2016

Beman, J. M., and Carolan, M. T. (2013). Deoxygenation alters bacterial diversity and community composition in the ocean's largest oxygen minimum zone. *Nat. Commun.* 4:2705. doi: 10.1038/ncomms3705

Berdalet, E., Packard, T., Lagacé, B., Roy, S., St-Amand, L., and Gagné, J.-P. (1995). CO_2 production, O_2 consumption and isocitrate dehydrogenase in the marine bacterium *Vibrio natriegens*. *Aquat. Microb. Ecol.* 9, 211–217. doi: 10.3354/ame009211

Berggren, M., Lapierre, J.-F., and del Giorgio, P. A. (2011). Magnitude and regulation of bacterioplankton respiratory quotient across freshwater environmental gradients. *ISME J.* 6, 984–993. doi: 10.1038/ismej.2011.157

Bertagnolli, A. D., and Stewart, F. J. (2018). Microbial niches in marine oxygen minimum zones. *Nat. Rev. Microbiol.* 16, 723–729. doi: 10.1038/s41579-018-0087-z

Biddanda, B., Opsahl, S., and Benner, R. (1994). Plankton respiration and carbon flux through bacterioplankton on the Louisiana shelf. *Limnol. Oceanogr.* 39, 1259–1275. doi: 10.4319/lo.1994.39.6.1259

Blight, S. P., Bentley, T. L., Lefevre, D., Robinson, C., Rodrigues, R., Rowlands, J., et al. (1995). Phasing of autotrophic and heterotrophic plankton metabolism in a temperate coastal ecosystem. *Mar. Ecol. Prog. Ser.* 128, 61–75. doi: 10.3354/meps128061

Bopp, L., Le Quéré, C., Heimann, M., Manning, A. C., and Monfray, P. (2002). Climate-induced oceanic oxygen fluxes: implications for the contemporary carbon budget. *Glob. Biogeochem. Cycles* 16, 6-1–6-13. doi: 10.1029/2001GB001445

Boyd, P. W., Collins, S., Dupont, S., Fabricius, K., Gattuso, J.-P., Havenhand, J., et al. (2018). Experimental strategies to assess the biological ramifications of multiple drivers of global ocean change – A review. *Glob. Change Biol.* 24, 2239–2261. doi: 10.1111/gcb.14102

Boyd, P. W., Dillingham, P. W., McGraw, C. M., Armstrong, E. A., Cornwall, C. E., Feng, Y.-Y., et al. (2016). Physiological responses of a Southern Ocean diatom to complex future ocean conditions. *Nat. Clim. Chang.* 6, 207–216. doi: 10.1038/nclimate2811

Boyle, R. A., Clark, J. R., Poulton, S. W., Shields-Zhou, G., Canfield, D. E., and Lenton, T. M. (2013). Nitrogen cycle feedbacks as a control on euxinia in the mid-Proterozoic ocean. *Nat. Commun.* 4:1533. doi: 10.1038/ncomms2511

Brandt, P., Bange, H. W., Banyte, D., Dengler, M., Didwischus, S.-H., Fischer, T., et al. (2015). On the role of circulation and mixing in the ventilation of oxygen minimum zones with a focus on the eastern tropical North Atlantic. *Biogeosciences* 12, 489–512. doi: 10.5194/bg-12-489-2015

Breitburg, D., Levin, L. A., Oschlies, A., Grégoire, M., Chavez, F. P., Conley, D. J., et al. (2018). Declining oxygen in the global ocean and coastal waters. *Science* 359:eaam7240. doi: 10.1126/science.aam7240

Brewer, P. G., and Peltzer, E. T. (2009). Limits to marine life. *Science* 324, 347–348. doi: 10.1126/science.1170756

Bristow, L. A., Callbeck, C. M., Larsen, M., Altabet, M. A., Dekaezemacker, J., Forth, M., et al. (2016). N2 production rates limited by nitrite availability in the Bay of Bengal oxygen minimum zone. *Nat. Geosci.* 10, 24–29. doi: 10.1038/NGEO2847

Bunse, C., Lundin, D., Karlsson, C. M. G., Akram, N., Vila-Costa, M., Palovaara, J., et al. (2016). Response of marine bacterioplankton pH homeostasis gene expression to elevated CO_2. *Nat. Clim. Chang.* 6, 483–487. doi: 10.1038/NCLIMATE2914

Canfield, D. E. (2006). Models of oxic respiration, denitrification and sulfate reduction in zones of coastal upwelling. *Geochim. Cosmochim. Acta* 70, 5753–5765. doi: 10.1016/j.gca.2006.07.023

Cavan, E. L., Trimmer, M., Shelley, F., and Sanders, R. (2016). Remineralization of particulate organic carbon in an ocean oxygen minimum zone. *Nat. Commun.* 8:14847. doi: 10.1038/ncomms14847

Collins, J. R., Fucile, P. D., McDonald, G., Ossolinski, J. E., Keil, R. G., Valdes, J. R., et al. (2018). An autonomous, *in situ* light-dark bottle device for determining community respiration and net community production. *Limnol. Oceanogr. Methods* 16, 323–338. doi: 10.1002/lom3.10247

Cram, J. A., Weber, T., Leung, S. W., McDonnell, A. M. P., Liang, J.-H., and Deutsch, C. (2018). The role of particle size, ballast, temperature, and oxygen in the sinking flux to the deep sea. *Glob. Biogeochem. Cycles* 32, 858–876. doi: 10.1029/2017GB005710

del Giorgio, P. A., and Duarte, C. M. (2002). Respiration in the open ocean. *Nature* 420, 379–384. doi: 10.1038/nature01165

del Giorgio, P. A., and Gasol, J. M. (2008). "Physiological structure and single-cell activity in marine bacterioplankton," in *Microbial Ecology of the Oceans*, 2nd Edn, ed. D. L. Kirchman (Hoboken, NJ: John Wiley & Sons, Inc).

Deutsch, C., Berelson, W., Thunell, R., Weber, T., Tems, C., and McManus, J. (2014). Centennial changes in North Pacific anoxia linked to tropical trade winds. *Science* 345, 665–668. doi: 10.1126/science.1252332

Deutsch, C., Brix, H., Ito, T., Frenzel, H., and Thompson, L. (2011). Climate-forced variability of Ocean Hypoxia. *Science* 333, 336–339. doi: 0.1126/science.1202422

Devol, A. H., and Hartnett, H. E. (2001). Role of oxygen-deficient zone in transfer of organic carbon to the deep ocean. *Limnol. Oceanogr.* 46, 1684–1690. doi: 10.4319/lo.2001.46.7.1684

DeVries, T., and Weber, T. (2017). The export and fate of organic matter in the ocean: new constraints from combining satellite and oceanographic tracer observations. *Glob. Biogeochem. Cycles* 31, 535–555. doi: 10.1002/2016GB005551

Diaz, R. J., and Rosenberg, R. (2008). Spreading dead zones and consequences for marine ecosystems. *Science* 321, 926–929. doi: 10.1126/science.1156401

Duteil, O., Koeve, W., Oschlies, A., Bianchi, D., Galbraith, E., Kriest, I., et al. (2013). A novel estimate of ocean oxygen utilization points to a reduced rate of respiration in the ocean interior. *Biogeosciences* 10, 7723–7738. doi: 10.5194/bg-10-7723-2013

Engel, A., Delille, B., Jacquet, S., Riebesell, U., Rochelle-Newall, E., Terbrüggen, A., et al. (2004). Transparent exopolymer particles and dissolved organic carbon production by *Emiliania huxleyi* exposed to different CO_2 concentrations: a mesocosm experiment. *Aquat. Microb. Ecol.* 34, 93–104. doi: 10.3354/ame034093

Feely, R. A., Sabine, C. L., Schlitzer, R., Bullister, J. L., Mecking, S., and Greeley, D. (2004). Oxygen utilization and organic carbon remineralization in the upper water column of the Pacific Ocean. *J. Oceanogr.* 60, 45–52. doi: 10.1023/B:JOCE.0000038317.01279.aa

Fernández-Castro, B., Arístegui, J., Anderson, L., Montero, M. F., Hernández-León, S., Marañón, E., et al. (2016). Mesopelagic respiration near the ESTOC (European Station for Time-Series in the Ocean, 15.5^{o}W, 29.1^{o}N) site inferred from a tracer conservation model. *Deep Sea Res. I Oceanogr. Res. Pap.* 115, 63–73. doi: 10.1016/j.dsr.2016.05.010

Filella, A., Baños, I., Montero, M. F., Hernández-Hernández, N., Rodriguez-Santos, A., Ludwig, A., et al. (2018). Plankton community respiration and ETS activity under variable CO_2 and nutrient fertilization during a mesocosm study in the Subtropical North Atlantic. *Front. Mar. Sci.* 5:310. doi: 10.3389/fmars.2018.00310

Garcia-Robledo, E., Borisov, S., Klimant, I., and Revsbech, N. P. (2016). Determination of respiration rates in water with sub-micromolar oxygen concentrations. *Front. Mar. Sci.* 3:244. doi: 10.3389/fmars.2016.00244

Garcia-Robledo, E., Padilla, C. C., Aldunate, M., Stewart, F. J., Ulloa, O., Paulmier, A., et al. (2017). Cryptic oxygen cycling in anoxic marine zones. *Proc. Natl. Acad. Sci. U.S.A.* 114, 8319–8324. doi: 10.1073/pnas.1619844114

Gasol, J. M., Alonso-Sáez, L., Vaqué, D., Baltar, F., Calleja, M. L., Duarte, C. M., et al. (2009). Mesopelagic prokaryotic bulk and single-cell heterotrophic activity and community composition in the NW Africa-Canary Islands coastal-transition zone. *Prog. Oceanogr.* 83, 189–196. doi: 10.1016/j.pocean.2009.07.014

Giering, S. L. C., Sanders, R., Lampitt, R. S., Anderson, T. R., Tamburini, C., Boutrif, M., et al. (2014). Reconciliation of the carbon budget in the ocean's twilight zone. *Nature* 507, 480–483. doi: 10.1038/nature13123

Gobler, C. J., and Baumann, H. (2016). Hypoxia and acidification in ocean ecosystems: coupled dynamics and effects on marine life. *Biol. Lett.* 12:20150976. doi: 10.1098/rsbl.2015.0976

Grossart, H.-P., Allgaier, M., Passow, U., and Riebesell, U. (2006). Testing the effect of CO_2 concentration on the dynamics of marine heterotrophic bacterioplankton. *Limnol. Oceanogr.* 51, 1–11. doi: 10.4319/lo.2006.51.1.0001

Gruber, N. (2011). Warming up, turning sour, losing breath: ocean biogeochemistry under global change. *Philos. Trans. A Math. Phys. Eng. Sci.* 369, 1980–1996. doi: 10.1098/rsta.2011.0003

Guidi, L., Legendre, L., Reygondeau, G., Uitz, J., Stemmann, L., and Henson, S. A. (2015). A new look at ocean carbon remineralization for estimating deepwater sequestration. *Glob. Biogeochem. Cycles* 29, 1044–1059. doi: 10.1002/2014GB005063

Hartnett, H. E., Kell, R. G., Hedges, J. I., and Devol, A. H. (1998). Influence of oxygen exposure time on organic carbon preservation in continental margin sediments. *Nature* 391, 572–574. doi: 10.1038/35351

Henson, S. A., Beaulieu, C., Ilyina, T., John, J. G., Long, M., Seferian, R., et al. (2017). Rapid emergence of climate change in environmental drivers of marine ecosystems. *Nat. Commun.* 8:14682. doi: 10.1038/ncomms14682

Henson, S. A., Sanders, R., and Madsen, E. (2012). Global patterns in efficiency of particulate organic carbon export and transfer to the deep ocean. *Glob. Biogeochem. Cycles* 26:GB1028. doi: 10.1029/2011GB004099

Hill, P. G., Warwick, P. E., and Zubkov, M. V. (2013). Low microbial respiration of leucine at ambient oceanic concentration in the mixed layer of the central Atlantic Ocean. *Limnol. Oceanogr.* 58, 1597–1604. doi: 10.4319/lo.2013.58.5.1597

Hofmann, E. E., and The IMBeR Scientific Steering Committee (2016). *IMBeR 2016-2025: Science Plan and Implementation Strategy*. Bergen: IMBeR International Project Office.

Holligan, P. M., Fernández, E., Aiken, J., Balch, W. M., Boyd, P., Burkill, P. H., et al. (1993). A biogeochemical study of the coccolithophore, *Emiliania huxleyi*, in the North Atlantic. *Glob. Biogeochem. Cycles* 7, 879–900. doi: 10.1029/93GB01731

Holtappels, M., Tiano, L., Kalvelage, T., Lavik, G., Revsbech, N. P., and Kuypers, M. M. M. (2014). Aquatic respiration rate measurements at low oxygen concentrations. *PLoS One* 9:e89369. doi: 10.1371/journal.pone.0089369

Honjo, S., Eglinton, T. I., Taylor, C. D., Ulmer, K. M., Sievert, S. M., Bracher, A., et al. (2014). Understanding the role of the biological pump in the global carbon cycle: an imperative for ocean science. *Oceanography* 27, 10–16. doi: 10.5670/oceanog.2014.78

Ito, T., Nenes, A., Johnson, M. S., Meskhidze, N., and Deutsch, C. (2016). Acceleration of oxygen decline in the tropical Pacific over the past decades by aerosol pollutants. *Nat. Geosci.* 9, 443–447. doi: 10.1038/NGEO2717

James, A. K., Passow, U., Brzezinski, M. A., Parsons, R. J., Trapani, J. N., and Carlson, C. A. (2017). Elevated pCO_2 enhances bacterioplankton removal of organic carbon. *PLoS One* 12:e0173145. doi: 10.1371/journal.pone.0173145

Jenkins, W. J. (1987). 3H and 3He in the Beta Triangle: observations of gyre ventilation and oxygen utilization rates. *J. Phys. Oceanogr.* 17, 763–783. doi: 10.1175/1520-0485(1987)017<0763:AITBTO>2.0.CO;2

Jiao, N., Herndl, G. J., Hansell, D. A., Benner, R., Kattner, G., Wilhelm, S. W., et al. (2010). Microbial production of recalcitrant dissolved organic matter: long-term carbon storage in the global ocean. *Nat. Rev. Microbiol.* 8, 593–599. doi: 10.1038/nrmicro2386

Jiao, N., Robinson, C., Azam, F., Thomas, H., Baltar, F., Dang, H., et al. (2014). Mechanisms of microbial carbon sequestration in the ocean – future research directions. *Biogeosciences* 11, 5285–5306. doi: 10.5194/bg-11-5285-2014

Jiao, N., Tang, K., Cai, H., and Mao, Y. (2011). Increasing the microbial carbon sink in the sea by reducing chemical fertilization on the land. *Nat. Rev. Microbiol.* 9, 75–75. doi: 10.1038/nrmicro2386-c2

Jørgensen, N. O. G., Kroer, N., Coffin, R. B., and Hoch, M. P. (1999). Relations between bacterial nitrogen metabolism and growth efficiency in an estuarine and an open-water ecosystem. *Aquat. Microb. Ecol.* 18, 247–261. doi: 10.3354/ame018247

Kalvelage, T., Lavik, G., Jensen, M. M., Revsbech, N. P., Löscher, C., Schunck, H., et al. (2015). Aerobic microbial respiration in oceanic oxygen minimum zones. *PLoS One* 10:e0133526. doi: 10.1371/journal.pone.0133526

Keeling, R. F., and Garcia, H. (2002). The change in oceanic O_2 inventory associated with recent global warming. *Proc. Natl. Acad. Sci. U.S.A.* 99, 7848–7853. doi: 10.1073/pnas.122154899

Keeling, R. F., Körtzinger, A., and Gruber, N. (2010). Ocean deoxygenation in a warming world. *Annu. Rev. Mar. Sci.* 2, 199–299. doi: 10.1146/annurev.marine.010908.163855

Laufkötter, C., John, J. G., Stock, C. A., and Dunne, J. P. (2017). Temperature and oxygen dependence of the remineralization of organic matter. *Glob. Biogeochem. Cycles* 31, 1038–1050. doi: 10.1002/2017GB005643

Lefèvre, D., Guigue, C., and Obernosterer, I. (2008). The metabolic balance at two contrasting sites in the Southern ocean: the iron-fertilised Kerguelen area and HNLC waters. *Deep Sea Res. II Top. Stud. Oceanogr.* 55, 766–776. doi: 10.1016/j.dsr2.2007.12.006

Lehner, P., Larndorfer, C., Garcia-Robledo, E., Larsen, M., Borisov, S. M., Revsbech, N.-P., et al. (2015). LUMOS – A sensitive and reliable optode system for measuring dissolved oxygen in the nanomolar range. *PLoS One* 10:e0128125. doi: 10.1371/journal.pone.0128125

Lehner, P., Staudinger, C., Borisov, S. M., and Klimant, I. (2014). Ultra-sensitive optical oxygen sensors for characterization of nearly anoxic systems. *Nat. Commun.* 5:4460. doi: 10.1038/ncomms5460

Letscher, R. T., Knapp, A. N., James, A. K., Carlson, C. A., Santoro, A. E., and Hansell, D. A. (2015). Microbial community composition and nitrogen availability influence DOC remineralization in the South Pacific Gyre. *Mar. Chem.* 177, 325–334. doi: 10.1016/j.marchem.2015.06.024

Levin, K., Cashore, B., Bernstein, S., and Auld, G. (2012). Overcoming the tragedy of super wicked problems: constraining our future selves to ameliorate global climate change. *Policy Sci.* 45, 123–152. doi: 10.1007/s11077-012-9151-0

Li, W., and Gao, K. (2012). A marine secondary producer respires and feeds more in a high CO_2 ocean. *Mar. Pollut. Bull.* 64, 699–703. doi: 10.1016/j.marpolbul.2012.01.033

López-Urrutia, A., and Móran, X. A. G. (2007). Resource limitation of bacterial production distorts the temperature dependence of oceanic carbon cycling. *Ecology* 88, 817–822. doi: 10.1890/06-1641

López-Urrutia, A., San Martin, E., Harris, R. P., and Irigoien, X. (2006). Scaling the metabolic balance of the ocean. *Proc. Natl. Acad. U.S.A.* 103, 8739–8744. doi: 10.1073/pnas.0601137103

Loucaides, S., Tyrrell, T., Achterberg, E. P., Torres, R., Nightingale, P. D., Kitidis, V., et al. (2012). Biological and physical forcing of carbonate chemistry in an upwelling filament off northwest Africa: results from a Lagrangian study. *Glob. Biogeochem. Cycles* 26:GB3008. doi: 10.1029/2011GB004216

Martínez-García, S. (2017). Microbial respiration in the mesopelagic zone at Station ALOHA. *Limnol. Oceanogr.* 62, 320–333. doi: 10.1002/lno.10397

Martínez-García, S., Fernández, E., Aranguren-Gassis, M., and Teira, E. (2009). In vivo electron transport system activity: a method to estimate respiration in natural marine microbial planktonic communities. *Limnol. Oceanogr. Methods* 7, 459–469. doi: 10.4319/lom.2009.7.459

Martínez-García, S., Fernández, E., Calvo-Díaz, A., Cermeño, P., Marañón, E., Morán, X. A. G., et al. (2013). Differential response of microbial plankton to nutrient inputs in oligotrophic versus mesotrophic waters of the North Atlantic. *Mar. Biol. Res.* 9, 358–370. doi: 10.1080/17451000.2012.745002

Maske, H., Cajal-Medrano, R., and Villegas-Mendoza, J. (2017). Substrate-limited and –unlimited coastal microbial communities show different metabolic responses with regard to temperature. *Front. Microbiol.* 8:2270. doi: 10.3389/fmicb.2017.02270

Mass, E. W., Law, C. S., Hall, J. A., Pickmere, S., Currie, K. I., Chang, F. H., et al. (2013). Effect of ocean acidification on bacterial abundance, activity and diversity in the Ross Sea, Antarctica. *Aquat. Microb. Ecol.* 70, 1–15. doi: 10.3354/ame01633

Maugendre, L., Gattuso, J.-P., Poulton, A. J., Dellisanti, W., Gaubert, M., Guieu, C., et al. (2017). No detectable effect of ocean acidification on plankton metabolism in the NW oligotrophic Mediterranean Sea: results from two

mesocosm studies. *Estuar. Coast. Shelf Sci.* 186, 89–99. doi: 10.1016/j.ecss.2015.03.009

Mazuecos, I. P., Arístegui, J., Vázquez-Dominguez, E., Ortega-Retuerta, E., Gasol, J. M., and Reche, I. (2015). Temperature control of microbial respiration and growth efficiency in the mesopelagic zone of the South Atlantic and Indian Oceans. *Deep Sea Res. I Oceanogr. Res. Pap.* 95, 131–138. doi: 10.1016/j.dsr.2014.10.014

McDonnell, A. M. P., Boyd, P. W., and Buesseler, K. O. (2015). Effects of sinking velocities and microbial respiration rates on the attenuation of particulate carbon fluxes through the mesopelagic zone. *Glob. Biogeochem. Cycles* 29, 175–193. doi: 10.1002/2014GB004935

Mercado, J. M., Sobrino, C., Neale, P. J., Segovia, M., Reul, A., Amorim, A. L., et al. (2014). Effect of CO_2, nutrients and light on coastal plankton. II. Metabolic rates. *Aquat. Biol.* 22, 43–57. doi: 10.3354/ab00606

Moore, J. K., Fu, W. W., Primeau, F., Britten, G. L., Lindsay, K., and Long, M. (2018). Sustained climate warming drives declining marine biological productivity. *Science* 359, 1139–1142. doi: 10.1126/science.aao6379

Motegi, C., Tanaka, T., Piontek, J., Brussard, C. P. D., Gattuso, J.-P., and Weinbauer, M. G. (2013). Effect of CO_2 enrichment on bacterial metabolism in an Arctic fjord. *Biogeosciences* 10, 8285–3296. doi: 10.5194/bg-10-3285-2013

Mukhanov, V., Rylkova, O., Lopukhina, O., and Kemp, R. B. (2003). Productivity and thermodynamics of marine bacterioplankton: an inter-ecosystem comparison. *Thermochim. Acta* 397, 31–35. doi: 10.1016/S0040-6031(02)00313-1

Nelson, C. E., and Carlson, C. A. (2012). Tracking differential incorporation of dissolved organic carbon types among diverse lineages of Sargasso Sea bacterioplankton. *Environ. Microbiol.* 14, 1500–1516. doi: 10.1111/j.1462-2920.2012.02738.x

Nguyen, D., Tremblay, J.-E., and Gosselin, M. (2012). Respiration and bacterial carbon dynamics in the Amundsen Gulf, western Canadian Arctic. *J. Geophys. Res.* 117:C00G16. doi: 10.1029/2011JC007343

Obernoster, I., Christaki, U., Lefèvre, D., Catala, P., van Wambeke, F., and Lebaron, P. (2008). Rapid bacterial mineralization of organic carbon produced during a phytoplankton bloom induced by natural iron fertilization in the Southern Ocean. *Deep Sea Res. II Top. Stud. Oceanogr.* 55, 777–789. doi: 10.1016/j.dsr2.2007.12.005

Oschlies, A., Brandt, P., Stramma, L., and Schmidtko, S. (2018). Drivers and mechanisms of ocean deoxygenation. *Nat. Geosci.* 11, 467–473. doi: 10.1038/s41561-018-0152-2

Osma, N., Fernández-Urruzola, I., Gómez, M., Montesdeoca-Esponda, S., and Packard, T. T. (2016). Predicting in vivo oxygen consumption rate from ETS activity and bisubstrate enzyme kinetics in cultured marine zooplankton. *Mar. Biol.* 163:146. doi: 10.1007/s00227-016-2923-x

Packard, T. T., Denis, M., Rodie, M., and Garfield, P. (1988). Deep-ocean metabolic CO_2 production: calculations from ETS activity. *Deep Sea Res. A Oceanogr. Res. Pap.* 35, 371–382. doi: 10.1016/0198-0149(88)90016-7

Packard, T. T., Osma, N., Fernández-Urruzola, I., Codispoti, L. A., Christensen, J. P., and Gómez, M. (2015). Peruvian upwelling plankton respiration: calculations of carbon flux, nutrient retention efficiency, and heterotrophic energy production. *Biogeosciences* 12, 2641–2654. doi: 10.5194/bg-12-2641-2015

Paulmier, A., Kriest, I., and Oschlies, A. (2009). Stoichiometries of remineralisation and denitrification in global biogeochemical ocean models. *Biogeosciences* 6, 923–935. doi: 10.5194/bg-6-923-2009

Paulmier, A., and Ruiz-Pino, D. (2009). Oxygen minimum zones (OMZs) in the modern ocean. *Prog. Oceanogr.* 80, 113–128. doi: 10.1016/j.pocean.2008.08.001

Paulmier, A., Ruiz-Pino, D., and Garcon, V. (2011). CO_2 maximum in the oxygen minimum zone (OMZ). *Biogeosciences* 8, 239–252. doi: 10.5194/bg-8-239-2011

Piontek, J., Borchard, C., Sperling, M., Schulz, K. G., Riebesell, U., and Engel, A. (2013). Response of bacterioplankton activity in an Arctic fjord system to elevated pCO2; results from a mesocosm perturbation study. *Biogeosciences* 10, 297–314. doi: 10.5194/bg-10-297-2013

Piontek, J., Lunau, M., Handel, N., Borchard, C., Wurst, M., and Engel, A. (2010). Acidification increases microbial polysaccharide degradation in the ocean. *Biogeosciences* 7, 1615–1624. doi: 10.5194/bg-7-1615-2010

Regaudie-de-Gioux, A., and Duarte, C. M. (2012). Temperature dependence of planktonic metabolism in the ocean. *Glob. Biogeochem. Cycles* 26:GB1015. doi: 10.1029/2010GB003907

Regaudie-de-Gioux, A., and Duarte, C. M. (2013). Global patterns in oceanic planktonic metabolism. *Limnol. Oceanogr.* 58, 977–986. doi: 10.4319/lo.2013.58.3.0977

Reinthaler, T., van Aken, H., Veth, C., Arístegui, J., Robinson, C., Williams, P. J., et al. (2006). Prokaryotic respiration and production in the meso- and bathypelagic realm of the eastern and western North Atlantic basin. *Limnol. Oceanogr.* 51, 1262–1273. doi: 10.4319/lo.2006.51.3.1262

Reinthaler, T., Winter, C., and Herndl, G. J. (2005). Relationship between bacterioplankton richness, respiration, and production in the southern North Sea. *Appl. Environ. Microbiol.* 71, 2260–2266. doi: 10.1128/AEM.71.5.2260-2266.2005

Revsbech, N. P., Larsen, L. H., Gundersen, J., Dalsgaard, T., Ulloa, O., and Thamdrup, B. (2009). Determination of ultra-low oxygen concentrations in oxygen minimum zones by the STOX sensor. *Limnol. Oceanogr. Methods* 7, 371–381. doi: 10.4319/lom.2009.7.371

Revsbech, N. P., Thamdrup, B., Dalsgaard, T., and Canfield, D. E. (2011). Construction of STOX oxygen sensors and their application for determination of O_2 concentrations in oxygen minimum zones. *Methods Enzymol.* 486, 325–341. doi: 10.1016/S0076-6879(11)86014-3

Riebesell, U., and Gattuso, J.-P. (2014). Lessons learned from ocean acidification research. *Nat. Clim. Chang.* 5, 12–14. doi: 10.1038/nclimate2456

Riebesell, U., Schulz, K. G., Bellerby, R. G. J., Botros, M., Fritsche, P., and Meyerhöfer, M. (2007). Enhanced biological carbon consumption in a high CO_2 ocean. *Nature* 450, 545–548. doi: 10.1038/nature06267

Riebesell, U., and Tortell, P. D. (2011). "Effects of ocean acidification on pelagic organisms and ecosystems," in *Ocean Acidification*, eds J.-P. Gattuso and L. Hansson (Oxford: Oxford University Press), 99–121.

Rivkin, R. B., and Legendre, L. (2001). Biogenic carbon cycling in the upper ocean: effects of microbial respiration. *Science* 291, 2398–2400. doi: 10.1126/science.291.5512.2398

Robertson, J. E., Robinson, C., Turner, D. R., Holligan, P., Watson, A. J., Boyd, P., et al. (1994). The impact of a coccolithophore bloom on oceanic carbon uptake in the northeast Atlantic during summer 1991. *Deep Sea Res. I Oceanogr. Res. Pap.* 41, 297–314. doi: 10.1016/0967-0637(94)90005-1

Robertson, J. I. (1989). *The Coulometric Determination of Total Inorganic Carbon in Seawater and the Study of the Inter-Relationship Between the Planktonic Metabolism of Carbon Dioxide and Oxygen*. Ph.D. Thesis, University College of North Wales, Bangor.

Robinson, C. (2008). "Heterotrophic bacterial respiration," in *Microbial Ecology of the Oceans*, 2nd Edn, ed. D. L. Kirchman (Hoboken, NJ: John Wiley & Sons, Inc).

Robinson, C., Archer, S. D., and Williams, P. J. (1999). Microbial dynamics in coastal waters of East Antarctica: plankton production and respiration. *Microb. Ecol. Prog. Ser.* 180, 23–36. doi: 10.3354/meps180023

Robinson, C., Serret, P., Tilstone, G., Teira, E., Zubkov, M. V., Rees, A. P., et al. (2002a). Plankton respiration in the Eastern Atlantic Ocean. *Deep Sea Res. I Oceanogr. Res. Pap.* 49, 787–813.

Robinson, C., Widdicombe, C. E., Zubkov, M. V., Tarran, G. A., Miller, A. E. J., and Rees, A. P. (2002b). Plankton community respiration during a coccolithophore bloom. *Deep Sea Res. II Top. Stud. Oceanogr.* 49, 2929–2950. doi: 10.1016/S0967-0645(02)00064-4

Robinson, C., Wallace, D., Hyun, J.-H., Polimene, L., Benner, R., Zhang, Y., et al. (2018). An implementation strategy to quantify the marine microbial carbon pump and its sensitivity to global change. *NatL. Sci. Rev.* 5, 474–480. doi: 10.1093/nsr/nwy070

Robinson, C., and Williams, P. J. (2005). "Respiration and its measurement in surface marine waters," in *Respiration in Aquatic Ecosystems*, eds P. A. del Giorgio and P. J. Williams (Oxford: Oxford University Press).

Robinson, C., and Williams, P. J. L. (1999). Plankton net community production and dark respiration in the Arabian Sea during September 1994. *Deep Sea Res. II Top. Stud. Oceanogr.* 46, 745–765. doi: 10.1016/S0967-0645(98)00126-X

Rodrigues, R. M. N. V., and Williams, P. J. (2001). Heterotrophic bacterial utilisation of nitrogenous and non-nitrogenous substrates determined from ammonia and oxygen fluxes. *Limnol. Oceanogr.* 46, 1675–1683. doi: 10.4319/lo.2001.46.7.1675

Romero-Kutzner, V., Packard, T. T., Berdalet, E., Roy, S. O., Gagné, J.-P., and Gómez, M. (2015). Respiration quotient variability: bacterial evidence. *Mar. Ecol. Prog. Ser.* 519, 47–59. doi: 10.3354/meps11062

Roy, S. O., Packard, T. T., Berdalet, E., and St-Amand, L. (1999). Impact of acetate, pyruvate, and physiological state on respiration and respiratory quotients in *Pseudomonas nautica*. *Aquat. Microb. Ecol.* 17, 105–110. doi: 10.3354/ame017105

Sanders, R., Henson, S. A., Martin, A. P., Anderson, T. R., Bernardello, R., and Enderlein, P. (2016). Controls over ocean mesopelagic interior carbon storage (COMICS): fieldwork, synthesis and modelling efforts. *Front. Mar. Sci.* 3:136. doi: 10.3389/fmars.2016.00136

Sarmiento, J. L., and Gruber, N. (2006). *Ocean Biogeochemical Dynamics*. Princeton, NJ: Princeton University Press.

Schmidtko, S., Strammar, L., and Visbeck, M. (2017). Decline in global oceanic oxygen content during the past five decades. *Nature* 542, 335–341. doi: 10.1038/nature21399

Sondergaard, M., Williams, P. J., Cauwet, G., Riemann, B., Robinson, C., Terzic, S., et al. (2000). Net accumulation and flux of dissolved organic carbon and dissolved organic nitrogen in marine plankton communities. *Limnol. Oceanogr.* 45, 1097–1111. doi: 10.4319/lo.2000.45.5.1097

Sonnerup, R. E., Mecking, S., and Bullister, J. L. (2013). Transit time distributions and oxygen utilization rates in the Northeast Pacific Ocean from chlorofluorocarbons and sulfur hexafluoride. *Deep Sea Res. I Oceanogr. Res. Pap.* 72, 61–71. doi: 10.1016/j.dsr.2012.10.013

Sonnerup, R. E., Mecking, S., Bullister, J. L., and Warner, M. J. (2015). Transit time distributions and oxygen utilization rates from chlorofluorocarbons and sulfur hexafluoride in the Southeast Pacific Ocean. *J. Geophys. Res. Oceans* 120, 3761–3776. doi: 10.1002/2015JC010781

Spilling, K., Paul, A. J., Virkkala, N., Hastings, T., Lischka, S., Stuhr, A., et al. (2016). Ocean acidification decreases plankton respiration: evidence from a mesocosm experiment. *Biogeosciences* 13, 4707–4719. doi: 10.5194/bg-13-4707-2016

Stanley, R. H. R., Doney, S. C., Jenkins, W. J., and Lott, D. E. III (2012). Apparent oxygen utilization rates calculated from tritium and helium-3 profiles at the Bermuda Atlantic Time-series Study site. *Biogeosciences* 9, 1969–1983. doi: 10.5194/bg-9-1969-2012

Steinberg, D. K., Van Mooy, B. A. S., Buesseler, K. O., Boyd, P. W., Kobari, T., and Karl, D. M. (2008). Bacterial vs. zooplankton control of sinking particle flux in the ocean's twilight zone. *Limnol. Oceanogr.* 53, 1327–1338. doi: 10.4319/lo.2008.53.4.1327

Stramma, L., Johnson, G. C., Sprintall, J., and Mohrholz, V. (2008). Expanding oxygen-minimum zones in the tropical oceans. *Science* 320, 655–658. doi: 10.1126/science.1153847

Tamburini, C., Boutrif, M., Garel, M., Colwell, R. R., and Deming, J. W. (2013). Prokaryotic responses to hydrostatic pressure in the ocean – a review. *Environ. Microbiol.* 15, 1262–1274. doi: 10.1111/1462-2920.12084

Tanaka, T., Alliouane, S., Bellerby, R. G. B., Czerny, J., de Kluijver, A., Riebesell, U., et al. (2013). Effect of increased pCO_2 on the planktonic metabolic balance during a mesocosm experiment in an Arctic fjord. *Biogeosciences* 10, 315–325. doi: 10.5194/bg-10-315-2013

Teira, E., Hernando-Morales, V., Martínez-García, S., Figueiras, F. G., Arbones, B., and Álvarez-Salgado, X. A. (2013). Response of bacterial community structure and function to experimental rainwater additions in a coastal eutrophic embayment. *Estuar. Coast. Shelf Sci.* 119, 44–53. doi: 10.1016/j.ecss.2012.12.018

Thomas, H. (2002). Remineralization ratios of carbon, nutrients, and oxygen in the North Atlantic Ocean: a field databased assessment. *Glob. Biogeochem. Cycles* 16:1051. doi: 10.1029/2001GB001452

Tiano, L., Garcia-Robledo, E., Dalsgaard, T., Devol, A. H., Ward, B. B., Ulloa, O., et al. (2014). Oxygen distribution and aerobic respiration in the north and south eastern tropical Pacific oxygen minimum zones. *Deep Sea Res. I Oceanogr. Res. Pap.* 94, 173–183. doi: 10.1016/j.dsr.2014.10.001

Van Mooy, B., Keil, R., and Devol, A. (2002). Impact of suboxia on sinking particulate organic carbon: enhanced carbon flux and preferential degradation of amino acids via denitrification. *Geochem. Cosmochim. Acta* 66, 457–465. doi: 10.1016/S0016-7037(01)00787-6

Wear, E. K., Carlson, C. A., Windecker, L. A., and Brzezinski, M. A. (2015). Roles of diatom nutrient stress and species identity in determining the short- and long-term bioavailability of diatom exudates to bacterioplankton. *Mar. Chem.* 177, 335–348. doi: 10.1016/j.marchem.2015.09.001

Weber, T., Cram, J. A., Leung, S. W., DeVries, T., and Deutsch, C. (2016). Deep ocean nutrients imply large latitudinal variation in particle transfer efficiency. *Proc. Natl. Acad. Sci. U.S.A.* 113, 8606–8611. doi: 10.1073/pnas.1604414113

Weinbauer, M. G., Liu, J., Motegi, C., Maier, C., Pedroti, M. L., Dai, M., et al. (2013). Seasonal variability of microbial respiration and bacterial and archaeal community composition in the upper twilight zone. *Aquat. Microb. Ecol.* 71, 99–115. doi: 10.3354/ame01666

Williams, P. J. B., and del Giorgio, P. A. (2005). "Respiration in aquatic ecosystems: history and background," in *Respiration in Aquatic Ecosystems*, eds P. A. del Giorgio and P. J. Williams (Oxford: Oxford University Press), 315.

Wohlers, J., Engel, A., Zöllner, E., Breithaupt, P., Jürgens, K., Hoppe, H.-G., et al. (2009). Changes in biogenic carbon flow in response to sea surface warming. *Proc. Natl. Acad. Sci. U.S.A.* 106, 7067–7072. doi: 10.1073/pnas.0812743106

Wood, E. S. (1992). *The Community Photosynthetic Quotient and the Assimilation of Nitrogen by Oceanic Plankton*. Ph.D. Thesis, University College of North Wales, Bangor.

Wright, J. J., Konwar, K. M., and Hallam, S. J. (2012). Microbial ecology of expanding oxygen minimum zones. *Nat. Rev. Microbiol.* 10, 381–394. doi: 10.1038/nrmicro2778

Yvon-Durocher, G., Caffrey, J. M., Cescatti, A., Dossena, M., del Giorgio, P., and Gasol, J. M. (2012). Reconciling the temperature dependence of respiration across timescales and ecosystem types. *Nature* 487, 472–476. doi: 10.1038/nature11205

Zhang, C., Dang, H., Azam, F., Benner, R., Legendre, L., Passow, U., et al. (2018). Evolving paradigms in biological carbon cycling in the ocean. *Natl. Sci. Rev.* 5, 481–499. doi: 10.1093/nsr/nwy074

Conflict of Interest Statement: The author declares that the research was conducted in the absence of any commercial or financial relationships that could be construed as a potential conflict of interest.

frontiers in Marine Science

ORIGINAL RESEARCH
published: 21 February 2019
doi: 10.3389/fmars.2019.00027

Rates and Pathways of N_2 Production in a Persistently Anoxic Fjord: Saanich Inlet, British Columbia

*Céline C. Michiels[1,2], Julia A. Huggins[1,2], Karina E. Giesbrecht[3], Jenifer S. Spence[1,2], Rachel L. Simister[1,2], Diana E. Varela[4], Steven J. Hallam[1,5,6,7,8] and Sean A. Crowe[1,2,8]**

[1] Department of Microbiology and Immunology, The University of British Columbia, Vancouver, BC, Canada, [2] Department of Earth, Ocean and Atmospheric Sciences, The University of British Columbia, Vancouver, BC, Canada, [3] School of Earth and Ocean Sciences, University of Victoria, Victoria, BC, Canada, [4] Department of Biology, School of Earth and Ocean Sciences, University of Victoria, Victoria, BC, Canada, [5] ECOSCOPE Training Program, The University of British Columbia, Vancouver, BC, Canada, [6] Graduate Program in Bioinformatics, The University of British Columbia, Vancouver, BC, Canada, [7] Genome Science and Technology Training Program, The University of British Columbia, Vancouver, BC, Canada, [8] Peter Wall Institute for Advanced Studies, The University of British Columbia, Vancouver, BC, Canada

OPEN ACCESS

Edited by:
Perran Cook, Monash University, Australia

Reviewed by:
Arvind Singh, Physical Research Laboratory, India
Annie Bourbonnais, University of South Carolina, United States

***Correspondence:**
Sean A. Crowe
sean.crowe@ubc.ca

Specialty section:
This article was submitted to Marine Biogeochemistry, a section of the journal Frontiers in Marine Science

Received: *05 October 2018*
Accepted: *21 January 2019*
Published: *21 February 2019*

Citation:
Michiels CC, Huggins JA, Giesbrecht KE, Spence JS, Simister RL, Varela DE, Hallam SJ and Crowe SA (2019) Rates and Pathways of N_2 Production in a Persistently Anoxic Fjord: Saanich Inlet, British Columbia. Front. Mar. Sci. 6:27. doi: 10.3389/fmars.2019.00027

Marine oxygen minimum zones (OMZs) support 30–50% of global fixed-nitrogen (N) loss but comprise only 7% of total ocean volume. This N-loss is driven by canonical denitrification and anaerobic ammonium oxidation (anammox), and the distribution and activity of these two processes vary greatly in space and time. Factors that regulate N-loss processes are complex, including organic matter availability, oxygen concentrations, and NO_2^- and NH_4^+ concentrations. While both denitrification and anammox produce N_2, the overall geochemical outcome of these processes are different, as incomplete denitrification, for example, produces N_2O, which is a potent greenhouse gas. Information on rates of anammox and denitrification and more detailed ecophysiological knowledge of the microorganisms catalyzing these processes are needed to develop more robust models of N-loss in OMZs. To this end, we conducted monthly incubations with ^{15}N-labeled N during under anoxic conditions and during a deep water renewal cycle in Saanich Inlet, British Columbia, a persistently anoxic fjord. Both denitrification and anammox operated throughout the low oxygen water column with depth integrated rates of anammox and denitrification ranging from 0.15 ± 0.03 to 3.4 ± 0.3 and 0.02 ± 0.006 to 14 ± 2 mmol N_2 m^{-2} d^{-1}, respectively. Most N_2 production in Saanich Inlet was driven by denitrification, with high rates developing in response to enhanced substrate supply from deep water renewal. Dynamics in rates of denitrification were linked to shifts in microbial community composition. Notably, periods of intense denitrification were accompanied by blooms in an Arcobacter population against a background community dominated by SUP05 and Marinimicrobia. Rates of N_2 production through denitrification and anammox, and their dynamics, were then explored through flux-balance modeling with higher rates of denitrification linked to the physiology of substrate uptake. Overall, both denitrification and anammox operated

throughout the year, contributing to an annual N-loss of 2×10^{-3} Tg N_2 yr^{-1}, 37% of which we attribute to anammox and 63% to complete denitrification. Extrapolating these rates from Saanich Inlet to all similar coastal inlets in BC (2478 km^2), we estimate that these inlets contribute 0.1% to global pelagic N-loss.

Keywords: anammox, denitrification, N_2 production, sulphidic, anoxia

INTRODUCTION

Nitrogen (N) is an essential element to life and is used as a building block for proteins and nucleic acids in all terrestrial and marine organisms. The bioavailability of N, therefore, can limit primary production in both terrestrial and aquatic compartments of the biosphere (Falkowski, 1997; Falkowski et al., 2008). The largest pool of N at the Earth's surface is N_2 in the atmosphere and this N_2 is made available to life mostly through energetically expensive microbial N-fixation (Canfield et al., 2010a). The abundance of fixed-N in the oceans is governed by the balance between N-fixation into biomass, biomass deposition and ultimate burial in marine sediments, and the return of fixed-N to the atmosphere through a modular series of redox reactions that ultimately lead to anaerobic N_2 production (Gruber, 2004). The processes that comprise the N-cycle are spatially decoupled with most N-fixation occurring in the euphotic surface ocean (Capone, 2001), the oxidative components distributed throughout much of the ocean, and anaerobic N_2 production partitioned between the low oxygen waters (30–50%) that typically develop at intermediate water depths and in eutrophic coastal regions, as well as in bottom sediments (50–70%) (Codispoti, 2007). The availability of N to marine life, therefore, depends on the relative rates of N-fixation versus N-loss, and N-loss is expected to scale with the extent and intensity of low oxygen marine waters, which are currently expanding throughout the global ocean with unconstrained feedbacks on marine N inventories (Keeling et al., 2010; Schmidtko et al., 2017; Breitburg et al., 2018).

Under low oxygen conditions (<20 μM O_2 concentration), NO_3^- is used as an electron acceptor in anaerobic microbial energy transduction leading, in part, to N_2 production and closure of the N- cycle. Such low oxygen conditions commonly develop in the open ocean at intermediate water depths, in restricted basins, and in eutrophic coastal regions, when respiratory oxygen consumption outpaces physical mixing and oxygenic photosynthesis. Low oxygen marine waters are commonly referred to as Oxygen Minimum Zones (OMZs), and are pervasive features of the modern oceans comprising 7% of current total ocean volume [with O_2 <20 μM] (Paulmier and Ruiz-Pino, 2009). The anoxic cores of OMZs, which contain oxygen concentrations below the limit of detection of oxygen sensors generally used in oceanographic research (<5 μM, but as low as 1 nM), constitute only 0.1% of the ocean's total volume (Codispoti et al., 2001; Ulloa et al., 2012). Despite their relatively low volumes, OMZs play an outsized role in N biogeochemistry driving up to 50% of marine fixed N-loss with a lower estimate of the annual pelagic N-sink of 150 Tg N (Codispoti, 2007).

N_2 production and thus N-loss in OMZs is driven by two entirely different microbial metabolisms: canonical denitrification and anaerobic ammonium oxidation (anammox). In denitrification a suite of either inorganic [sulfide (HS^-), ferrous iron (Fe(II))] or organic electron donors is used to reduce NO_3^- through a series of intermediates; NO_2^-, NO, and N_2O to ultimately produce N_2 (see Eqs. 1 and 2).

Organoheterotrophic denitrification (Mucciet al., 2000) :

$$84.8NO_3^- + (CH_2O)_{106}(NH_3)_{16}(H_3PO_4) \rightarrow 106\,HCO_3^- + 16\,NH_4^+ + 42.4\,N_2 + HPO_4^{2-} + 42.4\,H_2O + 7.2\,H^+ \quad (1)$$

Chemotrophic denitrification :

$$8NO_3^- + 5\,HS^- + 3\,H^+ \rightarrow 5\,SO_4^{2-} + 4\,N_2 + 4\,H_2O \quad (2)$$

Anammox directly couples NO_2^- reduction to the oxidation of NH_4^+ through hydroxylamine and hydrazine intermediates to produce N_2 (see Eq. 3).

$$\text{Anammox}: NO_2^- + NH_4^+ \rightarrow N_2 + 2H_2O \quad (3)$$

Both pathways are fuelled, in part, by relatively oxidized N species and yield N_2 as their ultimate metabolic products, and thus can occupy overlapping niches. Denitrification and anammox, however, diverge in both their ecophysiology and their biogeochemical outcomes including possible leakages of intermediate N species and their overall influence on the carbon (C) cycle (Voss et al., 2013). Denitrification, for example, can either consume or produce CO_2 depending on the electron donor used, as denitrifiers can be heterotrophic or autotrophic. Anammox, on the other hand, is considered exclusively autotrophic and only consumes CO_2. Denitrification, furthermore, yields N_2O as an intermediate, a potent greenhouse gas, that may accumulate during partial denitrification and play a role in global climate forcing (Fowler et al., 2013). The differing ecophysiologies of the organisms conducting denitrification and anammox are thus expected to interact with one another in different ways across a spectrum of anaerobic conditions. These differences confound attempts to model N-cycle dynamics and its interactions with other cycles, without explicit descriptions for both anammox and denitrification and their regulation.

Process rate measurements are beginning to define the relationships between anammox, denitrification and the N-cycle.

In OMZs globally, anammox appears to support most N_2 production (Kuypers et al., 2005; Thamdrup et al., 2006; Hamersley et al., 2007; Lam et al., 2009; Canfield et al., 2010b; Jensen et al., 2011; Kalvelage et al., 2013; De Brabandere et al., 2014), while denitrification may dominate ephemerally (Ward et al., 2009; Bulow et al., 2010; Dalsgaard et al., 2012; Babbin et al., 2014). In open ocean OMZs, the relative contributions of anammox and denitrification to N_2 production are theoretically constrained by the stoichiometry of settling organic matter and the NH_4^+ supply from remineralization of organic matter to anammox (Codispoti et al., 2001; Van Mooy et al., 2002; Devol, 2003; Koeve and Kähler, 2010; Babbin et al., 2014). This constraint develops when anammox is limited by NH_4^+ supplied through ammonification of organic N during heterotrophic NO_3^- respiration (organotrophic denitrification). In this case, N_2 production should occur 71% through denitrification and 29% through anammox based on Redfieldian organic matter stoichiometry of 106C:16N (Van Mooy et al., 2002; Dalsgaard et al., 2003; Devol, 2003).

Coupling of organotrophic denitrification and anammox in open ocean OMZ :

$$94.4\,NO_3^- + (CH_2O)_{106}(NH_3)_{16}(H_3PO_4) \rightarrow 106\,HCO_3^- + 55.2\,N_2 + HPO_4^{2-} + 71.2\,H_2O + 13.6\,H^+ \quad (4)$$

Here, denitrification produces 16 moles of NH_4^+ and 16 moles of NO_2^- that fuel anammox, producing 16 moles out of a total 55.2 moles N_2, hence 29% of the total N_2 production (Eqs. 5 and 6).

Denitrification products fuel anammox entirely through organic matter degradation :

$$94.4\,NO_3^- + (CH_2O)_{106}(NH_3)_{16}(H_3PO_4) \rightarrow 106\,HCO_3^- + 31.2\,N_2 + 16\,NH_4^+ + 16\,NO_2^- + HPO_4^{2-} + 39.2\,H_2O + 13.6\,H^+ \quad (5)$$

Anammox consumes NH_4^+ and NO_2^- from denitrification

$$16NH_4^+ + 16NO_2^- \rightarrow 16\,N_2 \quad (6)$$

This expected ratio between anammox and denitrification, however, is rarely observed in the ocean and deviations from the ratio can be at least partially explained through variability in organic matter composition and departures from the Redfield ratio (Babbin et al., 2014). While this stoichiometric variability appears to account for differences observed in the role of anammox in N_2 production in some open ocean OMZs, it remains unclear to what extent organic matter stoichiometry can explain the apparently outsized role of anammox in global N_2 production, more generally. Denitrification is commonly undetected in many OMZs, and this then raises the question as to what supplies NH_4^+ to anammox when denitrification appears absent. One possibility is microbial NO_3^- reduction to NH_4^+ (DNRA), which has been detected in the Peruvian OMZ and above the Omani shelf, and could be partially responsible for directly supplying NH_4^+ to anammox (Lam et al., 2009; Jensen et al., 2011). While DNRA could provide NH_4^+ for anammox in some cases, it is unlikely the universal source as the rates of DNRA measured are generally insufficient to fully support the NH_4^+ requirements of concurrent anammox (Lam et al., 2009). Other possible sources of NH_4^+ include remineralization of organic matter through NO_3^- reduction to NO_2^-, microaerobic respiration, and sulfate reduction (Canfield et al., 2010b), and in certain shallow settings, benthic release of NH_4^+ (Lam et al., 2009; Kalvelage et al., 2013). While we are gaining a clearer picture of the controls on rates of anammox and denitrification in OMZs, there remain no universal rules that allow quantitative prediction of the partitioning between these two pathways.

Beyond observations from canonical OMZs, anammox and denitrification have been reported from other anoxic environments, including marine sediments, anoxic fjords and lakes, and wastewater treatment facilities. In marine sediments for example, it has been shown that the relative contribution of anammox to N_2 production increases dramatically with both distance from the coast and water depth (Thamdrup and Dalsgaard, 2002; Trimmer and Nicholls, 2009) with anammox comprising up to 80% of the total N-loss at 700 m depth (Engstrom et al., 2005). This trend may be attributed to decreased organic matter content in deeper sediments (Trimmer and Nicholls, 2009). Indeed, availability of organic matter, rather than its reactivity or quality, appears to regulate the relative importance of denitrification and anammox in estuarine sediments (Nicholls and Trimmer, 2009). The relative contribution of anammox to sediment N_2 production also appears to increase when NO_3^- concentrations are persistently high in overlying waters (Rich et al., 2008; Nicholls and Trimmer, 2009). Notably, in sediments underlying low oxygen marine waters, nearly all N_2 production was supported by anammox (Prokopenko et al., 2013). In these sediments, NH_4^+ was supplied to anammox through DNRA. This implies then that the relative importance of anammox to sediment N_2 production may in part depend on the activity of DNRA. HS^- may also play a role in regulating anammox and denitrification. While HS^- is a common electron donor and thus a suitable substrate for denitrification, it has been shown to inhibit anammox at micromolar levels, possibly through toxicity (Jensen et al., 2009). This is consistent with the distribution of anammox, which appears to operate above the sulphidic zone in the Black Sea (Jensen et al., 2008). Likewise, anammox contributes up to 30% of the N_2 production in lacustrine water columns, but the highest rates of anammox occur in nearly hydrogen sulfide (HS^-) free waters (Wenk et al., 2013). In contrast, anammox appears entirely excluded from ferruginous (iron-rich) lake waters and sediments (Michiels et al., 2017; Robertson and Thamdrup, 2017), and ferruginous estuarine sediments (Roberts et al., 2014; Robertson et al., 2016). Taken together, the emerging picture suggests that the regulation of the relative importance of anammox and denitrification to total N_2 production is convoluted and development of predictive knowledge will require comprehensive and detailed studies across the broad range of systems where these processes are known to operate.

We have conducted a time-series study of the rates of denitrification and anammox and their relative contribution to N_2 production in Saanich Inlet (SI). SI is a persistently anoxic fjord that provides a tractable ecosystem in which to study anaerobic microbial metabolisms that are relevant and extensible to low oxygen environments, globally. Biogeochemical research has been conducted in SI since 1965 (Richards, 1965) and has culminated with instrumented real-time monitoring and a more than 10 years continuous time-series experiment (Walsh et al., 2009; Zaikova et al., 2010; Hawley et al., 2017b; Torres-Beltrán et al., 2017), making it one of the best studied anoxic fjords on Earth. The inlet is situated on the southern tip of Vancouver Island (see **Figure 1A**) and is up to 228 m deep with a 75 m deep glacial sill at its entrance that restricts hydrological connection to the Strait of Georgia and the mixing of deep basin waters. Similar to OMZs, aerobic respiration in the SI water column outpaces O_2 supply through physical water mixing and photosynthesis in the surface waters, rendering low oxygen conditions below 100 m for most of the year (**Figure 1B**). In contrast to most open ocean OMZs, however, sulphidic conditions develop in the bottom waters of SI as a result of either water column sulfate reduction (Anderson and Devol, 1973) and/or sulfide efflux from underlying sediments (Devol et al., 1984). Most years, SI stagnant deep waters transition from sulphidic to oxic at the end of the summer (late August – early September) in response to upwelling off the coast of Vancouver Island that forces dense well-oxygenated waters into the Strait of Georgia and over the sill into the inlet (Anderson and Devol, 1973), in connection to weak tidal currents (Manning et al., 2010). The inlet thus can exist in two main states during the year if renewal occurs: a state of "stagnation" referring to low oxygen concentrations in the deep-waters and a state of renewal when oxygenated waters penetrate the inlet and mix with low oxygen deep-waters. These physical–chemical characteristics combine to support microbial communities with anaerobic metabolisms that couple the C, N and S-cycles and are broadly analogous to those we expect to find in other low oxygen and anoxic marine waters globally (Wright et al., 2012).

N-cycling and its interactions with the other cycles in SI have been previously interrogated using a variety of geochemical and microbiological analyses. Geochemical data indirectly imply that SI supports relatively high rates of both pelagic and benthic N-loss (Manning et al., 2010; Bourbonnais et al., 2013) that vary seasonally, with the highest rates in the winter (December–February, 8.1 mmol m^{-2} d^{-1}) and lowest in the summer (May–August, 1.7 mmol m^{-2} d^{-1}) (Manning et al., 2010). Multi-omic analyses revealed that microbial communities in SI harbor the metabolic potential to catalyze many components of the N-cycle and to link N to cycling of C and S (Walsh et al., 2009; Hawley et al., 2014, 2017a). These metabolic pathway reconstructions have led to a conceptual model describing the microbial interactions that underpin N-cycling in SI, and low oxygen waters more broadly. Specifically, this model (reproduced in **Figure 1C** from Hawley et al., 2014) proposes that Thaumarchaeota are responsible for the first step of nitrification (NH_4^+ to NO_2^-) and that two different species of bacteria, *Nitrospina gracilis* and *Nitrospira defluvii*, oxidize NO_2^- to NO_3^-. Along with nitrification, the SAR11 are the most abundant aerobic heterotrophs, and they are thought to degrade settling organic matter and release NH_4^+ to the oxic water column (**Figure 1C**). Lower in the water column, the model suggests that Planctomycetes produce N_2 through the anammox process, while bacteria from the SUP05 clade (Gammaproteobacteria) were implicated in reducing NO_3^- to N_2O (**Figure 1C**). The final step of denitrification remained more elusive but analyses of Single Cell Amplified Genomes (SAGs) reveal metabolic potential for N_2O reduction to N_2 in the Marinimicrobia ZA3312c-A and SHBH1141 (previously known as Marine Group-A) (Hawley et al., 2017a). Notably, the taxonomic affiliations and genomic make-up of the key organisms that drive N-cycling in SI are closely related to those found across OMZs and other anoxic marine environments globally (Wright et al., 2012). For example, the Gammaproteobacteria SUP05 - with a single cultivated strain, *Ca. Thioglobus autotrophicus* strain EF1 (Shah et al., 2017) – appears to be a ubiquitous member of OMZ microbial communities with

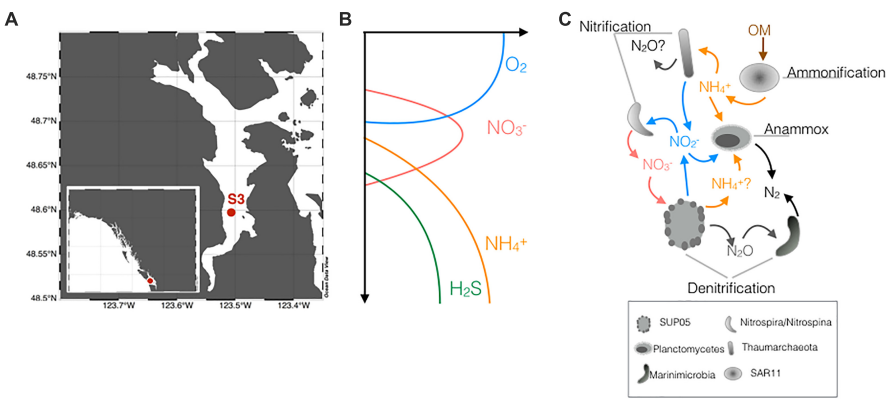

FIGURE 1 | (A) Sampling of Station S3 in Saanich Inlet, on Vancouver Island, British Columbia (Canada). Sampling of S3 happened once a month within a historic time series data collection. **(B)** Typical redox gradients found in SI. These gradients move vertically depending on the season. **(C)** Active microbial metabolisms of the N-cycle present along the redox gradients of SI, modified from Hawley et al. (2014).

the metabolic potential for partial denitrification (Stevens and Ulloa, 2008; Walsh et al., 2009; Hawley et al., 2014), along with bacteria from the group Marinimicrobia that reduce N_2O to N_2 (Hawley et al., 2017a) and are some of the most widely distributed and abundant taxa in marine OMZs.

The conceptual metabolic model for coupled C, N, and S cycling in OMZs was recently expanded into a quantitative 'gene-centric' model that integrates metabolic potential derived from multi-omic information with geochemical data to predict process rates (Louca et al., 2016). Modeled rates were validated through direct measurements, but these rates were an order of magnitude lower than the rates needed to support previous geochemical data (Manning et al., 2010). These observations highlight a discontinuity between current conceptual and quantitative models of the N-cycle in SI and a need for data that more fully capture and integrate the dynamics of N-cycling across multiple seasons.

Here, we used isotope labeling experiments to directly quantify rates and pathways of anaerobic N cycling in SI over an entire year. These measurements allowed us to calculate annual N-loss from Saanich inlet, determine the specific microbial pathways that are responsible, and to assess the biogeochemical controls on the rates and pathways of N-loss in the inlet. Overall, our data reveal that fixed N-loss from SI has strong seasonality and that periods of intense N-loss during the summer are driven primarily through sulfide-dependent denitrification, which is likely fuelled by benthic sulfide supply and new input of NO_3^- from a partial renewal of the water column. Anammox also contributed to N-loss at relatively constant rates throughout the year.

MATERIALS AND METHODS

Study Site and Sampling

Saanich Inlet (SI) is a marine fjord located on the west coast of Vancouver Island, British Columbia, Canada (**Figure 1**). We conducted a monthly time series experiment between January and December 2015 (**Table 1**) and sampled at station S3 (**Figure 1** – 48° 35.5 N and 123° 30.3 W, 227 m deep). A standard profile of 16 depths was sampled every month with 12L GO-FLO bottles attached in-series to a steel cable (10, 20, 40, 60, 75, 85, 90, 97, 100, 110, 120, 135, 150, 165, 185, and 200 m). Depths were set using a metered winch cable with a precision of plus or minus 0.5 m and the accuracy of the depth reached was checked with the CTD depth profile. CTD profiles [pressure (SBE 29), conductivity (SBE 4C), temperature (SBE 3F), and oxygen (SBE 43)] were obtained with the SBE25 Sealogger CTD (SBE). Oxygen concentrations measured with the SBE 43 sensor were calibrated monthly against Winkler titrations (Grasshoff et al., 1999) with a limit of detection <1 μM. The CTD, attached at the end of the winch cable, and the bottles were lowered to their final depths and left there to equilibrate with surrounding water for at least a minute before closing.

Samples for nutrient concentration measurements were immediately filtered and put on ice for later analysis. Samples for sulfide analyses were fixed in 0.5% zinc acetate final concentration without prior filtration and frozen at −20°C for later analysis. 250 mL serum bottles destined for isotope labeling experiments were overfilled three times with water from 7 depths (90, 100, 120, 135, 150, 165, and 200 m). The overfilling of the bottle as well as capping with blue halobutyl stoppers (previously boiled in NaOH, Bellco, United Kingdom) minimized oxygen contamination (De Brabandere et al., 2012). Samples for chlorophyll *a* determination were collected in carboys from four depths corresponding to 100, 50, 15, and 1% of the surface incident irradiance as measured by the PAR sensor on the CTD. Carboys were kept cool and dark until further subsampling back in the lab. 500 mL subsamples from each carboy were filtered for phytoplankton biomass (chl *a*). Filters were kept frozen at −20°C until analysis.

Nutrient and Process Rate Measurements

Samples for NO_2^-, NH_4^+ and HS^- determinations were thawed immediately prior to analysis and measured with

TABLE 1 | Addition of labeled N-species and electron donors to incubations in 2015.

	Exact date of sampling	Type of ^{15}N labeled-incubation
January 2015	January 14, 2015	$^{15}NO_3^-$ (10 μM), $^{15}NH_4^+$ and $^{14}NO_3^-$ (10 and 10 μM)
February 2015	February 11, 2015	/
March 2015	March 11, 2015	$^{15}NO_3^-$ (10 μM), $^{15}NH_4^+$ and $^{14}NO_3^-$ (10 and 10 μM)
April 2015	April 08, 2015	$^{15}NO_3^-$ (10 μM), $^{15}NH_4^+$ and $^{14}NO_3^-$ (10and 10 μM)
May 2015	May 13, 2015	$^{15}NO_3^-$ (10 μM), $^{15}NH_4^+$ and $^{14}NO_3^-$ (10 and 10 μM)
June 2015	June 03, 2015	$^{15}NO_3^-$ (10 μM), $^{15}NH_4^+$ and $^{14}NO_3^-$ (10 and 10 μM), $^{15}NO_3^-$ (10 μM) and HS^- (1, 5, 10, 15, and 20 μM)
July 2015	July 08, 2015	$^{15}NO_3^-$ (10 μM), $^{15}NH_4^+$ and $^{14}NO_3^-$ (10 and 10 μM)
August 2015	August 12, 2015	$^{15}NO_3^-$ (2.5, 5, 10, 15, and 25 μM), $^{15}NH_4^+$ and $^{14}NO_3^-$ (10 and 10 μM)
September 2015	September 09, 2015	$^{15}NO_3^-$ (10 μM), $^{15}NH_4^+$ and $^{14}NO_3^-$ (10 and10 μM)
October 2015	October 22, 2015	$^{15}NO_3^-$ (10 μM), $^{15}NH_4^+$ and $^{14}NO_3^-$ (10 and 10 μM)
November 2015	November 18, 2015	$^{15}NO_3^-$ (10 μM), $^{15}NH_4^+$ and $^{14}NO_3^-$ (10 and 10 μM)
December 2015	December 09, 2015	$^{15}NO_3^-$ (10 μM), $^{15}NH_4^+$ and $^{14}NO_3^-$ (10 and 10 μM)

spectrophotometric assays: the Griess assay, the indophenol blue method, and the Cline assay, respectively (Grasshoff et al., 1999). NOx concentrations (NO_3^- and NO_2^-) was measured by chemiluminescence following reduction to NO with vanadium (Braman and Hendrix, 1989), and we subtracted NO_2^- from the total NOx concentrations to obtain NO_3^- concentrations (Antek instruments 745 and 1050, Houston, TX, United States). Chlorophyll *a* samples collected on filters (0.7 μm nominal porosity) were extracted for 24 h with 90% acetone at −20°C, and the extracted chlorophyll *a* measured in a Turner Designs 10AU fluorometer, using an acidification method and corrected for phaeopigment interference Parsons et al. (1984). DIN deficit (DIN_{def}) was calculated according to Bourbonnais et al. (2013) and corrected for the release and dissolution of iron and manganese oxyhydroxide-bound PO_4^{3-} under anoxic conditions.

Dark carbon fixation rates were measured by overfilling 60 mL serum bottles 3 times to minimize O_2 contamination and amending ^{14}C-HCO_3 to the incubation bottles following the JGOFS protocol (Knap et al., 1996).

The protocol used for measuring rates of denitrification and anammox was modified from Thamdrup and Dalsgaard (2002), using ^{15}N-labeled incubations. In an attempt to minimize bottle effects arising from the use of small sample volumes, we incubated the water in 250 mL serum bottles closed with blue butyl rubber stoppers. At the start of the incubation, we inserted a 20 mL helium headspace into the bottle and then added the ^{15}N labeled N-species (10 μM $^{15}NO_3^-$ or 10 μM $^{15}NH_4^+$, see **Table 1** for details) and electron donors to the bottles (**Table 1**). Helium gas entering the serum bottle was passed through an oxygen scrubber (Cu-CuO, Glasgerätebau Ochs - Germany) to limit O_2 from being introduced to the incubation vessels. Oxygen in the incubation vessels remained below our detection limit (<0.2 μmol L^{-1}), which was measured with flow-through cell oxygen optode (Pyroscience). For incubations of oxygen contaminated water, adding a 20 mL headspace decreases the amount of oxygen in the seawater by about 30 times due to preferential partitioning of O_2 into the headspace gas. In contrast, given the distribution of sulfide between aqueous and gaseous species in seawater, less than 2% of the total sulfide in our incubation vessels resides in the headspace. Samples were collected approximately every 6, 12, 24, and 48 h during the incubations to both allow maximum sensitivity and capture intervals with constant rates. In between time points, incubations were kept in the dark at 15°C. To determine the time-course of ^{15}N labeled-N_2 production, gas samples were taken with a 1 mL gas-tight syringe (Hamilton) previously flushed with He and then with the headspace gas. Gas samples were stored in 3 mL exetainers previously filled with milliQ water. Liquid samples were taken to follow the production or consumption of NO_2^-, NO_3^-, or NH_4^+. Liquid samples were collected with a plastic 5 mL syringe previously flushed with He, filtered and then stored at −20°C for later analysis. The ^{15}N content of N_2 was determined in gas samples collected during the incubations on an isotope-ratio mass spectrometer (Delta V with continuous flow inlet, Thermo Scientific). Concentrations of N_2 were calibrated with standards by injecting different amounts of gas from N_2 flushed exetainer vials at 1 atmosphere. The excess $^{14}N^{15}N$ and $^{15}N^{15}N$ in the gas samples was calculated as described by Thamdrup and Dalsgaard (2000). Then, rates were calculated through least squares fitting of the slope of ^{15}N accumulation versus time for the linear region of ^5N excess ingrowth (i.e., constant rates), correcting for the ^{15}N labeling percentages of the initial substrate pool and accounting for the initial pool of substrate present. Rates were determined to be significant if the slope of the linear regression was considered different from 0 ($p < 0.05$). Denitrification rates were determined from the accumulation of $^{30}N_2$ in the bottle headspace from the $^{15}NO_3^-$ additions, and anammox rates were calculated from the accumulation of $^{29}N_2$ from the $^{15}NH_4^+ + ^{14}NO_3^-$ additions according to Thamdrup et al. (2006) with modifications and compared to the accumulation of $^{29}N_2$ from the $^{15}NO_3^-$ additions. The detection limit on these rates were calculated as the median of the standard error on the slope used to calculate all significant rates (De Brabandere et al., 2014; Bonaglia et al., 2016) and was determined to be 0.04 and 0.4 nM h^{-1} for anammox and denitrification, respectively. To produce integrated rates of denitrification and anammox for each month, we first scaled potential rates (R_{pot}) to *in situ* rates or "corrected rates" (R_{cor}) by using Michaelis–Menten half saturation constants K_m and *in situ* substrate concentrations for each process, respectively (see Eq. 7).

$$R_{cor} = \frac{[S]^* R_{pot}}{[S] + K_m} \quad (7)$$

For denitrification, we used K_m determined through the addition of different $^{15}NO_3^-$ concentrations in the incubations (see **Table 1** and **Figure 4A**). For anammox, we used a K_m from the literature (Awata et al., 2013). Then, we integrated the corrected rates over the sampling depth intervals to attain area specific process rates.

Microbial Community Profiling

Six different depths (10, 100, 120, 135, 150, and 200 m) were sampled for microbial community profiling and water from these depths was returned to the lab for same-day filtering. 10 L of water was filtered onto 0.22 μm Sterivex (Millipore) filters with a 2.7 μm glass fiber pre-filter. Filtered biomass was soaked in lysis buffer then frozen immediately in liquid nitrogen. Filters were stored at −80°C until further analysis. DNA was extracted according to Wright et al. (2009). Extracted DNA was quantified using the picogreen assay (Invitrogen) and checked for amplification of the small subunit ribosomal RNA (SSU or 16S rRNA) gene using universal primers targeting the V4–V5 region (515F-Y/926R) (Walters et al., 2016). DNA was sent to the Joint Genome Institute (Walnut Creek, CA, United States) for 16S rRNA amplicon sequencing on the Illumina MiSeq platform[1].

Once sequenced, amplicons were quality filtered using the JGI "itaggerReadQC" pipeline[2,3]. Quality filtered reads were run through USEARCH (Edgar et al., 2011) and QIIME (Caporaso et al., 2010). First, we identified chimeras using UCHIME (Edgar

[1]https://jgi.doe.gov/wp-content/uploads/2016/06/DOE-JGI-iTagger-methods.pdf
[2]https://bitbucket.org/berkeleylab/jgi_itagger/
[3]https://jgi.doe.gov/wp-content/uploads/2016/06/DOE-JGI-iTagger-methods.pdf

et al., 2011). We then picked OTUs *de novo* with the sumaclust method at 97% OTU threshold (Kopylova et al., 2016). We filtered singletons from the OTU table and assigned taxonomy to a representative set of sequences with rdp classifier using the QIIME release Silva database V128 (Quast et al., 2013). Chao1 diversity indices were calculated with R. Clustering of the samples was performed in R based on a dissimilarity matrix using the Euclidean method[4].

We also quantified total bacterial and archaeal 16S rRNA genes present in our samples via qPCR by targeting the V1–V3 region of the 16S rRNA genes with the primers 27F(bacterial)/20F(archaeal) (5′-AGAGTTTGATCCTGGCTCAG, 5′-TTCCGGTTGATCCY GCCRG) and DW519R (5′-GNTTTACCGCGGCKGCTG) (Zaikova et al., 2010). Standards used for total bacteria and total archaea quantification were obtained from SSU rRNA gene clone libraries as described in Zaikova et al. (2010). qPCR program was as followed: (1) 95° for 3 min, (2) 95° for 20 s, (3) 55° for 30 s, (4) plate read, repeat (2) to (4) 44 times, measuring the melting curve by incremental increases by 0.5° from 55 to 95° every second. qPCR reactions were performed in low-profile PCR 96 well-plates (Bio-Rad) in a 20 μL reaction volume on a CFX Connect Real-Time thermocycler (Bio-Rad). Results can be found in the **Supplementary Material**.

Flux Balance Modeling

Flux balance modeling was conducted to describe rates of anammox, NO_3^- reduction to NO_2^- and complete denitrification (NO_2^- to N_2) based on cell abundance, input fluxes of substrates, and kinetic descriptions of these processes. The script for the simulation was written in Matlab (version R2015b) and can be found in the **Supplementary Material**. More details can be found in the discussion section that follows as well as in the **Supplementary Material**.

RESULTS

General Water Column Physical, Chemical, and Biological Properties

A salinity profile (**Figure 2A**), shows relatively uniform bottom waters with monthly variability in the surface waters. **Figure 2B** shows the relatively homogeneous temperature in the SI water column with a warming in the surface waters during the summer (June–September 2015) and the extension of this warming to deeper water depths in the following months. The chlorophyll *a* data (**Figure 2C**) shows peaks of fluorescence in the surface waters in March, May, and September 2015 with the highest concentrations, at 44 μg L^{-1} chlorophyll *a* in March just below the surface. O_2 concentration profiles (**Figure 2D**) were also determined with the CTD probe, revealing O_2 depletion to less than the sensor limit of detection (<1 μM) in the deep-waters for all of 2015. The upper boundary of the oxycline (depths where there is a sharp gradient in oxygen concentration) is generally around 80m and oxygen penetrates to at least 120 m, though penetration can be as deep as 150 m, as seen in July and September. Low O_2 concentrations and anoxia thus characterize the deeper waters of SI (>120 m depth) throughout 2015. NO_3^- concentrations (**Figure 2E**) are high in surface waters (up to 32 μM) and generally decline with increasing depth within the oxycline and often remain detectable in deeper low-oxygen waters. A peak in NO_2^- concentrations (**Figure 2F**) can be detected sporadically in both the surface waters and/or around 120–135 m where it can reach concentrations as high as 2.5 μM. Surface waters are largely devoid of any NH_4^+ (**Figure 2G**), which tends to accumulate below 140 m in anoxic waters and reaches the highest measured concentrations (up to 32 μM) by 200 m. Sulfide (HS^-) was only present in bottom waters, reaching concentrations up to 41 μM in February 2015, and was generally detected at 135 m and below (**Figure 2H**). In **Figure 2I**, we show DIN deficit (Bourbonnais et al., 2013) calculated for the year 2015 with values varying from 0 in the surface waters to 60 in the bottom waters for February 2015. Overall, values reflected a DIN deficit in the anoxic waters and increased with depth (**Figure 2I**).

Rates of Denitrification, Anammox and Dark Carbon Fixation

Both anammox and denitrification were active throughout the year in the low oxygen waters where we conducted ^{15}N-labeled incubations. Rates of denitrification, corrected for *in situ* substrate concentrations, varied between 0.28 ± 0.03 and 140 ± 14 nM hr^{-1} (**Figure 3B**) based on the accumulation of $^{30}N_2$ in $^{15}NO_3^-$ amended incubations (see **Table 1**). Similarly, rates of anammox varied throughout the year, between 0.07 ± 0.01 and 13.2 ± 0.4 nM hr^{-1} (**Figure 3C**) based on the accumulation of $^{29}N_2$ in $^{15}NH_4^+ + {}^{14}NO_3^-$ amended incubations. We also compared rates of anammox obtained through the accumulation of $^{29}N_2$ with the addition of $^{15}NO_3^-$ (**Figure 3A**) and found that they were of the same order of magnitude as rates obtained from $^{15}NH_4^+ + {}^{14}NO_3^-$ incubations (**Figure 3C**). Overall, rates of denitrification, when detected, were equal to or higher than rates of anammox, although anammox dominated N_2 production in 55% of the measurements made. However, the fact that rates of denitrification were generally higher, when detected, led to a higher annual proportion of N_2 production through denitrification (see section "Depth-Integrated Rates of N-Loss"). Dark carbon fixation rates were measured for most of the water column and ranged between 0.24 and 400 nmoles C L^{-1} hr^{-1} (**Figure 3D**).

Response of Denitrification and Anammox to Amendments

Between 1 and 20 μM $^{15}NO_3^-$ was amended to seawater collected from 165 m depth in August 2015. This depth contained 1 μM NO_3^- *in situ* and was therefore at the lower end of NO_3^- concentrations found within the anoxic waters of Saanich Inlet. Hence, NO_3^- concentrations may be expected to limit denitrification, NO_3^- reduction to NO_2^-, and anammox at this depth. Rates of denitrification, based

[4]https://uc-r.github.io/hc_clustering

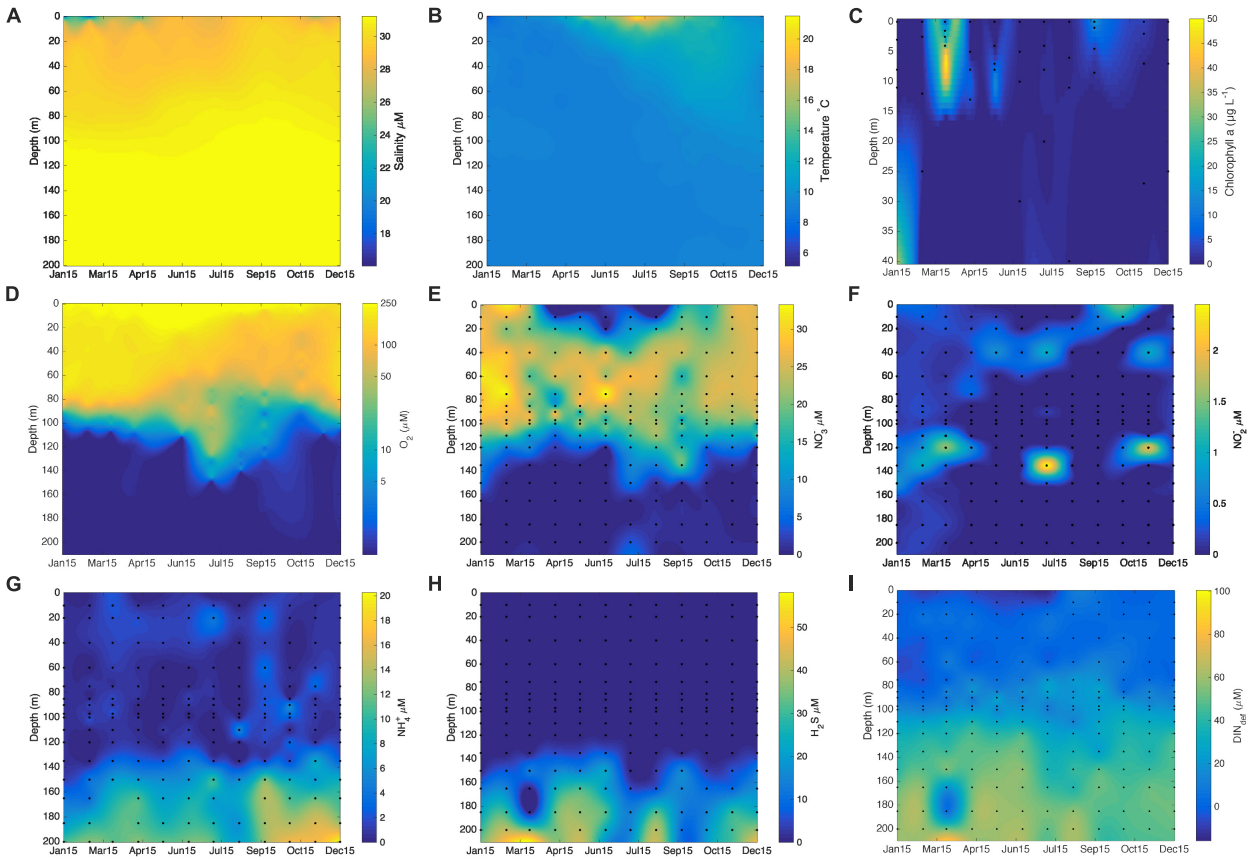

FIGURE 2 | (A) Salinity (g kg^{-1}); **(B)** temperature (°C); **(C)** chlorophyll *a* (µg L^{-1}); **(D)** oxygen profiles (µM); **(E)** NO_3^- concentrations (µM); **(F)** NO_2^- concentrations (µM); **(G)** NH_4^+ concentrations (µM); **(H)** HS^- concentrations (µM); **(I)** calculated DIN deficit values (see section "Materials and Methods" in main text) for Saanich Inlet during the year 2015 at station S3. **(A,B,D)** Values have been obtained from the CTD profiles monthly. Intermediate values have been interpolated in matlab using the gridfit function (specifically the nearest neighbor). **(C–G)** Values were obtained from discrete sampled depths as indicated by black dots on graphs and interpolated in matlab using the gridfit function (specifically the nearest neighbor). Note that figure **(C)** only goes down to 40 m depth as the values obtained for the chlorophyll *a* profile were sampled mostly above 40 m.

on the accumulation of $^{30}N_2$, increased with increasing NO_3^- concentrations up to 20 µM (**Figure 4A**), and the relationship between rates and NO_3^- concentration could be modeled with a Michaelis–Menten formulation. Our data could be described with a maximum rate of denitrification (V_{max}) and a half-saturation constant, K_m, for NO_3^- of 112 nM hr^{-1} and 5 µM (**Figures 4D,F** and **Table 2**), respectively. The rate of denitrification found at 20 µM NO_3^-, however, is lower than for 15 µM and did not follow predictions from the Michaelis–Menten model in **Figure 4F**. Anammox was not detected. We also determined changes in the concentrations of NO_x and NH_4^+ when we added different $^{15}NO_3^-$ concentrations (**Figures 4A,B**). We observed that NO_2^- accumulates with increasing $^{15}NO_3^-$ concentrations reaching a maximum of 9 µM when 20 µM $^{15}NO_3^-$ was added (**Figures 4A,E**). NH_4^+ concentrations, on the other hand, remain relatively constant between 8 and 12 µM (**Figure 4B**). Rates of NO_3^- reduction varied, between 0 and 430 nM hr^{-1}, and rates of NO_2^- accumulation varied between 0 and 286 nM hr^{-1} (**Figure 4E**). The latter rates combined with the rates of denitrification are enough to explain the rates of NO_3^- reduction and thus no accumulation of other intermediates such as N_2O is expected.

We also amended seawater collected from 120 m depth in June 2015 with HS^- ranging from 1 to 10 µM, in addition to 10 µM $^{15}NO_3^-$ to examine the influence of HS^- on rates of denitrification and anammox. This depth was chosen because it does not contain any detectable sulfide *in situ*. Instead, it immediately overlies the sulphidic deep waters and thus likely receives a flux of HS^- from below that fails to accumulate to detectable concentrations at 120 m depth and implies sulfide oxidation at this depth. Results show an increase in denitrification rates with increasing HS^- concentrations (see **Figures 5D,F**) above an apparent threshold of 2.5 µM HS^-. These experiments reveal a seemingly linear trend, but scarcity in data precludes the delineation of the precise relationship (**Figures 5E,F**). Anammox occurs (**Figures 5C,E**) with 1 and 2.5 µM HS^- amendments but was not detected with 5 and 10 µM HS^- amendments. NOx concentrations were constant over time in these

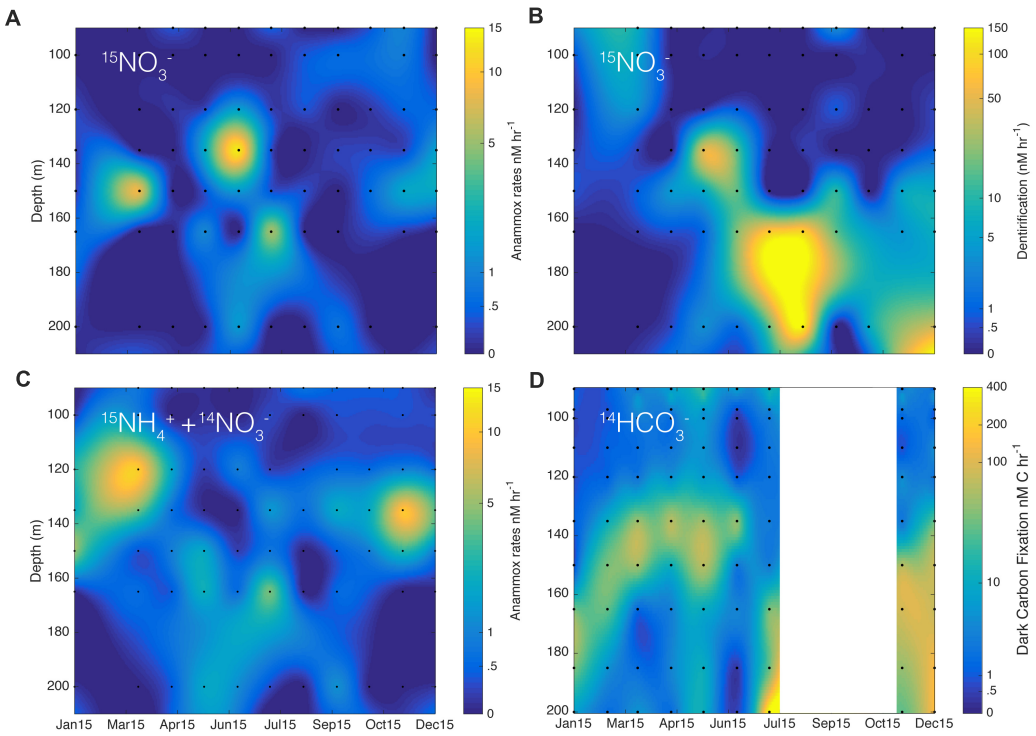

FIGURE 3 | Potential rates of **(A)** anammox (nM hr^{-1}) and **(B)** denitrification (nM hr^{-1}) calculated from the incubated samples with $^{15}NO_3^-$ for the year 2015 at station S3. **(C)** Shows potential rates of anammox of samples incubated with $^{15}NH_4^+ + ^{14}NO_3^-$. In **(D)**, graph shows rates of dark carbon fixation from incubation with $H^{14}CO_3^-$ in nM hr^{-1}. The scale bar is in log scale.

experiments except for the highest HS^- concentrations (**Figure 5A**), and NH_4^+ concentrations decreased over time (**Figure 5B**).

Depth-Integrated Rates of N-Loss

Depth-integrated rates of N_2 production varied over the year, with a greater contribution from denitrification (63%) than anammox (37%) (**Figure 6**). Rates of denitrification ranged between from 0.02 ± 0.006 to 14 ± 2 mmol m^{-2} d^{-1} (**Figure 6**), with the highest rates following renewal in July and August. Anammox rates, on the other hand, were comparatively constant throughout the year, and varied between 0.15 ± 0.03 and 3.4 ± 0.3 mmol m^{-2} d^{-1} (**Figure 6**). Anammox dominated N_2 production in January, April, May, June, October, and November (>50% of N_2 production). Nevertheless, results show that denitrification dominates the yearly N_2 production in the water column (**Figure 6**).

Microbial Community Composition

From a total of 6,889,880 sequences quality filtered by the JGI, 0.3% of the reads were discarded because they were too short or too long and 2% of the sequences were identified as chimeras and discarded. The final read count per sample can be found in **Supplementary Table S1** of the **Supplementary Material**. After clustering at the 97% identify threshold, 28,947 OTUs were resolved across 72 samples. The estimated community diversity (chao1) was low and variable in the surface waters and comparably higher and more stable at deeper depths. These results are summarized in **Supplementary Figure S1** and **Supplementary Table S1** of the **Supplementary Material**.

The microbial community in SI is vertically stratified with strong shifts in community compositions apparent between the surface waters (10 m) and the deeper waters (100 m and below) (**Figures 7**, **8**). In particular, there is a shift between high relative abundances of Alphaproteobacteria and Bacteroidetes (together, 42–85.3%) in the surface to a higher relative abundance of Gammaproteobacteria (23.4–68.5%) in the deeper waters (between 100 and 200 m) (**Figure 7**). In the surface waters, Alphaproteobacteria were mainly comprised of the SAR11 clade and Bacteroidetes of the Flavobacteriales. The cyanobacterial population present early in the year decreased to <1% during the spring bloom (April, May, and June), along with a sharp increase in Flavobacteriales for these 3 months (**Figure 7**). In deeper waters, the overwhelming majority of Gammaproteobacteria are associated with two OTUs belonging to the SUP05 cluster (Oceanospiralles clade) (**Figures 7**, **9**, and **Supplementary Material**). This trend was constant throughout the year. Another Gammaproteobacterial group – Ectothiorhodospiraceae (purple sulfur bacteria) – were present throughout the year in deeper waters (100–200 m), with one OTU representing between 1 and 30% (**Supplementary Figure S3**). Thaumarchaeotal (Marine

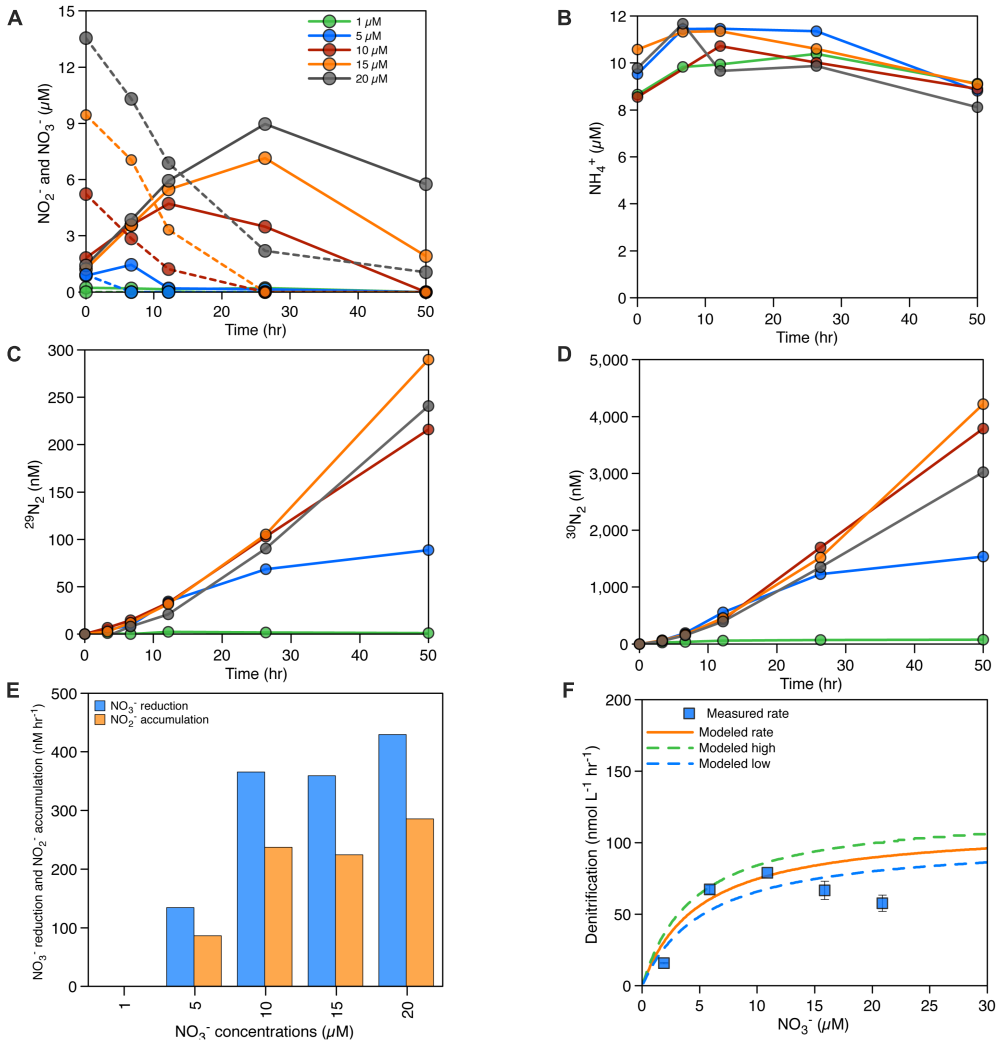

FIGURE 4 | (A) NOx accumulation/consumption over time with the addition of different NO_3^- concentrations – NO_3^- concentrations in dashed lines, NO_2^- concentrations in solid lines. **(B)** NH_4^+ accumulation/consumption over time with the addition of different NO_3^- concentrations. **(C)** Production of $^{29}N_2$ in the incubations (nM). **(D)** Production of $^{30}N_2$ in the incubations (nM), **(E)** rates of NO_3^- reduction and NO_2^- accumulation (nM hr^{-1}). **(F)** Michaelis–Menten curve and measured denitrification rates for different NO_3^- concentrations in August 2015, see **Table 2** for details on the Michaelis–Menten parameters used in **(F)**.

Group 1) relative abundance was generally low in the surface waters and increased up to 28% at 100 m where NO_3^- concentrations generally peaked (**Figure 7** and **Supplementary Figures S2**, **S3**). In the deeper waters (100–200 m), the Marinimicrobia clade totalled a few percent throughout the year and increased to up to 12% in November at 135 m. Epsilonproteobacteria were mostly comprised of an OTU from the genus Arcobacter, which reached up to 30% at 200 m in July 2015 during deep water renewal and remained present at relatively high abundances until September (**Figures 7**, **9** and **Supplementary Figure S3**). Several OTUs from the genera *Ca.* Scalindua (Planctomycetes) were present throughout the water column with a total up to 5.7% at 100 m in December 2015 (**Figures 7**, **9**). Members of the Woesearchaeota phylum were most abundant at depths from 100 to 200 m (0.3–12.2%). These results indicate a strong vertical stratification of the water column

TABLE 2 | Michaelis–Menten parameters, K_m (μM) and V_{max} (nmol L^{-1} hr^{-1}) for NO_3^- dependency of denitrification at 165 m in August 2015.

	Denitrification
K_m (μM)	5 ± 0.5
V_{max} (nmol L^{-1} hr^{-1})	112 ± 10

Note that anammox are not following Michaelis–Menten model in this case.

microbial community and relative consistency in this stratified community throughout the year, with notable exceptions (**Figure 8**). Surface waters, for example, exhibited considerable dynamics in microbial communities during the spring blooms (April–June), and deeper waters shifted composition following renewal in July (**Figure 8**).

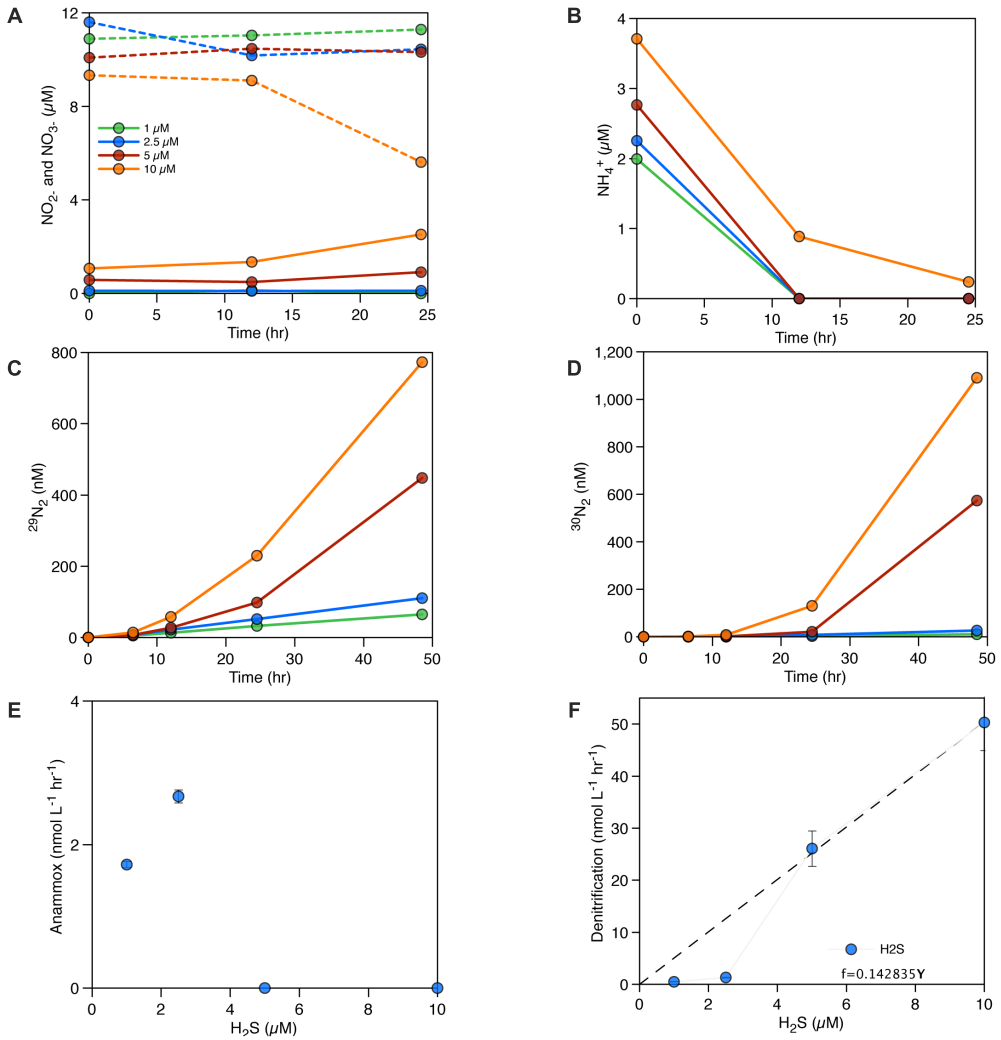

FIGURE 5 | (A) NOx accumulation/consumption over time with the addition of different HS^- concentrations – NO_3^- concentrations in dashed lines, NO_2^- concentrations in solid lines. **(B)** NH_4^+ accumulation/consumption over time with the addition of different HS^- concentrations. **(C)** Production of $^{29}N_2$ in the incubations (nM). **(D)** Production of $^{30}N_2$ in the incubations (nM), **(E)** measured anammox rates (nM hr^{-1}) for different HS^- concentrations in June 2015, **(F)** measured denitrification rates (nM hr^{-1}) for different HS^- concentrations in June 2015.

DISCUSSION

Partitioning of N-Loss in SI, and the Seasonality of Anammox and Denitrification

^{15}N-labeled incubations indicate that both anammox and denitrification operated simultaneously throughout the year in the anoxic water column of SI. Although anammox dominated (responsible for >50% N-loss) in 55% of the measurements in which N_2 production was detected (**Figures 3A–C**), depth-integrated rates of denitrification show that it accounts for up to 63% of the total N-loss from SI (**Figure 6**). Overall, depth-integrated rates of denitrification and anammox ranged between 0.02 and 14.4 mmol m^{-2} d^{-1} and 0.15 and 3.36 mmol m^{-2} d^{-1}, respectively (**Figure 6**). Annual pelagic N-loss from the inlet was calculated using these measurements by taking the average of the depth-integrated rates, and multiplying these by the surface area of SI's anoxic basin (33 km^2). Annual N-loss totalled 0.002 Tg N yr^{-1} in 2015. N-loss rates previously reported based solely on geochemical measurements (Manning et al., 2010) implied N-loss of between 1.7 and 8.1 mmol m^{-2} d^{-1}. Given that 50% of the N-loss previously reported is from benthic N_2 production, the rates that we measure here, that only capture pelagic N-loss, appear appreciably higher and may thus suggest inter-annual variability in N_2 production rates. Rates of denitrification and anammox were previously reported for 2 months during peak "stagnation" in SI in 2010 (Louca et al., 2016) and while these are at the lower end of the range of rates measured here, they generally agree with the rates we detected during peak stagnation.

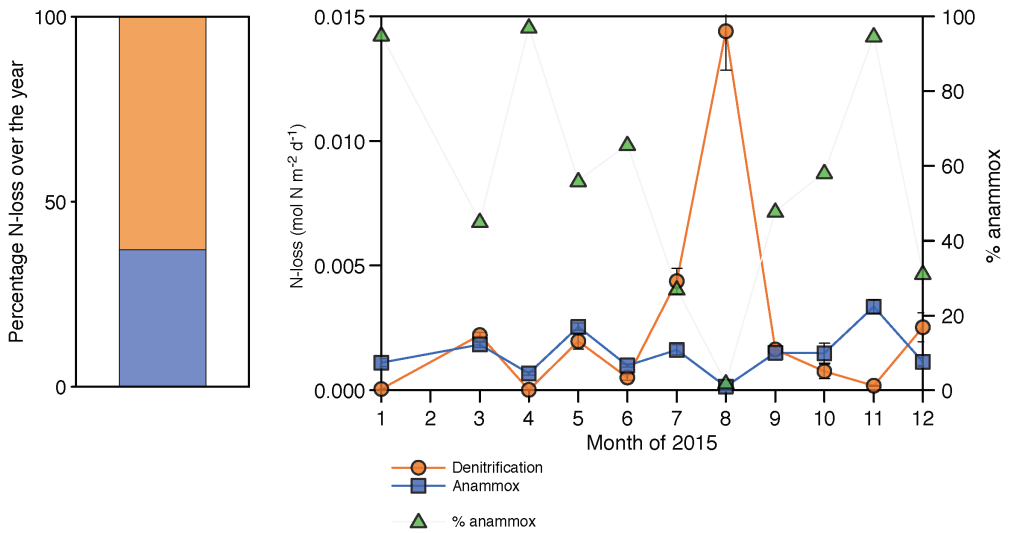

FIGURE 6 | Integrated N-loss rates over the year through denitrification in orange and through anammox in blue. The black dotted line represents the percentage of N-loss occurring through anammox (in %). The stacked bar represents the averaged N-loss over the entire year.

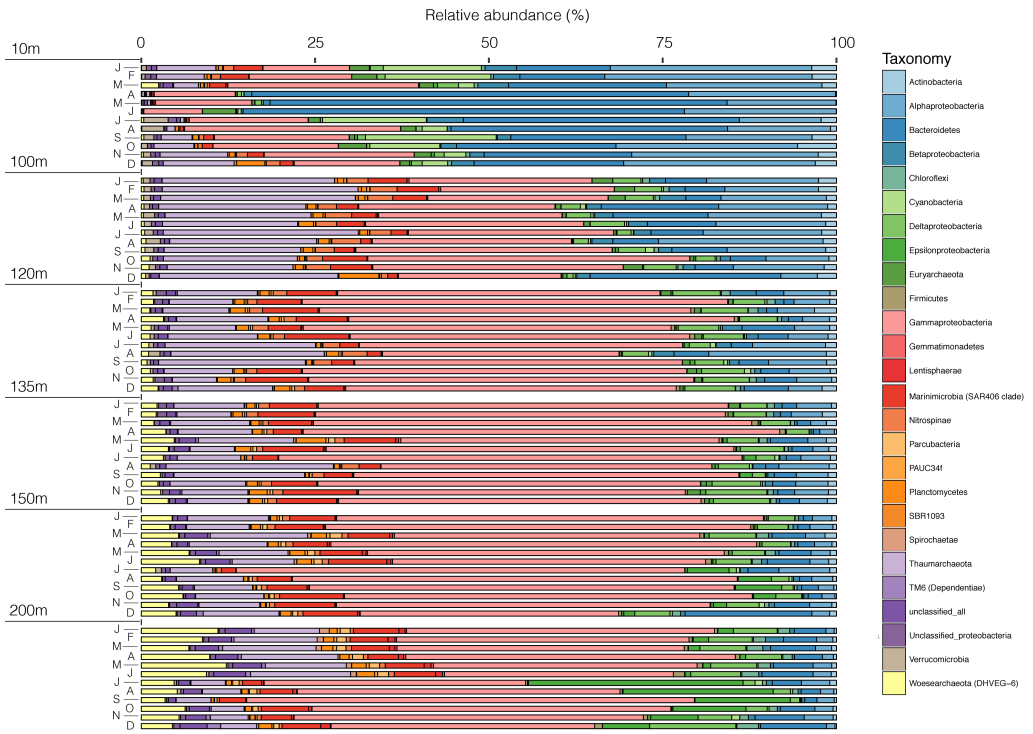

FIGURE 7 | Microbial community composition of SI in 2015 for 6 depths (10, 100, 120, 135, 150, and 200 m) at the phylum level in relative abundance.

The monthly variability in rates of N-loss from Saanich inlet are driven through dynamics in rates of both anammox and denitrification. Thus, knowledge on the regulation of both anammox and denitrification is key to knowing how N-budgets in Saanich inlet, and by extension, other anoxic fjords, vary. Partitioning of N-loss between these pathways for the entire year reveals 63% denitrification and 37% anammox. This ratio is close to the theoretical ratio calculated for the partitioning of N-loss in the open ocean through anammox and denitrification (29–71% anammox/denitrification ratio). This ratio applies when substrate (NH_4^+) supply rates for anammox are constrained by the stoichiometry of settling organic matter (Codispoti et al., 2001; Van Mooy et al., 2002; Devol, 2003; Koeve and Kähler, 2010; Babbin et al., 2014). Excursions beyond this ratio might

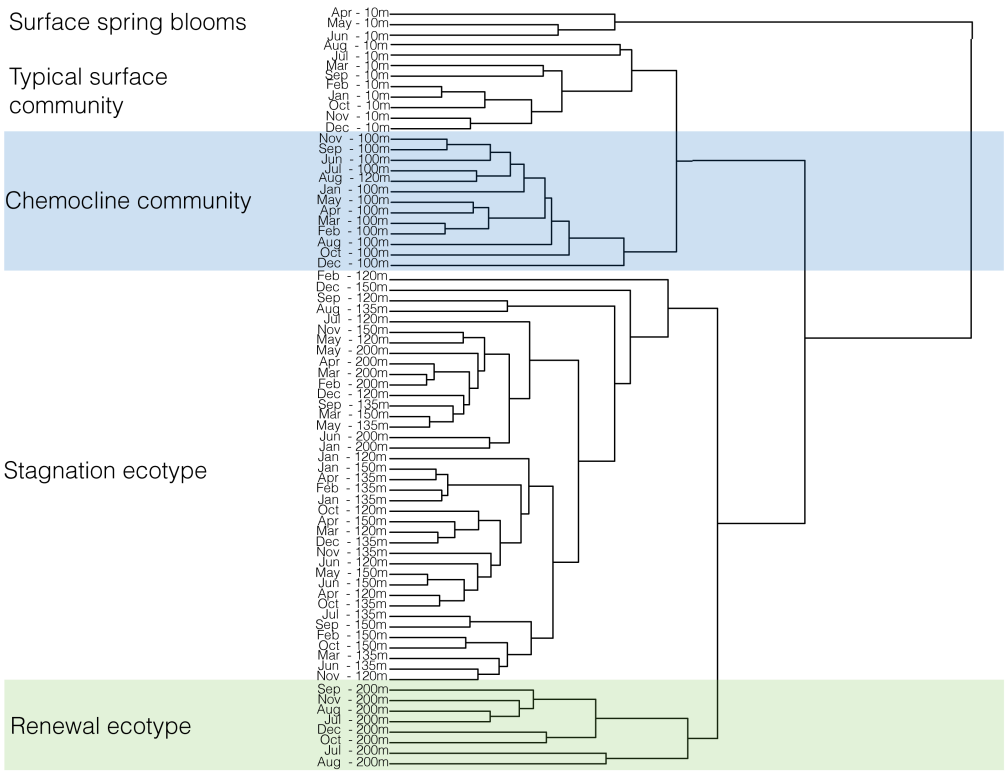

FIGURE 8 | Clustering of the microbial community composition of SI in 2015 for 6 depths (10, 100, 120, 135, 150, and 200 m) and 12 months. Dissimilarities between samples is shown by the height of the fusion of the dendrogram: the higher the fusion, the more dissimilar samples are between each other. Clustering of samples was performed in R with the Euclidean method.

FIGURE 9 | Comparison of the relative abundance of Planctomycetes, SUP05 cluster, Marinimicrobia, and newly highlighted Arcobacter bacteria. In addition to the relative abundance of these clades, we added total 16S counts (16S L^{-1}) for each of these samples.

indicate additional sources of NH_4^+, such as sulfate reduction, and/or an input of NH_4^+ from the underlying sediments. Excursion below this ratio more likely signals competition for nitrite or chemoautotrophic denitrification, which would not liberate NH_4^+. In July and December of 2015, N-loss was close to the theoretical ratio (27 and 31%, respectively), which is consistent with the canonical scenario in which heterotrophic denitrification supplies anammox with NH_4^+. The ratio deviates from this throughout much of the rest of the year, with generally higher proportions of anammox (40% and beyond), implying that an additional supply of NH_4^+, beyond that supplied through heterotrophic denitrification, is needed.

Rates of denitrification and anammox are expected to respond to supply of the principal substrates: NO_3^-, organic matter or HS^- for denitrification, and NH_4^+ and NO_2^- for anammox; as well as possible inhibitors like HS^- for anammox and O_2 for both anammox and denitrification. In July 2015, O_2 and NO_3^- both penetrate to 150 m (**Figures 2D,E**) signaling the intrusion of oxygenated NO_3^- rich waters to intermediate depths, and although devoid of O_2, deep waters (185 and 200 m) contain detectable NO_3^-. These observations indicate intermediate- and deep-water renewal in July. Although our monthly nutrient profiles do not record a strong deep-water renewal that would have oxygenated the deep waters, we do observe changes in nutrient concentrations, which coincide with higher rates of denitrification in July and August (**Figure 6**). Thus, the regulation of denitrification in SI appears linked to renewal, and is further enhanced by the accumulation of HS^- in August.

A dramatic increase in deep water NH_4^+ concentrations is reflected by relatively high rates of anammox recorded in September, October, and November (**Figure 6**), along with lower concentrations of HS^-, implying that increased deep-water NH_4^+ leads to higher rates of anammox. The NH_4^+ in the deep waters could originate from the remineralization of sinking organic matter supplied through primary production in the surface waters. Chlorophyll *a* peaks in the surface waters of SI, a proxy for the abundance of photosynthetic organisms, vary over the year, and peak during the spring/early summer (**Figure 2C**). Organic matter from primary production is exported to the deep waters and sediments as particles and fecal pellets. Given that both particles and fecal pellets would sediment to the deep waters in less than a week (Sancetta and Calvert, 1988), we expect deep water NH_4^+ concentrations to respond to blooms in the surface waters within 15 days. As we sampled approximately every 4 weeks, it is possible that we lacked the temporal resolution to capture intense degradation activity following a bloom. However, as blooms are a common occurrence during the summer months (Takahashi et al., 1977; Grundle et al., 2009), the increase in the deep-water NH_4^+ concentrations in September (**Figure 2G**) likely originates from a corresponding increase in surface water primary production. Therefore, the combination of relatively high productivity in surface water and the ensuing high NH_4^+ concentrations in the deep waters likely support relatively high rates of anammox toward the end of the summer.

Though ultimately sourced from primary production, the detailed biogeochemical pathways through which the NH_4^+ is made available to anammox can vary. These pathways include: ammonification due to organotrophic denitrification; DNRA; ammonification associated with sulfate reduction; or benthic NH_4^+ efflux. We thus consider these possible sources and their relative fluxes in relation to rates of anammox. Rates of denitrification measured in SI could have supplied 25% of the NH_4^+ needed to support co-occurring anammox on average, assuming Redfieldian OM stoichiometry and 100% organotrophic denitrification (in August 2015, **Figure 6**). This is unlikely as HS^- clearly influences rates of denitrification, and is consistent with previously reported genomic information (Walsh et al., 2009; Hawley et al., 2014), which implies chemoautotrophic denitrification in SI. Another source of NH_4^+ could be organotrophic NO_3^- reduction to NO_2^-.

We calculate that the highest potential rates of NO_3^- reduction to NO_2^- recorded in August 2015 (**Figure 4E**, 400 nM N hr^{-1} for 20 μM NO_3^- addition), are sufficiently high such that all of the NH_4^+ needed to support the highest rates of anammox could come from this reaction (13.7 nM hr^{-1}). However, *in situ* NO_3^- concentrations are generally not as high as the concentrations in these amended incubations, and thus rates of NO_3^- reduction to NO_2^- might not supply all the NH_4^+. Remineralization of organic matter through partial or complete denitrification is thus likely only partly responsible for NH_4^+ supply to anammox. Similarly, SO_4^{2-} reduction could also produce NH_4^+ through remineralization of organic matter in the water column. In SI, however, sulfate reduction remains unmeasured through direct process rate experiments and the functional markers for canonical sulfate reduction were absent from the metaproteomes generated to date (Hawley et al., 2014). DNRA can also supply NH_4^+ to anammox, as it does in the Peruvian OMZ (Lam et al., 2009). A DNRA catalyzing-like protein, hydroxylamine-oxidoreductase, was recovered in metaproteomes and appears to be associated with the denitrifier– SUP05 (Hawley et al., 2014). DNRA, however, has not been detected in SI to date, though modeling predicts appreciable DNRA for September 2009, and DNRA, if operating in SI, could thus contribute to dynamics in anammox activity (Louca et al., 2016). Given that the pelagic pathways for NH_4^+ delivery to anammox appear insufficient to support the measured rates, we consider the possibility that NH_4^+ efflux from the bottom sediments also contributes NH_4^+ to anammox. Indeed, high rates of organic matter remineralization through sulfate reduction characterize SI sediments (Devol et al., 1984). Some of the NH_4^+ liberated in the process would diffuse from the sediment and could advect upward to fuel anammox in the overlying water. Based on our calculations (see **Supplementary Section 1**), NH_4^+ fluxes from the sediment in SI could fuel 88 to 100% of the NH_4^+ required to support anammox. We thus expect a combination of these multiple NH_4^+ sources fuels anammox and contributes to its variability throughout the year.

Kinetics of Denitrification and Anammox

External forcing by substrate supply rates places overall constraints on material fluxes and thus microbial community metabolism, but microbial community structure and function also depend on the specific ecophysiologies of relevant organisms, such as an organism's ability to take up and metabolize a given

substrate. We showed that denitrification in SI appears to depend on NO_3^- concentrations (**Figure 4C** and **Table 2**), and the K_m for NO_3^- obtained at 165 m in August 2015 was 5 μM and in the same range as earlier reports from both environmental measurements and cultured denitrifiers (1.7–10 μM) (Jensen et al., 2009). These prior kinetic constants come from pure cultures of organotrophic denitrifiers (Parsonage et al., 1985; Christensen and Tiedje, 1988), sediment microbial communities (Murray et al., 1989; Dalsgaard and Thamdrup, 2002), and an anoxic sulfidic fjord (Jensen et al., 2009). When NO_3^- concentrations exceeded 15 μM, however, the rates of complete denitrification decreased (**Figure 4F**). This is in line with the observation that microorganism tend to favor the first step of denitrification, NO_3^- reduction to NO_2^-, over complete NO_3^- reduction to N_2, when NO_3^- concentrations are high. Similar observations were made previously in Mariager fjord (Jensen et al., 2009) where NO_3^- reduction to NO_2^- took over when NO_3^- concentrations exceeded 5 μM.

Rates of denitrification and anammox in SI are sensitive to the HS^- concentrations present. When seawater from 120 m (June 2015) was amended with HS^-, rates of denitrification increased with respect to HS^- concentrations (**Figure 5**) for HS^- concentrations higher than 2.5 μM. The rates then seemed to exhibit a linear response, possibly because the enzyme saturation for sulfide oxidation is much higher (Jensen et al., 2009). This observation is similar to reports of a linear dependency of denitrification on HS^- concentrations, with no sign of saturation, up to 40 μM HS^- in Mariager Fjord, Denmark (Jensen et al., 2009). Measurements of NO_3^- and NO_2^- indicate low or no NO_2^- accumulation during these incubations and, given the low rates of denitrification for 2.5 μM HS^-, this implies a shunting of the NO_2^- produced to anammox. Indeed, anammox occurs at low HS^- concentrations (**Figure 5D**). Anammox occurrence at low HS^- concentrations was previously observed in a sulphidic alpine lake (Wenk et al., 2013). This stands in contrast to most previous marine observations, which found that anammox was inhibited by HS^- at concentrations as low as 1.6 μM (Dalsgaard et al., 2003; Jensen et al., 2008). The stimulation of anammox at low HS^- concentrations in SI may reflect the production of NO_2^- through partial denitrification and the bypass of complete denitrification due to a higher affinity of anammox bacteria for NO_2^- (Dalsgaard and Thamdrup, 2002). This is supported by the fact that NO_2^- did not accumulate during these incubations (**Figure 5A**), implying that sulfide dependent partial denitrification (NO_3^- to NO_2^-) underpins nitrite leakage to anammox in SI when HS^- is low.

As rates of anammox appear to be sensitive to higher fluxes of NH_4^+ in the water column (see above), we plotted the rates of anammox obtained for the whole year vs. the *in situ* NH_4^+ concentrations (**Figure 10**). However, the lack of a coherent positive relationship between rates of anammox and NH_4^+ concentrations generally implies insensitivity of anammox to NH_4^+ concentrations higher than 2 μM. These results could indicate that the K_m for NH_4^+ of anammox bacteria is lower than the *in situ* NH_4^+ concentrations. Alternatively, this could also indicate that anammox bacteria could obtain the NH_4^+ needed through tight coupling between anammox and DNRA (Prokopenko et al., 2013) or through ammonification in particle-associated processes (Ganesh et al., 2014), which would not be specifically recorded in the ambient NH_4^+ concentrations in SI.

Vertical Partitioning of the Microbial Communities in SI

The strongest difference in microbial community composition was between the surface waters at 10 m depth and deep waters below 100 m depth (**Figure 8**), while temporal variations were most notable in the surface waters (**Figure 8**). Variation in community composition between 120 and 200 m depth was comparatively small as were dynamics in deep water community composition throughout the year, with the exception of OTUs assigned to the Epsilonproteobacterium, Arcobacter (**Figures 7**, **9**). Such vertical stratification in microbial community composition is typical for aquatic ecosystems including OMZs (Stevens and Ulloa, 2008; Wright et al., 2012; İnceoğlu et al., 2015), and has been previously observed in SI (Zaikova et al., 2010; Hawley et al., 2014). Indeed, niche partitioning along redox gradients is generally expected (Wright et al., 2012). A conceptual model previously developed (Hawley et al., 2014) describes microbial community structure and function in SI and provides a benchmark framework through which to view temporal and vertical dynamics in microbial community composition (**Figures 1C**, **7**–**9** and **Supplementary Figures S2**, **S3**). The key taxa that comprise this model, including SUP05, Marinimicrobia, Thaumarchaeota, SAR11, and Planctomycetes were prevalent SI community members in 2015. These taxa were present throughout the water column, with Thaumarchaeota and SAR11 most abundant at 100 m and SUP05 increasing in abundance with depth. Planctomycetes were low in the surface water and increased to a few percent in the deeper waters, similar to Marinimicrobia. In addition to these taxa, our community profiles reveal dynamics in relatively abundant Bacteroidetes, which increase in the surface waters during the spring bloom (from 20 to 65% in April, May, and June), and Arcobacter that appears to bloom in the deep waters (from <1% up to 30% at 200 m) in association with renewal in July and subsequently decreases in relative abundance in the following month.

A closer analysis of microbial community dynamics in the surface waters reveals that of the 15 most abundant OTUs, there were high relative abundances of 3 OTUs of the Flavobacteriaceae and 1 OTU of the Rhodobacterales family in April, May, and June, and correspondingly low abundances of an OTU belonging to the SAR11 clade (see **Supplementary Figure S3**). This particular microbial community composition appears contemporaneous with photosynthetic blooms. Flavobacteriaceae and Rhodobacterales are generally considered participants in biomass degradation (Bergauer et al., 2018) and their relatively high abundance in the spring may thus be a response to relatively strong photosynthetic activity (**Figure 2C**). While photosynthetic blooms are evident from pigment distributions (**Figure 2C**), we did not observe correspondingly high relative abundances of photosynthetic

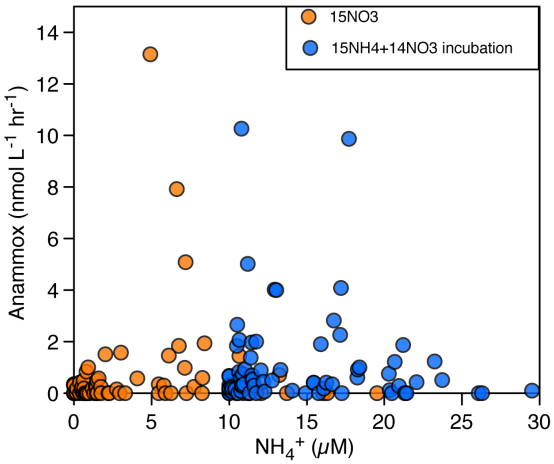

FIGURE 10 | Comparison of anammox rates vs. *in situ* NH_4^+ concentrations (taking into account the addition of $^{15}NH_4^+$). In orange, rates of anammox obtained through the production of $^{29}N2$ with the addition of $^{15}NH_4^+$ and $^{15}NO_3^-$. In blue, rates of anammox obtained through the production of $^{29}N2$ with the addition of $^{15}NO_3^-$.

bacterial taxa (cyanobacteria) at this time. This likely indicates that cyanobacteria play a limited role in this bloom, which instead is the response of diatom growth, as previously reported (Sancetta and Calvert, 1988). Diatom blooms in April, May and June thus appear to stimulate a number of microbial taxa linked to organic matter degradation in the surface waters, while cyanobacterial contributions to microbial community composition are marginalized at this time.

One of the most abundant OTUs present throughout the water column was assigned to the SUP05 cluster (**Supplementary Figure S3**), which varied between a few percent in the surface water to a maximum of 48% in July and September at 150 and 200 m, respectively (**Figure 9** and **Supplementary Figure S3**). Based on its metabolic potential to couple sulfide oxidation to NO_2^- reduction to N_2O and its relatively high abundance, SUP05 has been implicated as a key-player in coupled C, N, and S cycling and N-loss from SI (Walsh et al., 2009; Hawley et al., 2014), and more broadly throughout low oxygen marine waters globally (Wright et al., 2012; Anantharaman et al., 2013; Glaubitz et al., 2013; Callbeck et al., 2018). Consistent with this, we find that N_2 production through denitrification was active throughout the year when SUP05 was a ubiquitously abundant community member (**Figures 7**, **9** and **Supplementary Figure S3**). Likewise, water collected from 120 m in June had a microbial community composition of 28% SUP05, and rates of denitrification in this water increased in response to HS^- addition, indirectly linking SUP05 to sulfide dependent denitrification. However, N_2O did not accumulate in our incubations, and we thus suspect that other taxa also play a role in denitrification, by reducing N_2O to N_2.

Some Marinimicrobia clades indeed possess the *nosZ* gene and have the metabolic potential to perform this last step in denitrification (Hawley et al., 2017a). Like SUP05, Marinimicrobia were relatively abundant in the deep waters where they comprised 4 different OTUs that together comprised up to 12% of the total microbial community at 135 m in November 2015 (**Figures 7**, **9**, **11A** and **Supplementary Figure S3**). These 4 OTUs were phylogenetically compared to previously identified Marinimicrobia genome bins and SAGs [**Figure 11B**, (Hawley et al., 2017a)] and were found to be affiliated to 4 different clades: 3 SI clones (SHBH1141, SHBH319, and SHAN400) as well as an Arctic clone (Arctic96B-7). Interestingly, only SHBH1141 appears to carry the *nosZ* gene (Hawley et al., 2017a), making it the most likely microorganism in SI to reduce N_2O to N_2 coupled to HS^- oxidation (Hawley et al., 2014). The SHBH1141 clade increased with depth, with the overall highest relative abundance at 150 m (**Figure 11A**). However, SHBH1141's relative abundance decreased in July, in association with the renewal event. Comparatively, the SHAN400 clade remained relatively constant between 100 and 200 m and both Arctic96B-7 and SHBH391 have higher relative abundances at 120 m than at 100 m and remain constant down to 200 m. From SAGs, SHAN400 and Arctic96B-7 were shown to carry NO_3^- reduction to NO coupled to HS^- oxidation, thus participating in partial denitrification, whereas no genes involved in the N-cycle were found for SHBH391 (Hawley et al., 2017a).

Anammox was also operative throughout the entire year in 2015, and accordingly, we found members of the Planctomycetes phylum were present at up to 5% in the water column (**Figures 7–9**). Indeed, Planctomycetes is the only phylum known to contain bacteria that perform anammox. The metabolic potential for anammox is restricted in the Planctomycetes to the order Brocadiales. SI hosts mainly *Ca.* Scalindua, a well-known marine anammox bacterium which comprised up to 2.6% of the community at 135 m in May (**Figure 9**). Altogether, microbial community profiling reveals that the key taxa that comprise previous conceptual models for coupled microbial C, N, and S cycling in SI are present and relatively abundant at depths between 100 and 200 m throughout the year. At the community level, these taxa collectively underpin N cycling and loss from Saanich inlet, which we demonstrate through contemporaneous process rate measurements.

In addition to the taxa discussed above, it appears that an OTU assigned to the Epsilonproteobacteria Arcobacter increases dramatically in relative abundance in the deep waters, notably at 200 m where it goes from <1% in June, to 30% in July, becoming one of the 15 most abundant OTUs in SI, and then drops to 20% in August. This increase in relative abundance appears to be a response to deep water renewal and is strongly correlated with the enhanced rates of denitrification found in July and August, relative to the rest of the year, as well as the highest rates of dark carbon fixation (**Figure 2D**). Indeed, a number of Arcobacter isolates are known to perform complete denitrification (NO_3^- to N_2) (Canion et al., 2013), as well as sulfide oxidation (Wirsen et al., 2002). The high relative abundances of Arcobacter in July and the fact that Marinimicrobia OTUs decreased at the same time posits an important role for Arcobacter in the SI N-cycle (**Figures 9**, **11A**).

Considering our observations of microbial community and biogeochemical dynamics across the year, we suggest that the inlet exists in two principle biogeochemical states: throughout much of the year, the inlet is relatively stagnant,

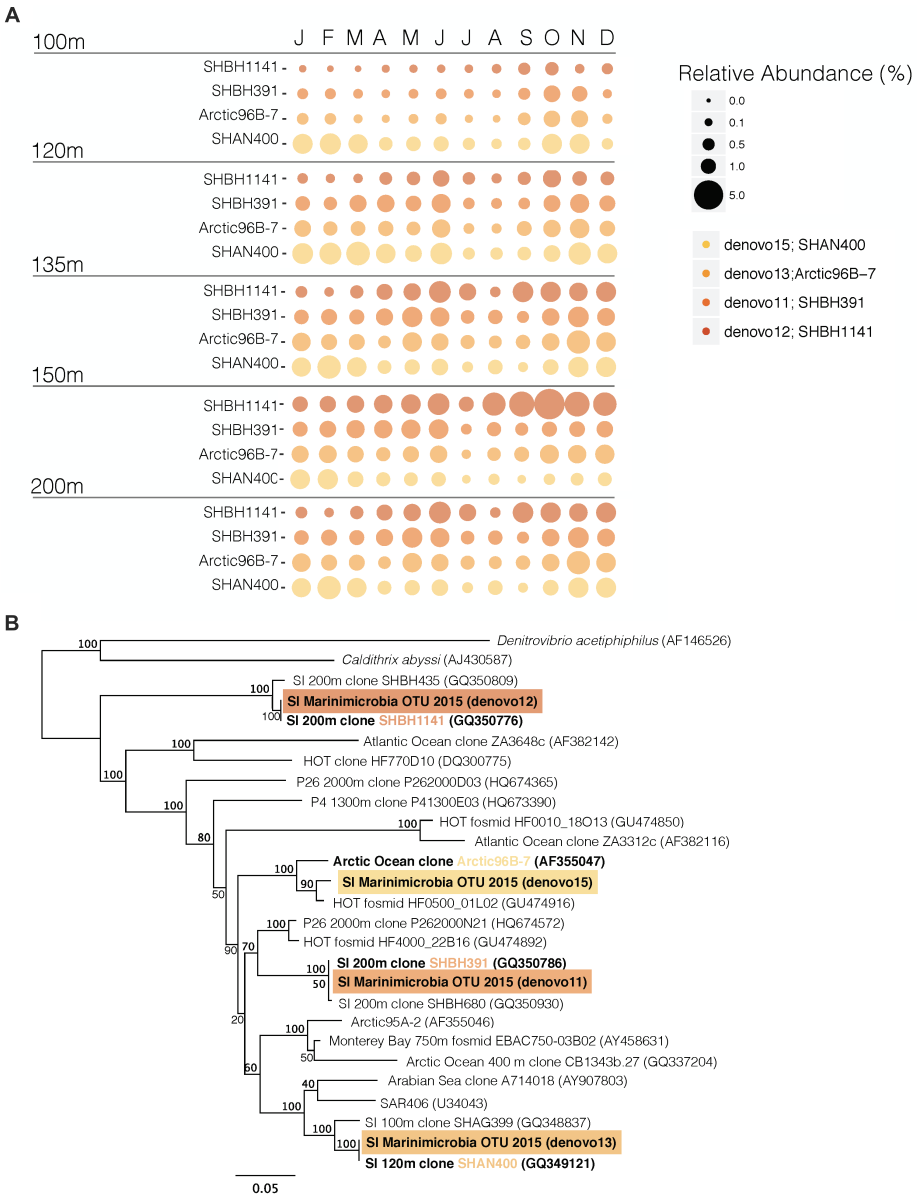

FIGURE 11 | OTUs from the Marinimicrobia phylum in SI. **(A)** Relative abundance of the 4 most abundant OTUs of the Marinimicrobia phylum in SI plotted by depths and months **(B)** maximum-likelihood phylogenetic tree of the small subunit rRNA for sequences of the Marinimicrobia clade (ML implemented with RaxML, 100 bootstraps). OTUs identified in this study are highlighted in a colored box. Previously identified SAGs or genome bins are in bold. The bar represents 5% estimated sequence divergence. Bootstrap value at the branch node indicate the robustness of the branching of the tree.

anaerobic N_2 production is distributed between anammox and denitrification and we suggest that *Ca.* Scalindua, SUP05, and Marinimicrobia are the key taxa responsible; during the summer renewal the input of NO_3^- to deep sulfide-rich waters stimulates the growth of Arcobacter, which drives most N_2 production through denitrification marginalizing anammox. These two states thus define microbial community phenotypes representing background or 'stagnation' periods and 'renewal' periods, respectively.

Shifts between stagnation and renewal phenotypes imply that the relevant community members possess differing ecophysiology. In particular, the bloom in Arcobacter in response to renewal implies that these organisms have higher maximum cell specific growth rates and/or lower biomass yield than the combination of SUP05 and Marinimicrobia. Without any existing information on biomass yield, we thus estimated cell-specific rates of N_2 production through denitrification during stagnation and renewal periods. We expect for the combined Marinimicrobia/SUP05 population to have lower cell specific rates in comparison to the Arcobacter population, which produces N_2 at higher rates for similar cell abundance. For the 'stagnation' phenotype we used

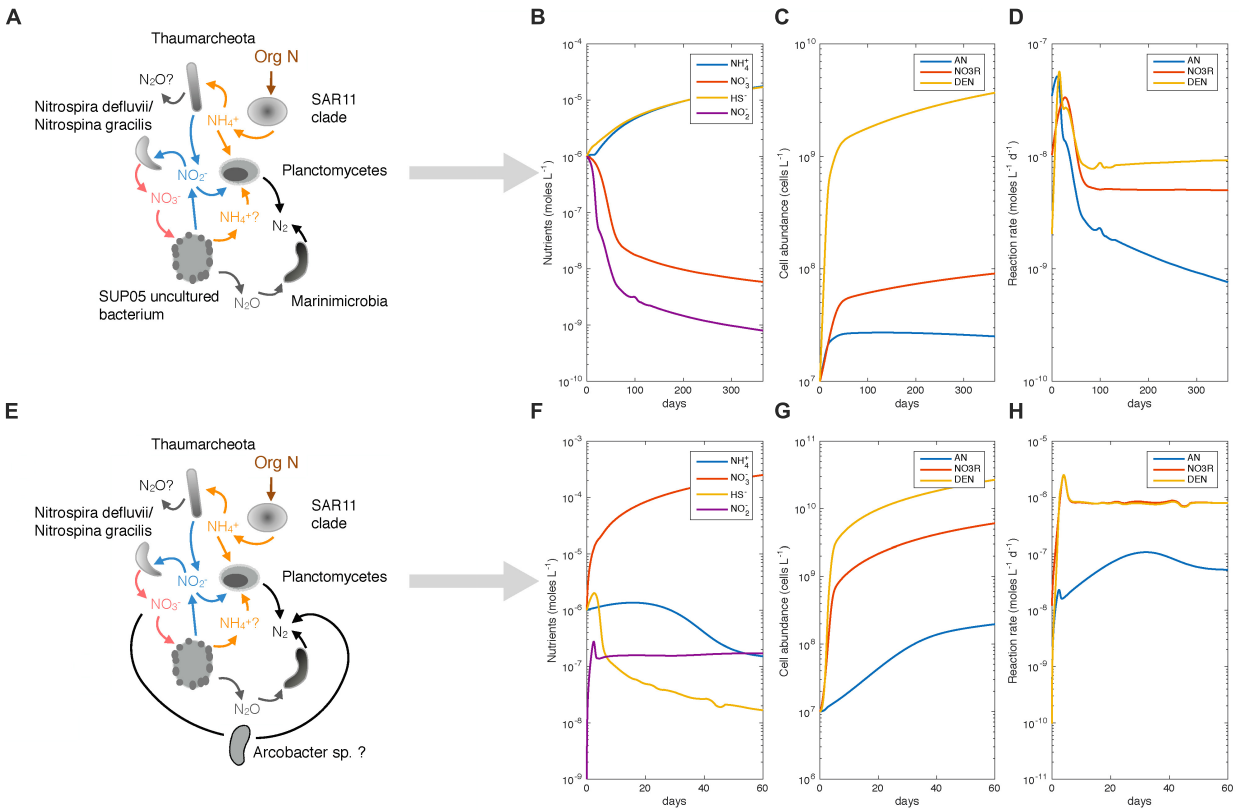

FIGURE 12 | Model of NO_2^- competition between anammox and complete denitrification for the 2 ecotypes found in SI, "stagnation phenotype" and "renewal phenotype". **(A)** Represents the ecotype found in SI during stagnant periods of time. **(B–D)** Shows a simulation of the model that tested to see if the phenotype of the ecotype could be reproduced through modeling. Parameters used to model this simulation can be found in **Table 3**. **(E)** Represents the second ecotype found in SI during renewal event, leading to higher N_2 production **(F–H)** shows that the model reproduced higher rates of N_2 production. Parameters used in this simulation can be found in **Table 3**.

an average cell abundance of 1.6×10^9 cells L^{-1} for the combined abundance of Marinimicrobia and SUP05, which we estimated by combining qPCR of the bacterial 16S rRNA gene as a proxy for total community size with the relative Marinimicrobia/SUP05 abundance from our amplicon sequence data (see **Supplementary Material**). Marinimicrobia, in association with SUP05, are likely responsible for the production of N_2 throughout most of the year, and we used the lowest and highest rates of denitrification in the stagnant period (0.01–38.45 nM hr^{-1}) to come up with a range of cell specific denitrification rates for Marinimicrobia/SUP05 between 0.0001 and 0.6 fmol N_2 $cell^{-1}$ d^{-1}.

To compare against the renewal phenotype, we estimated Arcobacter cell abundance (based on total bacterial 16S rRNA gene copies for July at 200 m, 3.05×10^9 cells L^{-1} combined with the relative abundance of Arcobacter from our amplicon sequence data— see **Supplementary Material**) and with the corresponding rates of denitrification obtained cell-specific rates of 1.08 fmol N_2 $cell^{-1}$ d^{-1} for Arcobacter. The cell-specific rates for Marinimicrobia are therefore lower than the cell-specific rate calculated for Arcobacter. Thus, it is likely that SUP05/Marinimicrobia population has a higher growth yield than Arcobacter, shown by similar cell abundance but lower cell-specific rate for the former.

The low relative abundance of Planctomycetes associated with lower N_2 production rates indicate that the anammox bacteria present in SI have a high cell-specific growth rate with a low growth yield. Again, based on the 16S abundance obtained from qPCR analysis (see **Supplementary Material**) applied to the average relative abundance of anammox bacteria, cell specific rates for anammox vary between 0.02 and 6.72 fmoles NH_4^+ $cell^{-1}$ d^{-1}, using average cell counts for anammox for the year (2.3×10^7 anammox cells L^{-1}) and the highest and lowest rates measured in SI in 2015. Our measured rates encompass the cell specific rates obtained from the Namibian OMZ [4.5 fmol NH_4^+ $cell^{-1}$ d^{-1}, (Kuypers et al., 2005)], the Black Sea [3–4 fmol NH_4^+ $cell^{-1}$ d^{-1}, (Jensen et al., 2008)], and diverse bioreactors [2–20 fmol NH_4^+ $cell^{-1}$ d^{-1}, (Strous et al., 1999)]. The lower end of our measured rates might be explained by small fractions of active versus total anammox bacteria present, which would increase the cell-specific rates calculated here. This highlights that, even though anammox bacteria are generally present in at lower relative abundances than denitrifiers (SUP05, Marinimicrobia and/or Arcobacter), they play a similar role in

N-species transformations and N_2 production as well as overall energy transduction in low-oxygen and anoxic marine waters.

Model of NO_2^- Competition Between Anammox and Complete Denitrification

Based on the results described above, we built a flux balance model to study the competition for NO_2^- between anammox and complete denitrification, testing if we could reproduce the rates corresponding to the two community phenotypes proposed (high or low N_2 production). Lower rates of denitrification are attributed to a 'stagnation' phenotype, whereas higher rates of denitrification correspond to a 'renewal' phenotype (**Figure 12**). The rates of anammox, NO_3^- reduction to NO_2^-, and complete denitrification (NO_2^- to N_2), are described through Michaelis–Menten equations, depending on both substrates (electron donors and electron acceptors), their respective kinetic parameters (K_m and V_{max}) for each of these substrates, cell abundance and biomass yield (Y) (see **Supplementary Material** for a complete description of the model). Both NO_3^- reduction to NO_2^-, and complete denitrification are sulfide-dependent. Nutrient concentrations of interest (NO_3^-, NO_2^-, NH_4^+, and HS^-) are calculated based on the rates of anammox, NO_3^- reduction to NO_2^-, and complete denitrification, as well as fixed input fluxes of the substrates through possible advection and diffusion (See **Supplemental Material**, section 3). These fluxes, however, are fixed throughout the simulation and do not reflect the highly dynamic nature of the nutrient fluxes found in SI, specifically through a renewal event. This model has thus been built to represent the two phenotypes introduced in the previous section in a steady-state scenario.

The stagnation phenotype represents the background state and characterizes the inlet throughout most of the year, with limited input of NO_3^- and higher fluxes of NH_4^+ and HS^- coming from the sediments underlying the anoxic water. To mimic this situation, we thus chose lower input flux of NO_3^- in comparison to NH_4^+ and HS^- (**Figure 12** and **Table 3**). Kinetic parameters (k_m and V_{max}) for anammox bacteria were taken from the literature (Awata et al., 2013). Kinetic parameters measured for denitrification in SI were determined during the renewal phenotype (August 2015, 165 m) and therefore, the stagnation phenotype kinetic parameters remained unconstrained. Thus, kinetic parameters for the SUP05/Marinimicrobia consortium (or stagnation ecotype) were fit to yield rates of the same order of magnitude for denitrification as those measured in SI during stagnation (**Figures 12A–D**, **Table 3**, and **Supplementary Material**). However, cell-specific growth rates (V_{max}) and growth yield (Y) were estimated based on rates of denitrification and cell abundance (see above). With nutrient fluxes appropriate for the stagnation period and reasonable physiological parameters for the relevant organisms, we find that rates of both denitrification and anammox are similar, and fall within the range observed in SI outside of a renewal period (**Figures 3**, **12A–D**). The dominance of one

TABLE 3 | Parameters used in model for competition of NO_2^- between anammox and complete denitrification (see **Figure 12**).

Ecotype	Parameters	Value and units	Reference
'Stagnation'	R_{NO3}	5×10^{-9} moles L^{-1} d^{-1}	State of stagnation in SI
	R_{NO2}	5×10^{-9} moles L^{-1} d^{-1}	"
	R_{NH4}	5×10^{-8} moles L^{-1} d^{-1}	"
	R_{HS}	5×10^{-8} moles L^{-1} d^{-1}	"
	K_{m_AN} for NH_4^+	3 μM	Awata et al., 2013
	K_{m_AN} for NO_2^-	0.45 μM	Awata et al., 2013
	$K_{m\_DEN\&NO3R}$ for HS^-	10 μM	Jensen et al., 2009 and this paper
	$K_{m\_DEN\&NO3R}$ for NO_2^- or NO_3^-	1 and 5 μM	Fit the rates in SI
	V_{max} (AN, NO3R)	2×10^{-14} moles N_2 $cell^{-1}$ d^{-1}	Strous et al., 1999
	V_{max} (DEN)	2×10^{-15} moles N_2 $cell^{-1}$ d^{-1}	Fit the rates in SI
	Y_{AN}	5×10^{13} cell (moles ED)$^{-1}$	Louca et al., 2016
	Y_{NO3R}	5×10^{14} cell (moles ED)$^{-1}$	Fit the rates in SI
	Y_{DEN}	5×10^{15} cell (moles ED)$^{-1}$	"
'Renewal'	R_{NO3}	5×10^{-6} moles L^{-1} d^{-1}	After renewal in SI
	R_{NO2}	5×10^{-8} moles L^{-1} d^{-1}	"
	R_{NH4}	5×10^{-7} moles L^{-1} d^{-1}	"
	R_{HS}	5×10^{-8} moles L^{-1} d^{-1}	"
	K_{m_AN} for NH_4^+	3 μM	Awata et al., 2013
	K_{m_AN} for NO_2^-	0.45 μM	Awata et al., 2013
	$K_{m\_DEN\&NO3R}$ for HS^-	10 μM	Jensen et al., 2009 and this paper
	$K_{m\_DEN\&NO3R}$ for NO_2^- or NO_3^-	5 μM	This paper, August 2015 (165 m)
	V_{max} (AN, NO3R)	2×10^{-14} moles N_2 $cell^{-1}$ d^{-1}	Strous et al., 1999
	V_{max} (DEN)	2×10^{-13} moles N_2 $cell^{-1}$ d^{-1}	Fit the rates in SI
	Y_{AN}	5×10^{13} cell (moles ED)$^{-1}$	Louca et al., 2016
	Y_{NO3R}	5×10^{14} cell (moles ED)$^{-1}$	Fit the rates in SI
	Y_{DEN}	1.5 × 1015 cell (moles ED)$^{-1}$	"

pathway over another could be inverted by changing the relative K_m values for denitrification and anammox, as these appear to be similar to one another in the stagnation period (see **Supplementary Material**). Modeled abundances of anammox bacteria were similar to those observed in SI (2.3×10^7 anammox cells L^{-1}) as were the modeled abundances of complete denitrifiers compared to abundances observed in SI (cell abundance of Marinimicrobia/SUP05 = 10^9 cells L^{-1}). Therefore, we could reproduce with a simple flux balance model rates of the same order of magnitude for anammox and complete denitrification measured during the year 2015 during peak stratification in SI.

Deep water renewal in SI introduces oxygenated water to the deep basin, where NO_3^- is produced through rapid nitrification, and the NO_3^- produced is in turn lost through anaerobic NO_3^- reduction and N_2 production following renewal. The renewal event is thus far from steady-state, and we therefore tried to reproduce the high rates of denitrification in 60 days of the simulation, corresponding to the approximate duration of the event based on the geochemical profiles and rate measurements. The kinetic parameters for anammox were identical to simulations of the stagnation phenotype, however, we changed the kinetic parameters for denitrification to represent Arcobacter in the renewal phenotype. As NO_3^- dependency was measured in August 2015, corresponding to higher rates of N_2 production, we chose to use the Michaelis–Menten constants modeled from this data to describe complete denitrification (NO_3^- to N_2) (**Tables 2**, **3**). We also chose a higher biomass yield than in the 'stagnation' phenotype (**Table 3**), as it appears that the Arcobacter population grows rapidly from <1% to 30% of relative abundance within a month's time (**Table 3**). The simulation reveals that under the conditions described here (**Figures 12E–H** and **Table 3**), rates of denitrification reach 10^{-6} N_2 M d^{-1}, which corresponds to the highest rates measured in July 2015 at 200 m (**Figure 3**). Rates of anammox remain similar to the rates that can be found after renewal in SI (**Figures 3**, **12E–H**). The abundance of complete denitrifiers reaches 10^9 cells L^{-1} after only 15 days of simulation, which is again similar to abundances observed in SI during renewal. However, to fully describe and model the input fluxes to SI, the model would need to have dynamic fluxes that can be changed over time. In addition to dynamic fluxes, competition between two different populations of complete denitrifiers should be implemented to fully describe and reconstruct the transition from one phenotype to the other.

SI as a Model Ecosystem for Coastal OMZs

We have extrapolated the annual N-loss calculated for SI (33 km^2) to all similar coastal inlets in BC (2478 km^2) in order to estimate the potential importance of BC coastal fjords to N-loss from the North Eastern Sub-Arctic Pacific Ocean. We estimate that these inlets could contribute up to 0.12 Tg N yr^{-1}, which constitutes 0.1% to global pelagic N-loss (Codispoti, 2007) if they are all anoxic and similar to SI. On an area-specific basis this is extremely high in comparison to the ETSP, for example, which has a surface area of 1.2×10^6 km^2 and supports up to 10 Tg N yr^{-1} (Kalvelage et al., 2013). This highlights that coastal OMZs are hotspots for N-loss and could also, in the near future, be subject to changes due to increased anthropogenic influence.

The low oxygen conditions in SI support pelagic anaerobic microbial metabolisms including denitrification and anammox that co-occur and underpin high rates of N-loss from the water column. We showed that denitrification is the most important contributor to N_2 production and its rates and the organisms responsible vary seasonally. Rates of anammox, in contrast, are relatively constant throughout the year, contributing 37% of the N-loss from SI. Anammox is often reported as the primary pathway of N-loss from OMZs (Kuypers et al., 2005; Thamdrup et al., 2006; Hamersley et al., 2007; Lam et al., 2009; Canfield et al., 2010b; Jensen et al., 2011; Kalvelage et al., 2013; De Brabandere et al., 2014), and our time-series observations from SI may be more broadly extensible to low oxygen marine waters globally. In SI, rates and pathways of N-loss and the responsible microbial taxa are dynamic responding to substrate fluxes driven by physical forcing. Analogous dynamics in upwelling and horizontal transport or large-scale eddies in open ocean OMZs may also lead to strong microbial responses with corresponding biogeochemical outcomes (Altabet et al., 2012; Bourbonnais et al., 2015). While sulphidic conditions that characterize SI are rare in modern open ocean OMZs, they could become more prevalent with progressive ocean deoxygenation (Ulloa et al., 2012; Callbeck et al., 2018). Information on microbial responses to system dynamics and on the ecophysiology the underpins coupled C, N, and S cycling in Saanich Inlet and other experimentally tractable coastal ecosystems is key for predicting broader global responses to ocean deoxygenation and the expansion of marine anoxia.

DATA AVAILABILITY

The datasets generated for this study can be found in the JGI – database (https://genome.jgi.doe.gov/portal/), Project ID: 1175277.

AUTHOR CONTRIBUTIONS

CM and SC designed the experiments, analyzed the data, and wrote the manuscript. CM performed the experiments. SH provided help in the design of the experiments and provided editorial support. JS, JH, and RS participated in the analysis of part of the data. DV and KG provided data regarding the chlorophyll *a* concentration.

FUNDING

This work was supported by the Natural Sciences and Engineering Research Council (NSERC) discovery grant 04867. Sequencing was performed at the DOE Joint Genome Institute under the CSP Program. The sequencing work was conducted in part by the United States Department of Energy Joint Genome Institute.

ACKNOWLEDGMENTS

We would like to thank all the people involved in the sampling and processing of samples for Saanich Inlet during the year 2015: the crew of the MSV Strickland, Chris Payne and Lora Pakhomova, Andreas Mueller, Melanie Scoffield, Jade Shiller, Diane Fairley, Sam Kheirandish, Alyse Hawley, Monica Torres-Beltran, Kohen Bauer, Kate Thompson, Andrew Hefford, Annie Cheng, Belle Cheng, and all of those who made the sampling easier by helping out before and after Saanich days.

SUPPLEMENTARY MATERIAL

The Supplementary Material for this article can be found online at: https://www.frontiersin.org/articles/10.3389/fmars.2019.00027/full#supplementary-material

REFERENCES

Altabet, M. A., Ryabenko, E., Stramma, L., Wallace, D. W. R., Frank, M., Grasse, P., et al. (2012). An eddy-stimulated hotspot for fixed nitrogen-loss from the Peru oxygen minimum zone. *Biogeosciences* 9, 4897–4908. doi: 110.5194/bg-9-4897-2012

Anantharaman, K., Breier, J. A., Sheik, C. S., and Dick, G. J. (2013). Evidence for hydrogen oxidation and metabolic plasticity in widespread deep-sea sulfur-oxidizing bacteria. *Proc. Natl. Acad. Sci. U.S.A.* 110, 330–335. doi: 10.1073/pnas.1215340110

Anderson, J. J., and Devol, A. H. (1973). Deep water renewal in Saanich Inlet, an intermittently anoxic basin. *Estuar. Coast. Mar. Sci.* 1, 1–10. doi: 10.1016/0302-3524(73)90052-2

Awata, T., Oshiki, M., Kindaichi, T., Ozaki, N., Ohashi, A., and Okabe, S. (2013). Physiological characterization of an anaerobic ammonium-oxidizing bacterium belonging to the "*Candidatus* Scalindua" group. *Appl. Environ. Microbiol.* 79, 4145–4148. doi: 10.1128/Aem.00056-13

Babbin, A. R., Keil, R. G., Devol, A. H., and Ward, B. B. (2014). Organic matter stoichiometry, flux, and oxygen control nitrogen loss in the ocean. *Science* 344, 406–408. doi: 10.1126/science.1248364

Bergauer, K., Fernandez-Guerra, A., Garcia, J. A. L., Sprenger, R. R., Stepanauskas, R., Pachiadaki, M. G., et al. (2018). Organic matter processing by microbial communities throughout the Atlantic water column as revealed by metaproteomics. *Proc. Natl. Acad. Sci. U.S.A.* 115, E400–E408. doi: 10.1073/pnas.1708779115

Bonaglia, S., Klawonn, I., De Brabandere, L., Deutsch, B., Thamdrup, B., and Bruchert, V. (2016). Denitrification and DNRA at the Baltic Sea oxic-anoxic interface: substrate spectrum and kinetics. *Limnol. Oceanogr.* 61, 1900–1915. doi: 10.1002/lno.10343

Bourbonnais, A., Altabet, M. A., Charoenpong, C. N., Larkum, J., Hu, H., Bange, H. W., et al. (2015). N-loss isotope effects in the Peru oxygen minimum zone studied using a mesoscale eddy as a natural tracer experiment. *Glob. Biogeochem. Cycles* 29, 793–811. doi: 10.1002/2014GB005001

Bourbonnais, A., Lehmann, M. F., Hamme, R. C., Manning, C. C., and Juniper, S. K. (2013). Nitrate elimination and regeneration as evidenced by dissolved inorganic nitrogen isotopes in Saanich Inlet, a seasonally anoxic fjord. *Mar. Chem.* 157, 194–207. doi: 10.1016/j.marchem.2013.09.006

Braman, R. S., and Hendrix, S. A. (1989). Nanogram nitrite and nitrate determination in environmental and biological materials by vanadium(III) reduction with chemiluminescence detection. *Anal. Chem.* 61, 2715–2718. doi: 10.1021/ac00199a007

Breitburg, D., Levin, L. A., Oschlies, A., Grégoire, M., Chavez, F. P., Conley, D. J., et al. (2018). Declining oxygen in the global ocean and coastal waters. *Science* 359:eaam7240. doi: 10.1126/science.aam7240

Bulow, S. E., Rich, J. J., Naik, H. S., Pratihary, A. K., and Ward, B. B. (2010). Denitrification exceeds anammox as a nitrogen loss pathway in the Arabian Sea oxygen minimum zone. *Deep Sea Res. Part I Oceanogr. Res. Pap.* 57, 384–393. doi: 10.1016/j.dsr.2009.10.014

Callbeck, C. M., Lavik, G., Ferdelman, T. G., Fuchs, B., Gruber-Vodicka, H. R., Hach, P. F., et al. (2018). Oxygen minimum zone cryptic sulfur cycling sustained by offshore transport of key sulfur oxidizing bacteria. *Nat. Commun.* 9:1729. doi: 10.1038/s41467-018-04041-x

Canfield, D. E., Glazer, A. N., and Falkowski, P. G. (2010a). The evolution and future of Earth's nitrogen cycle. *Science* 330, 192–196. doi: 10.1126/science.1186120

Canfield, D. E., Stewart, F. J., Thamdrup, B., De Brabandere, L., Dalsgaard, T., Delong, E. F., et al. (2010b). A cryptic sulfur cycle in oxygen-minimum-zone waters off the Chilean coast. *Science* 330, 1375–1378. doi: 10.1126/science.1196889

Canion, A., Prakash, O., Green, S. J., Jahnke, L., Kuypers, M. M. M., and Kostka, J. E. (2013). Isolation and physiological characterization of psychrophilic denitrifying bacteria from permanently cold Arctic fjord sediments (Svalbard, Norway). *Environ. Microbiol.* 15, 1606–1618. doi: 10.1111/1462-2920.12110

Capone, D. G. (2001). Marine nitrogen fixation: what's the fuss? *Curr. Opin. Microbiol.* 4, 341–348. doi: 10.1016/S1369-5274(00)00215-0

Caporaso, J. G., Kuczynski, J., Stombaugh, J., Bittinger, K., Bushman, F. D., Costello, E. K., et al. (2010). QIIME allows analysis of high-throughput community sequencing data. *Nat. Methods* 7, 335–336. doi: 10.1038/nmeth.f.303

Christensen, S., and Tiedje, J. M. (1988). Sub-parts-per-billion nitrate method: use of an N(2)O-producing denitrifier to convert NO(3) or NO(3) to N(2)O. *Appl. Environ. Microbiol.* 54, 1409–1413.

Codispoti, L. A. (2007). An oceanic fixed nitrogen sink exceeding 400 Tg Na-1 vs the concept of homeostasis in the fixed-nitrogen inventory. *Biogeosciences* 4, 233–253.

Codispoti, L. A., Brandes, J. A., Christensen, J. P., Devol, A. H., Naqvi, S. W. A., Paerl, H. W., et al. (2001). The oceanic fixed nitrogen and nitrous oxide budgets: moving targets as we enter the anthropocene? *Sci. Mar.* 65, 85–105.

Dalsgaard, T., Canfield, D. E., Petersen, J., Thamdrup, B., and Acuna-Gonzalez, J. (2003). N2 production by the anammox reaction in the anoxic water column of Golfo Dulce, Costa Rica. *Nature* 422, 606–608. doi: 10.1038/nature01526

Dalsgaard, T., and Thamdrup, B. (2002). Factors controlling anaerobic ammonium oxidation with nitrite in marine sediments. *Appl. Environ. Microbiol.* 68, 3802–3808.

Dalsgaard, T., Thamdrup, B., Farias, L., and Revsbech, N. P. (2012). Anammox and denitrification in the oxygen minimum zone of the eastern South Pacific. *Limnol. Oceanogr.* 57, 1331–1346. doi: 10.4319/lo.2012.57.5.1331

De Brabandere, L., Canfield, D. E., Dalsgaard, T., Friederich, G. E., Revsbech, N. P., Ulloa, O., et al. (2014). Vertical partitioning of nitrogen-loss processes across the oxic-anoxic interface of an oceanic oxygen minimum zone. *Environ. Microbiol.* 16, 3041–3054. doi: 10.1111/1462-2920.12255

De Brabandere, L., Thamdrup, B., Revsbech, N. P., and Foadi, R. (2012). A critical assessment of the occurrence and extend of oxygen contamination during anaerobic incubations utilizing commercially available vials. *J. Microbiol. Methods* 88, 147–154. doi: 10.1016/j.mimet.2011.11.001

Devol, A. H. (2003). Nitrogen cycle: solution to a marine mystery. *Nature* 422, 575–576.

Devol, A. H., Anderson, J. J., Kuivila, K., and Murray, J. W. (1984). A model for coupled sulfate reduction and methane oxidation in the sediments of Saanich inlet. *Geochim. Cosmochim. Acta* 48, 993–1004. doi: 10.1016/0016-7037(84)90191-1

Edgar, R. C., Haas, B. J., Clemente, J. C., Quince, C., and Knight, R. (2011). UCHIME improves sensitivity and speed of chimera detection. *Bioinformatics* 27, 2194–2200. doi: 10.1093/bioinformatics/btr381

Engstrom, P., Dalsgaard, T., Hulth, S., and Aller, R. C. (2005). Anaerobic ammonium oxidation by nitrite (anammox): implications for N-2 production in coastal marine sediments. *Geochim. Cosmochim. Acta* 69, 2057–2065. doi: 10.1016/j.gca.2004.09.032

Falkowski, P. G. (1997). Evolution of the nitrogen cycle and its influence on the biological sequestration of CO2 in the ocean. *Nature* 387, 272–275. doi: 10.1038/387272a0

Falkowski, P. G., Fenchel, T., and Delong, E. F. (2008). The microbial engines that drive Earth's biogeochemical cycles. *Science* 320, 1034–1039. doi: 10.1126/science.1153213

Fowler, D., Coyle, M., Skiba, U., Sutton, M. A., Cape, J. N., Reis, S., et al. (2013). The global nitrogen cycle in the twenty-first century. *Philos. Trans. R. Soc. B Biol. Sci.* 368:20130165.

Ganesh, S., Parris, D. J., DeLong, E. F., and Stewart, F. J. (2014). Metagenomic analysis of size-fractionated picoplankton in a marine oxygen minimum zone. *ISME J.* 8, 187–211. doi: 10.1038/ismej.2013.144

Glaubitz, S., Kießlich, K., Meeske, C., Labrenz, M., and Jürgens, K. (2013). SUP05 dominates the gammaproteobacterial sulfur oxidizer assemblages in pelagic redoxclines of the central baltic and black seas. *Appl. Environ. Microbiol.* 79, 2767–2776. doi: 10.1128/aem.03777-12

Grasshoff, K., Ehrhardt, M., Kremling, K., and Anderson, L. G. (1999). *Methods of Seawater Analysis*. New York, NY: Wiley-VCH.

Gruber, N. (2004). "The dynamics of the marine nitrogen cycle and its influence on atmospheric CO_2 variations," in *The Ocean Carbon Cycle and Climate*, eds M. Follows and T. Oguz (Dordrecht: Kluwer Academic), 97–148.

Grundle, D. S., Timothy, D. A., and Varela, D. E. (2009). Variations of phytoplankton productivity and biomass over an annual cycle in Saanich Inlet, a British Columbia fjord. *Cont. Shelf Res.* 29, 2257–2269. doi: 10.1016/j.csr.2009.08.013

Hamersley, M. R., Lavik, G., Woebken, D., Rattray, J. E., Lam, P., Hopmans, E. C., et al. (2007). Anaerobic ammonium oxidation in the Peruvian oxygen minimum zone. *Limnol. Oceanogr.* 52, 923–933. doi: 10.4319/lo.2007.52.3.0923

Hawley, A. K., Brewer, H. M., Norbeck, A. D., Pasa-Tolic, L., and Hallam, S. J. (2014). Metaproteomics reveals differential modes of metabolic coupling among ubiquitous oxygen minimum zone microbes. *Proc. Natl. Acad. Sci. U.S.A.* 111, 11395–11400. doi: 10.1073/pnas.1322132111

Hawley, A. K., Nobu, M. K., Wright, J. J., Durno, W. E., Morgan-Lang, C., Sage, B., et al. (2017a). Diverse Marinimicrobia bacteria may mediate coupled biogeochemical cycles along eco-thermodynamic gradients. *Nat. Commun.* 8:1507. doi: 10.1038/s41467-017-01376-9

Hawley, A. K., Torres-Beltrán, M., Zaikova, E., Walsh, D. A., Mueller, A., Scofield, M., et al. (2017b). A compendium of multi-omic sequence information from the Saanich Inlet water column. *Sci. Data* 4:170160. doi: 10.1038/sdata.2017.160

İnceoğlu, Ö., Llirós, M., García-Armisen, T., Crowe, S. A., Michiels, C., Darchambeau, F., et al. (2015). Distribution of bacteria and Archaea in meromictic tropical lake Kivu (Africa). *Aquat. Microb. Ecol.* 74, 215–233.

Jensen, M. M., Kuypers, M. M. M., Gaute, L., and Thamdrup, B. (2008). Rates and regulation of anaerobic ammonium oxidation and denitrification in the Black Sea. *Limnol. Oceanogr.* 53, 23–36. doi: 10.4319/lo.2008.53.1.0023

Jensen, M. M., Lam, P., Revsbech, N. P., Nagel, B., Gaye, B., Jetten, M. S. M., et al. (2011). Intensive nitrogen loss over the Omani Shelf due to anammox coupled with dissimilatory nitrite reduction to ammonium. *ISME J.* 5, 1660–1670. doi: 10.1038/ismej.2011.44

Jensen, M. M., Petersen, J., Dalsgaard, T., and Thamdrup, B. (2009). Pathways, rates, and regulation of N-2 production in the chemocline of an anoxic basin, Mariager Fjord, Denmark. *Mar. Chem.* 113, 102–113. doi: 10.1016/j.marchem.2009.01.002

Kalvelage, T., Lavik, G., Lam, P., Contreras, S., Arteaga, L., Loscher, C. R., et al. (2013). Nitrogen cycling driven by organic matter export in the South Pacific oxygen minimum zone. *Nat. Geosci.* 6, 228–234. doi: 10.1038/Ngeo1739

Keeling, R. F., Kortzinger, A., and Gruber, N. (2010). Ocean deoxygenation in a warming world. *Annu. Rev. Mar. Sci.* 2, 199–229. doi: 10.1146/annurev.marine.010908.163855

Knap, A. H., Michaels, A., Close, A. R., Ducklow, H., and Dickson, A. G. (1996). *Protocols for the Joint Global Ocean Flux Study (JGOFS) Core Measurements*. Paris: UNESCO.

Koeve, W., and Kähler, P. (2010). Heterotrophic denitrification vs. autotrophic anammox – quantifying collateral effects on the oceanic carbon cycle. *Biogeosciences* 7, 2327–2337. doi: 10.5194/bg-7-2327-2010

Kopylova, E., Navas-Molina, J. A., Mercier, C., Xu, Z. Z., Mahe, F., He, Y., et al. (2016). Open-source sequence clustering methods improve the state of the art. *mSystems* 1:e00003-15. doi: 10.1128/mSystems.00003-15

Kuypers, M. M. M., Lavik, G., Woebken, D., Schmid, M., Fuchs, B. M., Amann, R., et al. (2005). Massive nitrogen loss from the Benguela upwelling system through anaerobic ammonium oxidation. *Proc. Natl. Acad. Sci. U.S.A.* 102, 6478–6483. doi: 10.1073/pnas.0502088102

Lam, P., Lavik, G., Jensen, M. M., van de Vossenberg, J., Schmid, M., Woebken, D., et al. (2009). Revising the nitrogen cycle in the Peruvian oxygen minimum zone. *Proc. Natl. Acad. Sci. U.S.A.* 106, 4752–4757. doi: 10.1073/Pnas.0812444106

Louca, S., Hawley, A. K., Katsev, S., Torres-Beltran, M., Bhatia, M. P., Kheirandish, S., et al. (2016). Integrating biogeochemistry with multiomic sequence information in a model oxygen minimum zone. *Proc. Natl. Acad. Sci. U.S.A.* 113, E5925–E5933. doi: 10.1073/pnas.1602897113

Manning, C. C., Hamme, R. C., and Bourbonnais, A. (2010). Impact of deep-water renewal events on fixed nitrogen loss from seasonally-anoxic Saanich Inlet. *Mar. Chem.* 122, 1–10. doi: 10.1016/j.marchem.2010.08.002

Michiels, C. C., Darchambeau, F., Roland, F. A. E., Morana, C., Lliros, M., Garcia-Armisen, T., et al. (2017). Iron-dependent nitrogen cycling in a ferruginous lake and the nutrient status of Proterozoic oceans. *Nat. Geosci.* 10, 217–221. doi: 10.1038/Ngeo2886

Mucci, A., Sundby, B., Gehlen, M., Arakaki, T., Zhong, S., and Silverberg, N. (2000). The fate of carbon in continental shelf sediments of eastern Canada: a case study. *Deep Sea Res. Part II Top. Stud. Oceanogr.* 47, 733–760. doi: 10.1016/S0967-0645(99)00124-1

Murray, R. E., Parsons, L. L., and Smith, M. S. (1989). Kinetics of nitrate utilization by mixed populations of denitrifying bacteria. *Appl. Environ. Microbiol.* 55, 717–721.

Nicholls, J. C., and Trimmer, M. (2009). Widespread occurrence of the anammox reaction in estuarine sediments. *Aquat. Microb. Ecol.* 55, 105–113. doi: 10.3354/ame01285

Parsonage, D., Greenfield, A. J., and Ferguson, S. J. (1985). The high affinity of *Paracoccus denitrificans* cells for nitrate as an electron acceptor. Analysis of possible mechanisms of nitrate and nitrite movement across the plasma membrane and the basis for inhibition by added nitrite of oxidase activity in permeabilised cells. *Biochim. Biophys. Acta* 807, 81–95. doi: 10.1016/0005-2728(85)90055-6

Parsons, T. R., Maita, Y., and Lalli, C. M. (eds). (1984). "4.3 - fluorometric determination of chlorophylls," in *A Manual of Chemical & Biological Methods for Seawater Analysis*, (Amsterdam: Pergamon), 107–109.

Paulmier, A., and Ruiz-Pino, D. (2009). Oxygen minimum zones (OMZs) in the modern ocean. *Prog. Oceanogr.* 80, 113–128. doi: 10.1016/j.pocean.2008.08.001

Prokopenko, M. G., Hirst, M. B., De Brabandere, L., Lawrence, D. J., Berelson, W. M., Granger, J., et al. (2013). Nitrogen losses in anoxic marine sediments driven by *Thioploca*-anammox bacterial consortia. *Nature* 500, 194–198. doi: 10.1038/nature12365

Quast, C., Pruesse, E., Yilmaz, P., Gerken, J., Schweer, T., Yarza, P., et al. (2013). The SILVA ribosomal RNA gene database project: improved data processing and web-based tools. *Nucleic Acids Res.* 41, D590–D596. doi: 10.1093/nar/gks1219

Rich, J. J., Dale, O. R., Song, B., and Ward, B. B. (2008). Anaerobic ammonium oxidation (anammox) in Chesapeake Bay sediments. *Microb. Ecol.* 55, 311–320. doi: 10.1007/s00248-007-9277-3

Richards, F. A. (1965). *Anoxic Basins and Fjords*. Cambridge, MA: Academic press.

Roberts, K. L., Kessler, A. J., Grace, M. R., and Cook, P. L. M. (2014). Increased rates of dissimilatory nitrate reduction to ammonium (DNRA) under oxic conditions in a periodically hypoxic estuary. *Geochim. Cosmochim. Acta* 133, 313–324.

Robertson, E. K., Roberts, K. L., Burdorf, L. D. W., Cook, P., and Thamdrup, B. (2016). Dissimilatory nitrate reduction to ammonium coupled to Fe(II) oxidation in sediments of a periodically hypoxic estuary. *Limnol. Oceanogr.* 61, 365–381. doi: 10.1002/lno.10220

Robertson, E. K., and Thamdrup, B. (2017). The fate of nitrogen is linked to iron(II) availability in a freshwater lake sediment. *Geochim. Cosmochim. Acta* 205, 84–99. doi: 10.1016/j.gca.2017.02.014

Sancetta, C., and Calvert, S. E. (1988). The annual cycle of sedimentation in Saanich inlet, British-Columbia - implications for the interpretation of diatom fossil

assemblages. *Deep Sea Res. Part A Oceanogr. Res. Pap.* 35, 71–90. doi: 10.1016/0198-0149(88)90058-1

Schmidtko, S., Stramma, L., and Visbeck, M. (2017). Decline in global oceanic oxygen content during the past five decades. *Nature* 542, 335–339. doi: 10.1038/nature21399

Shah, V., Chang, B. X., and Morris, R. M. (2017). Cultivation of a chemoautotroph from the SUP05 clade of marine bacteria that produces nitrite and consumes ammonium. *ISME J.* 11, 263–271. doi: 10.1038/ismej.2016.87

Stevens, H., and Ulloa, O. (2008). Bacterial diversity in the oxygen minimum zone of the eastern tropical South Pacific. *Environ. Microbiol.* 10, 1244–1259. doi: 10.1111/j.1462-2920.2007.01539.x

Strous, M., Fuerst, J. A., Kramer, E. H. M., Logemann, S., Muyzer, G., van de Pas-Schoonen, K. T., et al. (1999). Missing lithotroph identified as new planctomycete. *Nature* 400, 446–449.

Takahashi, M., Seibert, D. L., and Thomas, W. H. (1977). Occasional blooms of phytoplankton during summer in Saanich Inlet, Bc, Canada. *Deep Sea Res.* 24, 775–780. doi: 10.1016/0146-6291(77)90499-4

Thamdrup, B., and Dalsgaard, T. (2000). The fate of ammonium in anoxic manganese oxide-rich marine sediment. *Geochim. Cosmochim. Acta* 64, 4157–4164. doi: 10.1016/S0016-7037(00)00496-8

Thamdrup, B., and Dalsgaard, T. (2002). Production of N(2) through anaerobic ammonium oxidation coupled to nitrate reduction in marine sediments. *Appl. Environ. Microbiol.* 68, 1312–1318.

Thamdrup, B., Dalsgaard, T., Jensen, M. M., Ulloa, O., Farías, L., and Escribano, R. (2006). Anaerobic ammonium oxidation in the oxygen-deficient waters off northern Chile. *Limnol. Oceanogr.* 51, 2145–2156. doi: 10.4319/lo.2006.51.5.2145

Torres-Beltrán, M., Hawley, A. K., Capelle, D., Zaikova, E., Walsh, D. A., Mueller, A., et al. (2017). A compendium of geochemical information from the Saanich Inlet water column. *Sci. Data* 4:170159. doi: 10.1038/sdata.2017.159

Trimmer, M., and Nicholls, J. C. (2009). Production of nitrogen gas via anammox and denitrification in intact sediment cores along a continental shelf to slope transect in the North Atlantic. *Limnol. Oceanogr.* 54, 577–589. doi: 10.4319/Lo.2009.54.2.0577

Ulloa, O., Canfield, D. E., DeLong, E. F., Letelier, R. M., and Stewart, F. J. (2012). Microbial oceanography of anoxic oxygen minimum zones. *Proc. Natl. Acad. Sci. U.S.A.* 109, 15996–16003. doi: 10.1073/pnas.1205009109

Van Mooy, B. A. S., Keil, R. G., and Devol, A. H. (2002). Impact of suboxia on sinking particulate organic carbon: enhanced carbon flux and preferential degradation of amino acids via denitrification. *Geochim. Cosmochim. Acta* 66, 457–465. doi: 10.1016/S0016-7037(01)00787-6

Voss, M., Bange, H. W., Dippner, J. W., Middelburg, J. J., Montoya, J. P., and Ward, B. (2013). The marine nitrogen cycle: recent discoveries, uncertainties and the potential relevance of climate change. *Philos. Trans. R. Soc. Lond. B Biol. Sci.* 368:20130121. doi: 10.1098/rstb.2013.0121

Walsh, D. A., Zaikova, E., Howes, C. G., Song, Y. C., Wright, J. J., Tringe, S. G., et al. (2009). Metagenome of a versatile chemolithoautotroph from expanding oceanic dead zones. *Science* 326, 578–582. doi: 10.1126/science.1175309

Walters, W., Hyde, E. R., Berg-Lyons, D., Ackermann, G., Humphrey, G., Parada, A., et al. (2016). Improved bacterial 16S rRNA gene (V4 and V4-5) and fungal internal transcribed spacer marker gene primers for microbial community surveys. *mSystems* 1:e00009-15. doi: 10.1128/mSystems.00009-15

Ward, B. B., Devol, A. H., Rich, J. J., Chang, B. X., Bulow, S. E., Naik, H., et al. (2009). Denitrification as the dominant nitrogen loss process in the Arabian Sea. *Nature* 461, 78–81. doi: 10.1038/nature08276

Wenk, C. B., Blees, J., Zopfi, J., Veronesi, M., Bourbonnais, A., Schubert, C. J., et al. (2013). Anaerobic ammonium oxidation (anammox) bacteria and sulfide-dependent denitrifiers coexist in the water column of a meromictic south-alpine lake. *Limnol. Oceanogr.* 58, 1–12. doi: 10.4319/lo.2013.58.1.0001

Wirsen, C. O., Sievert, S. M., Cavanaugh, C. M., Molyneaux, S. J., Ahmad, A., Taylor, L. T., et al. (2002). Characterization of an autotrophic sulfide-oxidizing marine *Arcobacter* sp. That produces filamentous sulfur. *Appl. Environ. Microbiol.* 68, 316–325. doi: 10.1128/aem.68.1.316-325.2002

Wright, J., Lee, S., Zaikova, E., Walsh, D. A., and Hallam, S. (2009). DNA extraction from 0.22 μM sterivex filters and cesium chloride density gradient centrifugation. *J. Vis. Exp.* 31:1352.

Wright, J. J., Konwar, K. M., and Hallam, S. J. (2012). Microbial ecology of expanding oxygen minimum zones. *Nat. Rev. Microbiol.* 10, 381–394. doi: 10.1038/nrmicro2778

Zaikova, E., Walsh, D. F., Stilwell, C. P., Mohn, W. W., Tortell, P. D., and Hallam, S. J. (2010). Microbial community dynamics in a seasonally anoxic fjord: Saanich Inlet, British Columbia. *Environ. Microbiol.* 12, 172–191. doi: 10.1111/j.1462-2920.2009.02058.x

Conflict of Interest Statement: The authors declare that the research was conducted in the absence of any commercial or financial relationships that could be construed as a potential conflict of interest.

frontiers in Marine Science

REVIEW
published: 22 March 2019
doi: 10.3389/fmars.2019.00139

Interactive Effects of Hypoxia and Temperature on Coastal Pelagic Zooplankton and Fish

Michael R. Roman[1], Stephen B. Brandt[2], Edward D. Houde[3] and James J. Pierson[1]*

[1] Horn Point Laboratory, University of Maryland Center for Environmental Science, Cambridge, MD, United States, [2] Department of Fisheries and Wildlife, Oregon State University, Corvallis, OR, United States, [3] Chesapeake Biological Laboratory, University of Maryland Center for Environmental Science, Solomons, MD, United States

Hypoxia, triggered in large part by eutrophication, exerts widespread and expanding stress on coastal ecosystems. Hypoxia is often specifically defined as water having dissolved oxygen (DO) concentrations < 2 mg L^{-1}. However, DO concentration alone is insufficient to categorize hypoxic stress or predict impacts of hypoxia on zooplankton and fish. Hypoxic stress depends on the oxygen supply relative to metabolic demand. Water temperature controls both oxygen solubility and the metabolic demand of aquatic ectotherms. Accordingly, to assess impacts of hypoxia requires consideration of effects of temperature on both oxygen availability and animal metabolism. Temperature differences across ecosystems or across seasons or years within an ecosystem can dramatically impact the severity of hypoxia even at similar DO concentrations. Living under sub-optimum DO can reduce temperature-dependent metabolic efficiencies, prey capture efficiency, growth and reproductive potential, thus impacting production and individual zooplankton and fish fitness. Avoidance of hypoxic bottom water can reduce or eliminate low-temperature thermal refuges for organisms and increase energy demands and respiration rates, and potentially reduce overall fitness if alternative habitats are sub-optimal. Moreover, differential habitat shifts among species can shift predator-prey abundance ratios or interactions and thus modify food webs. For example, more tolerant zooplankton prey may use hypoxic waters as a refuge from fish predation. In contrast, zooplankton avoidance of hypoxic bottom waters can result in prey aggregations at oxyclines sought out by fish predators. Hypoxic conditions that affect spatial ecology can drive taxonomic and size shifts in the zooplankton community, affecting foraging, consumption and growth of fish. Advances in understanding the ecological effects of low DO waters on pelagic zooplankton and fish and comparisons among ecosystems will require development of generic models that estimate the oxygen demand of organisms in relation to oxygen supply which depends on both DO and temperature. We provide preliminary analysis of a metric (Oxygen Stress Level) which integrates oxygen demand in relation to oxygen availability for a coastal copepod and compare the prediction of oxygen stress to actual copepod distributions in areas with hypoxic bottom waters.

Keywords: deoxygenation, climate change, food-webs, stressor, metabolism

OPEN ACCESS

Edited by:
Arthur Capet,
MAST – University of Liège, Belgium

Reviewed by:
John Patrick Dunne,
Geophysical Fluid Dynamics Laboratory (GFDL), United States
Andrew Altieri,
University of Florida, United States
José Lino Vieira De Oliveira Costa,
Universidade de Lisboa, Portugal

****Correspondence:***
Michael R. Roman
roman@umces.edu

Specialty section:
This article was submitted to Coastal Ocean Processes, a section of the journal Frontiers in Marine Science

Received: *03 June 2018*
Accepted: *05 March 2019*
Published: *22 March 2019*

Citation:
Roman MR, Brandt SB, Houde ED and Pierson JJ (2019) Interactive Effects of Hypoxia and Temperature on Coastal Pelagic Zooplankton and Fish. Front. Mar. Sci. 6:139. doi: 10.3389/fmars.2019.00139

INTRODUCTION

Dissolved oxygen (DO) has been declining in coastal waters since the middle of the 20th century (Diaz and Rosenberg, 2008; Vaquer-Sunyer and Duarte, 2008; Rabalais et al., 2009; Breitburg et al., 2018). Hypoxia occurs naturally in many marine and freshwater systems that are characterized by high productivity and stratification (Rabalais et al., 2010). However, human activities such as intensive agriculture practices, land use changes, and point-source nutrient loading have caused the frequency, magnitude and extent of coastal hypoxia to increase (Turner et al., 2008; Bianchi et al., 2010).

Seasonal deoxygenation of sub-pycnocline coastal waters is driven primarily by nutrient stimulation of largely ungrazed phytoplankton blooms that decay below a stratified water column. These blooms sink or are eaten and processed by zooplankton, and are subsequently decomposed by microbial activity, consuming much of the available DO in the lower water column isolated from aeration (Malone, 1991; Nixon, 1995; Howarth et al., 1996; Diaz and Rosenberg, 2008). Since 1950, more than 500 sites in coastal waters have reported DO $\leq$ 2 mg l^{-1}, with fewer than 10 percent of these systems reporting such low DO values prior to 1950 (Diaz and Rosenberg, 2008; Vaquer-Sunyer and Duarte, 2008; Isensee et al., 2015). While more observations have likely contributed to this increase in reporting, a greater diversity of coastal hypoxic sites suggests that increased eutrophication is primarily responsible for expanding coastal hypoxia (Vaquer-Sunyer and Duarte, 2008). Coastal zooplankton and fish do not appear to have developed specific physiological adaptations to low DO in these new coastal systems experiencing seasonal hypoxia (Childress and Seibel, 1998; Dam, 2013; McBryan et al., 2013). Instead, these organisms suffer direct mortality, or reside in the low DO waters and tolerate some deleterious effects, or avoid low DO bottom waters through behavioral avoidance. Global warming can increase coastal hypoxia by increasing water column density stratification, decreasing oxygen solubility, and increasing the oxygen demand of ectotherms (Altieri and Gedan, 2014).

Hypoxia is often specifically defined as water having DO concentrations < 2 mg L^{-1} (at 18°C in seawater = 1.5 ml L^{-1} = 5.6 kPa oxygen partial pressure), although more biologically relevant definitions are required to define its impacts (Davis, 1975; Vaquer-Sunyer and Duarte, 2008; Breitburg et al., 2009; Ekau et al., 2010; Verberk et al., 2011; Elliott et al., 2013). Physiologists usually express DO in terms of partial pressure because oxygen availability to aquatic organisms is dependent on the rate of diffusion across integuments or gills and is controlled by the partial pressure of O_2 (mm Hg or kPa). In contrast, aquatic ecologists and oceanographers usually express DO in terms of concentration (mg L^{-1} or ml L^{-1}).

Temperature directly influences oxygen solubility in seawater and thus DO concentration and oxygen partial pressure as well as the metabolic demand of aquatic ectotherms, yet is often overlooked as a controlling factor in hypoxic assessments. A meta-analysis by Vaquer-Sunyer and Duarte (2011) suggests that the survival time of benthic macrofauna in low DO is reduced with increasing temperature and that the DO concentration which results in mortality increases. Thus, in order to effectively assess the impacts of hypoxic stress, it is necessary to consider the effects of temperature on both oxygen availability and animal metabolism. We contend that temperature is an essential component defining hypoxic conditions. Temperature differences across ecosystems or across seasons or years within an ecosystem can dramatically impact the severity of hypoxia even at similar DO concentrations.

Although hypoxic events have been shown to cause mortality of more sedentary benthic species and crabs (Grantham et al., 2004), less is known about the impact of hypoxia on pelagic species, which is the focus of this paper. Pelagic species have behavioral capabilities to generally avoid hypoxic water and must either move out of the way or suffer the consequences of reduced oxygen (Ekau et al., 2010). The physiological and ecological consequences of moving to non-hypoxic, perhaps adjacent habitats are important to understand broader impacts of hypoxia at the species and ecosystem level. Physiological consequences include changes in energy demand, respiration rates and overall fitness if adjacent habitats have different temperatures. Ecological consequences include shifts in densities and spatial overlaps of predators and prey that modify food webs.

EFFECTS OF LOW DISSOLVED OXYGEN ON ZOOPLANKTON AND FISH METABOLISM AND VITAL RATES

Research on ecological effects of hypoxia in coastal systems typically has considered DO in terms of the concentration of oxygen in water (ml L^{-1} or mg L^{-1}). However, it is also essential to consider the partial pressure and diffusivity of oxygen in water because these properties determine the rate of oxygen supply and, ultimately, the rate of oxygen uptake by organisms (Verberk et al., 2011). The solubility of oxygen in water (i.e., concentration at atmospheric equilibrium) declines at both higher temperatures and higher salinities. Considering potential biological and ecological effects of hypoxia on coastal zooplankton and fish, reduced rates of oxygen uptake are ultimately responsible for direct adverse effects such as reduced growth and increased mortality. Under low oxygen conditions (with oxygen supply low relative to oxygen demand), aerobic respiration may not be fully supported by the consequent lower oxygen uptake rates, and respiration becomes oxygen limited (Gnaiger, 1991; Childress and Seibel, 1998; McAllen et al., 1999; Pörtner and Knust, 2007; Seibel, 2011; Elliott et al., 2013). As a result, zooplankton and fish residing in hypoxic water must either implement specific adaptations to maintain the rate of oxygen uptake, make up the energy deficit through anaerobic respiration, or reduce their energy demand and oxygen requirements by lowering metabolic rate such as through reduced activity (Gnaiger, 1991; Childress and Seibel, 1998; McAllen et al., 1999; Perry, 2011; Seibel, 2011; Friedman et al., 2012; Elliott et al., 2013). In aquatic ectotherms, temperature controls respiration and metabolic rates and thus the ambient temperature of low oxygen water will affect the specific response rates of an organism.

Two useful metrics to assess the effects of low DO on zooplankton and fish are the critical (P_{crit}) and lethal (P_{leth}) oxygen thresholds (Prosser and Brown, 1962; Connett et al., 1990; Gnaiger, 1991; Childress and Seibel, 1998; McAllen et al., 1999; Pörtner and Knust, 2007; Seibel, 2011; Elliott et al., 2013). When maximum potential respiration rate drops below an organism's "target" respiration rate (P_{crit}), respiration rate becomes limited by oxygen supply, and sub-lethal effects of hypoxia can be expected. When the oxygen supply drops below an organism's "basal" respiration rate (P_{leth}), acute lethal effects of hypoxia can be expected. Both of these thresholds reflect the balance between oxygen *supply* to the organism, a function of the rate of molecular diffusion, and oxygen *demand* by the organism, a function of respiration rate (and ultimately metabolic rate). Typically, these are expressed in terms of oxygen partial pressures. According to Fick's Law for diffusion across a membrane, oxygen uptake and maximum potential aerobic respiration rate will depend on oxygen supply as governed by the external (environmental) oxygen solubility, partial pressure, and diffusivity (Verberk et al., 2011). Thus, corresponding critical and lethal oxygen supply thresholds can be defined that account for oxygen solubility, partial pressure and diffusivity. These thresholds will depend on an organism's non-oxygen-limited (target) respiration rate, and the lowest sustainable (basal) respiration rate, respectively (Elliott et al., 2013). For coastal zooplankton and fish lacking specialized adaptations to live under low environmental DO, oxygen uptake is more or less constant at the target level when pO_2 is above P_{crit}, then declines linearly as DO declines to below the P_{crit} level (**Figure 1**). Because zooplankton and most newly hatched larval fish lack gills, their oxygen uptake is a function of diffusion through the body surface. Under low oxygen conditions relative to oxygen requirements, species with a higher surface/volume ratio would be favored because of their greater oxygen diffusion potential.

It has been established for decades that there is a critical oxygen level for fishes at which metabolism and other processes are limited by oxygen. The use of P_{crit} as a measure of the relative tolerance of a fish to low oxygen also has a long history (Prosser and Brown, 1962; Chapman et al., 2002; Nilsson and Östlund-Nilsson, 2008; Mandic et al., 2009; Richards, 2011; Speers-Roesch et al., 2013; and see review by Rogers et al., 2016). Early fish literature often referred to P_{crit} as the 'incipient limiting tension or level' (Davis, 1975). The classic work of Fry (1957) concludes "Any reduction of the oxygen content below the level where the active metabolic rate begins to be restricted is probably unfavorable to the species concerned. From the ecological point of view, the 'incipient limiting level' (the critical level under conditions of activity) can be taken as the point where oxygen content becomes unsuitable."

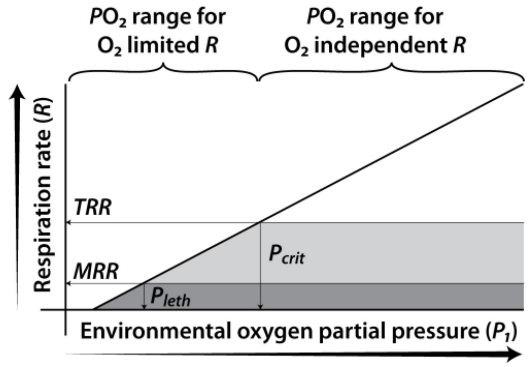

FIGURE 1 | Adapted from Elliott et al. (2013). Relationship between an organism's respiration rate and the environmental oxygen partial pressure. Target Respiration Rate (TRR); Minimum survivable Respiration Rate (MRR), critical oxygen partial pressure (Pcrit) and lethal oxygen partial pressure (Pleth) are shown.

Specific adaptations that help maintain oxygen uptake under low DO (or increasing oxygen demand) include increased ventilation of the respiratory surfaces (e.g., gills), increased heart rate, reduced activity and production of high-affinity oxygen uptake molecules (Herreid, 1980; Childress and Seibel, 1998; Pörtner and Knust, 2007; Richards, 2009; Seibel, 2011). These types of responses are common among zooplankton and fishes in oceanic oxygen minimum zones, which likely have co-evolved with low DO concentrations for thousands of years. However, among coastal organisms, exposure to hypoxia is generally more ephemeral (seasonal) and in many cases is a relatively new stressor associated with eutrophication (Diaz and Rosenberg, 2008). Consequently, planktivorous fish and their zooplankton prey do not appear to have developed specific physiological adaptations to hypoxia in typical coastal systems (Childress and Seibel, 1998; Dam, 2013; McBryan et al., 2013). Instead, these organisms must either avoid hypoxia through behavioral mechanisms or reside in stressful hypoxic water.

With 33 times less oxygen and 3×10^5 times lower diffusion rates in water (at saturation) compared to air, DO can be the proximate cause of reduced growth in zooplankton and fish (e.g., Prosser and Brown, 1962; Pörtner, 2010; Bertrand et al., 2011; Verberk et al., 2011). Warming seas will result in increased oxygen demand by zooplankton and fishes which can result in shifts in spatial distributions, reduced body size and changes in species composition (e.g., Beaugrand et al., 2002; Pörtner and Knust, 2007; Cheung et al., 2012; Deutsch et al., 2015). Because warming temperatures and oxygen limitation are inextricably linked, investigating the impacts of low DO on coastal zooplankton and fishes can provide valuable insights into future ocean warming effects on pelagic ecosystems.

LOW OXYGEN IMPACTS ON COASTAL ZOOPLANKTON

The general observation of reduced copepod abundances (integrated over the entire water column) in hypoxic water columns (Roman et al., 1993; Keister et al., 2000; Kimmel et al., 2012) suggests lower population growth, greater copepod mortality, predation and/or emigration in water columns with hypoxic bottom waters. Laboratory experiments have demonstrated that copepod survival, growth rate, egg production and ingestion rate all decline with lowered oxygen availability. Low DO reduces the survival of copepods

(Vargo and Sastry, 1977; Roman et al., 1993; Stalder and Marcus, 1997; Marcus et al., 2004; Richmond et al., 2006). In laboratory experiments, Marcus et al. (2004) and Richmond et al. (2006) demonstrated that *Acartia* egg production and population growth rate were reduced in low DO waters (0.7 and 1.5 ml O_2 L^{-1}) compared to normoxic (DO > 2 mg L^{-1}) controls. Low DO conditions have also been shown to reduce the ingestion rates of copepods fed in laboratory experiments (Elliott et al., 2013), as well as reduce their escape response (Decker et al., 2004).

Hypoxia can directly affect the earliest life stages of copepods. Copepods can be divided into two groups with respect to reproduction: those that carry their eggs until hatching (brooders) and those that release their eggs (broadcast spawners). Copepod eggs are denser than seawater and thus sink to bottom waters where they can be affected by low DO conditions. Copepods in estuarine and coastal waters produce two types of eggs: diapause (resting) eggs which must complete a dormancy (refractory) period before hatching and non-diapause (subitaneous) eggs which hatch within hours-days of being spawned, depending on temperature (Grice and Marcus, 1981). Low DO has been shown in laboratory experiments to severely reduce the hatching success of non-diapause copepod eggs (Lutz et al., 1992; Roman et al., 1993; Marcus et al., 1994, 1997; Marcus and Lutz, 1994; Invidia et al., 2004; Richmond et al., 2006). The eggs of dominant coastal copepods have sinking rates which range from 15 to 35 m d^{-1} (Uye, 1980; Knutsen et al., 2001; Jiang et al., 2006). Thus, if hatching times are sufficiently long, non-diapause (subitaneous) copepod eggs may sink into low DO bottom waters in shallow systems (Tang et al., 1998; Jiang et al., 2006). Low DO conditions can sometimes induce dormancy in these non-diapause eggs, which is reversed with increases in DO (Katajisto, 2004). Thus, the potential exists for non-diapause eggs to hatch if hypoxia dissipates or they are resuspended into normoxic waters. The length of time that non-diapause eggs can withstand hypoxia/anoxia and remain viable to hatch varies with copepod species and abiotic conditions such as temperature and hydrogen sulfide (Katajisto, 2004; Hansen and Drillet, 2013; Broman et al., 2017). Copepod diapause eggs have an obligatory "refractory phase" and sink to the sediment which is typically anoxic below a depth of several millimeters. Diapause eggs can withstand considerable periods of anoxia and toxic hydrogen sulfide (Marcus, 2001). In general, non-diapause eggs are less able to withstand prolonged exposure to low oxygen than diapause eggs because of their higher metabolic demand (Hansen and Drillet, 2013). Coastal and estuarine waters which experience seasonal hypoxia in bottom waters may develop a significant "egg bank" of copepod eggs which, if reaerated, could hatch and make important contributions to copepod populations and their predators. A combined laboratory and modeling study by Broman et al. (2017) demonstrated that re-oxygenation of anoxic sediments activated copepod egg hatching, indicating that re-oxygenation could result in substantial contributions to copepod populations in the Baltic, and perhaps in other similar systems.

Generally, hypoxic bottom waters truncate zooplankton vertical migration behaviors, reducing the excursion distance (Roman et al., 1993, 2012; Pierson et al., 2009a, 2017; Keister and Tuttle, 2013). For example, zooplankton in the Gulf of Mexico avoided hypoxic near-bottom waters in their diel vertical migrations and the median depth of their daytime distribution was 7 m higher in the water column compared to daytime distributions of zooplankton in water columns with no hypoxic bottom waters (Roman et al., 2012). In the Chesapeake Bay, moderate levels of hypoxia (P_{crit} > DO > P_{leth}) coincided with stronger migration responses than did lethal or fully oxygenated conditions (Pierson et al., 2017). Thus, along with food levels (Huntley and Brooks, 1982; Roman et al., 1988; Pearre, 2000; Hays et al., 2001) and predators (Ohman, 1988; Bollens and Frost, 1989; Frost and Bollens, 1992), the presence of hypoxic bottom waters can influence diel shifts in the vertical distribution of neritic copepods (e.g., Roman et al., 1993; Keister et al., 2000; Qureshi and Rabalais, 2001; North and Houde, 2004). Decker et al. (2003) reported that behavioral responses of copepods to hypoxia may differ depending on environmental history: *Acartia tonsa* from Chesapeake Bay appeared to avoid hypoxic bottom waters in laboratory mesocosms whereas *A. tonsa* from Florida, not typically exposed to hypoxia, did not avoid low-oxygen concentrations in the same mesocosms. Temporal analysis of vertical distributions of copepods has suggested that individuals display considerable variation in their vertical movements, often taking brief (hours) excursions between the surface mixed layer and sub-pycnocline depths (Pearre, 2000; Hays et al., 2001; Pierson et al., 2009a). Thus, it may be common for copepods in coastal waters with hypoxia to experience a range of oxygen concentrations over the day.

Zooplankton may change their vertical position in the water column to avoid low DO bottom waters. However, the vertical compression of their distribution to the upper water column can increase their vulnerability to predation by visually feeding fish and thus alter food-web processes (e.g., Pothoven et al., 2012). Vertical movements can increase zooplankton concentrations or visibility and move them into warmer temperatures with a different array of predators. In general, depth-stratified zooplankton sampling has shown that copepod abundances are higher in the surface mixed layer and within the pycnocline compared to hypoxic bottom water in coastal environments (Roman et al., 1993; Keister et al., 2000; North and Houde, 2004; Kimmel et al., 2009; Pierson et al., 2009b, 2017; Keister and Tuttle, 2013). However, this is not always the case (Qureshi and Rabalais, 2001; Taylor and Rand, 2003) and even if most zooplankton are above the oxycline, significant amounts can occur in hypoxic near-bottom water for part of the day (Roman et al., 1993; North and Houde, 2004; Taylor et al., 2007; Keister and Tuttle, 2013; Pierson et al., 2017). In most coastal and estuarine waters, copepods exhibit diel vertical migrations, presumably to reduce predation by visual feeders by residing at depth during the day, and returning to the surface layer at night (Cahoon, 1981; Roman et al., 1988). Bottom-water hypoxia can clearly disrupt vertical migration behavior. For example, when a wind event mixed the water column and re-aerated hypoxic bottom water in Chesapeake Bay, copepods migrated to a deeper depth during the day (Roman et al., 1993).

Low oxygen waters have been associated with changes in zooplankton species assemblages. These assemblage shifts could be due to direct effects of low DO on the metabolic functions

of the animal or indirect effects due to selective predation by zooplanktivores. Long-term seasonal presence of bottom-water hypoxia may favor copepod species which brood their eggs as compared to broadcast spawners whose eggs would sink into anoxic/hypoxic bottom waters. For example, increased eutrophication and low oxygen bottom waters have resulted in an increase in the abundance of the small, egg-carrying copepod *Oithona davisae* in Tokyo Bay and decline in the occurrence of *Acartia omorii* and *Paracalanus* sp., copepods that release their eggs into the water column (Uye, 1994). A similar decline in the broadcast egg spawner, *Acartia tonsa* has been associated with the increase in bottom water hypoxia in Chesapeake Bay (Kimmel et al., 2012). Egg-carrying copepods in the Gulf of Mexico showed more relative abundance in water columns with hypoxic bottom waters compared to nearby well-oxygenated water columns (Elliott et al., 2012).

In general, smaller copepods have a higher surface to volume ratio which would favor their oxygen uptake over larger copepods in hypoxic waters and warmer waters where oxygen solubility is lower and oxygen demand (respiration) is higher. In laboratory experiments, Stalder and Marcus (1997) showed that the smaller copepod, *Acartia tonsa,* survived low oxygen conditions better than the larger *Labidocera aestiva* and *Centropages hamatus*. In similar types of laboratory experiments, Roman et al. (1993) found that the smaller copepod *Oithona colcarva* survived low oxygen conditions better than the larger *Acartia tonsa*. In addition to species differences there may be gender differences in tolerance to hypoxia. Pierson et al. (2017) reported that male *Acartia tonsa* were found in lower oxygen waters than females in Chesapeake Bay. Males are smaller (Pierson et al., 2017) and thus have a higher surface/volume ratio than females that may also have a higher respiratory demand because of egg production (e.g., Castellani and Altunbas, 2014).

LOW OXYGEN IMPACTS ON COASTAL PELAGIC FISHES

Exploration of the impacts of low DO on fish date back over a century (e.g., Shelford and Allee, 1913; Wells, 1913) which, early on, documented that fish can often behaviorally avoid low DO and that the tolerance of fish to low DO can vary with species and body size (e.g., Fry, 1957; Brett, 1964, 1970). Research on the physiological response of fish to DO is extensive and research on the impact of hypoxia on fish in coastal ecosystems has exploded in the last few decades (see reviews by Pauly, 2010; Richards, 2011; Rogers et al., 2016). Hypoxia directly affects fish physiological rates and fish must either move out of the way or suffer the consequences of reduced DO. The consequences of moving to non-hypoxic environments, while often poorly understood, is a key to understanding hypoxic impacts at the species or ecosystem level. To predict/forecast how hypoxia-driven changes in habitat conditions will affect fish populations, we need to understand how vital habitat requirements of a species are related to hypoxia and other environmental drivers.

Physiological responses of fishes to low DO have been well studied under laboratory conditions (e.g., Rogers et al., 2016). Low DO has been shown to reduce fish consumption, growth, reproduction and recruitment in the laboratory (e.g., Aku and Tonn, 1997; Breitburg et al., 1999; Taylor and Miller, 2001; Shang and Wu, 2004; Craig and Crowder, 2005; Eby et al., 2005; Diaz and Breitburg, 2009; Brandt et al., 2011; Thomas and Rahman, 2012; Zhang et al., 2014) and increases susceptibility to other stressors (Breitburg et al., 2009). Reductions in abundance of sensitive, less-mobile fish species may occur due to fish kills (Graham et al., 2004; Thronson and Quigg, 2008). Effects may be direct via increased mortality through prolonged exposure to low DO (Breitburg et al., 1999, 2003; Turner, 2001; Diaz and Breitburg, 2009) or indirect via reduction of benthic (Turner, 2001) and water column (Wang, 1998; Breitburg et al., 1999; Chesney et al., 2000; Turner, 2001) habitat availability and alteration of food web structure (Graham, 2001). However, such research rarely considers the interactive effects of temperature and low DO on the fish.

If ambient DO is below the P_{crit} level, fish can respond to lowered oxygen in a number of ways that range from avoiding the hypoxic region to increasing oxygen intake (increased ventilation) to physiological shifts (e.g., Gamperl and Driedzic, 2009; Richards, 2009; Wells, 2009; Speers-Roesch et al., 2012) to reducing metabolic costs (e.g., lowered appetite, reduced activity levels). Eggs and larvae have fewer options; eggs can only respond passively while larvae can migrate vertically or adjust their feeding and activity levels. Most responses to hypoxia will have consequences for consumption and growth rates (e.g., Wang et al., 2009) and thus ultimately survival rates and/or reproduction (Craig and Crowder, 2005; Beauchamp et al., 2007; Searcy et al., 2007; Daewel et al., 2008; Wu, 2009).

Hypoxia can drive changes in spatial distribution of coastal and estuarine fishes (Craig and Crowder, 2005; Hazen et al., 2009; Ludsin et al., 2009; Zhang et al., 2009). Hypoxia-induced changes in food webs may result from changes in the abundances of some species and/or the distributional overlap of predators and prey (Breitburg et al., 1997; Ekau et al., 2010). Diets of fishes can differ in hypoxic water as shown for Atlantic bumper in the Gulf of Mexico (Glaspie et al., 2018). Some fishes may even benefit from hypoxia if their prey are forced into more vulnerable predatory habitats as suggested for Chesapeake Bay where striped bass may benefit from concentration of bay anchovy prey in the well-oxygenated mixed layer (Costantini et al., 2008). Clearly, these effects differ across species, life stages, and ecosystems and are particularly dependent on the prevailing water temperatures and species-specific bioenergetics tolerances (Brandt et al., 2009).

Whether effects of hypoxia on fish populations are positive or negative is likely species-specific and ecosystem-dependent (Breitburg et al., 1997, 2001; Costantini et al., 2008) and also depend on the severity of the low oxygen coupled to the prevailing temperatures. For example, species less tolerant of hypoxia may be forced to reside where habitat (e.g., food, refuge from predators, and temperature) critical for growth, reproduction, and/or survival are suboptimal (Roman et al., 1993; Aku et al., 1997; Keister et al., 2000; Wannamaker and Rice, 2000; Costantini et al., 2008; Ludsin et al., 2009; Wu, 2009) which may reduce individual consumption and fitness, ultimately leading to lower population sizes (Aku and Tonn, 1997; Wu, 2002;

Breitburg et al., 2003). In contrast, species more tolerant of low DO could prosper in hypoxic waters, using it as a refuge from predation or for feeding (Breitburg et al., 2001; Klumb et al., 2004; Prince and Goodyear, 2006; Prince et al., 2010; Vejøík et al., 2016). Some fish predators may benefit if low DO forces their prey to move into habitats easily exploited by the predators (e.g., Costantini et al., 2008; Brandt et al., 2011).

It has been demonstrated that year-class success in fishes is largely determined during the larval or early juvenile stage, and that variability in vital rates (e.g., growth and mortality rates), attributable to a wide variety of environmental stressors, including low DO, can lead to order of magnitude fluctuations in survival during early life (Cowan and Shaw, 2002; Houde, 2008). As such, even subtle changes in survival potential of early life stages may lead to declines in regional fish production if hypoxia affects the distribution and physiological ecology of a significant fraction of the population.

In coastal ecosystems, fish are likely to be most susceptible to the effects of hypoxia during their egg and larval stages (Breitburg, 2002). In coastal upwelling ecosystems subject to variable DO conditions, early life stages of pelagic fish species differ in their distributions, a reflection of species-specific tolerances to low DO (Ekau and Verheye, 2005; Geist et al., 2013, 2015). Pelagic fish eggs may have different exposures to bottom hypoxia, depending on the species, sinking rates and density structure of the water column (Nissling and Vallin, 1996; Ekau and Verheye, 2005). Larvae are generally planktonic and thus are primarily able to migrate vertically in response to hypoxia (Breitburg, 2002). Hypoxia may affect eggs and larvae through direct mortality or indirectly as a consequence of reduced growth and higher mortality resulting from altered spatial distributions, availability of suitable prey for larvae, and susceptibility to predators. Even small changes in daily growth and mortality rates of early life stages can have order of magnitude effects on levels of recruitment (Houde, 1989b, 2016).

ECOSYSTEM COMPARISONS OF HYPOXIA IMPACTS ON COASTAL ZOOPLANKTON AND FISH

Global comparisons of the effects of low DO on pelagic ecosystems need to consider and evaluate the role of temperature in controlling oxygen availability, metabolic demand, organism behavior, and the consequences of moving to alternative habitats. For example, temperatures of hypoxic (<2 mg L^{-1}) bottom water in the Gulf of Mexico can exceed 28°C (Pierson et al., 2009b) in contrast to the Baltic Sea where hypoxic water temperatures are 8–10°C (Carstensen et al., 2014; **Figure 2**). Such differences in bottom temperatures affect oxygen availability (partial pressure and solubility) for organisms, and drive differences in respiratory demands (Q_{10} for respiration for most zooplankton is around 2). Perhaps equally important is the contrast in temperatures between hypoxic water and the

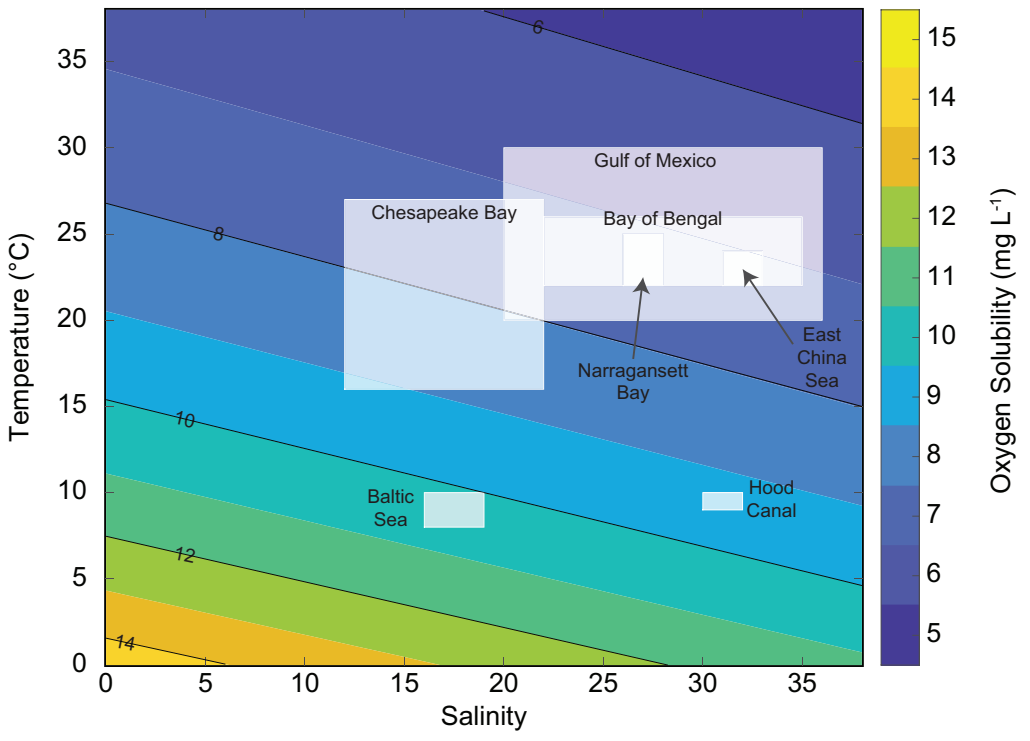

FIGURE 2 | Oxygen solubility (mg L^{-1}) is shown by the color scale at different salinity and temperature (°C) conditions, with boxes indicating the range of salinity and temperature during periods of seasonal deoxygenation for seven coastal and estuarine bodies of water around the world. Oxygen solubility calculated using the equations of Benson and Krause (1980, 1984), assuming surface water pressure.

overlying mixed layer (alternative habitats) which can be small (1–3°C in the Gulf of Mexico; Pierson et al., 2009b, East China Sea; Zhang et al., 2015) or large (up to 10°C) in the Baltic Sea (Carstensen et al., 2014), Hood Canal (Sato et al., 2016), and Lake Erie (Pothoven et al., 2012). Salinity also has an effect on oxygen solubility, but the effect of temperature per degree °C is nearly three times that of a change of one salinity unit.

Thus, all "hypoxic" bottom waters do not pose the same level of stress on zooplankton and zooplanktivorous fishes and can generate different responses in spatial ecology and predator-prey interactions. For example, using the predictive response to decreasing oxygen (P_{crit}) developed for the copepod *Acartia tonsa* by Elliott et al. (2013), 2 mg L^{-1} bottom water in the Baltic Sea (9°C) would have an oxygen partial pressure of 4.24 kPa, which is slightly below the limiting P_{crit} of *A. tonsa* predicted for this temperature (5.07 kPa). In contrast, 2 mg L^{-1} bottom water in the Gulf of Mexico (30°C) would have an oxygen partial pressure of 6.37 kPa, which is substantially below the limiting P_{crit} = 18.31 kPa of *A. tonsa* predicted for this temperature and is approximately the same as the predicted lethal P_{leth} = 6.77 kPa oxygen partial pressure. These predicted differences in oxygen supply and demand provide a useful way to assess how low oxygen waters directly determine habitat availability for estuarine and coastal zooplankton. Field surveys have shown that zooplankton generally avoid the warmer low DO waters of the Gulf of Mexico (e.g., Qureshi and Rabalais, 2001; Roman et al., 2012) but reside in the colder low oxygen waters of the Baltic Sea for significant portions of the day, affording the zooplankton a potential refuge from predation (e.g., Appeltans et al., 2003; Webster et al., 2015). Because of the higher oxygen demand by coastal zooplankton and fish in warm tropical and subtropical waters, the loss of habitat space due to low oxygen waters is expected to be more severe in these regions.

Research in ecosystems such as the Great Lakes and Chesapeake Bay has identified water temperature as a critical factor in the assessment of hypoxia impacts for fish (e.g., Costantini et al., 2008; Brandt et al., 2009, 2011). Temperature is a fundamental driver of fish bioenergetics, behavior, and feeding and large-scale changes in ocean temperature trigger large-scale regime shifts in fish abundances (e.g., Cheung et al., 2013; Kilduff et al., 2014; Ito et al., 2015). The temperatures at which hypoxia occurs will determine the species most likely affected by the hypoxia. For example, if hypoxia occurs at temperatures that are largely unsuitable (too cold or too warm) to a particular species, then hypoxia is unlikely to directly impact that species. Also, if fish are forced to avoid hypoxic areas then temperatures of nearby alternative habitats may determine the consequences of shifts in distributions.

The direct consequences of lowered oxygen to fishes are also highly dependent on the prevailing water temperatures. Normally, the sensitivity of fish to low oxygen is higher at higher water temperatures due to higher metabolic demand. But the relationships are species-dependent, life stage-dependent and non-linear. For example, a set of laboratory experiments showed that juvenile striped bass growth was highly responsive to the interaction between oxygen and temperature (**Figure 3**). It is probable that striped bass would be more vulnerable to low DO in some ecosystems than others depending on respective temperature-DO levels (see **Figure 2**).

ZOOPLANKTON RESPIRATION, METABOLISM AND ALLOMETRIC SCALING

Oxygen availability to coastal zooplankton and fish is a function of the rate of diffusion across their integument or gills, thus allometric relationships for surface/volume, body mass, and gill area, among others, should be explored for similar groups of zooplankton and fish to predict oxygen limitation and its consequences. For zooplankton, copepods have been studied extensively and provide a robust example. The respiration of copepods is an exponential function of temperature (Ikeda, 1970). Whereas there are differences due to species, latitude and acclimation period, published Q_{10} values for copepod respiration range from 1.0 to 2.7 (Mauchline, 1998; Teuber et al., 2013). Temperature also influences the oxygen availability to copepods. While oxygen solubility in seawater decreases with temperature, oxygen partial pressure increases with temperature because of the greater kinetic energy of the oxygen molecules. As temperatures increase, the linear increase in partial pressure may initially satisfy the increased oxygen demand by copepods but, because respiration increases exponentially with respect to temperature, oxygen demand eventually exceeds supply and organisms become oxygen stressed (Verberk et al., 2011). An example of this is shown using the relationships from Elliott et al. (2013; **Figure 4**) for *A. tonsa* at a salinity of 25. The curve showing the relationship of P_{crit} with temperature crosses the line describing the oxygen partial pressure for concentrations of 2 mg L^{-1} at approximately 10°C. The P_{leth} curve crosses at approximately 25°C. Consequently, above 10

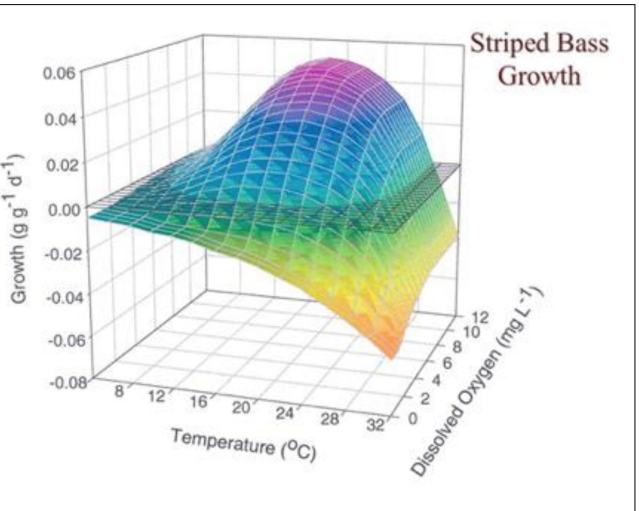

FIGURE 3 | The relationships between striped bass growth rate, temperature, and dissolved oxygen from Brandt et al. (2009).

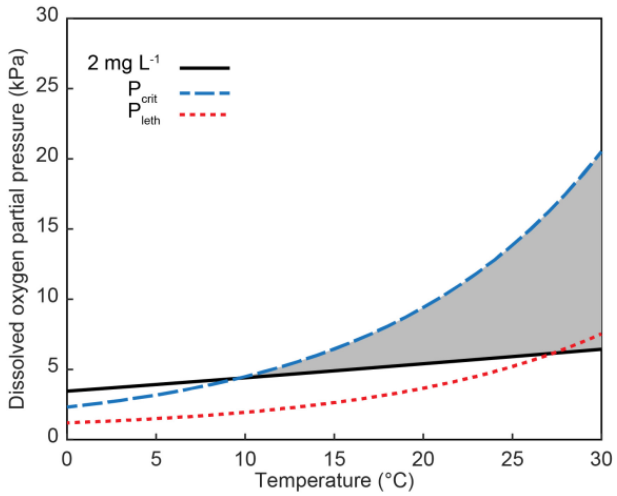

FIGURE 4 | Partial pressure of dissolved oxygen over a range of temperatures for an oxygen concentration of 2 mg L^{-1} (solid black line), the P_{crit} (dashed blue line) and P_{leth} (dotted red line) for the copepod *A. tonsa* (Elliott et al., 2013). Gray area shows region where values for P_{crit} and P_{leth} are greater than the PO_2 at 2 mg L^{-1}, and thus where water may not be classified as hypoxic but DO would be below the critical or lethal threshold. The partial pressures of 2 mg L^{-1} were calculated as the percent saturation of O2 (Benson and Krause, 1980, 1984) at the given temperature (at assumed salinity of 25), and then multiplying that by 21.198 kPa, the assumed partial pressure of O_2 at the surface.

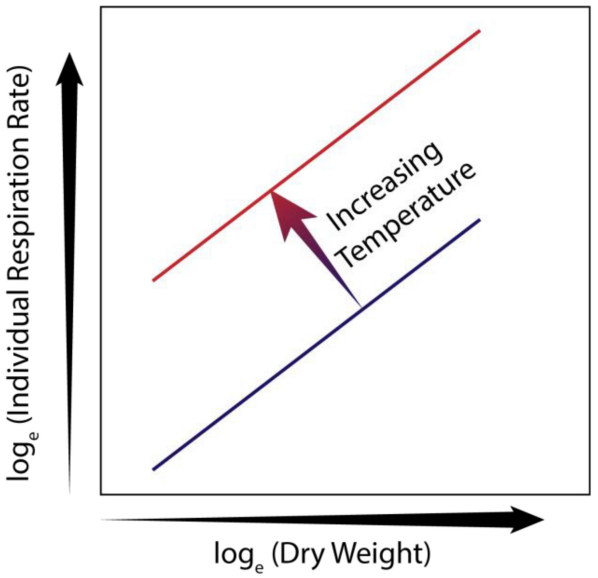

FIGURE 5 | Conceptual figure showing natural log transformed respiration rate (ln R) of a copepod versus copepod dry weight (ln DW), and the effect of temperature on the relationship, based on data from Castellani and Altunbas (2014). Lines represent the relationship between ln R, ln DW for different temperatures. Note the slope remains the same but the overall respiration at a given size increases with temperature.

and 25°C, DO concentrations even when above 2 mg L^{-1} may be below the critical or lethal thresholds, respectively, for *A. tonsa*.

The mass-specific metabolic activity and respiration of copepods decrease with body size (see reviews by Marshall, 1973; Hirst and Sheader, 1997; Mauchline, 1998). Thus, to compare respiration in different developmental stages of a particular species or to compare different zooplankton species over wide size ranges, investigators have developed empirical, allometric scaling models that predict respiration rates from body mass (Raymont and Gauld, 1951; Marshall, 1973; Ikeda, 1985). Within copepod species, body sizes in nature are inversely related to temperature (Deevey, 1960; McLaren, 1963; Uye, 1982), due largely to different temperature-dependent rates of growth and development (Miller et al., 1977; Forster et al., 2011). Since oxygen uptake by copepods takes place through the integument and surface to volume ratio decreases with increasing size, smaller copepods, with a higher surface area to volume ratio may be favored in warmer waters where oxygen solubility is lower but respiratory demand is higher. Similarly, in low-oxygen environments, smaller copepods may be favored because of their higher surface area to volume ratio and thus more efficient oxygen diffusion per unit mass (Pörtner, 2010).

Taken together, copepod body mass and habitat temperature can account for 72 – 96% of the variability in measured weight-specific copepod respiration rate (Ikeda, 1985; Ikeda et al., 2007; Bode et al., 2013; Castellani and Altunbas, 2014; **Figure 5**). Thus, for copepods, temperature dependence of growth rates and presumably respiration usually outweigh species-specific differences (Huntley and Lopez, 1992; Hirst and Sheader, 1997). To provide global assessments of seasonal hypoxia effects on coastal zooplankton, one could develop generic species models for copepods based solely on allometry and assess patterns of low DO effects based on size and ambient temperature.

PLANKTIVOROUS FISH RESPIRATION, METABOLISM AND ALLOMETRIC SCALING

There is an extensive body of literature demonstrating that metabolic rates of fish also are strongly dependent on both body mass and temperature (e.g., Fry, 1971; Clarke and Johnston, 1999; Claireaux and Lefrançois, 2007; Pauly, 2010; Peck et al., 2012; Evans et al., 2014). Within a species, the allometric relationship of metabolic demand to fish mass or weight is well established (Rombough, 1988; Clarke and Johnston, 1999). Larger fish have a higher demand for oxygen but the weight-specific rate of oxygen consumption decreases as weight increases. Thus warmer temperatures and lower DO would favor smaller fish (e.g., Ekau et al., 2010; Pauly, 2010; Verberk et al., 2011; Cheung et al., 2012).

Scaling relationships have been developed for body mass, metabolic rate and temperature in fishes and broader taxa categories (e.g., Gillooly et al., 2001; Brown et al., 2004). For example, Clarke and Johnston (1999) derived a generalized allometric relationship of standard (resting) metabolism for 69 species of post-larval fishes. The taxa covered 12 orders

and 28 families of fishes ranging from Myctophidae, to Salmonidae, to Gobiidae to Ictaluridae. The mean coefficient b for allometric scaling ($R = aM^b$) was 0.79 and the mean Q_{10} for the effect of temperature was 1.83. After adjusting for body mass, the relationship of metabolic rate (oxygen consumption) was a curvilinear relationship to temperature that the authors noted was "strikingly similar to relationships established previously for aquatic invertebrates" (Clarke, 1991). They also provided evidence that the relationship of metabolism to temperature had different mean rates but overall similar slopes across related species at the fish order level. Killen et al. (2010) examined the scaling of metabolic rate and fish body mass across temperature and fish 'lifestyles' among 89 species of fish and concluded that the metabolic scaling b exponent shifted with lifestyle changes from bathyal to benthic to benthopelagic to pelagic and the authors related this shift to energy requirements associated with swimming and predator-prey interactions. At a standardized temperature, oxygen consumption levels were generally high for pelagic fishes (46% higher than for benthic fishes; b = 0.698 benthic versus b = 0.856 pelagic). Highly active pelagic fishes may require more muscle mass and respiratory surface areas (Muir, 1969).

In larval-stage fishes, scaling relationships for respiration and metabolism also have been investigated and reviewed. Relationships may differ from those in juvenile and adult fishes, probably because of the shift from cutaneous to gill respiration during ontogeny (Rombough, 1988). The exponent in the allometric relationship between respiration rate and body mass is variable among taxa, generally lying in the range 0.6–1.2 (Houde and Zastrow, 1993; Peck et al., 2012), with some authors contending that the relationship is isometric (b = 1.0) in fish larvae (Giguere et al., 1988). As expected, temperature strongly affects respiration rates in embryonic and larval-stage fishes (Houde, 1989a; Houde and Zastrow, 1993). Peck et al. (2012) suggested there is an ontogenetic shift in the scaling relationship, with the power exponent in the allometric relationship declining as larvae transition to the juvenile stage. The Q_{10} for respiration rates in fish larvae may, in many cases, be lower than the 2.0–3.0 values typically seen in juvenile and adult fishes (Rombough, 1988). Houde (1989a) reported mean Q_{10} of 1.46 for marine fish larvae although Peck et al. (2012), with an expanded database, estimated a mean Q_{10} of 2.31, noting that taxa-specific Q_{10} always was < 1.70 for species living at $> 25°$ C but was > 2.60 for species living at $\leq 18°$C.

Bioenergetics relationships in pelagic fishes have been investigated and feeding, energy budgets, oxygen uptakes and metabolic demand in relation to temperature, diet level, and body size are reasonably well understood for some taxa, for example anchovy life stages (Houde and Schekter, 1983; Houde et al., 1989; Vazquez and Houde, 1989). Bioenergetic models for bay anchovy (Luo and Brandt, 1993; Houde and Madon, 1995), based on our previous research, suggest that temperature-dependent, weight-specific metabolism of different anchovy species is similar (Vazquez and Houde, 1989; **Figure 6**), implying similar dependencies on ambient temperatures and DO.

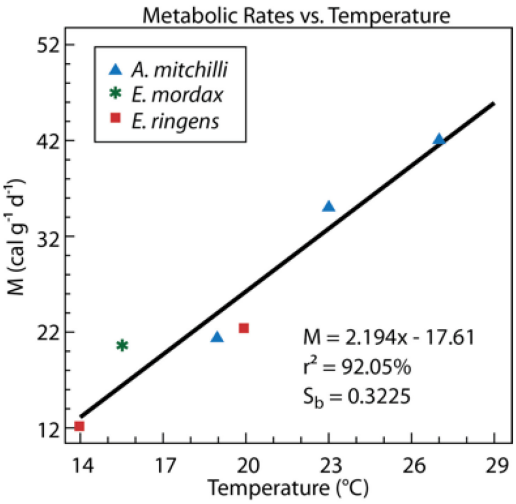

FIGURE 6 | Weight-specific metabolic rates (M, calories g-1 day-1) at different temperatures (T, °C) for three anchovy species, *A. mitchilli* the bay anchovy, a coastal species; *Engraulis mordax* the northern anchovy from the California current; *Engraulis ringens*, the *Peru anchoveta*, from the Humboldt Current. Figure adapted from Vazquez and Houde (1989).

COMPARING HYPOXIA IMPACTS ACROSS ECOSYSTEMS AND SPECIES

To assess effects of globally expanding, coastal low oxygen zones, we need to determine if generic models and unifying metrics can be developed to evaluate and predict how low DO imposes temporal and spatial limitations on metabolic functioning of zooplankton and their fish predators. An oxygen concentration of 2 mg L^{-1} has routinely been used to define the presence, areal extent, volume, duration and inter-annual variability of hypoxia within and across ecosystems. This concentration does not consider the important role of temperature in defining oxygen supply. **Figure 2** demonstrates the large differences in ecosystems with similar oxygen concentrations. We recommend that habitat characterization be done using oxygen partial pressure to define hypoxia and the approach outlined in **Figure 2** adopted to compare ecosystems.

Hypoxic stress must be considered in the context of oxygen supply relative to oxygen demand. Oxygen supply, being determined by rate of diffusion, will scale with temperature based on Fick's Law (Verberk et al., 2011) and would be expected to scale linearly with body/gill surface area, or approximately to the 2/3 power with body volume or mass. Estimates of oxygen supply relative to demand can be derived from existing knowledge of an organism's P_{crit} (see **Figure 4**). Because P_{crit} is essentially the external oxygen partial pressure at which supply equals demand, the rate of oxygen supply at this threshold will equal that of oxygen demand (i.e., the respiration rate). Values of P_{crit} have been measured for copepods and fish of various body masses and respiration rates have been related to both temperature and body mass in numerous studies. Thus, ample data exist to derive estimates of the rate of oxygen supply and demand

for zooplankton (mainly copepods) and fishes across a range of temperatures and body masses, allowing parameterization of the expected scaling relationships. Deutsch et al. (2015) developed an integrated "metabolic index" projected over the global ocean to predict how the supply of and demand for DO will change in the future with regard to all of the potential impacts of climate change on DO. Their findings suggest large decreases in the metabolic index over large swaths of the globe, meaning organisms in a particular region are likely to exist in less favorable conditions in the future. Although this research was directed to the open ocean, it is probable that coastal and estuarine systems experiencing seasonal hypoxia at increasing water temperatures are likely to have similar prospects for the future.

Similar to the metabolic index of Deutsch et al., 2015, the general, broadly applicable relationships of temperature and body mass with oxygen supply and demand can be parameterized to develop an Oxygen Stress Level (OSL, a dimensionless number), either for individual taxa or for groups of organisms. This ratio of oxygen supply to demand could be calculated for study regions as a simple metric indicating the predicted occurrence and severity of hypoxic stress. Oxygen stress levels can be defined as:

$$\mathrm{OSL} = [\text{ambient pO2} - P_{leth}] / [P_{crit} - P_{leth}]$$

For OSL > 1, supply exceeds demand and no oxygen stress, sub-lethal or lethal effects would be predicted. Conversely, for OSL < 1, oxygen demand exceeds supply and sub-lethal or lethal effects of oxygen stress would be predicted. For OSL < 0 oxygen demand is below the basal respiration rate. Thus, OSL = 1 indicates DO conditions equal to the organism's P_{crit} and for OSL = 0 it indicates DO conditions equivalent to the organism's P_{leth}.

As an example, we examined the spatial extent and temporal variability of OSL based on high resolution profiles of temperature, salinity and DO collected in July of each of 4 years along axial transects in Chesapeake Bay (Zhang et al., 2006). DO concentrations were converted to partial pressure by first calculating the DO solubility for each temperature and salinity value (Benson and Krause, 1984), and multiplying the percent saturation by 21.198, the partial pressure of oxygen in the air. P_{crit} and P_{leth} for *Acartia tonsa* (Elliott et al., 2013) were calculated to determine OSL values for *A. tonsa* at each data point (**Figure 7**). The along-channel patterns in OSL are similar among years; however, 1996 was a wet year with high streamflow, which led to very low OSL in the upper Chesapeake Bay. In contrast, 1999 was a dry year with low streamflow, and OSL values were higher in the mid-bay and the lower-bay reaches than in any of the other years.

We also examined whether the concentration of *A. tonsa* varied with respect to OSL in this same system. Using data from zooplankton samples collected in summer of 2010 and 2011 from depth stratified net tows and simultaneously collected hydrographic data (Pierson et al., 2017), we determined the relationship between stage-specific *A. tonsa* concentrations and OSL using a regression tree analysis (**Figure 8**).

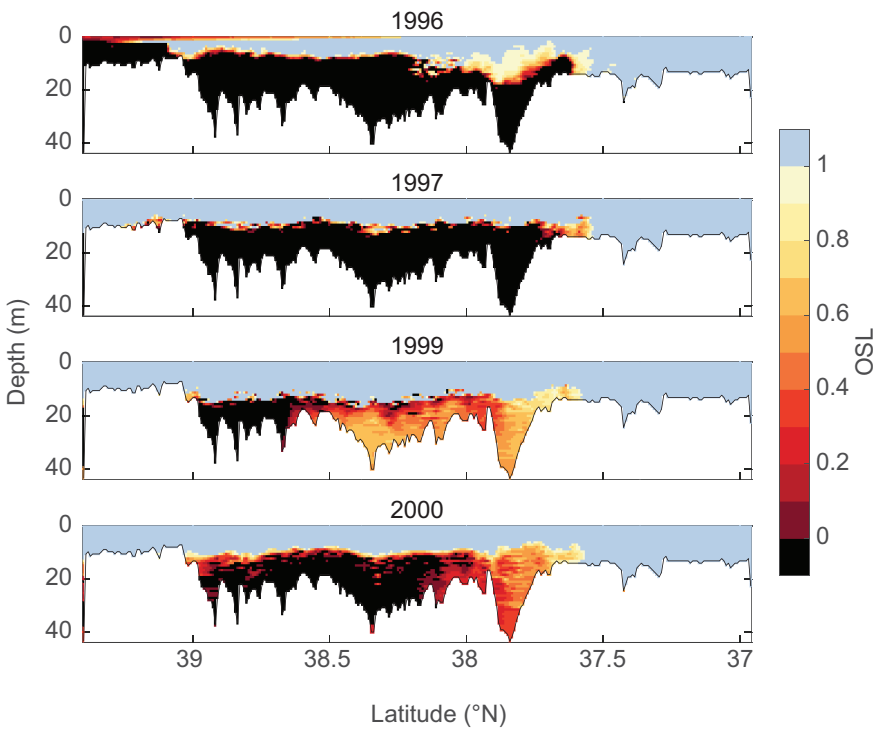

FIGURE 7 | OSL index for the copepod *A. tonsa* in the main channel of the Chesapeake Bay for 4 years, calculated using high resolution hydrographic data (temperature, salinity, and dissolved oxygen) collected with a Scanfish (Zhang et al., 2006). Calculations of P_{crit} and P_{leth} were made using equations from Elliott et al. (2013).

The *A. tonsa* data were sorted to include only data from samples collected in the oxycline and below the oxycline, and not in the surface, to avoid biases related to general patterns of depth distribution. In general, *A. tonsa* concentrations were lowest where OSL < 0 and highest where OSL > 1 (**Figure 8**). Specifically, the regression tree analysis identified cut points at OSL = −0.26 and OSL = 0.84 for all three stages. Mean concentrations values of copepodites, females, and males at each of the nodes ranged from 4.7 – 10.6 m^{-3} for OSL < −0.26, 333 – 770 m^{-3} for −0.26 < OSL < 0.84, and 1652 – 3467 m^{-3} for OSL > 0.84. This suggests that the OSL metric may be a useful tool to assess available and usable habitat.

In addition to this simple metric OSL, there are temperature-specific and allometric relationships describing P_{crit} and P_{leth}. Because P_{crit} and P_{leth} are direct reflections of the balance between oxygen supply and demand, these low oxygen thresholds will scale with temperature and body size in the same manner as OSL. Effects of temperature on these thresholds, through effects on respiration, can be described using specific respiratory Q_{10} values available from the literature (e.g., Rombough, 1988; Peck et al., 2012; Elliott et al., 2013). For calibration, absolute values of P_{crit} and P_{leth} at various body masses can be taken or derived from the available literature using methods similar to Elliott et al. (2013). The methods of Killen et al. (2010) to derive P_{crit} and temperature-oxygen specific respiration rates may be appropriate for pelagic planktivores which are likely to have similar energy requirements and oxygen demands (Clarke and Johnston, 1999; Killen et al., 2010). Results from published literature on fishes such as herring, sardines, anchovies and smelt (e.g., Kiørboe et al., 1987; Tanaka et al., 2006; Bernreuther et al., 2013) could be critically evaluated and combined to define generic relationships. Using the techniques employed by Elliott et al. (2013), one could convert vital rate data collected at different oxygen and temperature conditions to estimate the values of P_{crit} and P_{leth}, and to determine OSL for fish taxa found in regions with hypoxic conditions. Such calculations are important because the relative impact of deoxygenation on an organism can be quantified and scaled to make it applicable to a wide variety of modeling efforts. de Mutsert et al. (2016) employed a similar approach to scale fish feeding to oxygen concentration and showed species-specific responses to hypoxia and to explicitly modeled drivers of hypoxia. Parameterizations of organismal responses to hypoxia for broader taxonomic (e.g., various zooplankton species) and ontogenetic stages (e.g., larvae and juveniles) as well as expanded parameterizations of the individual responses of organisms to hypoxia (e.g., reproductive output, predator avoidance) will further improve our predictive capabilities for ecosystem and food-web models.

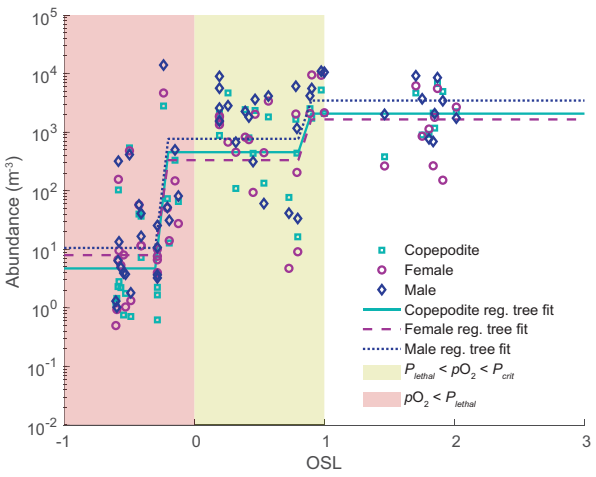

FIGURE 8 | Concentration (m^{-3}) of *Acartia tonsa* in the Chesapeake Bay at various values of OSL, determined from simultaneously collected vertically stratified zooplankton samples and hydrographic data. Green squares show data for copepodite stages, purple circles show data for adult females, and blue diamonds show data for adult males. Lines show results from regression tree analysis to examine the relationship between log10 transformed concentration and OSL, with solid green lines for copepodites, dashed purple lines for adult females, and dotted blue lines for adult males. Yellow shaded area shows where $P_{leth} < pO_2 < P_{crit}$, and pink shaded region shows where $pO_2 < P_{leth}$. Regression trees were created in Matlab using the "fitrtree.m" function, with a minimum leaf size of 8 and pruned to a level of 2.

IMPACTS OF HYPOXIA ON ZOOPLANKTON-FISH INTERACTIONS

Low DO bottom waters can influence the spatial overlap and trophic coupling of pelagic zooplankton and fish populations. For example, more hypoxia-tolerant zooplankton may use low DO bottom waters as a refuge from fish predation (Appeltans et al., 2003; Taylor and Rand, 2003; Webster et al., 2015; **Figure 9**). In contrast, zooplankton avoidance of hypoxic bottom waters can result in prey aggregations at oxyclines where fish and invertebrate predators may aggregate (Qureshi and Rabalais, 2001; Taylor and Rand, 2003; Roman et al., 2012). As fish and zooplankton differentially distribute across oxygen gradients within the water column based on their DO tolerances, there will likely be a disruption in the food web as encounter rates among predators and prey will change (e.g., Vanderploeg et al., 2009; Pothoven et al., 2012).

In coastal ecosystems with shears and differential flow between surface and deep layers, avoidance of low oxygen bottom waters can influence spatial dynamics of zooplankton and fish populations by altering emigration and immigration patterns, and residence times. As more information becomes available on the oxygen demand of dominant estuarine and coastal zooplankton and fish at different temperatures, we will be able to better assess if low oxygen bottom waters influence their trophic interactions.

Several lines of evidence suggest that hypoxic bottom waters do effect pelagic food-web interactions in coastal waters. Glaspie et al. (2018) found the diet of a pelagic fish, the Atlantic bumper (*Chloroscombrus chrysurus*), to differ significantly between hypoxic and non-hypoxic waters. The vertical distribution of DO within the water column affects spatial overlap between zooplankton and their fish and gelatinous zooplankton predators (e.g., Keister et al., 2000; Breitburg et al., 2003). Predators may make short excursions into hypoxic water to take advantage

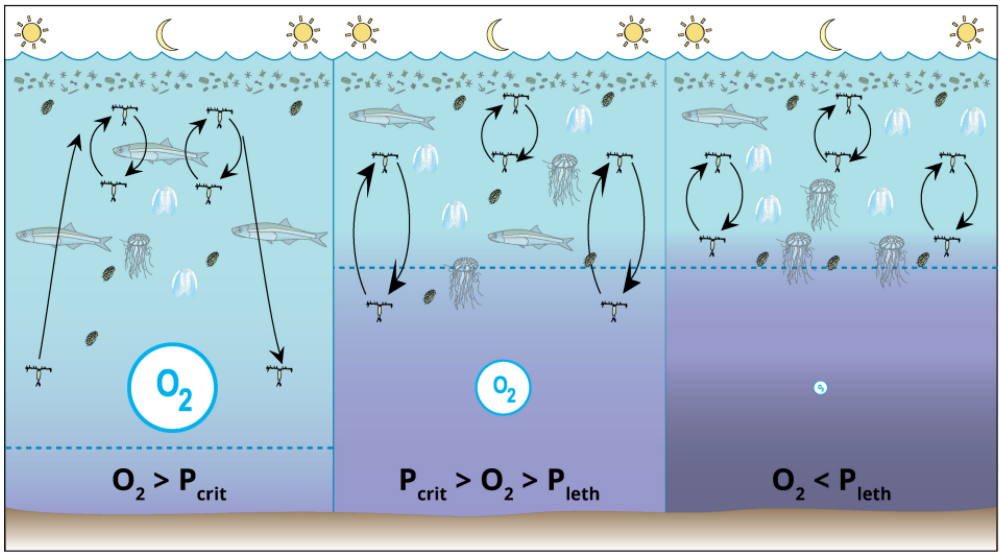

FIGURE 9 | Conceptual diagram of food web changes that may occur over diel cycles between normoxic conditions **(left)**, sub-lethal deoxygenation conditions **(middle)**, and lethal conditions **(right)**. The size of the symbol for O_2 and the color indicates the relative amount of dissolved oxygen under each condition (with light blue indicating high oxygen concentration and purple indicating lower oxygen concentration). With decreasing oxygen concentration comes reduced habitat, truncated magnitude of copepod vertical migration (shown by length of arrows), increased gelatinous zooplankton abundance, and decreased forage fish abundance. Symbols Courtesy of the Integration and Application Network, University of Maryland Center for Environmental Science (ian.umces.edu/symbols/).

of aggregated prey (Taylor et al., 2007) and predation rates of fish and gelatinous zooplankton feeding on mesozooplankton are affected by DO concentrations (Breitburg et al., 1997; Decker et al., 2004).

Hypoxic conditions that affect spatial ecology and population dynamics can drive taxonomic and size shifts in the zooplankton community which will affect foraging, consumption and growth of fish species. Smaller zooplankton may be favored in low-oxygen conditions because their higher surface/volume ratio. If hypoxic conditions result in a community shift to smaller zooplankton, there may be negative consequences for fish that then must feed on smaller prey items. It is this type of shift in the Peru Current that is believed to control hypoxia-related species shifts that favor sardine over anchoveta (Bertrand et al., 2011). Similar food web consequences from shifts in zooplankton species could occur if there was a succession to favor copepods that carry their eggs in systems with hypoxic bottom waters (Uye, 1994). Furthermore, low oxygen waters may favor jellyfish over planktivorous fish (**Figure 9**) because of the higher oxygen requirements of fish. Shifts in the zooplankton food available to fish and greater competition by jellyfish can work together to alter pelagic food webs in estuarine and coastal waters experiencing seasonal bottom-water hypoxia.

An important issue related to bottom water hypoxia in estuarine and coastal waters is determining whether zooplankton use the low-DO areas as a critical habitat to avoid predation or must avoid it and remain in the upper water column where they may be subject to greater predation (**Figure 9**). In theory, zooplankton could reside in hypoxic bottom waters if the oxygen supply is greater than its critical oxygen demand (i.e., P_{crit}, OSL > 1) but not if the oxygen availability is well below P_{crit} or the lethal oxygen partial pressure (i.e., P_{leth}, OSL < 0). In both the Gulf of Mexico and Chesapeake Bay, the size distribution of zooplankton as measured with an Optical Plankton Counter (OPC) was shifted to smaller individuals in surface normoxic waters compared to bottom hypoxic waters where there was larger zooplankton (Kimmel et al., 2009). Kimmel et al. (2009) interpreted these patterns to be a consequence of larger copepods having been removed from surface waters by visual predators (fish) which did not forage in the hypoxic bottom waters. Analysis of depth-stratified zooplankton collections in the Gulf of Mexico confirmed OPC results, with larger copepod species more prevalent in low-oxygen bottom waters and smaller copepod species assemblages more prevalent in the oxygenated surface waters where selective predation by fish would likely reduce the abundance of larger copepod species (Elliott et al., 2012). A recent illustration of oxygen tolerances and predator-prey interactions is provided by Sato et al. (2016) for Hood Canal, a fjord in the Northwest U.S. The authors hypothesized that moderate 2–4 mg L^{-1} DO bottom waters would be avoided by fish but not zooplankton, providing a separation of predators and prey. However, field sampling did not support this hypothesis because daytime peak distributions of zooplankton (copepods and euphausiids) and fish (herring and hake) co-occurred in the low-DO bottom waters. The authors suggested that the cold (9°C) waters reduced fish metabolism such that the available oxygen was greater than their P_{crit}.

The spatial relationships of relative stress (OSL < 1) between zooplankton and planktivorous fish can provide insight into potential effects on predator-prey interactions. Determining and

comparing the P_{crit} and P_{leth} for each will be important because the relative behaviors that control prey and predator interactions are likely to be responsive to P_{crit} and P_{leth}. Habitats that have high potential stress for fishes but not for zooplankton may provide a refuge for the zooplankton. In contrast, habitats where DO is above the P_{crit} for jellyfish but is below the P_{crit} for zooplankton may increase predation rates on zooplankton as escape response is reduced in low DO (Decker et al., 2004). If P_{crit} and P_{leth} differ substantially for copepods and their predators, this result can explain how predator-prey interactions are regulated by combined effects of DO and temperature and provide a means to map potential areas of relative predation risk.

CONCLUSION AND RECOMMENDATIONS

The scientific literature does not clearly explain or define how hypoxia affects pelagic zooplankton and planktivorous fishes and their occurrences in hypoxic waters, nor have the interactive effects of temperature and hypoxia been addressed in the context of multiple stressors on organisms in coastal ecosystems. To assess effects of the globally expanding coastal low-oxygen zones, often termed "dead zones," generic approaches and unifying metrics that include ambient water temperatures are needed to assess and predict when and how oxygen limits occurrence and metabolic functioning of zooplankton and their fish predators. Considering oxygen and temperature as a combined and interactive driver in coastal ecosystems will provide a unifying approach for ecosystem comparisons. The P_{crit}, P_{leth} and OSL characterization of habitat provides a direct measure of habitat quality (or stress level) that should have broad appeal and direct applications in water quality monitoring and fisheries management. These metrics should be applicable to pelagic ecosystems in general, and once developed they can provide a quantitative and meaningful measure to define tipping points, evaluate external perturbations and resilience, nutrient reduction strategies, ecosystem physical dynamics, restoration potential, and impacts of a warming climate. Because oxygen availability is dependent on diffusion across integument or gills of aquatic organisms, allometric relationships such as surface area/volume, body mass, and gill area for similar groups of zooplankton and fishes offer a generalized approach to characterize effects of hypoxia and predict oxygen limitation. Allometric scaling models that predict temperature-dependent oxygen supply and demand from the perspectives of zooplankton and planktivorous fishes will lead to improved ability to assess effects of increasing coastal hypoxia on pelagic food webs and allow standardized, quantitative approaches to evaluate and compare hypoxia impacts across coastal ecosystems.

AUTHOR CONTRIBUTIONS

MR had overall responsibility for manuscript preparation. SB and EH wrote the section on fish ecology and physiology and contributed sections on the fish-zooplankton interactions. JP prepared sections on zooplankton ecology and physiology.

FUNDING

The following grants supported our efforts to prepare this work: NOAA-NGOMEX NA06NOS4780148 and NA09NOS4780198 (SB, JP, and MR), NA16NOS4780202 (SB), NSF OCE-0961942 (EH, JP, and MR) and OCE-1259691 (MR and JP), and NAS-2000006418 (MR, JP, and SB).

ACKNOWLEDGMENTS

We are grateful to Catherine Fitzgerald who helped prepare the Figures and References for this manuscript.

REFERENCES

Aku, P. M. K., Rudstam, L. G., and Tonn, W. M. (1997). Impact of hypolimnetic oxygenation on the vertical distribution of cisco (*Coregonus artedi*) in Amisk Lake, Alberta. *Can. J. Fish. Aquat. Sci.* 54, 2182–2195. doi: 10.1139/f97-124

Aku, P. M. K., and Tonn, W. M. (1997). Changes in population structure, growth, and biomass of cisco (*Coregonus artedi*) during hypolimnetic oxygenation of a deep, eutrophic lake, Amisk Lake, Alberta. *Can. J. Fish. Aquat. Sci.* 54, 2196–2206. doi: 10.1139/f97-118

Altieri, A. H., and Gedan, K. B. (2014). Climate change and dead zones. *Glob. Change Biol.* 21, 1395–1406. doi: 10.1111/gcb.12754

Appeltans, W., Hannouti, A., van Damme, S., Soetaert, K., Vanthomme, R., and Tackx, M. (2003). Zooplankton in the Schelde estuary (Belgium/The Netherlands). The distribution of Eurytemora affinis: effect of oxygen? *J. Plankton. Res.* 25, 1441–1445. doi: 10.1093/plankt/fbg101

Beauchamp, D. A., Cross, A. D., Armstrong, J. L., Myers, K. W., Moss, J. H., Boldt, J. L., et al. (2007). Bioenergetic responses by Pacific salmon to climate and ecosystem variation. *North Pac. Anadromous Fish Commission Bull.* 4, 257–269.

Beaugrand, G., Reid, P. C., Ibañez, F., Lindley, J. A., and Edwards, M. (2002). Reorganization of North Atlantic marine copepod diversity and climate. *Science* 296, 1692–1694. doi: 10.1126/science.1071329

Benson, B., and Krause, D. (1980). The concentration and isotopic fractionation of gases dissolved in freshwater in equilibrium with the atmosphere. 1. Oxygen. *Limnol. Oceanogr.* 25, 662–671. doi: 10.4319/lo.1980.25.4.0662

Benson, B. B., and Krause, D. (1984). The concentration and isotopic fractionation of oxygen dissolved in freshwater and seawater in equilibrium with the atmosphere. *Limnol. Oceanogr.* 29, 620–632. doi: 10.4319/lo.1984.29.3.0620

Bernreuther, M., Herrmann, J. P., Peck, M. A., and Temming, A. (2013). Growth energetics of juvenile herring, *Clupea harengus* L.: food conversion efficiency and temperature dependency of metabolic rate. *J. Appl. Ichthyol.* 29, 331–340. doi: 10.1016/j.marpolbul.2010.02.011

Bertrand, A., Chaigneau, A., Peraltilla, S., Ledesma, J., Graco, M., Monetti, F., et al. (2011). Oxygen: a fundamental property regulating pelagic ecosystem structure in the coastal southeastern tropical pacific. *PLoS One* 6:e29558. doi: 10.1371/journal.pone.0029558

Bianchi, T. S., DiMarco, S. F., Cowan, J. H., Hetland, R. D., Chapman, P., Day, J. W., et al. (2010). The science of hypoxia in the northern Gulf of Mexico: a review. *Sci. Total Environ.* 408, 1471–1484. doi: 10.1016/j.scitotenv.2009.11.047

Bode, M., Schukat, A., Hagen, W., and Auel, H. (2013). Predicting metabolic rates of calanoid copepods. *J. Exp. Mar. Biol. Ecol.* 444, 1–7. doi: 10.1016/j.jembe.2013.03.003

Bollens, S. M., and Frost, B. W. (1989). Predator-induced diel vertical migration in a planktonic copepod. *J. Plankton Res.* 11, 1047–1065. doi: 10.1093/plankt/11.5.1047

Brandt, S. B., Costantini, M., Kolesar, S., Ludsin, S. A., Mason, D. M., Rae, C. M., et al. (2011). Does hypoxia reduce habitat quality for Lake Erie walleye (*Sander vitreus*)? A bioenergetics perspective. *Can. J. Fish. Aquat. Sci.* 68, 857–879. doi: 10.1139/f2011-018

Brandt, S. B., Gerken, M., Hartman, K. J., and Demers, E. (2009). Effects of hypoxia on food consumption and growth of juvenile striped bass (*Morone saxatilis*). *J. Exp. Mar. Biol. Ecol.* 381, S143–S149. doi: 10.1016/j.jembe.2009.07.028

Breitburg, D. (2002). Effects of hypoxia, and the balance between hypoxia and enrichment, on coastal fishes and fisheries. *Estuaries* 25, 767–781. doi: 10.1007/BF02804904

Breitburg, D., Levin, L. A., Oschlies, A., Grégoire, M., Chavez, F. P., Conley, D. J., et al. (2018). Declining oxygen in the global ocean and coastal waters. *Science* 359, 7240. doi: 10.1126/science.aam7240

Breitburg, D. L., Adamack, A., Rose, K. A., Kolesar, S. E., Decker, B., Purcell, J. E., et al. (2003). The pattern and influence of low dissolved oxygen in the Patuxent River, a seasonally hypoxic estuary. *Estuaries* 26, 280–297. doi: 10.1007/BF02695967

Breitburg, D. L., Hondorp, D. W., Davias, L. A., and Diaz, R. J. (2009). Hypoxia, nitrogen, and fisheries: integrating effects across local and global landscapes. *Annu. Rev. Mar. Sci.* 1, 329–349. doi: 10.1146/annurev.marine.010908.163754

Breitburg, D. L., Loher, T., Pacey, C. A., and Gerstein, A. (1997). Varying effects of low dissolved oxygen on trophic interactions in an estuarine food web. *Ecol. Monogr.* 67, 489–507. doi: 10.1890/0012-9615(1997)067[0489:VEOLDO]2.0.CO;2

Breitburg, D. L., Pihl, L., and Kolesar, S. E. (2001). "Effects of low dissolved oxygen on the behavior, ecology and harvest of fishes: a comparison of the chesapeake bay and baltic-kattegat systems," in *The Effects of Hypoxia on Living Resources, with Emphasis on the Northern Gulf of Mexico Coastal Hypoxia: Consequences for Living Resources and Ecosystems*, eds N. C. Rabalais and E. Turner (Washington, DC: American Geophysical Union), 241–267.

Breitburg, D. L., Rose, K. A., and Cowan, J. H. (1999). Linking water quality to larval survival: predation mortality of fish larvae in an oxygen-stratified water column. *Mar. Ecol.* 178, 39–54. doi: 10.3354/meps178039

Brett, J. R. (1964). The respiratory metabolism and swimming performance of young sockeye salmon. *J. Fish. Board Can.* 21, 1183–1226. doi: 10.1139/f64-103

Brett, J. R. (1970). *Fish-the Energy Cost of Living*. Oregon: Oregon State University Press.

Broman, E., Brusin, M., Dopson, M., and Hylander, S. (2017). Oxygenation of anoxic sediment triggers hatching of copepod eggs. *Proc. R. Soc.* 282, 2015–2025. doi: 10.1098/rspb.2015.2025

Brown, J. H., Gillooly, J. F., Allen, A. P., Savage, V. M., and West, G. B. (2004). Toward a metabolic theory of ecology. *Ecology* 85, 1771–1789. doi: 10.1890/03-9000

Cahoon, L. B. (1981). Reproductive response of *Acartia tonsa* to variations in food ration and quality. *Deep Sea Res. Part A Oceanogr. Res. Papers* 28, 1215–1221. doi: 10.1016/0198-0149(81)90057-1

Carstensen, J., Andersen, J. H., Gustasson, B. G., and Conley, D. J. (2014). Deoxygenation of the Baltic Sea during the last century. *Proc. Natl. Acad. Sci. U.S.A.* 111, 5628–5633. doi: 10.1073/pnas.1323156111

Castellani, C., and Altunbas, Y. (2014). Seasonal change in acclimatized respiration rate of *Temora longicornis*. *Mar. Ecol. Prog. Ser.* 500, 83–101. doi: 10.3354/meps10661

Chapman, L. J., Chapman, C. A., Nordlie, F. G., and Rosenberger, A. E. (2002). Physiological refugia: swamps, hypoxia tolerance and maintenance of fish diversity in the Lake Victoria region. *Comp. Biochem. Physiol. A* 133, 421–437. doi: 10.1016/S1095-6433(02)00195-2

Chesney, E. J., Baltz, D. M., and Thomas, R. G. (2000). Louisiana estuarine and coastal fisheries and habitats: perspectives from a fish's eye view. *Ecol. Appl.* 10, 350–366. doi: 10.1890/1051-0761(2000)010[0350:LEACFA]2.0.CO;2

Cheung, W. W. L., Sarmiento, J. L., Dunne, J., Frölicher, T. L., Lam, V. W. Y., Deng Palomares, M. L., et al. (2012). Shrinking of fishes exacerbates impacts of global ocean changes on marine ecosystems. *Nat. Clim. Change* 3, 254–258. doi: 10.1038/NCLIMATE1691

Cheung, W. W. L., Watson, R., and Pauly, D. (2013). Signature of ocean warming in global fish catch. *Nature* 497, 365–368. doi: 10.1038/nature12156

Childress, J. J., and Seibel, B. A. (1998). Life at stable low oxygen levels: adaptations of animals to oceanic oxygen minimum layers. *J. Exp. Biol.* 201, 1223–1232.

Claireaux, G., and Lefrançois, C. (2007). Linking environmental variability and fish performance: integration through the concept of scope for activity. *Philos. Trans. R. Soc. B Biol. Sci.* 362, 2031–2041. doi: 10.1098/rstb.2007.2099

Clarke, A. (1991). What is cold adaptation and how should we measure it? *Am. Zool.* 31, 81–92. doi: 10.1093/icb/31.1.81

Clarke, A., and Johnston, N. M. (1999). Scaling of metabolic rate with body mass and temperature in teleost fish. *J. Anim. Ecol.* 68, 893–905. doi: 10.1046/j.1365-2656.1999.00337.x

Connett, R. J., Honig, C. R., Gayeski, T. E., and Brooks, G. A. (1990). Defining hypoxia: a systems view of VO2, glycolysis, energetics, and intracellular PO2. *J. Appl. Physiol.* 68, 833–842. doi: 10.1152/jappl.1990.68.3.833

Costantini, M., Ludsin, S. A., Mason, D. M., Zhang, X., Boicourt, W. C., and Brandt, S. B. (2008). Effect of hypoxia on habitat quality of striped bass (*Morone saxatilis*) in Chesapeake Bay. *Can. J. Fish. Aquat. Sci.* 65, 989–1002. doi: 10.1139/f08-021

Cowan, J. H. Jr., and Shaw, R. F. (2002). "Recruitment," in *Fishery Science: The Unique Contributions of Early Life Stages*, eds L. A. Fuiman and R. G. Werner (Bodmin: MPG Books), 88–111.

Craig, J. K., and Crowder, L. B. (2005). Hypoxia-induced habitat shifts and energetic consequences in Atlantic croaker and brown shrimp on the Gulf of Mexico shelf. *Mar. Ecol. Prog. Ser.* 294, 79–94. doi: 10.3354/meps294079

Daewel, U., Peck, M. A., Kühn, W., Michael, A., Alekseeva, I., and Schrum, C. (2008). Coupling ecosystem and individual-based models to simulate the influence of environmental variability on potential growth and survival of larval sprat *(Sprattus sprattus* L.) in the North Sea. *Fish. Oceanogr.* 17, 333–351. doi: 10.1111/j.1365-2419.2008.00482.x

Dam, H. G. (2013). Evolutionary adaptation of marine zooplankton to global change. *Annu. Rev. Mar. Sci.* 5, 349–370. doi: 10.1146/annurev-marine-121211-172229

Davis, J. C. (1975). Minimal dissolved oxygen requirements of aquatic life with emphasis on Canadian species: a review. *J. Fish. Board Can.* 32, 2295–2332. doi: 10.1139/f75-268

de Mutsert, K., Steenbeek, J., Lewis, K., Buszowski, J., Cowan, J. H. Jr., and Christensen, V. (2016). Exploring effects of hypoxia on fish and fisheries in the northern Gulf of Mexico using a dynamic spatially explicit ecosystem model. *Ecol. Model* 331, 142–150. doi: 10.1016/j.ecolmodel.2015.10.013

Decker, M. B., Breitburg, D. L., and Marcus, N. H. (2003). Geographical differences in behavioral responses to hypoxia: local adaptation to an anthropogenic stressor? *Ecol. Appl.* 13, 1104–1109. doi: 10.1890/1051-0761(2003)13[1104:GDIBRT]2.0.CO;2

Decker, M. B., Breitburg, D. L., and Purcell, J. E. (2004). Effects of low dissolved oxygen on zooplankton predation by the ctenophore *Mnemiopsis leidyi*. *Mar. Ecol. Prog. Ser.* 280, 163–172. doi: 10.3354/meps280163

Deevey, G. B. (1960). Relative effects of temperature and food on seasonal variations in length of marine copepods in some eastern American and western European waters. *Bull. Bingham Oceanogr. Collect.* 17, 54–86.

Deutsch, C., Ferrel, A., Seibel, B., Pörtner, H. O., and Huey, R. B. (2015). Climate change tightens a metabolic constraint on marine habitats. *Science* 348, 1132–1135. doi: 10.1126/science.aaa1605

Diaz, R. J., and Breitburg, D. L. (2009). The hypoxic environment. *Fish Physiol.* 27, 1–23. doi: 10.1016/S1546-5098(08)00001-0

Diaz, R. J., and Rosenberg, R. (2008). Spreading dead zones and consequences for marine ecosystems. *Science* 321, 926–929. doi: 10.1126/science.1156401

Eby, L. A., Crowder, L. B., McClellan, C. M., Peterson, C. H., and Powers, M. J. (2005). Habitat degradation from intermittent hypoxia: impacts on demersal fishes. *Mar. Ecol. Prog. Ser.* 291, 249–262. doi: 10.3354/meps291249

Ekau, W., Auel, H., Pörtner, H.-O., and Gilbert, D. (2010). Impacts of hypoxia on the structure and processes in pelagic communities (zooplankton, macro-invertebrates and fish). *Biogeosciences* 7, 1669–1699. doi: 10.5194/bg-7-1669-2010

Ekau, W., and Verheye, H. M. (2005). Influence of oceanographic fronts and low oxygen on the distribution of ichthyoplankton in the Benguela and southern Angola currents. *Afr. J. Mar. Sci.* 27, 629–639. doi: 10.2989/18142320509504123

Elliott, D. T., Pierson, J. J., and Roman, M. R. (2012). Relationship between environmental conditions and zooplankton community structure during

summer hypoxia in the northern Gulf of Mexico. *J. Plankton Res.* 34, 602–613. doi: 10.1093/plankt/fbs029

Elliott, D. T., Pierson, J. J., and Roman, M. R. (2013). Predicting the effects of coastal hypoxia on vital rates of the planktonic copepod *Acartia tonsa* Dana. *PLoS One* 8:e63987. doi: 10.1371/journal.pone.0063987

Evans, D. H., Claiborne, J. B., and Currie, S. (eds). (2014). *The Physiology of Fishes*, 4th Edn. Boca Raton, FL: CRC Press.

Forster, J., Hirst, A. G., and Woodward, G. (2011). Growth and development rates have different thermal responses. *Am. Nat.* 178, 668–678. doi: 10.1086/662174

Friedman, J. R., Condon, N. E., and Drazen, J. C. (2012). Gill surface area and metabolic enzyme activities of demersal fishes associated with the oxygen minimum zone off California. *Limnol. Oceanogr.* 57, 1701–1710. doi: 10.4319/lo.2012.57.6.1701

Frost, B. W., and Bollens, S. M. (1992). Variability of diel vertical migration in the marine planktonic copepod *Pseudocalanus newmani* in relation to its predators. *Can. J. Fish. Aquat. Sci.* 49, 1137–1141. doi: 10.1139/f92-126

Fry, F. E. (1957). "The aquatic respiration of fish," in *The Physiology of Fishes*, Vol. 1, ed. M. E. Brown (New York, NY: Academic Press), 1–63.

Fry, F. E. J. (1971). "The Effect of environmental factors on the physiology of fish," in *Fish Physiology*, Vol. 6, eds W. S. Hoar and D. J. Randall (New York, NY: Academic Press), 1–98.

Gamperl, A. K., and Driedzic, W. R. (2009). Cardiovascular function and cardiac metabolism. *Fish Physiol.* 27, 301–360. doi: 10.1016/S1546-5098(08)00007-1

Geist, S. J., Ekau, W., and Kunzmann, A. (2013). Energy demand of larval and juvenile Cape horse mackerels, *Trachurus capensis*, and indications for hypoxia tolerance as benefit in a changing environment. *Mar. Biol.* 160, 3221–3232. doi: 10.1007/s00227-013-2309-2

Geist, S. J., Kunzmann, A., Verheye, H. M., Eggert, A., Schukat, A., and Ekau, W. (2015). Distribution, feeding behaviour, and condition of Cape horse mackerel early life stages, *Trachurus capensis*, under different environmental conditions in the northern Benguela upwelling ecosystem. *ICES J. Mar. Sci.* 72, 543–557. doi: 10.1093/icesjms/fsu087

Giguere, L. A., Côté, B., and St-Pierre, J.-F. (1988). Metabolic rates scale isometrically in larval fishes. *Mar. Ecol. Prog. Ser.* 50, 13–19. doi: 10.3354/meps050013

Gillooly, J. F., Brown, J. H., West, G. B., Savage, V. M., and Charnov, E. L. (2001). Effects of size and temperature on metabolic rate. *Science* 293, 2248–2251. doi: 10.1126/science.1061967

Glaspie, C. N., Clouse, M., Adamack, A. T., Cha, Y. K., Ludsin, S. A., Mason, D. M., et al. (2018). Effect of hypoxia on diet of Atlantic bumper *Chloroscombrus chrysurus* in the Northern Gulf of Mexico. *Trans. Am. Fish. Soc.* 147, 740–748. doi: 10.1002/tafs.10063

Gnaiger, E. (1991). "Animal energetics at very low oxygen: information from calorimetry and respirometry," in *Physiological Strategies for Gas Exchange and Metabolism*, eds A. J. Woakes, M. K. Grieshaber, and C. R. Bridges (Cambridge: Cambridge University Press), 141–171.

Graham, B. A., Chan, F., Nielsen, K. J., Fox, D. S., Barth, J. A., Huyer, A., et al. (2004). Upwelling-driven nearshore hypoxia signals ecosystem and oceanographic changes in the northeast Pacific. *Nature* 429, 749–751. doi: 10.1038/nature02605

Graham, W. M. (2001). "Numerical increases and distributional shifts of *Chrysaora quinquecirrha* (Desor) and *Aurelia aurita* (Linné)(Cnidaria: Scyphozoa) in the northern Gulf of Mexico," in *Developments in Hydrobiology, Jellyfish Blooms: Ecological and Societal Importance*, eds J. E. Purcell, W. M. Graham, and H. J. Dumont (Dordrecht: Kluwer Academic Publishers), 97–111.

Grantham, B. A., Chan, F., Nielsen, K. J., Fox, D. S., Barth, J. A., Huyer, A., et al. (2004). Upwelling-driven nearshore hypoxia signals ecosystem and oceanographic changes in the northeast Pacific. *Nature* 429, 749–754. doi: 10.1038/nature02605

Grice, G. D., and Marcus, N. H. (1981). Dormant eggs of marine copepods. *Oceanogr. Mar. Biol. Annu. Rev.* 19, 125–140.

Hansen, B. W., and Drillet, G. (2013). Comparative oxygen consumption rates of subitaneous and delayed hatching eggs of the calanoid copepod *Acartia tonsa* (Dana). *J. Exp. Mar. Biol. Ecol.* 442, 66–96. doi: 10.1016/j.jembe.2013.01.029

Hays, G. C., Kennedy, H., and Frost, B. W. (2001). Individual variability in diel vertical migration of a marine copepod: why some individuals remain at depth when others migrate. *Limnol. Oceanogr.* 46, 2050–2054. doi: 10.4319/lo.2001.46.8.2050

Hazen, E. L., Craig, J. K., Good, C. P., and Crowder, L. B. (2009). Vertical distribution of fish biomass in hypoxic waters on the Gulf of Mexico shelf. *Mar. Ecol. Prog. Ser.* 375, 195–207. doi: 10.3354/meps07791

Herreid, C. F. (1980). Hypoxia in invertebrates. *Comp. Biochem. Physiol. A Physiol.* 67, 311–320. doi: 10.1016/S0300-9629(80)80002-8

Hirst, A. G., and Sheader, M. (1997). Are in situ weight specific growth rates body-size independent in marine planktonic copepods? Are-ananlysis of the global syntheses and a new empirical model. *Mar. Ecol. Prog. Ser.* 154, 155–165. doi: 10.3354/meps154155

Houde, E. D. (1989a). Comparative growth, mortality, and energetics of marine fish larvae: temperature and implied latitudinal effects. *Fish. Bull.* 87, 471–495.

Houde, E. D. (1989b). Subtleties and episodes in the early life of fishes. *J. Fish Biol.* 35(Suppl. A), 29–38. doi: 10.1111/j.1095-8649.1989.tb03043.x

Houde, E. D. (2008). Emerging from Hjort's shadow. *J. Northwest Atlantic Fish. Sci.* 41, 53–70. doi: 10.2960/J.v41.m634

Houde, E. D. (2016). "Recruitment variability," in *Reproductive Biology of Fishes: Implications for Assessment and Management*, 2nd Edn, eds T. Jakobsen, M. Fogarty, B. Megrey, and E. Moksness (Hoboken, NJ: John Wiley & Sons, Ltd), 98–187. doi: 10.1002/9781118752739.ch3

Houde, E. D., Chesney, E. J., Newberger, T. A., Vazquez, A. V., Zastrow, C. E., Morin, L. G., et al. (1989). *Population biology of bay anchovy in mid-Chesapeake Bay (Final Report to Maryland Sea Grant, Reference Number [UMCES]CBL 89-141)*. Solomons, MD: Chesapeake Biological Laboratory.

Houde, E. D., and Madon, S. P. (1995). *Fish in MEERC: Top-Down Controls-Bioenergetics Models and Experimental Protocols*. Cambridge, MD: University of Maryland Center for Environmental Science.

Houde, E. D., and Schekter, R. C. (1983). Oxygen uptake and comparative energetics among eggs and larvae of three subtropical marine fishes. *Mar. Biol.* 72, 283–293. doi: 10.1007/BF00396834

Houde, E. D., and Zastrow, C. E. (1993). Ecosystem-and taxon-specific dynamic and energetics properties of larval fish assemblages. *Bull. Mar. Sci.* 53, 290–335.

Howarth, R. W., Billen, G., Swaney, D., Townsend, A., Jaworski, N., Lajtha, K., et al. (1996). "Regional nitrogen budgets and riverine N and P fluxes for the drainages to the North Atlantic Ocean: Natural and human influences," in *Nitrogen Cycling in the North Atlantic Ocean and its Watersheds*, ed. R. W. Howarth (Dordrecht: Kluwer Academic Publishers), 75–139.

Huntley, M., and Brooks, E. R. (1982). Effects of age and food availability on diel vertical migration of *Calanus pacificus*. *Mar. Biol.* 71, 23–31. doi: 10.1007/BF00396989

Huntley, M. E., and Lopez, M. D. (1992). Temperature-dependent production of marine copepods: a global synthesis. *Am. Nat.* 140, 201–242. doi: 10.1086/285410

Ikeda, T. (1970). Relationship between respiration rate and body size in marine plankton animals as a function of the temperature of habitat. *Bull. Fac. Fish. Hokkaido Univ.* 21, 91–112.

Ikeda, T. (1985). Metabolic rates of epipelagic marine zooplankton as a function of body mass and temperature. *Mar. Biol.* 85, 1–11. doi: 10.1007/BF00396409

Ikeda, T., Sano, F., and Yamaguchi, A. (2007). Respiration in marine pelagic copepods: a global-bathymetric model. *Mar. Ecol. Prog. Ser.* 339, 215–219. doi: 10.3354/meps339215

Invidia, M., Sei, S., and Gorbi, G. (2004). Survival of the copepod *Acartia tonsa* following egg exposure to near anoxia and to sulfide at different pH values. *Mar. Ecol. Prog. Ser.* 276, 187–196. doi: 10.3354/meps276187

Isensee, K., Levin, L. A., Breitburg, D., Gregoire, M., Garçon, V., and Valdés, L. (2015). *The Ocean is Losing its Breath. Ocean and Climate, Scientific notes*. Available at: www.ocean-climate.org

Ito, S.-I., Rose, K., Megrey, B. A., Schweigert, J. F., Hay, D. E., Werner, F. E., et al. (2015). Geographic variation in Pacific herring growth in response to regime shifts in the North Pacific Ocean. *Prog. Oceanogr.* 138, 331–347. doi: 10.1016/j.pocean.2015.05.022

Jiang, X. D., Wang, G. H., and Li, S. J. (2006). Population dynamics of *Acartia pacifica* (Copepods: calanoida) the importance of benthic-pelagic coupling. *Acta Oceanol. Sin.* 25, 88–98.

Katajisto, T. (2004). Effects of anoxia and hypoxia on the dormancy and survival of subitaneous eggs of *Acartia bifilosa* (Copepods: Calanoidia). *Mar. Biol.* 145, 751–757.

Keister, J. E., Houde, E. D., and Breitburg, D. L. (2000). Effects of bottom-layer hypoxia on abundances and depth distributions of organisms in Patuxent River, Chesapeake Bay. *Mar. Ecol. Prog. Ser.* 205, 43–59. doi: 10.3354/meps205043

Keister, J. E., and Tuttle, L. B. (2013). Effects of bottom-layer hypoxia on spatial distributions and community structure of mesozooplankton in a sub-estuary of Puget Sound, Washington, USA. *Limnol. Oceanogr.* 58, 667–680. doi: 10.4319/lo.2013.58.2.0667

Kilduff, D. P., Botsford, L. W., and Teo, S. L. H. (2014). Spatial and temporal covariability in early ocean survival of Chinook salmon (*Oncorhynchus tshawytscha*) along the west coast of North America. *ICES J. Mar. Sci.* 71, 1671–1682. doi: 10.1093/icesjms/fsu031

Killen, S. S., Atkinson, D., and Glazier, D. S. (2010). The intraspecific scaling of metabolic rate with body mass in fishes depends on lifestyle and temperature. *Ecol. Lett.* 13, 184–193. doi: 10.1111/j.1461-0248.2009.01415.x

Kimmel, D. G., Boynton, W. R., and Roman, M. R. (2012). Long-term decline in the calanoid copepod *Acartia tonsa* in central Chesapeake Bay, USA: An indirect effect of eutrophication? *Estuar. Coast. Shelf Sci.* 101, 76–85. doi: 10.1016/j.ecss.2012.02.019

Kimmel, D. G., Miller, W. D., Harding, L. W. Jr., Houde, E. D., and Roman, M. R. (2009). Estuarine ecosystem response captured using a synoptic climatology. *Estuar. Coasts* 32, 403–409. doi: 10.1007/s12237-009-9147-y

Kiørboe, T., Munk, P., and Richardson, K. (1987). Respiration and growth of larval herring *Clupea harengus*: relation between specific dynamic action and growth efficiency. *Mar. Ecol. Prog. Ser.* 40, 1–10. doi: 10.3354/meps040001

Klumb, R. A., Bunch, K. L., Mills, E. L., Rudstam, L. G., Brown, G., Knauf, C., et al. (2004). Establishment of a metalimnetic oxygen refuge for zooplankton in a productive Lake Ontario embayment. *Ecol. Appl.* 14, 113–131. doi: 10.1890/02-5054

Knutsen, T., Melle, W., and Calise, L. (2001). Determining the mass density of marine copepods and their eggs with a critical focus on some of the previously used methods. *J. Plankton Res.* 23, 859–873. doi: 10.1093/plankt/23.8.859

Ludsin, S. A., Zhang, X., Brandt, S. B., Roman, M. R., Boicourt, W. C., Mason, D. M., et al. (2009). Hypoxia-avoidance by planktivorous fish in Chesapeake Bay: implications for food web interactions and fish recruitment. *J. Exp. Mar. Biol. Ecol.* 381, S121–S131. doi: 10.1016/j.jembe.2009.07.016

Luo, J., and Brandt, S. B. (1993). Bay anchovy *Anchoa mitchilli* production and consumption in mid-Chesapeake Bay based on a bioenergetics model and acoustic measures of fish abundance. *Mar. Ecol. Prog. Ser.* 98, 223–223. doi: 10.3354/meps098223

Lutz, R. V., Marcus, N. H., and Chanton, J. P. (1992). Effects of low oxygen concentrations on the hatching and viability of eggs of marine calanoid copepods. *Mar. Biol.* 114, 241–247. doi: 10.1007/BF00349525

Malone, T. C. (1991). "River flow, phytoplankton production and oxygen depletion in Chesapeake Bay," in *Modern and Ancient Continental Shelf Anoxia: An Overview*, Vol. 58, eds R. V. Tyson and T. H. Pearson (London: Geological Society of London Special Publications), 83–93. doi: 10.1144/GSL.SP.1991.058.01.06

Mandic, M., Todgham, A. E., and Richards, J. G. (2009). Mechanisms and evolution of hypoxia tolerance in fish. *Proc. R. Soc. B Biol. Sci.* 276, 735–744. doi: 10.1098/rspb.2008.1235

Marcus, N. H. (2001). "Zooplankton: responses to and consequences of hypoxia," in *Coastal Hypoxia: Consequences for Living Resources and Ecosystems*, eds N. N. Rabalais and R. E. Turner (Washington, DC: American Geophysical Union), doi: 10.1029/CE058p0049

Marcus, N. H., and Lutz, R. V. (1994). Effects of anoxia on the viability of subitaneous eggs of planktonic copepods. *Mar. Biol.* 121, 83–87. doi: 10.1007/BF00349476

Marcus, N. H., Lutz, R., Burnett, W., and Cable, P. (1994). Age, viability, and vertical distribution of zooplankton resting eggs from an anoxic basin: evidence of an egg bank. *Limnol. Oceanogr.* 39, 154–158. doi: 10.4319/lo.1994.39.1.0154

Marcus, N. H., Lutz, R. V., and Chanton, J. P. (1997). Impact of anoxia and sulfide on the viability of eggs of three planktonic copepods. *Mar. Ecol. Prog. Ser.* 146, 291–295. doi: 10.3354/meps146291

Marcus, N. H., Richmond, C., Sedlacek, C., Miller, G. A., and Oppert, C. (2004). Impact of hypoxia on the survival, egg production and population dynamics of *Acartia tonsa* Dana. *J. Exp. Mar. Biol. Ecol.* 301, 111–128. doi: 10.1016/j.jembe.2003.09.016

Marshall, S. M. (1973). Respiration and feeding in copepods. *Adv. Mar. Biol.* 11, 57–120. doi: 10.1016/S0065-2881(08)60268-0

Mauchline, J. (1998). *The Biology of Calanoid Copepods*. San Diego, CA: Academic Press.

McAllen, R., Taylor, A. C., and Davenport, J. (1999). The effects of temperature and oxygen partial pressure on the rate of oxygen consumption of the high-shore rock pool copepod *Tigriopus brevicornis*. *Comp. Biochem. Physiol. A Mol. Integr. Physiol.* 123, 195–202. doi: 10.1016/S1095-6433(99)00050-1

McBryan, T. L., Anttila, K., Healy, T. M., and Schulte, P. M. (2013). Responses to temperature and hypoxia as interacting stressors in fish: implications for adaptation to environmental change. *Integr. Comp. Biol.* 53, 648–659. doi: 10.1093/icb/ict066

McLaren, I. (1963). Effects of temperature on growth of zooplankton and the adaptive value of vertical migration. *J. Fish. Res. Board Can.* 20, 685–727. doi: 10.1139/f63-046

Miller, C. B., Johnson, J. K., and Heinle, D. R. (1977). Growth rules in the marine copepod genus Acartia. *Limnol. Oceanogr.* 22, 326–335. doi: 10.4319/lo.1977.22.2.0326

Muir, B. S. (1969). Gill dimensions as a function of fish size. *J. Fish. Res. Board. Can.* 26, 165–170. doi: 10.1139/f69-018

Nilsson, G. E., and Östlund-Nilsson, S. (2008). Does size matter for hypoxia tolerance in fish? *Biol. Rev.* 83, 173–189. doi: 10.1111/j.1469-185X.2008.00038.x

Nissling, A., and Vallin, L. (1996). The ability of Baltic cod eggs to maintain neutral buoyancy and the opportunity for survival in fluctuating conditions in the Baltic Sea. *J. Fish. Biol.* 48, 217–227. doi: 10.1111/j.1095-8649.1996.tb01114.x

Nixon, S. W. (1995). Coastal marine eutrophication: a definition, social causes, and future concerns. *Ophelia* 41, 199–219. doi: 10.1080/00785236.1995.10422044

North, E. W., and Houde, E. D. (2004). Distribution and transport of bay anchovy (*Anchoa mitchilli*) eggs and larvae in Chesapeake Bay. *Estuar. Coast. Shelf Sci.* 60, 409–429. doi: 10.1016/j.ecss.2004.01.011

Ohman, M. D. (1988). Behavioral responses of zooplankton to predation. *Bull. Mar. Sci.* 43, 530–550.

Pauly, D. (2010). *Gasping Fish and Panting Squids: Oxygen, Temperature and the Growth of Water-Breathing Animals. International Ecology Institute. Excellence in Ecology*, Vol. 22. Germany: Oldendorf/Luhe, 216.

Pearre, S. (2000). Long-term changes in diel vertical migration behavior: more ups and downs. *Mar. Ecol. Prog. Ser.* 197, 305–307. doi: 10.3354/meps197305

Peck, M. A., Huebert, K. B., and Llopiz, J. K. (2012). Intrinsic and extrinsic factors driving match-mismatch dynamics during the early life history of marine fishes. *Adv. Ecol. Res.* 47, 177–302. doi: 10.1016/B978-0-12-398315-2.00003-X

Perry, P. C. (2011). *The Role of Compensatory Dynamics AND Influence of Environmental Factors Across Multiple Spatial Scales in Structuring Fish Populations (Order No. 1510259). Available from ProQuest Dissertations & Theses Global. (1015396170).* Available at: https://search.proquest.com/docview/1015396170?accountid=28934

Pierson, J. J., Frost, B. W., Thoreson, D., Leising, A. W., Postel, J. R., and Nuwer, M. (2009a). Trapping migrating zooplankton. *Limnol. Oceanogr. Methods* 7, 334–346. doi: 10.4319/lom.2009.7.334

Pierson, J. J., Roman, M. R., Kimmel, D. G., Boicourt, W. C., and Zhang, X. (2009b). Quantifying changes in the vertical distribution of mesozooplankton in response to hypoxic bottom waters. *J. Exp. Mar. Biol. Ecol.* 381(Suppl.), S74–S79. doi: 10.1016/j.jembe.2009.07.013

Pierson, J. J., Slater, W. C. L., Elliott, D., and Roman, M. R. (2017). Synergistic effects of seasonal deoxygenation and temperature truncate copepod vertical migration and distribution. *Mar. Ecol. Prog. Ser.* 575, 57–68. doi: 10.3354/meps12205

Pörtner, H. O. (2010). Oxygen-and capacity-limitation of thermal tolerance: a matrix for integrating climate-related stressor effects in marine ecosystems. *J. Exp. Biol.* 213, 881–893. doi: 10.1242/jeb.037523

Pörtner, H. O., and Knust, R. (2007). Climate change affects marine fishes through the oxygen limitation of thermal tolerance. *Science* 315, 95–97. doi: 10.1126/science.1135471

Pothoven, S. A., Vanderploeg, H. A., Höök, T. O., and Ludsin, S. A. (2012). Hypoxia modifies planktivore-zooplankton interactions in Lake Erie. *Can. J. Fish. Aquat. Sci.* 69, 2018–2028. doi: 10.1139/cjfas-2012-0144

Prince, E. D., and Goodyear, C. P. (2006). Hypoxia-based habitat compression of tropical pelagic fishes. *Fish. Oceanogr.* 15, 451–464. doi: 10.1111/gcb.13799

Prince, E. D., Luo, J., Goodyear, C. P., Hoolihan, J. P., Snodgrass, D., Orbesen, E. S., et al. (2010). Ocean scale hypoxia-based habitat compression of Atlantic istiophorid billfishes. *Fish. Oceanogr.* 19, 448–462. doi: 10.1111/j.1365-2419.2010.00556.x

Prosser, C. L., and Brown, F. A. Jr. (1962). *Comparative Animal Physiology*. Philadelphia, PA: Saunders.

Qureshi, N. A., and Rabalais, N. N. (2001). "Distribution of zooplankton on a seasonally hypoxic continental shelf," in *Coastal Hypoxia: Consequences for Living Resources and Ecosystems*, Vol. 58, eds N. N. Rabalais and R. E. Turner (Washington, DC: American Geophysical Union), 61–76. doi: 10.1029/CE058p0061

Rabalais, N. N., Diaz, R. J., Levin, L. A., Turner, R. E., Gilbert, D., and Zhang, J. (2010). Dynamics and distribution of natural and human-caused hypoxia. *Mar. Ecol. Prog. Ser.* 445, 75–95. doi: 10.5194/bg-7-585-2010

Rabalais, N. N., Turner, R. E., Díaz, R. J., and Justiæ, D. (2009). Global change and eutrophication of coastal waters. *ICES J. Mar. Sci.* 66, 1528–1537. doi: 10.1093/icesjms/fsp047

Raymont, J. E. G., and Gauld, D. T. (1951). The respiration of some planktonic copepods. *J. Mar. Biol. Assoc. U. K.* 29, 681–693. doi: 10.1017/S0025315400052863

Richards, J. G. (2009). "Chapter 10 metabolic and molecular responses of fish to hypoxia," in *Fish Physiology*, Vol. 27, eds J. G. Richards, A. P. Farrell, and C. J. Brauner (Amsterdam: Elsevier), 443–485. doi: 10.1016/S1546-5098(08)00010-1

Richards, J. G. (2011). Physiological, behavioral and biochemical adaptations of intertidal fishes to hypoxia. *J. Exp. Biol.* 214, 191–199. doi: 10.1242/jeb.047951

Richmond, C., Marcus, N. H., Sedlacek, C., Miller, G. A., and Oppert, C. (2006). Hypoxia and seasonal temperature: short-term effects and long-term implications for *Acartia tonsa* dana. *J. Exp. Mar. Biol. Ecol.* 328, 177–196. doi: 10.1016/j.jembe.2005.07.004

Rogers, N. J., Urbina, M. A., Reardon, E. E., McKenzie, D. J., and Wilson, R. W. (2016). A new analysis on hypoxia tolerance in fishes using a database of critical oxygen level (Pcrit). *Conserv. Physiol.* 4:cow12. doi: 10.1093/conphys/cow012

Roman, M. R., Ashton, K. A., and Gauzens, A. L. (1988). "Day/night differences in the grazing impact of marine copepods," in *Developments in Hydrobiology: Biology of Copepods*, eds G. Boxshall and H. K. Schminke (Dordrecht: Kluwer Academic Publishers), 21–30.

Roman, M. R., Gauzens, A. L., Rhinehart, W. K., and White, J. R. (1993). Effects of low oxygen waters on Chesapeake Bay zooplankton. *Limnol. Oceanogr.* 38, 1603–1614. doi: 10.4319/lo.1993.38.8.1603

Roman, M. R., Pierson, J. J., Kimmel, D. G., Boicourt, W. C., and Zhang, X. (2012). Impacts of hypoxia on zooplankton spatial distributions in the northern Gulf of Mexico. *Estuar. Coasts* 35, 1261–1269. doi: 10.1007/s12237-012-9531-x

Rombough, P. J. (1988). Growth, aerobic metabolism, and dissolved oxygen requirements of embryos and alevins of steelhead, *Salmo gairdneri*. *Can. J. Zool.* 66, 651–660. doi: 10.1139/z88-097

Sato, M., Horne, J. K., Parker-Stetter, S. L., Essington, T. E., Keister, J. E., Moriarty, P. E., et al. (2016). Impacts of moderate hypoxia on fish and zooplankton prey distributions in a coastal fjord. *Mar. Ecol. Prog. Ser.* 560, 57–72. doi: 10.3354/meps11910

Searcy, S. P., Eggleston, D. B., and Hare, J. A. (2007). Environmental influences on the relationship between juvenile and larval growth of Atlantic croaker Micropogonias undulatus. *Mar. Ecol. Prog. Ser.* 349, 81–88. doi: 10.3354/meps07124

Seibel, B. A. (2011). Critical oxygen levels and metabolic suppression in oceanic oxygen minimum zones. *J. Exp. Biol.* 214, 326–336. doi: 10.1242/jeb.049171

Shang, E. H., and Wu, R. S. (2004). Aquatic hypoxia is a teratogen and affects fish embryonic development. *Environ. Sci. Technol.* 38, 4763–4767. doi: 10.1021/es0496423

Shelford, V. E., and Allee, W. C. (1913). The reactions of fishes to gradients of dissolved atmospheric gases. *J. Exp. Zool.* 14, 207–266. doi: 10.1002/jez.1400140203

Speers-Roesch, B., Mandic, M., Groom, D. J. E., and Richards, J. G. (2013). Critical oxygen tensions as predictors of hypoxia tolerance and tissue metabolic responses during hypoxia exposure in fishes. *J. Exp. Mar. Biol. Ecol.* 449, 239–249. doi: 10.1016/j.jembe.2013.10.006

Speers-Roesch, B., Richards, J. G., Brauner, C. J., Farrell, A. P., Hickey, A. J., Wang, Y. S., et al. (2012). Hypoxia tolerance in elasmobranchs. I. Critical oxygen tension as a measure of blood oxygen transport during hypoxia exposure. *J. Exp. Biol.* 215, 93–102. doi: 10.1242/jeb.059642

Stalder, L. C., and Marcus, N. H. (1997). Zooplankton responses to hypoxia: behavioral patterns and survival of three species of calanoid copepods. *Mar. Biol.* 127, 599–607. doi: 10.1007/s002270050050

Tanaka, H., Aoki, I., and Ohshimo, S. (2006). Feeding habits and gill raker morphology of three planktivorous pelagic fish species off the coast of northern and western Kyushu in summer. *J. Fish Biol.* 68, 1041–1061. doi: 10.1111/j.0022-1112.2006.00988.x

Tang, K. W., Dam, H. G., and Feinberg, L. R. (1998). The relative importance of egg production rate, hatching success, hatching duration and egg sinking in population recruitment of two species of marine copepods. *J. Plankton Res.* 20, 1971–1987. doi: 10.1093/plankt/20.10.1971

Taylor, J. C., and Miller, J. M. (2001). Physiological performance of juvenile southern flounder, Paralichthys lethostigma (Jordan and Gilbert, 1884), in chronic and episodic hypoxia. *J. Exp. Mar. Biol. Ecol.* 258, 195–214. doi: 10.1016/S0022-0981(01)00215-5

Taylor, J. C., and Rand, P. S. (2003). Spatial overlap and distribution of anchovies (Anchoa spp.) and copepods in a shallow stratified estuary. *Acoust. Fish. Aquat. Ecol.* 16, 191–196. doi: 10.1016/S0990-7440(03)00012-3

Taylor, J. C., Rand, P. S., and Jenkins, J. (2007). Swimming behavior of juvenile anchovies (Anchoa spp.) in an episodically hypoxic estuary: implications for individual energetics and trophic dynamics. *Mar. Biol.* 152, 939–957. doi: 10.1007/s00227-007-0745-6

Teuber, L., Kiko, R., Séguin, F., and Auel, H. (2013). Respiration rates of tropical Atlantic copepods in relation to the oxygen minimum zone. *J. Exp. Mar. Biol. Ecol.* 448, 28–36. doi: 10.1371/journal.pone.0077590

Thomas, P., and Rahman, S. (2012). Extensive reproductive disruption, ovarian masculinization and aromatase suppression in Atlantic Croaker in the northern Gulf of Mexico hypoxic zone. *Proc. R. Soc. B* 1726, 28–38. doi: 10.1098/rspb.2011.0529

Thronson, A., and Quigg, A. (2008). Fifty-five years of fish kills in Coastal Texas. *Estuar. Coasts.* 31, 802–813. doi: 10.1007/sl2237-008-9056-5

Turner, R. E. (2001). "Some effects of nutrient loading and hypoxia on pelagic and demersal marine food webs," in *Coastal Hypoxia: Consequences for Living Resources and Ecosystems, Coastal and Estuarine Studies*, Vol. 58, eds N. N. Rabalais and R. E. Turner (Washington, DC: American Geophysical Union), 371–398.

Turner, R. E., Rabalais, N. N., and Justic, D. (2008). Gulf of Mexico hypoxia: alternate states and a legacy. *Environ. Sci. Technol.* 42, 2323–2327. doi: 10.1021/es071617k

Uye, S. (1980). Development of neritic copepods *Acartia clausi* and *A. steuri*. 1. Some environmental factors affecting egg development and the nature of resting eggs. *Bull. Plankton Soc. Jpn.* 27, 1–9.

Uye, S. (1994). "Replacement of large copepods by small ones with eutrophication of embayments: cause and consequence," in *Developments in Hydrobiology: Ecology and Morphology of Copepods*, Vol. 102, eds F. D. Ferrari and B. P. Bradley (Dordrecht: Kluwer Academic Publishers), 513–519. doi: 10.1007/978-94-017-1347-4_64

Uye, S. I. (1982). Length-weight relationships of important zooplankton from the Inland Sea of Japan. *J. Oceanogr. Soc. Jpn.* 38, 149–158. doi: 10.1007/BF02110286

Vanderploeg, H. A., Ludsin, S. A., Ruberg, S. A., Hook, T. O., Pothoven, S. A., Brandt, S. B., et al. (2009). Hypoxia affects spatial distributions and overlap of pelagic fish, zooplankton, and phytoplankton in Lake Erie. *J. Exp. Mar. Biol. Ecol.* 381, S92–S107. doi: 10.1016/j.jembe.2009.07.027

Vaquer-Sunyer, R., and Duarte, C. M. (2008). Thresholds of hypoxia for marine biodiversity. *Proc. Natl. Acad. Sci. U.S.A.* 105, 15452–15457. doi: 10.1073/pnas.0803833105

Vaquer-Sunyer, R., and Duarte, C. M. (2011). Temperature effects on oxygen thresholds for hypoxia in marine benthic organisms. *Glob. Change Biol.* 17, 1788–1797. doi: 10.1111/j.1365-2486.2010.02343.x

Vargo, S. L., and Sastry, A. N. (1977). Acute temperature and low dissolved oxygen tolerances of brachyuran crab (*Cancer irroratus*) larvae. *Mar. Biol.* 40, 165–171. doi: 10.1007/BF00396263

Vazquez, A. V., and Houde, E. D. (1989). "Chapter 6. Energetics of bay anchovy, Anchoa mitchilli: ration levels and temperature effects," in *Population biology*

of bay anchovy in mid-Chesapeake Bay, eds E. D. Houde et al. (Solomons, MD: Center for Environmental and Estuarine Studies, Chesapeake Biological Laboratory), 108–148.

Vejřík, L., Matějíčková, I., Jůza, T., Frouzová, J., Seïa, J., Blabolil, P., et al. (2016). Small fish use the hypoxic pelagic zone as a refuge from predators. *Fresh. Biol.* 61, 899–913. doi: 10.1111/fwb.12753

Verberk, W. C., Bilton, D. T., Calosi, P., and Spicer, J. I. (2011). Oxygen supply in aquatic ectotherms: partial pressure and solubility together explain biodiversity and size patterns. *Ecology* 92, 1565–1572. doi: 10.1890/10-2369.1

Wang, S. B. (1998). Comparative studies of the life history and production potential of bay anchovy *Anchoa mitchilli* and northern anchovy *Engraulis mordax*: an individual-based modeling approach. *Diss. Abstr. Int. B Sci. Eng.* 59, 4555.

Wang, T., Lefevre, S., Thanh Huong, D. T., Cong, N., and van Bayley, M. (2009). "Chapter 8 The Effects of Hypoxia On Growth and Digestion," in *Fish Physiology*, Vol. 27, eds J. G. Richards, A. P. Farrell, and C. J. Brauner (Amsterdam: Academic Press), 361–396.

Wannamaker, C. M., and Rice, J. A. (2000). Effects of hypoxia on movements and behavior of selected estuarine organisms from the southeastern United States. *J. Exp. Mar. Biol. Ecol.* 249, 145–163. doi: 10.1016/S0022-0981(00)00160-X

Webster, C. N., Hansson, S., Didrikas, T., Gorokhova, E., Peltonen, H., Brierley, A. S., et al. (2015). Stuck between a rock and a hard place: zooplankton vertical distribution and hypoxia in the Gulf of Finland. Baltic Sea. *Mar. Biol.* 162, 1429–1440. doi: 10.1007/s00227-015-2679-8

Wells, M. M. (1913). The resistance of fishes to different concentrations and combinations of oxygen and carbon dioxide. *Biol. Bull.* 25, 323–347. doi: 10.1086/BBLv25n6p323

Wells, R. M. (2009). "Blood-Gas Transport and Hemoglobin Function: Adaptations for Functional and Environmental Hypoxia," in *Fish Physiology*, Vol. 27, eds J. G. Richards, A. P. Farrell, and C. J. Brauner (Amsterdam: Academic Press), 255–299.

Wu, R. S. (2002). Hypoxia: from molecular responses to ecosystem responses. *Mar. Pollut. Bull.* 45, 35–45. doi: 10.1016/S0025-326X(02)00061-9

Wu, R. S. (2009). "Effects of hypoxia on fish reproduction and development," in *Fish Physiology*, Vol. 27, eds J. G. Richards, A. P. Farrell, and C. J. Brauner (Amsterdam: Academic Press), 79–141.

Zhang, C., Zhang, W., Ni, X., Zhao, Y., Huang, L., and Xiao, T. (2015). Influence of different water masses on planktonic ciliate distribution on the East China Sea shelf. *J. Mar. Syst.* 141, 98–111. doi: 10.1016/j.jmarsys.2014.09.003

Zhang, H., Ludsin, S. A., Mason, D. M., Adamack, A. T., Brandt, S. B., Zhang, X., et al. (2009). Hypoxia-driven changes in the behavior and spatial distribution of pelagic fish and mesozooplankton in the northern Gulf of Mexico. *J. Exp. Mar. Biol. Ecol.* 381, S80–S91. doi: 10.1016/j.jembe.2009.07.014

Zhang, H., Mason, D. M., Stow, C. A., Adamack, A. T., Brandt, S. B., Zhang, X., et al. (2014). Effects of hypoxia on habitat quality of pelagic planktivorous fishes in the northern Gulf of Mexico. *Mar. Ecol. Prog. Ser.* 505, 209–226. doi: 10.3354/meps10768

Zhang, X., Roman, M., Kimmel, D., McGilliard, C., and Boicourt, W. (2006). Spatial variability in the plankton biomass and hydrographic variables along an axial transect in Chesapeake Bay. *J. Geophys. Res.* 111:CO5S11. doi: 10.1029/2005JC003085

Conflict of Interest Statement: The authors declare that the research was conducted in the absence of any commercial or financial relationships that could be construed as a potential conflict of interest.

frontiers in Marine Science

ORIGINAL RESEARCH
published: 22 March 2019
doi: 10.3389/fmars.2019.00132

Sampling and Processing Methods Impact Microbial Community Structure and Potential Activity in a Seasonally Anoxic Fjord: Saanich Inlet, British Columbia

*Mónica Torres-Beltrán[1], Andreas Mueller[1], Melanie Scofield[1], Maria G. Pachiadaki[2,3], Craig Taylor[3], Kateryna Tyshchenko[4], Céline Michiels[1], Phyllis Lam[5,6], Osvaldo Ulloa[6,7], Klaus Jürgens[6,8], Jung-Ho Hyun[6,9], Virginia P. Edgcomb[2,6], Sean A. Crowe[1,6,10,11] and Steven J. Hallam[1,6,11,12,13]**

[1] Department of Microbiology and Immunology, The University of British Columbia, Vancouver, BC, Canada, [2] Bigelow Laboratory for Ocean Sciences, Boothbay, ME, United States, [3] Woods Hole Oceanographic Institute, Woods Hole, MA, United States, [4] Terry Fox Laboratory, BC Cancer Agency, Vancouver, BC, Canada, [5] Department of Ocean and Earth Science, National Oceanography Centre, University of Southampton, Southampton, United Kingdom, [6] The Scientific Committee on Oceanographic Research, Working Group 144, Vancouver, BC, Canada, [7] Departamento de Oceanografía and Instituto Milenio de Oceanografía, Universidad Concepción, Concepción, Chile, [8] Department of Biological Oceanography, Leibniz Institute for Baltic Sea Research, Warnemünde, Germany, [9] Department of Marine Sciences and Convergent Technology, Hanyang University, Seoul, South Korea, [10] Department of Earth, Ocean and Atmospheric Sciences, The University of British Columbia, Vancouver, BC, Canada, [11] ECOSCOPE Training Program, The University of British Columbia, Vancouver, BC, Canada, [12] Graduate Program in Bioinformatics, The University of British Columbia, Vancouver, BC, Canada, [13] Peter Wall Institute for Advanced Studies, The University of British Columbia, Vancouver, BC, Canada

OPEN ACCESS

Edited by:
Raquel Vaquer-Sunyer, Instituto Mediterráneo de Estudios Avanzados (IMEDEA), Spain

Reviewed by:
Dennis A. Bazylinski, University of Nevada, Las Vegas, United States
Jun Sun, Tianjin University of Science and Technology, China
Carolin Regina Löscher, University of Southern Denmark, Denmark

***Correspondence:**
Steven J. Hallam
shallam@mail.ubc.ca

Specialty section:
This article was submitted to Marine Biogeochemistry, a section of the journal Frontiers in Marine Science

Received: *10 October 2018*
Accepted: *04 March 2019*
Published: *22 March 2019*

Citation:
Torres-Beltrán M, Mueller A, Scofield M, Pachiadaki MG, Taylor C, Tyshchenko K, Michiels C, Lam P, Ulloa O, Jürgens K, Hyun J-H, Edgcomb VP, Crowe SA and Hallam SJ (2019) Sampling and Processing Methods Impact Microbial Community Structure and Potential Activity in a Seasonally Anoxic Fjord: Saanich Inlet, British Columbia. Front. Mar. Sci. 6:132. doi: 10.3389/fmars.2019.00132

The Scientific Committee on Oceanographic Research (SCOR) Working Group 144 *Microbial Community Responses to Ocean Deoxygenation* workshop held in Vancouver, B.C on July 2014 had the primary objective of initiating a process to standardize operating procedures for compatible process rate and multi-omic (DNA, RNA, protein, and metabolite) data collection in marine oxygen minimum zones and other oxygen depleted waters. Workshop attendees participated in practical sampling and experimental activities in Saanich Inlet, British Columbia, a seasonally anoxic fjord. Experiments were designed to compare and cross-calibrate *in situ* versus bottle sampling methods to determine effects on microbial community structure and potential activity when using different filter combinations, filtration methods, and sample volumes. Resulting biomass was preserved for small subunit ribosomal RNA (SSU or 16S rRNA) and SSU rRNA gene (rDNA) amplicon sequencing followed by downstream statistical and visual analyses. Results from these analyses showed that significant community shifts occurred between *in situ* versus on ship processed samples. For example, Bacteroidetes, Alphaproteobacteria, and Opisthokonta associated with on-ship filtration onto 0.4 μm filters increased fivefold compared to on-ship in-line 0.22 μm filters or 0.4 μm filters processed and preserved *in situ*. In contrast, Planctomycetes associated with 0.4 μm *in situ* filters increased fivefold compared to on-ship filtration onto 0.4 μm filters and on-ship in-line 0.22 μm filters. In addition, candidate divisions and Chloroflexi

were primarily recovered when filtered onto 0.4 μm filters *in situ*. Results based on rRNA:rDNA ratios for microbial indicator groups revealed previously unrecognized roles of candidate divisions, Desulfarculales, and Desulfuromandales in sulfur cycling, carbon fixation and fermentation within anoxic basin waters. Taken together, filter size and *in situ* versus on-ship filtration had the largest impact on recovery of microbial groups with the potential to influence downstream metabolic reconstruction and process rate measurements. These observations highlight the need for establishing standardized and reproducible techniques that facilitate cross-scale comparisons and more accurately assess *in situ* activities of microbial communities.

Keywords: microbial ecology, oxygen minimum zone, standards of practice, filtration methods, amplicon sequencing

INTRODUCTION

Among the many environmental perturbations associated with global climate change is a decrease in dissolved oxygen (O_2) concentrations in coastal and interior regions of the ocean. As dissolved O_2 concentrations decline, oxygen minimum zones (OMZs) expand (Arrigo, 2005; Whitney et al., 2007; Diaz and Rosenberg, 2008; Stramma et al., 2008; Paulmier and Ruiz-Pino, 2009; Keeling et al., 2010; Schmidtko et al., 2017). The expansion of OMZs shifts energy away from higher trophic levels, impacting ecosystem functions and services through changes in food web structure and biodiversity (Diaz and Rosenberg, 2008; Stramma et al., 2010; Gruber, 2011; Bijma et al., 2013; Levin and Breitburg, 2015; Gallo and Levin, 2016). These changes are reflected in an increasing role for microbial metabolism in nutrient and energy cycling through the use of alternative terminal electron acceptors (TEAs) including nitrate (NO_3^-), sulfate (SO_4^{2-}), and carbon dioxide (CO_2) (Diaz and Rosenberg, 2008). Among other changes, the use of these TEAs in respiration results in fixed nitrogen loss and the production of climate active trace gasses including nitrous oxide (N_2O) and methane (CH_4) with potential feedback on the climate system (Lam et al., 2009; Ward et al., 2009; Canfield et al., 2010; Naqvi et al., 2010; Lam and Kuypers, 2011). Current research efforts are defining the interaction networks underlying microbial metabolism in OMZs and generating new insights into coupled biogeochemical processes driving nutrient and energy flow among and between trophic levels on local scales (Hawley et al., 2014; Cram et al., 2015; Louca et al., 2016; Torres-Beltrán et al., 2016). However, marine microbial responses at the individual, population and community levels to OMZ expansion, and the concomitant impact of these responses on global-scale nutrient and energy cycling remain poorly constrained due in part to inconsistent, and perhaps inadequate sampling methods that limit cross-scale comparisons between locations and may cloud our view of *in situ* microbial processes.

Over the past 20 years, oceanographic researchers have increasingly used multi-omic (DNA, RNA, protein, and metabolites) methods to determine microbial community structure, function and activity in relation to physical, chemical, and biological oceanographic processes (**Supplementary Figure 1**). While large-scale microbial community composition patterns appear to be consistent between studies with respect to major taxonomic groups and water column compartments, our ecological perspective is blurred by inconsistencies in marker gene selection and coverage.

Recent reports have begun to evaluate potential biases in OMZ microbial community structure, function, and activity with emphasis on sample collection and filtration methods. Water column sampling typically involves the use of collection bottles (Niskin or GO-FLO) and on-ship filtration to concentrate microbial biomass into two primary size fractions, a larger particle associated (>1–30 μm) and smaller free-living (<1–0.2 μm) fraction (Padilla et al., 2015). Size fractionation surveys conducted in the Eastern Tropical South Pacific (ETSP) and Eastern Tropical North Pacific (ETNP) showed differential microbial community structure and nitrogen cycling functional gene distribution and expression across size fractions (Ganesh et al., 2014, 2015). In addition to filter fractionation, Padilla et al. (2015) working in the Manzanillo Mexico OMZ observed variation in microbial community structure based on filtered water volume. Most recently, a study in the Cariaco Basin observed that particles sinking on timescales relevant to sample collection and filtration can influence microbial community structure in Niskin or GO-FLO bottles (Suter et al., 2016). A comparison of metatranscriptome data obtained from bathypelagic Mediterranean Sea samples collected using Niskin bottles followed by shipboard filtration vs. filtration and fixation *in situ* found significant shifts in gene expression for particular groups of microorganisms (Edgcomb et al., 2016). These findings reinforce the need for continued evaluation of the methods used for sample collection and processing. This is particularly relevant when conducting process rate measurements in which community structure variation due to bottle effects can result in potential rates that do not reflect *in situ* microbial activity (Stewart et al., 2012a).

The Scientific Committee on Oceanographic Research (SCOR) initiated Working Group 144 *Microbial Community Responses to Ocean Deoxygenation* to investigate and recommend community standards of practice for compatible multi-omic and process rate measurements in OMZs and other oxygen deficient waters in order to facilitate and promote future cross-scale comparisons that more accurately reflect *in situ* microbial

community structure, function, and activity[1]. The inaugural workshop of SCOR Working Group 144 was held in British Columbia Canada during the week of July 14, 2014. During the workshop, attendees participated in practical sampling and experimental activities in Saanich Inlet (SI), a seasonally anoxic fjord on the coast of Vancouver Island, British Columbia. During spring and summer months, restricted circulation and high levels of primary production lead to progressive deoxygenation and the accumulation of methane (CH_4), ammonium (NH_4^+), and hydrogen sulfide (H_2S) in deep basin waters. In late summer and fall, oxygenated nutrient rich waters flow into the inlet from the Haro Strait "renewing" deep basin waters (Carter, 1932, 1934; Herlinveaux, 1962; Anderson and Devol, 1973; Zaikova et al., 2010; Walsh and Hallam, 2011; Torres-Beltrán et al., 2017). The seasonal pattern of water column anoxia and renewal makes the inlet a model ecosystem for evaluating changes in microbial community structure, function and activity in response to changing levels of water column deoxygenation. Saanich Inlet is thus a tractable environment to test different water sample collection and processing methods relevant to OMZs.

Experiments carried out during the workshop were designed to compare and cross-calibrate *in situ* sampling with conventional bottle sampling methods including the use of different filter combinations and sample volumes. Here, we describe the effect of these parameters on microbial community structure and potential activity and discuss community standards development to facilitate and promote future cross-scale comparisons that more accurately reflect *in situ* microbial community structure, function and activity in OMZs and other oxygen deficient waters.

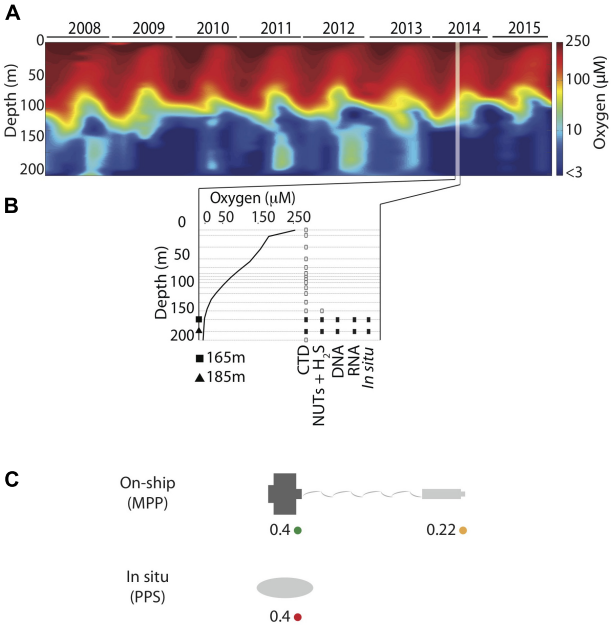

FIGURE 1 | (A) Saanich Inlet time-series CTD oxygen (O_2) concentration contour (2008–2015) showing seasonal water column stratification and deep-water renewal events. **(B)** Sample inventory for SCOR workshop held in July 2014 includes CTD, nutrients (NO_3, NO_2, NH_4, PO_4, and SiO_2), hydrogen sulfide (H_2S), and multi-omic on-ship and *in situ* data. Data shown in this survey is depicted as solid symbols (*in situ* and on ship DNA and RNA (rectangle) collected at 165 (square) and 185 (triangle) meters. **(C)** Schematic model for filter combinations and filtration methods showing on-ship [MasterFlex peristaltic pump (MPP)] filtration onto 0.4 µm pre-filters (green), filtration onto 0.22 µm filters with in-line pre-filtration using the 0.4 µm pre-filters (yellow), and *in situ* filtration (PPS) onto 0.4 µm filters without pre-filtration (red).

MATERIALS AND METHODS

Environmental Sampling

Sampling methods used during the workshop were similar to those previously described (Zaikova et al., 2010; Walsh and Hallam, 2011; Torres-Beltrán et al., 2017). In brief, waters for analysis of dissolved gasses and nutrients were collected aboard the *MSV John Strickland* at station SI03 (48° 35.500 N, 123° 30.300 W) on July 16, 2014 using 12 L GO-FLO bottles attached in series to a steel winch cable and closed at depth via messenger. A CTD was attached to the cable below the bottles and was used to measure temperature, salinity, PAR/Irradiance, fluorescence, conductivity, density, and dissolved O_2 at 165 and 185 m depth intervals spanning anoxic (<1 µmol O_2 kg^1) and sulfidic water column compartments (**Figures 1A,B** and **Supplementary Table 2**).

Workshop Microbial Biomass Collection

For comparison to Niskin bottle sampling, water samples were collected and preserved *in situ* in duplicate using a McLane Phytoplankton Sampler (PPS) system deployed at 165 and 185 m depth intervals spanning anoxic (<1 µmol O_2 kg^1) and sulfidic water column compartments (**Figure 1B**). Sample volumes of 2 L were filtered onto 0.4 µm GFF membrane filters (47 mm diameter). Filter biomass was directly frozen and stored at −80°C for downstream DNA and RNA extraction. On-ship samples were collected using Niskin bottles from 165 to 185 m as described above (**Figure 1B**) and concentrated for DNA and RNA extractions with a MasterFlex peristaltic pump (MPP) (∼60 mL min^{-1}). Biomass was concentrated using different filter combinations (0.4 µm polycarbonate or 2.7 µm GF/D pre-filters in-line with a 0.22 µm Sterivex polycarbonate filter cartridge) (**Figure 1C**) and water volumes (250 ml, 500 ml, 1 and 2 L) (**Table 1**) to test significance of sample volume and filtration method, on community structure (see section "Statistical Analysis and Data Visualization"). Filtered biomass on Sterivex filters was preserved in 1.8 ml of sucrose lysis buffer (DNA analyses) or RNA later (RNA analyses) prior to storage at −80°C. Pre-filters (0.4 µm only) were also preserved in 1.8 ml of lysis buffer (DNA) or RNA later (RNA) prior to storage at −80°C.

Time-Series Microbial Biomass Collection

Time-series samples were collected as previously described (Walsh et al., 2009; Zaikova et al., 2010;

[1]http://omz.microbiology.ubc.ca/page4/index.html

TABLE 1 | Biomass collection scheme for DNA and RNA *in situ* and on-ship samples.

Filtration type	Pre-filter size (μm)	Collection filter size (μm)	Volume (L)	Molecular sample
In situ		0.4	2	DNA, RNA
On ship	0.4	0.22	2	DNA, RNA*
			1.5	
			0.5	
			0.25	
	2.7	0.22	2	DNA
			1.5	
			0.5	
			0.25	

**RNA samples used in the present study were only from 0.25, 0.5, and 2 L on-ship 0.22 μm filters with in-line 0.4 μm prefilters.*

Torres-Beltrán et al., 2016; Hawley et al., 2017). Briefly, large volume (10 L) samples were collected from February 2006 to February 2011 at six depths (10, 100, 120, 135, 150, and 200 m) and filtered with an in-line 2.7 μm GDF glass fiber pre-filter onto a 0.22 μm Sterivex polycarbonate cartridge filter. High-resolution (2 L) samples were collected from May 2008 to July 2010 from 16 depths (10 to 200 m) and filtered directly onto a 0.22 μm Sterivex polycarbonate cartridge filter. All time-series samples were preserved in 1.8 ml of sucrose lysis buffer (DNA) prior to storage at −80°C.

Nucleic Acid Extraction

Genomic DNA was extracted from Sterivex filters (**Table 1**) as previously described (Zaikova et al., 2010; Hawley et al., 2017). Briefly, after defrosting Sterivex on ice, 100 μl lysozyme (0.125 mg ml^{-1}; Sigma) and 20 μl of RNAse (1 μl ml^{-1}; Thermo Fisher) were added and incubated at 37°C for 1 h with rotation followed by addition of 50 μl Proteinase K (Sigma) and 100 μl 20% SDS and incubation at 55°C for 2 h with rotation. Lysate was removed by pushing through with a syringe into 15 mL falcon tube (Corning) and with an additional rinse of 1 mL of lysis buffer. Filtrate was subject to chloroform extraction (Sigma) and the aqueous layer was collected and loaded onto a 10 K 15 ml Amicon filter cartridge (Millipore), washed three times with TE buffer (pH 8.0) and concentrated to a final volume of between 150 and 400 μl. Total DNA concentration was determined by PicoGreen assay (Life Technologies) and genomic DNA quality determined by visualization on 0.8% agarose gel (overnight at 16V). Genomic DNA was extracted from 0.4 to 2.7 μm pre-filters (**Table 1**) as follows. The filter was cut in half using sterile scissors. One half was minced into smaller pieces and used for DNA extraction while the remaining half was stored at −80°C. Filter pieces were transferred to a 15 mL falcon tube followed by addition of 1.8 mL lysis buffer and 150 μL 20% SDS. In order to ensure biomass removal from the filter, 3 and 2 mm zirconium beads were added for bead beating using a vortex mixer at maximum speed. Filters were shaken for a total of 4 min, in two 2-min laps then subjected to chloroform extraction and processed as described above for Sterivex filters.

Total RNA was extracted from Sterivex filters (**Table 1**) using the mirVana Isolation kit (Ambion) (Shi et al., 2009; Stewart et al., 2010) protocol modified for Sterivex filters (Hawley et al., 2017). Briefly, after thawing the filter cartridge on ice, RNA later was removed by pushing through with a 3 ml syringe followed by rinsing with an additional 1.8 mL of Ringer's solution and incubation at room temperature for 20 min with rotation. Ringer's solution was evacuated with a 3 ml syringe followed by addition of 100 μl of 0.125 mg ml^{-1} lysozyme and incubation at 37°C for 30 min with rotation. Lysate was removed from the filter cartridge and subjected to organic extraction following the mirVana kit protocol. DNA removal and clean up and purification of total RNA were conducted following the TURBO DNA-free kit (Thermo Fisher) and the RNeasy MinElute Cleanup kit (Qiagen) protocols respectively. Total RNA concentration was determined by RiboGreen analysis (Life Technologies) prior to synthesis of first strand cDNA using the SuperScript III First-Strand Synthesis System for RT-qPCR (Invitrogen) according to manufacturer instructions. Total RNA was extracted from 0.4 to 2.7 μm filters (**Table 1**) as follows. The filter was cut in half using sterile scissors. One half was minced into smaller pieces and used for RNA extraction while the remaining half was stored at −80°C. Filter pieces were transferred to a 15 mL falcon tube followed by addition 1.8 ml MirVana Lysis Buffer and 100 μl of 0.125 mg ml^{-1} lysozyme. In order to ensure biomass removal from the filter, 3 and 2 mm zirconium beads were added for bead beating using a vortex mixer at maximum speed. Filters were shaken for 4 min in two, 2 min laps followed by incubation at 37°C for 30 min with rotation, then processed in the same way as described above for Sterivex filters.

Small Subunit Ribosomal RNA Sequencing

Extracted DNA and cDNA corresponding to 2.7, 0.4, and 0.22 μm filters from 165 to 185 m depth intervals (**Table 1**) was used to generate SSU rDNA and rRNA amplicon sequences with three domain resolution on the 454 pyrosequencing platform. PCR amplification procedures were carried out as previously described (Hawley et al., 2017). In brief, SSU rDNA and rRNA amplicon libraries (pyrotags) were generated by PCR amplification using multi-domain primers targeting the V6–V8 region of the SSU rRNA gene (Allers et al., 2013): 926F (5′-cct atc ccc tgt gtg cct tgg cag tct cag AAA CTY AAA KGA ATT GRC GG-3′) and 1392R (5′-cca tct cat ccc tgc gtg tct ccg act cag-<**XXXXX**>-ACG GGC GGT GTG TRC-3′). Primer sequences were modified by the addition of 454 A or B adapter sequences (lower case). In addition, the reverse primer included a 5 bp barcode designated <**XXXXX**> for multiplexing of samples during sequencing Twenty-five microliter PCR reactions were performed in triplicate and pooled to minimize PCR bias. Each reaction contained between 1 and 10 ng of target DNA, 0.5 μl Taq DNA polymerase (Bioshop, Inc.), 2.5 μL Bioshop 10x buffer, 1.5 μl 25 mM Bioshop $MgCl_2$, 2.5 μL 10 mM dNTPs (Agilent Technologies) and 0.5 μL 10 mM of each primer. The thermal cycler protocol started with an initial denaturation at 95°C for 3 min and then 25 cycles of 30 s at 95°C, 45 s at 55°C, 90 s at

72°C and 45 s at 55°C. Final extension at 72°C for 10 min. PCR products were purified using the QiaQuick PCR purification kit (Qiagen), eluted in 25 μL, and quantified using the PicoGreen assay (Life Technologies). SSU rDNA and rRNA amplicons were pooled at 100 ng for each sample. Emulsion PCR and sequencing of the PCR amplicons was conducted on a Roche 454 GS FLX Titanium sequencer at the Department of Energy Joint Genome Institute (DOE-JGI), or the McGill University and Génome Québec Innovation Center.

A total of 1,027,601 small subunit ribosomal rDNA and rRNA pyrotags were processed together using the Quantitative Insights Into Microbial Ecology (QIIME) software package (Caporaso et al., 2010). Reads with length shorter than 200 bases, ambiguous bases, and homopolymer sequences were removed prior to chimera detection. Chimeras were detected and removed using chimera slayer provided in the QIIME software package. Sequences were then clustered into operational taxonomic units (OTUs) at 97% identity using UCLUST with average linkage algorithm. Prior to taxonomic assignment, singleton OTUs (OTUs represented by one read) were omitted, leaving 29,589 OTUs. Representative sequences from each non-singleton OTU were queried against the SILVA database release 111 using the BLAST algorithm (Altschul et al., 1990).

Statistical Analysis and Data Visualization

Statistical analyses were conducted using the R software package (R Core Team, 2013). Pyrotag data sets were normalized to the total number of reads per sample. Hierarchical cluster analysis (HCA) and non-metric multidimensional scaling (NMDS) were conducted to identify community compositional profiles associated with water column compartments using the pvclust (Suzuki and Shimodaira, 2015) and MASS (Venables and Ripley, 2002) packages with Manhattan Distance measures, and statistical significance to the resulting clusters as bootstrap score distributions with 1,000 iterations and NMDS stress value ≤ 0.05. Diversity indices (Shannon and alpha diversity) were calculated to identify changes in community structure based on filtration parameters using the vegan (Oksanen et al., 2015) package (**Supplementary Figure 3** and **Supplementary Table 1**). Microbial community richness on HC selected samples was determined using the vegan (Oksanen et al., 2015) package. The OTU table was rarefied starting with 10 sequences to the total maximum number of sequences found in the dataset and 10 iterations per sample were calculated with 100 sequences between each step (**Supplementary Figure 4**). Non-parametric Friedman block tests were conducted to determine the significance of volume variation and filtration method on community structure using the base stats package (R Core Team, 2013). In addition, one-way ANOVA was conducted to test the significance of filter combinations on taxa relative abundance using the ggpbur package (Kassambara, 2017).

Multi-level indicator species analysis (ISA) was conducted to identify OTUs specifically associated with different experimental parameters based on groups resolved in HCA using the indicspecies package (De Caceres and Legendre, 2009). The ISA/multi-level pattern analysis calculates *p*-values with Monte Carlo simulations and returns indicator values (IVs) and *p*-values with $\alpha \leq 0.05$. The IVs range between 0 and 1, where indicator OTUs considered in the present study for further community analysis shown an IV ≥ 0.7 and *p*-value ≤ 0.001. ISA groups abundance was visualized as dot plots using the *bubble.pl* pearl script[2]. Taxonomic distribution of identified OTUs was visualized using the ggplot2 (Wickham, 2009) package. The total rRNA:rDNA ratios were calculated for the subset of matching samples (165 m 250 mL and 2 L on-ship 0.22 μm filters with in-line 0.4 μm pre-filtration, and 185 m 500 mL and 2 L on-ship 0.22 μm filters with in-line 0.4 μm pre-filtration) to account for variation in taxon abundance in the DNA pool (Frias-Lopez et al., 2008; Stewart et al., 2012b) and compared for a subset of microbial groups to explore how filtration parameters influence recovery of potentially active OTUs. We then selected OTUs based on ISA results and their shifts in abundance among filtering conditions.

Data Deposition

SSU rDNA and rRNA pyrotag sequences have been submitted to the National Center for Biotechnology Information (NCBI) under BioSample Nos. SAMN05392373–SAMN05392466.

RESULTS

Water Column Conditions

Samples were collected during a stratification period characteristic of summer months (June–August) in SI (Carter, 1932, 1934; Herlinveaux, 1962; Zaikova et al., 2010). Below 150 m, water column CTD O_2 concentrations were below < 3 μM, consistent with previous observations of water column anoxia during peak stratification (**Figure 1A** and **Supplementary Table 2**). In addition, increasing concentrations of H_2S (13.95 μM) and NH_4^+ (6.1 μM) at 185 m were also observed, indicating anoxic and sulfidic conditions in deep basin waters. NO_3^- and NO_2^- concentrations peaked at 150 m reaching 12 and 0.6 μM, respectively. Phosphate concentrations ranged between 4.5 and 5.8 μM from 150 to 185 m, and SiO_2 concentration peaked at 185 m reaching 110 μM (**Supplementary Table 2**).

Benchmarking Workshop and Saanich Inlet Time-Series Results

We evaluated microbial community structure using 521 time-series samples traversing the SI water column (**Supplementary Figure 2**) and 29 samples collected during the workshop using rDNA pyrotag sequences to compare and cross-calibrate *in situ* sampling with the McLane PPS system and bottle sampling methods. Different water volumes from the same depth interval and filtration method showed no significant difference ($p = 0.1405$ and $p = 0.2545$, respectively) in richness based on Friedman block test results and were therefore treated as pseudo-replicates. NMDS indicated workshop samples clustered together primarily with high-resolution suboxic and anoxic samples from

[2]http://hallam.microbiology.ubc.ca/LabResources/Software.html

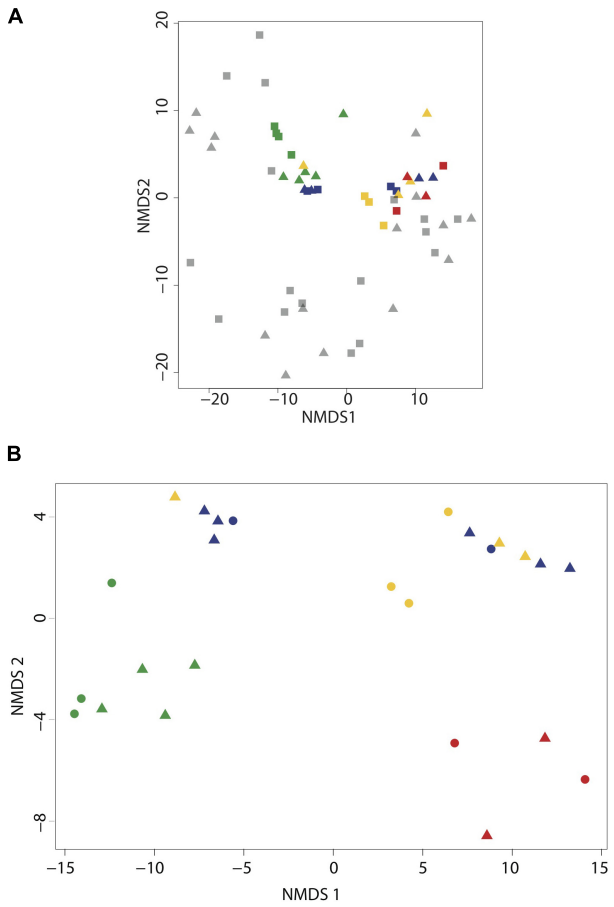

FIGURE 2 | Cluster analysis of small subunit ribosomal RNA (SSU rDNA) gene pyrotag data for the Saanich Inlet time-series (2006–2011) and SCOR workshop samples collected at 165 and 185 m. **(A)** NMDS based on Manhattan distance (1000 iterations) of time-series and SCOR pyrotag data showing microbial community partitioning based on oxygen gradients spanning suboxic (20–1 $\mu molO_2$ kg^{-1}) and anoxic-sulfidic (<1 μmol O_2 kg^{1}). **(B)** NMDS based on Manhattan distance (1000 iterations) of SCOR pyrotag data showing microbial community partitioning based on filtering conditions. In both biplots samples are depicted by depth (165 m = square and 185 m = triangle) and filter type [PPS *in situ* 0.4 μm (red), MPP on-ship 0.4 μm (green), 0.22 μm with in-line 0.4um prefilters (yellow), 0.22 μm with in-line 2.7 μm prefilters (blue), and time-series 0.22 μm (black)].

165 to 200 m depth intervals (0.22 μm Sterivex filters without pre-filtration) collected during summer months (**Figure 2A**). Similarities between time-series and workshop samples provided an internal check on experimental design and a rationale for examining more granular differences between community structure and potential activity resulting from different filtration parameters. Workshop samples collected at 165 and 185 m depth intervals formed three groups in NMDS analyses associated with on-ship 0.4 μm filters (group I), on-ship 0.22 μm filters with either 0.4 or 2.7 μm in-line pre-filtration (group II), and *in situ* 0.4 μm filters (group III) (**Figure 2B**). For the most part, samples within groups partitioned by depth. Consistent with NMDS, HCA resolved three groups (AU ≥ 70, 1000 iterations) associated with on-ship 0.4 μm filters (group I), on-ship 0.22 μm filters with in-line 0.4 μm pre-filters (group II), and *in situ* filtration 0.4 μm filters (group III) (**Figure 3A**). Within each filtration group, samples partitioned primarily by depth.

Size-Fractionation Effects on Community Structure

Based on NMDS and HCA results, we focused on changes in OTU relative abundance and taxon identity between groups. Microbial community structure was primarily comprised of OTUs (>0.1% relative abundance) affiliated with ubiquitous OMZ taxa including Marine Group A, SAR11, SAR324, SUP05 (Field et al., 1997; Fuhrman and Davis, 1997; Brown and Donachie, 2007; Tripp et al., 2008; Lam et al., 2009; Walsh et al., 2009; Zaikova et al., 2010; Walsh and Hallam, 2011; Wright et al., 2012) as well as Bacteroidetes, Desulfobacterales, and Euryarchaeota (**Figure 3B**). Interestingly, several of these groups were not detected in on-ship 0.4 μm pre-filter samples but were recovered from in-line 0.22 μm filters (group II). These included Marine Benthic Group E and Halobacteriales, SAR406 within the Marine Group A, Methylophilales within the Betaproteobacteria, Desulfuromonadales, and Desulfarculales within the Deltaproteobacteria and SUP05 within the Gammaproteobacteria. Conversely, Acidimicrobiales within the Actinobacteria, Cyanobacteria, Rhodobacterales within the Alphaproteobacteria, OM190 within the Planctomycetes, and eukaryotic phyla including Cnidaria and Arthropoda within the Opisthokonta and Diatoms within the Stramenopiles were detected in on-ship 0.4 μm filter samples but not recovered on in-line 0.22 μm filters or *in situ* 0.4 μm filters. Eukaryotic phyla affiliated with Alveolata were recovered on 0.22 μm filter samples with in-line 0.4 μm pre-filters (group I) and Phycisphaerales within the Planctomycetes were detected in *in situ* 0.4 μm filter samples (group III), respectively (**Figure 3B**).

Filtration methods, including the use of different pre-filters, resulted in a significant source of variation ($p < 0.001$) for the relative abundance of several bacterial phyla including Bacteroidetes, Deferribacteres, Alpha-, Delta- and Gamma-proteobacteria, Planctomycetes, archaeal phyla including Thaumarchaeota, and eukaryotic phyla including Opisthokonta and Rhizaria (**Figure 4** and **Table 2**). For example, the relative abundance of Bacteroidetes (Flavobacteriales), Alphaproteobacteria (SAR11, Rhodobacterales and Rhodospirillales) and Opisthokonta (Maxillopoda) associated with on-ship 0.4 μm filters increased fivefold compared to 0.22 μm filters with in-line 0.4 μm pre-filters and *in situ* 0.4 μm filters, while the relative abundance of Deferribacteres, Deltaproteobacteria (SAR324, Desulfobacterales and Desulfarculales) and Gammaproteobacteria (Oceanospirillales mainly affiliated with SUP05, Pseudomonadales and Alteromonadales) associated with on-ship 0.4 μm filters decreased fivefold compared to 0.22 μm filters with in-line 0.4 μm pre-filters and *in situ* 0.4 μm filters (**Figure 4**). Conversely, the relative abundance of Planctomycetes (Phycisphaerales and OM190) associated with *in situ*

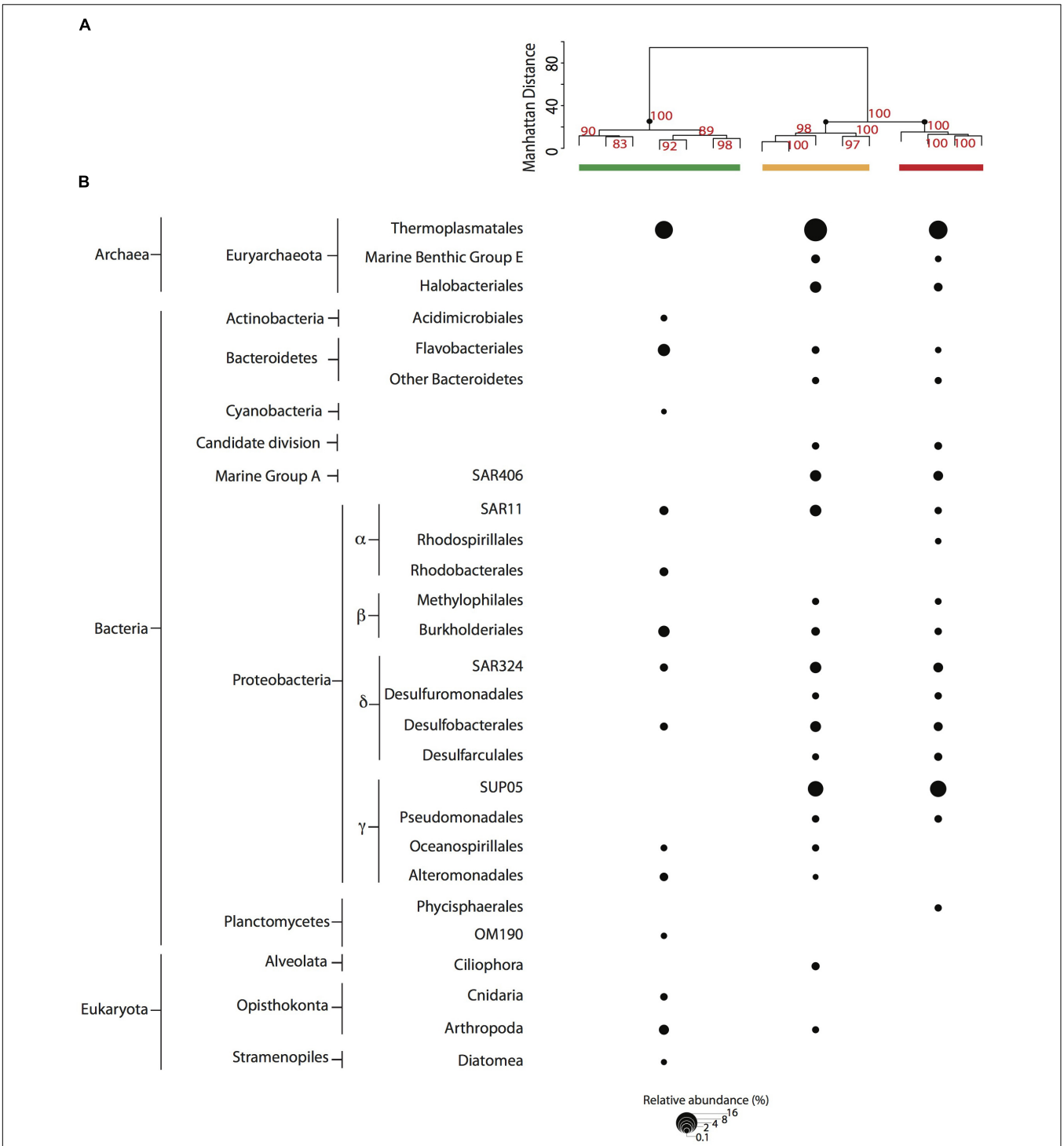

FIGURE 3 | (A) Cluster analysis (AU > 70, 1000 iterations) for 0.4 μm filter fractions. Samples are depicted with a colored bar by filter type [PPS *in situ* 0.4 μm (red), and MPP on-ship 0.4 μm (green), and 0.22 μm with in-line 0.4 μm prefilters (yellow)]. **(B)** Abundant taxa (>0.1% relative abundance from total reads in sample) observed among filter combinations for PPS *in situ* 0.4 μm (red), and MPP on-ship 0.4 μm (green) and 0.22 μm with in-line 0.4 μm prefilters (yellow). The size of dots depicts the relative abundance for each taxa as indicated in key.

0.4 μm filters increased fivefold compared to on-ship 0.22 μm filters with in-line 0.4 μm pre-filters and 0.4 μm filters (**Figure 4**).

Together these results indicate that filter selection and in-line positioning can introduce bias into microbial community structure data and reinforce the idea that filtration methods

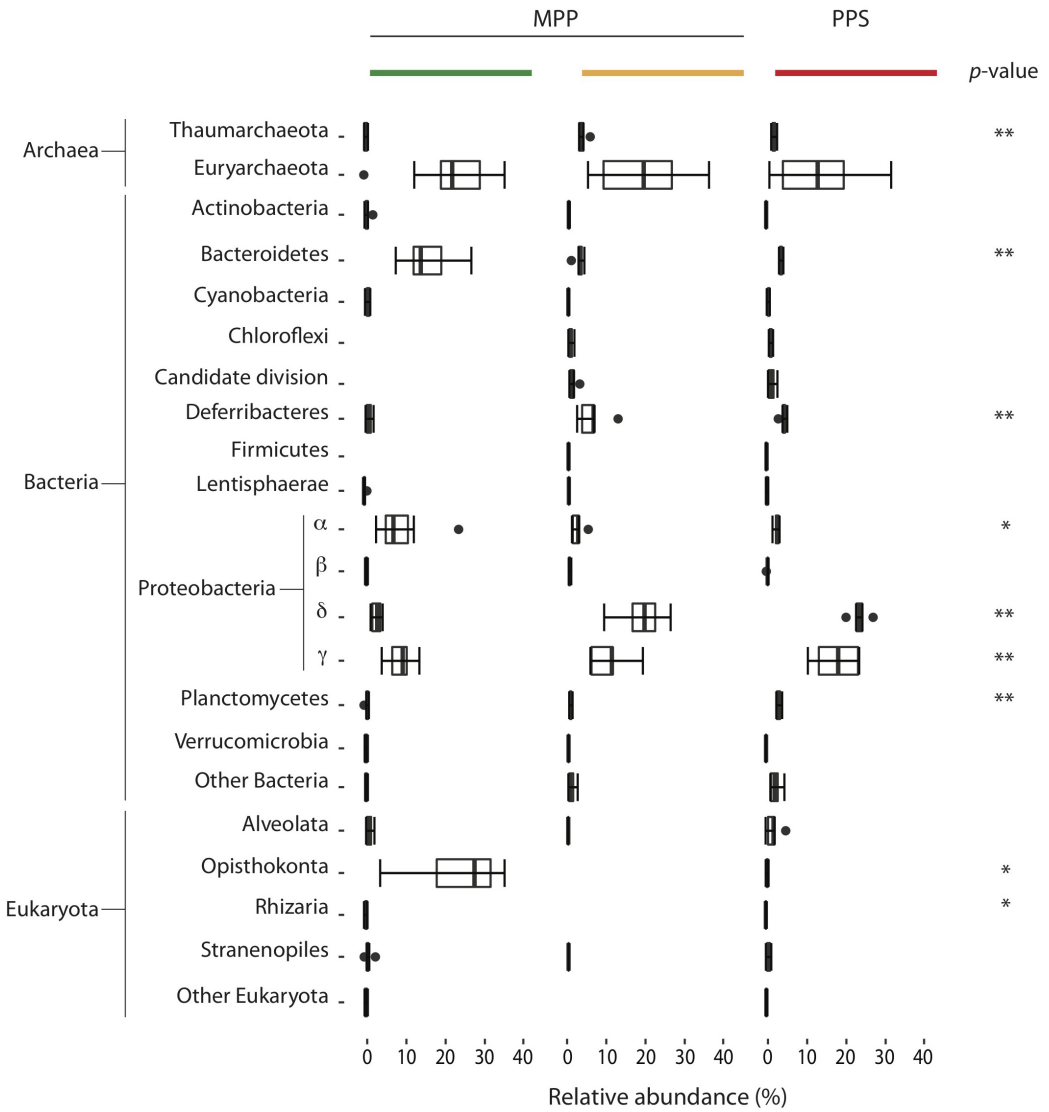

FIGURE 4 | Community shifts occurred among and within filter combinations for PPS *in situ* 0.4 μm (red), and MPP on-ship 0.4 μm (green), and 0.22 μm with in-line 0.4 μm prefilters (yellow). The size of each box represents the average of the percentage of relative abundance throughout the water column over this period. For both plots, extended dashed lines (whiskers) represent at the base the lower and upper quartiles (25 and 75%) and at the end the minimum and maximum values encountered. The middle line represents the median. *p*-Values for significant relative abundance shifts among filter groups are depicted as $^{*}p < 0.01$ and $^{**}p < 0.001$ aside corresponding taxa.

should be taken into consideration more carefully when interpreting microbial count data.

Size Fractionation Effects on Indicator OTUs (DNA Analyses)

To identify OTUs associated with specific filtration methods we conducted multi-level ISA on HCA groups I–III. As expected, resulting indicator OTUs varied with respect to filtration methods used (**Figure 5**). The largest differences with respect to indicators were detected between *in situ* and on-ship 0.4 μm filter samples. Indicator OTUs detected in on-ship 0.4 μm filter samples were mostly affiliated with bacterial phyla including Actinobacteria, Bacteroidetes, Cyanobacteria, Deferribacteres, Proteobacteria, and Verrucomicrobia, archaeal phyla including Euryarchaetoa, and eukaryotic phyla including Alveolata, Opisthokonta, Rhizaria, and Stramenopiles (**Figure 5**). Indicator OTUs detected in *in situ* 0.4 μm filter samples were mostly affiliated with bacterial phyla including Candidate divisions (WS3, OD1, and BRC1), Chloroflexi, Deferribacteres, Firmicutes, Lentisphareae, Nitrospirae, Alpha-, Beta-, Delta- and Gamma-proteobacteria, and Planctomycetes, archaeal phyla including Euryarchaeota, and eukaryotic phyla including Alveolata, Excavata, and Opisthokonta (**Figure 5**). Indicator OTUs detected in 0.22 μm filter samples with in-line 0.4 μm pre-filter were mostly affiliated with bacterial phyla including

TABLE 2 | *p*-values for taxa showing significant relative abundance shifts between filter conditions and filtration methods.

Taxa	*p*-value
Thaumarchaeota	$3e^{-6}$
Bacteroidetes	$5.1e^{-5}$
Deferribacteres	0.001
Alphaproteobacteria	0.01
Deltaproteobacteria	$2.1e^{-8}$
Gammaproteobacteria	0.0004
Planctomycetes	$4.1e^{-8}$
Opisthokonta	0.01
Rhizaria	0.01

Deferribacteres and Bacteroidetes, and archaeal phyla including Euryarchaeota (**Figure 5**). The differences observed between *in situ* and on-ship indicator OTUs reinforce the effect of size fractionation on microbial community structure and raise important questions about metabolic reconstruction efforts based solely on on-ship filtration methods.

Size-Fractionation Effects on Expressed OTUs Within Specific Populations (rRNA Analyses)

To further evaluate the impact of size fractionation on detection of active microbial groups we compared SSU rRNA:rDNA ratios of OTUs between 0.4 μm filters collected and preserved *in situ* vs. on-ship 0.22 μm filters with in-line 0.4 μm pre-filters. We focused on OTUs exhibiting ratios ≥ 1 as a proxy for cellular activity (Blazewicz et al., 2013). Ratios for Candidate divisions, Desulfobacterales, SUP05, Phycisphaerae, and Halobacteria were highest in 0.4 μm *in situ* filter samples while SAR11, Rhodospirillales, Methylophilales and Burkholderiales within Betaproteobacteria, and Verrucomicrobia and eukaryotic phyla affiliated with Alveolata, Opisthokonta, Rhizaria, and Stramenopiles were highest in on-ship 0.22 μm filter samples with in-line 0.4 μm pre-filtration (**Supplementary Figure 5**).

We detected OTUs affiliated with SUP05, Marine Group A, SAR11 and SAR324 that showed ratios ≥ 1, with differential expression between *in situ* and on-ship filters. For instance, a total of 4 SUP05 OTUs with ratios ranging from 1 to 2, and 3 SAR324 OTUs with ratios equal to 3 were exclusively detected in 0.4 μm *in situ* filter samples (**Figure 6**). We also observed six Marine Group A OTUs with ratios equal to 2 in on-ship 0.22 μm filter samples with in-line 0.4 μm pre-filtration and 1 exclusively active *in situ* OTU (**Figure 6**). Interestingly, we observed eight SAR11 OTUs with ratios ranging from 1 to 3 exclusively in on-ship 0.22 μm filter samples with in-line 0.4 μm pre-filtration (**Figure 6**). Candidate divisions BCR1 and WS3, Delta- and Gammaproteobacteria, and Planctomycetes OTUs also manifested higher ratios in 0.4 μm *in situ* filter samples than in on-ship samples (**Figure 7**). These differences showed some depth specificity. For example, we observed BCR1 and WS3 OTUs with high ratio values at 165 m while Desulfovibrionales and Desulfarculales within the Deltaproteobacteria had the highest ratio values at 185 m (**Figure 7**). Similarly, most OTUs affiliated with Planctomycetes (Phycisphaerae, OM190, Brocadiales, and Plactomycetales) had the highest ratio values at 185 m (**Figure 7**). In contrast, Flavobacteriales within Bacteroidetes and Alphaproteobacteria had higher ratio values in on-ship 0.22 μm filter samples with in-line 0.4 μm pre-filtration than 0.4 μm *in situ* sampled at both 165 and 185 m (**Figure 7**).

DISCUSSION

In this study we used SSU rDNA and rRNA count data generated to determine the effects of collection and filtration methods on microbial community structure and potential activity in the anoxic water column of Saanich Inlet (SI). Observed differences in microbial community structure and potential activity associated with *in situ* versus on-ship size fractionation suggest potential sources of error when linking field processes to microbial agents based on genomic sequence information in isolation. In particular, *in situ* results detected several microbial groups implicated in the sulfur-cycle that are underrepresented in public amplicon and shotgun sequencing data sets. Overall, results from this study provide useful information on how different sampling methods can contribute to bias in experimental outcomes and reinforce the need for more integrated studies based on standardized sampling protocols that increasingly incorporate *in situ* measurements.

Microbial Community Shifts Associated With Filter Type and Volume

For *in situ* sampling we used GFF filters certified with the instrument and the recommended filtration volume in duplicate. For on-ship sampling we adopted standard sampling protocols using filters available to us at the time including 0.4 μm polycarbonate or 2.7 μm GF/D pre-filters in-line with a 0.22 μm Sterivex polycarbonate filter cartridge. While we cannot strictly rule out potential membrane effects on the resulting microbial community composition profiles associated with GFF versus polycarbonate filters at the same size cut-off, a previous study by Djurhuus et al. (2017) suggests a minimal effect based on the nucleic acid extraction methods used. The use of different volumes filtered for a given depth and filter combination was intended to test the significance of volume variation on microbial community composition. We set the maximum volume to be 2 L in order to keep filtering time on ship to a minimum and for samples to be comparable to previous time-series environmental observations. Water volumes between 250 ml and 2 L from the same depth interval and filtration method showed no significant difference in richness based on Friedman block test results.

Microbial Community Shifts Associated With Size Fractionation

Understanding how microorganisms interact within the ocean at different scales is integral to linking microbial food webs to nutrient and energy flow processes (Azam and Malfatti, 2007). Particles play a salient role in structuring microbial community interactions and the interplay between "particle-associated" and "free-living" microbiota creates a dynamic metabolic network

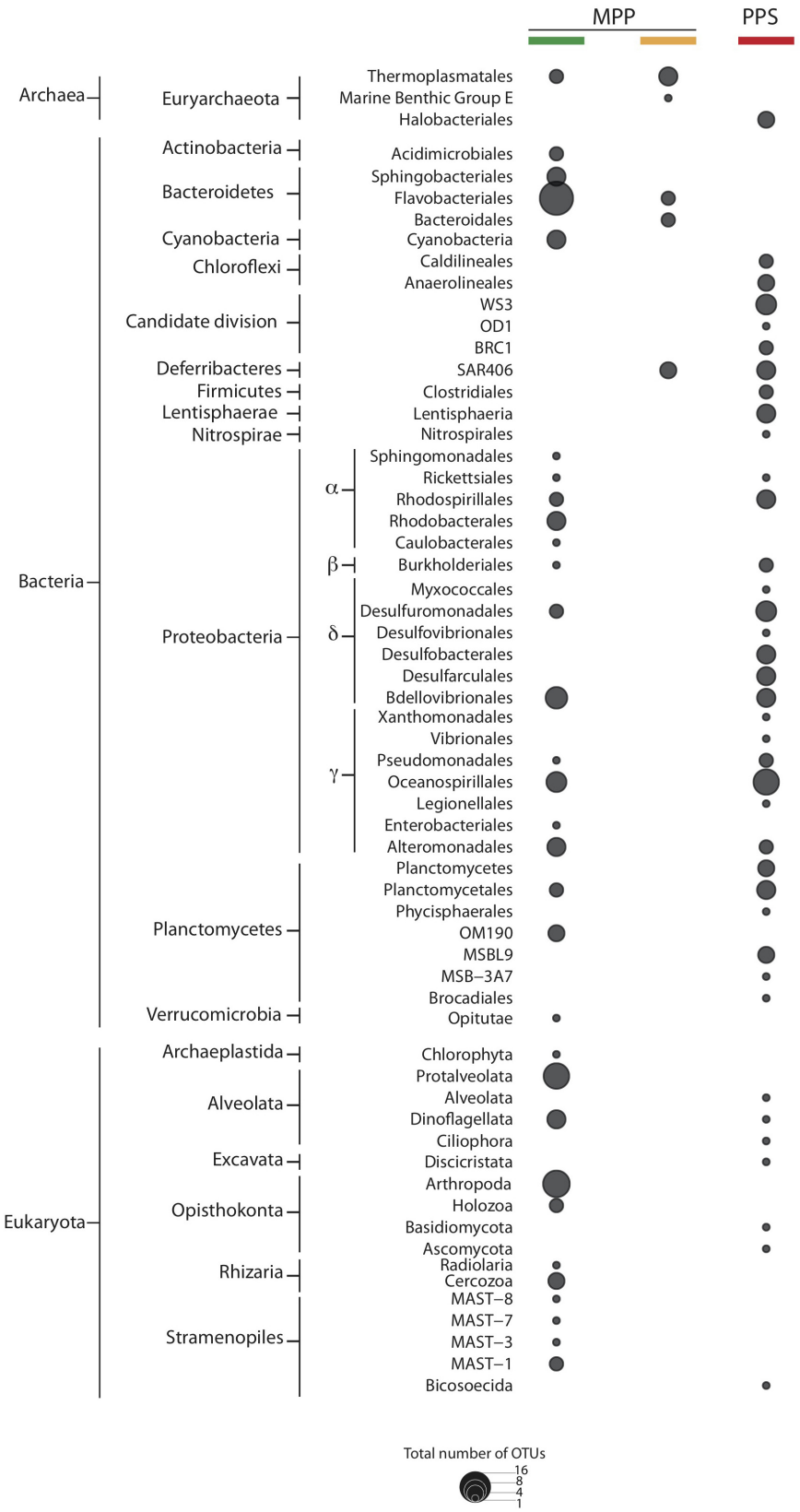

FIGURE 5 | Indicator OTUs for filter groups PPS *in situ* 0.4 μm (red), and MPP on-ship 0.4 μm (green), and 0.22 μm with in-line 0.4 μm prefilters (yellow). The size of dots depicts the total number of indicator OTUs affiliated to specific taxa.

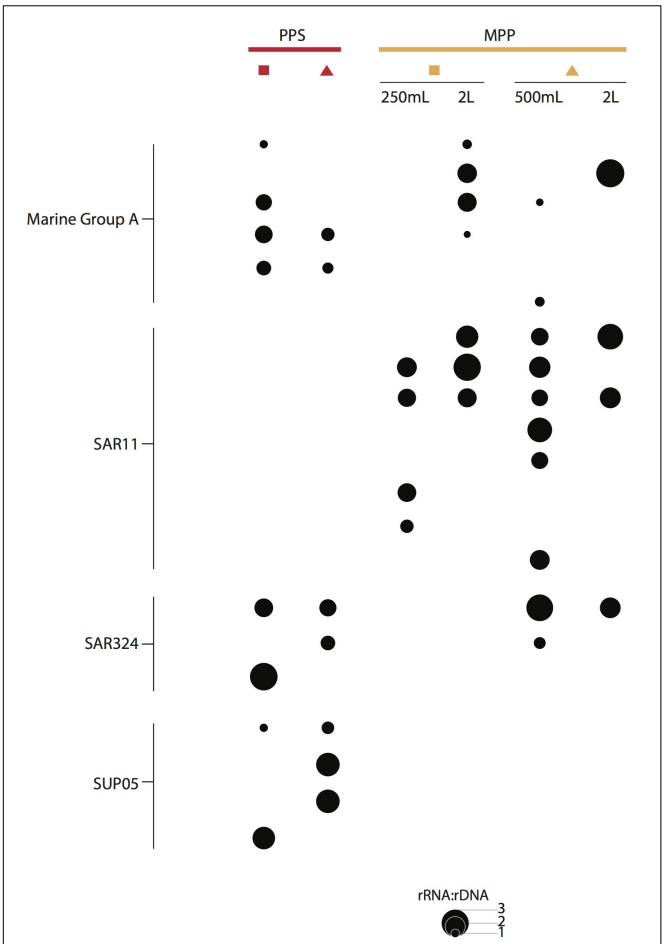

FIGURE 6 | RNA:DNA ratio for abundant and ubiquitous taxa in OMZs, i.e., SUP05, SAR406, SAR11, and SAR324, observed at PPS *in situ* 0.4 μm (red) and MPP on-ship 0.22 μm with in-line 0.4 μm prefilters (yellow). The size of dots depicts ratio values for individual OTUs as indicated on plot size key.

driving biogeochemical transformations (Smith et al., 1992; DeLong et al., 1993; Crump et al., 1999; Simon et al., 2002; Grossart, 2010; Ganesh et al., 2014). Previous observations from OMZ waters implicate particle maxima as hotspots for metabolic coupling (Garfield et al., 1983; Naqvi et al., 1993; Whitmire et al., 2009; Ganesh et al., 2014). However, the definition of "particle-associated" versus "free-living" can sometimes seem arbitrary and the degree to which microorganisms alternate between these two fractions in different water compartments is not firmly established. Typically, anything > 0.4 μm has been considered particle associated (Azam and Malfatti, 2007) although most studies use different combinations of 0.2–1.6 and 2.7 μm cut-offs to concentrate microbial biomass. Here, we compared 0.4 μm *in situ* filtration without a pre-filtration step to on-ship 0.22 μm filtration with in-line 0.4 μm pre-filtration to better evaluate "particle-associated" versus "free-living" fractions.

The core microbial community detected *in situ* versus on-ship was similar to time-series observations in suboxic-anoxic water column compartments (165–185 m) during summer months. However, at a more granular OTU level important differences in community structure and potential activity for a number of microbial groups were resolved that reinforce and expand on previous size fractionation studies in open ocean OMZs. For example, Padilla et al. (2015) have shown that mode and magnitude of sampling bias depends on filter type and pore size, particle load, and community complexity. Our results expand on these observations indicating that wire time and filtration duration likely impacted richness and particle size, as did potential bottle effects due to settling when processing on-ship samples (**Supplementary Figures 3**, **4**). Several studies have shown that particles can settle in sampling bottles on timescales relevant to on-ship processing (Gardner, 1977; Suter et al., 2016).

With respect to size fractionation, community structure differences were driven by shifts in abundance and activity of many known microorganisms. For example, as observed in the ETNP OMZ, OTUs affiliated with Deferribacteres were enriched in the smaller size fraction (<0.4 μm) consistent with an autotrophic lifestyle (Ganesh et al., 2014). Similarly, indicator OTUs affiliated with Bacteroidetes (Bacteroidales and Flavobacteriales), Lentisphareae, Deltaproteobacteria (Myxococcales and Desulfobacterales), Planctomycetes, and Verrucomicrobia were enriched in the larger size fraction (>0.4 μm) as observed in both ETNP and ETSP OMZs, consistent with attachment to sinking aggregates or zooplankton (Crump et al., 1999; Simon et al., 2002; Eloe et al., 2011; Allen et al., 2012; Fuchsman et al., 2012; Ganesh et al., 2014; Padilla et al., 2015). These similarities transcended domain boundaries with eukaryotic phyla including Dinoflagellata (Alveolata), Radiolaria (Rhizaria), and Syndiniales (Stramenopiles) enriched in the 0.4 μm filter samples (Guillou et al., 2008; Duret et al., 2015).

With respect to *in situ* versus bottle collection methods, previous studies have identified changes in community gene expression profiles (Feike et al., 2012; Stewart et al., 2012a) and process rate measurements (Taylor and Doherty, 1990; Stewart et al., 2012a; Taylor et al., 2015; Edgcomb et al., 2016). Here we identified changes in microbial community richness and structure (**Figure 4** and **Supplementary Figure 4**) that potentially explain variance in gene expression or process rates. For example, indicator OTUs detected in *in situ* samples suggests a potential unrecognized role for sulfate-reducers and candidate divisions WS3, OD1, and BRC1 in the SI water column. Previous studies have implicated WS3 and OD1 metabolism in sulfur cycling and methanogen provisioning (Kirkpatrick et al., 2006; Wrighton et al., 2012). Similarly, Desulfobacterales and Desulfovibrionales, are commonly underestimated in abundance in OMZs waters (Suter et al., 2016) as they are more prevalent on particles that likely settle during on-ship processing.

Working in the Cariaco Basin OMZ, Suter et al. (2016) provide a compelling description of bottle settling rates (approximately 12 min for a 1 mm particle to sink into below-spout space of an 8 L Niskin bottle or 18 min for a 12 L bottle) that can result in sampling bias. On-ship processing during the workshop took between 20 and 30 min. Shipboard processing times can often be even longer than this. In addition, wire-time and turbulence associated with sampling moment and vibration (Suter et al., 2016), and filtration across the membrane

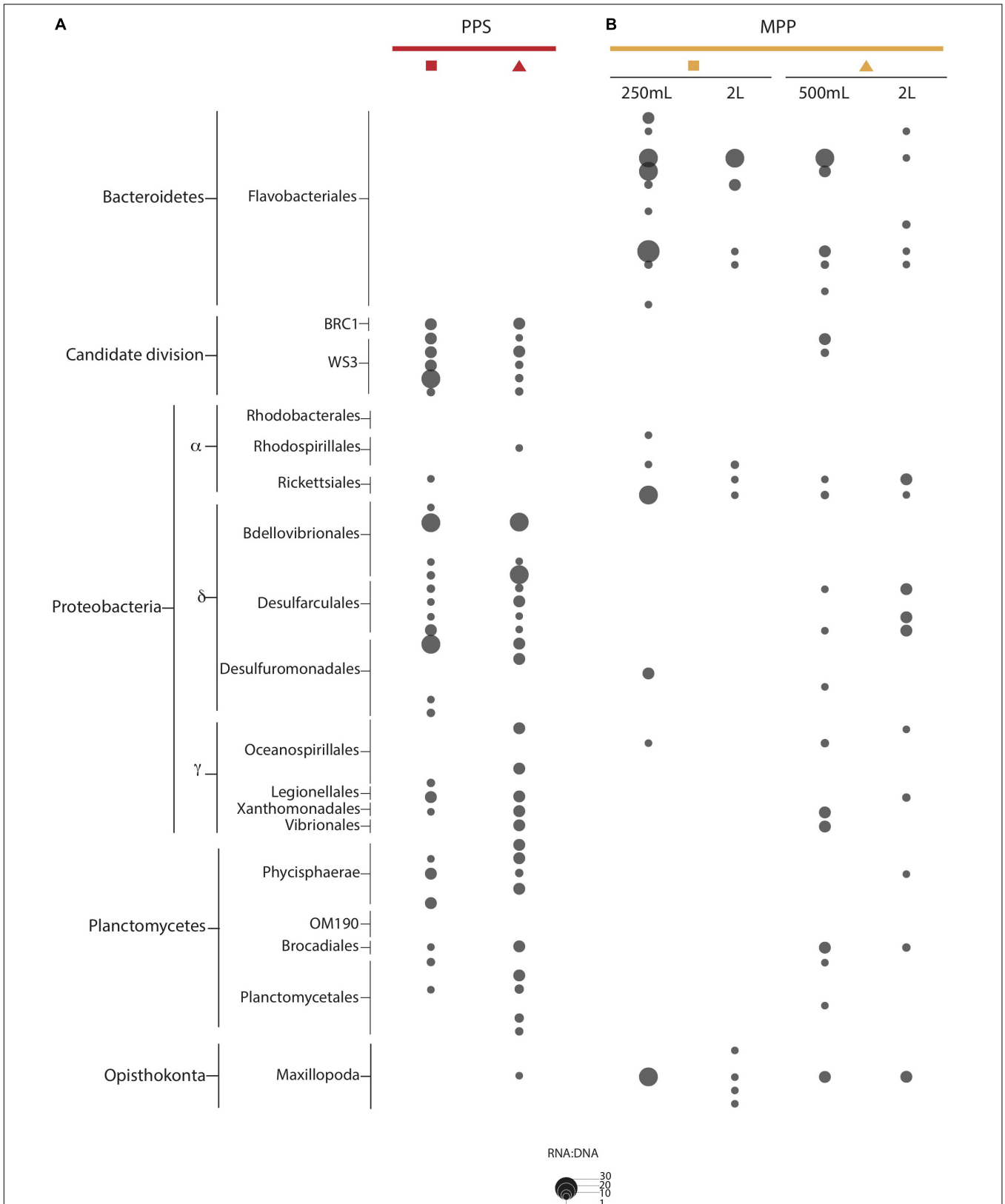

FIGURE 7 | RNA:DNA ratio for indicator OTUs observed at PPS *in situ* 0.4 μm (**A**: red) and MPP on-ship 0.22 μm with in-line 0.4 μm prefilters (**B**: yellow). The size of dots depicts ratio values for individual OTUs as indicated on plot size key.

(Duret et al., 2015) can impact particle size and stability in bottles, e.g., production of smaller particles derived from larger aggregates. Based on sinking rates estimated in the Cariaco Basin it is possible that observed community structure differences between *in situ* and on-ship samples in SI could be explained by a combination of particle settling and turbulence associated with sample collection and filtration. This could affect how we perceive the microbial metabolic network with respect to transient spatial interactions that are altered or disrupted using on-ship methods.

Implications of Size Fractionation for Inferring Microbial Activity in OMZs

In contrast to only examining rDNA sequences, combining those with analysis of rRNA sequences can provide a robust proxy for past, and present or emerging cellular activities (Blazewicz et al., 2013) that can inform hypotheses related to life strategies and metabolic interactions within microbial communities (Lepp and Schmidt, 1998; Barnard et al., 2013). Here, we considered rRNA:rDNA ratio values ≥ 1 as an indicator for potentially active microbial community members. While, using ratios to infer activity at higher taxonomic levels, e.g., Phylum, Class, Order, can promote inconsistent results (Blazewicz et al., 2013; Ganesh et al., 2015), focusing on the OTU level can identify ecologically relevant populations with the potential to play integral roles in nutrient and energy cycling within the ecosystem under study. For example, SUP05 has been determined to be an abundant member of the SI microbial community comprising between 20 and 30% of total bacteria at 165 and 185 m, respectively (Walsh et al., 2009; Zaikova et al., 2010; Walsh and Hallam, 2011). We detected 85 OTUs affiliated with SUP05 based on rDNA sequences. However, only 4 had rRNA:rDNA ratio values > 1 indicating population level variation in potential activity.

Consistent with previous observations in the ETSP using metatranscriptomic data (Padilla et al., 2015), examination of the taxonomic affiliation of indicator OTUs produced using *in situ* versus on-ship methods identified differences between the active microbial community in samples. Some candidate divisions recovered in *in situ* samples have not been previously well-described in the SI water column based on rDNA sequences due to their low abundance (<0.1%). Interestingly, the rRNA:rDNA ratios observed for indicator WS3 and BCR1 OTUs (ratios equal to 7 and 2, respectively) were greater than those observed for OTUs affiliated with ubiquitous and abundant taxa, including SUP05. Similar observations were made for OTUs affiliated with Deltaproteobacteria, Chloroflexi, Firmicutes, Lentisphaera, Nitrospina and Marine Group A, reinforcing the idea that multi-omic sequences and process rate measurements sourced from on-ship samples have the potential to underestimate the contribution of some active microbial groups present in the water column. Such groups may be sensitive to settling, turbulence or other factors including oxygen exposure, necessitating *in situ* sampling to reveal their contributions to the metabolic network.

Hawley et al. (2014) used metaproteomics to develop a conceptual model of coupled carbon, nitrogen and sulfur cycling. Louca et al. (2016) incorporated these ideas into a numerical model integrating multi-omic sequence and geochemical information to predict metabolic fluxes and growth yields under near steady-state conditions. Both conceptual and numerical models were based on interactions between Thaurmarchaeota, SAR11, SUP05 and Planctomycetes (Walsh et al., 2009; Zaikova et al., 2010; Walsh and Hallam, 2011; Wright et al., 2012). Although, the metabolic potential of WS3, OD1 and sulfate-reducing Deltaproteobacteria in the SI water column remains to be determined, the potential role of these groups at the nexus of sulfur cycling and methanogenesis (Kirkpatrick et al., 2006) presents an opportunity for new hypothesis development and testing to integrate these groups into prevailing conceptual and numerical models for coupled biogeochemical cycling.

CONCLUSION

As the research community transitions away from descriptive studies of marine microorganisms to more quantitative comparisons at ecosystem scales integrating multi-omic information with process rates and modeling, the need for standards of practice that reduce sampling bias becomes increasingly important.

Currently most microbial community studies use a combination of bottle sampling and filtration to collect biomass for nucleic acid extraction and sequencing. However, the specific details of how samples are collected including wire and bottle time, filter type, and method can have a discernable impact on resulting microbial community composition profiles. This is an important consideration when comparing data sets between studies and when trying to link microbial agents to defined field processes, e.g., denitrification, sulfur oxidation, carbon fixation, etc. Based on our analysis of both *in situ* and on-ship sample collection and processing methods the following practical considerations can be identified. For amplicon-based studies, use a consistent filtration volume between 1 and 2 L and record the precise volume filtered to back calculate nucleic acid yield per unit volume of water collected. Depending on the size fraction you are interested in profiling consult the literature to determine a consensus filter type and method. For cross-scale studies use the same filtration method for all locations. Take advantage of current library production methods that allow for low-input samples, and use the coverage provided by next generation sequencing platforms to sample with depth and replication. When possible, consider using single-cell amplified genome (SAG) approaches when more functional information is required (Stepanauskas, 2015). Samples for SAG sequencing are easy to replicate and do not require more than a 1–2 ml per sample that can be stored for extended periods of time at −80°C (Rinke et al., 2014). Most important, minimize wire time including on-ship bottle sampling duration. Particles are settling as the waters in the bottle rise. Consider inverting the bottle before collecting waters for more even biomass sampling or filtering samples directly in the water column.

In situ sampling approaches have the potential to limit many biases by providing a more authentic representation of microbial activity than on-ship sampling methods. Several promising devices such as the PPS (Edgcomb et al., 2016), Environmental Sample Processor (ESP) (Jones et al., 2008; Preston et al., 2009;

Ottesen et al., 2011; Robidart et al., 2014), Automatic Flow Injection Sampler (AFIS) (Feike et al., 2012), and the autonomous vertical sampling vehicle Clio (Jakuba et al., 2014) have been developed with the potential to support *in situ* sampling and direct fixation of samples under a variety of operational scenarios. For example, recent studies with the ESP have enabled dynamic intermittent sampling during light dark cycles in surface waters revealing conserved patters of gene expression on ocean basin scales (Ottesen et al., 2014; Aylward et al., 2015). Although community adoption of these new technologies remains in early stages due in part to accessibility, price point, and operating constraints, these devices and their "descendants" likely reflect the future of microbial sampling in the ocean given their autonomous and programmable designs extensible to time series or event response monitoring. Looking forward, we recommend replicated studies of different *in situ* sampling technologies that incorporate multi-omic sequencing and process rate measurements focused on coupled carbon, nitrogen, and sulfur cycling in coastal and open ocean OMZs.

AUTHOR CONTRIBUTIONS

MT-B collected and processed samples, analyzed data, and wrote the manuscript under SH supervision. AM and MS collected and processed samples and assisted data analysis. MP, CT, and VE collected and processed PPS samples. KT processed samples for sequencing. CM collected and processed samples. PL, OU, J-HH, KJ, VE, SC, and SH organized the SCOR 144 working group workshop, collected and processed samples, and provided input for data analysis and manuscript development.

FUNDING

This work was performed under the auspices of the Scientific Committee on Oceanographic Research (SCOR), the United States Department of Energy (DOE) Joint Genome Institute, an Office of Science User Facility, supported by the Office of Science of the United States Department of Energy under Contract DE-AC02- 05CH11231, the G. Unger Vetlesen and Ambrose Monell Foundations, the Tula Foundation-funded Centre for Microbial Diversity and Evolution, the Natural Sciences and Engineering Research Council of Canada, Genome British Columbia, the Canada Foundation for Innovation, and the Canadian Institute for Advanced Research through grants awarded to SH. McLane Research Laboratories and Connie Lovejoy contributed access to instrumentation for field work. Ship time support was provided by NSERC between 2007 and 2014 through grants awarded to SC, SH and Philippe Tortell MT-B was funded by Consejo Nacional de Ciencia y Tecnología (CONACyT) and the Tula Foundation.

ACKNOWLEDGMENTS

We thank Captain Ken Brown and his crew for their engaged effort on every cruise aboard the *RSV* Strickland. We also thank past and present members of the Hallam, Crowe and Tortell labs and the many undergraduate trainees, aka minions, for contributions to cruise preparation and clean up, water filtration, DNA extraction and QC. We thank our sea-going technicians at UBC, Chris Payne and Larysa Pakhomova for their contributions to cruise preparation and sample analyses. Special thanks to Ed Urban at SCOR for administrative support and guidance and to the entire SCOR Working Group 144: Bess Ward (Chair), Sean Crowe, Virginia Edgcomb, Vernonique Garcon, Steven Hallam, KJ, Elsabe Julies, Phyllis Lam, Nagappa Ramaiah, Matthew Sullivan, OU and associate members: Mark Altabet, Annie Bourbonnais, Karen Casciotti, Francis Chan, David Conley, Robinson (Wally) Fulweiler, J-HH, David Karl, John Kaye, Konstantinos Kormas, SWA Naqvi, Nancy Rabalais, Mak Saito, Frank Stewart, RV-S, Jennifer Brum, and Jody Wright for their efforts to develop a community of practice for OMZ research.

SUPPLEMENTARY MATERIAL

The Supplementary Material for this article can be found online at: https://www.frontiersin.org/articles/10.3389/fmars.2019.00132/full#supplementary-material

REFERENCES

Allen, L. Z., Allen, E. E., Badger, J. H., Mccrow, J. P., Paulsen, I. T., Elbourne, L. D. H., et al. (2012). Influence of nutrients and currents on the genomic composition of microbes across an upwelling mosaic. *ISME J.* 6, 1403–1414. doi: 10.1038/ismej.2011.201

Allers, E., Wright, J. J., Konwar, K. M., Howes, C. G., Beneze, E., Hallam, S. J., et al. (2013). Diversity and population structure of marine group A bacteria in the Northeast subarctic Pacific Ocean. *ISME J.* 7, 256–268. doi: 10.1038/ismej.2012.108

Altschul, S. F., Gish, W., Miller, W., Myers, E. W., and Lipman, D. J. (1990). Basic local alignment search tool. *J. Mol. Biol.* 215, 403–410. doi: 10.1016/S0022-2836(05)80360-2

Anderson, J. J., and Devol, A. H. (1973). Deep water renewal in Saanich Inlet, an intermittently anoxic basin. *Estuar. Coast. Mar. Sci.* 1, 1–10. doi: 10.1016/0302-3524(73)90052-2

Arrigo, K. R. (2005). Marine microorganisms and global nutrient cycles. *Nature* 437, 349–355. doi: 10.1038/nature04159

Aylward, F. O., Eppley, J. M., Smith, J. M., Chavez, F. P., Scholin, C. A., and Delong, E. F. (2015). Microbial community transcriptional networks are conserved in three domains at ocean basin scales. *Proc. Natl. Acad. Sci. U.S.A.* 112:5443. doi: 10.1073/pnas.1502883112

Azam, F., and Malfatti, F. (2007). Microbial structuring of marine ecosystems. *Nat. Rev. Microbiol.* 5, 966–966. doi: 10.1038/nrmicro1798

Barnard, R. L., Osborne, C. A., and Firestone, M. K. (2013). Responses of soil bacterial and fungal communities to extreme desiccation and rewetting. *ISME J.* 7, 2229–2241. doi: 10.1038/ismej.2013.104

Bijma, J., Pörtner, H.-O., Yesson, C., and Rogers, A. D. (2013). Climate change and the oceans – what does the future hold? *Mar. Pollut. Bull.* 74, 495–505. doi: 10.1016/j.marpolbul.2013.07.022

Blazewicz, S. J., Barnard, R. L., Daly, R. A., and Firestone, M. K. (2013). Evaluating rRNA as an indicator of microbial activity in environmental communities: limitations and uses. *ISME J.* 7, 2061–2068. doi: 10.1038/ismej.2013.102

Brown, M. V., and Donachie, S. P. (2007). Evidence for tropical endemicity in the Deltaproteobacteria marine group B/SAR324 bacterioplankton clade. *Aquat. Microb. Ecol.* 46, 107–115. doi: 10.3354/ame046107

Canfield, D. E., Stewart, F. J., Thamdrup, B., De Brabandere, L., Dalsgaard, T., Delong, E. F., et al. (2010). A cryptic sulfur cycle in oxygen-minimum-zone waters off the Chilean coast. *Science* 330, 1375–1378. doi: 10.1126/science.1196889

Caporaso, J. G., Kuczynski, J., Stombaugh, J., Bittinger, K., Bushman, F. D., Costello, E. K., et al. (2010). QIIME allows analysis of high-throughput community sequencing data. *Nat. Methods* 7, 335–336. doi: 10.1038/nmeth.f.303

Carter, N. M. (1932). The oceanography of the fjords of southern British Columbia. *Fish. Res. Bd. Canada Prog. Rept. Pacific Coast. Sta.* 12, 7–11.

Carter, N. M. (1934). Physiography and oceanography of some british columbia fjords. *Proc. Fifth Pacific Sci. Cong.* 1, 721–733.

Cram, J. A., Xia, L. C., Needham, D. M., Sachdeva, R., Sun, F., and Fuhrman, J. A. (2015). Cross-depth analysis of marine bacterial networks suggests downward propagation of temporal changes. *ISME J.* 9, 2573–2586. doi: 10.1038/ismej.2015.76

Crump, B. C., Armbrust, E. V., and Baross, J. A. (1999). Phylogenetic analysis of particle-attached and free-living bacterial communities in the columbia river, its estuary, and the adjacent coastal Ocean. *Appl. Environ. Microbiol.* 65, 3192–3204.

De Caceres, M., and Legendre, P. (2009). Associations between species and groups of sites: indices and statistical inference. *Ecology* 90, 3566–3574. doi: 10.1890/08-1823.1

DeLong, E. F., Franks, D. G., and Alldredge, A. L. (1993). Phylogenetic diversity of aggregate-attached vs. free-living marine bacterial assemblages. *Limnol. Oceanogr.* 38, 924–934. doi: 10.4319/lo.1993.38.5.0924

Diaz, R. J., and Rosenberg, R. (2008). Spreading dead zones and consequences for marine ecosystems. *Science* 321, 926–929. doi: 10.1126/science.1156401

Djurhuus, A., Port, J., Closek, C. J., Yamahara, K. M., Romero-Maraccini, O., Walz, K. R., et al. (2017). Evaluation of filtration and DNA extraction methods for environmental DNA biodiversity assessments across multiple trophic levels. *Front. Mar. Sci.* 4:314. doi: 10.3389/fmars.2017.00314

Duret, M. T., Pachiadaki, M. G., Stewart, F. J., Sarode, N., Christaki, U., Monchy, S., et al. (2015). Size-fractionated diversity of eukaryotic microbial communities in the Eastern Tropical North Pacific oxygen minimum zone. *FEMS Microbiol. Ecol.* 91:fiv037. doi: 10.1093/femsec/fiv037

Edgcomb, V. P., Taylor, C., Pachiadaki, M. G., Honjo, S., Engstrom, I., and Yakimov, M. (2016). Comparison of Niskin vs. in situ approaches for analysis of gene expression in deep Mediterranean Sea water samples. *Deep Sea Res. Part II Top. Stud. Oceanogr.* 129, 213–222. doi: 10.1016/j.dsr2.2014.10.020

Eloe, E. A., Shulse, C. N., Fadrosh, D. W., Williamson, S. J., Allen, E. E., and Bartlett, D. H. (2011). Compositional differences in particle-associated and free-living microbial assemblages from an extreme deep-ocean environment. *Environ. Microbiol. Rep.* 3, 449–458. doi: 10.1111/j.1758-2229.2010.00223.x

Feike, J., Jurgens, K., Hollibaugh, J. T., Kruger, S., Jost, G., and Labrenz, M. (2012). Measuring unbiased metatranscriptomics in suboxic waters of the central Baltic Sea using a new in situ fixation system. *ISME J.* 6, 461–470. doi: 10.1038/ismej.2011.94

Field, K. G., Gordon, D., Wright, T., Rappé, M., Urback, E., Vergin, K., et al. (1997). Diversity and depth-specific distribution of SAR11 cluster rRNA genes from marine planktonic bacteria. *Appl. Environ. Microbiol.* 63, 63–70.

Frias-Lopez, J., Shi, Y., Tyson, G. W., Coleman, M. L., Schuster, S. C., Chisholm, S. W., et al. (2008). Microbial community gene expression in ocean surface waters. *Proc. Natl. Acad. Sci. U.S.A.* 105, 3805–3810. doi: 10.1073/pnas.0708897105

Fuchsman, C. A., Staley, J. T., Oakley, B. B., Kirkpatrick, J. B., and Murray, J. W. (2012). Free-living and aggregate-associated Planctomycetes in the Black Sea. *FEMS Microbiol. Ecol.* 80, 402–416. doi: 10.1111/j.1574-6941.2012.01306.x

Fuhrman, J. A., and Davis, A. A. (1997). Widespread Archaea and novel bacteria from the deep sea as shown by 16S rRNA gene sequences. *Mar. Ecol. Prog. Ser.* 150, 275–285. doi: 10.3354/meps150275

Gallo, N. D., and Levin, L. A. (2016). "Chapter three - Fish ecology and evolution in the world's oxygen minimum zones and implications of ocean deoxygenation," in *Advances in Marine Biology*, ed. E. C. Barbara (Cambridge, MA: Academic Press), 117–198.

Ganesh, S., Bristow, L. A., Larsen, M., Sarode, N., Thamdrup, B., and Stewart, F. J. (2015). Size-fraction partitioning of community gene transcription and nitrogen metabolism in a marine oxygen minimum zone. *ISME J.* 9, 2682–2696. doi: 10.1038/ismej.2015.44

Ganesh, S., Parris, D. J., Delong, E. F., and Stewart, F. J. (2014). Metagenomic analysis of size-fractionated picoplankton in a marine oxygen minimum zone. *ISME J.* 8, 187–211. doi: 10.1038/ismej.2013.144

Gardner, W. D. (1977). Incomplete extraction of rapidly settling particles from water samplers1. *Limnol. Oceanogr.* 22, 764–768. doi: 10.4319/lo.1977.22.4.0764

Garfield, P. C., Packard, T. T., Friederich, G. E., and Codispoti, L. A. (1983). A subsurface particle maximum layer and enhanced microbial activity in the secondary nitrite maximum of the northeastern tropical Pacific Ocean. *J. Mar. Res.* 41, 747–768. doi: 10.1357/002224083788520496

Grossart, H.-P. (2010). Ecological consequences of bacterioplankton lifestyles: changes in concepts are needed. *Environ. Microbiol. Rep.* 2, 706–714. doi: 10.1111/j.1758-2229.2010.00179.x

Gruber, N. (2011). Warming up, turning sour, losing breath: ocean biogeochemistry under global change. *Philos. Trans. A Math. Phys. Eng. Sci.* 369:1980–1996. doi: 10.1098/rsta.2011.0003

Guillou, L., Viprey, M., Chambouvet, A., Welsh, R., Kirkham, A., Massana, R., et al. (2008). Widespread occurrence and genetic diversity of marine parasitoids belonging to Syndiniales (Alveolata). *Environ. Microbiol.* 10, 3349–3365. doi: 10.1111/j.1462-2920.2008.01731.x

Hawley, A. K., Brewer, H. M., Norbeck, A. D., Paša-Tolić, L., and Hallam, S. J. (2014). Metaproteomics reveals differential modes of metabolic coupling among ubiquitous oxygen minimum zone microbes. *Proc. Natl. Acad. Sci. U.S.A.* 111, 11395–11400. doi: 10.1073/pnas.1322132111

Hawley, A. K., Torres-Beltrán, M., Zaikova, E., Walsh, D. A., Mueller, A., Scofield, M., et al. (2017). A compendium of multi-omic sequence information from the Saanich Inlet water column. *Sci. Data* 4:170160. doi: 10.1038/sdata.2017.160

Herlinveaux, R. H. (1962). Oceanography of Saanich Inlet in Vancouver Island, British Columbia. *J. Fish. Res. Board Can.* 19, 1–37. doi: 10.1139/f62-001

Jakuba, M., Gomez-Ibanez, D., Saito, M. A., Dick, G., and Breier, J. A. Jr. (2014). *Clio: An Autonomous Vertical Sampling Vehicle for Global Ocean Biogeochemical Mapping*. Washington, DC: American Geophysical Union.

Jones, W. J., Preston, C. M., Marin Iii, R., Scholin, C. A., and Vrijenhoek, R. C. (2008). A robotic molecular method for in situ detection of marine invertebrate larvae. *Mol. Ecol. Resour.* 8, 540–550. doi: 10.1111/j.1471-8286.2007.02021.x

Kassambara, A. (2017). *ggpubr: 'ggplot2' Based Publication Ready Plots. R Package Version 0.1.5*. Available at: https://rdrr.io/cran/ggpubr/.

Keeling, R. E., Kortzinger, A., and Gruber, N. (2010). Ocean deoxygenation in a warming world. *Ann. Rev. Mar. Sci.* 2, 199–229. doi: 10.1146/annurev.marine.010908.163855

Kirkpatrick, J., Oakley, B., Fuchsman, C., Srinivasan, S., Staley, J. T., and Murray, J. W. (2006). Diversity and distribution of planctomycetes and related bacteria in the suboxic zone of the black Sea. *Appl. Environ. Microbiol.* 72, 3079–3083. doi: 10.1128/AEM.72.4.3079-3083.2006

Lam, P., and Kuypers, M. M. M. (2011). Microbial nitrogen cycling processes in oxygen minimum zones. *Annu. Rev. Mar. Sci.* 3, 317–345. doi: 10.1146/annurev-marine-120709-142814

Lam, P., Lavik, G., Jensen, M. M., Van De Vossenberg, J., Schmid, M., Woebken, D., et al. (2009). Revising the nitrogen cycle in the Peruvian oxygen minimum zone. *Proc. Natl. Acad. Sci. U.S.A.* 106, 4752–4757. doi: 10.1073/pnas.0812444106

Lepp, P. W., and Schmidt, T. M. (1998). Nucleic acid content of Synechococcus spp. during growth in continuous light and light/dark cycles. *Arch. Microbiol.* 170, 201–207. doi: 10.1007/s002030050634

Levin, L. A., and Breitburg, D. L. (2015). Linking coasts and seas to address ocean deoxygenation. *Nat. Clim. Change* 5, 401–403. doi: 10.1038/nclimate2595

Louca, S., Hawley, A. K., Katsev, S., Torres-Beltran, M., Bhatia, M. P., Kheirandish, S., et al. (2016). Integrating biogeochemistry with multiomic sequence information in a model oxygen minimum zone. *Proc. Natl. Acad. Sci. U.S.A.* 113, E5925–E5933. doi: 10.1073/pnas.1602897113

Naqvi, S. W. A., Bange, H. W., Farías, L., Monteiro, P. M. S., Scranton, M. I., and Zhang, J. (2010). Marine hypoxia/anoxia as a source of CH4 and N2O. *Biogeosciences* 7, 2159–2190. doi: 10.5194/bg-7-2159-2010

Naqvi, S. W. A., Kumar, M. D., Narvekar, P. V., De Sousa, S. N., George, M. D., and D'silva, C. (1993). An intermediate nepheloid layer associated with high

microbial metabolic rates and denitrification in the northwest Indian Ocean. *J. Geophys. Res.* 98, 16469–16479. doi: 10.1029/93JC00973

Oksanen, J., Blanchet, F. G., Kindt, R., Legendre, P., Minchin, P. R., O'hara, R. B., et al. (2015). *vegan: Community Ecology Package*. Available at: http://CRAN.R-project.org/package=vegan R package version 2.3-1

Ottesen, E. A., Marin, R., Preston, C. M., Young, C. R., Ryan, J. P., Scholin, C. A., et al. (2011). Metatranscriptomic analysis of autonomously collected and preserved marine bacterioplankton. *ISME J.* 5, 1881–1895. doi: 10.1038/ismej.2011.70

Ottesen, E. A., Young, C. R., Gifford, S. M., Eppley, J. M., Marin, R., Schuster, S. C., et al. (2014). Multispecies diel transcriptional oscillations in open ocean heterotrophic bacterial assemblages. *Science* 345:207. doi: 10.1126/science.1252476

Padilla, C. C., Ganesh, S., Gantt, S., Huhman, A., Parris, D. J., Sarode, N., et al. (2015). Standard filtration practices may significantly distort planktonic microbial diversity estimates. *Front. Microbiol.* 6:547. doi: 10.3389/fmicb.2015.00547

Paulmier, A., and Ruiz-Pino, D. (2009). Oxygen minimum zones (OMZs) in the modern ocean. *Prog. Oceanogr.* 80, 113–128. doi: 10.1016/j.pocean.2008.08.001

Preston, C. M., Marin, R., Jensen, S. D., Feldman, J., Birch, J. M., Massion, E. I., et al. (2009). Near real-time, autonomous detection of marine bacterioplankton on a coastal mooring in Monterey Bay, California, using rRNA-targeted DNA probes. *Environ. Microbiol.* 11, 1168–1180. doi: 10.1111/j.1462-2920.2009.01848.x

R Core Team (2013). *R: A Language and Environment for Statistical Computing*. Vienna: R Foundation for Statistical Computing.

Rinke, C., Lee, J., Nath, N., Goudeau, D., Thompson, B., Poulton, N., et al. (2014). Obtaining genomes from uncultivated environmental microorganisms using FACS–based single-cell genomics. *Nat. Protoc.* 9:1038. doi: 10.1038/nprot.2014.067

Robidart, J. C., Church, M. J., Ryan, J. P., Ascani, F., Wilson, S. T., Bombar, D., et al. (2014). Ecogenomic sensor reveals controls on N2-fixing microorganisms in the North Pacific Ocean. *ISME J.* 8:1175. doi: 10.1038/ismej.2013.244

Schmidtko, S., Stramma, L., and Visbeck, M. (2017). Decline in global oceanic oxygen content during the past five decades. *Nature* 542, 335–339. doi: 10.1038/nature21399

Shi, Y., Tyson, G. W., and Delong, E. F. (2009). Metatranscriptomics reveals unique microbial small RNAs in the ocean/'s water column. *Nature* 459, 266–269. doi: 10.1038/nature08055

Simon, M., Grossart, H.-P., Schweitzer, B., and Ploug, H. (2002). Microbial ecology of organic aggregates in aquatic ecosystems. *Aquat. Microb. Ecol.* 28, 175–211. doi: 10.3354/ame028175

Smith, D. C., Simon, M., Alldredge, A. L., and Azam, F. (1992). Intense hydrolytic enzyme activity on marine aggregates and implications for rapid particle dissolution. *Nature* 359, 139–142. doi: 10.1038/359139a0

Stepanauskas, R. (2015). Wiretapping into microbial interactions by single cell genomics. *Front. Microbiol.* 6:258. doi: 10.3389/fmicb.2015.00258

Stewart, F. J., Dalsgaard, T., Young, C. R., Thamdrup, B., Revsbech, N. P., Ulloa, O., et al. (2012a). Experimental incubations elicit profound changes in community transcription in OMZ bacterioplankton. *PLoS One* 7:e37118. doi: 10.1371/journal.pone.0037118

Stewart, F. J., Ulloa, O., and Delong, E. F. (2012b). Microbial metatranscriptomics in a permanent marine oxygen minimum zone. *Environ. Microbiol.* 14, 23–40. doi: 10.1111/j.1462-2920.2010.02400.x

Stewart, F. J., Ottesen, E. A., and Delong, E. F. (2010). Development and quantitative analyses of a universal rRNA-subtraction protocol for microbial metatranscriptomics. *ISME J.* 4, 896–907. doi: 10.1038/ismej.2010.18

Stramma, L., Johnson, G. C., Sprintall, J., and Mohrholz, V. (2008). Expanding oxygen-minimum zones in the tropical Oceans. *Science* 320:655. doi: 10.1126/science.1153847

Stramma, L., Schmidtko, S., Levin, L. A., and Johnson, G. C. (2010). Ocean oxygen minima expansions and their biological impacts. *Deep Sea Res. Part I Oceanogr. Res. Pap.* 57, 587–595. doi: 10.1016/j.dsr.2010.01.005

Suter, E. A., Scranton, M. I., Chow, S., Stinton, D., Medina Faull, L., and Taylor, G. T. (2016). Niskin bottle sample collection aliases microbial community composition and biogeochemical interpretation. *Limnol. Oceanogr.* 62, 606–617. doi: 10.1002/lno.10447

Suzuki, R., and Shimodaira, H. (2015). *pvclust: Hierarchical Clustering with P-Values via Multiscale Bootstrap Resampling. R Package Version 2.0-0*. Available at: http://CRAN.R-project.org/package=pvclust

Taylor, C. D., and Doherty, K. W. (1990). Submersible Incubation Device (SID), autonomous instrumentation for the in situ measurement of primary production and other microbial rate processes. *Deep Sea Res. Part A Oceanogr. Res. Pap.* 37, 343–358. doi: 10.1016/0198-0149(90)90132-F

Taylor, C. D., Edgcomb, V. P., Doherty, K. W., Engstrom, I., Shanahan, T., Pachiadaki, M. G., et al. (2015). Fixation filter, device for the rapid in situ preservation of particulate samples. *Deep Sea Res. Part A Oceanogr. Res. Pap.* 96, 69–79. doi: 10.1016/j.dsr.2014.09.006

Torres-Beltrán, M., Hawley, A., Capelle, D., Bhatia, M., Durno, E., Tortell, P., et al. (2016). Methanotrophic community dynamics in a seasonally anoxic fjord: saanich inlet, British Columbia. *Front. Mar. Sci.* 3:268. doi: 10.3389/fmars.2016.00268

Torres-Beltrán, M., Hawley, A. K., Capelle, D., Zaikova, E., Walsh, D. A., Mueller, A., et al. (2017). A compendium of geochemical information from the Saanich Inlet water column. *Sci. Data* 4:170159. doi: 10.1038/sdata.2017.159

Tripp, H. J., Kitner, J. B., Schwalbach, M. S., Dacey, J. W. H., Wilhelm, L. J., and Giovannoni, S. J. (2008). SAR11 marine bacteria require exogenous reduced sulphur for growth. *Nature* 452, 741–744. doi: 10.1038/nature06776

Venables, W. N., and Ripley, B. D. (2002). *Modern Applied Statistics with S*, 4th Edn. New York, NY: Springer. doi: 10.1007/978-0-387-21706-2

Walsh, D. A., and Hallam, S. J. (2011). "Bacterial Community Strucuture and Dynamics in a seasonally anoxic fjord: Saanich Inlet, British Columbia," in *Handbook of Molecular Microbial Ecology II: Metagenomics in Different Habitats*, ed. F. J. De Brujin (Hoboken, NJ: Wiley-Blackwell), 253–267.

Walsh, D. A., Zaikova, E., Howes, C. G., Song, Y. C., Wright, J. J., Tringe, S. G., et al. (2009). Metagenome of a versatile chemolithoautotroph from expanding oceanic dead zones. *Science* 326, 578–582. doi: 10.1126/science.1175309

Ward, B. B., Devol, A. H., Rich, J. J., Chang, B. X., Bulow, S. E., Naik, H., et al. (2009). Denitrification as the dominant nitrogen loss process in the Arabian Sea. *Nature* 461, 78–81. doi: 10.1038/nature08276

Whitmire, A. L., Letelier, R. M., Villagrán, V., and Ulloa, O. (2009). Autonomous observations of in vivo fluorescence and particle backscattering in an oceanic oxygen minimum zone. *Opt. Express* 17, 21992–22004. doi: 10.1364/OE.17.021992

Whitney, F. A., Freeland, H. J., and Robert, M. (2007). Persistently declining oxygen levels in the interior waters of the eastern subarctic Pacific. *Prog. Oceanogr.* 75, 179–199. doi: 10.1016/j.pocean.2007.08.007

Wickham, H. (2009). *ggplot2: Elegant Graphics for Data Analysis*. New York, NY: Springer-Verlag. doi: 10.1007/978-0-387-98141-3

Wright, J. J., Konwar, K. M., and Hallam, S. J. (2012). Microbial ecology of expanding oxygen minimum zones. *Nat. Rev. Microbiol.* 10, 381–394. doi: 10.1038/nrmicro2778

Wrighton, K. C., Thomas, B. C., Sharon, I., Miller, C. S., Castelle, C. J., Verberkmoes, N. C., et al. (2012). Fermentation, hydrogen, and sulfur metabolism in multiple uncultivated bacterial phyla. *Science* 337:1661. doi: 10.1126/science.1224041

Zaikova, E., Walsh, D. A., Stilwell, C. P., Mohn, W. W., Tortell, P. D., and Hallam, S. J. (2010). Microbial community dynamics in a seasonally anoxic fjord: Saanich Inlet, British Columbia. *Environ. Microbiol.* 12, 172–191. doi: 10.1111/j.1462-2920.2009.02058.x

Conflict of Interest Statement: The authors declare that the research was conducted in the absence of any commercial or financial relationships that could be construed as a potential conflict of interest.

frontiers in Marine Science

ORIGINAL RESEARCH
published: 29 May 2019
doi: 10.3389/fmars.2019.00270

Multidecadal Changes in Marine Subsurface Oxygenation Off Central Peru During the Last ca. 170 Years

Jorge Cardich[1,2], Abdelfettah Sifeddine[3], Renato Salvatteci[4], Dennis Romero[5], Francisco Briceño-Zuluaga[6], Michelle Graco[5], Tony Anculle[5], Carine Almeida[2] and Dimitri Gutiérrez[1,5]**

[1] LID-CIDIS-Facultad de Ciencias y Filosofía, Universidad Peruana Cayetano Heredia, Lima, Peru, [2] Departamento de Geoquimica, Universidade Federal Fluminense, Rio de Janeiro, Brazil, [3] Centre IRD France-Nord, LOCEAN, Paris, France, [4] Institute of Geoscience, Kiel University, Kiel, Germany, [5] Dirección General de Investigaciones Oceanográficas y Cambio Climático, Instituto del Mar del Perú – IMARPE, Callao, Peru, [6] Programa de Geociencias, Instituto de Investigaciones Marinas y Costeras – INVEMAR, Santa Marta, Colombia

Subsurface water masses with permanent oxygen deficiency (oxygen minimum zones, OMZ) are typically associated with upwelling regions and exhibit a high sensitivity to climate variability. Over the last decade, several studies have reported a global ocean deoxygenation trend since 1960 and a consequent OMZ expansion. However, some proxy records suggest an oxygenation trend for the OMZ over the margins of the Tropical North East Pacific since ca. 1850. At the Tropical South East Pacific, the upper Peruvian margin is permanently impinged by a shallow and intense OMZ. In this study, we aim to (1) reconstruct the (multi)decadal oxygenation variability off central Peru, and (2) to identify the influence of both largescale and local factors and the potential underlying mechanisms driving subsurface oxygenation in the Eastern Pacific. We combined a multiproxy approach in multiple paleoceanographic records for the last ∼170 years with instrumental records of subsurface oxygen concentrations since 1960. We analyzed benthic foraminiferal assemblages, redox-sensitive metals (Mo, Re, U), $\delta^{15}N$ and contents of total organic carbon and biogenic silica in multiple sediment cores collected in the upper margin off Callao (180 m) and Pisco (∼300 m). An OMZ weakening over the Peruvian central margin can be inferred from 1865 to 2004. The records can be divided in three major periods, based on responses of local productivity and subsurface ventilation: (i) the mid to late 19th century, with enhanced siliceous productivity, a strong oxygen-deficient and reducing sedimentary conditions; (ii) the late 19th century to mid-twentieth century, with less oxygen-deficient and reducing sedimentary conditions, superimposed to a slight decadal-scale variability; and (iii) the late 20th century until the early 2000's, with a slight oxygenation trend. We attribute the centennial-scale oxygenation trend in the Tropical East Pacific to ventilation processes by undercurrents that decreased subsurface oxygenation even when during the same period an overall increase in export production was inferred off Peru. Unlike other upwelling areas in the Tropical East Pacific, subsurface oxygenation off Peru does not show a decrease in the last decades, instead a subtle oxygenation trend was observed close to the core of the OMZ at 200 m depth.

Keywords: deoxygenation, OMZ, redox metals, benthic foraminifera, Peru

OPEN ACCESS

Edited by:
Emilio Garcia-Robledo, University of Cádiz, Spain

Reviewed by:
Annie Bourbonnais, University of South Carolina, United States
Thomas Smith Weber, University of Rochester, United States

****Correspondence:***
Jorge Cardich
jorge.cardich.s@upch.pe
Dimitri Gutiérrez
dgutierrez@imarpe.gob.pe;
dimitri.gutierrez.a@upch.pe

Specialty section:
This article was submitted to Marine Biogeochemistry, a section of the journal Frontiers in Marine Science

Received: *10 August 2018*
Accepted: *03 May 2019*
Published: *29 May 2019*

Citation:
Cardich J, Sifeddine A, Salvatteci R, Romero D, Briceño-Zuluaga F, Graco M, Anculle T, Almeida C and Gutiérrez D (2019) Multidecadal Changes in Marine Subsurface Oxygenation Off Central Peru During the Last ca. 170 Years. Front. Mar. Sci. 6:270. doi: 10.3389/fmars.2019.00270

INTRODUCTION

Massive oceanic midwaters with permanent oxygen-deficiency are found in the open ocean and in regions influenced by coastal upwelling (e.g., East Pacific, Arabian Sea). These areas are known as oxygen minimum zones (OMZ) and are produced by the combination of high oxygen demand, sluggish circulation, and low-oxygen source waters (Helly and Levin, 2004; Karstensen et al., 2008). The OMZs show strong variability at multiple time scales, ranging from interannual (Cabré et al., 2015; Graco et al., 2017) to geological scales (Jaccard and Galbraith, 2012). OMZs play a relevant role in the global cycles of carbon and nitrogen, and related greenhouse gasses (Paulmier and Ruiz-Pino, 2008) and constrain productivity and biodiversity (Levin et al., 2009).

Over the last decade, several studies have reported global ocean deoxygenation trends since the middle of the 20th century (Bograd et al., 2008; Stramma et al., 2008; Keeling et al., 2010; Horak et al., 2016; Schmidtko et al., 2017). The main drivers of deoxygenation in the upper water column are increased stratification, reduction of oxygen solubility and acceleration of oxygen consumption, all due to global warming (Keeling and Garcia, 2002; Breitburg et al., 2018). As a result, an expansion of OMZs have been documented (Stramma et al., 2008). Another type of oxygen loss occurs in coastal waters, where dead zones are caused by human-caused eutrophication. These zones have increased in number (Breitburg et al., 2018) and their interaction with expanding OMZs represent a global threat for ecosystems and coastal fisheries (Stramma et al., 2010). Global deoxygenation is expected to continue in the future with climate change, as most of numerical models predict (Bopp et al., 2013). However, several global models fail to reproduce recent regional deoxygenation trends and differ in the prediction of future regional trends, particularly in the tropics where most of OMZs are hosted (Schmidtko et al., 2017).

The Peruvian upwelling system is one of the most productive areas of the world ocean (Chávez and Messié, 2009) and is associated with a permanent, intense and shallow OMZ (Gutiérrez et al., 2008; Graco et al., 2017). The source of low oxygen waters and nutrients that feeds coastal upwelling is the Peru–Chile Undercurrent (PCUC; Montes et al., 2014). The OMZ is wider off central Peru and impinges the continental margin, generating strong biogeochemical gradients in the surface sediments (Gutiérrez et al., 2006). The Peruvian upwelling system is also subjected to a significant interannual variability linked to equatorial Kelvin waves and the El Niño-Southern Oscillation (ENSO) that affects upwelling, nutrient availability and coastal ventilation (Chavez et al., 2008; Espinoza-Morriberón et al., 2017). The oxycline and the coastal subsurface oxygenation off Peru are modulated by this interannual variability and temporal regimes can be defined by the occurrence, frequency and intensity of El Niño (EN) events and Kelvin waves (Gutiérrez et al., 2008; Graco et al., 2017). The seasonal cycle is driven by local respiration, vertical mixing/stratification and mesoscale circulation as eddies and filaments (Thomsen et al., 2016; Vergara et al., 2016; Graco et al., 2017).

Several geochemical and biogenic proxies are used to infer geochemical conditions. Redox-sensitive metals are usually used to infer paleo-redox conditions. Poorly oxygenated overlying waters and the flux of organic matter control sedimentary reducing conditions (McManus et al., 2006). Metal enrichment (excess part from a background) occurs during or after deposition, and each metal presents different sensitivities in the redox gradient (Tribovillard et al., 2006). In general, higher metal enrichment in the sediments suggest more reducing conditions (Tribovillard et al., 2006). Scholz et al. (2011) summarized the behavior of main redox-sensitive metals in the Peruvian margin. Among them, molybdenum and uranium show different sensitivities to redox conditions that can be used to depict sulfidic (Mo) to suboxic (U) conditions. Rhenium is another metal that behaves as U (Colodner et al., 1995; Crusius et al., 1996). Benthic foraminiferal assemblages represent another reliable proxy for paleo-redox reconstructions. The living community is abundant in marine sediments, is highly sensitive to environmental changes and their calcareous tests are preserved in the sediment record (Gooday, 2003). Calcareous benthic foraminifera are abundant in OMZ sediments such as off California (Phleger and Soutar, 1973), Peru (Mallon et al., 2012; Cardich et al., 2015), and in the Arabian Sea (Caulle et al., 2014, 2015). Calcareous tests of dead foraminifera are typically well preserved in low-oxygen sediments, but oxygenation events might promote carbonate diagenesis (Jahnke et al., 1997). In the Peruvian margin, the foraminiferal assemblages are associated with particular biogeochemical states defined by the interplay of porewater sulfide concentration and the quality of sedimentary organic matter (Cardich et al., 2015).

Large changes in OMZ intensity have been reconstructed in the Eastern Tropical South Pacific during the Late Quaternary (Gutiérrez et al., 2009; Scholz et al., 2014; Salvatteci et al., 2016). Based on multiproxy records (e.g., trace metals, foraminifera, organic carbon, $\delta^{15}N$) from two sites located in the current OMZ core (dissolved oxygen ~0.2 ml/l), centennial-scale biogeochemical regimes were evidenced (Gutiérrez et al., 2009). For instance, a major shift from low productivity and suboxic bottom waters to nutrient-rich, oxygen-depleted waters is evidenced toward the ending of the Little Ice Age period (early 19th century). The current low oxygen levels in the OMZ off Peru were established after a large climatic reorganization in the tropical Pacific involving the Intertropical Convergence Zone, the South Pacific Subtropical High and the Walker circulation (Sifeddine et al., 2008; Gutiérrez et al., 2009; Salvatteci et al., 2014b). Changes in this ocean-atmosphere circulation controls the Humboldt system variability at longer time-scales (Salvatteci et al., 2016, 2019).

Here, we studied the decadal to multidecadal subsurface oxygenation variability from the central Peruvian continental margin using a multiproxy approach combining multiple proxies from sediment records and oxygen measurements. First, we assessed the oxygenation trends at 60, 150, and 200 m depth based on instrumental data for the 1960 – 2010 period. Second, we assessed benthic foraminiferal records in order to depict sedimentary redox changes associated with variations in OMZ intensity throughout the 180-year record. The interpretation of benthic foraminiferal indicators is achieved through a calibration with ecological distribution data shown by Cardich et al. (2015)

and complemented with new data presented in this work. Our goal is to determine the relative importance of large-scale (i.e., ocean-atmosphere) versus local processes (i.e., export production) driving sub-surface oxygenation off Peru. To do so, we compared our results to other geochemical proxies analyzed in the same box cores (described in detail in Sifeddine et al., 2008; Gutiérrez et al., 2009, 2011; Salvatteci et al., 2014b, 2016; Briceño Zuluaga et al., 2016) and to regional paleo-records.

MATERIALS AND METHODS

Study Area

The central Peruvian upper margin presents some geomorphological differences: the shelf (200-m isobath) north of 13°S is relatively wide (∼50 km) with a pronounced break to the slope, while south of 14°S is narrow (∼15 km) and with a soft transition to the slope (**Figure 1B**). Sediments in the central Peruvian upper margin contain fine grains, are rich in organic carbon (Gutiérrez et al., 2006) and are highly reduced (Suits and Arthur, 2000). Sediment records show different structures, but laminations are common (Salvatteci et al., 2014a). Muddy laminated areas are found between Huacho and Callao (11 – 12°S; Reinhardt et al., 2002), but sedimentary records retrieved in the OMZ core off Pisco (14°S) are better laminated (Gutiérrez et al., 2006; Salvatteci et al., 2014a). ^{210}Pb sedimentation rates vary from 0.4 mm/y to 4 mm/y in the shelf and slope (Levin et al., 2002; Gutiérrez et al., 2009; Salvatteci et al., 2018). **Figure 1B** shows the main three equatorial currents arriving the Eastern Tropical Pacific. The Equatorial Undercurrent (EUC) and the primary and secondary Southern Subsurface Countercurrents feed the Peru Undercurrent (PUC) (Montes et al., 2010). **Figure 1B** also shows the two main subsurface currents off Chile and Peru, the PUC and the equatorward Chile-Peru Deep Coastal Current (CPDCC, Chaigneau et al., 2013) with an upper limit at ∼500 m is depicted as well.

Dissolved Oxygen Concentration

To assess the oxygen variability in the last decades, we used instrumental data of dissolved oxygen by Winkler titration *in situ* analysis (Strickland and Parsons, 1968; Grasshoff et al., 1999) from multiple cruises carried out by the Peruvian Institute of Marine Research (IMARPE) and from the World Ocean Database for the 1960 – 2017 period (WOD 2018) (**Figure 2A**). In order to avoid bias we do not include information available in the last decades by other instrument (e.g., CTD, Argos). Quarterly data from 1960 to 2010 between 11 and 15° S for the oceanic area (30 – 100 nautical miles) were analyzed in different water column depths (60, 80, 100, 150, and 200 m). These depths were chosen after evaluating the dissolved oxygen (DO) mean profile for central Peru (**Figure 2B**). Data of DO were downloaded from the WOD 2018 for the 1960 – 2017 period and is available at https://www.nodc.noaa.gov/OC5/woa18/. For the depth time series, data with >3 replicates were used in the analysis. Afterward, measurements were integrated to show semi-annual variability. A regression analysis was performed for the time series to evaluate significant temporal trends in the time series.

Core Sampling

Soutar box cores were collected off Callao (B0405-13, 12°00′S, 72°42′W, 184 m) and off Pisco (B0405-06, 14°07′S, 76°30′W, 299 m) in May 2004 on board of the R/V José Olaya Balandra (**Figure 1B**). Hereafter both cores will be referred as B-13 and B-6, respectively. The processing of the box cores is described in detail in Gutiérrez et al. (2006). The length of B-13 and B-6 is ∼78 and ∼74 cm, respectively. Both box cores were longitudinally sectioned in six slabs (I – VI) and each of those were used to determine physical characteristics (e.g., X radiography), chronology and geochemical and biogenic proxies. Subsampling for proxies was done following the laminae or bands in the record (Gutiérrez et al., 2006; Morales et al., 2006). Geochronology in both records was solved with radiocarbon dating of bulk organic sedimentary carbon and ^{210}Pb measurements (Gutiérrez et al., 2009; **Supplementary Material** therein). The last ∼33 cm (B-13) and ∼34 cm (B-6) represent the period from ∼1830 to 2004 (∼180 years). This time period consisted of a total of 37 and 41 subsamples (0.25 – 0.8 cm of thickness) in B-13 and B-6, respectively. A third box core nearby B-6 is considered in this study: B0506 – 14, 14°27′S, 76°43′W, 301 m (hereafter referred as B-14). The subsampling and processing of B-14 is described in detail in Salvatteci et al. (2014b). X-ray images of the three box cores are shown in **Supplementary Figure S1A**. The three box cores show laminated sections and the period from ∼1830 to 2004 starts after a shift in physical properties (e.g., dry bulk density and percentage of calcite, **Supplementary Figure S1**). The Pisco box cores (B-6 and B-14) are located in the core of the SE Pacific OMZ (**Figures 1A,C**) while the Callao box core (B-13) is closer to the upper limit of the OMZ.

Benthic Foraminifera

Pre-treatment for box core subsamples for foraminifera is described in Salvatteci et al. (2012). These subsamples were treated with oxygen peroxide (30%) and sodium pyrophosphate under temperatures of 40–50°C for 5–10 minutes to disaggregate the organic matter. Residual material was later sieved through sieves of 355, 125, and 63 μm mesh size. The material retained in the 125 and 63 μm sieves was dried for about an hour at 40° C. Foraminifera were sorted and counted at the lowest taxonomical level, if possible, in the 63 – 125 μm size fraction under a stereoscopic microscope. Counts from this fraction were then integrated to the counts from the >125 μm size fraction published in Morales et al. (2006) and Gutiérrez et al. (2009). Splitting of large subsamples was performed using an Otto micro-splitter. A minimum of 300 tests was sorted in the splits. We calculated diversity indices on the raw abundance of foraminifera. The Shannon-Wiener index (H') was calculated as an indicator of diversity; while the Pielou index (J') was used to show how similar the abundances of the species are in a sample. Foraminiferal standing stocks were expressed in number of individuals per gram of dry sediment (#ind. g^{-1}). Species with percentages > 0.5% in at least three samples (5% of the total number of samples) were included in subsequent statistical analyses. In addition to counts of benthic foraminifera in the box cores, counts of planktonic foraminifera from the >125 μm

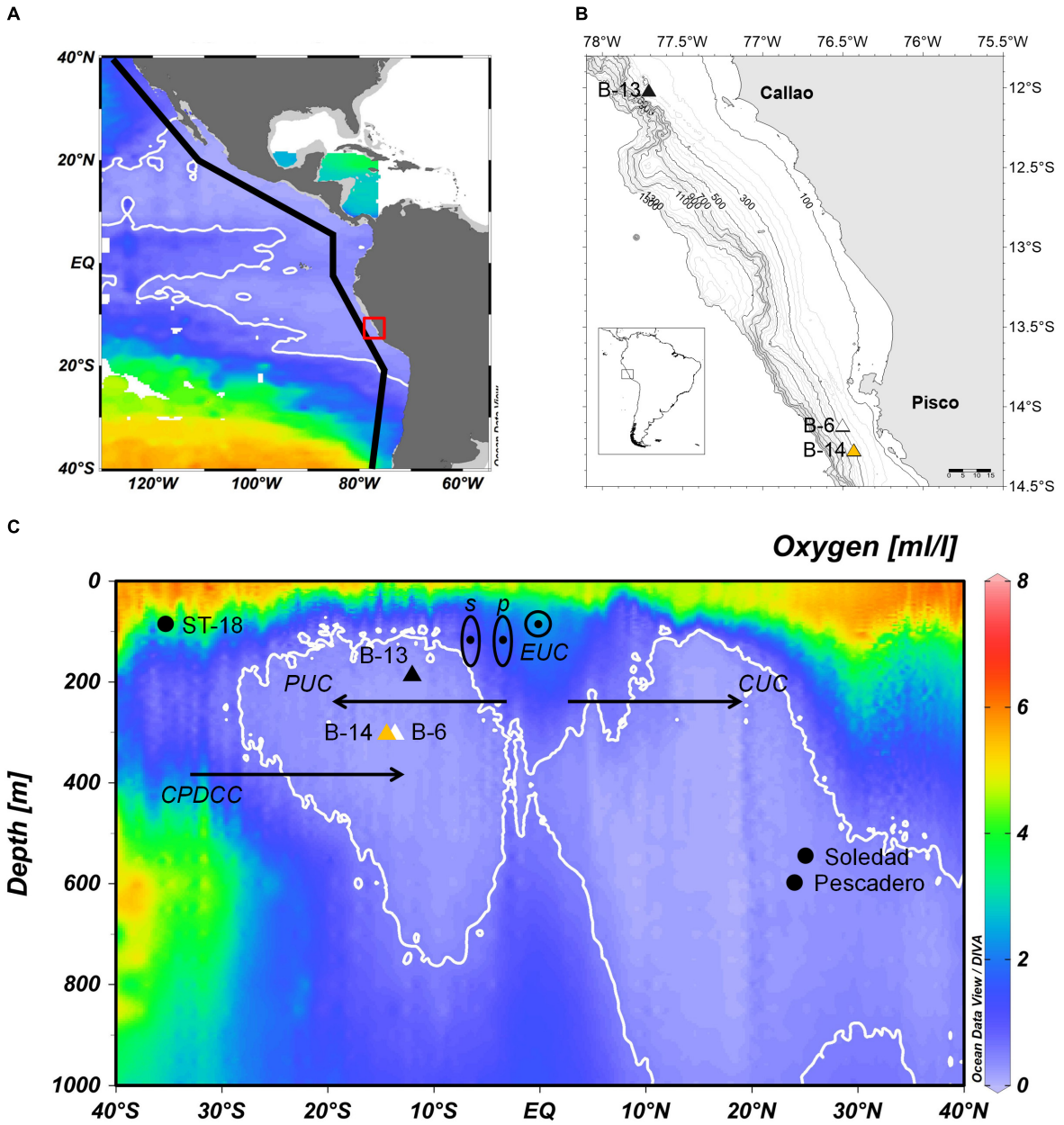

FIGURE 1 | Site location and description of box cores used in this study. **(A)** Mean dissolved oxygen concentration (ml l^{-1}) at 400 m depth at the Tropical East Pacific (data available in World Ocean Database 2013). **(B)** Map of central Peru indicating the location of B0405-13 (B-13; 12°00' S, 77°42′ W, 184 m), B0405-06 (B-6; 14°07′ S, 76°30′ W, 299 m) and B0506-14 (B-14; 14°27′S, 76°43′W, 301 m). **(C)** Dissolved oxygen concentration in an oceanographic section along the coast of America (black line in inset in A), showing the position of the cores in relation to the OMZ and the principal subsurface currents. Triangles are our box cores (B-13, B-6 and B-14) and black circles are other sites considered in the discussion: Soledad and Pescadero (Deutsch et al., 2014) and ST-18 (Srain et al., 2015).

fraction (published in Morales et al., 2006) were used to calculate the planktonic to benthic ratio (P/B) to assess calcite preservation in the sediment. We only applied the P/B in the >125 μm fraction as planktonic foraminifera are well preserved here.

In order to understand the foraminiferal assemblages in the cores, we calibrated the living foraminiferal stocks with oxygen and sedimentary redox gradients. For this purpose, we compiled abundance data of the main calcareous benthic foraminifera off Callao and Pisco. We complemented the dataset from Cardich et al. (2015) with new samples of living calcareous foraminiferal stocks from 2012 to 2016. These samples were taken during IMARPE surveys and during the Meteor 92 cruise. We also include other studies from the upper margin of central Peru: Pérez et al. (2002) and Mallon et al. (2012) to better represent the fauna zonation of benthic foraminifera.

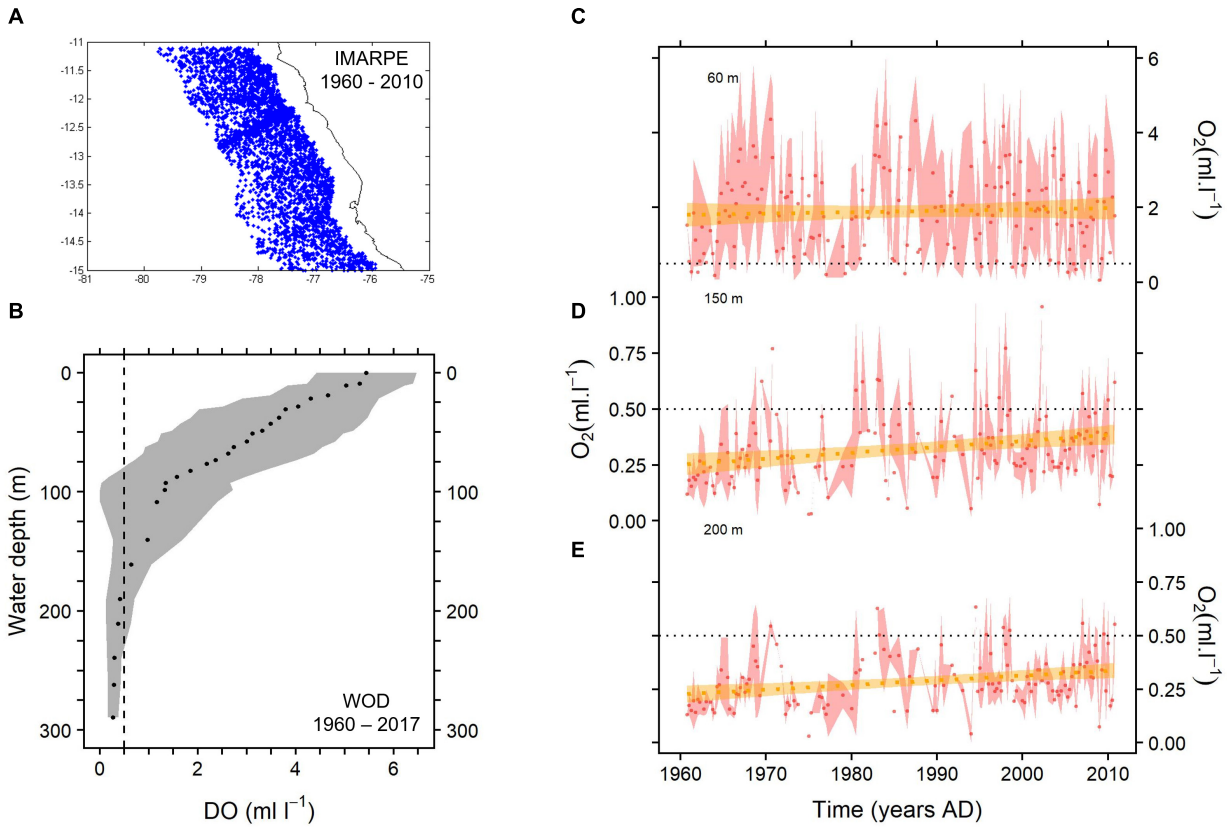

FIGURE 2 | Time series (1960 – 2010) of dissolved oxygen off central Peru. **(A)** Map showing the IMARPE oceanographical stations between 30 and 100 NM and 11 and 15° S. **(B)** Mean dissolved oxygen profile with error values in the water column for the area depicted in **(A)** (data available in World Ocean Database 2018). Time series of dissolved oxygen at 60 m **(C)**, 150 m **(D)** and 200 m **(E)** depth. Red areas indicate error values. Trend lines with confidence intervals (orange) for each depth are indicated.

Geochemical Proxies

We compiled published geochemical information for B-13, B-6, and B-14 to assess the temporal variability of benthic redox conditions (trace metals), water column denitrification ($\delta^{15}N$) and export production (TOC and biogenic silica). The methodology and data for the geochemical (Mo and $\delta^{15}N$) and organic concentrations [total organic carbon (TOC), biogenic silica] for B-13 and B-6 are shown in Gutiérrez et al. (2009). Data for B-14 (TOC, biogenic silica, Mo, Re and $\delta^{15}N$) were published in Salvatteci et al. (2014b, 2018). Subsampling for geochemical proxies in B-13 and B-6 was done every centimeter for trace elements and every two centimeters for TOC, biogenic silica and $\delta^{15}N$ (Gutiérrez et al., 2009). Subsampling resolution was higher for B-14 (Salvatteci et al., 2014b, 2018). In cores B-13 and B-6, TOC was determined from total carbon measurements with a Thermo Electron CNS elemental analyzer, corrected for carbonate content (Gutiérrez et al., 2009) while in B-14 it was determined by RockEval (Salvatteci et al., 2014b). $\delta^{15}N$ in B-6 and B-13 was determined by mass spectrometry after acidification at the Department of Geosciences, University of Arizona, United States. $\delta^{15}N$ analyses in B-14 were measured on a continuous flow gas-ratio mass spectrometer at ALYSES laboratory (Bondy, France). Trace metals' concentrations were analyzed by ICP-MS after hot-plate acid digestion in Polytetrafluoroethylene vessels and elimination of organic matter and removal of silica using acid treatments (HF, HNO_3^- and $HClO_4^-$). Besides Molybdenum, Uranium concentrations were measured in B-13 and B-6 and were not published before. Rhenium was only measured in B-14. The detrital (background, usually lithogenic) and authigenic (the excess part) fractions of all three metals were estimated. Authigenic Mo is a proxy for temporal to permanent sulfidic conditions (Scholz et al., 2011). Re and U are enriched under less reducing conditions (Algeo and Tribovillard, 2009), and can be used as a proxy for anoxic, but non-sulfidic, conditions. The enrichment factor (EF) of Mo, Re, and U was calculated using background values of andesite as an adequate representation of detrital material in the Peruvian margin. Mo, Re, and U to aluminum mass ratios in andesite are: 0.25×10^{-4}, 1.93×10^{-9}, and 0.34×10^{-4}, respectively (GEOROC database). The EFs were calculated with the formula: $EF_{element\ x} = (X/Al)_{sample}/(X/Al)_{andesite}$ (Tribovillard et al., 2006). Additionally, Mo/U (for B-13 and B-6) and Re/Mo (for B-14) ratios were used as indicators of redox states.

Statistical Analyses

We performed two principal component analysis (PCA) in order to detect structure in the relationships between variables. The first PCA was performed, in both cores, on a matrix of species data with a prior Hellinger transformation (squared root of relative abundances). Foraminiferal principal components were then compared with living assemblages to reconstruct past redox conditions. The second PCA was performed on a matrix of both foraminiferal and geochemical data. This PCA was used to understand the relationship between the foraminiferal assemblages and the different proxies for environmental changes. A varimax rotation was applied to the loadings. Finally, a non-parametric r Spearman correlation was applied to both foraminiferal and geochemical data. For multiple comparisons, the probability level was corrected by dividing the probability level α ($p < 0.05$) by the number of tests performed (Glantz, 2002). All statistical analyses were conducted using R statistical software version 3.5.1.

RESULTS

Dissolved Oxygen Off Central Peru in 1960–2010

Water column mean DO is highly variable down to ∼125 m depth (**Figure 2B**). Below this depth, DO values are homogenous, more stable and always < 0.5 ml l^{-1}. We chose data from 60, 150, and 200 m (**Figures 2C–E**) as they are in the depth gradient from the oxycline to the OMZ core (**Figure 2B**). The trend of DO values from 1960 to 2010 at 60 m water depth (**Figure 2B**) differed from the trends at 150 and 200 m (**Figures 2C,D**). At 60 m, oxygen values were usually > 1.0 ml l^{-1}, showed high variation and amplitude, and there was not a clear trend in the time series. On the other hand, at 150 and 200 m, oxygen values were usually below 0.5 ml l^{-1} and presented little variation. Both 150 and 200 m time series presented a slight positive trend from 1960 to 2010 ($p < 0.01$). Both time series had an estimated increase of ∼0.02 ml l^{-1} per decade.

Benthic Foraminifera in the Box Cores (∼1835–2005 Period)

The abundance of benthic foraminifera was higher in Callao compared with Pisco, but both sites display similar temporal trends (**Figure 3A**). Densities of benthic foraminifera ranged from 2,504 to 73,660 ind. g^{-1} in B-13 and from 117 to 24,498 ind. g^{-1} in B-6. Four samples of B-6 were discarded from the analysis as they presented low unrealistic values (1 – 15 ind. g^{-1}). Both records presented similar patterns until ca. 1960, with three high peaks in B-13 (1834, 1847, and 1861) and two peaks in B-6 (1843 and 1856) and an increasing trend during the 20th century to reach the maximum abundance in ca. 1950. In the last decades of the records, densities in B-6 decreased, whereas densities increased in B-13 until 1990.

The diversity indices and the P/B ratio presented temporal and spatial changes (**Table 1**). A total of 68 species was identified in both records and a higher species richness was observed in Callao than in Pisco (**Table 1**). The species richness in B-13 (Callao) ranged from 14 to 35 species, while in B-6 (Pisco) it ranged from 5 to 21. The lowest diversity was found between ca. 1865 and ca. 1885 in B-13 (**Table 1**). The diversity then increased from 1910 to 2004 in B-13. The number of species did not change downcore in B-6. Species diversity (H_S) ranged from 1.3 to 2.1 in B-13 and from 0.3 to 1.9 in B-6. In both records, the Pielou's evenness index (J') increased from ca. 1835 to ca. 1870, then decreased until 1950 – 1960. In the last period, H_S and J' increased again in B-6 and remained homogenous in B-13. Finally, P/B ratio values were higher in B-13 than in B-6 from the beginning of the records to ca. 1910 (**Figure 3B**), while from 1910 to 2004, the P/B was similar in both records. After a rise in both records from 1920 to 1945, the values rapidly decreased and remained low in B-6, while those in B-13 did it a decade later.

TABLE 1 | Diversity indices of benthic foraminifera for box cores B-13 and B-6.

	Callao (B-13)			Pisco (B-6)		
	I	II	III	I	II	III
S	20 – 29	14 - 30	16 – 30	5 – 18	6 – 21	13 – 20
H'	1.42 – 1.95	1.39 – 2.07	1.32 – 2.06	0.82 – 1.61	0.32 – 1.79	1.16 – 1.88
J'	0.44 – 0.61	0.44 – 0.67	0.42 – 0.68	0.31 – 0.83	0.18 – 0.61	0.43 – 0.71

Temporal changes in the relative abundance of benthic foraminifera can help to determine the state of sediment redox conditions given that each species have a preferred habitat. The foraminiferal fauna in both records was greatly dominated by *Bolivina seminuda* and *Buliminella tenuata* (>50% of total abundance, **Figures 3C,D**). Both species presented a decadal to multidecadal negative co-variation (B-13: Spearman's ρ = −0.79, $p < 0.001$; B-6: Spearman's ρ = −0.93, $p < 0.001$), especially after ca. 1875 A.D. (**Figure 3C**). *Bolivina costata* (**Figure 3E**) and *Nonionella auris* (**Figure 3F**) presented high densities between ca. 1820 and ca. 1865 in B-13, but were not abundant in B-6. *Bolivina pacifica* showed an increasing trend from ca. 1865 to ca. 1960 in both records (**Figure 3H**). Other species presented different patterns between records (**Figures 3I–M**). The relative abundance of *Suggrunda eckisi* and *Bolivina plicata* was higher in the XX century compared with the XIX century. *Buliminella elegantissima* showed high relative abundances in some time periods in both records (**Figure 3I**). Finally, the presence of *Virgulinella fragilis* was rare and low abundances were recorded only in the last 40 years of the records (**Figure 3G**).

The mean spatial distribution of living benthic foraminifera in sediments between 45 and 300 m depth is shown in **Figure 4A**. The selected species presented a gradual zonation across the upper margin: some species were more abundant near the coast (*B. costata* and *N. auris*), some in the outer shelf (*B. tenuata*, *B. elegantissima,* and *Epistominella* sp.), and others thriving in the upper slope (*B. seminuda*, *B. pacifica,* and others).

The PCA results, based on the different species of benthic foraminifera, indicate that most of the variance of the data set can be explained by two principal components (**Figures 4B,C**). In Callao (B-13) and Pisco (B-6), 56.9 and 66.8% of the total variance of the downcore records was explained by two principal

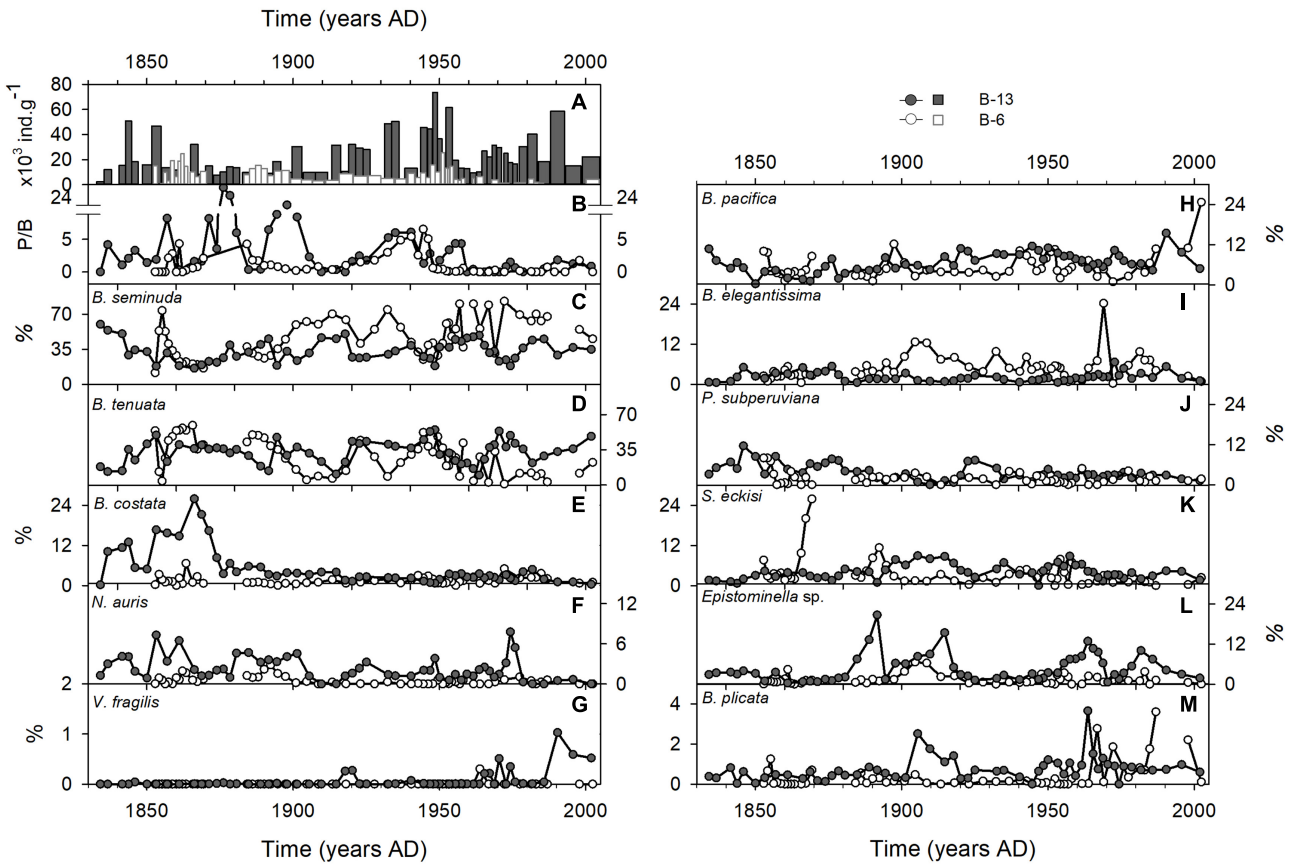

FIGURE 3 | Records of foraminifera in in Callao (B-13, black circles) and Pisco (B-6, white circles) box cores: **(A)** Total densities; **(B)** P/B ratio and **(C–M)** relative abundances (%) of main benthic foraminiferal species.

components. The PC1 in both B-13 (36.8%) and in B-6 (58.8%) was explained mainly by *Bolivina seminuda* and *Buliminella tenuata* (**Figures 4B,C**). PC1 resembles the negative covariation between *B. seminuda* and *B. tenuata* as observed in **Figures 3B,C**. In B-13, *Epistominella* sp. also contributed to PC1 (loading factor = 0.45; **Figure 4B**). PC2 in B-13 (20.1%) and in B-6 (8%) reflected the contrast of *B. pacifica* to different assemblages of species (**Figures 4B,C**). For B-13, *B. pacifica* and *B. tenuata* showed opposite loadings in comparison to *B. costata*. For B-6, loadings of *B. pacifica* were opposed to those of *B. elegantissima* and *Epistominella* sp. These observations are in agreement with the relative position of the sediment cores and the zonation in the recent samples (**Figure 4A**). In B-6, *B. costata* is absent given that it is a coastal species, while *B. elegantissima* and *Epistominella* sp. are present as they thrive in the shelf.

Principal Components of Geochemical and Biogenic Proxies in the Box Cores (∼1835–2005 Period)

The results of the Varimax rotated PCA using geochemical and foraminifera-based proxies in both B-13 and B-6 are shown in **Figure 5**. Values for TOC, Si, δ^{15}N, Mo EF, and Mo/U were used along the selected species in **Figure 4** and the P/B ratio. In B-13 (**Figure 5A**), TOC and *B. pacifica* were opposed to Mo/U, Mo EF, Si, *B. costata* and *N. auris* (Varimax rotated PC1 – RC1). On the other axis, *B. tenuata* was contrasted to *B. seminuda* and the foraminiferal assemblage of deep sites (Varimax rotated PC2 – RC2). A similar pattern is observed in B-6, but with an inversion of the components: *B. seminuda* was contrasted to *B. tenuata* and other outer shelf species (RC1); while Mo/U, Mo EF, and Si were distributed in an opposite direction of *B. pacifica* (RC2). Additionally, TOC was distributed closer to δ^{15}N in Pisco (B-6) than in Callao (B-13).

DISCUSSION

Understanding the Benthic Foraminiferal Assemblages in the Cores

The new observations of living foraminiferal assemblages in addition to the findings in Cardich et al. (2015) helped to determine the temporal changes in sedimentary redox conditions. The distribution of the main species across the upper margin of the central Peru region presented a bathymetrical zonation responding to gradients of OM quality and sulfide

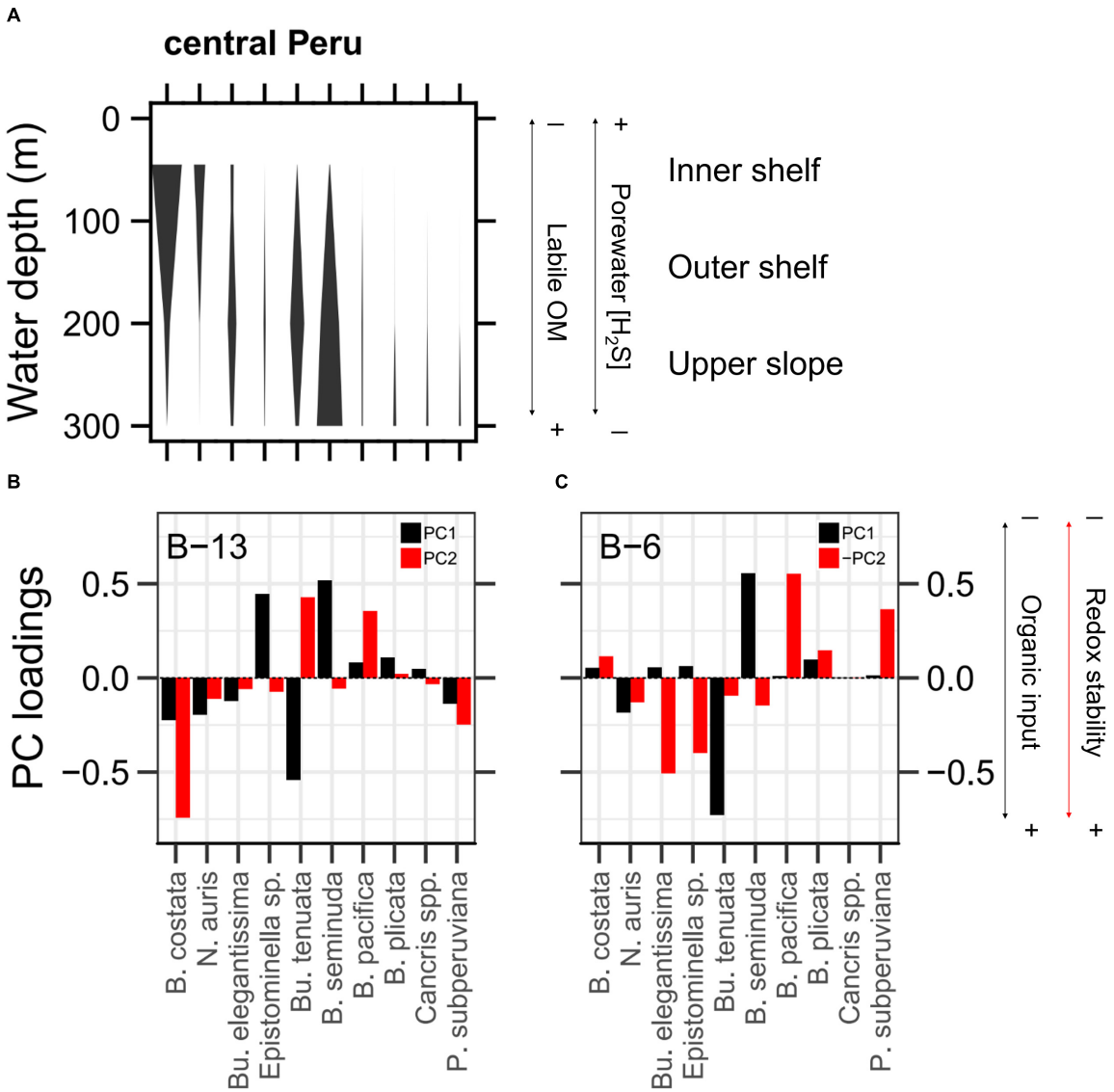

FIGURE 4 | Interpretation of benthic foraminiferal assemblages. **(A)** Distribution of living species in central Peru from several databases: Callao and Pisco upper margin for the 2009 – 2011 period (Cardich et al., 2015) and for the 2012 – 2017 period (Benthos Lab of IMARPE); Callao and Huacho upper margin (M77-2 cruise, 2008; Mallon et al., 2012); Callao upper slope (Panorama Leg3a cruise, 1997; Pérez et al., 2002) and (M92-2 cruise, 2013; Cardich et al., un published). Width of bars indicate mean relative abundance for each species. **(B,C)** Loadings of principal component 1 (black bars) and principal component 2 (red bars) for B-13 (Callao) and B-6 (Pisco). Opposite values of B-6's PC2 scores are shown to maintain coherence in the axes.

concentration. A first group of coastal species (*B. costata* and *N. auris*) is more abundant toward the inner shelf (**Figure 4A**), where sediments are typically sulfidic and rich in fresh phytodetritus (Cardich et al., 2015) but are also exposed to interannual oxygenation events (Gutiérrez et al., 2008). A second group (*Buliminella tenuata*, *B. elegantissima,* and *Epistominella* sp.) is present across the margin, but concentrates in the outer shelf, which is less exposed to oxygenation events, but typically presents sediments with less labile OM, low sulfide tenors and *Thioploca* spp. mats. In third place, there is a group of species more abundant in the upper slope where the low oxygen values are not affected by high frequency temporal variability (OMZ core). In this area, the bottom waters are suboxic (dissolved nitrate is present and nitrite is high, Sommer et al., 2016) and the sediments are postoxic (anoxic, non-sulfidic) and rich in preserved OM (Dale et al., 2015). Within this last group, *Bolivina seminuda* shows a steep growing dominance from the inner shelf toward the upper slope, along the increase of nitrate and nitrite in the overlying waters. This pattern is consistent with the nitrate or nitrite respiration of *B. seminuda* (Piña-Ochoa et al., 2010; Glock et al., 2019). *Bolivina pacifica* is in general less abundant and follows *B. seminuda*'s distribution, but is absent in the inner shelf sulfidic sediments. Finally, *B. plicata*, *Cancris* spp. and *P. subperuviana* are only present in the upper slope.

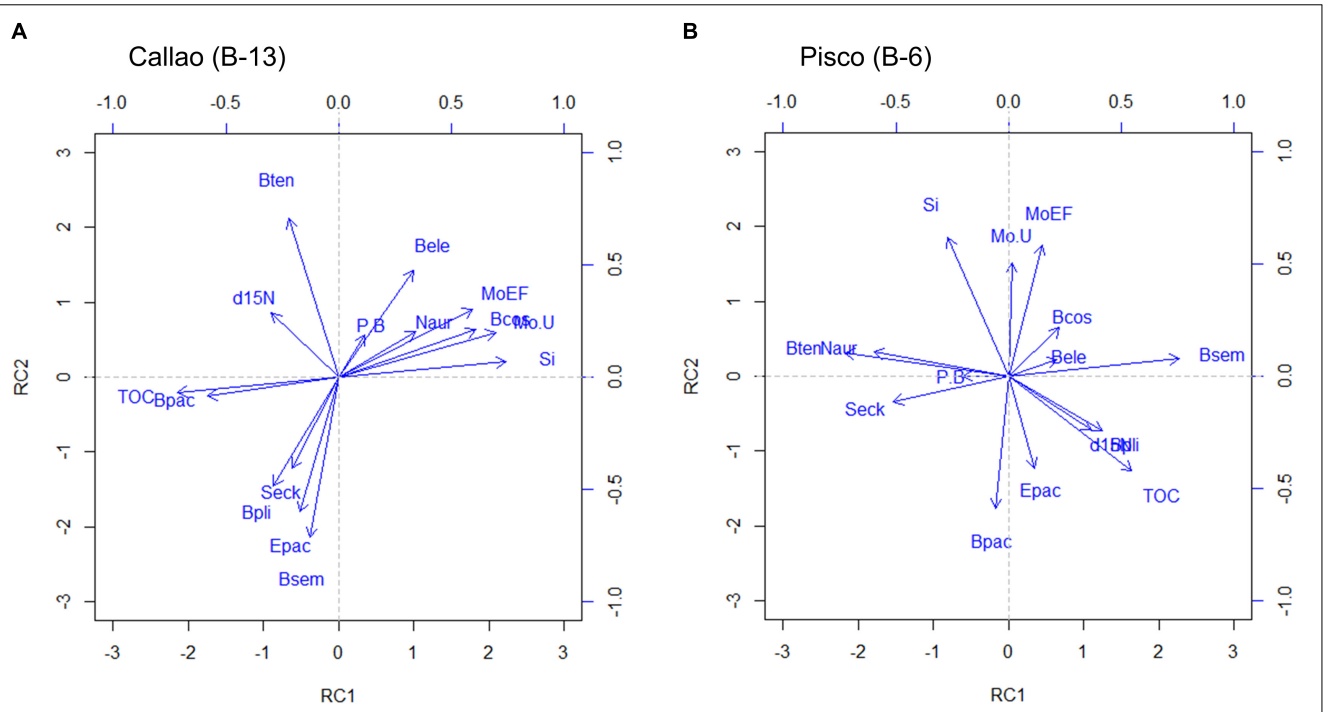

FIGURE 5 | Principal component analysis based on both geochemical and foraminiferal matrices for B-13 **(A)** (Callao; left) and B-6 **(B)** (Pisco; right). Geochemical proxies are: Total organic carbon (TOC), δ^{15}N, biogenic silica (Si), Mo/U, Mo enrichment factor (Mo EF). Foraminiferal proxies are the same benthic species in **Figure 4**, plus the planktonic to benthic ratio (P/B).

Based on the observations from the foraminiferal ecological zonation (Cardich et al., 2015), the species composing the first two principal components of both B-13 and B-6 are part of the main living assemblages of the reduced shelf sediments off Callao and Pisco (**Figure 4**). Moreover, the foraminiferal PCs are in closely agreement with the faunal zonation. This assures the use of the PCs as proxies for biogeochemical gradients (e.g., redox) in our cores. Given that the variance of the PCs can be explained by no more than two or three dominant species (**Figures 4B,C**), we use these species ratios in the sediment cores to reconstruct the redox conditions. The use of ratios simplifies this interpretation of the PCs which is in agreement with the abiotic – biotic relationships (**Figure 5**). Thus, PC1 is expressed as the *B. tenuata* to (*B. tenuata* + *B. seminuda*) ratio [Bt/(Bt+Bs)] for both box cores. On the other hand, PC2 can be expressed as the P*sp* to (A*spx* + P*sp*) ratio, A*sp* representing the anoxia assemblages: *B. costata* for the inner shelf (B-13) and *Bu. elegantissima* and *Epistominella* sp. for the outer shelf (B-6); and P*sp* representing the postoxia species *B. pacifica*. We did not use *B. tenuata* in the P*sp*/(A*spx* + P*sp*) because this species was already present in the first ratio (**Figure 4**).

Principal component analysis results on geochemical and foraminiferal data (**Figure 5**) and Spearman correlations (**Table 2**) in the box cores confirm the above ecological interpretation. Moreover, there is a clear relationship between the different foraminiferal assemblages with reducing conditions in RC2 of both box cores (**Figures 5A,B**). This indicates that the sedimentary geochemical zonation in the margin is consistent and that more reducing conditions (e.g., sulfidic) are typically found near the coast. From the faunal distribution (**Figure 4A**) and the PCA results (**Figure 5**), an association between *B. tenuata* and mild reducing conditions is detected.

The co-variation of *B. tenuata* and *B. seminuda* may be associated with the water column denitrification (WCD). When comparing the *B. tenuata* to (*B. tenuata* + *B. seminuda*) ratio in B-13 and B-6 (**Figures 6E,L**) to the δ^{15}N records (**Figures 6B,I**), a slight co-variation between the dominance of *B. tenuata* (*B. seminuda*) and stronger (weaker) WCD is noticed. This connection might be explained by changes in local export production to the sediments. A greater organic input is translated in prevailing anoxic sediments with no nitrate, low sulfide tenors and more labile OM. The thriving of *B. tenuata* is evident in this type of condition, which is typical of outer shelf sediments (**Figure 4A**; Cardich et al., 2015). On the other hand, postoxic sediments with preserved OM and available dissolved nitrate are found under lower organic input. *B. seminuda* and associated species thriving in the upper slope appear to be associated with availability of dissolved nitrate in the bottom waters (Glock et al., 2019; Cardich et al., unpublished results). The association of *B. tenuata* with δ^{15}N exists in B-13 (**Figure 5A**) but not in B-6 (**Figure 5B**), giving more evidence that the intensity of WCD over the shelf and its effect on reducing conditions is mediated by local export production.

On the other hand, the ratio of shelf versus slope species is associated with redox extremes and environmental stability.

TABLE 2 | Spearman correlation matrix for biogenic and geochemical proxies from B-13 and B-06.

B-13	Bcos	Bpac	Bsem	Bele	Bten	Bpli	Naur	Epac	Seck	P.B	TOC	Si	$\delta^{15}N$	MoEF
Bcos														
Bpac	−0.78													
Bsem	−0.19	0.26												
Bele	0.36	−0.46	**−0.67**											
Bten	−0.39	0.19	**−0.73**	0.28										
Bpli	−0.41	0.24	0.56	−0.48	−0.30									
Naur	0.30	−0.28	−0.40	0.34	0.04	−0.39								
Epac	−0.13	0.13	**0.72**	−0.36	**−0.67**	0.53	−0.13							
Seck	−0.19	0.16	0.30	−0.34	−0.28	0.33	−0.27	0.36						
P.B	0.22	0.03	−0.24	0.13	0.07	−0.54	0.20	−0.31	−0.09					
TOC	**−0.78**	**0.66**	0.32	−0.23	0.14	0.52	−0.38	0.30	0.15	−0.39				
Si	**0.80**	**−0.68**	−0.26	0.35	−0.14	−0.48	0.41	−0.25	−0.41	0.27	**−0.86**			
$\delta^{15}N$	−0.05	−0.07	−0.33	0.19	0.30	0.09	−0.26	−0.20	0.07	0.03	−0.01	−0.07		
MoEF	0.48	−0.31	−0.51	0.43	0.31	**−0.69**	0.32	−0.51	−0.41	0.41	−0.58	**0.71**	0.01	
Mo.U	**0.68**	−0.49	−0.44	0.32	0.10	−0.64	0.41	−0.43	−0.31	0.41	**−0.85**	**0.87**	−0.02	**0.90**
B-6	**Bcos**	**Bpac**	**Bsem**	**Bele**	**Bten**	**Bpli**	**Naur**	**Epac**	**Seck**	**P.B**	**TOC**	**Si**	**$\delta^{15}N$**	**MoEF**
Bpac	−0.18													
Bsem	0.35	−0.19												
Bele	−0.06	−0.20	0.29											
Bten	−0.28	0.03	**−0.93**	−0.29										
Bpli	0.08	0.13	0.39	0.09	−0.52									
Naur	−0.16	−0.09	−0.62	−0.20	**0.67**	−0.46								
Epac	−0.11	0.04	0.44	0.05	−0.49	0.29	−0.45							
Seck	−0.29	0.08	**−0.70**	−0.29	0.61	−0.24	0.61	−0.31						
P/B	0.01	0.03	−0.41	0.16	0.43	−0.10	0.34	−0.20	0.22					
TOC	0.18	0.25	0.58	0.07	**−0.64**	0.43	**−0.59**	0.25	−0.44	−0.44				
Si	0.04	−0.38	−0.11	−0.33	0.25	−0.39	0.21	−0.17	0.12	−0.10	−0.41			
$\delta^{15}N$	−0.01	0.11	0.29	0.46	−0.23	0.31	−0.24	0.31	−0.28	0.16	0.17	**−0.57**		
MoEF	0.12	−0.25	0.21	−0.04	−0.03	−0.27	0.07	0.04	−0.18	−0.10	−0.22	0.52	0.04	
Mo.U	0.23	−0.36	0.06	0.06	0.06	−0.09	0.03	−0.05	0.12	0.32	−0.27	0.46	−0.10	0.25

Statistically significant values are shown in bold (p-value < 0.003).

Thus, lower (higher) values of the P*sp*/(P*sp* + A*sp*) ratio for Callao indicates sulfidic (mild postoxic) sediments with high labile (preserved) OM. Lower (higher) values also indicate exposition to coastal oxygenation events (stable bottom water suboxia). Likewise, lower (higher) values of the P*sp*/(P*sp* + A*sp*) for Pisco indicates light sulfidic (postoxic) sediments with labile (preserved) OM and less (more) stable conditions. These local disparities are a product of the bathymetric difference between the study sites. B-13 (180 m, outer shelf) is more exposed to coastal oxygenation processes than B-6 (300 m, upper slope), reflecting a biogeochemical gradient for coastal species. Meanwhile B-6 is more prone to register changes in the OMZ core of central Peru.

(Multi)Decadal Sedimentary Patterns and Response to Climatic Variability

From the patterns of geochemical proxies along the records (Gutiérrez et al., 2009; Salvatteci et al., 2014b; **Supplementary Figure S2**), we differentiated three distinct time periods after ca. 1835:

(i) From ca. 1835 to ca. 1875, with high export productivity (large peaks of biogenic silica), intense water column denitrification (high values of $\delta^{15}N$) and sulfidic sediments (high Mo EF and low Mo/U values);
(ii) From ca. 1875 to ca. 1960, with increasing export productivity, a decreasing trend of water column denitrification and a relaxation of reducing sedimentary conditions; and
(iii) From ca. 1960 to ca. 2005, the increasing trend of export productivity continues, but with local differences of reducing sedimentary conditions and water column denitrification.

Benthic foraminiferal ratios (**Figures 6E,F**) and rotated principal components (**Figures 6G,N**) for B-13 and B-6 also indicated the variability of redox and OM quality. The first time period (ca. 1835 to ca. 1875) showed a dominance of anoxia-tolerant foraminiferal assemblages inhabiting reduced sediments off Callao and Pisco, which evolved to sulfidic conditions off Callao. Average reducing conditions off Pisco (B-6) in the first period were as intense as in Callao (B-13), however, strong

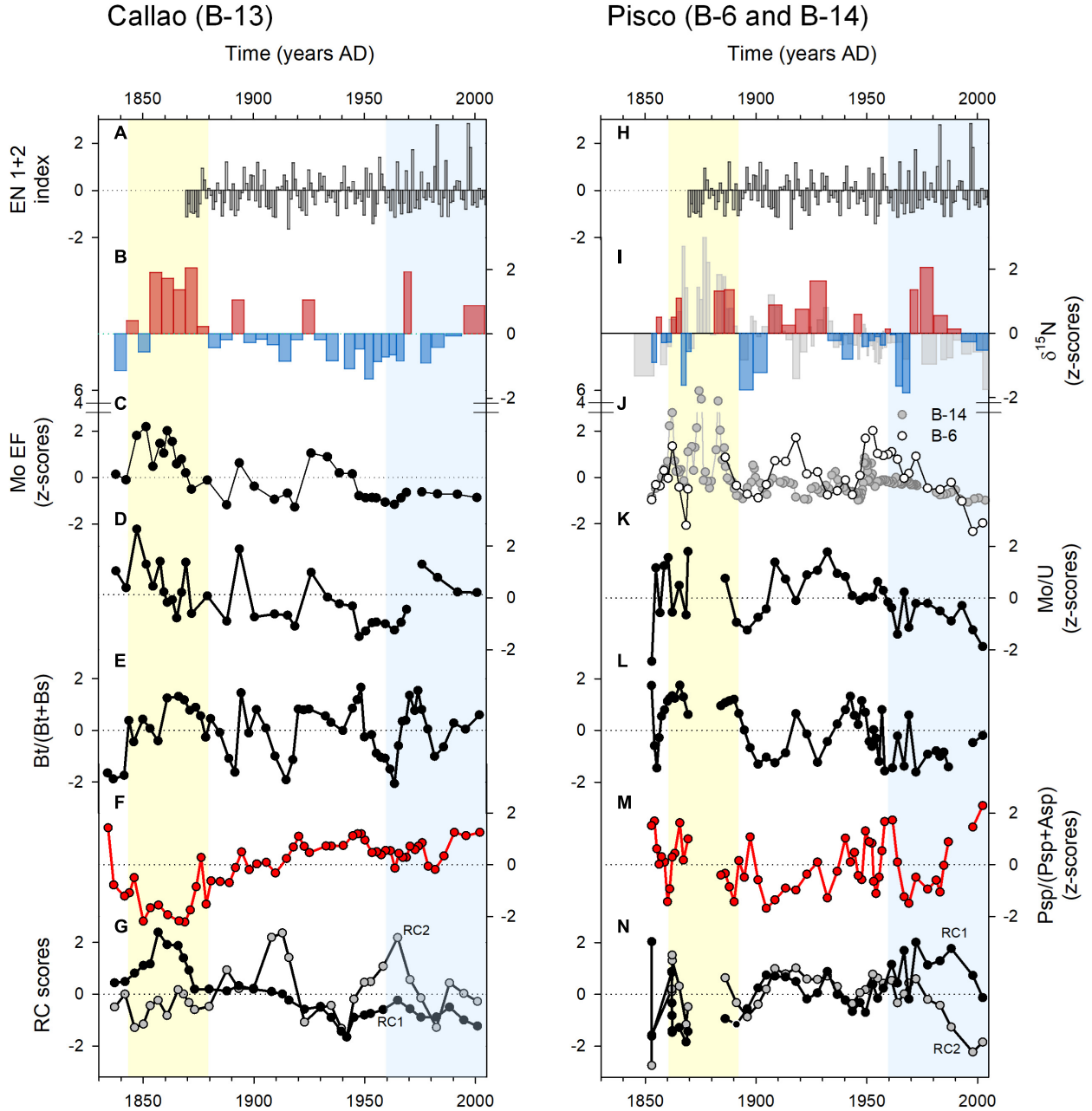

FIGURE 6 | Trends of geochemical and foraminiferal proxies in Callao (left panel) and Pisco (right panel) along to ENSO index (EN 1+2; **A,H**): δ^{15}N anomalies **(B,I)**, as a proxy of water-column denitrification; Mo EF **(C,J)** as proxy of intensity of anoxia; Mo/U ratio **(D,K)** as proxy of suboxic (low values) vs. sulfidic (high values) conditions; Bt/(Bt+Bs) index **(E,L)**; *Asp*/(*Asp*+*Psp*) index **(F,M)**; and PC scores from **Figure 5** as indicators of redox conditions [RC1 of B-13 **(G)** and RC2 of B-6 **(N)**].

sulfidic conditions are observed in B-14. This suggests that the cause of reducing sediments come from the neritic water column (i.e., local productivity). The presence of diatom bands in B-13 and B-14 in this period (not visible in B-6 because of a hiatus; Salvatteci et al., 2014a) and peaks of biogenic silica content indicate that massive algal blooms were frequent. Algal blooms in this period might be enhanced by a prevailing water column stratification, inferred from the warm sea surface temperatures (Gutiérrez et al., 2011) and weak surface winds (Briceño Zuluaga et al., 2016). The second time period was represented by a (multi)decadal oscillation of the WCD and organic input (co-variation of *B. seminuda* and *B. tenuata*) and a sustained relaxation of reducing conditions to non-sulfidic sediments off Callao and Pisco (**Figure 6**). Weakening of sulfidic conditions (settling of postoxic sediments) continues during the last time period. However, the WCD off Pisco shows a strong weakening trend. Being situated in the shelf, the Callao site (B-13) is influenced mainly by coastal productivity fluctuations and

the Pisco site (B-6) is more exposed to the oceanic variability. This implies that the variations of water column $\delta^{15}N$ is affected by both local and regional processes. Thus, WCD multidecadal changes off Pisco can be attributed to variations of the OMZ intensity, since this signature is more marked off Pisco than it is off Callao. From the latter, we can attribute the variability of the OMZ off Pisco to the variability in subsurface circulation.

We interpret the OMZ weakening (from ca. 1875 to 2004) as a result of ventilation arriving either from the equator or from the south, or as an interplay of both sources. Equatorial oceanic circulation linked to the Peruvian upwelling system is complex. The EUC fuels the PCUC with relatively oxygen-richer waters in comparison to the primary and secondary Southern Subsurface Countercurrents (p and s in **Figure 1C**; Montes et al., 2014). A major and sustained contribution of the EUC to the PCUC would ventilate the Peruvian OMZ. However, ultimately "the water mass properties within the PCUC core result from a delicate balance between different sources in terms of oxygen" (Montes et al., 2014). Overall, the oxygen supply is low to the PCUC, but it contributes to the ventilation of the OMZ (Karstensen et al., 2008). An intensification of the EUC took place since 1900 according to a SODAS reanalysis in the central Equatorial Pacific (**Figure 7A**; Drenkard and Karnauskas, 2014). The velocity of the EUC increased in 16 – 47% per century since the half of the 19th century (Drenkard and Karnauskas, 2014). Nevertheless, a reconstruction of the variability of the Tsuchiya Jets in the same time period is needed. It is known that the PCUC is the main nutrient source for the coastal upwelling off Peru and northern Chile, favoring primary productivity and subsequent export production. As the latter processes presented an enhancement since ca. 1900 (Gutiérrez et al., 2011; Salvatteci et al., 2018), dissolved oxygen arriving in the PCUC might have been rapidly consumed. The equatorward subsurface current CPDCC may be another source of ventilation. At about 500 m depth (Chaigneau et al., 2013), the CPDCC transports relatively fresh and cold Antartic Intermediate Water (AAIW) northward (Pietri et al., 2014). Pietri et al. (2014) suggested that deep equatorward flow off Peru may be modulated by coastal trapped waves at intraseasonal time scales, enhancing the transport of AAIW to the tropics. This suggests that Equatorial circulation might drive intermediate circulation. However, this process needs more research at (multi)decadal time scales.

At this point, our observations suggest that the variability of subsurface oxygenation over the Peruvian margin at (multi)decadal to centennial scales might be a result of an interplay of subsurface ventilation and local productivity. The PCA performed on the geochemical and foraminiferal data (**Figure 5**) showed a close association between the proxies of anoxia (Mo EF and Mo/U) and Si contents. This correlation is stronger in B-13 (outer shelf), indicating that local siliceous productivity drives the bottom oxygenation variability. Besides, IMARPE instrumental data shows evidence of a slightly subsurface oxygenation at 200 m depth since 1960 (**Figure 2**; red lines in **Figure 7C**). In the same time period, a positive trend in chlorophyll-a contents has been reported within 100 km off the coast (13.5 – 14.5°S) (Gutiérrez et al., 2011). Oxygenation might have been more intense at intermediate waters, which could explain the reduction of the OMZ strength.

We compared our records with the main regional climatic indices to assess their influence on the OMZ variability. In that way, we used the Interdecadal Pacific Oscillation (IPO; Henley et al., 2015), the ENSO 1+2 index and the core velocity of the EUC from the SODA reanalysis (Drenkard and Karnauskas, 2014). The IPO integrates sea surface temperature anomalies of the Pacific Ocean with weak trade winds during its warm (positive) phase and strong trade winds during its cool (negative) phase. The IPO resembles a multidecadal "El Niño-like" pattern of climate variability (Henley et al., 2015). The ENSO 1+2 index is used to show how ocean-atmospheric circulation in the northern part of the Peruvian upwelling system impacts the study area. The velocity of the EUC is also shown as a possible consequent ventilation process driven by both IPO and ENSO 1+2 indices.

Deutsch et al. (2011) and Ito and Deutsch (2013) related the (multi)decadal variability of the Tropical Pacific OMZ to the natural variation of biogeochemical and physical processes. The authors explained that the suboxic zone of this region expands during La Niña events or during the cold phase of the Pacific Decadal Oscillation (PDO) by means of a shallower thermocline that promotes nutrient supply to the surface, a higher organic flux to the seafloor and an elevated respiration. The opposite occurs during EN events or the warm phase of PDO. These environmental changes might be associated with the $\delta^{15}N$ records and the foraminiferal ratios [Bt/(Bt+Bs)] off Callao and Pisco in some degree. However, because of the difference in resolution between the climate indices and the proxies in the box cores, possible correlations might be masked. We suggest that additional time series analysis, such as cross-correlations, is needed to better infer cause-effect relationships at a finer scale.

As discussed above (see Understanding the Benthic Foraminiferal Assemblages in the Cores), a possible indirect link between the co-variation of *B. tenuata* and *B. seminuda* and WCD exists. An intensified WCD/OMZ over the margin during periods of frequent and strong LN events is associated with a high input of silica to the sediments. On the other hand, when strong EN events are frequent, the OMZ is deepened, WCD decreases, dissolved nitrate is more available in the bottom water and the upper margin sediments have less labile organic carbon. These oceanographical changes and their impact in the sedimentary geochemistry determine the dominance of either *B. tenuata* or *B. seminuda*. This suggests that there might be a link between species dominance and ENSO and IPO, possibly mediated by changes in the exported organic carbon and/or in oxygenation/denitrification.

Regional Trend of Oxygenation in the Eastern Pacific

Records of oxygenation/redox-proxies from other East Pacific upwelling zones are included in **Figure 7**: California (NE Pacific; Deutsch et al., 2014) and Concepción (SE Pacific; Srain et al., 2015). The weakening trend of the OMZ from a multidecadal to centennial scale is a feature present in both the

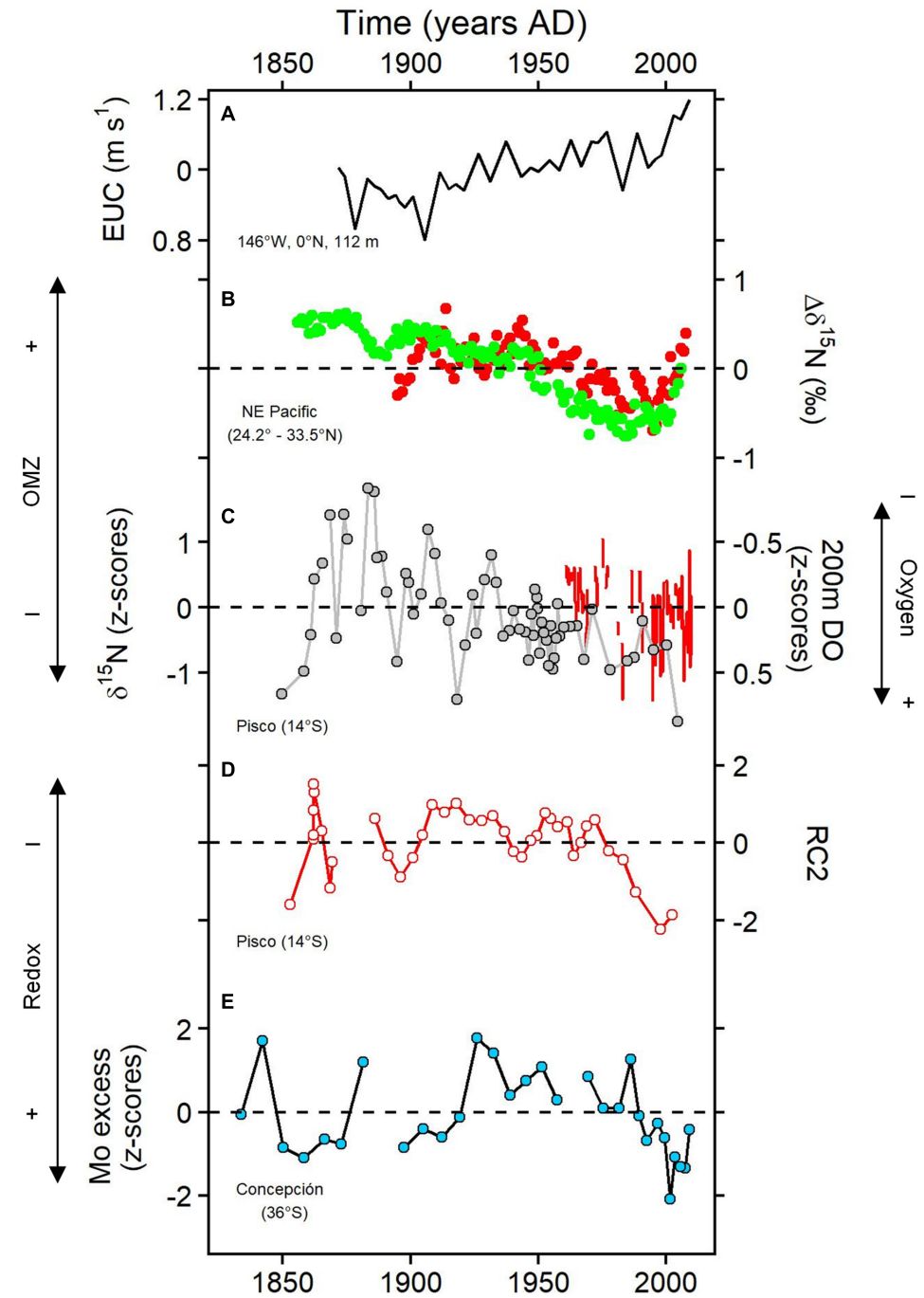

FIGURE 7 | Ocean circulation indices and records for (de)oxygenation in the East Pacific upwelling systems: **(A)** Equatorial Undercurrent (EUC) zonal velocity (Drenkard and Karnauskas, 2014); **(B)** mean anomalies of $\delta^{15}N$ in two locations off California (black dots in **Figure 2B**; Deutsch et al., 2014); **(C)** $\delta^{15}N$ record in B-14 (gray circles, this study) and instrumental dissolved oxygen anomalies at 200 m depth off central Peru (red line, inverse axis, this study); **(D)** P*sp*/(P*sp*+A*sp*) index anomalies (this study); and **(E)** Mo excess content anomalies off Concepción (Srain et al., 2015).

NE Pacific and the SE Pacific (**Figures 7B–E**). Deutsch et al. (2014) conclude that the main factor controlling OMZ intensity in the NE Pacific is Walker Circulation through variation in thermocline depth as a natural variability not related to global warming. These records show a recent OMZ expansion since the mid-1990s (**Figure 7B**) because of the strengthening of the Walker Circulation (England et al., 2014). Deutsch et al. (2014) also suggest that when a new declining trend of trade winds settle, the NE Pacific OMZ will contract again. The reactivation of the OMZ expansion in the last decade is apparent off Concepción,

Chile (**Figure 7E**), but not that evident as it is in California (**Figure 7B**). The sediments in Concepción shelf display a more reducing condition after 2000 (Srain et al., 2015). Despite the Concepción site being more representative of the variations of the oxycline and local productivity because of its location (∼100 m depth), it shows the general picture of the regional OMZ variations. The OMZ off Peru (based on the Pisco records), during the last decades, does not present the same pattern as Concepción and California given that suboxic waters are maintained in the core of the OMZ (**Figures 7C,D**).

The slight oxygenation trend near the equator (central Peru) as observed in the oxygen data and the paleo data (**Figures 7C,D**), and the OMZ expansion in the subtropics during the last 10 – 15 years appear to be regulated in some degree by EUC intensification. Subsurface equatorial source waters of the EUC are oxygen-rich for Peru but simultaneously result in oxygen-poor for higher latitudes (24.2 – 33.5°S, California and 36°S, Concepción). However, a shoaling trend of the oxycline off central Peru during the last decades has been determined indicating a vertical OMZ expansion (Bertrand et al., 2011; Espinoza-Morriberón, 2018). An alternate explanation for our results is deeper ventilation over the margin driven by intermediate circulation (e.g., CPDCC) occurring at the same as oxycline shoaling. The expansion of the volume of hypoxic waters off California during the last decades (since 1960s; Bograd et al., 2008) has been associated with changes in the source of water masses (EUC and northern subtropics) which affected ventilation in the basin (Bograd et al., 2015). This scenario might be the same at high subtropical latitudes in the SE Pacific. It must be noticed also that the Concepción record is shallower and might show a signal of local processes. Other coastal records from Callao (68 m, unpublished) and from Chile [100 m deep, Mejillones Bay (23°S); Díaz-Ochoa et al., 2011] exhibit a strong trend toward reducing conditions in the last decades. These results indicate that the progressive local productivity increase (among other factors) controls coastal hypoxia.

CONCLUSION

We show evidence for a subtle oxygenation trend from 1960 to 2010 in the core of the OMZ off central Peru. This trend is part of the OMZ variability at (multi)decadal to centennial time scales since the second half of the 19th century evidenced by a multiproxy approach. Near the coast, an intensification of the subsurface deoxygenation during the mid-nineteenth century resulted from the interplay of local and regional factors. Decadal to multidecadal variability of redox conditions might be controlled by local productivity changes affecting the OMZ intensity. At a larger scale, subsurface ventilation through the EUC and/or CPDCC is the ultimate factor controlling OMZ variability at multidecadal to centennial scale off Peru and probably in the Tropical South Eastern Pacific region. To be fully understood, the mechanisms behind the subsurface (de)oxygenation trends in Eastern Boundary Upwelling Ecosystems during past periods need the use of subsurface circulation proxies together with earth models at regional scale in addition to geochemical/biogenic proxies.

AUTHOR CONTRIBUTIONS

JC and DG designed the manuscript and landed the original idea of the manuscript. AS, RS, and FB-Z participated in data interpretation and discussion since the conception of the idea. RS analyzed the geochemical proxies. DR and CA analyzed the benthic foraminifera from the Pisco box core. JC analyzed benthic foraminifera in the Callao box core. MG and TA analyzed the oceanographic data from Peru and in its interpretation. All authors participated in the general discussion of the manuscript.

FUNDING

This project was funded by the MAGNET Program of CONCYTEC N°007-2017. This work was supported by the International Joint Laboratory "PALEOTRACES" (IRD, France; UPMC, France; UFF, Brazil; UA, Chile; UPCH, Peru), the Department of Geochemistry of the Universidade Federal Fluminense (UFF, Brazil), and the Peruvian Marine Research Institute (IMARPE). JC acknowledges the financial support from CNPq (Grant 142001/2013-9).

ACKNOWLEDGMENTS

We give special thanks to Ioanna Bouloubassi and Myriam Khodri for their comments and suggestions. We also thank the crews aboard the RVs 'SNP 2' and 'José Olaya Balandra' during the sampling cruises.

SUPPLEMENTARY MATERIAL

The Supplementary Material for this article can be found online at: https://www.frontiersin.org/articles/10.3389/fmars.2019.00270/full#supplementary-material

REFERENCES

Algeo, T. J., and Tribovillard, N. (2009). Environmental analysis of paleoceanographic systems based on molybdenumeuranium covariation. *Chem. Geol.* 268, 211–225. doi: 10.1016/j.chemgeo.2009.09.001

Bertrand, A., Chaigneau, A., Peraltilla, S., Ledesma, J., Graco, M., and Monetti, F. (2011). Oxygen: a fundamental property regulating pelagic ecosystem structure in the coastal southeastern tropical pacific. *PLoS One* 6:e29558. doi: 10.1371/journal.pone.0029558

Bograd, S. J., Castro, C. G., Di Lorenzo, E., Palacios, D. M., Bailey, H., Gilly, W., et al. (2008). Oxygen declines and the shoaling of the hypoxic boundary in the California Current. *Geophys. Res. Lett.* 35:L12607. doi: 10.1029/2008GL034185

Bopp, L., Resplandy, L., Orr, J. C., Doney, S. C., Dunne, J. P., and Gehlen, M. (2013). Multiple stressors of ocean ecosystems in the 21st century: projections with CMIP5 models. *Biogeosciences* 10, 6225–6245. doi: 10.5194/bg-10-6225-2013

Breitburg, D., Levin, L. A., Oschlies, A., Grégoire, M., Chavez, F. P., Conley, D. J., et al. (2018). Declining oxygen in the global ocean and coastal waters. *Science* 359:eaam7240. doi: 10.1126/science.aam7240

Briceño Zuluaga, F., Sifeddine, A., Caquineau, S., Cardich, J., Salvatteci, R., Gutierrez, D., et al. (2016). Terrigenous material supply to the Peruvian central continental shelf (Pisco 14° S) during the last 1000 yr: paleoclimatic implications. *Clim. Past* 12, 787–798. doi: 10.5194/cpd-12-787-2016

Cabré, A., Marinov, I., Bernardello, R., and Bianchi, D. (2015). Oxygen minimum zones in the tropical Pacific across CMIP5 models: mean state differences and climate change trends. *Biogeosciences* 12, 5429–5454. doi: 10.5194/bg-12-5429-2015

Cardich, J., Gutiérrez, D., Romero, D., Pérez, A., Quipúzcoa, L., Marquina, L., et al. (2015). Calcareous benthic foraminifera from the upper central Peruvian margin: control of the assemblage by pore water redox and sedimentary organic matter. *Mar. Ecol. Prog. Ser.* 535, 63–87. doi: 10.3354/meps11409

Caulle, C., Koho, K. A., Mojtahid, M., Reichart, G. J., and Jorissen, F. J. (2014). Live (Rose Bengal stained) foraminiferal faunas from the northern Arabian Sea: faunal succession within and below the OMZ. *Biogeosciences* 11, 1155–1175. doi: 10.5194/bg-11-1155-2014

Caulle, C., Mojtahid, M., Gooday, A. J., Jorissen, F. J., and Kitazato, H. (2015). Living (Rose-Bengal-stained) benthic foraminiferal faunas along a strong bottom-water oxygen gradient on the Indian margin (Arabian Sea). *Biogeosciences* 12, 5005–5019. doi: 10.5194/bg-12-5005-2015

Chaigneau, A., Dominguez, N., Eldin, G., Vasquez, L., Flores, R., and Grados, C. (2013). Near-coastal circulation in the northern humboldt current system from shipboard ADCP data. *J. Geophys. Res.* 118, 1–16. doi: 10.1002/jgrc.20328

Chavez, F. P., Bertrand, A., Guevara-Carrasco, R., Soler, P., and Csirke, J. (2008). The northern Humboldt current system: brief history, present status and a view towards the future. *Prog. Oceanogr.* 79, 95–412.

Chávez, F. P., and Messié, M. A. (2009). comparison of eastern boundary upwelling ecosystems. *Prog. Oceanogr.* 83, 80–96. doi: 10.7717/peerj.5339

Colodner, D., Edmond, J., and Boyle, E. (1995). Rhenium in the Black Sea: comparison with molybdenum and uranium. *Earth Planet. Sci. Lett.* 131, 1–15. doi: 10.1016/0012-821x(95)00010-a

Crusius, J., Calvert, S., Pedersen, T., and Sage, D. (1996). Rhenium and molybdenum enrichments in sediments as indicators of oxic, suboxic and sulfidic conditions of deposition. *Earth Planet. Sci. Lett.* 145, 65–78. doi: 10.1016/s0012-821x(96)00204-x

Dale, A. W., Sommer, S., Lomnitz, U., Montes, I., Treude, T., Liebetrau, V., et al. (2015). Organic carbon production, mineralisation and preservation on the Peruvian margin. *Biogeosciences* 12, 1537–1559. doi: 10.5194/bg-12-1537-2015

Deutsch, C., Berelson, W., Thunell, R., Weber, T., Tems, C., McManus, J., et al. (2014). Centennial changes in North Pacific anoxia linked to tropical trade winds. *Science* 345, 665–668. doi: 10.1126/science.1252332

Deutsch, C., Brix, H., Ito, T., Frenzel, H., and Thompson, L. (2011). Climateforced variability of ocean hypoxia. *Science* 333, 336–339. doi: 10.1126/science.1202422

Díaz-Ochoa, J. A., Pantoja, S., De Lange, G. J., Lange, C. B., Sánchez, G. E., Acuña, V. R., et al. (2011). Oxygenation variability in Mejillones Bay, off northern Chile, during the last two centuries. *Biogeosciences* 8, 137–146. doi: 10.5194/bg-8-137-2011

Drenkard, E. J., and Karnauskas, K. B. (2014). Strengthening of the Pacific equatorial undercurrent in the SODA reanalysis: mechanisms, ocean dynamics, and implications. *J. Clim.* 27, 2405–2416. doi: 10.1175/jcli-d-13-00359.1

England, M. H., McGregor, S., Spence, P., Meehl, G. A., Timmermann, A., Cai, W., et al. (2014). Recent intensification of wind-driven circulation in the Pacific and the ongoing warming hiatus. *Nat. Clim. Change* 4, 222–227. doi: 10.1038/nclimate2106

Espinoza-Morriberón, D. (2018). *Interannual and Decadal Variability of the Primary Productivity and Oxygen Minimum Zone in the Peruvian Upwelling System. 2018*. PhD Thesis. Paris: Sorbonne Université.

Espinoza-Morriberón, D., Echevin, V., Colas, F., Tam, J., Ledesma, J., Vásquez, L., et al. (2017). Impacts of El Nino events on the Peruvian upwelling system productivity. *J. Geophys. Res. Oceans* 122, 5423–5444. doi: 10.1002/2016JC012439

Forsgren, K. L., Bay, S. M., Vidal-Dorsch, D. E., Deng, X., Lu, G., Armstrong, J., et al. (2015). Changes in source waters to the Southern California Bight. *Deep Sea Res. II* 112, 42–52. doi: 10.1002/etc.2006

Glantz, S. A. (2002). *Primer of Biostatistics*. New York, NY: McGraw-Hill Medical.

Glock, N., Roy, A. S., Romero, D., Wein, T., Weissenbach, J., Revsbech, N. P., et al. (2019). Metabolic preference of nitrate over oxygen as an electron acceptor in foraminifera from the Peruvian oxygen minimum zone. *Proc. Natl. Acad. Sci. U.S.A.* 116, 2860–2865. doi: 10.1073/pnas.1813887116

Gooday, A. J. (2003). Benthic foraminifera (protista) as tools in deep-water palaeoceanography: environmental influences on faunal characteristics. *Adv. Mar. Biol.* 46, 1–90. doi: 10.1016/s0065-2881(03)46002-1

Graco, M., Purca, S., Dewitte, B., Castro, C., Morón, O., Ledesma, J., et al. (2017). The OMZ and nutrient features as a signature of interannual and low-frequency variability in the Peruvian upwelling system. *Biogeosciences* 14, 4601–4617. doi: 10.5194/bg-14-4601-2017

Grasshoff, K. K., Kremling, K., and Ehrhardt, M. (eds) (1999). *Methods of Seawater Analysis Third, Completely Revised and Extended Edition*. Weinheim: Wiley-VCH.

Gutiérrez, D., Bouloubassi, I., Sifeddine, A., Purca, S., Goubanova, K., Graco, M., et al. (2011). Coastal cooling and increased productivity in the main upwelling zone off Peru since the mid-twentieth century. *Geophys. Res. Lett.* 38:L07603.

Gutiérrez, D., Enriquez, E., Purca, S., Quipuzcoa, L., Marquina, R., Flores, G., et al. (2008). Oxygenation episodes on the continental shelf of central Peru: remote forcing and benthic ecosystem response. *Prog. Oceanogr.* 79, 177–189. doi: 10.1016/j.pocean.2008.10.025

Gutiérrez, D., Sifeddine, A., Field, D. B., Ortlieb, L., Vargas, G., Chavez, F., et al. (2009). Rapid reorganization in ocean biogeochemistry off Peru towards the end of the little ice age. *Biogeosciences* 6, 835–848. doi: 10.5194/bg-6-835-2009

Gutiérrez, D., Sifeddine, A., Reyss, J. L., Vargas, G., Velazco, F., Salvatteci, R., et al. (2006). Anoxic sediments off Central Peru record interannual to multidecadal changes of climate and upwelling ecosystem during the last two centuries. *Adv. Geosci.* 6, 119–125. doi: 10.5194/adgeo-6-119-2006

Helly, J. J., and Levin, L. A. (2004). Global distribution of naturally occurring marine hypoxia on continental margins. *Deep Sea Res.* 51, 1159–1168. doi: 10.1016/j.dsr.2004.03.009

Henley, B. J., Gergis, J., Karoly, D. J., Power, S. B., Kennedy, J., and Folland, C. K. (2015). A tripole index for the interdecadal pacific oscillation. *Clim. Dyn.* 45, 3077–3090. doi: 10.1007/s00382-015-2525-1

Horak, R. E. A., Ruef, W., Ward, B. B., and Devol, A. H. (2016). Expansion of denitrification and anoxia in the eastern tropical North Pacific from 1972 to 2012. *Geophys. Res. Lett.* 43, 5252–5260. doi: 10.1002/2016GL068871

Ito, T., and Deutsch, C. (2013). Variability of the oxygen minimum zone in the tropical North Pacific during the late twentieth century. *Glob. Biogeochem. Cycles* 27, 1119–1128. doi: 10.1002/2013gb004567

Jaccard, S. L., and Galbraith, E. D. (2012). Large climate-driven changes of oceanic oxygen concentrations during the last deglaciation. *Nat. Geosci.* 5, 151–156. doi: 10.1038/ngeo1352

Jahnke, R. A., Craven, D. B., McCorkle, D. C., and Reimers, C. E. (1997). CaCO3 dissolution in California continental margin sediments: the influence of organic matter remineralization. *Geochim. Cosmochim. Acta* 61, 3587–3604. doi: 10.1016/s0016-7037(97)00184-1

Karstensen, J., Stramma, L., and Visbeck, M. (2008). Oxygen minimum zones in the eastern tropical Atlantic and Pacific oceans. *Prog. Oceanogr.* 77, 331–350. doi: 10.1016/j.pocean.2007.05.009

Keeling, R. E., Körtzinger, A., and Gruber, N. (2010). Ocean deoxygenation in a warming world. *Annu. Rev. Mar. Sci.* 2, 199–229. doi: 10.1146/annurev.marine.010908.163855

Keeling, R. F., and Garcia, H. (2002). The change in oceanic O2 inventory associated with recent global warming. *Proc. Natl. Acad. Sci. U.S.A.* 99, 7848–7853. doi: 10.1073/pnas.122154899

Levin, L. A., Ekau, W., Gooday, A. J., Jorissen, F., Middelburg, J. J., and Naqvi, S. W. A. (2009). Effects of natural and human-induced hypoxia on coastal benthos. *Biogeosciences* 6, 2063–2098. doi: 10.5194/bg-6-2063-2009

Levin, L. A., Gutiérrez, D., Rathburn, A. E., Neira, C., Sellanesand, J., Muñoz, P., et al. (2002). Benthic processes on the Peru margin: a transect across the oxygen minimum zone during the 1997-98 El Niño. *Prog. Oceanogr.* 53, 1–27. doi: 10.1016/s0079-6611(02)00022-8

Mallon, J., Glock, N., and Schonfed, J. (2012). "The response of benthic foraminifera to lowoxygen conditions of the Peruvian oxygen minmum zone," in *Anoxia: Evidence for Eukaryote Survival and Paleontological Strategies*,

Vol. 21, eds A. V. Altenbach, J. M. Bernhard, and J. Seckbach (Dordrecht: Springer),

McManus, J., Berelson, W. M., Severmann, S., Poulson, R. L., Hammond, D. E., Klinkhammer, G. P., et al. (2006). Molybdenum and uranium geochemistry in continental margin sediments: paleoproxy potential. *Geochim. Cosmochim. Acta* 70, 4646–4662.

Montes, I., Colas, F., Capet, X., and Schneider, W. (2010). On the pathways of the equatorial subsurface currents in the Eastern Equatorial Pacific and their contributions to the Peru-Chile Undercurrent. *J. Geophys. Res.* 115:C09003. doi: 10.1029/2009JC005710

Montes, I., Dewitte, B., Gutknecht, E., Paulmier, A., Dadou, I., and Oschlies, A. (2014). High-resolution modeling of the Eastern Tropical Pacific oxygen minimum zone: sensitivity to the tropical oceanic circulation. *J. Geophys. Res. Oceans* 119, 5515–5532. doi: 10.1002/2014JC009858

Morales, M. C., Field, D., Pastor, S. M., Gutierrez, D., Sifeddine, A., Ortlieb, L., et al. (2006). Variations in foraminifera over the last 460 years from laminated sediments off the coast of Peru. *Bol. Soc. Peru* 101, 5–18.

Paulmier, A., and Ruiz-Pino, D. (2008). Oxygen minimum zones (OMZs) in the modern ocean. *Prog. Oceanogr.* 80, 113–128. doi: 10.1016/j.pocean.2008.08.001

Pérez, M. E., Rathburn, A. E., Levin, L. A., and Deng, W. B. (2002). The ecology of benthic foraminifera of the Peru oxygen minimum zone. *Geolog. Soc. Am.* 34:352. doi: 10.1073/pnas.1813887116

Phleger, F. B., and Soutar, A. (1973). Production of benthic foraminifera in three east Pacific oxygen minima. *Micropaleontology* 19, 110–115.

Pietri, A., Echevin, V., Testor, P., Chaigneau, A., Mortier, L., Grados, C., et al. (2014). Impact of a coastal-trapped wave on the near-coastal circulation of the Peru upwelling system from glider data. *J. Geophys. Res. Oceans* 119, 2109–2120. doi: 10.1002/2013JC009270

Piña-Ochoa, E., Høgslund, S., Geslin, E., Cedhagend, T., Revsbech, N. P., Nielsen, L. P., et al. (2010). Widespread occurrence of nitrate storage and denitrification among Foraminifera and Gromiida. *Proc. Natl. Acad. Sci. U.S.A.* 107, 1148–1153. doi: 10.1073/pnas.0908440107

Reinhardt, L., Kudrass, H.-R., Luckge, A., Wiedicke, M., Wunderlich, J., and Wendt, G. (2002). High-resolution sediment echosounding off Peru: late quaternary depositional sequences and sedimentary structures of a current-dominated shelf. *Mar. Geophys. Res.* 23, 335–351.

Salvatteci, R., Field, D. B., Baumgartner, T., Ferreira, V., and Gutiérrez, D. (2012). Evaluating fish scale preservation in sediment records from the oxygen minimum zone off Peru. *Paleobiology* 38, 52–78. doi: 10.1666/10045.1

Salvatteci, R., Field, D., Gutiérrez, D., Baumgartner, T., Ferreira, V., Ortlieb, L., et al. (2018). Multifarious anchovy and sardine regimes in the humboldt current system during the last 150 years. *Glob. Change Biol.* 24, 1055–1068. doi: 10.1111/gcb.13991

Salvatteci, R., Field, D., Sifeddine, A., Ortlieb, L., Ferreira, V., Baumgartner, T., et al. (2014a). Cross-stratigraphies from a seismically active mud lens off Peru indicate horizontal extensions of laminae, missing sequences, and a need for multiple cores for high resolution records. *Mar. Geol.* 357, 72–89. doi: 10.1016/j.margeo.2014.07.008

Salvatteci, R., Gutierrez, D., Field, D., Sifeddine, A., Ortlieb, L., Bouloubassi, I., et al. (2014b). The response of the peruvian upwelling ecosystem to centennial-scale global change during the last two millennia. *Clim. Past* 10, 715–731. doi: 10.5194/cp-10-715-2014

Salvatteci, R., Gutierrez, D., Sifeddine, A., Ortlieb, L., Druffel, E., Boussafir, M., et al. (2016). Centennial to millennial-scale changes in oxygenation and productivity in the eastern tropical South Pacific during the last 25,000 years. *Quat. Sci. Rev.* 131, 102–117. doi: 10.1016/j.quascirev.2015.10.044

Salvatteci, R., Schneider, R. R., Blanz, T., and Mollier-Vogel, E., (2019). Deglacial to holocene ocean temperatures in the humboldt current system as indicated by alkenone paleothermometry. *Geophys. Res. Lett.* 46, 281–292. doi: 10.1029/2018GL080634

Schmidtko, S., Stramma, L., and Visbeck, M. (2017). Decline in global oceanic oxygen content during the past five decades. *Nature* 542, 335–339. doi: 10.1038/nature21399

Scholz, F., Hensen, C., Noffke, A., Rohde, A., Liebetrau, V., and Wallmann, K. (2011). Early diagenesis of redox-sensitive trace metals in the Peru upwelling area e response to ENSO-related oxygen fluctuations in the water column. *Geochim. Cosmochim. Acta* 75, 7257–7276. doi: 10.1016/j.gca.2011.08.007

Scholz, F., McManus, J., Mix, A. C., Hensen, C., and Schneider, R. R. (2014). The impact of ocean deoxygenation on iron release from continental margin sediments. *Nat. Geosci.* 7, 433–437. doi: 10.1038/ngeo2162

Sifeddine, A., Gutiérrez, D., Ortlieb, L., Boucher, H., Velazco, F., Field, D., et al. (2008). Laminated sediments from the central Peruvian continental slope: a 500 year record of upwelling system productivity, terrestrial runoff and redox conditions. *Prog. Oceanogr.* 79, 190–197. doi: 10.1016/j.pocean.2008.10.024

Sommer, S., Gier, J., Treude, T., Lomnitz, U., Dengler, M., Cardich, J., et al. (2016). Depletion of oxygen, nitrate and nitrite in the Peruvian oxygen minimum zone cause an imbalance of benthic nitrogen fluxes. *Deep Sea Res. I* 112, 113–122. doi: 10.1016/j.dsr.2016.03.001

Srain, B., Pantoja, S., Sepúlveda, J., Lange, C. B., Muñoz, P., Summons, R. E., et al. (2015). Interdecadal changes in intensity of the oxygen minimum zone off Concepción, Chile (∼36° S), over the last century. *Biogeosciences* 12, 6045–6058. doi: 10.5194/bg-12-6045-2015

Stramma, L., Johnson, G. C., Sprintall, J., and Mohrholz, V. (2008). Expanding oxygen-minimum zones in the tropical oceans. *Science* 320, 655–658. doi: 10.1126/science.1153847

Stramma, L., Schmidtko, S., Levin, L. A., and Johnson, G. C. (2010). Ocean oxygen minima expansions and their biological impacts. *Deep Sea Res. Part I* 57, 587–595. doi: 10.1016/j.dsr.2010.01.005

Strickland, J. D. H., and Parsons, T. R. (1968). *A Practical Handbook of Seawater Analyses*. Ottawa: Fisheries Research Board of Canada, 311.

Suits, N. S., and Arthur, M. A. (2000). Bacterial production of anomalously high dissolved sulfate concentrations in Peru slope sediments: steady-state sulfur oxidation, or transient response to end of El Niño? *Deep Sea Res I* 47, 1829–1853. doi: 10.1016/s0967-0637(99)00120-x

Thomsen, S., Kanzow, T., Colas, F., Echevin, V., Krahmann, G., and Engel, A. (2016). Do submesoscale frontal processes ventilate the oxygen minimum zone off Peru? *Geophys. Res. Lett.* 43, 8133–8142. doi: 10.1002/2016GL070548

Tribovillard, N., Algeo, T. J., Lyons, T., and Riboulleau, A. (2006). Trace metals as paleoredox and paleoproductivity proxies: an update. *Chem. Geol.* 232, 12–32. doi: 10.1016/j.chemgeo.2006.02.012

Vergara, O., Dewitte, B., Montes, I., Garçon, V., Ramos, M., Paulmier, A., et al. (2016). Seasonal variability of the oxygen minimum zone off Peru in a high-resolution regional coupled model. *Biogeosciences* 13, 4389–4410. doi: 10.5194/bg-13-4389-2016

Conflict of Interest Statement: The authors declare that the research was conducted in the absence of any commercial or financial relationships that could be construed as a potential conflict of interest.

frontiers in Marine Science

ORIGINAL RESEARCH
published: 24 July 2019
doi: 10.3389/fmars.2019.00459

Ventilation of the Upper Oxygen Minimum Zone in the Coastal Region Off Mexico: Implications of El Niño 2015–2016

Pablo N. Trucco-Pignata[1,2], José Martín Hernández-Ayón[1], Eduardo Santamaria-del-Angel[3], Emilio Beier[4], Laura Sánchez-Velasco[5], Victor M. Godínez[6] and Orión Norzagaray[1]*

[1] Instituto de Investigaciones Oceanológicas, Universidad Autónoma de Baja California, Ensenada, Mexico, [2] Ocean and Earth Science, National Oceanography Centre, University of Southampton, Southampton, United Kingdom, [3] Facultad de Ciencias Marinas, Universidad Autónoma de Baja California, Ensenada, Mexico, [4] CICESE, Unidad La Paz, La Paz, Mexico, [5] Departamento de Plancton y Ecología Marina, Centro Interdisciplinario de Ciencias Marinas, Instituto Politécnico Nacional, La Paz, Mexico, [6] Departamento de Oceanografía Física, CICESE, Ensenada, Mexico

OPEN ACCESS

Edited by:
Emilio Garcia-Robledo, University of Cádiz, Spain

Reviewed by:
GVM Gupta, Centre for Marine Living Resources & Ecology (CMLRE), India
Manuel Flores Montes, Universidade Federal de Pernambuco (UFPE), Brazil

***Correspondence:**
José Martín Hernández-Ayón
jmartin@uabc.edu.mx

Specialty section:
This article was submitted to Marine Biogeochemistry, a section of the journal Frontiers in Marine Science

Received: *02 August 2018*
Accepted: *09 July 2019*
Published: *24 July 2019*

Citation:
Trucco-Pignata PN, Hernández-Ayón JM, Santamaria-del-Angel E, Beier E, Sánchez-Velasco L, Godínez VM and Norzagaray O (2019) Ventilation of the Upper Oxygen Minimum Zone in the Coastal Region Off Mexico: Implications of El Niño 2015–2016. Front. Mar. Sci. 6:459. doi: 10.3389/fmars.2019.00459

As a result of anthropogenic activities, it has been predicted that the ocean will be challenged with rising temperature, increased stratification, ocean acidification, stronger more frequent tropical storms, and oxygen depletion. In the tropical Pacific off central Mexico all these phenomena are already occurring naturally, providing a laboratory from which to explore ocean biogeochemical dynamics that are predicted under future anthropogenic forcing conditions. Here, seasonally anomalous surface tropical waters were detected as a result of the developing "Godzilla El Niño 2015–2016." The incursion of this oxygenated water modified the local structure of an intense and shallow oxygen minimum zone (OMZ), partially eroding and intensifying the oxycline while having an associated impact on the carbon maximum zone. The core of the OMZ ($<$4.4 μmol kg^{-1}) was centered around 474 m, with a variant upper level between 50 and 360 m depth. Below the dominance of Tropical Surface Waters, the thickness of the oxycline varied between 10 and 325 m, with intensity values up to 11 μmol kg^{-1} m^{-1}. The change in dissolved inorganic carbon (DIC) and apparent oxygen utilization yielded a molar ratio of δDIC = 0.98 $\times$ δAOU during June 2015 and of δDIC = 1.08 $\times$ δAOU for March 2016. A further decrease in the average content of DIC was observed in the carbon maximum zone for 2016. Traditionally, different explanations have been proposed to account for changing oxygen concentrations in the ocean rather than considering the interactions between multiple forcing factors. Our results highlight the significance of an episodic event like El Niño in the distribution and concentration of O_2 and DIC and as a plausible mechanism of ventilation and increased oxygen availability in the upper OMZ of the tropical Pacific off central Mexico.

Keywords: oxygen minimum zones, dissolved inorganic carbon, El Niño 2015–2016, oxycline, eastern tropical North Pacific

INTRODUCTION

Knowledge of the main hydrographic features of the northeastern tropical Pacific Ocean, spanning from the Gulf of California entrance to Panama, have been summarized by Fiedler and Talley (2006). The principal characteristics in the surface are: a warm low-salinity poleward flowing Tropical Surface Water (TSW) over a strong and shallow pycnocline, and a cool, low-salinity eastern boundary current water flowing from the north. In the subsurface, a pronounced oxygen minimum layer flows into the region, as a warm high salinity subtropical water, subducted into the thermocline primarily in the southern Subtropical Convergence (Fiedler and Talley, 2006). Afterward, this broad review is refined at a sub-basin scale by Portela et al. (2016). Focusing their analysis on the tropical Pacific off central Mexico (TPCM), the authors describe the seasonality of the water masses and the current pattern in the regional circulation scheme.

The TPCM forms part of the northern limit of one of the most extensive and intense (O_2 < 20 μmol kg^{-1}) oxygen minimum zone (OMZ) in the world (Paulmier and Ruiz-Pino, 2009; Stramma et al., 2010; Cepeda-Morales et al., 2013). Multiple studies have highlighted the role of OMZs in the biogeochemical cycles of nitrogen and sulfur (Canfield et al., 2010; Kalvelage et al., 2013), in the distribution and boundaries of pelagic ecosystems (Wishner et al., 2013; Davies et al., 2015), and as important reservoirs of inorganic carbon (Paulmier et al., 2011; Franco et al., 2014). Given increased atmospheric CO_2 and thermal stratification in the ocean, OMZs have intensified and expanded (Stramma et al., 2008; Rabalais et al., 2010). Explore these zones provides a window through which to study and to understand the potential future conditions of our oceans, as well as their respective role in the climate system (Keeling and Garcia, 2002).

Our study area extends from 25.5°N in the Gulf of California, off the coasts of Baja California Sur and Sinaloa, to 18°N in front of the coasts of Nayarit and Jalisco, between 105.5 and 110°W (**Figure 1**). This is an oceanographically complex area in which hydrographic conditions depend on the interactions between the surrounding water masses (Portela et al., 2016), the intensity of seasonal and interannual variability (Kurczyn et al., 2012, 2013), and the prevailing mesoscale physical processes (Lavín et al., 2006; Godínez et al., 2010).

In the northern region of the study area, circulation is dominated by both the entry of Transitional Water (TW) along Sinaloa and the exit of Gulf of California Water (GCW) down the peninsular side of the Gulf (**Figure 1**; Castro and Durazo, 2000; Kurczyn et al., 2012; Lavín et al., 2013; Portela et al., 2016). The dynamics of this area are strongly modulated by the presence of cyclonic and anticyclonic eddies (Castro et al., 2006; Lavín et al., 2009, 2013; Kurczyn et al., 2012; Collins et al., 2015), which significantly influence primary production and the distribution of the zooplankton [i.e., larval fish and squid paralarvae (Apango-Figueroa et al., 2015; Sánchez-Velasco et al., 2016)].

Off the coasts of Nayarit and Jalisco in the southern region, the water column is highly stratified and TSW dominates from the surface to 70 m depth (Franco et al., 2014). TSW is transported northward by the Mexican Coastal Current (MCC) primarily during summer and autumn, traveling over the continental platform (Gómez-Valdivia et al., 2015) while interacting and mixing with TW, GCW, and California Current Water (CCW). Due to the presence of cyclonic eddies near the tip of the Baja California peninsula, CCW is advected to the east (Lavín et al., 2009). In summary, the TPCM receives GCW in the surface layer during spring and TSW during summer and autumn (Portela et al., 2016).

The coastal oxycline is generally shallow, between 50 and 100 m depth (Fernández-Álamo and Färber-Lorda, 2006; Cepeda-Morales et al., 2009, 2013), as is the carbocline (Franco et al., 2014). These waters enriched with dissolved inorganic carbon (DIC) and low dissolved oxygen (DO) are associated with Subtropical Subsurface Water (StSsW), which dominates zonally and meridionally below the waters previously mentioned. The depth of the oxycline, along with upwelling events and cyclonic eddy pumping, can have a significant influence on the partial pressure of CO_2 (pCO_2) and important consequences for the estimation of ocean-atmosphere CO_2 fluxes.

The overall objective of this paper is to understand the main processes that are affecting the measured distribution of DIC and DO in the upper part of the OMZ in the TPCM. Observations were performed during two contrasting temporal (seasonal) and spatial distribution on the OMZ, and during the development of an El Niño event, providing a wide range of oceanographic conditions to explore the mechanism that controls the OMZ dynamics. We started with the assumption that the distribution of DIC (determined for the first time in this region) and DO will be strongly correlated with the seasonal distribution of the different water masses (Kurczyn et al., 2012, 2013; Portela et al., 2016), each one with a particular chemical composition upon its origin and history. Our emphasis on the present study is about the repercussions of the "Godzilla El Niño 2015–2016" event on the structure of the OMZ in the TPCM, and how these oceanographic processes may concomitantly affect the distribution of the Carbon Maximum Zone (CMZ; Paulmier et al., 2011). The structure of the paper is as follows. In section "Data and Methods" we describe the sample collection methodology, measurements technics and the data analysis performed. In section "Results" we analyze the water masses distribution and their DIC and DO content, followed by a description of the vertical distribution oceanographic variables along a latitudinal transect. In section "Discussion" we discuss our observations differentiating the processes into oceanographic regions. Finally, in section "Conclusion" we summarize our findings and conclusions.

DATA AND METHODS

Data Collection and Analysis

Two oceanographic cruises were carried out aboard the R/V "Alpha Helix" (CICESE). Hydrographic data were collected with an SBE-911 plus CTD and water samples were collected at different depths (typically from the surface to 200 m) using a rosette arranged with 12-L Niskin bottles. From a total of 83 hydrographic stations, 29 stations were analyzed for June 2015 to determine DIC, pH, and total alkalinity (TA), while

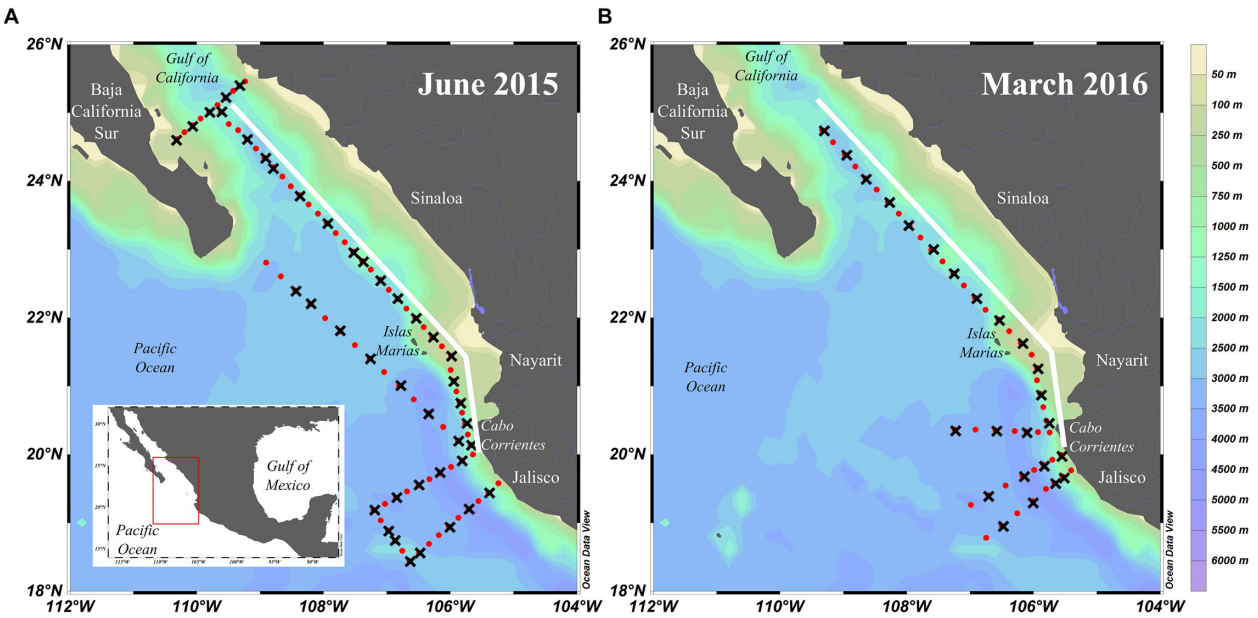

FIGURE 1 | Hydrographic transects in the studied region over the bathymetric map. **(A)** June 3–16, 2015, **(B)** March 2–8, 2016. Black crosses depict stations with water sampling for chemical analysis, while red dots indicate only hydrographic stations. Latitudinal transect 1 appears as a white line.

24 of 48 stations were analyzed for March 2016 (**Figure 1**). The samples of DIC and pH analysis were taken and preserved according to the protocols specified in the best practices manual SOP 1 (Dickson et al., 2007).

Dissolved inorganic carbon measurements were carried out in laboratory conditions using a CO_2 (CO_2/H_2O LI-7000, LICOR) infrared gas analyzer. The analyzer was linked to a semiautomatic dispenser system. The sample was dosified with a Kloehn syringe and acidified with phosphoric acid at 8.5%. Due to this acidification, the DIC present in the sample was taken to a gaseous state. CO_2 was then subsequently transferred to the infrared analyzer using N_2 as a carrier and its absorbency value was quantified. To convert the absorbance values, samples were calibrated with a certified DIC standard provided by the laboratory of Dr. Andrew Dickson of Scripps Institution of Oceanography (Dickson et al., 2003). The precision obtained with this methodology was ± 2 μmol kg^{-1} with a measurement error of ±0.2%.

In this work, spectrophotometric measurements of pH in total proton scale (pH_T) were implemented following the methodology established by Clayton and Byrne (1993) and the modifications made by Liu et al. (2011). The proton concentration in the total ion concentration scale was measured using 10 mM meta-Cresol purple (mCP) following the recommendations described in the best practices manual SOP 6b (Dickson et al., 2007). The absorbance measurements were carried out using a spectrophotometer (USB 4000, Ocean Optics) linked to a tungsten lamp (HL-2000, Ocean Optics). The temperature of the samples was controlled at 25 ± 0.2°C. A Tris pH standard from the laboratory of Dr. Andrew Dickson of Scripps Institution of Oceanography was used as quality control. A correction was applied for the absorbance of impurities present in mCP (Douglas and Byrne, 2017); specifically, a correction factor of$_{434}A_{imp}$ of 8.527 × 10^{-3} for a final mCP concentration in sample of 1.7 μM. Finally the pH_T is converted to *in situ* conditions using the software CO2sys_v2.2.xls (Lewis and Wallace, 1998) The obtained precision was ±0.005 pH units with an accuracy of ±0.002 and a measurement error of ±0.023%.

A *SBE43* type oxygen electrode (with a precision 4.46 μmol $kg^{-1}$and a resolution of 0.446 μmol kg^{-1}) was attached to the CTD and calibrated at Seabird in December 2011. Routine cleaning of the oxygen electrode was performed during the cruises. The sensor was rinsed with a 0.1% solution of Triton X-100 after every cast, followed by a flush of 500 ppm solution of bleach and finally rinsed with fresh water. The sensor was kept from direct sunlight and humidified. The oxygen electrode data were not compared with chemical oxygen determinations since the electrode was factory calibrated prior to cruises. Similar (O_2) measurement values in the core of the StSsW for both winter and spring reflects a good performance of the DO sensor during both cruises (**Table 2**).

From these oxygen data, apparent oxygen utilization (AOU) was calculated. AOU is defined as the saturated DO concentration, estimated from temperature and salinity (Garcia and Gordon, 1992), minus the observed DO concentration. It has to be seen as an estimation of the amount of oxygen consumed since seawater was last under the air-sea equilibrium.

The international equation of the state of seawater (TEOS-10) allows to consistently evaluate all thermodynamic properties of pure water, ice, seawater and humid air. At the same time, variations in the composition of seawater around the world are accounted for; this spatial variation in its composition

causes density differences that are equivalent to ten times the precision of practical salinity (S_P) measurements made at sea (McDougall and Barker, 2017). The absolute salinity (S_A) and the conservative temperature (Θ) are included in this new system of equations and should be used in the scientific literature replacing the use of potential temperature and practical salinity (IOC et al., 2010). The S_A has units of grams per kilogram, and has a non-trivial effect on the horizontal density gradients, affecting all the variables derived from it. On the other hand, the conservative temperature Θ represents more accurately the heat content per unit mass of seawater. In this paper, we apply this recommendation and use these variables following the criteria defined by Portela et al. (2016) (see **Table 1**) to identify the water masses present during the different sampling periods. TW is the result of the mixing and interaction of the water masses present in this Table (**Figure 3**). As Pacific Intermediate Water (PIW) is found at depths much greater than 400 m, it was not included in the present analysis. The calculations of Θ and S_A were carried out using the Thermodynamic Equation of Seawater 2010 (TEOS-10; IOC et al., 2010) included in the Ocean Data View program V4.7.8[1]. The calculations of mixed layer depth were carried out using the methodology described by Kara et al. (2000) and a criterion of 0.2°C in $\Delta\Theta$ for the equation of state was used to find the density variation ($\Delta\sigma_t$). The stratification parameter was calculated following Simpson (1981). It represents the amount of work per volume ($J{\cdot}m^{-3}$) needed to mix the water column up to a particular depth (300 m for this study).

In order to contrast the vertical distribution of oceanographic variables observed in each cruise, seasonal average profiles were extracted from the World Ocean Atlas 2009 (WOA09), specifically for spring and winter corresponding to June 2015 and March 2016 cruises, respectively. Also, to evaluate spatial variability in the study zone, the daily composition of the mean sea level anomaly (MSLA) from Aviso[2], sea surface temperature from GHRSST[3], and satellite chlorophyll ($Chla_{sat}$) distributed by Copernicus platform[4] were obtained.

[1]http://odv.awi.de

[2]https://www.aviso.altimetry.fr/

TABLE 1 | Water mass limits in the Tropical Pacific in front of Mexico.

				Mixed layer (m)	
	Θ (°C)	**S_A (g kg^{-1})**	**Depth (m)**	**Winter**	**Summer**
California Current Water	10–21	<34.6	0–150	45 ± 7	18 ± 8
Tropical Surface Water	>25.1	<34.6	0–50	32 ± 14	24 ± 10
Gulf of California Water	>12	>35.1	0–150	23 ± 7	15 ± 4
Subtropical Subsuperficial Water	9–18	34.6–35.1	75–400	–	–
Pacific Intermediate Water	4–9	34.6–34.9	400–1000	–	–

Taken and modified from Portela et al. (2016).

RESULTS

Water Masses

Five water masses were detected in the first 400 m during the June 2015 cruise. TSW was observed in front of Cabo Corrientes, between 18 and 21.5°N (blue colors in **Figure 2A**). The water column exhibited a strong thermal stratification in this zone. Conversely, GCW was observed from the surface to 176 m and confined within the entrance to the gulf at latitudes greater than 24°N (**Table 2**). In addition, the presence of the Tropical Branch of Californian Current was detected in five oceanic stations between 34 and 53 m depth near the tip of the peninsula (23.5°N). However, due to the previously defined objectives of the cruise, samples were not taken for this water mass and its DIC and pH content were unable to be characterized (**Table 2**). The water column is oftentimes unstable in this region and water column profiles in the T-S diagram (**Figure 2**) exhibit abrupt changes in salinity over a few meters. This pattern is typically associated with the presence of eddies that modify and disturb the vertical structure of the ocean. The presence of TW was detected in latitudes greater than 22°N where TSW loses its surface influence, as well as in the northern region within the Gulf of California up to 25.5°N. Toward the interior of the ocean, StSsW was present across all latitudes between 45 and 520 m depth (**Figure 2A** and **Table 2**).

The March 2016 cruise was comprised of fewer sampling stations (48 compared to 83 during 2015), with the notable absence of a cross gulf transect within the Gulf of California and another oceanic northwest-southeast section. However, the cruise comprised nearly the same latitudinal coverage as the previous year (**Figure 1**). GCW was only registered in four northern stations between 24 and 26°N and between 40 and 110 m depth. TSW was registered from 18–22°N, showing a relatively greater spatial coverage than during June 2015, although 30 m shallower (**Table 2**). In addition, TSW presented a lower average salinity and temperature than during the previous cruise. StSsW was present below superficial waters along with all latitudes in the study region (**Figure 2A**); in addition, the upper and lower limits of StSsW were like to those for June 2015 (**Table 2**). CCW was not registered during this period.

A comparison between the seasonal average taken from the World Ocean Atlas 2009 (WOA09) database and data from the June 2015 (spring) and March 2016 (winter) cruises shows that, for our particular region of the TPCM, TSW is typically absent during spring (**Figure 2C**) while water with characteristics similar to GCW was present during winter. Portela et al. (2016) indicate that the similarity to GCW is more pronounced below 250 m. Typical seasonality was not observed during spring when TSW was present in various southern stations and a large portion of TW was found to have thermohaline characteristics

[3]https://www.ghrsst.org/

[4]http://marine.copernicus.eu/

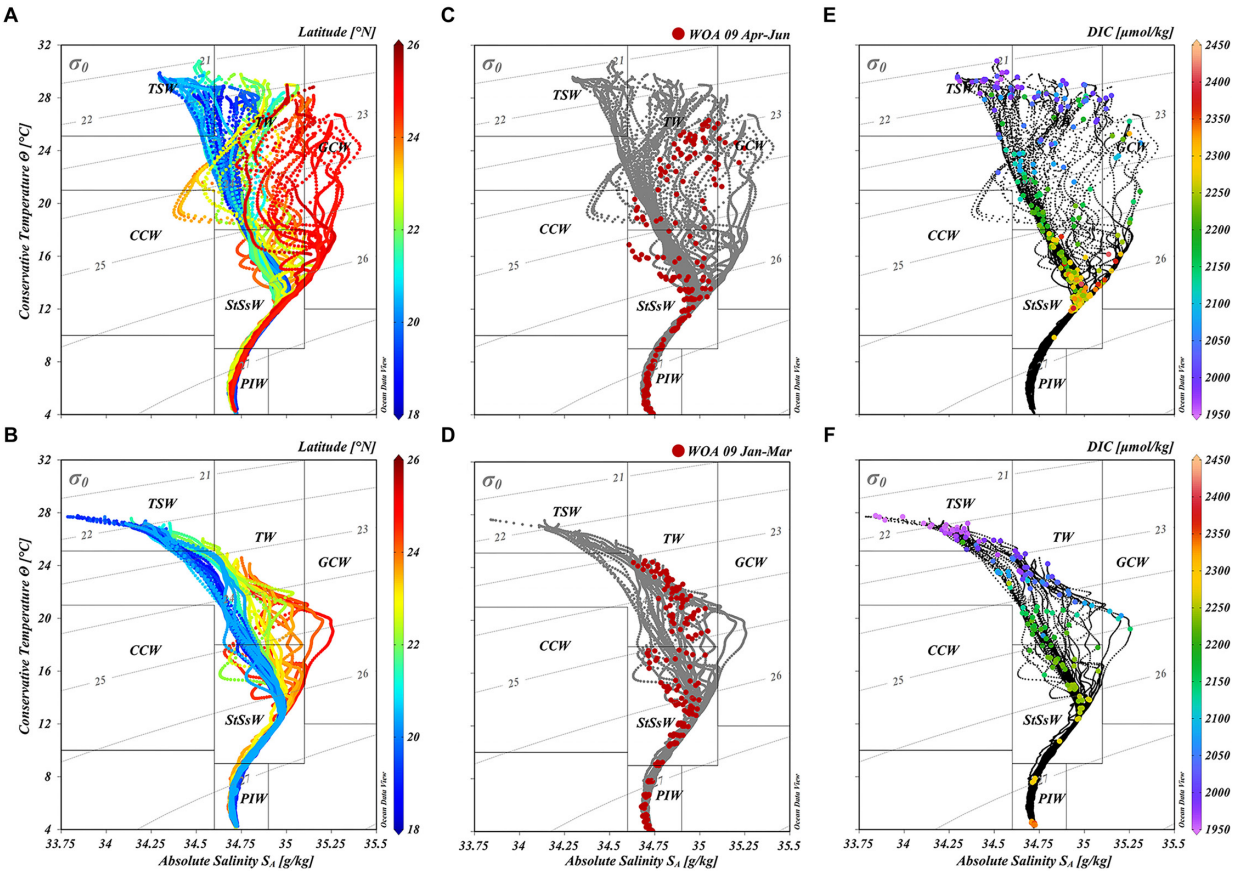

FIGURE 2 | Conservative temperature (Θ,°C) and absolute salinity (S_A, g/kg) diagram. Top figures, June 2015; bottom figures, March 2016. In color: **(A,B)** latitude in °N, **(C,D)** seasonal climatology was taken from World Ocean Atlas 2009, **(E,F)** dissolved inorganic carbon (DIC). The acronyms utilized are Gulf of California Water (GCW), California Current Water (CCW), Transitional Water (TW), Tropical Surface Water (TSW), Subtropical Subsuperficial Water (StSsW), and Pacific Intermediate Water (PIW). Water masses were classified according to Portela et al. (2016).

TABLE 2 | Physical and chemical characteristics of the water masses in the Tropical Pacific in front of Mexico.

Water mass	Month	Mean depth range (m)	Mixed layer depth (m)	Average Absolute Salinity (g/kg)	Average Conservative Temperature (°C)	DIC (µmol/kg)	pH_T	*n*	DO (µmol/kg)
GCW	Jun-15	0–176	10 ± 4	35.18 ± 0.05	18.09 ± 4.17	2199 ± 118	7.696 ± 0.219	22	107 ± 61
	Mar-16	42–112	–	35.17 ± 0.05	19.02 ± 1.52	2108 ± 30	7.967 ± 0.041	4	135 ± 56
CCW	Jun-15	34–53	–	34.46 ± 0.07	19.77 ± 0.73	–	–	–	178 ± 21
	Mar-16	–	–	–	–	–	–	–	–
TW	Jun-15	0–115	10 ± 6	34.78 ± 0.13	23.73 ± 3.56	2115 ± 78	7.786 ± 0.155	88	144 ± 69
	Mar-16	0–100	13 ± 6	34.73 ± 0.12	21.79 ± 1.75	2089 ± 77	7.888 ± 0.147	68	130 ± 69
TSW	Jun-15	0–74	25 ± 13	34.48 ± 0.09	28.35 ± 1.19	2016 ± 60	7.887 ± 0.12	35	196 ± 13
	Mar-16	0–44	12 ± 6	34.27 ± 0.15	26.44 ± 0.66	1971 ± 48	8.01 ± 0.087	35	198 ± 8
StSsW	Jun-15	45–520	–	34.09 ± 0.07	11.92 ± 1.94	2269 ± 42	7.551 ± 0.099	108	5 ± 10
	Mar-16	51–448	–	34.9 ± 0.07	12.05 ± 2.05	2232 ± 24	7.674 ± 0.053	35	5 ± 9

The salinity and average temperature of each water mass are presented. The acronyms utilized are Gulf of California Water (GCW), California Current Water (CCW), Transitional Water (TW), Tropical Surface Water (TSW), and Subtropical Subsuperficial Water (StSsW).

similar to TSW. Expanding this comparison, the winter season climatology (**Figure 2D**) showed a distribution where water mass characteristics were close to TSW. However, TSW is typically not present in the study region during this season; instead, a strong presence of TSW was detected during March 2016. In summary, for the June 2015 and March 2016 cruises, the presence of seasonally anomalous TSW was found within the study region.

The DIC concentration for each of the water masses defined is shown in **Figures 2E,F**. Most notably, superficial peaks and a greater variation in DIC were present in June 2015 when compared with March 2016, which presented less variability and a typical gradient in DIC concentration toward the interior of the ocean. The concentration of DIC in TSW during March 2016 was largely homogenous with values typically below 2000 $\mu mol \cdot kg^{-1}$. TW presented similar superficial DIC concentrations (between the 23 and 24 isopycnals) in all profiles, with increases in DIC up to 2200 $\mu mol \cdot kg^{-1}$nearing StSsW. For June 2015, TSW presented values in the same range as those present in 2016 but with greater superficial variability. The same occurred with the TW for this period, when values of up to 2200 $\mu mol \cdot kg^{-1}$ were present in surface waters. Finally, GCW presented the greatest variability, both near the surface with values of 2200 and 2300 $\mu mol \cdot kg^{-1}$, as in the deeper portion where concentrations similar to the maximums present in StSsW ($\sim$2400 $\mu mol \cdot kg^{-1}$) were observed (**Table 2**).

Profiles

Conservative Temperature and Absolute Salinity

Conservative temperature (O°C) and absolute salinity (S_A g/kg) profiles along transect 1 (white line in **Figure 1**) are shown in **Figure 3**. In June 2015 (**Figure 3A**), the temperature in the first 200 m of the water column was greater than during March 2016 (**Figure 3C**) and also notably, in the southern portion where the incursion of TSW was detected. The thermocline also appeared to be more intense during June 2015. Markedly, the 18°C isotherm deepened from 50 m near the entrance to the Gulf of California to 100 m under TSW toward the south. In this transect, the haline limits of the water masses were also detectable (white lines in **Figures 3B,D** and **Table 1**). TSW ventured to the north as a surface layer of low salinity (<34.6 $g \cdot kg^{-1}$) with greater depth during June 2015 (**Figure 3B**), but was shallower and less saline during March 2016. In June 2015, the exit of GCW (>35.1 $g \cdot kg^{-1}$) can also be noted, dominating above 150 m and extending 50 km outside the Gulf of California. In addition, the intrusion of CCW (<34.6 $g \cdot kg^{-1}$) at approximately 40 m depth was observed, which generated instability and mixing. During March 2016, the intrusion of GCW between 50 and 150 m depth near the entrance to the Gulf of California was also detected.

Positive sea surface temperature (SST) anomalies along the North Pacific were reported for winter 2014 (Hartmann, 2015; Stramma et al., 2016) and due to their intensity and extension, these anomalies have been referred to as "The Blob" (Bond et al., 2015). Following its establishment in the region, intense signals indicating the development of an El Niño-Southern Oscillation (ENSO) event were detected in the tropical Pacific[5]. Sánchez-Velasco et al. (2017) constructed an index of standardized SST anomalies using satellite images from 1981 to 2016 to determine if the local warming of surface waters was present in the TPCM as a result of the advance of the ENSO along the Mexican coast. The results of this index are shown in **Figure 2** of their article where a relationship between low southern oscillation index values (SOI) associated to strong ENSO events and positive and intense local anomalies in SST for the TPCM during 2015 and part of 2016 can be observed.

These temperature anomalies did not only appear on the surface. In **Figure 4**, these temperature anomalies are apparent along transect 1 toward the subsurface layer. The same database comparison was carried out, as with **Figures 2C,D**, to evaluate

[5]http://www.cpc.ncep.noaa.gov/

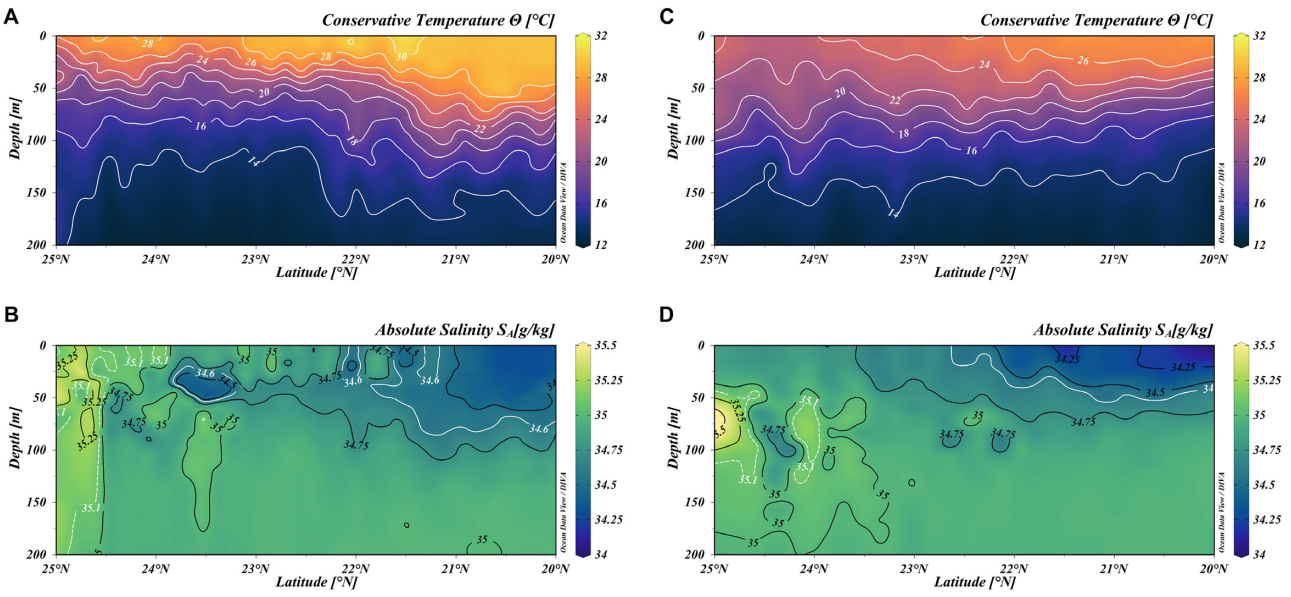

FIGURE 3 | Vertical distribution of conservative temperature (Θ,°C) and absolute salinity (S_A, g/kg) over transect 1 (see **Figure 1**). Respectively, **(A,B)** correspond to June 2015 and **(C,D)** to March 2016. Isohaline limits for Tropical Surface Water and Californian Current Water (<34.6 g/kg) and Gulf of California Water (>35.1 g/kg) appear in white.

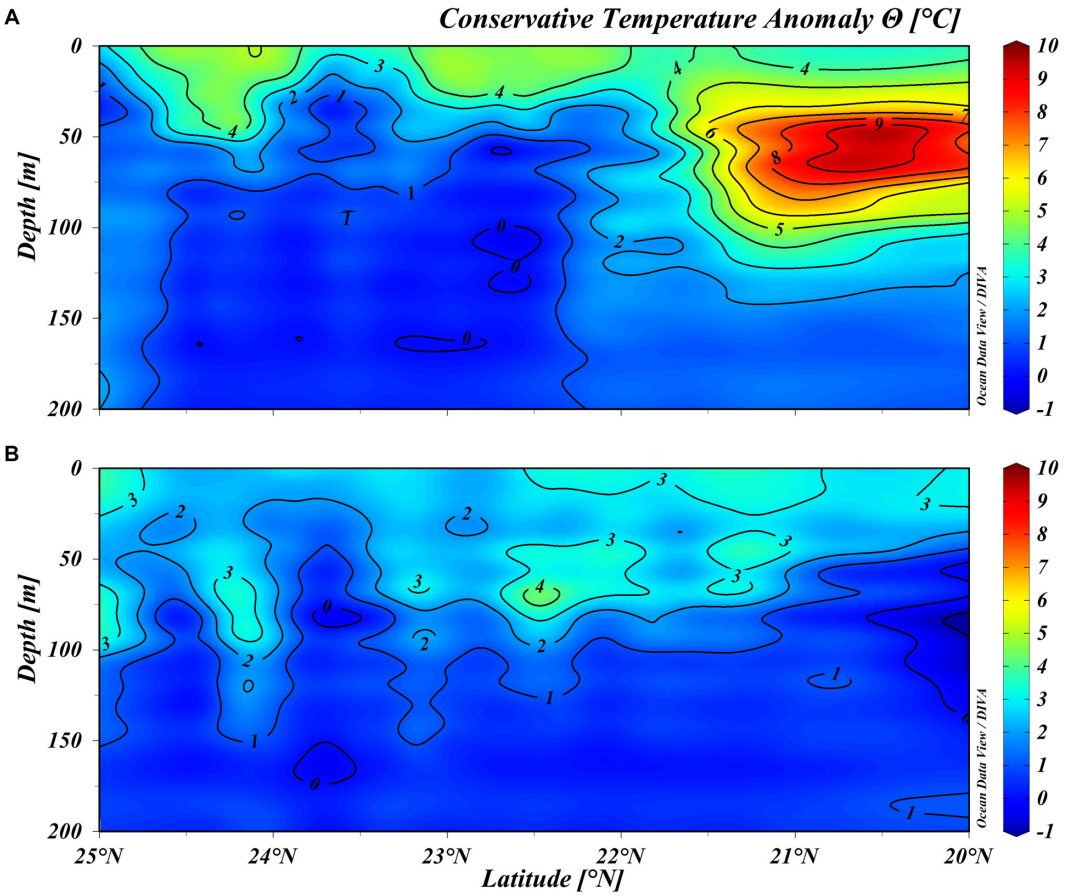

FIGURE 4 | Vertical distribution of conservative temperature (Θ,°C) anomalies along transect 1 (see **Figure 1**). **(A)** June 2015 and **(B)** March 2016. Refer to text for anomaly construction.

the temperature anomalies present, namely observed values from each cruise minus the corresponding seasonal climatology obtained from WOA09. For June 2015, the most intense positive anomalies were registered for either period in southern latitudes (21.5–20°N; **Figure 4A**) around Islas Marías (**Figure 1**). There we observed positive anomalies throughout the first 200 m, with values above 4°C from 100 m depth toward the surface. The greatest anomaly intensity in this area was near the vertical limit between TSW and StSsW (**Figures 3B**, **4A**), between 50 and 75 m depth. For the rest of transect to the north, positive anomalies were principally registered in the surface layer from 50 m depth. During March 2016, positive temperature anomalies in the water column were also registered. Despite being of lower intensity than the previous season (2–4°C), the positive anomaly manifested along the entire transect, from the surface to 100 m depth in northern latitudes and decreasing in depth toward southern latitudes (**Figure 4B**). This behavior is observed during an ENSO in decline (Abellán et al., 2017; Santoso et al., 2017), with superficial temperature anomalies that are still positive but with oceanographic conditions close to those of the seasonal climatology (**Figure 2D**). The weakest thermal anomaly signal observed during March 2016 may be due to the residual effect of the dissipating ENSO and the onset of conditions that are closer to the expected climatology.

Dissolved Oxygen

There is no consensus regarding the definition of OMZ limits (Hofmann et al., 2011); however, in order to understand their distribution, characteristics, and biogeochemical relevance, it is important to define reference boundaries as a function of the concentration of DO. These horizons have been established from different biological and chemical approximations and they have been assigned different terms (Hofmann et al., 2011). In the present study, we follow the limits established by Paulmier et al. (2011) for oxic levels (>200 $\mu mol \cdot kg^{-1}$) and Sánchez-Velasco et al. (2017) for hypoxic (<44 $\mu mol \cdot kg^{-1}$) and suboxic levels (<4.4 $\mu mol \cdot kg^{-1}$). These levels have been set on the function of the possible effects on the biology present. This is, under hypoxic conditions, epipelagic species may be subject to stressful conditions, while suboxic conditions can result in the death of epipelagic and mesopelagic species.

In June 2015, a narrowing of a layer with DO concentrations greater than suboxic levels but below oxic levels was observed from 50 m to below 175 m depth around 24.5°N (gray color

in **Figure 5A**). This may be associated with the exit of GCW (>35.1 g·kg^{-1}, **Figure 3B**), which rapidly loses its influence a few kilometers south of the entrance to the Gulf of California. Adjacent to this front, two relevant structures were observed, namely a downward 100 m displacement of the suboxic horizon to 200 m depth and an intrusion throughout the surface layer of waters from 50 m with oxygen concentrations between 140–160 μmol·kg^{-1}. For the remainder of the surface layer (>75 m) waters with oxic conditions dominated, except in the southern zone around Islas Marías were the advance of TSW was detected (<34.6 g·kg^{-1} in **Figure 3B**, and >25.1°C in **Figure 3A**). The upper horizon of the OMZ is defined by Cepeda-Morales et al. (2013) as a concentration of 9 μmol·L^{-1}and despite the fact that it is not shown in **Figure 5**, the 4.4 μmol·kg^{-1} isoline follows nearly the same distribution and is the one that will be used to define the upper and lower limit of the OMZ throughout this study. The upper portion of the OMZ is found shallower in the central portion of the transect (∼70 m), gradually deepening toward the south underneath TSW. The depth of the oxycline was defined as described by Maske et al. (2010), taking the depth of the maximum difference in DO calculated in a range of 4 m.

In contrast, March 2016 exhibited a scenario in accordance with oxygen winter climatology (Cepeda-Morales et al., 2013). A latitudinal gradient, where the OMZ deepens from its most shallow area around Cabo Corrientes (∼60 m) until it reaches approximately 300 m in front of the entrance to the Gulf of California.

Important anomalies in the concentration of DO were also observed latitudinally and toward the interior of the ocean. The analysis was carried out in the same manner as that for the T-S diagrams, taking into account only those depths that had more than four observations for the construction of the seasonal climatology (typically six observations, with a maximum of 15 observations, were used for oxygen, while 60 observations, with a maximum of 250 observations, were used for temperature). In **Figure 6A**, it can be noted that during June 2015, the incursion of TSW (from 20° to 21.5°N and from 75 m to the surface) appeared as a superficial wedge of low salinity (isohaline of 34.6 g·kg^{-1}) that brought a relatively high concentration of subsurface DO with values >75 μmol·kg^{-1}. In the northern region around the entrance to the Gulf of California (∼25°N), a similar behavior was observed to what was described for the southern region. The exit of GCW (>35.1 g·kg^{-1}) generated a near-vertical

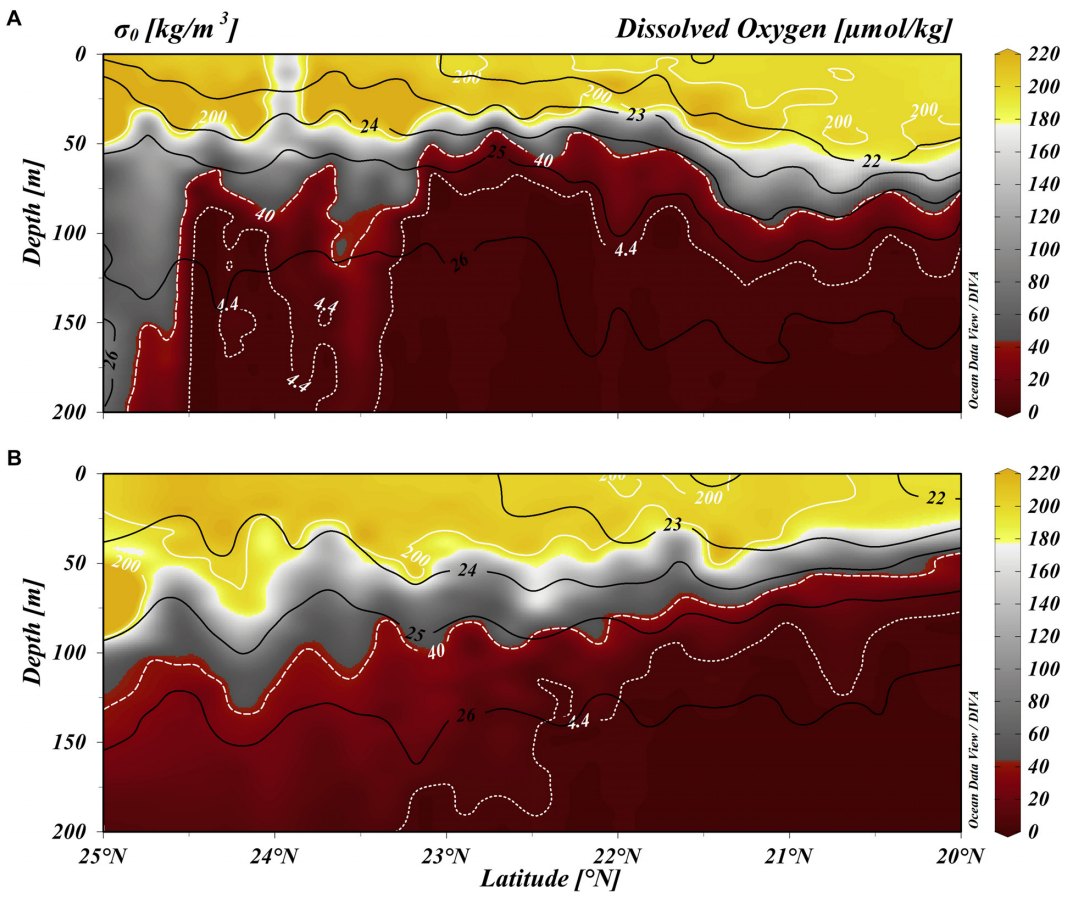

FIGURE 5 | Vertical distribution of dissolved oxygen (DO, μmol/kg) and potential density anomaly (σ_0, kg/m^3) along transect 1 (see **Figure 1**). **(A)** June 2015, **(B)** March 2016. Refer to text for DO limits.

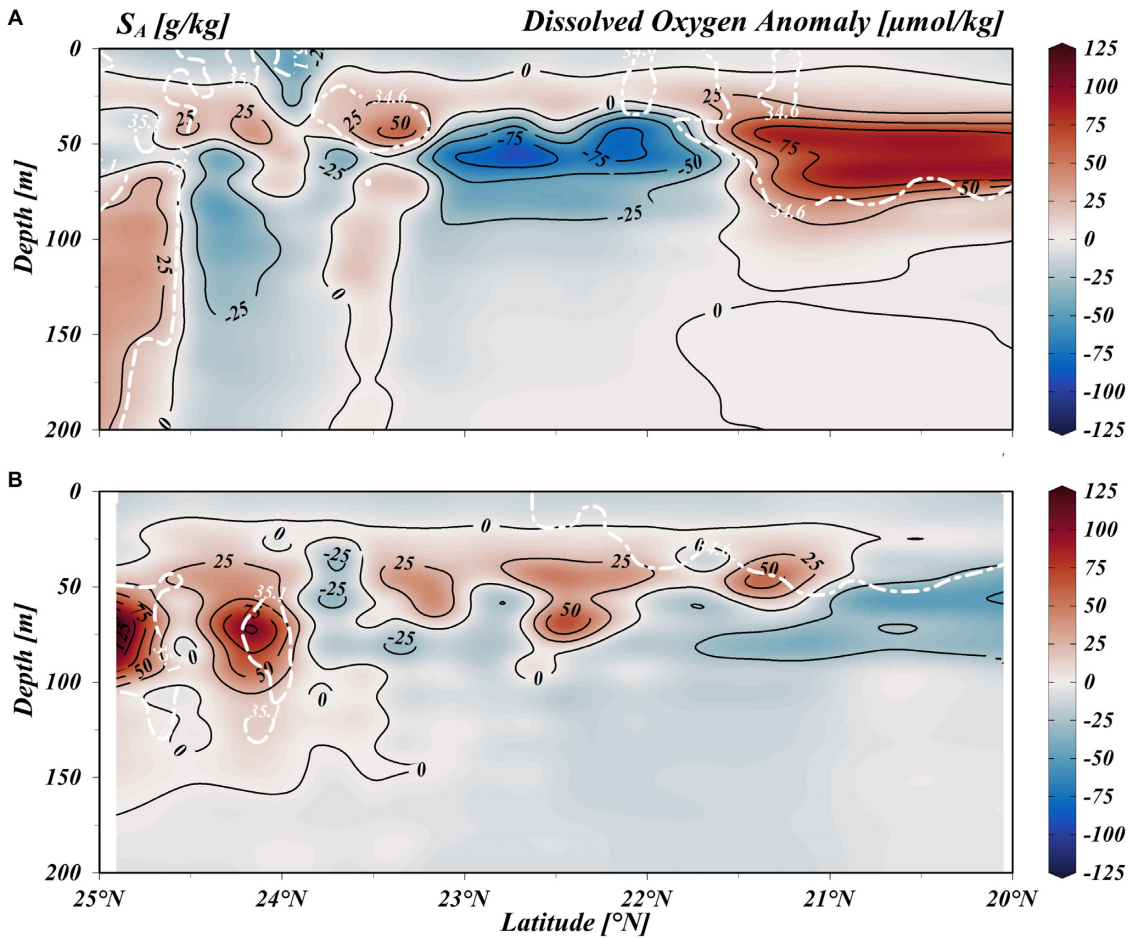

FIGURE 6 | Vertical distribution of dissolved oxygen (DO, µmol/kg) anomalies and absolute salinity (S_A, g/kg) along transect 1 (see **Figure 1**). **(A)** June 2015, **(B)** March 2016. Isohaline limits for Tropical Surface Water and Californian Current Water (<34.6 g/kg) and Gulf of California Water (>35.1 g/kg) appear in white. Refer to text for anomaly construction.

saline front that extended to 200 m depth. Collins et al. (2015) reported and described the mechanisms that participated in the formation of these fronts, highlighting that their generation is more prone to occur during autumn. The front associated with GCW generated positive DO anomalies with values above 25 µmol·kg^{-1} at depths between 50 and 200 m. Adjacent to where we observed the presence of GCW, between 50 and 150 m and between 25 m and the surface, anomalous values of DO below −25 µmol·kg^{-1} were detected. This occurs where an incursion throughout the surface layer of waters from 50 m depth with DO concentrations between 140 and 160 µmol·kg^{-1} (**Figure 5A**) was found. Further south (∼24°N), an intrusion was observed around 50 m depth of CCW (<34.6 g·kg^{-1}) that generated positive anomalies above 25 µmol·kg^{-1}.

For the following year in March 2016 (**Figure 5B**), the distribution of DO returned to near-seasonal conditions. However, a band of a positive anomaly (>25 µmol·kg^{-1}) along the entire transect around 50 m depth was present (**Figure 6B**). A plausible explanation for this process is (as also previously observed with temperature anomalies) that this band is the remnant effect of the incursion of warm southern oxygenated waters registered in the previous period. Moreover, around 25°–24°N, we observe positive DO anomalies of 50–125 µmol·kg^{-1} between 50–100 m depth that is related to the presence of GCW.

Despite the dispersion of data between the relationship of DO and DIC, these variables were highly correlated (r_p = 0.851, p < 0.001 for June 2015 and r_p = 0.867, p < 0.001 for March 2016; **Figure 7**), showing a clear tendency toward a decrease in DO as DIC values increase. For June 2015, the dispersion of the data clearly shows DO above 200 µmol·kg^{-1} (i.e., surface values; **Figure 5A**) and below 40 µmol·kg^{-1} (hypoxic concentration near the OMZ; **Figure 5A**). This dispersion is mainly attributed to the instability of the water column observed throughout this period (**Figure 2A**). TSW was mainly characterized by being well oxygenated (∼ 200 µmol·kg^{-1}), with greater dispersion in the concentration of DIC during June 2015 (2016 ± 60 µmol·kg^{-1}) than in March 2016 (1971 ± 48 µmol·kg^{-1}; **Table 2**). This pattern was observed for StSsW, with DO values below 50 µmol·kg^{-1} and greater variability during late spring 2015 than during winter 2016.

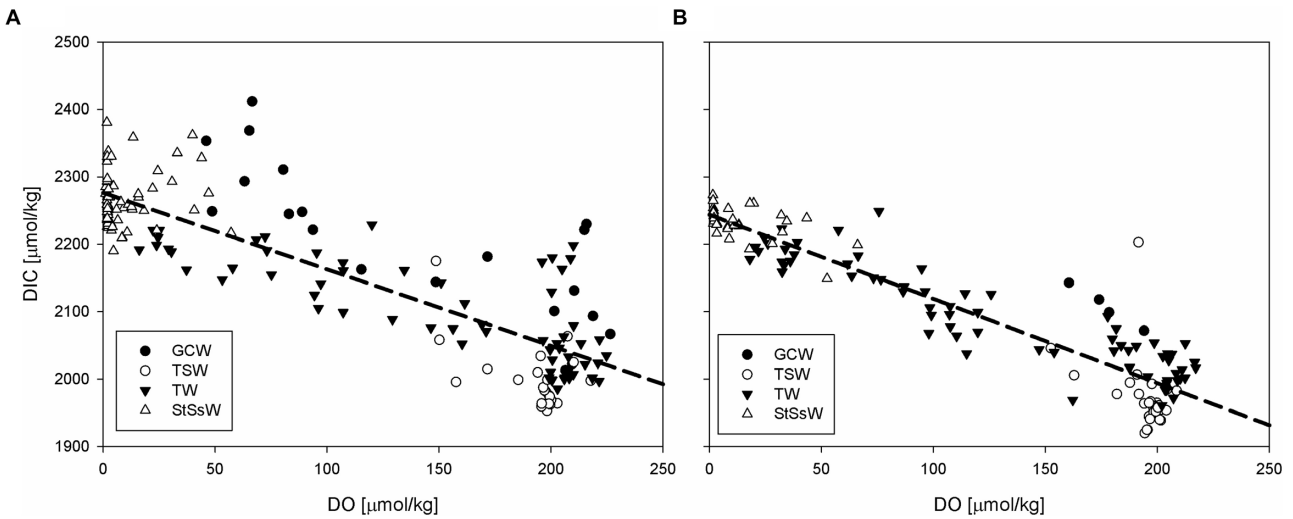

FIGURE 7 | Comparison between dissolved oxygen (DO, μmol/kg) and dissolved inorganic carbon (DIC, μmol/kg).The acronyms utilized are Gulf of California Water (GCW), California Current Water (CCW), Transitional Water (TW), Tropical Surface Water (TSW), and Subtropical Subsuperficial Water (StSsW). **(A)** June 2015, **(B)** March 2016.

DISCUSSION

Brewer (2018) exhorts that changing ocean oxygen field to be viewed and dealt with as a complex process of multiple forcing factors acting simultaneously. Furthermore, Respandly (2018) discuss the possible shifts in time between the expansions and contractions of the OMZ. Here we present another plausible forcing factor for the local ventilation of the upper OMZ that should be contemplated, according to Brewer's statement, in our understanding of the variability of these zones. An anomalous incursion of tropical water during El Niño 2015–2016 increased the availability of oxygen in previously deprived depths. This oxygen availability is reflected in the intensification of the oxycline where the intrusion was detected and in a higher molar ratio of DIC/AOU than prior studies have been reported (Maske et al., 2010).

Spatial Differentiation of DO and DIC Dynamics

In our analysis, we have identified three principal regions (I, II, and III in **Figure 8**), with regard to the processes that distribute and modify the spatial structure of DO and DIC. In this section, we have constructed the discussion about the characteristics observed during spring 2015 and we contrasted those characteristics with the scenario found during winter 2016.

June 2015

Cabo Corrientes (Region I)

In southern latitudes, below 22°N for coastal stations and 20.5°N for oceanic stations, the surface layer was dominated by the incursion of TSW. Its anomalous presence was related to the seasonally expected pattern, associated with a developing ENSO event (Sánchez-Velasco et al., 2017). In this region, the greatest stratification in our study period was registered, from 1000 to 1400 J·m^{-3} along an ocean-coast gradient (**Figure 9A**). These values are typically found in front of the coasts of Oaxaca (Chapa-Balcorta et al., 2015) and in the eastern Pacific warm pool (Fiedler et al., 2013), progressively decreasing toward our study region with values around 1200 J·m^{-3} (Fiedler et al., 2013; Franco et al., 2014). Temperature is the main factor controlling stratification in our region (Fiedler et al., 2013) and in the TPCM area, we can observe that the intensification of stratification was associated with an ocean-coast and north-south temperature gradient (**Figures 10**, **11**). However, for some coastal stations, where the influx of fresh water was detected (around Cabo Corrientes; **Figure 1**), salinity becomes the most relevant factor controlling stratification.

The oxycline has been proposed as a local mechanism where the OMZ is maintained through intense remineralization processes (Paulmier et al., 2006). Given the proximity of the oxycline to the surface and the wide range of DO concentrations present (from oxic $>$ 200 μmol·kg^{-1} to suboxic $<$ 4.4 μmol·kg^{-1}), aerobic/anaerobic and photic/aphotic processes can coexist within the oxycline, which may have concomitant repercussions in DIC and carbocline distributions (Paulmier et al., 2011). In **Figure 9E** we can observe how the depth of the oxycline is displaced from 40 m in the oceanic areas to below 80 m in front of Cabo Corrientes. The depth of the oxycline is closely associated with the distribution of stratification, caused by the entry of TSW with characteristics that were previously defined. This mechanism of the deepening and partial erosion of the oxycline has been described for equatorial zones (Fuenzalida et al., 2009) and Peruvian coasts (Stramma et al., 2016). The mixed later is associated with local processes, like winds, insolation, and rain (Fiedler et al., 2013). The greatest variability in the depth of the mixed layer can be found in the region of Cabo Corrientes, where sampling was carried out after the close passage of hurricane Blanca. Despite the high variability,

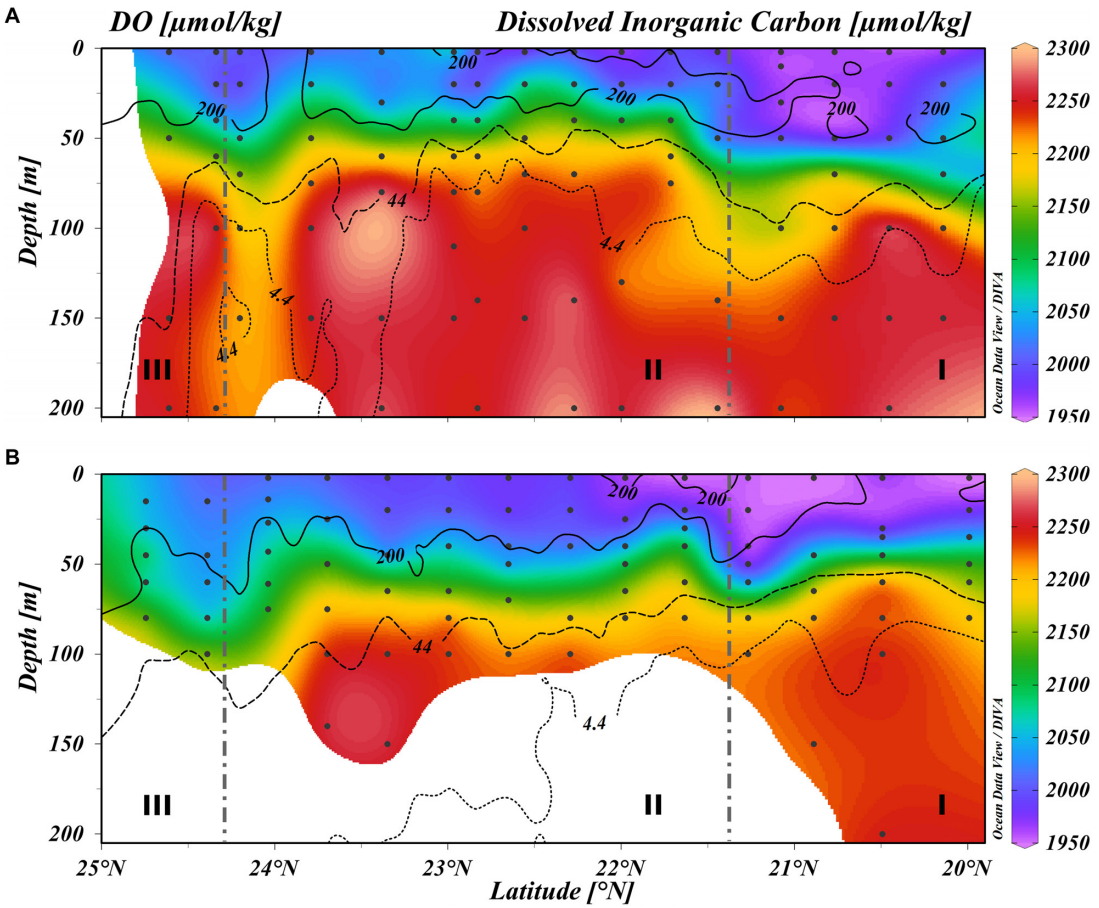

FIGURE 8 | Vertical distribution of dissolved inorganic carbon (DIC, µmol/kg) and dissolved oxygen (DO, µmol/kg) along transect 1 (see **Figure 1**). **(A)** June 2015, **(B)** March 2016. Refer to text for DO limits. Cabo Corrientes region **(I)**, Transitional region **(II)**, and entrance to the Gulf of California region **(III)**.

an ocean-coast pattern can be observed (**Figure 9C**) where the oxycline appears close (∼10 m) to the mixed layer in the oceanic sections yet separated by 60 m near the coast. Paulmier et al. (2006) hypothesize that remineralization is more sensitive to the availability of O_2 than to superficial biomass, suggesting that remineralization is "driven by oxygen." Our results support this hypothesis as the most intense oxyclines are found when the depth of the mixed layer is close to the depth of the oxycline and stratification is reduced, favoring the availability of oxygen in this layer and driving remineralization.

In **Figure 8** we presented the variation of DIC and DO along transect 1 for both latitude and depth. We also showed the established limits as a function of the analyses that were presented in this section. These limits were established according to physical-chemical characteristics determined during June 2015 and they were conserved to observe changes in the same sector during March 2016. These characteristics are dynamic and their presence can vary seasonally, principally as a function of the extension of the water masses present, but also due to forcing factors that favor dispersion and mixing.

In the region of Cabo Corrientes (region I, **Figure 8A**), TSW showed low DIC concentrations (∼1950 µmol·kg^{-1}) associated with slightly lower dissolved oxygen concentrations (180–200 µmol·kg^{-1}) than other superficial waters in the TPCM (typically > 200 µmol·kg^{-1}). OMZs present associated CMZs and analogous to OMZs, CMZs also contain a carbocline in their structures (Paulmier et al., 2011; Franco et al., 2014). The vertical resolution of our sampling does not allow for a detailed description of the carbocline and, as was mentioned in the observations carried out for **Figure 8**, there is a certain degree of dispersion between the relationship between DIC and DO depending on the water mass observed and on the latitude in which it is found. This is mainly due to the fact that DIC, in contrast to O_2, is a buffered system and responds more slowly to vertical perturbations (Paulmier et al., 2011). However, in part of the Cabo Corrientes region, a good association between the oxiplets of 4.4 and 44 µmol·kg^{-1} with DIC concentrations of 2300 and 2150 µmol·kg^{-1} was observed, related to StSsW that deepened due to the entry of TSW.

Transitional (Region II)

As the name suggests, this region is dominated at the surface by TW, which reached depths of up to 100 m (**Table 2**), and is the region in which the greatest instability in the water column

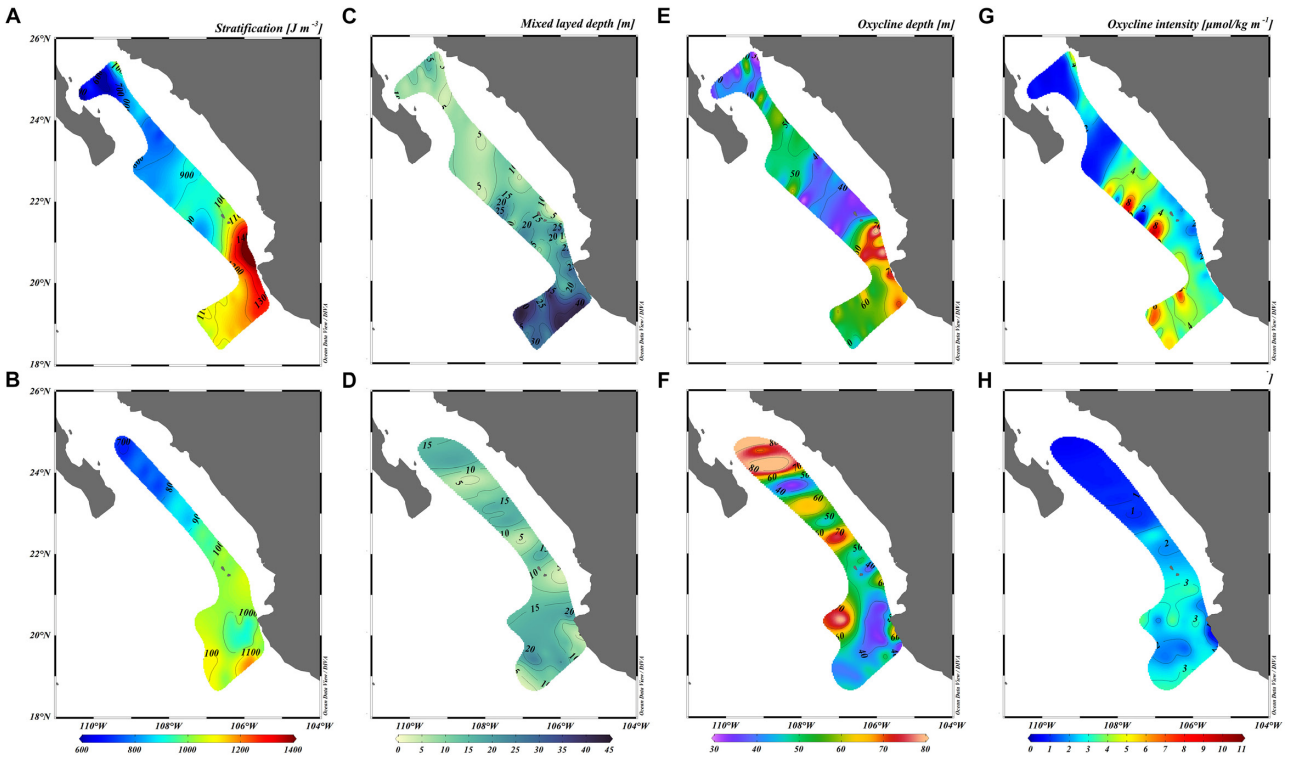

FIGURE 9 | Isosurfaces of stratification **(A,B)** calculated for the first 300 m, mixed layer depth **(C,D)**, oxycline depth **(E,F)**, and oxycline intensity **(G,H)**. Top figures, June 2015; bottom figures, March 2016.

is observed (**Figure 2**). The region is bounded to the north at 24.5°N by the exit of GCW as an oceanic front (**Figure 3**), while the southern border next to the Cabo Corrientes region is defined by the incursion of TSW (observable in **Figure 9A** as a stratification >1000 $J{\cdot}m^{-3}$). Stratification is lower in the transitional region, with an average of 850 $J{\cdot}m^{-3}$ and declines in a south-north gradient (∼900–700 $J{\cdot}m^{-3}$, **Figure 9**). In addition, this area can be divided into two separate sections by the depth of the oxycline, one section with the shallowest oxycline in all TPCM with depths less than 35 m (i.e., purple colors in **Figure 9E**) and another section with oxycline depths between 40 and 60 m (i.e., green colors in **Figure 9E**). In this region, a shallow oxycline occurred with a deep mixed layer (**Figure 9C**) and it is here that the greatest intensities in the oxycline were observed for all the TPCM (>8 $\mu mol{\cdot}kg^{-1}{\cdot}m^{-1}$; **Figure 9G**). Godínez et al. (2010) reported that 30% of the global variance in the observed circulation of the TPCM can be explained by mesoscale processes, such as the presence of eddies that can have relevant effects on the distribution of chemical variables in this region. Taking into consideration the closeness of the oxycline to the mixed layer, a lifting of the 22 $kg{\cdot}m^{-3}$ isopycnal from 50 m to the surface was found, which was also seen with the 26 $kg{\cdot}m^{-3}$ isopycnal (between 23.5 and 22°N in **Figure 5A**) and was associated with the passing of a cyclonic eddy between 21°N and 107°W in the days prior to beginning the cruise (**Figure 10**). It is around this area that we also found the greatest values of superficial pCO_2 (data not presented).

Two relevant structures were observed in the vertical distribution of DIC and DO (**Figure 8**). The first was a lifting of waters with greater DIC concentrations and lower DO concentrations around 23–22°N associated with a reduction in the influence of highly stratified TSW waters and the presence of a cyclonic eddy (**Figure 10**). The second was a highly unstable zone between 23.5 and 24.5°N where a pronounced sinking of the 4.4 $\mu mol{\cdot}kg^{-1}$oxiplet of ∼100 m was detected, without a comparable disturbance in the CMZ (>2200 $\mu mol{\cdot}kg^{-1}$), along with a simultaneous lifting from 50 m depth to the surface of water with concentrations below oxygenated levels centered around 24°N. In this region, we found an intrusion at 50 m depth of CCW and the instability that was found along the border was attributed to a front between a cyclonic and an anticyclonic eddy (**Figure 11**).

Entrance to the Gulf of California (Region III)

This area behaved in a similar manner to what has been reported in the literature. Here, the lowest stratification for the entire TPCM was detected, with values around 600 $J{\cdot}m^{-3}$. The exit of GCW was observed on the peninsular side as a front with high salinity (Castro et al., 2006; Collins et al., 2015) as was the entrance of TW over the continental platform in front of the coasts of Sonora, in accordance with the typical circulation scheme for this zone (Lavín et al., 2009). The depth of the oxycline was shallow in comparison to the region of Cabo Corrientes, but the intensity of the oxycline was amongst the

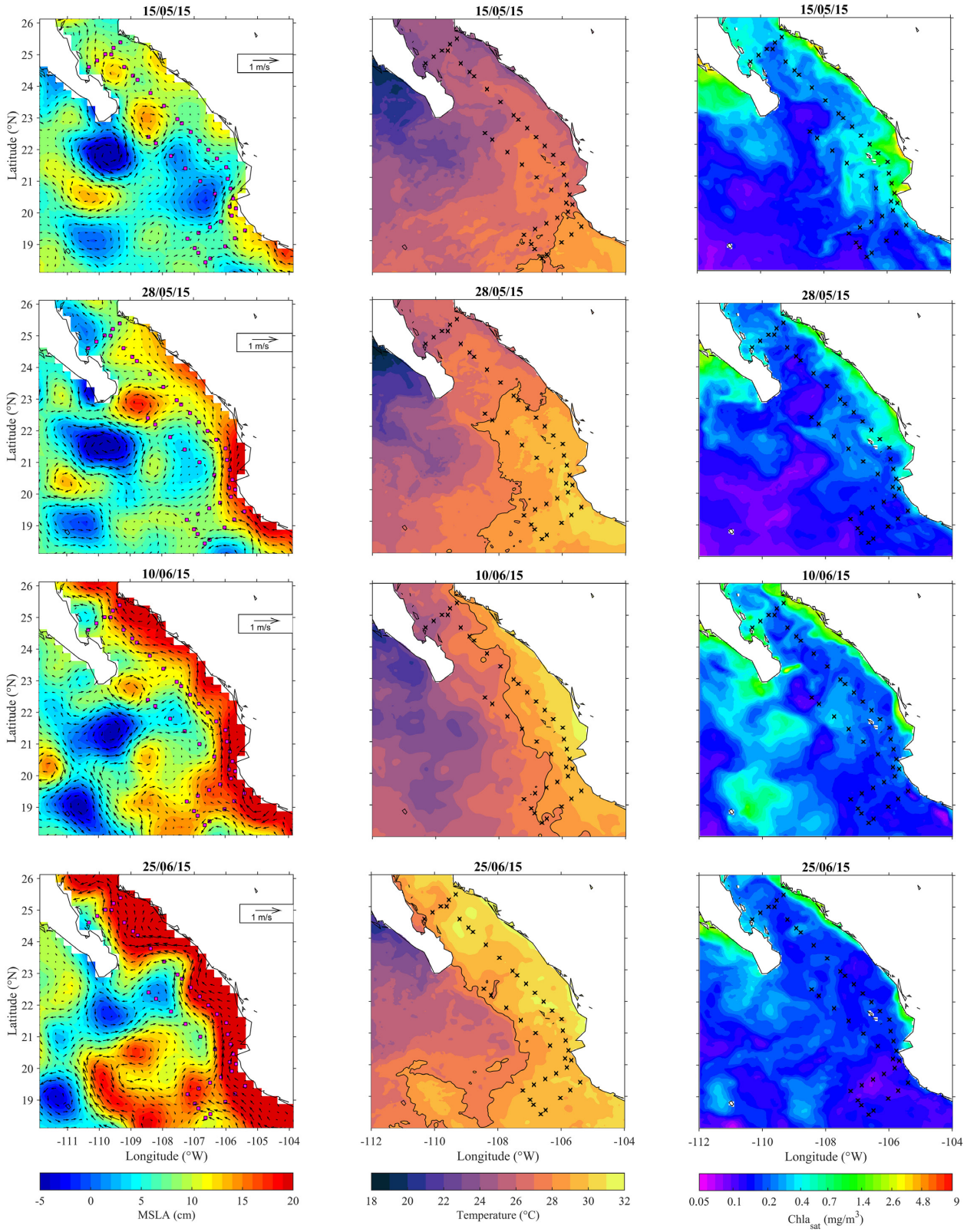

FIGURE 10 | Daily composition of mean sea level anomaly (MSLA, distributed by Aviso), sea surface temperature (GHRSST, the isotherm of 28°C in solid line), and satellite chlorophyll ($Chla_{sat}$ distributed by Copernicus).

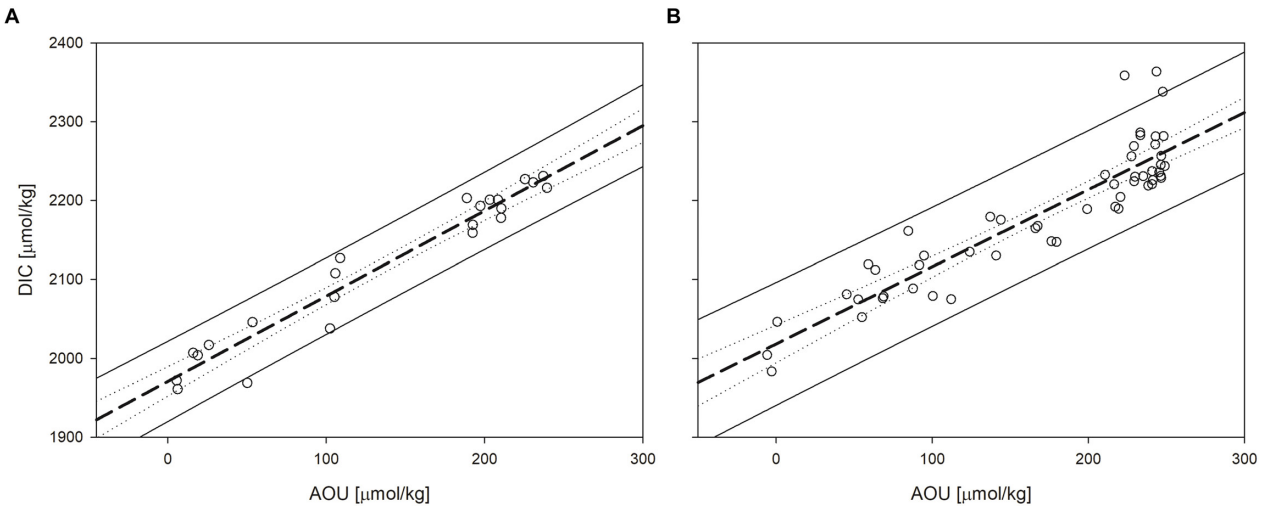

FIGURE 11 | Comparison between apparent oxygen utilization (AOU) and dissolved inorganic carbon (DIC) along the oxycline. See text for references. **(A)** June 2015 and **(B)** March 2016.

lowest recorded (Sánchez-Velasco et al., 2017). This is due to the GCW being more oxygenated and dominating depths below 150 m (**Figures 3**, **5**), causing the oxycline to become the thickest in this region. StSsW presented shallowly on the continental side, generating a likewise shallow oxycline with intensities of 5 $\mu mol \cdot kg^{-1} \cdot m^{-1}$ and consequently, the superficial pCO_2 was greater for this zone (data not shown).

March 2016

Cabo Corrientes (Region I)

With an ENSO in decline (Abellán et al., 2017; Santoso et al., 2017) and with lower stratification than the previous year (**Figure 9B**; ∼1100 $J \cdot m^{-3}$), the TSW area of influence was recorded up to 22°N (**Figures 2C,D**). In contrast to what occurred during spring 2015, the shallowest depth of the oxycline was found in this region (<40 m). The relationship between the intensity of the oxycline with respect to the depth of the mixed layer was not as direct as during 2016, and despite maximum intensities being lower compared with 2015 (50% less), it is in the area under the influence of TSW where we find the greatest values of oxycline intensity (2–4 $\mu mol \cdot kg^{-1} \cdot m^{-1}$; Paulmier et al. (2006) define as intense those oxycline > 1 $\mu mol \cdot kg^{-1} \cdot m^{-1}$). The vertical structure of the OMZ appeared to recover toward average conditions (**Figure 5**), where the oxyplets of 40 and 4.4 $\mu mol \cdot kg^{-1}$deepen in a south-north gradient (Cepeda-Morales et al., 2013). The content of DIC in the CMZ decreased with regard to the previous year (**Figure 3** and **Table 2**), probably due to a reduced presence of StSsW during March 2016. This same reduction is observed by Franco et al. (2014) for pCO_2 in oceanic sampling stations during August 2010.

Transitional (Region II)

The transitional region proved to be more stable than during the previous year; however, fluctuations in various characteristics were still present. The depth of the oxycline was variable throughout the entire region, as shown in **Figure 9F**, and in the undulations of the 44 $\mu mol \cdot kg^{-1}$oxyplet shown in **Figure 5B**. This area shows stratification lower than 900 $J \cdot m^{-3}$ and the depth mixed layer varies between 5 and 15 m. There is also a lifting of the CMZ (**Figure 8B**), principally due to the entry of GCW between 50 and 100 m (**Figure 3D**). However, this shallowing does not show significant repercussions in the superficial values of pCO_2 (not shown). The region of the entrance to the Gulf of California was only limited to the structure described in the previous sentence.

Ventilation of the OMZ Due to ENSO 2015–2016

For March 2016, in contrast to spring of the previous year, the presence of TSW did not originate apparent variations in the climatological seasonal distribution of DO. This is due to the relaxation of local ENSO effects (Sánchez-Velasco et al., 2017) and to the return of oceanographic conditions closer to the seasonal climatology (**Figure 2B**), where the influence of TSW in the TPCM during winter periods was still present and was the result of the incursions of this water mass during spring and autumn (Portela et al., 2016).

Cepeda-Morales et al. (2013) showed that a transition zone exists between 23 and 20°N where the influence of StSsW disappears and the upper portion of the OMZ is forced toward greater depths due to the intrusion of CCW transported by the interaction between eddies and the Tropical Branch of the CC. This intrusion has been observed and reported previously (Lavín et al., 2009). This mechanism may explain the positive DO anomaly related to the incursion of CCW and to the presence of two eddies, one cyclonic and one anticyclonic around this area (**Figure 10**).

Fuenzalida et al. (2009) report the erosion of the oxycline due to ENSO effects along the Peruvian coasts, observing a rapid re-establishment of a shallow mixed layer associated with an intense

oxycline. Even though we did not detect a complete erosion of the oxycline during the incursion of TSW in June 2016, our data show that there was an intensification of the same where this water mass was detected (**Figure 9G**). The latter suggests that in **Figure 5B** we might be observing the reestablishment of the oxycline in the region.

Due to the relatively high variability in the relationship between DIC and DO, a selection of the stations that presented the greatest intensities of the oxycline (>3 $\mu mol \cdot kg^{-1} \cdot m^{-1}$for June 2015 and >2.5 $\mu mol \cdot kg^{-1} \cdot m^{-1}$for March 2016) and that were contained within the depth range of the oxycline was carried out. This was done to evaluate the relationship between the production of DIC and biological activity in this layer. To do this, a linear regression of DIC versus apparent oxygen utilization (AOU) was carried out. The results are presented in **Figure 11** and show a relationship of: $DIC = 0.9777 \times AOU + 2018.34$ ($r_P = 0.9075$, $p < 0.0001$) for March 2015 and $DIC = 1.0807 \times AOU + 1970.81$ ($r_P = 0.9727$, $p < 0.0001$) for June 2016. Maske et al. (2010) report a molar relationship for the zone between DIC and AOU of 0.79 during March 2005. It is complicated to interpret this molar relationship in terms of which metabolic activity is acting given the wide range in oxygen concentration. However, we can observe a tendency of AOU to increase in the TPCM with the passage of the ENSO.

In addition, the pH_T values were strongly correlated with DIC values for both cruises (**Figure 12**; $r_p = 0.90$ for June 2015 and $r_p = 0.88$ for March 2016) and the distribution of pH_T presented in the same manner throughout each cruise. However, differences are present in the relationship between these two variables and between one year and the next. In general terms, greater pH_T values were present during March 2016 for the same observed concentration of DIC than in June 2015. This is more notable for greater concentrations of DIC (>2200 $\mu mol \cdot kg^{-1}$), while for DIC values close to typical surface values (1900–2000 $\mu mol \cdot kg^{-1}$), the data for both cruises tend to present greater similarity. This could be possibly explained as the result of a lower presence of StSsW and a relative greater contribution of TSW toward the end of the El Niño 2015–2016. Alternatively, the suppression of nutrient availability as a presence of oligotrophic, warmer, and higher stratified water could cause a drop in the biological pump. Evidence of this explanation is observed in **Figure 11**, by the presence of the incursion of warmer water ($>28°C$, solid line) associated to positive MSLA and a marked drop in chlorophyll in the coastal area where this water was present.

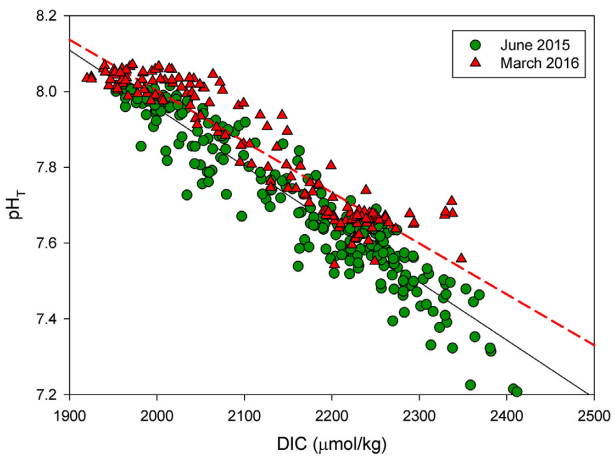

FIGURE 12 | Comparison between dissolved inorganic carbon (DIC) and pH in total scale (pH_T).

Paulmier et al. (2006) suggests control over biological activity in the OMZ as a function of the availability of oxygen. Ito and Deutsch (2013), from the results of their biogeochemical modeling of the tropical Pacific, highlight that heat content and respiration rates are highly correlated with the ENSO, suggesting that a deeper and warmer thermocline contains a greater quantity of oxygen because of changes in the biological consumption of oxygen due to a reduction in supply of nutrients from the surface. This mechanism, in conjunction with the sinking of StSsW to below the depth of incursion of TSW, may be operating in the southern portion of our study area, where the greatest anomalies of DO were present (**Figure 6**) as well as where the lowest values of DIC were found during the sampling periods (**Table 2** and **Figure 2**). These results agree with what has been reported in the literature for other areas, where the influence of the ENSO on the depth and structure of the OMZ and oxycline has been established (Morales et al., 1999; Fuenzalida et al., 2009; Czeschel et al., 2012).

CONCLUSION

The southern region of the TPCM was dominated at the surface by seasonally anomalous TSW as a result of a developing ENSO. Its presence modified the structure of the OMZ, partially eroding it while intensifying the oxycline, which had repercussions for the structure of the CMZ.

In the transition region, the carbon system was modulated by mesoscale processes. This region was dominated by TW and presented subsurface intrusions of more oxygenated CCW, which deepened the OMZ without altering the distribution of the CMZ. The presence of cyclonic eddies resulted in a lifting of the isopycnals in the central portion and the superficial enrichment of DIC.

The northern region was dominated by the exit of GCW on the peninsular side, where the OMZ deepened to below 200 m, and by the entry of TW on the continental side. In the latter, StSsW was close to the surface resulting in greater concentrations of DIC.

After these events, a return to close-to-average conditions was observed with regard to the structure of the OMZ during winter 2016. DIC concentrations diminished toward the interior of StSsW.

There is a strong regionalization of physical factors that control the distribution of dissolved oxygen and the variables of the seawater CO_2 system, which is principally modulated by the advection of water masses in the northern and southern regions and by the presence of mesoscale processes in the central region.

AUTHOR CONTRIBUTIONS

The conceptualization and arrangement of the original manuscript were under the charge of PT-P, JH-A, ES-d-A, and EB. The conceptual design and financial support of the oceanographic expeditions were under the direction of LS-V. All CTD data were facilitated through LS-V. Preprocessing of all data was carried out by VG. Laboratory analyses were conducted by PT-P and ON. All authors contributed equally to the reworking of the original manuscript toward the submitted version.

FUNDING

This work was supported by the project (2014-236864) "Influencia de remolinos de mesoescala sobre hábitats de larvas de peces (con énfasis en especies de importancia comercial) en la zona de mínimo de oxígeno del océano Pacífico frente a México: Océano abierto y efecto de islas," the project SEP – CONACyT (#2011-168034-T) "Un estudio de la Corriente Costera Mexicana y el Pacífico adyacente, con un 'SeaGlider,' cruceros oceanográficos y datos de satélite," and the project CONACyT Fronteras de la Ciencia 180 "Probando paradigmas sobre la expansión de la zona de mínimo de oxigeno: reducción del hábitat vertical del zooplancton y su efecto en el ecosistema pelágico mediante métodos autónomos." Funding came from CONACyT, Mexico, through the Grant 412049 for the M.Sc. studies of PT-P.

ACKNOWLEDGMENTS

We would like to thank the crew on board of the R/V Alpha Helix for their support during the sampling cruises. We would also like to give special recognition to Dr. María del Carmen Avila López and José Jonatan Santander Cruz, M.Sc., for their support in analyzing the TA samples, and to the researchers and students in the aquatic biogeochemistry seminar for their comments enriched this work. Finally we want to give special thanks to the reviewers for their excellent comments and suggestions.

REFERENCES

Abellán, E., McGregor, S., England, M. H., and Santoso, A. (2017). Distinctive role of ocean advection anomalies in the development of the extreme 2015–16 El Niño. *Clim. Dyn.* 51, 2191–2208. doi: 10.1007/s00382-017-4007-0

Apango-Figueroa, E., Sánchez-Velasco, L., Lavín, M. F., Godínez, V. M., and Barton, E. D. (2015). Larval fish habitats in a mesoscale dipole eddy in the gulf of California. *Deep Res. Part I* 103, 1–12. doi: 10.1016/j.dsr.2015.05.005

Bond, N. A., Cronin, M. F., Freeland, H., and Mantua, N. (2015). Causes and impacts of the 2014 warm anomaly in the NE Pacific. *Geophys. Res. Lett.* 42, 3414–3420. doi: 10.1002/2015GL063306

Canfield, D. E., Stewart, F. J., Thamdrup, B., De Brabandere, L., Dalsgaard, T., Delong, E. F., et al. (2010). A cryptic sulfur cycle in oxygen-minimum-zone waters off the chilean coast. *Science* 330, 1375–1379. doi: 10.1126/science.1196889

Castro, R., and Durazo, R. (2000). Variación estacional de la temperatura y salinidad en la entrada del Golfo de California, México. *Ciencias Mar.* 26, 561–583.

Castro, R., Durazo, R., Mascarenhas, A., Collins, C. A., and Trasviña, A. (2006). Thermohaline variability and geostrophic circulation in the southern portion of the Gulf of California. *Deep Res. Part I Oceanogr. Res. Pap.* 53, 188–200. doi: 10.1016/j.dsr.2005.09.010

Cepeda-Morales, J., Beier, E., Gaxiola-Castro, G., Lavín, M. F., and Godínez, V. M. (2009). Efecto de la zona del mínimo de oxígeno en el segundo máximo de clorofila en el Pacífico Oriental Tropical Mexicano. *Ciencias Mar.* 35, 389–403.

Cepeda-Morales, J., Gaxiola-Castro, G., Beier, E., and Godínez, V. M. (2013). The mechanisms involved in defining the northern boundary of the shallow oxygen minimum zone in the eastern tropical Pacific Ocean off Mexico. *Deep Res. Part I Oceanogr. Res. Pap.* 76, 1–12. doi: 10.1016/j.dsr.2013.02.004

Chapa-Balcorta, C., Hernandez-Ayon, J. M., Durazo, R., Beier, E., Alin, S. R., and López-Pérez, A. (2015). Influence of post-Tehuano oceanographic processes in the dynamics of the CO2 system in the Gulf of Tehuantepec. *Mexico J. Geophys. Res. Ocean* 120, 7752–7770. doi: 10.1002/2015JC011249

Clayton, T. D., and Byrne, R. H. (1993). Spectrophotometric seawater pH measurements: total hydrogen results. *Deep Sea Res. Part I Oceanogr. Res. Pap.* 40, 2115–2129. doi: 10.1016/0967-0637(93)90048-8

Collins, C. A., Castro, R., and Mascarenhas, A. (2015). Properties of an upper ocean front associated with water mass boundaries at the entrance to the Gulf of California, November 2004. *Deep Sea Res. Part II Top. Stud. Oceanogr.* 119, 48–60. doi: 10.1016/j.dsr2.2014.06.002

Czeschel, R., Stramma, L., and Johnson, G. C. (2012). Oxygen decreases and variability in the eastern equatorial Pacific. *J. Geophys. Res. Ocean* 117, 1–12. doi: 10.1029/2012JC008043

Davies, S. M., Sánchez-Velasco, L., Beier, E., Godínez, V. M., Barton, E. D., and Tamayo, A. (2015). Three-dimensional distribution of larval fish habitats in the shallow oxygen minimum zone in the eastern tropical Pacific Ocean off Mexico. *Deep Res. Part I Oceanogr. Res. Pap.* 101, 118–129. doi: 10.1016/j.dsr.2015.04.003

Dickson, A. G., Afghan, J. D., and Anderson, G. C. (2003). Reference materials for oceanic CO2 analysis: a method for the certification of total alkalinity. *Mar. Chem.* 80, 185–197. doi: 10.1016/S0304-4203(02)00133-130

Dickson, A. G., Sabine, C. L., and Christian, J. R. (2007). *Guide to Best Practices for Ocean CO2 Measurements*. Sidney, BC: North Pacific Marine Science Organization.

Douglas, N. K., and Byrne, R. H. (2017). Achieving accurate spectrophotometric pH measurements using unpurified meta-cresol purple. *Mar. Chem.* 190, 66–72. doi: 10.1016/j.marchem.2017.02.004

Fernández-Álamo, M. A., and Färber-Lorda, J. (2006). Zooplankton and the oceanography of the eastern tropical Pacific: a review. *Prog. Oceanogr.* 69, 318–359. doi: 10.1016/j.pocean.2006.03.003

Fiedler, P. C., Mendelssohn, R., Palacios, D. M., and Bograd, S. J. (2013). Pycnocline variations in the eastern tropical and north pacific, 1958-2008. *J. Clim.* 26, 583–599. doi: 10.1175/JCLI-D-11-00728.1

Fiedler, P. C., and Talley, L. D. (2006). Hydrography of the eastern tropical Pacific: a review. *Prog. Oceanogr.* 69, 143–180. doi: 10.1016/j.pocean.2006.03.008

Franco, A. C., Hernández-Ayón, J. M., Beier, E., Garçon, V., Maske, H., Paulmier, A., et al. (2014). Air-sea CO2 fluxes above the stratified oxygen minimumzone in the coastal region offMexico. *J. Geophys. Res. Ocean.* 119, 1–15. doi: 10.1002/2013JC009337

Fuenzalida, R., Schneider, W., Garcpes-Vargas, J., Bravo, L., and Lange, C. (2009). Vertical and horizontal extension of the oxygen minimum zone in the eastern South Pacific Ocean. *Deep. Res. Part II* 56, 992–1008. doi: 10.1016/j.dsr2.2008.11.001

Garcia, H. E., and Gordon, L. I. (1992). Oxygen solubility in seawater: better fitting equations. *Limnol. Oceanogr.* 37, 1307–1312. doi: 10.4319/lo.1992.37.6.1307

Godínez, V. M., Beier, E., Lavín, M. F., and Kurczyn, J. A. (2010). Circulation at the entrance of the Gulf of California from satellite altimeter and hydrographic observations. *J. Geophys. Res. Ocean* 115, 1–15. doi: 10.1029/2009JC005705

Gómez-Valdivia, F., Parés-Sierra, A., and Flores-Morales, A. L. (2015). The mexican coastal current: a subsurface seasonal bridge that connects the tropical and subtropical Northeastern Pacific. *Cont. Shelf Res.* 110, 100–107. doi: 10.1016/j.csr.2015.10.010

Hartmann, D. L. (2015). Pacific sea surface temperature and the winter of 2014. *Geophys. Res. Lett.* 42, 1894–1902. doi: 10.1002/2015GL063083

Hofmann, A. F., Peltzer, E. T., Walz, P. M., and Brewer, P. G. (2011). Hypoxia by degrees: establishing definitions for a changing ocean. *Deep Res. Part I Oceanogr. Res. Pap.* 58, 1212–1226. doi: 10.1016/j.dsr.2011.09.004

Ito, T., and Deutsch, C. (2013). Variability of the oxygen minimum zone in the tropical North Pacific during the late twentieth century. *Glob. Biogeochem. Cycles* 27, 1119–1128. doi: 10.1002/2013GB004567

Kalvelage, T., Lavik, G., Lam, P., Contreras, S., Arteaga, L., Löscher, C. R., et al. (2013). Nitrogen cycling driven by organic matter export in the South Pacific oxygen minimum zone. *Nat. Geosci.* 6, 228–234. doi: 10.1038/ngeo1739

Kara, A. B., Rochford, P. A., and Hurlburt, H. E. (2000). An optimal definition for ocean mixed layer depth. *J. Geophys. Res.* 105821, 803–816. doi: 10.1029/2000JC900072

Keeling, R. F., and Garcia, H. E. (2002). The change in oceanic O 2 inventory associated with recent global warming. *Proc. Natl. Acad. Sci. U.S.A.* 99, 7848–7853. doi: 10.1073/pnas.122154899

Kurczyn, J. A., Beier, E., Lavín, M. F., and Chaigneau, A. (2012). Mesoscale eddies in the northeastern Pacific tropical-subtropical transition zone: statistical characterization from satellite altimetry. *J. Geophys. Res. Ocean* 117:C10021. doi: 10.1029/2012JC007970

Kurczyn, J. A., Beier, E., Lavín, M. F., Chaigneau, A., and Godínez, V. M. (2013). Anatomy and evolution of a cyclonic mesoscale eddy observed in the northeastern Pacific tropical-subtropical transition zone. *J. Geophys. Res. Ocean* 118, 5931–5950. doi: 10.1002/2013JC20437

Lavín, M. F., Beier, E., Gómez-Valdés, J., Godínez, V. M., and García, J. (2006). On the summer poleward coastal current off SW México. *Geophys. Res. Lett.* 33, 2–5. doi: 10.1029/2005GL024686

Lavín, M. F., Castro, R., Beier, E., and Godínez, V. M. (2013). Mesoscale eddies in the southern Gulf of California during summer: characteristics and interaction with the wind stress. *J. Geophys. Res. Ocean* 118, 1367–1381. doi: 10.1002/jgrc.20132

Lavín, M. F., Castro, R., Beier, E., GodInez, V. M., Amador, A., and Guest, P. (2009). SST, thermohaline structure, and circulation in the southern gulf of California in june 2004 during the north american monsoon experiment. *J. Geophys. Res. Ocean* 114, 1–22.

Lewis, E., and Wallace, D. (1998). *Program Developed for CO2 System Calculations*. Washington, DC: United States Department of Energy.

Liu, X., Patsavas, M. C., and Byrne, R. H. (2011). Purification and characterization of meta-cresol purple for spectrophotometric seawater ph measurements. *Environ. Sci. Technol.* 45, 4862–4868. doi: 10.1021/es200665d

Maske, H., Medrano, R. C., Castro, A. T., Mercado, A. J., Jauregui, C. O. A., Castro, G. G., et al. (2010). Inorganic carbon and biological oceanography above a shallow oxygen minimum in the entrance to the Gulf of California in the Mexican Pacific. *Limnol. Oceanogr.* 55, 481–491. doi: 10.4319/lo.2009.55.2.0481

McDougall, T. J., and Barker, P. M. (2017). *Getting Started with TEOS-10 and the Gibbs Seawater (GSW) Oceanographic Toolbox*. Paris: SCOR.

Morales, C. E., Hormazábal, S. E., and Blanco, J. (1999). Interannual variability in the mesoscale distribution of the depth of the upper boundary of the oxygen minimum layer off northern Chile (18–24S): implications for the pelagic system and biogeochemical cycling. *J. Mar. Res.* 57, 909–932. doi: 10.1357/002224099321514097

Paulmier, A., and Ruiz-Pino, D. (2009). Oxygen minimum zones (OMZs) in the modern ocean. *Prog. Oceanogr.* 80, 113–128. doi: 10.1016/j.pocean.2008.08.001

Paulmier, A., Ruiz-Pino, D., and Garçon, V. (2011). CO2 maximum in the oxygen minimum zone (OMZ). *Biogeosciences* 8, 239–252. doi: 10.5194/bg-8-239-2011

Paulmier, A., Ruiz-Pino, D., Garçon, V., and Farías, L. (2006). Maintaining of the eastern south pacific oxygen minimum zone (OMZ) off Chile. *Geophys. Res. Lett.* 33, 2–7. doi: 10.1029/2006GL026801

Portela, E., Beier, E. J., Barton, E. D., Castro, R., Godínez, V., Palacios-Hernández, E., et al. (2016). Water masses and circulation in the tropical Pacific off central Mexico and surrounding areas. *J. Phys. Oceanogr.* 46, 3069–3081. doi: 10.1175/JPO-D-16-0068.1

Rabalais, N. N., Díaz, R. J., Levin, L. A., Turner, R. E., Gilbert, D., and Zhang, J. (2010). Dynamics and distribution of natural and human-caused hypoxia. *Biogeosciences* 7, 585–619. doi: 10.5194/bg-7-585-2010

Respandly, L. (2018). Climate change and oxygen in the ocean. *Nature* 557, 314–315.

Sánchez-Velasco, L., Beier, E., GodInez, V. M., Barton, E. D., Santamaría-del-Angel, E., Jiménez-Rosenberg, S. P. A., et al. (2017). Hydrographic and fish larvae distribution during the "Godzilla El Niño 2015–2016" in the northern end of the shallow oxygen minimum zone of the Eastern Tropical Pacific Ocean. *J. Geophys. Res. Ocean* 122, 2156–2170. doi: 10.1002/2016JC012622

Sánchez-Velasco, L., Ruvalcaba-Aroche, E. D., Beier, E., Godínez, V. M., Barton, E. D., Díaz-Viloria, N., et al. (2016). Paralarvae of the complex *Sthenoteuthis oualaniensis*-Dosidicus gigas (Cephalopoda: Ommastrephidae) in the northern limit of the shallow oxygen minimum zone of the Eastern Tropical Pacific Ocean (April 2012). *J. Geophys. Res. Ocean* 121, 1998–2015. doi: 10.1002/2015JC011534

Santoso, A., McPhaden, M. J., and Cai, W. (2017). The defining characteristics of ENSO extremes and the strong 2015/16 El Niño. *Rev. Geophys.* 55, 1079–1129. doi: 10.1002/2017RG000560

IOC, SCOR, and IAPSO. (2010). *The International Thermodynamic Equation of Seawater – 2010: Calculation and use of Thermodynamic Properties*. Paris: UNESCO.

Simpson, J. H. (1981). The shelf-sea fronts: implications of their existence and behaviour. *Philos. Trans. R. Soc. Lond Ser. A* 302, 531–546. doi: 10.1098/rsta.1981.0181

Stramma, L., Fischer, T., Grundle, D. S., Krahmann, G., and Bange, H. W. (2016). Observed El Niño conditions in the eastern tropical Pacific in October 2015. *Ocean Sci.* 12, 861–873. doi: 10.5194/os-12-861-2016

Stramma, L., Johnson, G. C., Sprintall, J., and Mohrholz, V. (2008). Expanding oxygen-minimum zones in the tropical oceans. *Science* 320, 655–658. doi: 10.1126/science.1153847

Stramma, L., Schmidtko, S., Levin, L. A., and Johnson, G. C. (2010). Ocean oxygen minima expansions and their biological impacts. *Deep. Res. Part I Oceanogr. Res. Pap.* 57, 587–595. doi: 10.1016/j.dsr.2010.01.005

Wishner, K. F., Outram, D. M., Seibel, B. A., Daly, K. L., and Williams, R. L. (2013). Zooplankton in the eastern tropical north Pacific: boundary effects of oxygen minimum zone expansion. *Deep Sea Res. Part I Oceanogr. Res. Pap.* 79, 122–140. doi: 10.1016/j.dsr.2013.05.012

Conflict of Interest Statement: The authors declare that the research was conducted in the absence of any commercial or financial relationships that could be construed as a potential conflict of interest.

frontiers in Earth Science

ORIGINAL RESEARCH
published: 26 September 2019
doi: 10.3389/feart.2019.00237

Scenarios of Deoxygenation of the Eastern Tropical North Pacific During the Past Millennium as a Window Into the Future of Oxygen Minimum Zones

Konstantin Choumiline[1]*, *Ligia Pérez-Cruz*[2], *Andrew B. Gray*[3], *Steven M. Bates*[1] and *Timothy W. Lyons*[1]

[1] Department of Earth and Planetary Sciences, University of California, Riverside, Riverside, CA, United States, [2] Instituto de Geofisica, Universidad Nacional Autonóma de México, Mexico City, Mexico, [3] Department of Environmental Sciences, University of California, Riverside, Riverside, CA, United States

Diverse studies predict global expansion of Oxygen Minimum Zones (OMZs) as a consequence of anthropogenic global warming. While the observed dissolved oxygen concentrations in many coastal regions are slowly decreasing, sediment core paleorecords often show contradictory trends. This is the case for numerous high-resolution reconstructions of oxygenation in the Eastern Tropical North Pacific (ETNP). While major shifts in redox conditions of the ETNP are dominated by glacial-interglacial cycling, important fluctuations also occur in response to minor climatic and oceanographic perturbations. It is important to understand these scenarios of past redox variation, as they are the closest analog for near future climate and oceanographic change. We present recently collected sediment core proxy records from the Gulf of California in which we reproduce the variability of productivity and oxygenation of the ETNP OMZ during the past millennium. We emphasize paleoproductivity (C_{org}, Ni, Ba_{excess}) and paleoredox indicators (Mo, Cd, V, U_{auth}) in sediment cores collected in Alfonso and La Paz basins and compare these OMZ records with other archives of the Eastern Pacific. Our findings indicate that the OMZ expanded in response to increased upwelling and productivity during cold intervals of the early 1400s, early 1500s, late 1600s, and early 1800s AD (evidenced by higher Ni, V, Cd, Mo, and U_{auth}). The most hypoxic times corresponded to the beginning of the Little Ice Age (expressed in elevated Mo). Significant OMZ contractions occurred around late 1300s, early 1700s, and late 1900s AD after reoxygenation events that were instigated by low productivity (lower Ni, V, Cd, Mo, and U_{auth}). The mechanisms that control decadal-to-centennial oxygen variability in the ETNP remain unidentified but are likely influenced by solar forcing not only driving migrations of the Intertropical Convergence Zone (ITCZ) but more importantly changes in the intensity of the Pacific Walker Circulation (PWC). During the Little Ice Age solar irradiance was at its lowest for the past millennium, which strengthened the PWC. This pattern contributed to more frequent La Niña-like conditions, which enhanced upwelling of nutrient-rich waters in the west coast of North America, driving productivity and reducing bottom oxygen levels, as seen in our ETNP records.

Keywords: Oxygen Minimum Zones (OMZs), Eastern Tropical North Pacific (ETNP), primary productivity, deoxygenation, hypoxia, paleoredox, redox-sensitive trace elements, authigenic uranium

OPEN ACCESS

Edited by:
Babette Hoogakker, Heriot-Watt University, United Kingdom

Reviewed by:
Nicolas Tribovillard, Lille University of Science and Technology, France
Laetitia Pichevin, University of Edinburgh, United Kingdom

***Correspondence:**
Konstantin Choumiline
konstantin.choumiline@email.ucr.edu

Specialty section:
This article was submitted to Marine Biogeochemistry, a section of the journal Frontiers in Earth Science

Received: *20 September 2018*
Accepted: *28 August 2019*
Published: *26 September 2019*

Citation:
Choumiline K, Pérez-Cruz L, Gray AB, Bates SM and Lyons TW (2019) Scenarios of Deoxygenation of the Eastern Tropical North Pacific During the Past Millennium as a Window Into the Future of Oxygen Minimum Zones. Front. Earth Sci. 7:237. doi: 10.3389/feart.2019.00237

INTRODUCTION

Numerous experimental, observational, and numerical model studies predict global expansion of Oxygen Minimum Zones (OMZ) linked to human induced climate change (Keeling et al., 2010; Gilly et al., 2013; Howes et al., 2015; Praetorius et al., 2015; Levin, 2018). The Eastern Tropical North Pacific (ETNP) hosts the largest OMZ in the world, and its economic importance for the coastal regions of North and South America is indisputable (Levin, 2018). Numerous *in-situ* measurements during recurring oceanographic campaigns (e.g., CalCOFI, IMECOCAL; Lynn and Simpson, 1987; Bograd et al., 2003; Durazo-Arvizu and Gaxiola-Castro, 2010) revealed declining O_2 trends during the last few decades (Bograd et al., 2003, 2008; Lavín et al., 2013; Breitburg et al., 2018; Levin, 2018). It is important to note that some of the decreasing patterns could be biased by improvements in O_2 measurement technologies that have decreased minimum detection thresholds. Despite this caveat, high-resolution reconstructions of changes in dissolved oxygen in the ETNP OMZ over the past century yield contrasting observations, with warming and increasing extent of anoxia (<0.1 mL/L O_2) not always correlated (Choumiline, 2011; Deutsch et al., 2014; Tems et al., 2016; Fu et al., 2018; Ontiveros-Cuadras et al., 2019). Ongoing discussions about the causes of OMZ intensification over the past decades typically invoke decreased O_2 solubility due to warming of the upper ocean, increased stratification slowing ventilation (Oschlies et al., 2008; Shaffer et al., 2009; Moffitt et al., 2015; Praetorius et al., 2015; Fu et al., 2018), and the strong effect of enhanced marine productivity on the formation of settling organic matter that undergoes decay and consumes more O_2 during remineralization (Wright et al., 2012; Levin, 2018). The latter relationship is the main mechanism by which some OMZ basins in the Eastern Pacific become anoxic (Moffitt et al., 2015; Breitburg et al., 2018; Levin, 2018). However, what causes increases in primary productivity is still debated, with initial results pointing to a complex interaction of factors involving increased upwelling rates and terrigenous discharge—both of which can provide the necessary nutrients for proliferation of primary producers (Howes et al., 2015).

Because the first analytical measurements of dissolved oxygen in seawater started in the late 1800s (Carpenter, 1965), data are not available for preceding portions of the nineteenth century. Nevertheless, multiple applications of well-established paleoceanographic proxies allow us to infer changes in earlier productivity and oxygenation by reconstructing past conditions preserved in the elemental composition of marine sedimentary records emphasizing organic carbon (C_{org}), Ba, Cd, Mo, Mn, Ni, U, and V (Calvert and Pedersen, 1993; Helz et al., 1996; Morford and Emerson, 1999; Zheng et al., 2000; Lyons and Severmann, 2006; Tribovillard et al., 2006; Algeo and Rowe, 2012; Schoepfer et al., 2015). Multiple lines of proxy evidence show that major oxygenation shifts in the ETNP are coupled to glacial-interglacial cycling, often leading to a decrease in dissolved O_2 concentrations in North Pacific Intermediate and North Pacific Deep waters during glacial stages (e.g., Last Glacial Maximum) as well as cold Dansgaard-Oeschger and/or Heinrich-like events (e.g., the Younger Dryas) (Ganeshram and Pedersen, 1998; Hendy and Kennett, 2000; Nameroff et al., 2004; Hendy and Pedersen, 2006; Tetard et al., 2017). Paleoceanographic changes are not only observed in sediment core records at OMZ-depths (400–1,000 m) but also in sediments collected at greater depths of the Pacific and shallower waters of the glacial Southern Ocean, which confirms the likelihood of widespread impacts on oxygenation far beyond intra-OMZ variability (Lu et al., 2016; Hoogakker et al., 2018). Important fluctuations of the upper OMZ also occurred. Rather than the traditional view of these fluctuations as lesser responses to minor climate perturbations, they may have dominated certain regions such as the ETNP. The Pacific Decadal Oscillation (PDO)—detected as decadal cyclic changes in climatic regime from warm to cold and vice versa—is one of these atmospheric effects with strong oceanographic implications (Mantua and Hare, 2002). The North Pacific Gyre Oscillation (NPGO) manifests in decadal fluctuations of nutrients, chlorophyll, and consequentially primary productivity that very often go hand to hand with atmospheric PDO changes in the Pacific (Di Lorenzo et al., 2008). Despite the similarities between the PDO and NPGO, they do not always co-vary.

High-resolution variability in paleoceanographic records, previously categorized by the scientific community as regional background noise, is now elucidating decadal- and centennial-scale OMZ fluctuations (Dean et al., 2004; Barron and Bukry, 2007; Choumiline, 2011; Deutsch et al., 2014; Tems et al., 2015, 2016). In the ETNP, cold PDO and/or NPGO phases cause intense upwelling off the western mainland of North America and lead to enhanced productivity, denitrification, and extreme water column anoxia (Di Lorenzo et al., 2008). However, numerous reports of marine sedimentary records in the literature typically lack the highly resolved age models needed to study decadal phenomena, which coupled with the absence of published multi-proxy records for denitrification ($\delta^{15}N$) and water column redox (Cd, Mn, V, Mo, U) make ETNP-wide redox reconstructions challenging (Moffitt et al., 2015; Borreggine et al., 2017). The importance of reconstructing OMZ reoxygenation and deoxygenation events and mechanistically explaining their climatic causes is essential in light of current and potential future responses of the ocean to modern global warming. These efforts encounter further challenges as redox-sensitive data can be compromised when sediment cores from anoxic settings are not carefully sampled or stored with adequate care in core repositories (Zheng et al., 2000; McManus et al., 2006; Scholz et al., 2011; Costa et al., 2018).

Here we reconstruct changes in the ETNP OMZ based on sediment cores collected at various depths in the Gulf of California. To achieve an ETNP-wide reconstruction, we integrate our multiproxy record of paleoproductivity and paleoredox with published sediment cores from the region. Further, to avoid misinterpreting local variability as global patterns, we apply geostatistical and numerical approaches to existing datasets to unmix local from larger-scale controls.

Strengths and Weaknesses of Geochemical Proxies as Applied to Oxygen Minimum Zone Reconstructions

In this section we provide background details for productivity and redox proxies as archived in marine sediments and as applied to OMZ reconstructions.

Productivity Proxies (C_{org}, Ba_{excess}, Ni)

Organic carbon (C_{org}) has long been used as a proxy for exported organic matter because of its analytical simplicity and wide range of applications (Schoepfer et al., 2015). While C_{org} could directly represent superficial primary productivity, this possibility is likely confounded by multiple controls on remineralization and burial that are tightly related to reactivity of organic matter, bioturbation, and oxygen availability (Calvert et al., 1996; Burdige, 2007; Bianchi et al., 2016).

Barite, Ba/Al, and excess barium (Ba_{excess}) have been used widely as productivity proxies (Dymond et al., 1992; Eagle et al., 2003; Anderson and Winckler, 2005; Schoepfer et al., 2015), although barite and Ba_{excess} relationships with productivity may be complicated by post-burial reprecipitation (McManus et al., 1998; Riedinger et al., 2006; Schoepfer et al., 2015). In some well-oxygenated marine settings, sedimentary Ba_{excess} corresponds well to changes in productivity established by other proxies (e.g., Ni, P, and biogenic silica) (Schoepfer et al., 2015). However, post-depositional diagenetic remobilization of Ba has been found both in regions with transient anoxia and where bottom waters are well-oxygenated (McManus et al., 1998; Riedinger et al., 2006; Schoepfer et al., 2015). Sedimentary records of Ba_{excess} can be further compromised over glacial-interglacial cycles when significant reoxygenation can cause redissolution and reprecipitation of barite along reaction fronts (McManus et al., 1998; Riedinger et al., 2006; Schoepfer et al., 2015).

Nickel is actively involved in biological cycling related to diatom export (Dupont et al., 2010; Twining et al., 2012). Dissolved Ni is removed from the water column by organic matter and supplied to the bottom sediments through particle settling (Böning et al., 2015). In sediments, Ni is the best-known analog for fresh organic matter because it mirrors the input of chlorins—one of the degradation products of chlorophyll (Böning et al., 2015). An advantage of Ni over other biologically active trace elements is its detachment from Mn and S cycling, compared to Cd and Zn, which more readily form insoluble sulfides (Morse and Luther, 1999; Böning et al., 2015). Potential complications for Ni as a productivity proxy include its elevated concentration in the detrital fraction (Wedepohl, 1995) and the possibility of anthropogenic contribution of Ni to marine sediments (Reck et al., 2008).

Redox Proxies (Mo, Cd, V, U)

Molybdenum enrichment processes are linked with incorporation into pyrite and associations with organic matter, which often require abundant hydrogen sulfide (Calvert and Pedersen, 1993; Tribovillard et al., 2008; Chappaz et al., 2014; Scholz et al., 2017). An important pathway for Mo enrichment is the transformation of molybdate to thiomolybdates ($MoO_xS^{2-}_{4-x}$, where $x = 0 \sim 4$), which are highly particle reactive (Helz et al., 1996; Erickson and Helz, 2000; Scholz et al., 2017). Additionally, Mo can be scavenged by Fe-Mo-S clusters (Helz et al., 2011) or adsorbed onto sulfide-rich organic matter (Helz et al., 1996). Molybdenum enrichments can occur diagenetically (within the sediments), in the water column, or in some cases near the sediment-water interface, which was reported for OMZs (Zheng et al., 2000). While widely used as an indicator of past anoxic and euxinic (anoxic and sulfidic) conditions, several complications have been reported for this proxy (Morford and Emerson, 1999; Chappaz et al., 2014), including localized Mo enriched in turbidites despite fully oxygenated water column conditions (McKay and Pedersen, 2014) and uptake exclusively within the sediments when significant amounts of sulfide are present solely in pore waters (Zheng et al., 2000; Scholz et al., 2017; Hardisty et al., 2018)—although these enrichments tend to fall below those typical of euxinic settings (e.g., Scott and Lyons, 2012).

Cadmium is a biologically active trace element supplied to marine sediments in association with organic matter (Morford and Emerson, 1999). It has been used as a proxy for strongly reducing waters (Calvert and Pedersen, 1993; Tribovillard et al., 2006). Cadmium can be precipitated in the presence of H_2S, which makes it a particularly good indicator of euxinia (Morse and Luther, 1999).

Vanadium is present in well-oxygenated seawater in its V(+5) form, usually as $H_2VO_4^-$, which is reduced to V(+4) as VO^{2+} under oxygen-deficient conditions (Calvert and Pedersen, 1993; Morford and Emerson, 1999). This V(+4) form is more effectively scavenged and can be adsorbed to Fe-(oxyhydr)oxides, which is one of its removal mechanisms from seawater (Bauer et al., 2017; Ho et al., 2018). Over sub-millennial and glacial-interglacial timescales, V is potentially one of the most reliable redox proxies, tightly following changes in oxygenation (Nameroff et al., 2004; Costa et al., 2018). The contribution of non-lithogenic V through particulate settling has not been fully constrained; however, slight enrichments in suspended and settling matter have been found (Rodríguez-Castañeda, 2008; Hakspiel-Segura et al., 2016; Bauer et al., 2017; Ho et al., 2018; Conte et al., 2019).

Uranium is widely used as paleoredox proxy; however, the pathways of its sedimentary enrichment are still not fully understood. Uranium is present in seawater in the dissolved U(+6) form as uranyl carbonate complexes $(UO_2)^{2+}$ that are reduced under anoxic conditions to the insoluble U(+4) form by inorganic and microbially mediated processes (Ku et al., 1977; Klinkhammer and Palmer, 1991; Dunk et al., 2002) resulting in the formation of solid particles. Uranium can also be adsorbed to organic matter and to Fe- and Mn-(oxyhydr)oxides (Anderson et al., 1989). While increases in particulate U are thought to mostly occur diagenetically in sediment pore waters underlying strongly anoxic and sulfidic (euxinic) waters (Klinkhammer and Palmer, 1991), some particulate non-lithogenic U can form very slowly in the water column (Zheng et al., 2002; Holmden et al., 2015). The extent to which non-lithogenic U can be enriched in marine particles is not well-established and may be more common in highly productive OMZ-type settings than previously thought. We propose an updated model for the behavior of U in OMZs, which will be discussed further in the paper.

METHODS

Depositional Setting

The Gulf of California (GC) is located within the ETNP OMZ and is well-connected to the Eastern Pacific through its southern entrance (Lavín et al., 2013). Circulation is not known to be limited in most GC basins, including Guaymas, Pescadero, and La Paz. Alfonso Basin is the only partially restricted setting in the GC, with a bathymetric sill extending today to a depth of 250 m (Nava-Sánchez et al., 2001). The sill restricts the incursion of North Pacific Intermediate Water (NPIW) and North Pacific Deep Water (NPDW) (**Figures 1A,B**). Primary productivity is higher on the eastern side of the GC because it is nourished by nutrients upwelled predominantly during dry and cold seasons with strong northwesterly winds (Lavín et al., 2013; Silverberg et al., 2014). Mesoscale eddies together with wind-driven coastal upwelling (primarily along the mainland margin during winter) promote primary productivity in the region (Badan-Dangon et al., 1991; Trasviña-Castro et al., 2003; Deutsch et al., 2014). A strong east-to-west gradient persists from autumn through spring (Lavín et al., 2013), which results in organic material produced in the upwelling system on the eastern margin being deposited as biogenic remains on the west side of the basin.

Particularly in Alfonso Basin, productivity is regulated by cyclonic flow that produces water divergence—transporting nutrients from the subsurface waters (>60 m) into the photic zone. This cyclonic gyre is semi-permanent and has been linked by past researchers to the increase in productivity (Monreal-Gómez et al., 2001; Coria-Monter et al., 2014). Satellite and *in-situ* measurements of Net Primary Productivity (NPP) in Alfonso Basin range from 0.5 to 3.5 gC $m^{-2}d^{-1}$ over the last decade and show an inverse correlation with surface temperature. Mesoscale transport processes explain why the Gulf of California, like most of the Eastern Pacific, is influenced by ENSO, PDO, and/or NPGO phenomena (Mantua and Hare, 2002; Di Lorenzo et al., 2008). During cold La Niña years, the Walker Circulation triggers upwelling and productivity in the Eastern Pacific—weakening the typical upper ocean stratification that dominates during normal and El Niño years (Thunell, 1998; McPhaden, 2004; Bustos-Serrano and Castro-Valdez, 2006). Atmospheric circulation is also an important mechanism that seems to control upwelling in the Gulf of California and is dictated by the North American Monsoon (NAM) (Metcalfe et al., 2015). When the North Pacific High (NPH) and the Intertropical Convergence Zone (ITCZ) migrate southward, intense upwelling is triggered by northwesterly winds (Schneider et al., 2014; Metcalfe et al., 2015; Staines-Urías et al., 2015). Longer-scale variability of similar nature is attributed to cold PDO and sometimes NPGO phases, but the atmospheric and oceanographic links are still unclear.

The water columns of Alfonso and La Paz basins show a pronounced decrease in oxygen with depth, reaching values below 0.1 ml/L O_2 (**Figure 1B**). To avoid the imprecise term "suboxic" (Canfield and Thamdrup, 2009), we classify the water column using the threshold O_2 values from Hofmann et al. (2011) and Moffitt et al. (2015), which yielded the following categories: oxic ([bottom O_2] > 1.5 mL/L), moderately hypoxic (0.5 mL/L < [bottom O_2] < 1.5 mL/L), severely hypoxic (0.1 mL/L < [bottom O_2] < 0.5 mL/L), and anoxic ([bottom O_2] < 0.1 mL/L). According to this classification, both Alfonso and La Paz basins fall within the "anoxic" category (**Figure 1B**).

Due to their locations near the open Pacific Ocean, the southern basins are a sensitive recorder of regional variation in the GC and the larger-scale climate circulation of the ETNP,

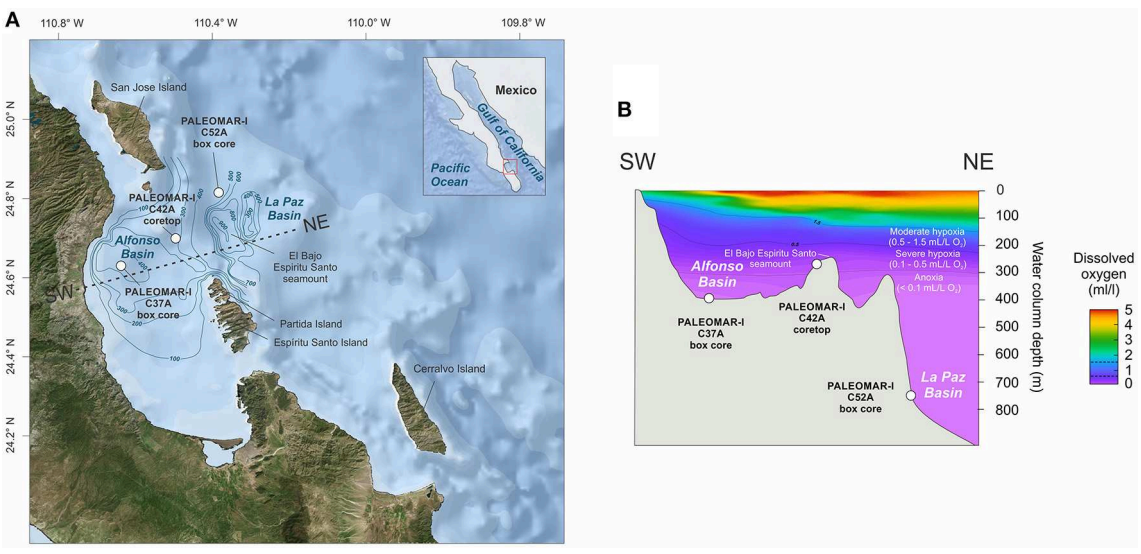

FIGURE 1 | (A) Location of the studied marine setting in the eastern margin of the Gulf of California including the anoxic Alfonso and La Paz basins. The line between SW and NE represents a cross section shown in **(B)**. **(B)** Cross section from the Baja California peninsula (SW) to the Gulf of California (NE) representing the basin morphology and dissolved oxygen (mL/L) concentration spanning Alfonso and La Paz basins.

capturing changes in productivity and redox conditions useful for tracking fluctuations of the OMZ (Dean et al., 2004; Barron and Bukry, 2007; Dean, 2007; Pérez-Cruz, 2013; Deutsch et al., 2014; Tems et al., 2015, 2016; Ontiveros-Cuadras et al., 2019).

Sampling

Laminated sediments from marine basins of the Gulf of California with varying degrees of deoxygenation were collected using a Reineck box corer during the PALEOMAR-I campaign in November 2014 aboard R/V "El Puma" owned by UNAM, Mexico (**Figures 1A,B**). The 50 cm sediment core PALEOMAR-I C37A was collected at 408 m water depth in the silled Alfonso Basin. Core PALEOMAR-I C52A represents a sedimentary sequence of the upper 24 cm of La Paz Basin at 785 m depth. Both cores show a clear, continuously laminated fabric. Additionally, the core top of PALEOMAR-I C42A was sampled from the shallower part of Alfonso Basin (265 m). This core did not show clear laminations. Poor recovery during retrieval limited its utility for paleoceanographic reconstructions. From this point forward, we will refer to these cores as C37A, C42A, and C52A.

Each core was extruded and subsampled immediately after collection, and pore waters were extracted from each section in a glove bag under N_2 atmosphere using CSS 5 cm Rhizon samplers attached to plastic syringes (Lyons and Berner, 1992; Dickens et al., 2007; Raiswell and Canfield, 2012; Riedinger et al., 2017). Each core segment yielded approximately 8 mL of pore waters, which were filtered at 0.2 μm, acidified with trace grade pure nitric acid (10 μL of acid per each 1 mL of sample), and stored at 4°C (Riedinger et al., 2014, 2017). Prior to analysis, solid-phase samples were dried, weighed, and homogenized.

Age Model

We use the present-day sedimentation rates previously reported in the literature for Alfonso Basin to generate the age model for the studied core C37A. Due to the extended timespan of the sedimentary section, the composite age model is based on ^{210}Pb and ^{14}C dating methods (**Figure 2**; **Table 1**). For this purpose, we selected box core DIPAL-II C44 (Choumiline, 2011) and gravity core DIPAL-III T43 (Pérez-Cruz, 2013). The dated materials were collected at the same location within the basin and span a matching sedimentary package (**Supplementary Figure 1**). High-resolution sections of the uppermost 10 cm (subsampled at <3 mm) of core DIPAL-II C44 were analyzed for ^{210}Pb at Flett Research Ltd. Laboratory (Winnipeg, Canada) (**Supplementary Figure 2**). The mean sedimentation rate for the upper 10 cm is 0.61 mm/year in Alfonso Basin (Choumiline et al., 2010; Choumiline, 2011). The sedimentary section of the gravity core DIPAL-III T43 corresponding to the lower part of C37 (between 15 and 50 cm) was dated using the ^{14}C method (Pérez-Cruz, 2013). Measurements were performed in benthic foraminifera *Bolivina subadvena* by accelerator mass spectrometry at Beta Analytic (Pérez-Cruz, 2013) and the radiocarbon values were calibrated using the Marine13 curve (Reimer et al., 2013). This part of the core yielded a mean sedimentation rate of 0.8 mm/year (Pérez-Cruz, 2013). In our age model for C37A we extrapolate the sedimentation rate of 0.61 mm/year to the uppermost core section (0–15 cm) and use 0.8 mm/year for the lowermost segment (15–50 cm) as shown in **Table 1** and **Supplementary Figure 1**. To demonstrate that the core sections are equivalent, we compared the total carbon (C_{tot}), calcium carbonate ($CaCO_3$) and Ca changes through time for cores C37A (this study), DIPAL-II C44 (Choumiline et al., 2010, 2017; Choumiline, 2011) and DIPAL-III T43 (Pérez-Cruz, 2013). The curves covary, confirming the consistency between age models for different core records (**Supplementary Figure 1**). Additionally, selected dry splits of sediment core C37A (Alfonso Basin) were dated using the ^{210}Pb and ^{137}Cs methods via gamma-ray spectroscopy in the Gray Lab (University of California, Riverside). The subsampling resolution of this core was too coarse to produce a robust age model using these methods. Despite known difficulties with radiocesium detection in the region (Ruiz-Fernández et al., 2009) it was still possible to find slightly elevated ^{137}Cs activity values around the 2–4 cm core horizon, very likely corresponding to the mid-1960s peak of nuclear testing in the atmosphere (Foster and Walling, 1994). The resulting linear sedimentation rate using the radiocesium method for core C37A was roughly 0.6 mm/year. The sedimentation rates determined for Alfonso Basin from different age models are consistent. Further, the age model for Alfonso Basin shows that the deepest sample of core C37A at 500 mm extends to 1300 AD (also called the Common Era or CE).

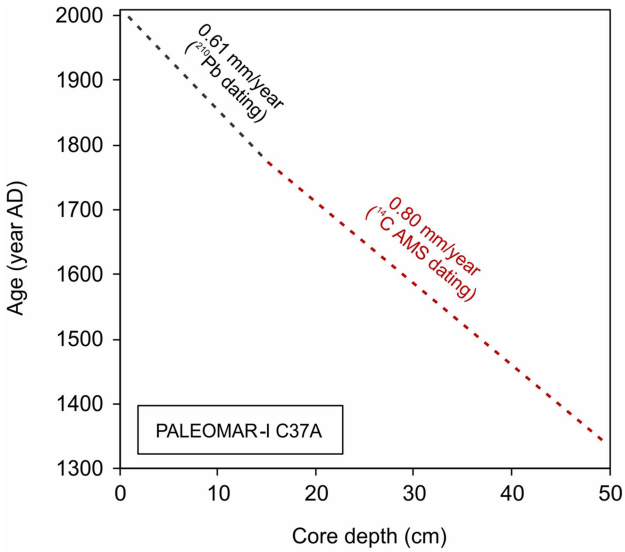

FIGURE 2 | Age model of core PALEOMAR-I C37A from Alfonso Basin.

Analytical Approaches

Total carbon (C_{tot}) and total inorganic carbon (C_{inorg}) in dry sediment subsamples were measured on an ELTRA CS-500. The CO_2 produced during subsample combustion at 1350°C (C_{tot}) or acidification with 20% HCl (C_{inorg}) was quantified with an infrared analyzer. The organic carbon (C_{org}) fraction was calculated by numerical difference: $C_{org} = C_{tot} - C_{inorg}$.

TABLE 1 | Age model for core C37A, constructed by a combination of extrapolated average sedimentation rates produced using the ^{210}Pb method on core DIPAL-II C44 (Choumiline et al., 2010; Choumiline, 2011) and acceleration mass spectrometry ^{14}C on core DIPAL-III T43 (Pérez-Cruz, 2013).

Depth range (cm)	Depth midpoint (cm)	Age in years AD	Dated material and method used	Corresponding sedimentation rate for C37A
0–2	1	1999	^{210}Pb dating of the uppermost 10 cm of bulk sediment from box core DIPAL-II C44	0.61 mm/year
2–4	3	1967		
4–6	5	1934		
6–8	7	1902		
8–10	9	1870		
10–12	11	1837		
12–14	13	1805		
14–16	15	1772		
16–18	17	1747	AMS ^{14}C dating with *Bolivina subadvena* in the following horizons of the gravity core DIPAL-III T43: Code: BETA320950 Interval: 17–18 cm Age: 1572 year AD Code: BETA322689 Interval: 41–43 cm Age: 1240 year AD	0.8 mm/year
18–20	19	1722		
20–22	21	1697		
22–24	23	1672		
24–26	25	1647		
26–28	27	1622		
28–30	29	1597		
30–32	31	1572		
32–34	33	1547		
34–36	35	1522		
36–38	37	1497		
38–40	39	1472		
40–42	41	1447		
42–44	43	1422		
44–46	45	1397		
46–48	47	1372		
48–50	49	1347		

The cores were collected at the same location in Alfonso Basin.

Prior to sample digestion, 100 mg splits were ashed in ceramic vessels for 8 h at 550°C in a high temperature oven. A two-step digestion procedure involved a mixture of HNO_3 and HF, followed by aqua regia (HCl and HNO_3) and acidification/drying cycles on temperature-controlled hot plates. A very low HF:HNO_3 ratio of 1:8 was employed during the first step to prevent insoluble fluoride formation. Careful evaluation of each sample revealed that no undissolved particles were detected, suggesting complete digestion (Durand et al., 2016). The final digested extracts were diluted in 2% HNO_3 and measured for major and trace elements (Al, Ba, Cd, Fe, Ni, Mo, V, U) on an Agilent 7900 Inductively Coupled Mass Spectrometer (ICP-MS).

Pore waters were analyzed for elemental composition on an Agilent 7900 ICP-MS, emphasizing dissolved Fe, Mn, and selected trace elements. The quality of our data was assessed by analyzing duplicates and certified reference materials USGS SGR-1B, USGS SDO-1, NIST 2702, AR4007, and AR4024. Analytical precision was always below 3%. Recoveries of measured sample relative to certified standard value ranged between 96 and 105%.

Numerical and Statistical Approaches

The productivity and redox proxy approaches used here rely heavily on authigenic enrichment of trace elements relative to detrital inputs through uptake in marine sediments during diagenesis and via scavenging from seawater during primary production and during particle settling. To assess enrichments relative to detrital contributions, each element was normalized to Al as a reliable crustal proxy (Wedepohl, 1995). Further, to account for dilution by $CaCO_3$, which can cause apparent elemental variability, we recalculated the data on a carbonate free basis (CFB) by dividing each concentration by the fraction of non-carbonate material. Elemental ratios were also calculated for selected elements. The authigenic uranium (U_{auth}) fraction was calculated as $U_{auth} = U_{total} - (Th/3)$ (Wignall and Myers, 1988).

Due to limited sample sizes, it was not possible to perform the barite sequential leach sometimes used as a productivity proxy in well-oxygenated marine settings (Dymond et al., 1992; Eagle et al., 2003; Schoepfer et al., 2015). Instead, we used our measurements for total Ba and Al to determine excess barium (Ba_{excess}) as the closest calculated alternative (Eagle et al., 2003; Anderson and Winckler, 2005): $Ba_{excess} = Ba_{total} - (Ba_{terrigenous}/Al_{terrigenous}) \times Al_{total}$. We assumed a $Ba_{terrigenous}/Al_{terrigenous}$ ratio of 0.0045 as suggested by Dymond et al. (1992) and Eagle et al. (2003).

In order to define proxy associations, we applied a multivariate statistical approach for the proxy datasets from Alfonso and La

Paz basins. Specifically, we performed R-mode Factor Analysis with Varimax rotation using the software STATISTICA by StatSoft. The analysis included the following variables: C_{org}, Ba_{excess}, Ni, U, U_{auth}, Cd, Mo, and V.

Geostatistical analyses and data extraction techniques were performed using ArcGIS 10.6 software by ESRI. We combined our data with previously published geochemical records obtained in part from the EarthChem SedDB database via the Interdisciplinary Earth Data Alliance (IEDA) repository. Estimated oceanographic data (dissolved O_2 and chlorophyll) were obtained for each core location in GIS and used in our statistical analysis. Global oceanic oxygen data are based on the World Ocean Atlas (2005) and Garcia et al. (2006); surficial chlorophyll estimates from the SeaWIFS satellite sensor were published by OBPG/NASA.

Paleoceanographic Proxies Used in This Study

To interpret past OMZ conditions preserved in marine sediments we used a combination of proxies assuming C_{org} as an indicator for organic carbon burial (Schoepfer et al., 2015); Ba_{excess} (despite the caveats described above) and Ni for export production (Böning et al., 2015; Schoepfer et al., 2015); Cd, Mo, and V for bottom water anoxia (Calvert and Pedersen, 1993; McManus et al., 2006; Tribovillard et al., 2006; Lyons et al., 2009). Due to a strong contribution of U_{auth} via settling particulates (Choumiline et al., 2010; Choumiline, 2011) potentially after its reduction or adsorption to organic matter, this proxy could trace both redox and productivity—as will be explained further in the paper.

While each proxy has distinct biogeochemistry and enrichment pathways, they are all affected by a circular relationship between productivity and redox (Tribovillard et al., 2006; Schoepfer et al., 2015; Bianchi et al., 2016). In transiently anoxic settings high productivity often leads to the development of water column anoxia, which favors organic preservation and reduces the mobility of productivity proxies (Schoepfer et al., 2015). Due to the latter, it is often common to expect a covariance between productivity and redox proxies (Tribovillard et al., 2006; Bianchi et al., 2016). The differences in proxy relationships are often helpful to unravel more specific biogeochemical processes tied to preservation biases, such as organic matter reactivity and post-depositional diagenetic transformations.

RESULTS AND DISCUSSION

Geochemistry of Modern Sediments From the Southwestern Gulf of California at Various OMZ Depths

The chemical compositions of core tops (upper 2 cm) represent the most recent sediments from Alfonso and La Paz basins (**Table 2**). A water depth transect from the 265 to 785 m through the study region revealed that dissolved O_2 values decreased from 0.3 mL/L (uppermost OMZ) to <0.1 mL/L (OMZ core) (**Figure 1B**). Most redox-sensitive elements increase in concentration in the deeper sites C37A and C52A relative to the shallower C42A. For all three sites the elemental concentrations range as follow: C_{org} (2.96–6.41%), Ba_{excess} (175.50–682.77 mg/kg), Ni (26.84–49.06 mg/kg), and Mo (0.75–6.75 mg/kg). In contrast, Cd and U_{auth} are enriched at the shallow, more oxygenated site C42A—reaching 13.17 mg/kg for Cd and 5.34 mg/kg for U_{auth}, compared to 7.24 mg/kg for U_{auth} in C52A and 2.48 mg/kg for Cd in C37A (**Table 2**). Although circulation in Alfonso Basin is slightly restricted due to the presence of a bathymetric sill at 250 m depth, restriction was apparently not severe enough to limit trace element enrichments in La Paz Basin relative to the more open ocean. We calculated U_{auth} values for the CFB fraction as 6.43 mg/kg in C42A, 7.26 mg/kg in C37A, and 7.24 mg/kg in C52A. Carbonate-free values were also calculated for the other proxies but did not produce major differences relative to either total or Al-normalized data (see **Supplementary Material**).

Bioturbation and Post-sampling Effects as Complicating Overprints on Primary Proxy Records

Visual observation confirmed that the sediments from Alfonso (C37A) and La Paz (C52A) basins are clearly laminated, with no evidence for bioturbation, which could obscure primary sedimentary features. Pore water profiles were used to establish the chemical zonation of electron acceptors at the time of sample collection (Canfield and Thamdrup, 2009). It is essential to evaluate diagenetic conditions before applying paleoreconstruction techniques because many proxies can be overprinted during diagenesis, obscuring records of primary water column conditions (Calvert and Pedersen, 1993; Tribovillard et al., 2006). Further, pore water data shed light on bioturbational overprints via burrow irrigation and sediment homogenization and disturbance during sediment collection and processing. At both Alfonso Basin (C37A) and La Paz Basin (C52A), concentrations of dissolved Fe (Fe_{diss}) and dissolved Mn (Mn_{diss}) show downcore decreases (**Figure 3**). The observed trend for Fe_{diss} is similar to those from analogous OMZ settings of the Gulf of California (Guaymas Basin), offshore California (San Pedro and Catalina basins), and the Peruvian margin—that is, pore water Fe_{diss} reaches its maximum a few centimeters below the sediment-water interface and gradually declines down core (Brumsack and Gieskes, 1983; McManus et al., 1997; Canfield and Thamdrup, 2009; Scholz et al., 2011; Scholz, 2018). Our recovery of expected trends suggests that proper techniques for sediment collection and preservation were employed in this study.

Downcore Records of Changing Productivity and Redox

Here we present downcore variations of productivity and redox proxies recorded in our sedimentary material from the ETNP (**Figure 1**). We found almost no difference between the trends for absolute concentrations and corrected data, so we present only absolute values. However, Al-normalized and CFB data are presented in **Supplementary Materials** for the interested reader.

TABLE 2 | Composition of modern sedimentary material represented by core tops from different OMZ depths in Alfonso (C42A and C37A) and La Paz basin (C52A).

Marine basin	Water column depth	Redox condition and bottom dissolved O_2 (mL/L)	Core top proxy data							
			Productivity/nutrients			Redox and/or Productivity		Redox		
			C_{org} (%)	Ba_{excess} (mg/kg)	Ni (mg/kg)	U (mg/kg)	U_{auth} (mg/kg)	Cd (mg/kg)	Mo (mg/kg)	V (mg/kg)
Alfonso Basin (C42A)	Uppermost OMZ (265 m)	Severe hypoxia (~0.3)	2.96	175.70	26.84	14.31	13.17	5.34	0.75	26.05
Alfonso Basin (C37A)	Upper OMZ (408 m)	Anoxia (<0.1)	6.01	406.37	40.25	9.85	8.14	2.48	6.34	124.67
La Paz Basin (C52A)	Middle OMZ (785 m)	Anoxia (<0.1)	6.41	682.77	49.06	8.84	7.24	2.60	6.75	75.048

The dissolved oxygen values presented here were obtained during the PALEOMAR-I oceanographic campaign.

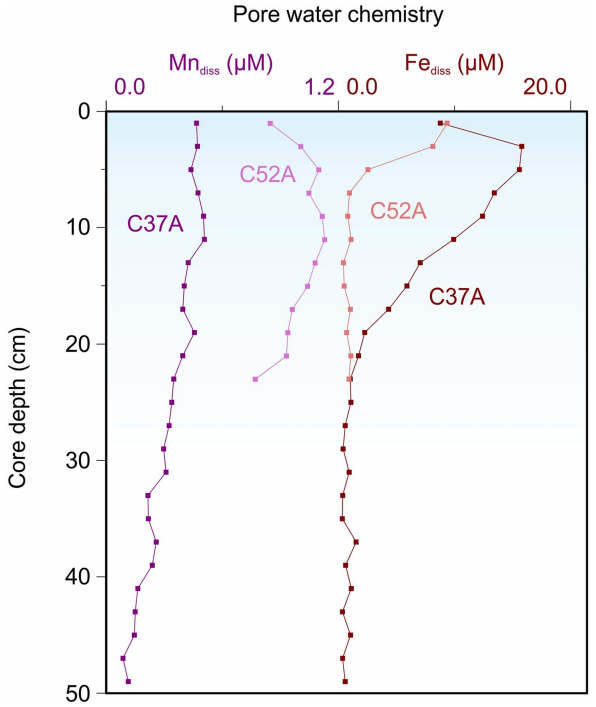

FIGURE 3 | Pore water chemical profiles in cores PALEOMAR-I C37A from Alfonso Basin and PALEOMAR-I C52A from La Paz Basin (Data: Choumiline et al., 2017).

Geochemistry of Sediments From the Upper OMZ in Alfonso Basin

Elemental profiles for C37A from Alfonso Basin are shown in **Table 3**. Data for C_{org} are in good agreement with Ba_{excess}, Ni, U_{auth}, and V as proxies for past oxygenation and/or primary productivity. Values range from 5.60 to 6.76% for C_{org}, 372.22–491.54 mg/kg for Ba_{excess}, 40.25–51.61 mg/kg for Ni, 9.23–14.15 mg/kg for U, 7.71–12.48 mg/kg for U_{auth}, and 115.81–172.40 mg/kg for V. Trends for Cd and Mo differ slightly from those for the other proxies and range from 2.48 to 7.04 mg/kg and 6.34–15.16 mg/kg, respectively (**Figure 4**).

Geochemistry of Sediment From the Mid-Depth OMZ of La Paz Basin

Downcore concentrations for the productivity and redox proxies in core C52A from La Paz Basin are presented in **Table 3**. Despite differences in core length and depositional setting, the records for C_{org}, Ni, U_{auth}, V, and Cd in C52A are similar to those from core C37A (**Supplementary Figure 3**). These elements range as follow: 6.51–7.12% for C_{org}, 47.34–53.25 mg/kg for Ni, 5.97–9.32 mg/kg for U_{auth}, and 74.31–102.80 mg/kg for V. In C52A, Ba_{excess} does not covary with Ni and U_{auth}, pointing to its potential remobilization during diagenesis. Excess-Ba concentrations range from 419.76 to 763.24 mg/kg but are mostly uniform over the length of the core—averaging 670.89 mg/kg. The trends for Cd and Mo decrease down core in the upper 6 cm of laminated sediments (**Supplementary Figure 3**; **Table 3**) and range from 2.38 to 2.97 and 4.90 to 12.55 mg/kg, respectively.

The lowest concentrations for most proxy data are found in the upper 5 cm, at ~14 cm, and below 23 cm—perhaps corresponding to well-ventilated past conditions. The highest values, indicating enhanced anoxia, were registered around 20 cm for all proxies, while the second anoxic horizon close to 10 cm was only captured by C_{org}, Ni, U_{auth}, V, and more subtly by Cd and Mo.

Variability of the Upper OMZ in Alfonso Basin Over the Last 700 Years

We present down-core elemental concentrations in the context of the age model described earlier in the paper. Due to multiple challenges during our efforts to date cores C42A and C52A, such as poor recovery, only core C37A from Alfonso Basin produced a robust age model. Core C37 will be emphasized for paleoceanographic reconstructions for the remainder of the report.

The geochemical profiles for C37A from Alfonso Basin record changes in the upper OMZ boundary dating back to 1300 AD

TABLE 3 | Elemental composition of the solid phase from cores C37A, C42A, and C52A collected during PALEOMAR-I expedition to the Gulf of California.

Core	Depth range (cm)	C_{org} (%)	Al (%)	Fe (%)	Ba (mg/kg)	Cd (mg/kg)	Mo (mg/kg)	Ni (mg/kg)	U (mg/kg)	V (mg/kg)	Ba_{excess} (mg/kg)	U_{auth} (mg/kg)
C37A (Alfonso Basin)	0–2	6.01	4.9	2.5	406.4	2.5	6.3	40.3	9.9	124.7	406.4	8.1
	2–4	6.18	5.1	2.6	419.3	2.6	6.4	41.9	10.1	115.8	419.2	8.3
	4–6	6.13	5.1	2.6	440.0	3.4	9.3	41.3	9.7	133.4	439.9	7.9
	6–8	6.42	5.0	2.5	454.3	3.4	10.2	44.2	10.1	137.1	454.3	8.4
	8–10		4.7	2.3	439.9	3.5	9.9	44.0	11.3	139.6	439.9	9.6
	10–12	6.39	4.8	2.3	430.4	3.8	9.0	45.3	13.0	150.6	430.4	11.3
	12–14	6.65	5.0	2.5	476.6	4.1	9.5	47.9	13.5	156.8	476.6	11.7
	14–16	6.66	5.3	2.6	479.3	3.8	9.2	48.3	12.4	141.8	479.3	10.6
	16–18	6.76	4.3	2.1	416.0	3.8	9.2	41.2	9.2	117.0	415.9	7.7
	18–20	6.26	4.9	2.4	458.0	3.9	8.7	45.8	11.6	149.7	458.0	9.9
	22–24	6.43	5.0	2.6	480.5	4.8	12.7	49.5	10.9	167.1	480.5	9.1
	24–26	6.05	4.8	2.4	458.3	4.6	11.2	46.3	12.9	157.0	458.3	11.2
	26–28	6.56	4.9	2.4	459.1	4.7	8.2	50.4	12.4	154.9	459.1	10.7
	28–30	6.25	5.0	2.5	461.5	5.4	13.4	46.9	10.8	160.0	461.4	9.0
	30–32	5.93	5.0	2.5	485.5	5.0	13.0	46.4	11.2	164.2	485.5	9.5
	32–34	5.89	4.9	2.5	468.1	4.8	11.2	47.7	11.8	160.6	468.1	10.1
	34–36	6.53	5.1	2.6	488.8	5.3	12.9	51.6	11.9	172.4	488.7	10.1
	36–38	6.18	5.1	2.5	470.3	4.3	10.7	48.9	11.1	167.5	470.3	9.4
	38–40	6.04	5.1	2.5	441.8	3.7	9.3	46.1	11.3	146.4	441.8	9.5
	40–42	6.30	5.1	2.5	472.7	4.7	13.5	48.9	10.1	161.0	472.7	8.3
	42–44	6.65	4.7	2.4	481.5	7.0	14.2	51.4	14.2	170.8	481.5	12.5
	44–46	5.60	4.6	2.4	372.2	2.9	6.8	42.8	14.0	124.0	372.2	12.3
	46–48	6.62	4.6	2.3	440.1	5.0	13.3	46.3	9.9	148.5	440.1	8.2
	48–50		4.8	2.4	491.6	5.2	15.2	50.0	12.9	165.9	491.5	11.2
C52A (La Paz Basin)	0–2	6.41	4.3	1.8	682.8	2.6	6.7	49.1	8.8	75.0	682.8	7.2
	2–4	6.58	4.3	1.9	681.1	2.4	4.9	49.4	7.5	76.0	681.1	6.0
	4–6	6.55	4.3	1.9	419.8	2.5	9.1	49.0	8.3	76.5	419.8	6.8
	6–8	6.68	4.3	1.9	580.4	2.5	10.7	49.9	8.4	86.8	580.4	6.8
	8–10	7.12	4.6	1.9	763.3	3.0	12.6	52.9	9.7	102.8	763.2	8.1
	10–12	6.61	4.4	1.8	689.6	2.8	11.8	50.7	10.4	93.4	689.5	8.8
	12–14	6.43	4.4	1.9	704.3	2.8	10.6	49.9	9.2	88.4	704.3	7.6
	14–16	6.54	4.6	1.9	723.0	2.8	9.9	51.7	9.6	83.9	722.9	8.0
	16–18	6.40	4.6	1.9	703.2	2.9	9.6	51.1	8.8	80.9	703.2	7.2
	18–20	6.49	4.8	2.0	728.1	2.9	10.3	53.2	11.1	94.7	728.1	9.3
	20–22	6.17	4.3	1.9	661.3	2.7	9.5	47.3	8.6	82.2	661.3	7.0
	22–24	6.10	4.5	2.0	714.1	2.4	10.9	50.2	9.1	74.3	714.1	7.5
C42A	-	2.96	2.3	1.0	175.7	5.3	0.8	26.8	14.3	26.0	175.7	13.2

(**Figure 4**; **Table 3**). Data for C_{org} are in good agreement with Ba_{excess}, Ni, U_{auth}, and V as proxies for past oxygenation and/or primary productivity. Unlike our other proxies, Mo and Cd remain high from 1300 to 1700 AD and then slowly transition toward lower values after 1700 AD. This slight decrease toward the present corresponds to the uppermost 20 cm of the record in the Alfonso Basin. The lowest concentrations for our proxies are generally concurrent with the late 1900s, early 1700s, and late 1300s AD. These times correspond to warm periods of the past millennium as reconstructed by multiple records (IPCC, 2014), including the anthropogenically caused warming trend that started around the beginning of the nineteenth century and extends to present day (**Figure 4**). Lower proxy values indicate decreased primary productivity and correspond to slightly more oxygenated times. In contrast, high proxy values occurred in the early 1800s, late 1600s, early 1500s, and early 1400s, with maxima between roughly 1700 and 1400 AD are likely associated with the prolonged cold period of the Little Ice Age. Higher values usually correspond to increased primary productivity in surface waters and enhanced anoxia.

Multivariate Statistical Associations of Paleoproxies in Alfonso and La Paz Basins

Factor analysis results for the combined geochemical datasets from Alfonso Basin (core C37A) and La Paz Basin (C52A) distinguished three elemental associations between Factor 1

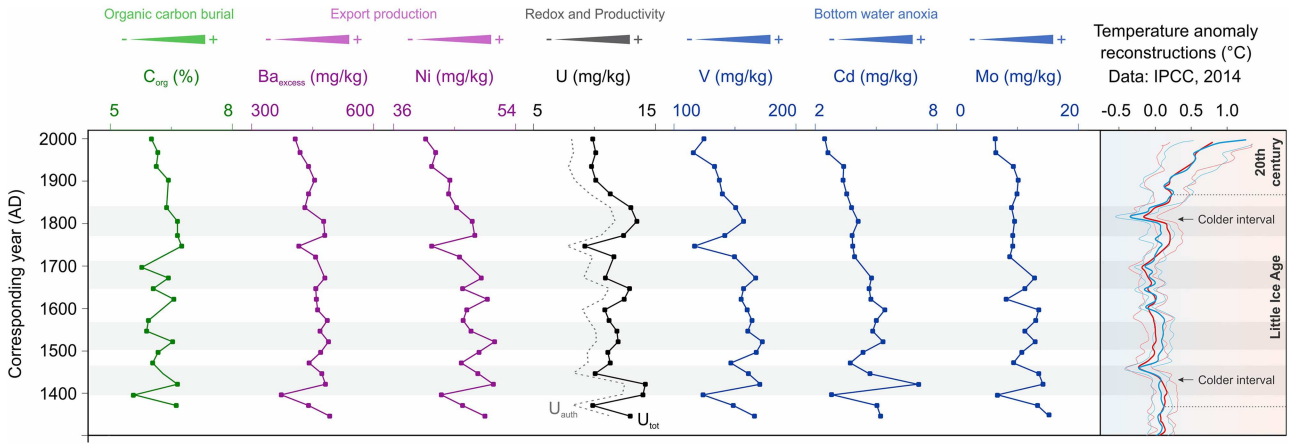

FIGURE 4 | Organic carbon, productivity, and redox proxies in core PALEOMAR-I C37A from Alfonso Basin. Data for temperature anomaly reconstructions of the last millennium taken from IPCC (2014).

TABLE 4 | Factor loadings of the R-mode Factor Analysis with Varimax rotation performed on a combined dataset of cores C37A (Alfonso Basin) and C52A (La Paz Basin).

Proxy	Factor 1	Factor 2
C_{org}	−0.1448	0.6978
Ba_{excess}	−0.5988	0.6615
Ni	−0.0413	0.9013
U	0.8700	−0.1489
U_{auth}	0.8611	−0.1366
V	0.9316	−0.1517
Cd	0.9046	0.1995
Mo	0.5406	0.6226
Explained variance	3.8581	2.2282
Proportion of total variance	48.23%	27.85%

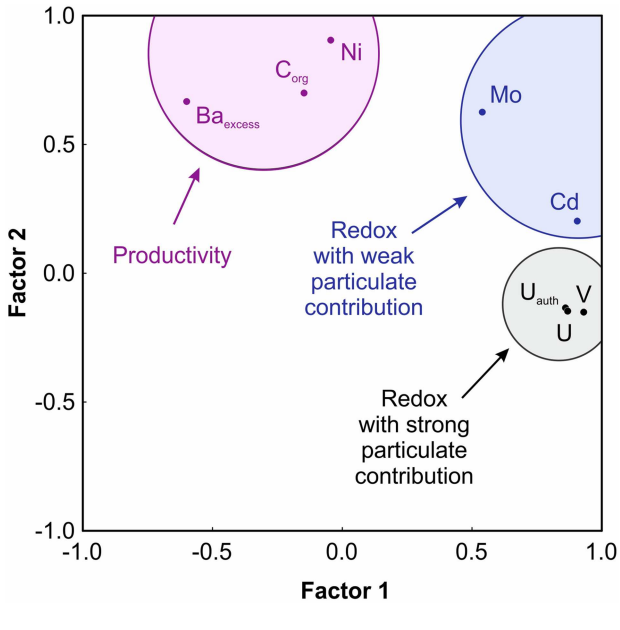

FIGURE 5 | Productivity and redox proxy associations defined by R-mode factor analysis of a combined geochemical dataset from Alfonso Basin (core C37A) and La Paz Basin (C52A).

(48.23% variance) and Factor 2 (27.85% variance) (**Table 4**; **Figure 5**). The "productivity" association is based on C_{org}, Ni and Ba_{excess}–elements related to organic matter production at shallow depths. The "redox with weak particulate contribution" defined by Cd and Mo, which require strongly reducing conditions in bottom waters for strong authigenic enrichments. The "redox with strong particulate contribution" links U, U_{auth}, and V—elements that can be supplied through particulate fluxes in oxygen-deficient water column depths and/or enriched diagenetically either under anoxic bottom waters or at the sediment-water interface.

Comparison of Productivity and Redox Proxies in Core Tops Across Varying OMZ Depths and Productivity Regimes in the ETNP

Here we present a compilation of data from core tops from this and previous studies (**Table 5**; **Figure 6** and **Supplementary Figure 4**). Comparing core tops, most of the cores collected at upper- and mid-OMZ depths have significantly stronger C_{org}, Ba_{excess}, Ni, Mo, and V enrichments compared to shallower cores (e.g., core C42A)—with the latter perhaps representing the fluctuating upper OMZ boundary often exposed to high O_2 levels (**Table 5**). These enrichments correspond to regions where high chlorophyll is reported in the surface waters associated with eastern North Pacific upwelling (**Table 5**; **Figure 6** and **Supplementary Figure 4**) (Badan-Dangon et al., 1991; Trasviña-Castro et al., 2003). The elevated C_{org}, Ba_{excess}, and Ni in these high-chlorophyll regions are likely to indicate enhanced primary productivity in the photic zone but could also reflect strong preservation of refractory organics delivered

from land (Calvert et al., 1996; Burdige, 2007; Bianchi et al., 2016) (**Table 5**). These productive coastal sectors correspond to severe hypoxia/anoxia in which trace element enrichments reach 75.05–149.08 mg/kg for V and 6.75–7.35 mg/kg for Mo in the deepest cores from La Paz and Pescadero basins, respectively (**Table 5**; **Figure 6**). Detrital contributions in such settings are relatively minor (Rodríguez-Castañeda, 2008; Choumiline, 2011). These enrichments are favored by oxygen-deficient conditions in the water column and, in the case of Mo, sulfide accumulation in seawater (Calvert and Pedersen, 1993; Zheng et al., 2000; Tribovillard et al., 2006). The studied core tops from the Eastern Pacific OMZ show Mo values sufficiently high to indicate anoxia but are too low to suggest euxinia (presence of H_2S) (**Table 5**; **Figure 6A**). For comparison, only certain places off the Peruvian margin, where water conditions are extremely reducing even for an OMZ, show Mo values as high as 70 mg/kg (McManus et al., 2006). In contrast, at 265 m depth in the upper portion of the OMZ, core C42A displays low V and Mo values of 26.05 and 0.75 mg/kg, respectively, indicating the presence of some oxygen in the overlying waters and that V and Mo are mostly supplied through detrital inputs.

Uranium is the exception. The U_{auth} concentrations are high in the shallower and more-oxygenated core (C42A), reaching 13.17 mg/kg—with values similar to those of the deeper, anoxic core tops (C37A and C52A). We hypothesize that the added contribution of uranium is through its uptake in settling particles and associated anoxic microenvironments. Under oxic and weakly oxic conditions, dissolved uranium is present in its +6 form but is reduced to the insoluble +4 form once oxygen declines further (moderate hypoxia) or disappears (anoxia). This authigenic U is preserved as the organic-rich marine aggregates settle through the water column, in the absence of U_{auth} reoxidation even in ventilated waters. This exported authigenic uranium is delivered to the sediments—often showing a stronger correlation with C_{org} compared to the relationships between the organic matter and V or Mo (Choumiline, 2011). Evidence for authigenic U enrichments in settling particles was reported by Zheng et al. (2002) in marine basins of the California Margin and also from Alfonso Basin, with particulate U concentrations reaching 40 mg/kg (Choumiline et al., 2010; Choumiline, 2011)—more than an order of magnitude higher than the crustal average of 2.5 mg/kg (Wedepohl, 1995).

Like U_{auth}, V is enriched in sediments from regions of the Pacific where bottom water anoxia is present. Additionally, its concentration in suspended particles also peaks seasonally at depths of 150–250 m in response to intra-annual changes in water column O_2 (Hakspiel-Segura et al., 2016). The contribution of V to the bottom via settling particles is usually lower than the average sedimentary concentration under low O_2 conditions but still within the same order of magnitude (Rodríguez-Castañeda, 2008).

To assess the contribution of authigenic U through settling, we contrast U and Mo sedimentary records published in the literature with ours from the ETNP (Ivanochko and Pedersen, 2004; McManus et al., 2006). Typically, Mo is used as an indicator for water euxinia (Calvert and Pedersen, 1993; Algeo and Lyons, 2006; Algeo and Tribovillard, 2009; Lyons et al., 2009; Algeo and Rowe, 2012; Scott and Lyons, 2012), but most of the enrichments in modern OMZs are likely tied to the presence of sulfide only in pore waters (Scholz et al., 2017; Hardisty et al., 2018). We are not using V because, like U, there could also be important contribution of the redox sensitive element through settling particles, associated to reducing microenvironments (**Table 5**; Choumiline, 2011). We expect good correlation between U and Mo records if both elements are enriched during burial (i.e., diagenetically or at the sediment-water interface; Klinkhammer and Palmer, 1991; Calvert and Pedersen, 1993; Zheng et al., 2002; Algeo and Tribovillard, 2009). A weak correlation is likely to be found for samples where significant amounts of non-lithogenic U are scavenged into particles and settle through the water column. In contrast, Mo uptake is typically limited to the sediments when oxygen is present in the water column. For the previously published data, we estimated bottom O_2 values for each sediment core in a GIS using an interpolated global oxygen database (World Ocean Atlas, 2005; Garcia et al., 2006). This approach allowed us to classify data in two main groups depending on the dominant redox conditions: oxic to moderately hypoxic (0.5 mL/L < [bottom O_2] < 1.5 mL/L) (**Figure 7A**) and severely hypoxic (0.1 mL/L < [bottom O_2] < 0.5 mL/L) to anoxic ([bottom O_2] < 0.1 mL/L) (**Figure 7B**). We found that sediments underlying oxic–moderately hypoxic waters do not show correlation between U and Mo—with an R^2 value close to 0.00 (**Figure 7A**). Some samples do, however, show significant enrichment above crustal values of 2.5 mg/kg that could be due to water column U authigenesis (Zheng et al., 2002; Choumiline, 2011). In contrast, sediments deposited under severely hypoxic to anoxic waters show strong correlation between Mo and U, with an R^2 value of 0.80. While most of the U concentrations for the oxygen-deficient sites correlate with Mo, some reach even higher values of 17 mg/kg U with no significant Mo increase. In many cases, the lack of Mo enrichments could be attributed to bottom water redox potentials that were not sufficiently reducing, especially for sites in the upper OMZ. These observations of high U and low Mo could also indicate a water column supply of authigenic U through settling particles. In this context of U-Mo relationships, the studied sites from Alfonso and La Paz basins fall above the trend line, showing potential surpluses in U_{auth} enrichments perhaps tied to high levels of productivity and associated particle scavenging (**Figure 7**).

Chronology of Reoxygenation and Deoxygenation Events Over the Past Millennium in a Predominantly Anoxic Marine Setting

In the following discussing, we use the term reoxygenation to imply a relative increase in dissolved O_2 at OMZ depths, usually corresponding to deepening of the upper OMZ boundary. Reoxygenation need not indicate disappearance of the OMZ, as no proxy record indicates fully oxygenated water conditions (Tems et al., 2016), including the data produced in our study—specifically, Mo, V, and U values are several times higher than their crustal average values (Wedepohl, 1995). The oxygenation chronology of the last millennium starts with the predominantly

TABLE 5 | Comparison of productivity and/or redox proxy values for selected sedimentary material from different OMZ depths in the Eastern Pacific.

Marine basin	Water column depth	Redox condition and bottom dissolved O_2 (mL/L)	Proxy data							
			Productivity/nutrients			Redox and/or Productivity		Redox		
			C_{org} (%)	Ba_{excess} (mg/kg)	Ni (mg/kg)	U (mg/kg)	U_{auth} (mg/kg)	Cd (mg/kg)	Mo (mg/kg)	V (mg/kg)
Alfonso Basin, Gulf of California (settling particles)[c]	Upper OMZ (360 m)	Anoxia (<0.1)	7.80 [16.37]	338.95* [2147.45]	37.49 [107.99]	4.65 [42.79]	4.16 [42.70]	1.42 [4.65]	1.40 [7.92]	38.96 [84.64]
Alfonso Basin, Gulf of California (core C42A)[a]	Uppermost OMZ (265 m)	Severe hypoxia (~0.3)	2.96	175.70	26.84	14.31	13.17	5.34	0.75	26.05
Alfonso Basin, Gulf of California (core C37A)[a]	Upper OMZ (408 m)	Anoxia (<0.1)	6.01	406.37	40.25	9.85	8.14	2.48	6.34	124.67
La Paz Basin, Gulf of California (core C52A)[a]	Middle OMZ (785 m)	Anoxia (<0.1)	6.41	682.77	49.06	8.84	7.24	2.60	6.75	75.05
Pescadero Slope, Gulf of California (core DIPAL-III T2)[b]	Upper OMZ (577 m)	Anoxia (<0.1)	6.42	654.95	54.10	8.09	5.05	-	7.35	149.08
Santa Barbara Basin, Eastern Pacific, 34°N (core ODP 893A)[d]	Upper OMZ (576.5 m)	Anoxia (<0.1)	3.00	513.2*	51.00	2.90	-	2.80	4.70	186.70
Mazatlan Margin, Eastern Pacific, 22.7°N (core Mazatlan)[e]	Upper OMZ (442 m)	Anoxia (<0.1)	-	-	-	4.29	-	-	6.26	-
Soledad Basin, Eastern Pacific, 25.2°N (core Soledad)[e]	Upper OMZ (542 m)	Anoxia (<0.1)	7.09	-	-	6.78	-	-	4.16	-
Gulf of Tehuantepec, Eastern Pacific, 15.7°N (core ME0005A 11PC)[f]	Upper OMZ (574 m)	Anoxia (<0.1)	4.74	-	-	-	-	3.05	6.51	-
Gulf of Tehuantepec, Eastern Pacific, 15.7°N (core ME0005A 3JC)[f]	Middle OMZ (740 m)	Anoxia (<0.1)	4.34	-	-	-	-	1.57	6.54	-
Peru Margin Eastern Pacific, 13.7°S (core MC82)[e]	Uppermost OMZ (264 m)	Anoxia (<0.1)	16.27	-	-	17.34	-	-	70.08	-
Upper Continental Crust Average[g]	-	-	-	668*	18.6	2.5	2.5*	0.102	1.4	53

The core top values represent the uppermost 2 cm of sedimentary record.

**Total concentration value (not enough supplementary data to calculate authigenic or excess values).*

[a] *This study.*

[b] *Gravity core (Choumiline et al., 2017).*

[c] *Sediment trap material; average and [maximum] values between 2002–2008 in 173 samples (Rodríguez-Castañeda, 2008; Choumiline, 2011; Silverberg et al., 2014).*

[d] *Drill core (Ivanochko and Pedersen, 2004).*

[e] *Multicore (McManus et al., 2006).*

[f] *Sediment core (Hendy and Pedersen, 2006).*

[g] *Wedepohl (1995).*

warm climatic trends of the Medieval Warm Period (or Medieval Climate Optimum), which ended as cooling began with gradual change in the insolation regime after the Wolf Minimum (**Figure 8**). This cooling transitioned the planet into the colder Little Ice Age, which started around 1300 AD (Bard et al., 2000; IPCC, 2014; Griffiths et al., 2016) and was the most anoxic period of the last millennium as indicated by our V, Cd, Mo, and U_{auth} data from Alfonso. The Little Ice Age coincides with the highest values of the SOI index, indicating more La Niña-like years and enhanced upwelling (Yan et al., 2011; Griffiths et al., 2016). Most marine basins of the ETNP experienced short-term reoxygenation events and corresponding decreases in water column denitrification during warm times around late 1300s, early 1700s, and the mid to late 1900s (**Figure 8**). These warm reoxygenation periods lasted from 100 to 150 years but reversed several times toward anoxic conditions in a matter of decades due

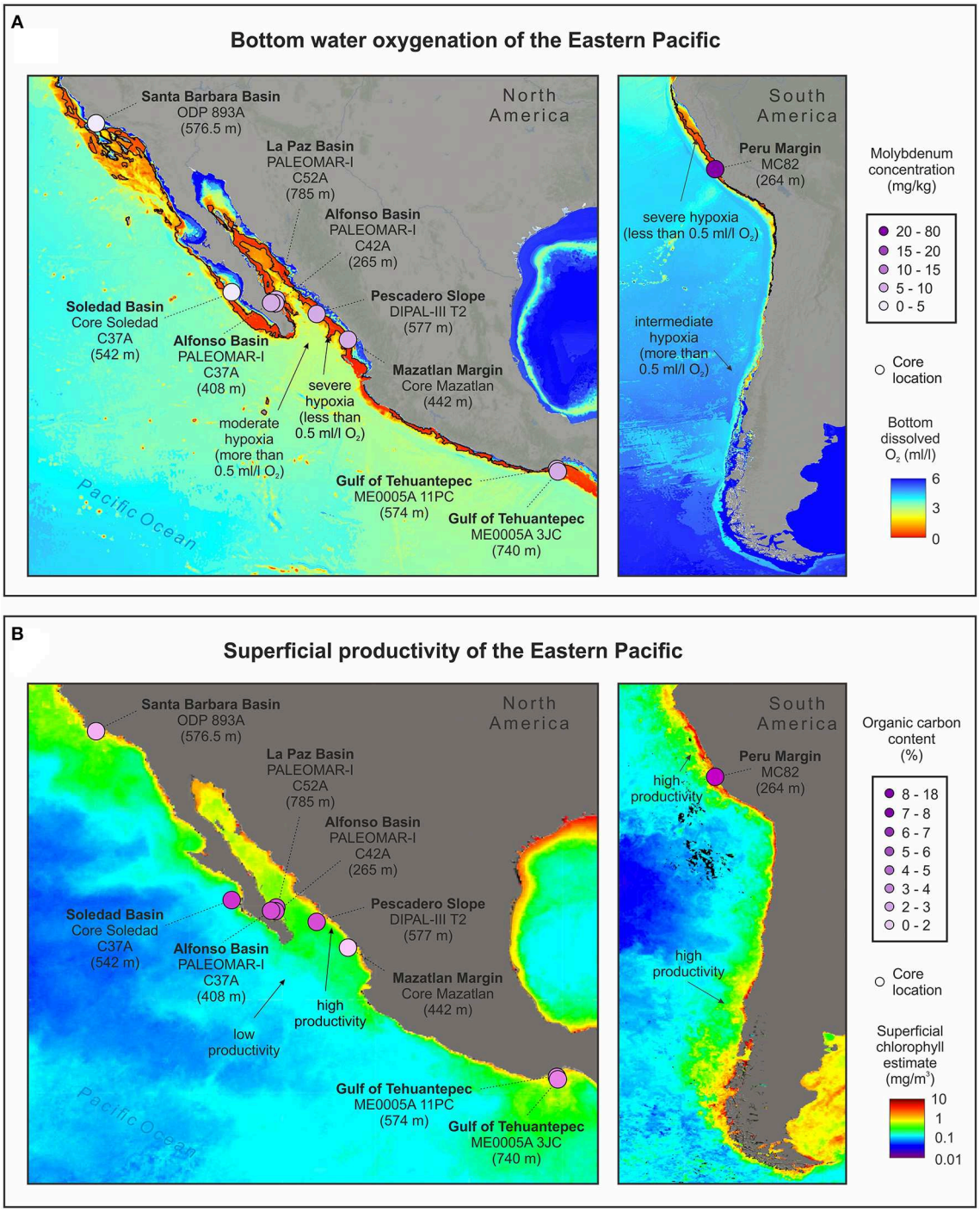

FIGURE 6 | Molybdenum and organic carbon in core tops from various locations across the Gulf of California and adjacent Pacific, **(A)** bottom dissolved oxygen, and **(B)** superficial chlorophyll estimate from the studied marine OMZ settings of ETNP (Alfonso Basin and La Paz Basin) (Oxygen based on World Ocean Atlas, 2005; Garcia et al., 2006; superficial chlorophyll estimates by SeaWIFS satellite sensor published by OBPG/NASA).

to cooling and strengthening of the OMZ (Tems et al., 2016). During the Little Ice Age, denitrification, and bottom anoxia were the strongest during the Spörer Minimum, leading to OMZ expansion (this study; Tems et al., 2016). Subsequent periods of lower solar irradiance (Maunder and Dalton minimums) also corresponded with expanded OMZs but to a lesser degree than during the Spörer (**Figure 8**). The most recent stage was marked by a gradual reoxygenation during the twentieth century toward

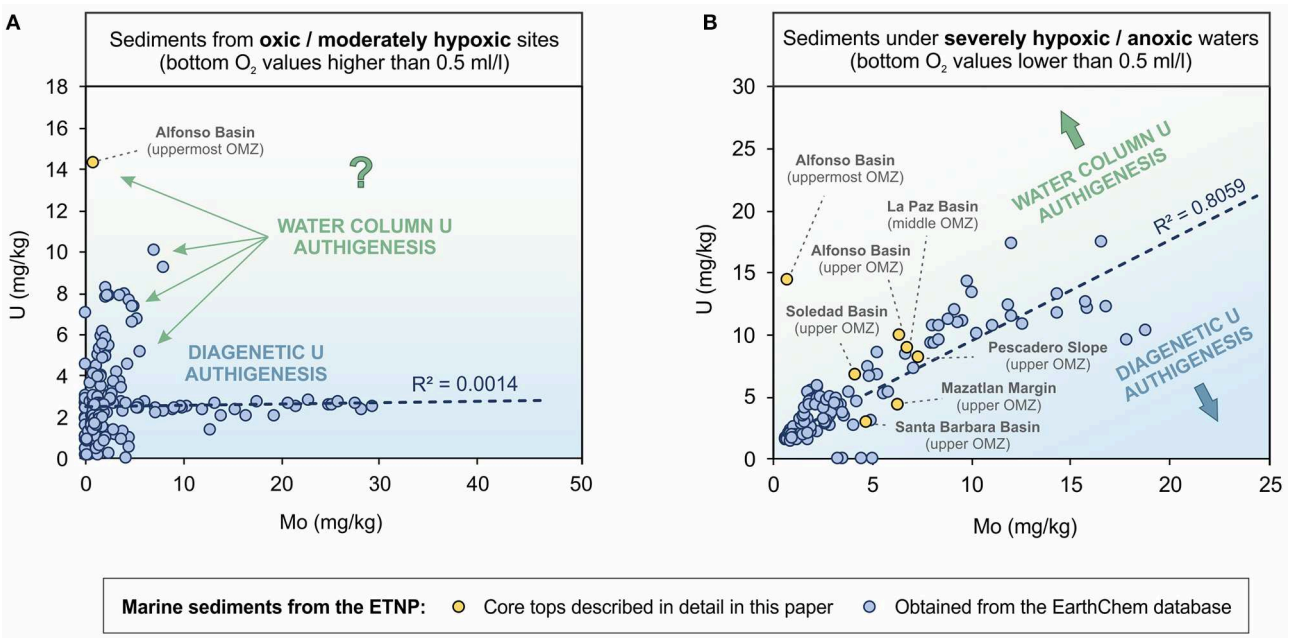

FIGURE 7 | Correlation between U and Mo in sediments collected under **(A)** oxic or moderately hypoxic waters and **(B)** severely hypoxic or anoxic waters from different basins of the Eastern Tropical North Pacific (Data from: this study; Ivanochko and Pedersen, 2004; McManus et al., 2006; Choumiline et al., 2017; EarthChem database with $n = 183$).

the mid-1990s, followed by a slight possible OMZ intensification over the last decade as shown by some of our proxy V and U_{auth} data from Alfonso and La Paz basins in accordance with the findings of Tems et al. (2016), Ontiveros-Cuadras et al. (2019) and a high-resolution U record of the last century by Choumiline et al. (2010) and Choumiline (2011).

Climatic Drivers of Historical OMZ Fluctuations in the ETNP Over the Last Millennium

As suggested by our data from marine basins of the southwestern Gulf of California, patterns of productivity tied to upwelling are one of the key drivers of oxygenation in coastal OMZs. Importantly, most of the variability in the ETNP is indirectly controlled by short and long-term variations of solar irradiance (Bard et al., 2000). La Niña years are known to positively impact productivity in coastal regions of the Eastern Pacific by increasing upwelling rates (Thunell, 1998; Chang et al., 2013). Atmospheric dynamics, also triggered by insolation changes, play a substantial role in controlling coastal wind-driven upwelling, caused by migrations of NPH and ITCZ (Schneider et al., 2014; Metcalfe et al., 2015; Staines-Urías et al., 2015). Southward position of the NPH and ITCZ would trigger more upwelling in the Eastern Pacific (Metcalfe et al., 2015). Our research suggests—based on the chronology of Ni, V, and U_{auth} variability—that one of the most important controls on upwelling in the ETNP leading to OMZ fluctuations is the position of the Walker Circulation and its effect on El Niño or La Niña years on longer time scales (**Figure 8**). Evidence for long-term ENSO trends are manifested in PDO and/or NPGO variability in the Eastern Tropical North Pacific (Mantua and Hare, 2002; Moy et al., 2002; Di Lorenzo et al., 2010; Choumiline, 2011; Tems et al., 2016). These changes control delivery of nutrients to the marine basins of the Eastern Pacific, subsequently enhancing productivity and favoring oxygen loss (deoxygenation) of these oceanic settings (and OMZs). The mechanistic links between changes in PWC and PDO and their impacts on upwelling variability are still not clear, mainly due to difficulties in the paleoreconstruction of these phenomena.

Our record of productivity and redox over the last millennium can be compared to changes in COCOC (Composite Coccolith Proxy) presented by Beaufort and Grelaud (2017) in an attempt to reconstruct long-term variation in the PDO (**Figure 8**). The Southern Oscillation Index (SOI) presented by Yan et al. (2011) and Griffiths et al. (2016) is proposed to represent changes in Walker Circulation through time (**Figure 8**). On decadal and centennial timescales, the driving force for the major and minor fluctuations in the PWC is solar irradiance (Bard et al., 2000). Colder periods corresponding to the solar irradiance minimums—known as Dalton, Maunder, Spörer, and Wolf minimums—are also times of higher productivity and lower oxygen concentrations (seen in the Alfonso, La Paz, and Pescadero records). Importantly, denitrification was also higher during times of low insolation, as evidenced by higher sedimentary $\delta^{15}N$ values on the Pescadero Slope (eastern side of the Gulf of California) published by Tems et al. (2016). Periods of high productivity are captured in records for Ba_{excess},

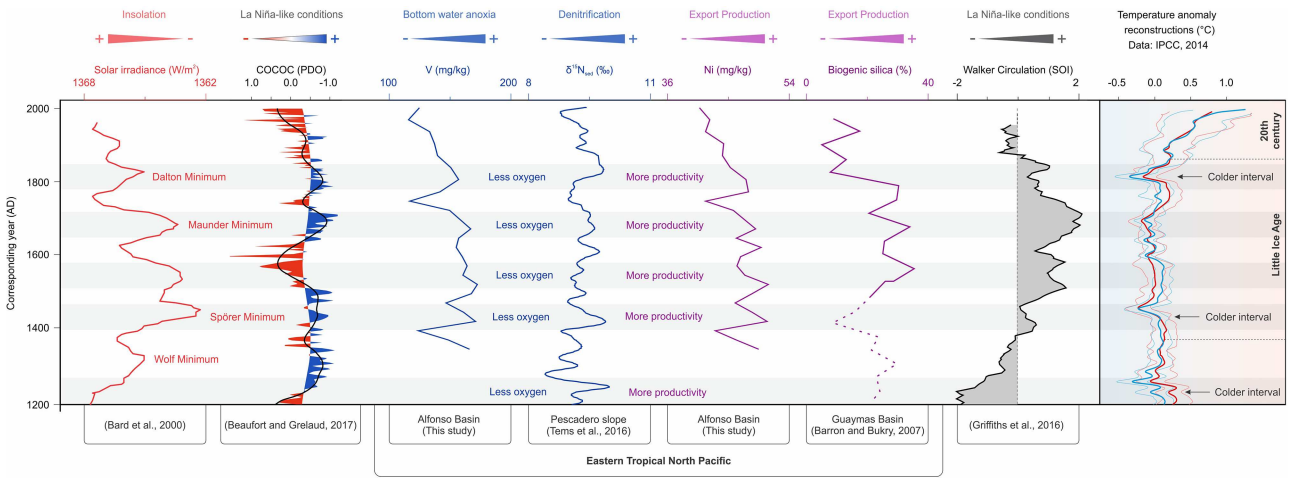

FIGURE 8 | Reconstruction of OMZ variability of the Eastern Pacific during the last 800 years based on proxies for water column denitrification, redox and productivity compared to major climatic forcings. Note that the solar irradiance plot is inverted for better visualization.

Ni, and U_{auth} in Alfonso and La Paz basins during the Little Ice Age—with maximum peaks of productivity during Spörer, Maunder, and Dalton solar minimums (Bard et al., 2000; Barron and Bukry, 2007). Independent records of biogenic silica from Guaymas Basin, central Gulf of California, confirm elevated export production during colder solar episodes (Barron and Bukry, 2007). These productive times led to enhanced bottom water anoxia manifested in high V and U_{auth} concentrations in marine sediments of Alfonso and La Paz basins (**Figures 8**, **9A**). The drivers of climatic change over the last millennium remain unclear, but the leading theories involve a combination of factors from orbital change to periods of strong volcanism that triggered a cooling phase during the Little Ice Age (Atwood et al., 2016). That cooling phase affected the strength of the PWC and led to lesser El Niño years.

Drivers of Redox in the Eastern Pacific and Apparent Contradictions With the Glacial-Interglacial Model for OMZ Expansions

The mechanisms that control decadal to centennial oxygen variability in the ETNP remain unresolved but are likely influenced by solar forcing. That forcing not only drives migration of the ITCZ (Schneider et al., 2014) but also, more importantly, variation in the intensity of the PWC. During the Little Ice Age, solar irradiance was at its lowest over the past millennium, which strengthened Walker Circulation (Bard et al., 2000; Yan et al., 2011; Griffiths et al., 2016). The result was La Niña-like conditions, which enhanced upwelling of colder nutrient-rich waters and favored elevated productivity and reduced bottom oxygen levels (**Figure 9A**), as seen in Alfonso and La Paz basins and on the Pescadero Slope (**Figure 8**). A smaller-scale form of PWC variability is expressed in changes in the PDO and/or NPGO indices, which control rates of denitrification in OMZ waters of the Eastern Pacific (Di Lorenzo et al., 2010; Tems et al., 2016; Beaufort and Grelaud, 2017). As indicated by Tems et al. (2016) and confirmed by our findings, despite a decline in measured O_2 values in the Eastern Pacific over the last few decades (Bograd et al., 2003, 2008; Levin, 2018), sedimentary records of the ETNP do not indicate increasing anoxia. Our geochemical proxy data from Alfonso from this study, Pescadero (Tems et al., 2016), and Mazatlan Margin (Ontiveros-Cuadras et al., 2019) also confirm that despite the recent warming trend and related anthropogenically triggered ocean-scale O_2 decline (Bograd et al., 2003, 2008; Breitburg et al., 2018; Levin, 2018), the sedimentary records of benthic foraminifera, $\delta^{15}N$, Cd, Mo, U_{auth}, and V do not suggest a significant increase in anoxia after the mid-1800s (**Figures 4**, **8**). Our evidence for gradually increasing dissolved oxygen levels are also supported by a decline in export production toward the beginning of the twenty-first century, evidenced by our C_{org} and Ni data from Alfonso and La Paz, as well as biogenic silica from Guaymas Basin (Barron and Bukry, 2007).

Despite a longstanding decrease of productivity and redox during the last century (**Figure 8**), a subtle regime change toward increased anoxia could have begun around the 1990s but is represented only by a few data points for the redox proxies (this study; Dean et al., 2004; IPCC, 2014; Tems et al., 2016). Remarkably, this relationship is only evidenced by $\delta^{15}N$, V, and Mo and not by productivity proxies, pointing at the global decline of O_2 (Tems et al., 2016; Breitburg et al., 2018; Levin, 2018). Rather than reflecting global warming, reoxygenation and deoxygenation scenarios of the last millennium in the ETNP are primarily controlled by coastal productivity and dominated by long-term persistence of La Niña conditions more often occurring during stronger PWC. Deutsch et al. (2014) proposed another mechanism for the apparent OMZ contraction despite declining O_2 trends in the North Pacific. The authors argued that global warming is resulting in a weakening of easterly trade winds and will continue to do so, leading to contraction of the ETNP OMZ rather than the previously predicted expansion (Deutsch et al., 2014; Tems et al., 2016). Regardless of the dominant mechanisms, our results (**Figure 8**) also support the

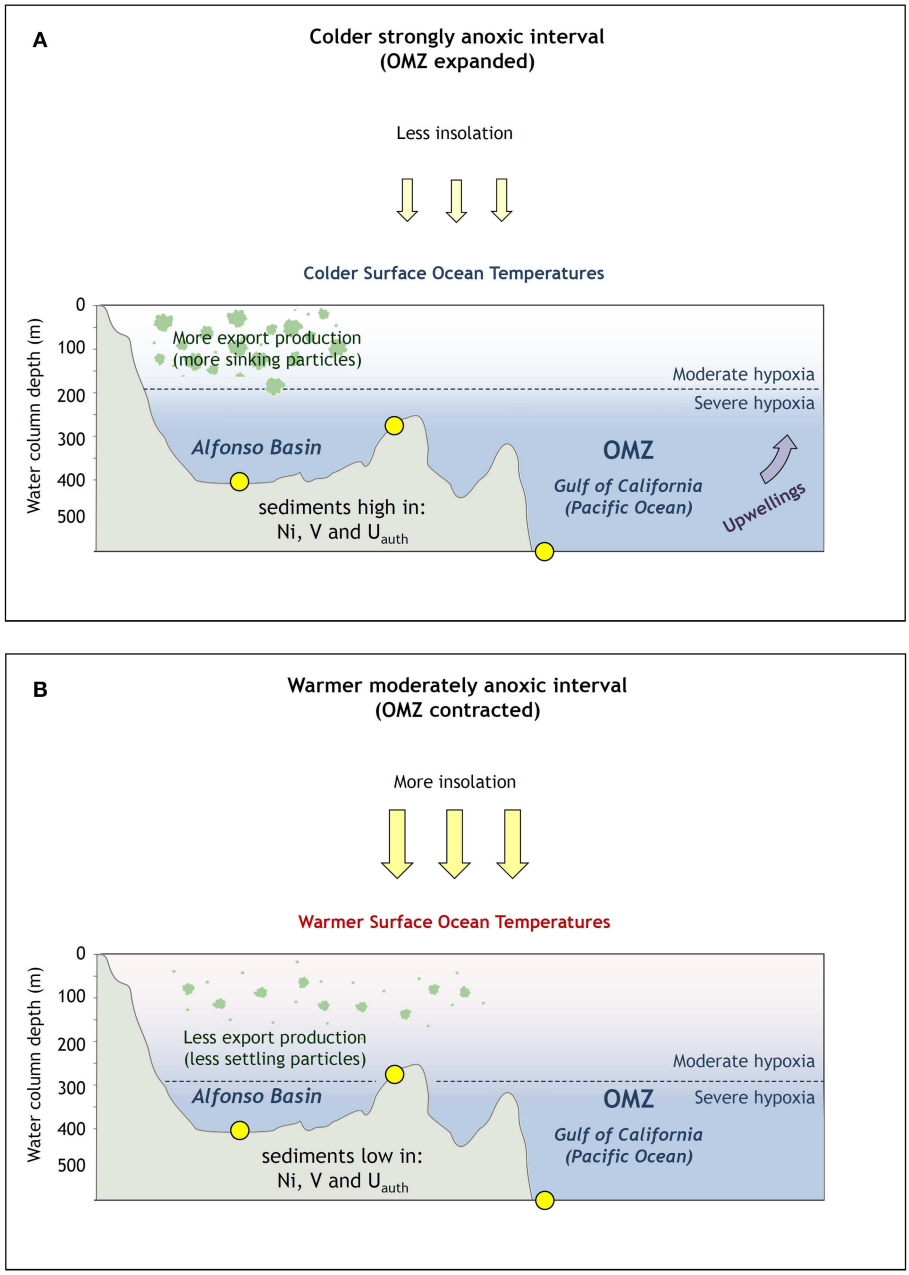

FIGURE 9 | Two dominating oceanographic regimes: **(A)** high productivity and enhanced anoxia during colder periods, **(B)** low productivity and reoxygenation during warm periods.

interpretation that OMZ expansion occurred during cooling periods rather than being a consequence of warming—at least over the last millennium (**Figure 9**).

A clear distinction should be made between the dominant mechanisms that control oxygenation in the ETNP over decadal-centennial timescales (Deutsch et al., 2014; Tems et al., 2015, 2016) and those that govern long-term glacial-interglacial variability (Ganeshram and Pedersen, 1998; Nameroff et al., 2004; Hendy and Pedersen, 2006; Ivanochko et al., 2008; Pichevin et al., 2012, 2014; Cartapanis et al., 2014; Umling and Thunell, 2017). High-amplitude variability (such as the one described in our results) is superimposed over the long-term millennial-multimillenial O_2 trends (Nameroff et al., 2004; Cartapanis et al., 2014; Chang et al., 2014; Moffitt et al., 2015; Praetorius et al., 2015; Tetard et al., 2017). In contrast, the long-term tendencies (e.g., transition from the Last Glacial Maximum toward the Holocene) are driven by global changes in temperature and circulation that control intermediate and deep-water oxygenation (Ganeshram and Pedersen, 1998; Hendy and Pedersen, 2006; Cartapanis et al., 2014; Praetorius et al.,

2015; Lu et al., 2016; Choumiline et al., 2017; Breitburg et al., 2018; Levin, 2018). In other words, short-term decreases in anoxia during warm times in response to the weakening of the Walker Circulation and increase abundance of ENSO years can counteract long-term warming of the upper ocean, which causes stratification and reduced ventilation and O_2 concentration on the global scale ocean.

Lagged Response of the Ocean to Climate Change and Future Scenarios

The effect of global warming on the world ocean is not expected to be spatially uniform. For example, latitudinal differences in the change of O_2 volume have been observed, with faster declines near the equator (0–20°N) compared to higher latitudes (20–90°N) (Schmidtko et al., 2017). Some vulnerable regions have experienced a rapid response (e.g., ETSP), while others (e.g., ETNP) show a lag of several decades (Chavez et al., 2011; Howes et al., 2015; Long et al., 2016). It has been suggested that the response time of the OMZs to ocean deoxygenation caused by a decrease in O_2 solubility and enhanced stratification linked to global warming (Praetorius et al., 2015) could be quicker than 25 years (Tems et al., 2016). However, the effects of climate change on OMZ oxygenation seem to only begin toward the end of the 20th century as preserved in multiple sediment records (Dean et al., 2004; Tems et al., 2016)—including ours—wherein the gradual oxygen increase in the beginning of the twentieth century shifts to a decline in O_2 toward the twenty-first century. The observed lagged response in O_2 trends to warming is consistent with current estimates of oceanic oxygen volume (Chavez et al., 2011; Long et al., 2016; Schmidtko et al., 2017).

Overall, there is still no consensus in the community about predicted OMZ behavior for the near future due to differences in the volume estimates among the models (Cocco et al., 2013; Long et al., 2016; Battaglia and Joos, 2018). A more recent study concludes that after the gradual increase of anoxia, the trend will be reversed globally, and the overall volume of OMZs will start declining (Fu et al., 2018). The mechanism proposed by Fu et al. (2018) involves a reduction of biological export linked to surface warming.

SYNTHESIS

Lessons Learned About the Utility of Productivity and Redox Proxies From Our ETNP OMZ Records

Our findings indicate that the efficacy of productivity and redox proxies in modern OMZs depends somewhat on the supply of non-detrital trace elements via settling due to biological uptake or scavenging, as well as their preservation potential during diagenetic overprinting. We conclude that Ni, U, and V are the most reliable, while Ba and Mo should be used with caution in OMZ-type settings. Barium is significantly enriched in sediment trap material, which could elevate its proxy potential in the region (**Table 5**; Rodríguez-Castañeda, 2008; Choumiline, 2011). However, its long-term preservation in sedimentary records is an important issue. For La Paz Basin, we can confirm that Ba_{excess} did not behave as a reliable productivity proxy—showing trends that differ significantly from those of the other indicators (**Table 3**). However, our Ba_{excess} record in Alfonso Basin does mirror other productivity proxies (C_{org} and Ni) and is statistically associated with them (**Figure 5**). This agreement could be because our Alfonso Basin core was not exposed to severe diagenetic remobilization of sedimentary barite as much as the La Paz basin core (McManus et al., 1998; Riedinger et al., 2006). Despite the good agreement between proxy records and Ba_{excess} in Alfonso Basin, long-term preservation of the Ba fraction remains a concern (Schoepfer et al., 2015).

In our studied cores, Ni shows good temporal agreement with both the productivity (C_{org} and Ba_{excess}) and water column redox proxies (V and U_{auth}). In Alfonso Basin, this element served as the best indicator for productivity—mirroring an independent biogenic SiO_2 record from Guaymas Basin generated by Barron and Bukry (2007) (**Figure 8**). Nickel does not follow Mo and Cd, which are bottom water and/or diagenetic redox proxies (**Figure 5**), which could be explained by a significant contribution of particulate Ni (**Table 5**), enriched in settling matter by biological uptake (Böning et al., 2015) and potentially related to diatom export (Twining et al., 2012).

In our sediment cores from Alfonso and La Paz basins, Mo covaries with Cd (**Figure 5**) and reaches high values. However, due to the low and transient concentrations of water column H_2S in most modern OMZs, it is unlikely that Mo enrichments are related to bottom water euxinia in such settings (Scott and Lyons, 2012; McKay and Pedersen, 2014; Costa et al., 2018). Nevertheless, Mo is commonly elevated in ETNP sediment cores, reaching maxima several times higher than the average crustal value of 1.4 mg/kg (Wedepohl, 1995) (**Figure 7**; **Table 5**). These values are likely linked to the presence of sulfide only in the pore waters, leading to diagenetic enrichments (Zheng et al., 2000; Scholz et al., 2017; Hardisty et al., 2018). Because of this diagenetic enrichment, Mo is a less sensitive indicator of very low and transient sulfide in the water column.

We confirm the utility of V as a water column redox proxy as expressed through strong correlation with water column denitrification records reconstructed from sedimentary $\delta^{15}N$ in the ETNP OMZ (Tems et al., 2016). Moreover, V is sensitive to O_2 changes occurring not only at upper OMZ depths but also those closer to the OMZ-core, which have less pronounced redox variations. It is worth noting that, as for U_{auth}, there is evidence for an important contribution of V through settling matter (Rodríguez-Castañeda, 2008; Hakspiel-Segura et al., 2016; Bauer et al., 2017; Ho et al., 2018). The source of such enrichments is yet unknown, but we hypothesize that it could be related to redox processes causing authigenic V enrichment in organic matter aggregates (Ho et al., 2018).

An important methodological distinction needs to be made for proper numerical treatment of sediments with highly variable $CaCO_3$ and biogenic silica contents. As previously suggested (Pichevin et al., 2012, 2014), proxy records can, in some cases, be significantly impacted by dilution with major components. In this study we have $CaCO_3$ values for the studied sediment cores, so CFB fraction calculations were possible. By comparing elemental

concentrations against CFB-corrected values, no substantial differences were found. Most importantly, the paleoceanographic and paleoclimatic trends described in this paper also prevailed for the carbonate-corrected values. We have no data to corroborate the dilution effect with biogenic opal, as it was not measured for the cores studied here. The consequences of the dilution effects with biogenic detritus need to be further investigated for Alfonso Basin and similar marine settings.

New Insights on Uranium Biogeochemistry in OMZs

In our study, uranium shows a consistently good correlation with C_{org} and the micronutrient Ni in both the deeper (mid OMZ) and shallow cores (upper OMZ) (**Figure 4** and **Supplementary Figure 3**). We attribute this observation to seasonal variation in dissolved O_2 and to the particulate authigenic U contribution during settling (Rodríguez-Castañeda, 2008; Choumiline, 2011). As particles settle deeper, there is more reaction time for dissolved U (+6) to be reduced to its particulate phase U (+4) and/or for adsorption to occur. This relationship is a consistent feature of vertical sediment trap moorings—that is, higher authigenic U enrichment in the particles collected in deeper waters (Zheng et al., 2002; Rodríguez-Castañeda, 2008; Huang and Conte, 2009; Choumiline, 2011). The extent to which U_{auth} enrichments are microbially mediated remains unknown, but evidence suggests that these biological interactions could be among the principal controls (Lovley et al., 1991; Cumberland et al., 2016). There is growing evidence that anaerobic metabolism can occur within aggregates of settling matter if conditions are energetically favorable (Wright et al., 2012; Lehto et al., 2014; Bianchi et al., 2018). Authigenic U formation is favored after the ferruginous (Fe reduction) and sulfidic (SO_4^{2-} reduction) chemical zones (Zheng et al., 2002; Canfield and Thamdrup, 2009). This range of redox conditions is common in marine aggregates of modern OMZs (Bianchi et al., 2018), which could explain the strong authigenic U enrichments in settling matter of the Gulf of California and California Margin (Zheng et al., 2002; Choumiline, 2011). Other marine settings, such as Saanich Inlet, also reveal the possibility of water column authigenic U enrichments, where up to one third of the estimated authigenic fraction is captured in particles in the water column (Holmden et al., 2015). It is worth mentioning that while ideal microenvironments for particulate-U_{auth} formation exist in strongly reducing and restricted settings in the Black and Baltic seas, as well as the Cariaco Basin (Dellwig et al., 2010; Calvert et al., 2015; Bauer et al., 2017), significant U_{auth} enrichments have not been detected (Anderson et al., 1989; Calvert et al., 2015). Perhaps the necessary conditions for authigenic U enrichments are favored in coastal upwelling sites, where high productivity and thus abundant particulate organic matter formation are common.

We propose an updated model for U_{auth} enrichments (**Figure 10**). This model points to a significant contribution of U_{auth}, beyond that linked to diagenesis, via settling matter in regions of high productivity and upwelling—such as the coastal regions of the ETNP.

In summary, the current understanding of U geochemistry in OMZs supports a significant contribution via settling particulates during times of high productivity. The actual enrichment mechanism could either be linked to localized reduction within organic-rich microenvironments or simply adsorption to organic

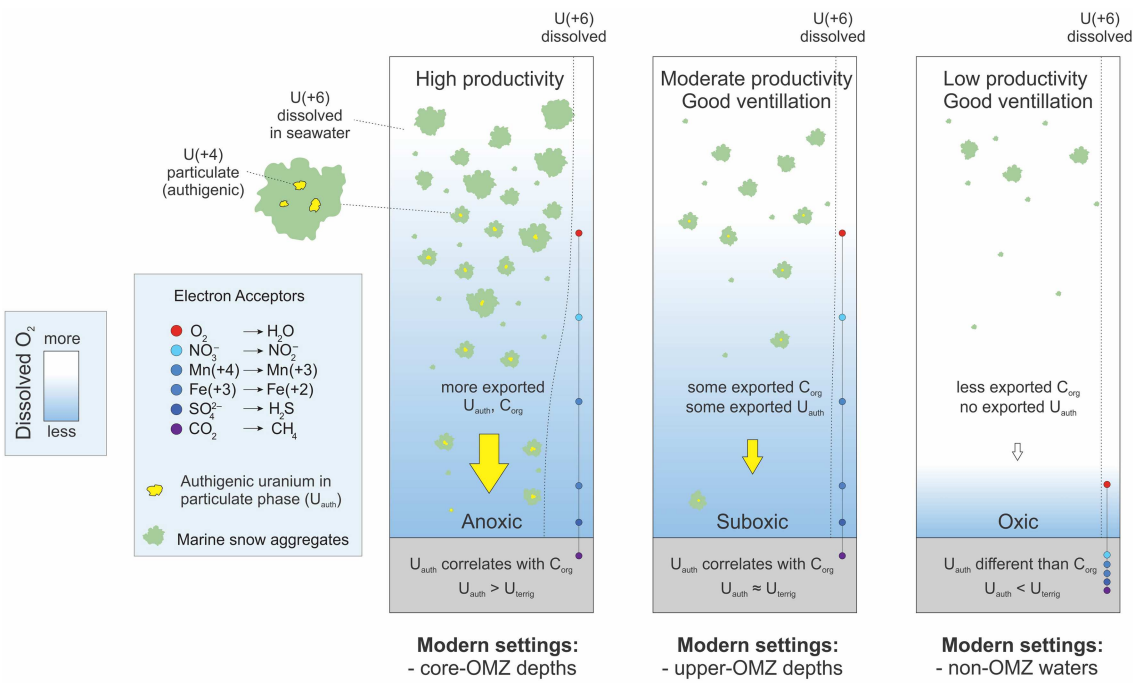

FIGURE 10 | Hypothetic scenarios of uranium biogeochemistry in modern OMZs.

matter. Both processes could explain the correlation with C_{org} and Ni and excessive U enrichments during well-ventilated times. Improved understanding of the details of U uptake will enhance its utility as a paleoproxy.

Suggestions for Future Work

This research highlights the importance of comparing high-resolution OMZ records of both modern and past oceanic conditions with global climatic trends. We have demonstrated it is possible to reconstruct high-resolution OMZ variability using a multiproxy approach. However, there are multiple caveats when interpreting deoxygenation and productivity trends because of the complex mechanisms by which trace elements are transferred to sedimentary records. We encourage particular caution for elements that demand an understanding of the relative contributions from diagenetic vs. water column processes and how specifically those inputs translate to regional patterns of redox and productivity. The importance of particulate supply of scavenged non-detrital trace elements in OMZ-type settings is clear, and further research, when possible, should include isotopic data as a source of additional mechanistic perspective.

CONCLUSIONS

In the modern Eastern Tropical North Pacific, marine sediments are mostly enriched in Cd, Mo, V at sites underlying severely hypoxic and anoxic waters—in contrast to shallower and oxygenated sites where these elements are present in low, mostly crustal, abundances. The exception is U, which is found to be enriched not only in sediments underlying anoxic waters but also in those of well-ventilated regions, suggesting a strong contribution of authigenic uranium through settling of marine snow aggregates.

Most of the sites located at present Oxygen Minimum Zone depths remained anoxic over the last millennium. The Eastern Tropical North Pacific Oxygen Minimum Zone expanded throughout the Little Ice Age, with the most anoxic events during the Spörer, Maunder, and Dalton insolation minima. Reoxygenation in the Eastern Tropical North Pacific occurred during warm periods around late 1300s, early 1700s, and late 1900s AD.

There is no clear effect of the temperature increase of twentieth century on the intensification of the Eastern Tropical North Pacific Oxygen Minimum Zone. The prevailing trend shows an increase in dissolved oxygen from the 1900s AD toward present time, with a subtle decrease in the beginning of the twenty-first century.

Redox and productivity changes reconstructed for the last millennium from marine basins of the Eastern Tropical North Pacific indicate a strong relationship with insolation fluctuations and the Pacific Walker Circulation that drive upwelling rates, productivity, and oceanic anoxia at Oxygen Minimum Zone depths.

The most reliable redox proxies for water column oxygenation in Oxygen Minimum Zones are vanadium and uranium. Uranium also shows strong potential to serve as a productivity proxy because it can be exported from the water column to sediments through settling particulate matter during periods of high primary productivity. Molybdenum is the least useful proxy for Oxygen Minimum Zone oxygenation because it is not sensitive to small redox variations and can be enriched diagenetically when pore water sulfide is present.

AUTHOR CONTRIBUTIONS

KC wrote the paper including comments by LP-C, AG, SB, and TL. Project planning logistics were performed by KC, TL, and LP-C. Samples used in this research were collected, preserved, and handled by KC and LP-C. Analytical measurements were performed by KC, SB, and AG.

ACKNOWLEDGMENTS

The authors acknowledge financial support granted by UC MEXUS - CONACYT Collaborative Research Grant "High resolution geochemical reconstructions of recent climate and oxygenation history in La Paz Bay, Gulf of California" that covered travel and analytical costs. The authors express gratitude to Coordinación de Plataformas Oceanográficas (UNAM, Mexico) for funding the PALEOMAR-I campaign and the crew members of R/V "El Puma" for exceptional support during the field stage. KC was thankful for the UC MEXUS – CONACYT Doctoral Fellowship for a fully funded scholarship during his Ph.D. studies and for the 2016 UC MEXUS Dissertation Grant award for analytical expenses. Partial support was received by TL, KC, and SB from the NASA Astrobiology Institute, and AG from the USDA NIFA Hatch program (project # CA-R-ENS-5120-H).

SUPPLEMENTARY MATERIAL

The Supplementary Material for this article can be found online at: https://www.frontiersin.org/articles/10.3389/feart.2019.00237/full#supplementary-material

REFERENCES

Algeo, T. J., and Lyons, T. W. (2006). Mo-total organic carbon covariation in modern anoxic marine environments: implications for analysis of paleoredox and paleohydrographic conditions. *Paleoceanogr. Paleoclimatol.* 21:PA1016 doi: 10.1029/2004PA001112

Algeo, T. J., and Rowe, H. (2012). Paleoceanographic applications of trace-metal concentration data. *Chem. Geol.* 324–325, 6–18. doi: 10.1016/j.chemgeo.2011.09.002

Algeo, T. J., and Tribovillard, N. (2009). Environmental analysis of paleoceanographic systems based on molybdenum–uranium covariation. *Chem. Geol.* 268, 211–225. doi: 10.1016/j.chemgeo.2009.09.001

Anderson, R. F., Fleisher, M. Q., and Lehuray, A. P. (1989). Concentration, oxidation state, and particulate flux of uranium in the Black Sea. *Geochim. Cosmochim. Acta* 53, 2215–2224. doi: 10.1016/0016-7037(89)90345-1

Anderson, R. F., and Winckler, G. (2005). Problems with paleoproductivity proxies. *Paleoceanogr. Paleoclimatol.* 20:PA3012. doi: 10.1029/2004PA001107

Atwood, A. R., Wu, E., Frierson, D. M. W., Battisti, D. S., and Sachs, J. P. (2016). Quantifying climate forcings and feedbacks over the Last Millennium in the CMIP5-PMIP3 Models. *J. Clim.* 29, 1161–1178. doi: 10.1175/JCLI-D-15-0063.1

Badan-Dangon, A., Dorman, C. E., Merrifield, M. A., and Winant, C. D. (1991). The lower atmosphere over the Gulf of California. *J. Geophys. Res.* 96, 16887–16896. doi: 10.1029/91JC01433

Bard, E., Raisbeck, G., Yiou, F., and Jouzel, J. (2000). Solar irradiance during the last 1200 years based on cosmogenic nuclides. *Tellus B* 52, 985–992. doi: 10.3402/tellusb.v52i3.17080

Barron, J. A., and Bukry, D. (2007). Solar forcing of Gulf of California climate during the past 2000 yr suggested by diatoms and silicoflagellates. *Mar. Micropaleontol.* 62, 115–139. doi: 10.1016/j.marmicro.2006.08.003

Battaglia, G., and Joos, F. (2018). Hazards of decreasing marine oxygen: the near-term and millennial-scale benefits of meeting the Paris climate targets. *Earth Syst. Dyn.* 9, 797–816. doi: 10.5194/esd-9-797-2018

Bauer, S., Blomqvist, S., and Ingri, J. (2017). Distribution of dissolved and suspended particulate molybdenum, vanadium, and tungsten in the Baltic Sea. *Mar. Chem.* 196, 135–147. doi: 10.1016/j.marchem.2017.08.010

Beaufort, L., and Grelaud, M. (2017). A 2700-year record of ENSO and PDO variability from the Californian margin based on coccolithophore assemblages and calcification. *Prog. Earth Planet. Sci.* 4:5. doi: 10.1186/s40645-017-0123-z

Bianchi, D., Weber, T. S., Kiko, R., and Deutsch, C. (2018). Global niche of marine anaerobic metabolisms expanded by particle microenvironments. *Nat. Geosci.* 11, 263–268. doi: 10.1038/s41561-018-0081-0

Bianchi, T. S., Schreiner, K. M., Smith, R. W., Burdige, D. J., Woodard, S., and Conley, D. J. (2016). Redox effects on organic matter storage in coastal sediments during the holocene: a biomarker/proxy perspective. *Annu. Rev. Earth Planet. Sci.* 44, 295–319. doi: 10.1146/annurev-earth-060614-105417

Bograd, S. J., Castro, C. G., Di Lorenzo, E., Palacios, D. M., Bailey, H., Gilly, W., et al. (2008). Oxygen declines and the shoaling of the hypoxic boundary in the California Current. *Geophys. Res. Lett.* 35:L12607. doi: 10.1029/2008GL034185

Bograd, S. J., Checkley, D. A., and Wooster, W. S. (2003). CalCOFI: a half century of physical, chemical, and biological research in the California Current System. *Deep Sea Res. Part II Top. Stud. Oceanogr.* 50, 2349–2353. doi: 10.1016/S0967-0645(03)00122-X

Böning, P., Shaw, T., Pahnke, K., and Brumsack, H.-J. (2015). Nickel as indicator of fresh organic matter in upwelling sediments. *Geochim. Cosmochim. Acta* 162, 99–108. doi: 10.1016/j.gca.2015.04.027

Borreggine, M., Myhre, S. E., Mislan, K. A. S., Deutsch, C., and Davis, C. V. (2017). A database of paleoceanographic sediment cores from the North Pacific, 1951-2016. *Earth Syst. Sci. Data* 9, 739–749. doi: 10.5194/essd-9-739-2017

Breitburg, D., Levin, L. A., Oschlies, A., Grégoire, M., Chavez, F. P., Conley, D. J., et al. (2018). Declining oxygen in the global ocean and coastal waters. *Science* 359:eaam7240. doi: 10.1126/science.aam7240

Brumsack, H.-J., and Gieskes, J. (1983). Interstitial water trace-metal chemistry of laminated sediments from the Gulf of California, Mexico. *Mar. Chem.* 14, 89–106. doi: 10.1016/0304-4203(83)90072-5

Burdige, D. J. (2007). Preservation of organic matter in marine sediments: controls, mechanisms, and an imbalance in sediment organic carbon budgets? *Chem. Rev.* 107, 467–485. doi: 10.1021/cr050347q

Bustos-Serrano, H., and Castro-Valdez, R. (2006). Flux of nutrients in the Gulf of California: geostrophic approach. *Mar. Chem.* 99, 210–219. doi: 10.1016/j.marchem.2005.09.012

Calvert, S. E., Bustin, R. M., and Ingall, E. D. (1996). Influence of water column anoxia and sediment supply on the burial and preservation of organic carbon in marine shales. *Geochimica Cosmochimica Acta* 60, 1577–1593.

Calvert, S. E., and Pedersen, T. (1993). Geochemistry of recent oxic and anoxic marine sediments: implications for the geological record. *Mar. Geol.* 113, 67–88. doi: 10.1016/0025-3227(93)90150-T

Calvert, S. E., Piper, D. Z., Thunell, R. C., and Astor, Y. (2015). Elemental settling and burial fluxes in the Cariaco Basin. *Mar. Chem.* 177, 607–629. doi: 10.1016/j.marchem.2015.10.001

Canfield, D. E., and Thamdrup, B. (2009). Towards a consistent classification scheme for geochemical environments, or, why we wish the term 'suboxic' would go away. *Geobiology* 7, 385–392. doi: 10.1111/j.1472-4669.2009.00214.x

Carpenter, J. H. (1965). The Chesapeake Bay Institute technique for the Winkler dissolved oxygen method. *Limnol. Oceanogr.* 10, 141–143. doi: 10.4319/lo.1965.10.1.0141

Cartapanis, O., Tachikawa, K., Romero, O. E., and Bard, E. (2014). Persistent millennial-scale link between Greenland climate and northern Pacific Oxygen Minimum Zone under interglacial conditions. *Clim. Past* 10, 405–418. doi: 10.5194/cp-10-405-2014

Chang, A. S., Bertram, M. A., Ivanochko, T., Calvert, S. E., Dallimore, A., and Thomson, R. E. (2013). Annual record of particle fluxes, geochemistry and diatoms in Effingham Inlet, British Columbia, Canada, and the impact of the 1999 La Niña event. *Mar. Geol.* 337, 20–34. doi: 10.1016/j.margeo.2013.01.003

Chang, A. S., Pedersen, T. F., and Hendy, I. L. (2014). Effects of productivity, glaciation, and ventilation on late Quaternary sedimentary redox and trace element accumulation on the Vancouver Island margin, western Canada. *Paleoceanography* 29, 730–746. doi: 10.1002/2013PA002581

Chappaz, A., Lyons, T. W., Gregory, D. D., Reinhard, C. T., Gill, B. C., Li, C., et al. (2014). Does pyrite act as an important host for molybdenum in modern and ancient euxinic sediments? *Geochim. Cosmochim. Acta* 126, 112–122. doi: 10.1016/j.gca.2013.10.028

Chavez, F. P., Messié, M., and Pennington, J. T. (2011). Marine primary production in relation to climate variability and change. *Ann. Rev. Mar. Sci.* 3, 227–260. doi: 10.1146/annurev.marine.010908.163917

Choumiline, K. (2011). *Geoquímica de la materia particulada en hundimiento y de los sedimentos recientes de Cuenca Alfonso, Bahía de La Paz.* (Master's thesis). Centro Interdisciplinario de Ciencias Marinas – Instituto Politécnico Nacional, La Paz, Mexico.

Choumiline, K., Lyons, T. W., Pérez-Cruz, L., Carriquiry, J. D., Raiswell, R., and Beaufort, L. (2017). "Sensitivity of redox proxies to rapid variability in Oxygen Minimum Zones. Goldschmidt 2017," in *Abstract Retrieved from Goldschmidt Conference Archive* (Paris).

Choumiline, K., Rodríguez-Castañeda, A. P., Silverberg, N., Shumilin, E., Aguirre-Bahena, F., Sapozhnikov, D., et al. (2010). "Arsenic and uranium in the settling particulate matter and sediments of Alfonso Basin, La Paz Bay," in *Proceedings of the 13th International Conference on Water-Rock Interaction. Reviewed Extended Abstract* (Guanajuato).

Cocco, V., Joos, F., Steinacher, M., Frölicher, T. L., Bopp, L., Dunne, J., et al. (2013). Oxygen and indicators of stress for marine life in multi-model global warming projections. *Biogeosciences* 10, 1849–1868. doi: 10.5194/bg-10-1849-2013

Conte, M. H., Carter, A. M., Koweek, D. A., Huang, S., and Weber, J. C. (2019). The elemental composition of the deep particle flux in the Sargasso Sea. *Chem. Geol.* 511, 279–313. doi: 10.1016/j.chemgeo.2018.11.001

Coria-Monter, E., Monreal-Gómez, M. A., Salas-de-León, D. A., Aldeco-Ramírez, J., and Merino-Ibarra, M. (2014). Differential distribution of diatoms and dinoflagellates in a cyclonic eddy confined in the Bay of La Paz, Gulf of California. *J. Geophys. Res.* 119, 6258–6268. doi: 10.1002/2014JC009916

Costa, K. M., Anderson, R. F., McManus, J. F., Winckler, G., Middleton, J. L., and Langmuir, C. H. (2018). Trace element (Mn, Zn, Ni, V) and authigenic uranium (aU) geochemistry reveal sedimentary redox history on the Juan de Fuca Ridge, North Pacific Ocean. *Geochim. Cosmochim. Acta* 236, 79–98. doi: 10.1016/j.gca.2018.02.016

Cumberland, S. A., Douglas, G., Grice, K., and Moreau, J. W. (2016). Uranium mobility in organic matter-rich sediments: a review of geological and geochemical processes. *Earth Sci. Rev.* 159, 160–185. doi: 10.1016/j.earscirev.2016.05.010

Dean, W., Pride, C., and Thunell, R. (2004). Geochemical cycles in sediments deposited on the slopes of the Guaymas and Carmen Basins of the Gulf of California over the last 180 years. *Quat. Sci. Rev.* 23, 1817–1833. doi: 10.1016/j.quascirev.2004.03.010

Dean, W. E. (2007). Sediment geochemical records of productivity and oxygen depletion along the margin of western North America during the past 60,000 years: teleconnections with Greenland Ice and the Cariaco Basin. *Quat. Sci. Rev.* 26, 98–114. doi: 10.1016/j.quascirev.2006.08.006

Dellwig, O., Leipe, T., März, C., Glockzin, M., Pollehne, F., Schnetger, B., et al. (2010). A new particulate Mn–Fe–P-shuttle at the redoxcline of anoxic basins. *Geochim. Cosmochim. Acta* 74, 7100–7115. doi: 10.1016/j.gca.2010.09.017

Deutsch, C., Berelson, W., Thunell, R., Weber, T., Tems, C., McManus, J., et al. (2014). Oceanography. *Centennial changes in North Pacific anoxia linked to tropical trade winds. Science* 345, 665–668. doi: 10.1126/science.1252332

Di Lorenzo, E., Cobb, K. M., Furtado, J. C., Schneider, N., Anderson, B. T., Bracco, A., et al. (2010). Central Pacific El Niño and decadal climate change in the North Pacific Ocean. *Nat. Geosci.* 3, 762–765. doi: 10.1038/ngeo984

Di Lorenzo, E., Schneider, N., Cobb, K. M., Franks, P. J. S., Chhak, K., Miller, A. J., et al. (2008). North Pacific Gyre Oscillation links ocean climate and ecosystem change. *Geophys. Res. Lett.* 35:L08607. doi: 10.1029/2007GL032838

Dickens, G. R., Koelling, M., Smith, D. C., and Schnieders, L. (2007). Rhizon sampling of pore waters on scientific drilling expeditions: an example from the IODP Expedition 302, Arctic Coring Expedition (ACEX). *Sci. Drilling* 4, 22–25. doi: 10.5194/sd-4-22-2007

Dunk, R. M., Mills, R. A., and Jenkins, W. J. (2002). A reevaluation of the oceanic uranium budget for the Holocene. *Chem. Geol.* 190, 45–67. doi: 10.1016/S0009-2541(02)00110-9

Dupont, C. L., Buck, K. N., Palenik, B., and Barbeau, K. (2010). Nickel utilization in phytoplankton assemblages from contrasting oceanic regimes. *Deep Sea Res. Part I Oceanogr. Res. Pap.* 57, 553–566. doi: 10.1016/j.dsr.2009.12.014

Durand, A., Chase, Z., Townsend, A. T., Noble, T., Panietz, E., and Goemann, K. (2016). Improved methodology for the microwave digestion of carbonate-rich environmental samples. *Int. J. Environ. Anal. Chem.* 96, 119–136. doi: 10.1080/03067319.2015.1137904

Durazo-Arvizu, R., and Gaxiola-Castro, G. (2010). *Dinámica del ecosistema pelágico frente a Baja California, 1997–2007. Diez años de investigaciones mexicanas de la Corriente de California*. Mexico, Distrito Federal: INE/CICESE/UABC/SEMARNAT.

Dymond, J., Suess, E., and Lyle, M. (1992). Barium in deep-sea sediment. *A geochemical proxy for paleoproductivity. Paleoceanography Paleoclimatol.* 7, 163–181. doi: 10.1029/92PA00181

Eagle, M., Paytan, A., Arrigo, K. R., van Dijken, G., and Murray, R. W. (2003). A comparison between excess barium and barite as indicators of carbon export. *Paleoceanogr. Paleoclimatol.* 18:1021. doi: 10.1029/2002PA000793

Erickson, B. E., and Helz, G. R. (2000). Molybdenum(VI) speciation in sulfidic waters:: Stability and lability of thiomolybdates. *Geochim. Cosmochim. Acta* 64, 1149–1158. doi: 10.1016/S0016-7037(99)00423-8

Foster, I. D. L., and Walling, D. E. (1994). Using reservoir deposits to reconstruct changing sediment yields and sources in the catchment of the Old Mill Reservoir, South Devon, UK, over the past 50 years. *Hydrol. Sci. J.* 39, 347–368. doi: 10.1080/02626669409492755

Fu, W., Primeau, F., Moore, J. K., Lindsay, K., and Randerson, J. T. (2018). Reversal of increasing tropical ocean hypoxia trends with sustained climate warming. *Global Biogeochem. Cycles* 32, 551–564. doi: 10.1002/2017GB005788

Ganeshram, R. S., and Pedersen, T. F. (1998). Glacial-interglacial variability in upwelling and bioproductivity off NW Mexico: implications for quaternary paleoclimate. *Paleoceanography Paleoclimatol.* 13, 634–645. doi: 10.1029/98PA02508

Garcia, H. E., Locarnini, R. A., Boyer, T. P., and Antonov, J. I. (2006). World Ocean Atlas 2005, Volume 3: Dissolved Oxygen, Apparent Oxygen Utilization, and Oxygen Saturation. S. Levitus, Ed. NOAA Atlas NESDIS 63, U.S. Government Printing Office, Washington, D.C., 342 pp.

Gilly, W. F., Beman, J. M., Litvin, S. Y., and Robison, B. H. (2013). Oceanographic and biological effects of shoaling of the oxygen minimum zone. *Ann. Rev. Mar. Sci.* 5, 393–420. doi: 10.1146/annurev-marine-120710-100849

Griffiths, M. L., Kimbrough, A. K., Gagan, M. K., Drysdale, R. N., Cole, J. E., Johnson, K. R., et al. (2016). Western Pacific hydroclimate linked to global climate variability over the past two millennia. *Nat. Commun.* 7:11719. doi: 10.1038/ncomms11719

Hakspiel-Segura, C., Martínez-López, A., Pinedo-González, P., Verdugo-Díaz, G., and Acevedo-Acosta, J. D. (2016). Composition of metals in suspended particulate matter of Alfonso basin, southern Gulf of California. *Reg. Stud. Mar. Sci.* 3, 144–153. doi: 10.1016/j.rsma.2015.07.001

Hardisty, D. S., Lyons, T. W., Riedinger, N., Isson, T. T., Owens, J. D., Aller, R. C., et al. (2018). An evaluation of sedimentary molybdenum and iron as proxies for pore fluid paleoredox conditions. *Am. J. Sci.* 318, 527–556. doi: 10.2475/05.2018.04

Helz, G. R., Bura-Nakić, E., Mikac, N., and Ciglenečki, I. (2011). New model for molybdenum behavior in euxinic waters. *Chem. Geol.* 284, 323–332. doi: 10.1016/j.chemgeo.2011.03.012

Helz, G. R., Miller, C. V., Charnock, J. M., Mosselmans, F. W., Pattrick, R., Garner, D., et al. (1996). Mechanism of molybdenum removal from the sea and its concentration in black shales: EXAFS evidence. *Geochim. Cosmochim. Acta* 60, 3631–3642. doi: 10.1016/0016-7037(96)00195-0

Hendy, I. L., and Kennett, J. P. (2000). Dansgaard-Oeschger cycles and the California current system: Planktonic foraminiferal response to rapid climate change in Santa Barbara Basin, Ocean Drilling Program Hole 893A. *Paleoceanogr. Paleoclimatol.* 15, 30–42. doi: 10.1029/1999PA000413

Hendy, I. L., and Pedersen, T. F. (2006). Oxygen minimum zone expansion in the eastern tropical North Pacific during deglaciation. *Geophys. Res. Lett.* 33:L20602. doi: 10.1029/2006GL025975

Ho, P., Lee, J.-M., Heller, M. I., Lam, P. J., and Shiller, A. M. (2018). The distribution of dissolved and particulate Mo and V along the U.S. GEOTRACES East Pacific Zonal Transect (GP16): the roles of oxides and biogenic particles in their distributions in the oxygen deficient zone and the hydrothermal plume. *Mar. Chem.* 201, 242–255. doi: 10.1016/j.marchem.2017.12.003

Hofmann, A. F., Peltzer, E. T., Walz, P. M., and Brewer, P. G. (2011). Hypoxia by degrees: establishing definitions for a changing ocean. *Deep Sea Res. Part I Oceanogr. Res. Pap.* 58, 1212–1226. doi: 10.1016/j.dsr.2011.09.004

Holmden, C., Amini, M., and Francois, R. (2015). Uranium isotope fractionation in Saanich Inlet: a modern analog study of a paleoredox tracer. *Geochim. Cosmochim. Acta* 153, 202–215. doi: 10.1016/j.gca.2014.11.012

Hoogakker, B. A. A., Lu, Z., Umling, N., Jones, L., Zhou, X., Rickaby, R. E. M., et al. (2018). Glacial expansion of oxygen-depleted seawater in the eastern tropical Pacific. *Nature* 562, 410–413. doi: 10.1038/s41586-018-0589-x

Howes, E. L., Joos, F., Eakin, C. M., and Gattuso, J.-P. (2015). An updated synthesis of the observed and projected impacts of climate change on the chemical, physical and biological processes in the oceans. *Front. Mar. Sci.* 2:36. doi: 10.3389/fmars.2015.00036

Huang, S., and Conte, M. H. (2009). Source/process apportionment of major and trace elements in sinking particles in the Sargasso sea. *Geochim. Cosmochim. Acta* 73, 65–90. doi: 10.1016/j.gca.2008.08.023

IPCC (2014). Climate Change 2014: Synthesis Report. *Contribution of Working Groups I, II and III to the Fifth Assessment Report of the Intergovernmental Panel on Climate Change [Core Writing Team, R.K. Pachauri and L.A. Meyer (eds.)]. IPCC, Geneva, Switzerland*, 151pp.

Ivanochko, T. S., Calvert, S. E., Southon, J. R., Enkin, R. J., Baker, J., Dallimore, A., et al. (2008). Determining the post-glacial evolution of a northeast Pacific coastal fjord using a multiproxy geochemical approach. *Can. J. Earth Sci.* 45, 1331–1344. doi: 10.1139/E08-030

Ivanochko, T. S., and Pedersen, T. F. (2004). Determining the influences of Late Quaternary ventilation and productivity variations on Santa Barbara Basin sedimentary oxygenation: a multi-proxy approach. *Quat. Sci. Rev.* 23, 467–480. doi: 10.1016/j.quascirev.2003.06.006

Keeling, R. E., Kortzinger, A., and Gruber, N. (2010). Ocean deoxygenation in a warming world. *Ann. Rev. Mar. Sci.* 2, 199–229. doi: 10.1146/annurev.marine.010908.163855

Klinkhammer, G. P., and Palmer, M. R. (1991). Uranium in the oceans: where it goes and why. *Geochim. Cosmochim. Acta* 55, 1799–1806. doi: 10.1016/0016-7037(91)90024-Y

Ku, T.-L., Knauss, K. G., and Mathieu, G. G. (1977). Uranium in open ocean: concentration and isotopic composition. *Deep Sea Res.* 24, 1005–1017. doi: 10.1016/0146-6291(77)90571-9

Lavín, M. F., Castro, R., Beier, E., and Godínez, V. M. (2013). Mesoscale eddies in the southern Gulf of California during summer: characteristics and interaction with the wind stress. *J. Geophys. Res. Oceans* 118, 1367–1381. doi: 10.1002/jgrc.20132

Lehto, N., Glud, R. N., Á., Norð*i, G., Zhang, H., and Davison, W. (2014). Anoxic microniches in marine sediments induced by aggregate settlement: biogeochemical dynamics and implications. *Biogeochemistry* 119, 307–327. doi: 10.1007/s10533-014-9967-0

Levin, L. A. (2018). Manifestation, drivers, and emergence of open ocean deoxygenation. *Ann. Rev. Mar. Sci.* 10, 229–260. doi: 10.1146/annurev-marine-121916-063359

Long, M. C., Deutsch, C., and Ito, T. (2016). Finding forced trends in oceanic oxygen. *Global Biogeochem. Cycles* 30, 381–397. doi: 10.1002/2015GB005310

Lovley, D. R., Phillips, E. J. P., Gorby, Y. A., and Landa, E. R. (1991). Microbial reduction of uranium. *Nature* 350, 413–416. doi: 10.1038/350413a0

Lu, Z., Hoogakker, B. A. A., Hillenbrand, C.-D., Zhou, X., Thomas, E., et al. (2016). Oxygen depletion recorded in upper waters of the glacial Southern Ocean. *Nat. Commun.* 7:11146. doi: 10.1038/ncomms11146

Lynn, R. J., and Simpson, J. J. (1987). The California Current system: the seasonal variability of its physical characteristics. *J. Geophys. Res. Atmos.* 92, 12947–12966. doi: 10.1029/JC092iC12p12947

Lyons, T. W., and Berner, R. A. (1992). Carbon-sulfur-iron systematics of the uppermost deep-water sediments of the Black Sea. *Chem. Geol.* 99, 1–27. doi: 10.1016/0009-2541(92)90028-4

Lyons, T. W., Reinhard, C. T., and Scott, C. (2009). Redox redux. *Geobiology* 7, 489–494. doi: 10.1111/j.1472-4669.2009.00222.x

Lyons, T. W., and Severmann, S. (2006). A critical look at iron paleoredox proxies: new insights from modern euxinic marine basins. *Geochim. Cosmochim. Acta* 70, 5698–5722. doi: 10.1016/j.gca.2006.08.021

Mantua, N. J., and Hare, S. R. (2002). The Pacific decadal oscillation. *J. Oceanogr.* 58, 35–44. doi: 10.1023/A:1015820616384

McKay, J. L., and Pedersen, T. F. (2014). Geochemical response to pulsed sedimentation: implications for the use of Mo as a paleo-proxy. *Chem. Geol.* 382, 83–94. doi: 10.1016/j.chemgeo.2014.05.009

McManus, J., Berelson, W. M., Coale, K. H., Johnson, K. S., and Kilgore, T. E. (1997). Phosphorus regeneration in continental margin sediments. *Geochim. Cosmochim. Acta* 61, 2891–2907. doi: 10.1016/S0016-7037(97)00138-5

McManus, J., Berelson, W. M., Klinkhammer, G. P., Johnson, K. S., Coale, K. H., Anderson, R. F., et al. (1998). Geochemistry of barium in marine sediments: implications for its use as a paleoproxy. *Geochim. Cosmochim. Acta* 62, 3453–3473. doi: 10.1016/S0016-7037(98)00248-8

McManus, J., Berelson, W. M., Severmann, S., Poulson, R. L., Hammond, D. E., Klinkhammer, G. P., et al. (2006). Molybdenum and uranium geochemistry in continental margin sediments: paleoproxy potential. *Geochim. Cosmochim. Acta* 70, 4643–4662. doi: 10.1016/j.gca.2006.06.1564

McPhaden, M. J. (2004). Evolution of the 2002/03 El Niño*. *Bull. Am. Meteorol. Soc.* 85, 677–695. doi: 10.1175/BAMS-85-5-677

Metcalfe, S. E., Barron, J. A., and Davies, S. J. (2015). The Holocene history of the North American Monsoon: 'known knowns' and 'known unknowns' in understanding its spatial and temporal complexity. *Quat. Sci. Rev.* 120, 1–27. doi: 10.1016/j.quascirev.2015.04.004

Moffitt, S. E., Moffitt, R. A., Sauthoff, W., Davis, C. W., Hewett, K., and Hill, T. M. (2015). Paleoceanographic insights on recent oxygen minimum zone expansion: lessons for modern oceanography. *PLoS ONE* 10: e0115246. doi: 10.1371/journal.pone.0115246

Monreal-Gómez, M. A., Molina-Cruz, A., and Salas-de-León, D. A. (2001). Water masses and cyclonic circulation in Bay of la Paz, Gulf of California, during June 1998. *J. Mar. Syst.* 30, 305–315. doi: 10.1016/S0924-7963(01)00064-1

Morford, J. L., and Emerson, S. (1999). The geochemistry of redox sensitive trace metals in sediments. *Geochim. Cosmochim. Acta* 63, 1735–1750. doi: 10.1016/S0016-7037(99)00126-X

Morse, J. W., and Luther, G. W. III. (1999). Chemical influences on trace metal-sulfide interactions in anoxic *sediments*. *Geochim. Cosmochim. Acta* 63, 3373–3378. doi: 10.1016/S0016-7037(99)00258-6

Moy, C. M., Seltzer, G. O., Rodbell, D. T., and Anderson, D. M. (2002). Variability of El Niño/Southern Oscillation activity at millennial timescales during the Holocene epoch. *Nature* 420, 162–165. doi: 10.1038/nature01194

Nameroff, T. J., Calvert, S. E., and Murray, J. W. (2004). Glacial-interglacial variability in the eastern tropical North Pacific oxygen minimum zone recorded by redox-sensitive trace metals. *Paleoceanogr. Paleoclimatol.* 19:PA1010. doi: 10.1029/2003PA000912

Nava-Sánchez, E. H., Gorsline, D. S., and Molina-Cruz, A. (2001). The Baja California peninsula borderland: structural and sedimentological characteristics. *Sediment. Geol.* 144, 63–82. doi: 10.1016/S0037-0738(01)00135-X

Ontiveros-Cuadras, J. F., Thunell, R., Ruiz-Fernández, A. C., Benitez-Nelson, C., Machain-Castillo, M. L., Tappa, E., et al. (2019). Centennial OMZ changes in the NW Mexican Margin from geochemical and foraminiferal sedimentary records. *Cont. Shelf Res.* 176, 64–75. doi: 10.1016/j.csr.2019.02.009

Oschlies, A., Schulz, K. G., Riebessel, U., Schmittner, A. (2008). Simulated 21st century's increase in oceanic suboxia by CO_2-enhanced biotic carbon export. *Global Biogeochem. Cycles* 22:GB4008. doi: 10.1029/2007GB003147

Pérez-Cruz, L. (2013). Hydrological changes and paleoproductivity in the Gulf of California during middle and late Holocene and their relationship with ITCZ and North American Monsoon variability. *Quat. Res.* 79, 138–151. doi: 10.1016/j.yqres.2012.11.007

Pichevin, L., Ganeshram, R. S., Reynolds, B. C., Prahl, F., Pedersen, T. F., Thunell, R., et al. (2012). Silicic acid biogeochemistry in the Gulf of California: Insights from sedimentary Si isotopes. *Paleoceanogr. Paleoclimatol.* 27:PA2201. doi: 10.1029/2011PA002237

Pichevin, L. E., Ganeshram, R. S., Geibert, W., Thunell, R., and Hinton, R. (2014). Silica burial enhanced by iron limitation in oceanic upwelling margins. *Nat. Geosci.* 7, 541–546. doi: 10.1038/ngeo2181

Praetorius, S. K., Mix, A. C., Walczak, M. H., Wolhowe, M. D., Addison, J. A., and Prahl, F. G. (2015). North Pacific deglacial hypoxic events linked to abrupt ocean warming. *Nature* 527, 362–366. doi: 10.1038/nature15753

Raiswell, R., and Canfield, D. E. (2012). The iron biogeochemical cycle past and present. *Geochem. Perspect.* 1, 1–220. doi: 10.7185/geochempersp.1.1

Reck, B. K., Müller, D. B., Rostkowski, K., and Graedel, T. E. (2008). Anthropogenic nickel cycle: insights into use, trade, and recycling. *Environ. Sci. Technol.* 42, 3394–3400. doi: 10.1021/es072108l

Reimer, P. J., Bard, E., Bayliss, A., Beck, J. W., Blackwell, P. G., Ramsey, C. B., et al. (2013). IntCal13 and Marine13 Radiocarbon Age Calibration Curves 0–50,000 Years cal BP. *Radiocarbon* 55, 1869–1887. doi: 10.2458/azu_js_rc.55.16947

Riedinger, N., Brunner, B., Krastel, S., Arnold, G. L., Wehrmann, L. M., Formolo, M. J., et al. (2017). Sulfur cycling in an iron oxide-dominated, dynamic marine depositional system: the Argentine continental margin. *Front. Earth Sci.* 5:33. doi: 10.3389/feart.2017.00033

Riedinger, N., Formolo, M. J., Lyons, T. W., Henkel, S., Beck, A., and Kasten, S. (2014). An inorganic geochemical argument for coupled anaerobic oxidation of methane and iron reduction in marine sediments. *Geobiology* 12, 172–181. doi: 10.1111/gbi.12077

Riedinger, N., Kasten, S., Gröger, J., Franke, C., and Pfeifer, K. (2006). Active and buried authigenic barite fronts in sediments from the Eastern Cape Basin. *Earth Planet. Sci. Lett.* 241, 876–887. doi: 10.1016/j.epsl.2005.10.032

Rodríguez-Castañeda, A. P. (2008). Variación de flujos de los elementos particulados en Cuenca Alfonso, Bahía de La Paz, en el periodo 2002–2005. [Ph.D. dissertation]. [La Paz, Mexico]: Centro Interdisciplinario de Ciencias Marinas – Instituto Politécnico Nacional

Ruiz-Fernández, A. C., Hillaire-Marcel, C., De Vernal, A., Machain-Castillo, M. L., Vásquez, L., Ghaleb, B., et al. (2009). Changes of coastal sedimentation in the Gulf of Tehuantepec, South Pacific Mexico, over the last 100 years from short-lived radionuclide measurements. *Estuar. Coast. Shelf Sci.* 82, 525–536. doi: 10.1016/j.ecss.2009.02.019

Schmidtko, S., Stramma, L., and Visbeck, M. (2017). Decline in global oceanic oxygen content during the past five decades. *Nature* 542, 335–339. doi: 10.1038/nature21399

Schneider, T., Bischoff, T., and Haug, G. H. (2014). Migrations and dynamics of the intertropical convergence zone. *Nature* 513, 45–53. doi: 10.1038/nature13636

Schoepfer, S. D., Shen, J., Wei, H., Tyson, R. V., Ingall, E., and Algeo, T. J. (2015). Total organic carbon, organic phosphorus, and biogenic barium fluxes as proxies for paleomarine productivity. *Earth Sci. Rev.* 149, 23–52. doi: 10.1016/j.earscirev.2014.08.017

Scholz, F. (2018). Identifying oxygen minimum zone-type biogeochemical cycling in Earth history using inorganic geochemical proxies. *Earth Sci. Rev.* 184, 29–45. doi: 10.1016/j.earscirev.2018.08.002

Scholz, F., Hensen, C., Noffke, A., Rohde, A., Liebetrau, V., and Wallmann, K. (2011). Early diagenesis of redox-sensitive trace metals in the Peru upwelling area – response to ENSO-related oxygen fluctuations in the water column. *Geochim. Cosmochim. Acta* 75, 7257–7276. doi: 10.1016/j.gca.2011.08.007

Scholz, F., Siebert, C., Dale, A. W., and Frank, M. (2017). Intense molybdenum accumulation in sediments underneath a nitrogenous water column and implications for the reconstruction of paleo-redox conditions based on molybdenum isotopes. *Geochim. Cosmochim. Acta* 213, 400–417. doi: 10.1016/j.gca.2017.06.048

Scott, C., and Lyons, T. W. (2012). Contrasting molybdenum cycling and isotopic properties in euxinic versus non-euxinic sediments and sedimentary rocks: refining the paleoproxies. *Chem. Geol.* 324–325, 19–27. doi: 10.1016/j.chemgeo.2012.05.012

Shaffer, G., Olsen, S. M., and Pedersen, J. O. P. (2009). Long-term ocean oxygen depletion in response to carbon dioxide emissions from fossil fuels. *Nat. Geosci.* 2, 105–109. doi: 10.1038/ngeo420

Silverberg, N., Aguirre-Bahena, F., and Mucci, A. (2014). Time-series measurements of settling particulate matter in Alfonso Basin, La Paz

Bay, southwestern Gulf of California. *Cont. Shelf Res.* 84, 169–187. doi: 10.1016/j.csr.2014.05.005

Staines-Urías, F., González-Yajimovich, O., and Beaufort, L. (2015). Reconstruction of past climate variability and ENSO-like fluctuations in the southern Gulf of California (Alfonso Basin) since the last glacial maximum. *Q. Res.* 83, 488–501. doi: 10.1016/j.yqres.2015.03.007

Tems, C. E., Berelson, W. M., and Prokopenko, M. G. (2015). Particulate δ15N in laminated marine sediments as a proxy for mixing between the California Undercurrent and the California Current: a proof of concept. *Geophys. Res. Lett.* 42, 419–427. doi: 10.1002/2014GL061993

Tems, C. E., Berelson, W. M., Thunell, R., Tappa, E., Xu, X., Khider, D., et al. (2016). Decadal to centennial fluctuations in the intensity of the eastern tropical North Pacific oxygen minimum zone during the last 1200 years. *Paleoceanography Paleoclimatol.* 31, 1138–1151. doi: 10.1002/2015PA002904

Tetard, M., Licari, L., and Beaufort, L. (2017). Oxygen history off Baja California over the last 80 kyr: a new foraminiferal-based record. *Paleoceanography Paleoclimatol*. doi: 10.1002/2016PA003034

Thunell, R. (1998). Seasonal and annual variability in particle fluxes in the Gulf of California. *A response to climate forcing. Deep Sea Res. Part I Oceanogr. Res. Pap.* 45, 2059–2083. doi: 10.1016/S0967-0637(98)00053-3

Trasviña-Castro, A., Gutierrez De Velasco, G., Valle-Levinson, A., González-Armas, R., Muhlia, A., and Cosio, M. A. (2003). Hydrographic observations of the flow in the vicinity of a shallow seamount top in the Gulf of California. *Estuar. Coast. Shelf Sci.* 57, 149–162. doi: 10.1016/S0272-7714(02)00338-4

Tribovillard, N., Algeo, T. J., Lyons, T., and Riboulleau, A. (2006). Trace metals as paleoredox and paleoproductivity proxies: an update. *Chem. Geol.* 232, 12–32. doi: 10.1016/j.chemgeo.2006.02.012

Tribovillard, N., Bout-Roumazeilles, V., Algeo, T., Lyons, T. W., Sionneau, T., Montero-Serrano, J. C., et al. (2008). Paleodepositional conditions in the Orca Basin as inferred from organic matter and trace metal contents. *Mar. Geol.* 254, 62–72. doi: 10.1016/j.margeo.2008.04.016

Twining, B. S., Baines, S. B., Vogt, S., and Nelson, D. M. (2012). Role of diatoms in nickel biogeochemistry in the ocean. *Glob. Biogeochem. Cycles* 26. doi: 10.1029/2011GB004233

Umling, N. E., and Thunell, R. C. (2017). Synchronous deglacial thermocline and deep-water ventilation in the eastern equatorial Pacific. *Nat. Commun.* 8:14203. doi: 10.1038/ncomms14203

Wedepohl, K. H. (1995). The composition of the continental crust. *Geochim. Cosmochim. Acta* 59, 1217–1232. doi: 10.1016/0016-7037(95)00038-2

Wignall, P. B., and Myers, K. J. (1988). Interpreting benthic oxygen levels in mudrocks: a new approach. *Geology* 16:452–455. doi: 10.1130/0091-7613(1988)016<0452:IBOLIM>2.3.CO;2

World Ocean Atlas (2005). http://www.nodc.noaa.gov/OC5/WOA05/pr_woa05.html

Wright, J. J., Konwar, K. M., and Hallam, S. J. (2012). Microbial ecology of expanding oxygen minimum zones. *Nat. Rev. Microbiol.* 10, 381–394. doi: 10.1038/nrmicro2778

Yan, H., Sun, L., Wang, Y., Huang, W., Qiu, S., and Yang, C. (2011). A record of the Southern Oscillation Index for the past 2,000 years from precipitation proxies. *Nat. Geosci.* 4, 611–614. doi: 10.1038/ngeo1231

Zheng, Y., Anderson, R. B., Van Geen, A., and Fleisher, M. Q. (2002). Preservation of particulate non-lithogenic uranium in marine sediments. *Geochim. Cosmochim. Acta* 66, 3085–3092. doi: 10.1016/S0016-7037(01)00632-9

Zheng, Y., Anderson, R. B., Van Geen, A., and Kuwabara, J. (2000). Authigenic molybdenum formation in marine sediments: a link to pore water sulfide in Santa Barbara Basin. *Geochim. Cosmochim. Acta* 64, 4165–4178. doi: 10.1016/S0016-7037(00)00495-6

Conflict of Interest Statement: The authors declare that the research was conducted in the absence of any commercial or financial relationships that could be construed as a potential conflict of interest.

frontiers in Marine Science

ORIGINAL RESEARCH
published: 16 October 2019
doi: 10.3389/fmars.2019.00617

Dynamics of the Carbonate System Across the Peruvian Oxygen Minimum Zone

Jose M. Hernandez-Ayon[1], Aurélien Paulmier[2], Veronique Garcon[2], Joel Sudre[2], Ivonne Montes[3], Cecilia Chapa-Balcorta[4], Giovanni Durante[1], Boris Dewitte[2,5,6,7], Cristophe Maes[2,8] and Marine Bretagnon[2]*

[1] Instituto de Investigaciones Oceanológicas, Universidad Autónoma de Baja California, Ensenada, Mexico, [2] LEGOS, CNRS/IRD/UPS/CNES UMR 5566, Université de Toulouse, Toulouse, France, [3] Instituto Geofisico del Peru, Lima, Peru, [4] Facultad de Ciencias Marinas, Universidad del Mar, Oaxaca, Mexico, [5] Centro de Estudios Avanzado en Zonas Áridas (CEAZA), Coquimbo, Chile, [6] Departamento de Biología, Facultad de Ciencias del Mar, Universidad Católica del Norte, Coquimbo, Chile, [7] Millennium Nucleus for Ecology and Sustainable Management of Oceanic Islands (ESMOI), Coquimbo, Chile, [8] LOPS (Univ. Brest/IRD/CNRS/IFREMER), Plouzané, France

OPEN ACCESS

Edited by:
Wolfgang Koeve, GEOMAR Helmholtz Center for Ocean Research Kiel, Germany

Reviewed by:
Raffaele Bernardello, Barcelona Supercomputing Center, Spain
John Patrick Dunne, Geophysical Fluid Dynamics Laboratory (GFDL), United States

***Correspondence:**
Jose M. Hernandez-Ayon
jmartin@uabc.edu.mx

Specialty section:
This article was submitted to Marine Biogeochemistry, a section of the journal Frontiers in Marine Science

Received: *10 August 2018*
Accepted: *18 September 2019*
Published: *16 October 2019*

Citation:
Hernandez-Ayon JM, Paulmier A, Garcon V, Sudre J, Montes I, Chapa-Balcorta C, Durante G, Dewitte B, Maes C and Bretagnon M (2019) Dynamics of the Carbonate System Across the Peruvian Oxygen Minimum Zone. Front. Mar. Sci. 6:617. doi: 10.3389/fmars.2019.00617

The oxygen minimum zone (OMZ) of Peru is recognized as a source of CO_2 to the atmosphere due to upwelling that brings water with high concentrations of dissolved inorganic carbon (DIC) to the surface. However, the influence of OMZ dynamics on the carbonate system remains poorly understood given a lack of direct observations. This study examines the influence of a coastal Eastern South Pacific OMZ on carbonate system dynamics based on a multidisciplinary cruise that took place in 2014. During the cruise, onboard DIC and pH measurements were used to estimate pCO_2 and to calculate the calcium carbonate saturation state (Ω aragonite and calcite). South of Chimbote (9°S), water stratification decreased and both the oxycline and carbocline moved from 150 m depth to 20–50 m below the surface. The aragonite saturation depth was observed to be close to 50 m. However, values <1.2 were detected close to 20 m along with low pH (minimum of 7.5), high pCO_2 (maximum 1,250 μatm), and high DIC concentrations (maximum 2,300 μmol kg^{-1}). These chemical characteristics are shown to be associated with Equatorial Subsurface Water (ESSW). Large spatial variability in surface values was also found. Part of this variability can be attributed to the influence of mesoscale eddies, which can modify the distribution of biogeochemical variables, such as the aragonite saturation horizon, in response to shallower (cyclonic eddies) or deeper (anticyclonic eddies) thermoclines. The analysis of a 21-year (1993–2014) data set of mean sea surface level anomalies (SSHa) derived from altimetry data indicated that a large variance associated with interannual timescales was present near the coast. However, 2014 was characterized by weak Kelvin activity, and physical forcing was more associated with eddy activity. Mesoscale activity modulates the position of the upper boundary of ESSW, which is associated with high DIC and influences the carbocline and aragonite saturation depths. Weighing the relative importance of each individual signal results in a better understanding of the biogeochemical processes present in the area.

Keywords: OMZ, DIC, pH, omega aragonite, upwelling peruvian system

INTRODUCTION

The upwelling region of Peru is one of the most important upwelling systems in the world due to its high productivity that supports abundant fisheries, particularly the Peruvian anchovy fishery (Chavez et al., 2008; Espinoza-Morriberon et al., 2017). Upwelling events mainly occur in spring and summer (Sobarzo and Djurfeldt, 2004; Franco et al., 2018). However, large and productive areas with important fisheries like Peru are considered to be zones that currently experience or that are projected to experience ocean acidification (Shen et al., 2017). The intense biological activity present in these areas produces a large quantity of organic matter (OM), some of which sinks and is degraded by catabolic processes (Bretagnon et al., 2018). Therefore, subsurface OM degradation contributes to the consumption of oxygen (O_2) and in conjunction with poor water mass ventilation, leads to the formation of an oxygen minimum zone (OMZ; Paulmier et al., 2008). The Peruvian OMZ presents a poorly oxygenated core (O_2 down to <1 μmol kg^{-1}: Revsbech et al., 2009), with significant anaerobic activity (e.g., Hamersley et al., 2007) that occurs in the thickest core (340 m in average; Paulmier et al., 2008).

Various studies have shown the existence of intense biogeochemical anomalies (e.g., in O_2, CO_2, pH, alkalinity, nitrate, nitrite, and N_2O) associated with microorganism (e.g., bacteria) as well as mesoorganism and microorganism (e.g., zooplankton) processes that take place near the oxycline. The seasonal cycle of O_2/oxycline depth is very weak when compared with that of interannual timescales. The OMZ off Peru is characterized by notable interannual variability that is particularly evident with regard to depth, an example of which is the 100 m deepening of the oxycline that is associated with trapped Kelvin waves and which is particularly apparent during El Niño events (Gutiérrez et al., 2011). Furthermore, primary production is 2- to 3-fold higher in summer than in winter (Graco et al., 2007). The Peruvian upwelling region is also considered to be a source of CO_2 to the atmosphere, with an estimated annual flux of 5.7 mol m^{-2} y^{-1} (Friederich et al., 2008).

In the Peruvian region, the OMZ is associated with high dissolved inorganic carbon (DIC) concentrations (mean of 2,330 ± 60 μmol kg^{-1}) and is defined as a carbon maximum zone (CMZ). High DIC concentrations (2,225–2,350 μmol kg^{-1}) have been reported over the entire OMZ, indicating that all studied OMZs may be classified as CMZs (Paulmier et al., 2011). In addition, the existence of the CMZ suggests that it is being formed by the same dynamics (low ventilation and upwelling) and biogeochemical (remineralization that produces DIC and consumes O_2) mechanisms (Paulmier et al., 2011) as an OMZ. Surface pCO_2 values in coastal regions can reach 1,500 μatm in subsurface waters, as can be observed in the California Current (Feely et al., 2008; Takahashi et al., 2009). However, in the Peruvian upwelling system, pCO_2 values that exceed those of other upwelling systems can be found in surface water (Friederich et al., 2008; Shen et al., 2017). When the ocean absorbs more CO_2, extremely high pCO_2 values (e.g., >1,000 μatm) imply a decrease in pH. "Hotspots" of acidification, like the Peruvian regions, are thus predicted to occur in major fishery zones by mid-century when atmospheric CO_2 is projected to reach 650 μatm (McNeil and Sasse, 2016; Shen et al., 2017). In addition, ocean acidification modeling studies based on the oceanic uptake of anthropogenic CO_2 indicate that the upper water of the Humboldt Current is likely to become more corrosive with regard to mineral $CaCO_3$ (Franco et al., 2018).

Biomineral saturation, such as omega calcite (Ω_{calc}) and omega aragonite (Ω_{arag}), is a function of the concentration of CO_3^{2-}, Ca^{2+}, and temperature and may be expressed with the pressure-dependent stoichiometric solubility product K^*_{sp} ($\Omega = [Ca^{2+}]\ [CO_3^{2-}]/K^*_{sp}$; Mucci, 1983). The aragonite and calcite saturation states respond directly to changes in the availability of the CO_3^{2-} ion. If the ocean absorbs more CO_2, pH decreases and Ω_{arag} and Ω_{calc} also decrease. For example, when $\Omega = 1$, seawater is saturated with respect to CO_3^{2-}. Conditions favor precipitation or the preservation of carbonate minerals when $\Omega > 1$, while conditions favor dissolution when $\Omega < 1$. If the aragonite and calcite saturation states decrease, greater physiological challenges for calcifying organisms are expected to be present (Fabry et al., 2008; Guinotte and Fabry, 2008). Often, large fisheries are present in regions in which ocean acidification has already occurred or is expected to occur (Shen et al., 2017). For example, the Peruvian anchovy (*Engraulis ringens*) is found in a region where the pCO_2 values can be higher than 1,000 ppm (Friederich et al., 2008). Furthermore, eggs from Peruvian anchovies that spawned in waters with high pCO_2 were found to have survival rate (Shen et al., 2017).

Coastal zones are connected to ocean areas in which OMZs are expanding (Stramma et al., 2008). Therefore, it is important to generate a better understanding of the different components of the carbon system that are involved in the formation and maintenance of OMZs. Very little is known about ocean acidification in Peruvian regions. Moreover, the mechanisms behind the existence of such an intense CO_2 maximum and its relationship with physical and biochemical processes must be elucidated. We evaluated the relevant physical processes that influence the spatial variability of carbonate chemistry and the aragonite saturation state of the Peruvian coastal region. We describe the patterns of relevant water masses with low pH and oxygen concentrations. In particular, we describe shoaling due to mesoscale activity that modulates the position of the upper boundary of the water masses. This shoaling is associated with high DIC and influences the carbocline and aragonite saturation depths. Our oceanographic and biogeochemical data show the effects of physical processes on the spatial and vertical distribution of the CO_2 variables. Due to the shallow OMZ and CMZ in the Peruvian upwelling system, this region can be considered a natural laboratory for investigations that are focused on the CO_2 system.

METHODS

Oceanographic sampling was carried out aboard the RV L'Atalante (**Figure 1**). The AMOP cruise was planned as a round trip from Callao that departed on January 26 and arrived on February 22, 2014. The first sampling stations were

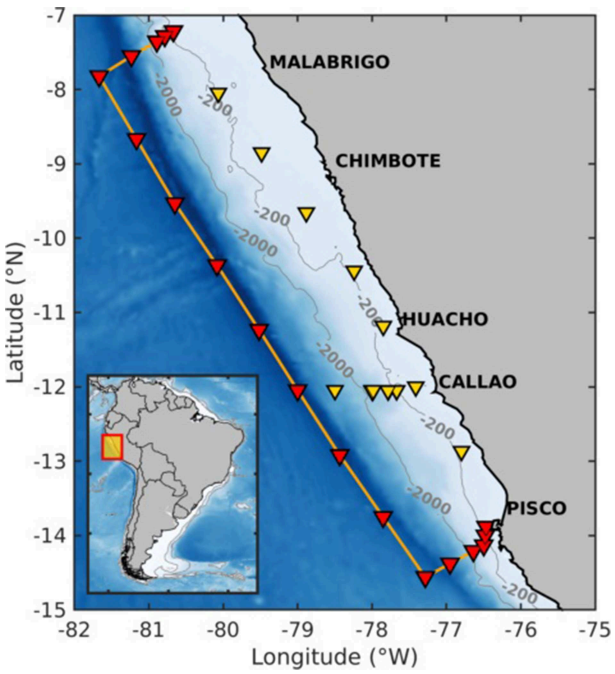

FIGURE 1 | Hydrographic casts in the study region over a bathymetric map of Peru. Yellow and red triangles depict stations with water sampling for chemical analysis, while the yellow line indicates the main offshore transect.

located near the coast. By following the 12°S transect, the cruise continued northward and sampled the water column in typical offshore stations (0–2,000 m depth). After which, the vessel returned to sample coastal stations following the main gradient of the bathymetry. The ship then headed southward to sample stations along the shelf (typical maximum depths of ∼150 m) until the vessel reached the Pisco sector (15°S). The last offshore transect was then sampled up to station 28 (14°34′S–77°16′W), which represents the southernmost point of the cruise (Maes et al., 2014).

Discrete samples for DIC and pH analysis were collected over depth gradients at coastal and offshore sites in the Peruvian OMZ area. A total of 31 station profiles of ∼500 meters depth were generated. At each station, vertical profiles were produced using standard oceanographic equipment (CTD-rosette at most stations). Seawater samples for DIC and pH samples were collected by a rosette casts covering the low-oxygen water with an average of 12 depths targeting the key water column features of the oxic photic zone, oxycline (upper), OMZ interface, and anoxic OMZ core.

Water samples for DIC analysis were collected in 250-ml sodium borosilicate bottles and preserved with 50 µl of $HgCl_2$ saturated solution. For pH analysis, the samples were collected directly from the Niskin bottles using 60-ml syringes. All samples were analyzed aboard the ship. For DIC analysis, a LI-7000 gas analyzer (CO_2/H_2O, LICOR, Lincoln, NE, USA) was used. The certificate reference material for DIC analysis was provided by the laboratory of Dr. Andrew Dickson of Scripps Institution of Oceanography (Dickson et al., 2003). The relative difference averaged ±2 µmol kg^{-1} (0.2% error).

The pH was measured using a glass electrode at 25°C on the seawater scale (pHsw) as described by Chapa-Balcorta et al. (2015). We use the program CO2SYS (Lewis and Wallace, 1998) and DIC-pH_{sw} to calculate pCO_2, *in situ* pHsw, and the aragonite saturation state (Ω_{Arg}). We use the constants proposed by Mehrbach et al. (1973) for these calculations. The uncertainty obtained for *in situ* pH_{sw}, Ω_{Arg}, and pCO_2 was ± 0.04 ± 0.2, and 56 µatm, respectively. The pCO_2 variability range observed in Peruvian waters was 25-fold greater than the error.

Wind Data

Wind speed data were obtained from the SeaWinds database provided by NOAA (Zhang et al., 2006a,b). Wind stress was computed using the bulk equation (Schwing et al., 1996). Monthly means of the wind speed field were also derived from the Copernicus level 4 multi-sensor blended wind product.

Vertical Velocities Due to Wind Stress Curl and Ekman Transport

The curl-driven vertical velocities (w_c) and coastal upwelling associated with Ekman offshore transport (w_e) at the limit of the mixed layer were estimated following Rykaczewski et al. (2015) using Equations (1) and (2):

$$w_c = \frac{1}{\rho_w f} \nabla_h \times \tau \quad (1)$$

$$w_e = \frac{\tau_a}{\rho_w f\, Rd} \quad (2)$$

where $\rho_w = 1{,}024\,\mathrm{kg\ m^3}$ is the seawater density, f is the coriolis parameter, τ is the wind stress vector field, τ_a is the wind stress parallel to the coastline, and Rd is the local Rossby radius of deformation. Note that using Rd to convert Ekman transport in upwelling rate yields an estimate that is in the low range values of the actual amplitude of vertical velocity since the upwelling scale is smaller than Rd [cf. Marchesiello and Estrade (2010)].

Variability of Sea Surface Height Anomalies

In order to calculate the relative importance of the different scales of variability for sea surface height anomalies (SSHa) in the study area, the seasonal, interannual, and mesoscale signals were derived following the methods of Godínez et al. (2010) and León-Chávez et al. (2015). A 21-year database (1993–2014) of mean SSHa distributed by AVISO was used (http://www.aviso.altimetry.fr).

The seasonal, mesoscale, and interannual signals were separated. The first was obtained using a harmonic fit, while the second and third were obtained by means of orthogonal empirical functions (Equations 3 and 4).

$$SSHa(\vec{x},t) = A_a(\vec{x})\cos(\omega t - \varphi_a(\vec{x})) + A_s(\vec{x})\cos(2\omega t - \varphi_s(\vec{x})) + F_1(\vec{x})f_1(t) + \sum_{n=2}^{N} F_n(\vec{x})f_n(t) \quad (3)$$

$$SSHa(\vec{x},t) = SSHa_{season}(\vec{x},t) + SSHa_{inter}(\vec{x},t) + SSHa_{meso}(\vec{x},t) \quad (4)$$

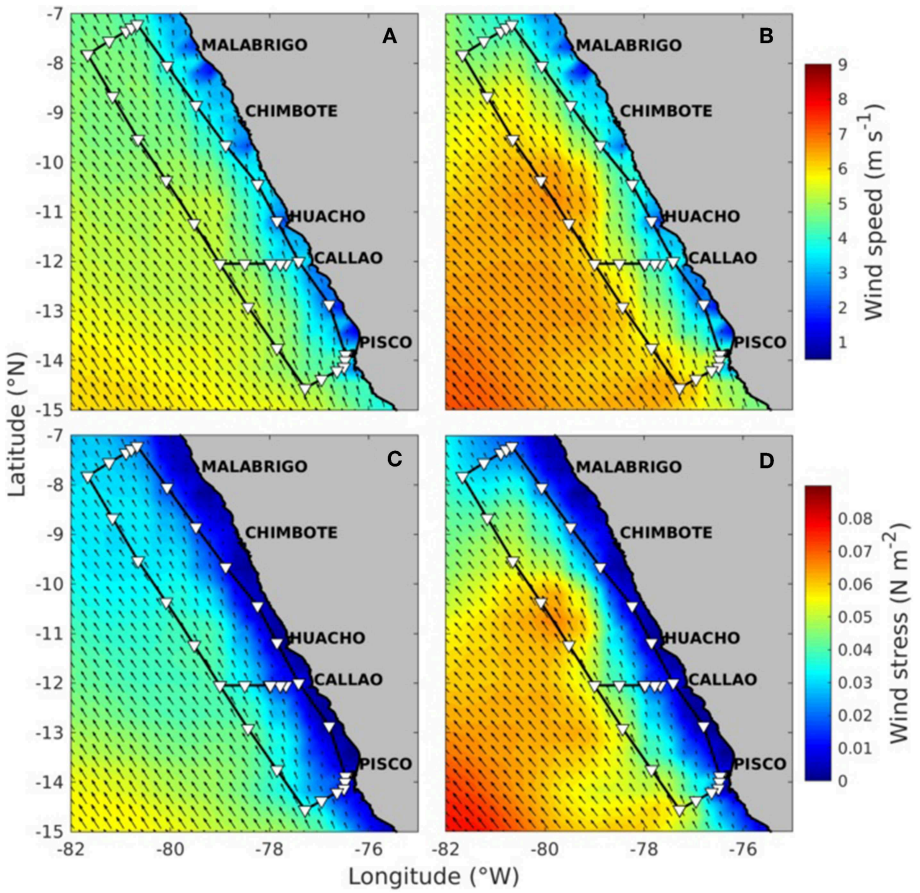

FIGURE 2 | Wind speed data were obtained from the NOAA SeaWinds database. The upper panels show the January **(A)** and February **(B)** 2014 monthly mean of the wind speed field derived from the Copernicus level 4 multi-sensor blended wind product. Lower panels show wind stress field monthly mean for January **(C)** and February **(D)** 2014.

A_a and A_s are the annual and semi-annual amplitudes of the harmonic fit, respectively, while $\vec{x}$ is the spatial vector, φ_a and φ_s are the annual and semi-annual phases, ω is the annual radian frequency, t is the time referred to the beginning of the year, and n is the number of EOF. The first two terms on the right of Equation (3) are the seasonal components ($SSHa_{season}$ is the first term in Equation 4), which were calculated using a least squares fitting. Fitting errors and uncertainties were calculated as in previous studies (Prentice et al., 2001; Ripa, 2002). $F_1(\vec{x})$ and $f_1(t)$ are the spatial and temporal series of the first EOF mode, which in the South Equatorial Tropical Pacific (SETP) typically contain the interannual signal ($SSHa_{inter}$ in Equation 4) that is characterized by ENSO-induced variability (Macharé and Ortlieb, 1993). In the last term of Equation (3), $F_n(\vec{x})$ and $f_n(t)$ are the spatial and temporal series of the nth EOF mode. The sum of these (2 to N) mainly contains mesoscale variability ($SSHa_{meso}$, third term of Equation 4), although it may include some interannual variability not captured by the first EOF. Analyzing this information enables us to identify the dominant processes in the region in general as well as during the time of our cruise, allowing us to weigh the significance of the measurements according to the predominant signal type. The local variance (LV) of each variability component (seasonal, interannual, and mesoscale) was calculated as follows:

$$LV_{season} = \frac{\sigma^2_{SSHa\ season} * 100}{\sigma^2_{SSHa}} \quad (5)$$

where LV_{season} indicates local variance, $\sigma^2_{SSHa_{season}}$ is the variance of the seasonal component of SSHa, and σ^2_{SSHa} is the variance of the original SSHa. LV was calculated per pixel for each time series. The same procedure was used for the interannual and mesoscale components. The complete series was used for this calculation (1992–2015). The signal decomposition during the cruise was obtained by reconstructing SSHa data of the separated variability scales for the dates corresponding to the sampling periods. The seasonal data were reconstructed from the harmonic analysis. The interannual data were reconstructed from the first EOF. The mesoscale data were constructed from the sum of the EOF from 2 to N.

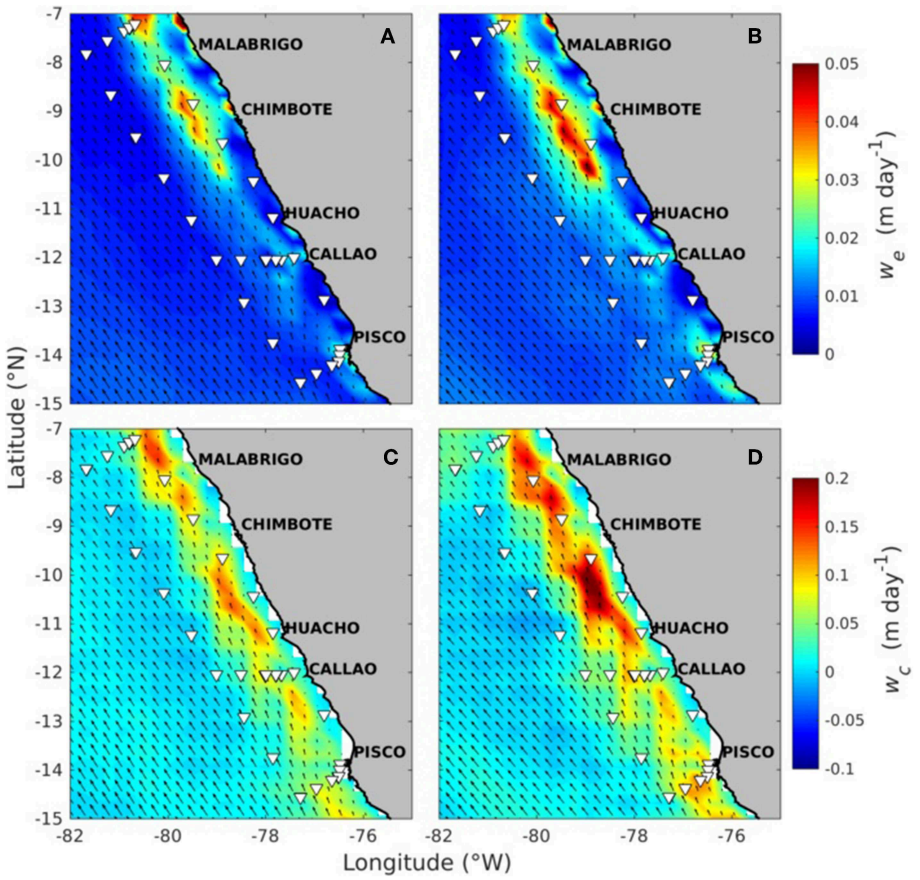

FIGURE 3 | The **(A,B)** show the mean vertical velocities associated with Ekman transport (w_e) for January and February, respectively (upper color scale). In the lower panels, monthly vertical transport (w_c) means due winds stress curl are shown (lower color scale) for January **(C)** and February **(D)**. For all the panels in this figure, the black arrows represent the mean wind stress vectors for the respective month.

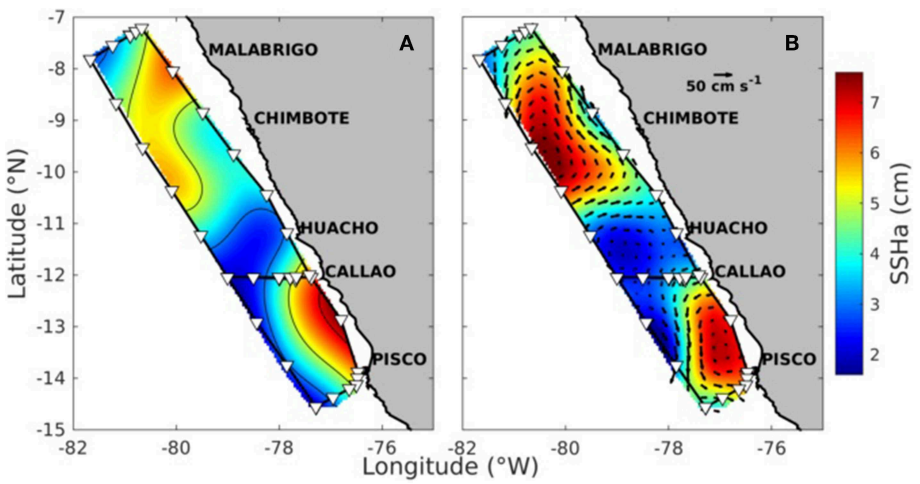

FIGURE 4 | (A) shows objectively interpolated SSHa values at the sampling date in a given position. **(B)** shows February 2014 mean SSHa in the color scale, and the black arrows represent the mean geostrophic velocity ($cm\ s^{-1}$).

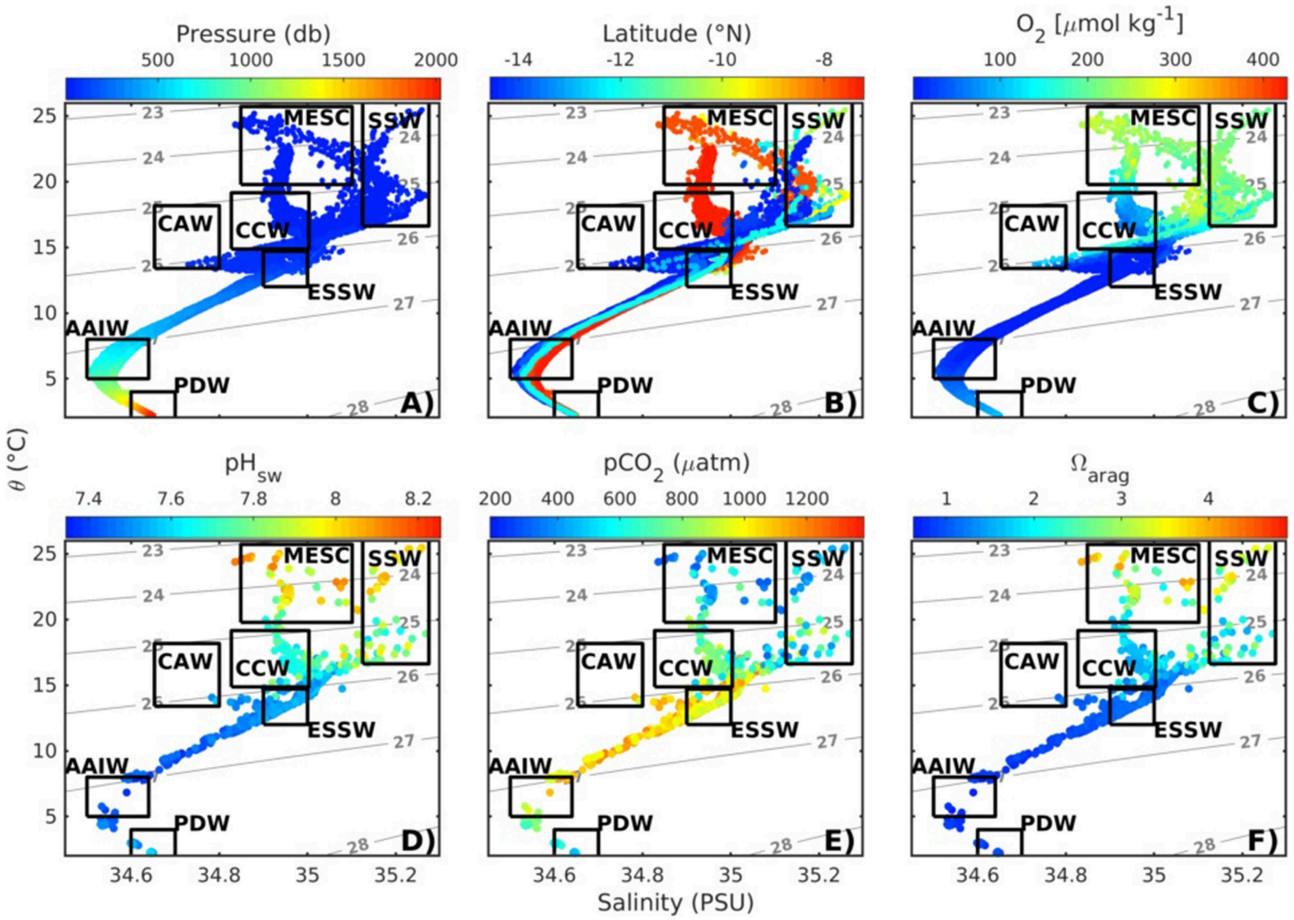

FIGURE 5 | Potential temperature and salinity diagram for the cruise. The color bar for each plot indicates **(A)** depth, **(B)** latitude, **(C)** oxygen, **(D)** pH_{SW}, **(E)** *in situ* pCO_2, and **(F)** omega aragonite. The water masses were detected based on the criteria of Silva and Neshyba (1976) and were Surface Subtropical Water (SSW), Equatorial Subsurface Water (ESSW), Antarctic Intermediate Water (AAIW), and Pacific Deep Water (PDW). The observed water types observed were Cold Coastal Water (CCW); Mixed Equatorial, Subtropical and Coastal Water (MESC); and Coastal Antarctic Water (CAW). CAW was reported by Swartzman et al. (2008).

Inferred Sea Surface Height Anomalies

With a deep level of no motion in the offshore transect (1,000 db), we used T and S to calculate density and thus inferred sea surface height anomalies, which we compared to the AVISO satellite product. The dynamic height calculation was performed using the functions of the TEOS-10 library (McDougall and Barker, 2011). The measured salinity and temperature data were interpolated vertically with an interval of 1 m using the objective interpolation of Barnes (1964).

RESULTS

We provide a description of the circulation patterns that drive the physical and biogeochemical patterns observed in the study region during the cruise, and we use this as a frame of reference to define the importance of each water mass in the region. We also provide a description of the oceanographic conditions during the cruise, which is interpreted considering the analysis of altimeter data to estimate anomalous conditions in seasonal and interannual timescales.

Wind, Wind Stress Curl, and Ekman Transport Conditions

At the beginning of the sampling period in January 2014, the wind speed was <5 m s^{-1} throughout the coastal area spanning from Pisco to Malabrigo. The wind speed was stronger offshore and presented values of 6–7 m s^{-1} (**Figures 2A,B**). The most intense winds 10 m s^{-1} were observed offshore in February, although winds of 7 m s^{-1} were observed in the coastal region near Pisco. During the January sampling period, the winds oscillated from $\sim$3 to 5 m s^{-1} and produced relatively weak upwelling compared to the remainder of the period (**Figure 2C**). Stronger yet opposite wind stress can be observed in February (**Figure 2D**). The combination of calm (**Figure 2A**) and subsequently strong winds (**Figure 2B**) produced different oceanographic conditions; namely, regions with high vertical mixing and areas with coastal upwelling (**Figure 3**). The mean vertical velocities associated with Ekman transport and the monthly vertical transport means due to winds stress curl for January and February are presented in **Figure 3**. Of note, February presented the highest Ekman offshore transport and

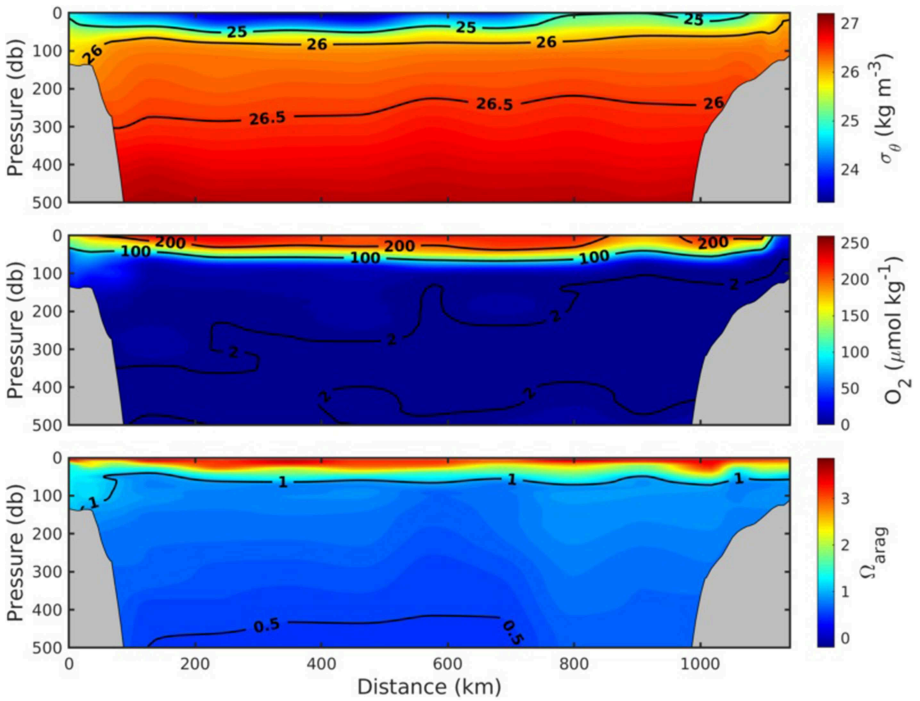

FIGURE 6 | Vertical distribution of the potential density anomaly (σ_θ, kg/m^3), dissolved oxygen (DO, μmol kg^{-1}), and omega aragonite (Ω_{arag}) along the transect.

vertical transport values. However, the vertical transport near to Chimbote did not occur because of the presence of an anticyclone eddy (**Figure 4**).

Variability in Sea Surface Height Anomalies

The SSHa in the study area for January and February 2014 are shown in **Figure 4**. The cruise track variability that was attributed to mesoscale eddies during February was present during the anticyclonic eddy from Malabrigo to the middle of Huacho for both odd shore and coastal stations. In front of Huacho and to the north of Callao, cyclonic eddy influence may be observed in both January and February (**Figures 4A,B**). While the effect of each of the conditions on the chemistry of the CO_2 system will be described later, the spatial distribution of the CO_2 variables was directly associated with the various oceanographic conditions.

Water Masses, Water Types, and Vertical Structure

The distribution of water masses was examined to analyze the potential effects on the carbonate chemistry in the study area. We also found it very useful to study the water-type distribution because of the broad T-S variability. The T-S plot in **Figure 5** incorporates several characteristics for comparison on the Z axis, such as latitudinal distribution, oxygen concentration, pH_{SW}, pCO_2, and omega aragonite (Ω_{Arg}). The T–S diagrams for all sections in the study area indicate the presence of four water masses in the first 500 m based on the classifications of Silva and Neshyba (1976), Silva et al. (2009). In addition, three water types were observed as defined by the conditions of Swartzman et al. (2008). The water masses that were detected were Subtropical Surface Water (SSW), Equatorial Subsurface Water (ESSW), Antarctic Intermediate Water (AAIW), and Pacific Deep Water (PDW). The water types that were observed were Cold Coastal Water (CCW); Mixed Equatorial, Subtropical and Coastal Water (MESC); and Coastal Antarctic Water (CAW). The CAW reported by Swartzman et al. (2008) was detected as a small intrusion between 55 and 80 m.

In surface waters, MESC and SSW were detected in the first 25 m (**Figure 5A**). MESC is less salty and it was located north of 8°N, while SSW had salinities >35 and was observed south of 12°N (**Figure 5B**). The corresponding MESC values following 24 kg m^{-3} isopycnal (located in <10 m) for oxygen, pH, pCO_2, and Ω_{arag} were 250 μmol Kg^{-1}, ~8.1, <500 μatm, and >3.5 units, respectively. The values for SSW between 10 and 60 m for the 25 kg m^{-3} isopycnal were >200 μmol Kg^{-1}, >7.8, ~550 μatm, and >2.0 units (**Figure 5**). CCW located below MESC was also found at 8°N between 20 and 60 m depth (**Figures 5A,B**). When following the 25 kg m^{-3} isopycnal in <20 m depth, the average values of CCW characteristics indicated that this water type presented less oxygen, lower pH, higher pCO_2, and lower Ω_{arag} (close to zero to 50 μmol Kg^{-1}, ~7.7, <1,000 μatm, and <2.0, respectively) when compared to that of MESC. The water type CAW was observed between 55 and 80 m. This water mass presented the lowest oxygen concentrations, low pH, higher pCO_2, and low Ω_{arag} (0 and 20 μmol kg^{-1}, ~7.7, >1,300 μatm, and <2.0, respectively). In subsurface waters, the main water mass of the OMZ and CMZ in the study area considering the observed characteristics (low

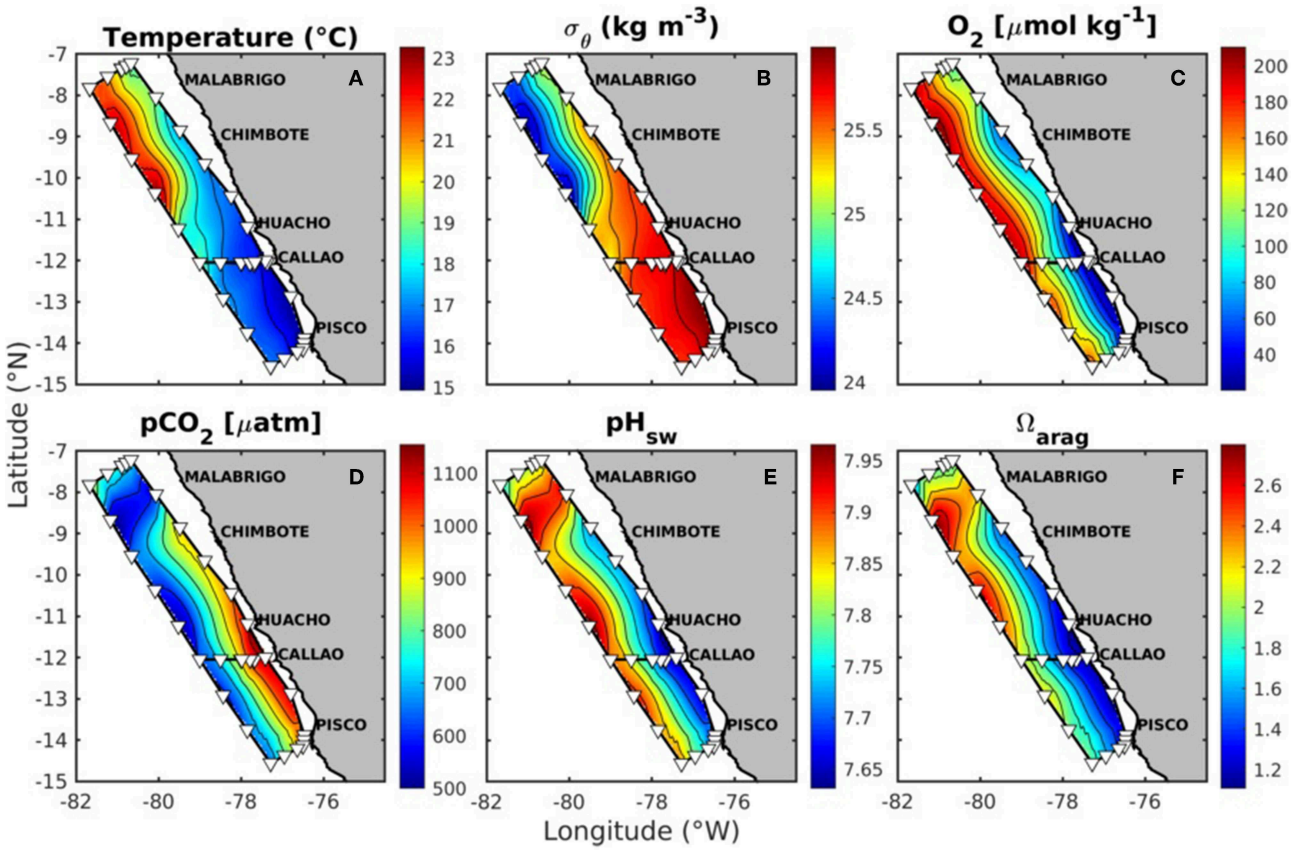

FIGURE 7 | Surface distribution maps of physical and chemical variables at 30 m depth. Top panels show **(A)** temperature, **(B)** density, and **(C)** oxygen. Bottom panels show **(D)** derived *in situ* pCO_2 (pH-DIC), **(E)** *in situ* pH_{SW}, and **(F)** omega aragonite (Ω_{arag}).

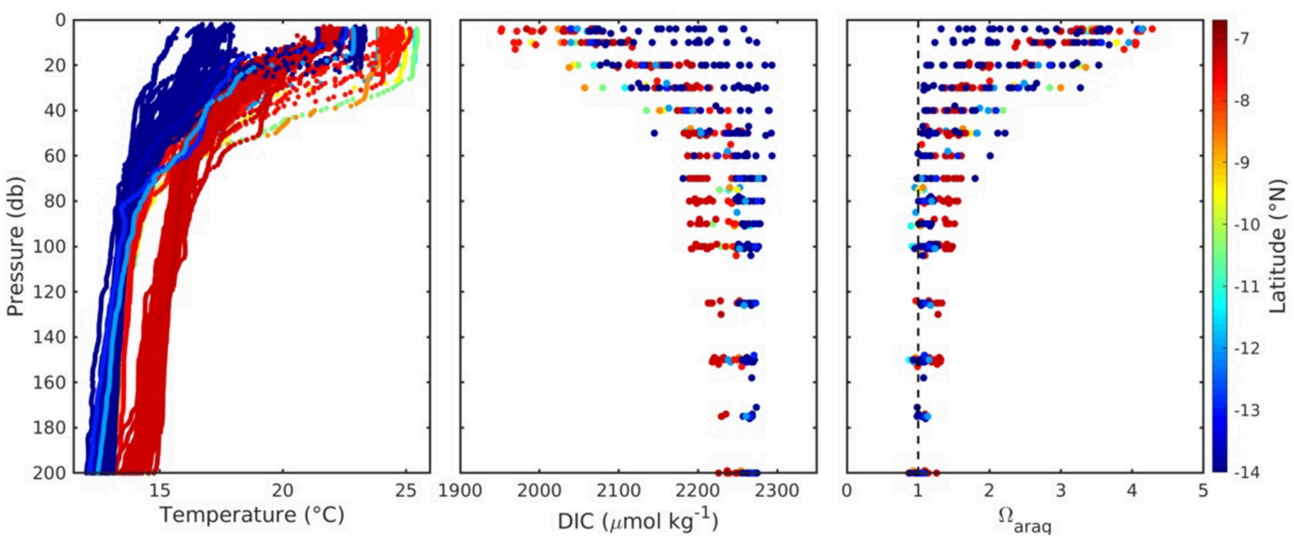

FIGURE 8 | Profiles of temperature (°C), dissolved inorganic carbon (DIC), and omega aragonite (Ω_{arag}). The color bar represents the latitude for all of the plots and the black dashed line for omega aragonite indicates the saturation value ($\Omega_{arag} = 1$).

oxygen and pH and high pCO_2 and DIC) was ESSW. The upper ESSW limit presented a potential density anomaly of 26 kg m^{-3} (**Figure 5**) in the offshore transect, and this isopycnal was found at ~70 m depth (**Figure 6**). However, the isopycnal was found at ~30 m near the coast at 14°S. The oxygen concentration declined to <20 μmol kg^{-1} at this depth but also presented pH values of 7.7 and <1.5 units for Ω_{arag} (**Figure 6**).

Figure 7 presents the spatial distribution at 30 m for temperature, density, oxygen, pCO_2, pH, and omega aragonite. With the exception of a few stations located in the offshore region between 8 and 11°S, the area was influenced by subsurface waters and was therefore characterized by low concentrations of oxygen (<10 μmol kg^{-1}), subsaturation values of omega aragonite (~1 near the coast Callao-Pisco), low pH (<7.5), and high pCO_2 (values from ~ 500 to 1,200 μatm). The highest values of pCO_2 were observed in the coastal region between Callao and Pisco at the southern end of the transect.

Vertical Mixing

Two different oceanographic scenarios were found during the cruise and consisted of the presence or absence of upwelling. The wind stress near the coast was low during January (<0.03 N m^{-2}) prior to sampling (**Figures 2**, **3**) and presented wind speed values <3 ms^{-1}. However, in February, the monthly wind speed mean was 7 ms^{-1} while the wind stress was ~0.07 N m^{-2}. In February we found the highest values for both Ekman offshore transport and vertical transport (**Figure 3**). During February, the upper ESSW limit was found near the surface between 20 and 50 m depth in the coastal area between 12 and 14°S. The lowest surface temperatures (~17°C), lower oxygen concentrations (<100 μmol kg^{-1}), the highest surface DIC concentrations (~2,300 μmol kg^{-1}), and low omega aragonite values (<1.5) were present at ~20 m depth (**Figure 8**).

During the cruise, weakly stratified regions were identified based on temperature profiles with a N-S gradient (**Figure 8**). The stratification parameter was calculated according to Simpson (1981) for the upper 300 m of the water column. This value expressed in J m^{-3} and represents the amount of work per volume that is needed to mix the water column to a specified depth. The lowest stratification values were detected (<200 J m^{-3}) between 11 and 15°S near the upwelling area found between Callao and Pisco (see vertical profiles in **Figure 8**). However, higher stratification values (>400 J m^{-3} were found between 8 and 11°S. For all sampled areas, the calculated stratification average was 350 J m^{-3}. This combination of upwelling and stratification plays an important role in the spatial and vertical distribution of DIC, omega aragonite, oxygen, and temperature.

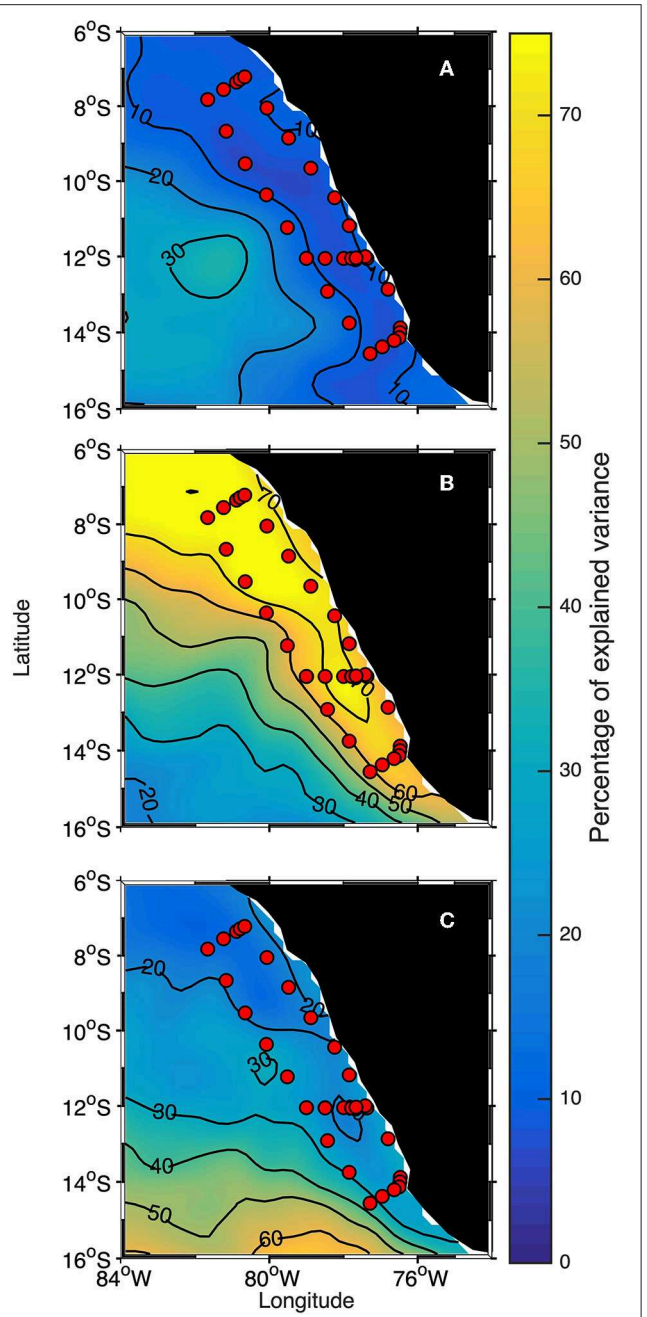

FIGURE 9 | Variance of the sea level anomaly for the three time scales: **(A)** seasonal, **(B)** interannual, and **(C)** mesoscale.

Circulation Based on SSHa Variability Scales

The decomposition of SSHa variability for the Peruvian area based on 21 years of AVISO data shows that the interannual signal is dominant (~30–80%), followed by the mesoscale signal (20–60%), and finally the seasonal signal (~7 and 30%; **Figure 9**). However, the cruise took place during a normal year. The seasonal cycle presented weak variance, which is consistent with previous studies in the eastern tropical Pacific (Takahashi et al., 2011).

Seasonality between 6 and 16°S had a greater effect on SSHa between 80 and 84°W in offshore areas while a small influence was observed near the coast between 8 and 13°S, which coincides with the location of the sampling network (**Figure 9A**). The interannual variability was mainly the result of ENSO as shown in **Figure 9B** where the temporal component

of the first mode (EOF1) can be seen to be correlated with the El Niño multivariate (MEI) and ONI indices. It should be noted that the region is partially located within the area referred to as El Niño region I (Trenberth and, 2019). **Figure 9B** also shows that the ENSO effect extended south of the study area near the coast with a local variance between 57–77%.

Mesoscale eddy activity is generated by variations in density that arise from coastal currents in their own vortices. The greatest effect of this activity was detected with SSHa in the southern region between 13 and 16°S, although mesoscale eddy activity presented latitudinal variation and minimum values were present in the northern region (**Figure 9C**). This is likely because most eddies are generated near the coastal region between 10–16°S and reach their greatest diameters between 13–16°S.

During neutral El Niño conditions, as in February 2014, the ENSO signal may be overshadowed by high mesoscale variability. The signal decomposition for the sampling dates during the cruise is shown in **Figure 10**. January and February were neutral ENSO periods (ONI = −0.4), and the interannual signal was weak (0.5–1.8 cm). The strongest driver of SSHa variability was the mesoscale signal (−5.9 to 5.1 cm), which was mainly due to the presence of eddies, with fluctuations of −1.3 to 3.0 cm generated by seasonality.

Inferred Sea Surface Height Anomalies, Satellite Product, and Cruise Track Variability Attributed to Mesoscale Eddies

To evaluate if mesoscale eddy activity played a large role in carbon system variability within the inner and outer transects, two approaches were considered. Inferred SSHa by calculate density and thus to compare with the satellite product (**Figures 11A,C,D**). We found that both estimations showed similar trends. However, a linear regression analysis was carried out to determine if the inferred SSHa were associated with the satellite dynamic height product. The R^2 value of this analysis was 0.78. Likewise, a statistically significant Pearson linear correlation coefficient of $r_p = 0.88$ was obtained, indicating that increases in sea surface height were associated with SSHa (confidence level of 95%).

After SSHa were estimated, they were used to geo-reference each carbonate system profile to determine the degree of variability in the carbonate system that may be attributed to mesoscale eddies (**Figures 11B,E**). For example, the large horizonal and vertical variability associated with DIC values of 2,250 μmol kg^{-1} was due to eddy presence. The linear regression was performed considering SSHa and DIC depth (Z). An association was found between $Z_{DIC=2250}$ (depth at which DIC = 2,250 μmol kg^{-1}) and SSHa for the deepest portions of the main offshore transect. The model obtained has $x_0 = -29.11$, $x_1 = 8.08$, $R^2 = 0.46$, and $r_p = -0.68$. We found that mesoscale processes change the upper depth limit of ESSW and the depth of this water mass, while affecting DIC, the aragonite saturation depth, and the upper limit of the OMZ.

DISCUSSION

This study describes the Peruvian upwelling conditions observed during January and February 2014 and the associated spatial variation of the CO_2 system. During upwelling events, the aragonite saturation depth was observed to be close to 50 m, but values of <1.2 were detected close to 20 m and were accompanied by low pH (<7.5), high pCO_2 (>1,250 μatm), and high DIC (>2,250 μmol kg^{-1}). These chemical characteristics were linked with the portion of the water-column that spanned from the upper limit of Equatorial Subsurface Water (ESSW) to the upper limit of the OMZ (<5 μmol kg^{-1}) and the carbocline (∼2,300 μmol kg^{-1}). Our analysis of the decomposition of SSHa variability also shows that the coastal-oceanic signal was dominated by interannual variability. However, during our sampling period, mesoscale processes were key drivers of surface water dynamics. In particular, the upper depth limit of ESSW may be altered by physical phenomena, such as eddies or interannual events. This results in changes in the depth of this water mass and affects DIC, the aragonite saturation depth, and the upper limit of the OMZ.

Vertical Mixing, Water Masses, and Water Types

Large spatial variability in sea surface anomalies were found (**Figure 4**). Part of this variability may be attributed to the influence of mesoscale eddies, which modify biogeochemistry. For example, shallower saturation horizons and high DIC values may be due to cyclonic eddy activity, while low DIC concentrations will be deeper due to anticyclonic eddy activity. The sampling area showed eddy production in the oceanic region, which may account for a large percentage of the variability that was observed in the offshore stations located south of 13°S (>40%) as may be seen in **Figure 9C**. Additional information regarding the effect of eddies on the biogeochemistry inside an OMZ has been reported by Bettencourt et al. (2015) who indicate that mesoscale structures have relevant dual roles at depths between 380 and 600 m. Firstly, their mean positions and paths delimit and maintain the boundaries of oxygen minimum zones. Secondly, their high frequency fluctuations entrain oxygen across these boundaries. As a result, these eddy fluxes contribute to the ventilation of the oxygen minimum zone. Eddy structures can introduce water types with different pH and Ω_{arag} values (**Figure 5**). For example, MESC and SSW at the surface were affected by anticyclonic and cyclonic eddies (**Figure 6**), respectively, and MESC had higher pH and oxygen values than SSW (**Figure 5**).

The offshore surface waters were saturated with regard to aragonite (Ω_{arag} >1.5 to >4.5) in the first 50 m of the water column (**Figures 6**, **7**). However, for depths below 150 m, the Ω_{arag} values were <1. These values are similar to those reported for the open ocean (300 km from the coast) in the Eastern South Pacific (Feely et al., 2012; Jiang et al., 2015). The upper limit of ESSW can be identified by the 26 kg m^{-3} isopycnal (**Figure 5**). The depth of this isopycnal surface was closely related to the thermocline and with the aragonite saturation horizon (**Figure 6**). Therefore, most of the chemical features associated

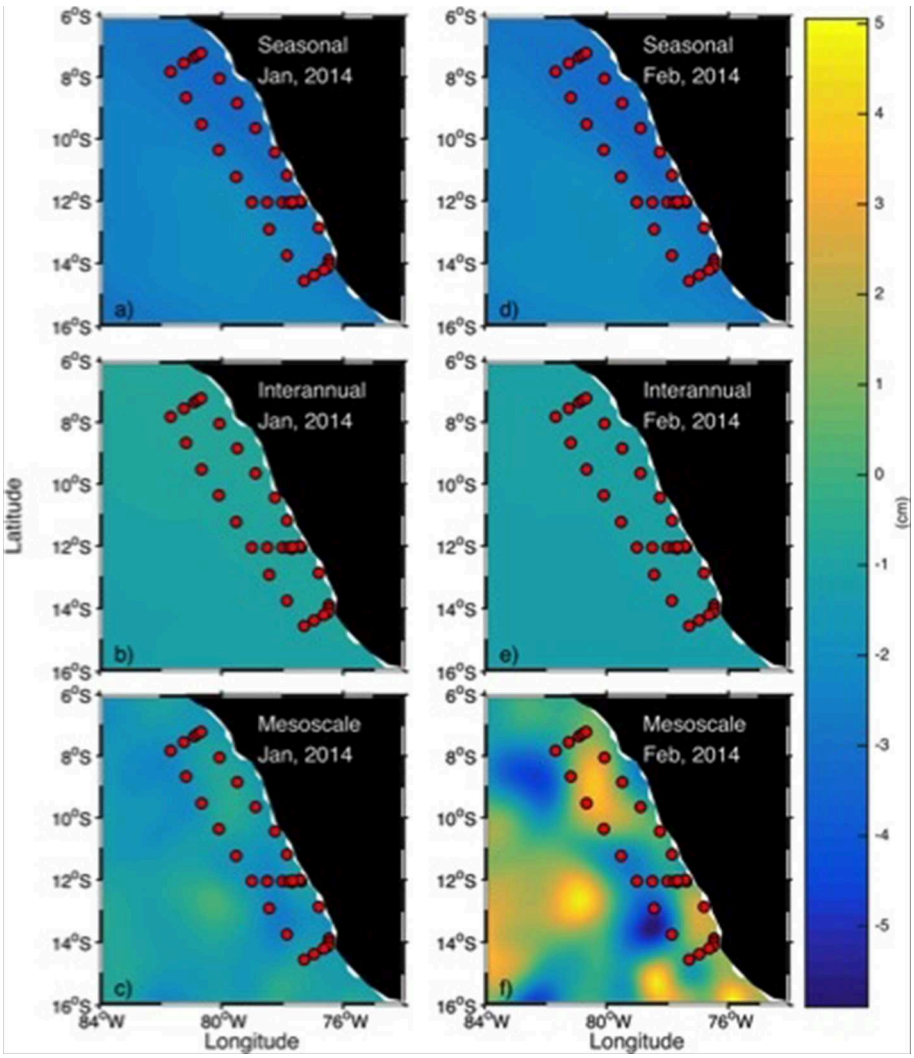

FIGURE 10 | Signal decomposition for January and February: **(a,d)** seasonal, **(b,e)** interannual, and **(c,f)** mesoscale.

with this isopycnal were similar regardless of depth. In most cases, the sinking of this density surface directly resulted in changes in the depth of the aragonite saturation horizon. Near Pisco, the upper limit of ESSW was as shallow as ∼20 m depth.

During the cruise, the low surface Ω_{arag} values (<1.2) that were observed near the coastal stations were due to the influence of upwelled water. However, a cyclonic eddy was present during sampling along the coast between 11 and 12°S (**Figure 4**; February). This eddy resulted in an upward vertical transport of aragonite-undersaturated ESSW, which reduced the surface values of Ω_{arag} (**Figures 6**, **7**). Furthermore, an anticyclone was observed in most of the oceanic region (8–12°S and 80–81°W) that resulted in a depression of the aragonite saturation horizon. The highest Ω_{arag} values (near 3) that were found in the Peruvian area were observed offshore in the northern transects. Nevertheless, the high offshore pH values (>8.1) and low pCO_2 values (<600 μatm) that were found in this region suggest that the aragonite saturation state is driven by two processes: outgassing of CO_2 and the biological consumption of dissolved inorganic carbon. However, submesoscale processes are another physical driver of CO_2 outgassing. Köhn et al. (2018) carried out a CO_2 variability study across an upwelling front near Peru using high-resolution underway measurements and provided evidence of the complex submesoscale distribution of surface CO_2 in the Peruvian upwelling system. Thus, physical processes may also influence the distribution of pCO_2 on different spatial and time scales.

Spatial Variability

In winter, the Peruvian Coastal Current (PCC) flows intensely toward the equator, while the Peruvian Coastal Under Current (PCUC) flows toward the pole (Bakun and Nelson, 1991; Penven et al., 2005; Croquette et al., 2007; Ayón et al., 2008; Dewitte et al., 2011). During normal conditions, upwelling transports water from the PCUC (Ayón et al., 2008; Montes et al., 2011). During La Niña conditions, the Cold Coastal

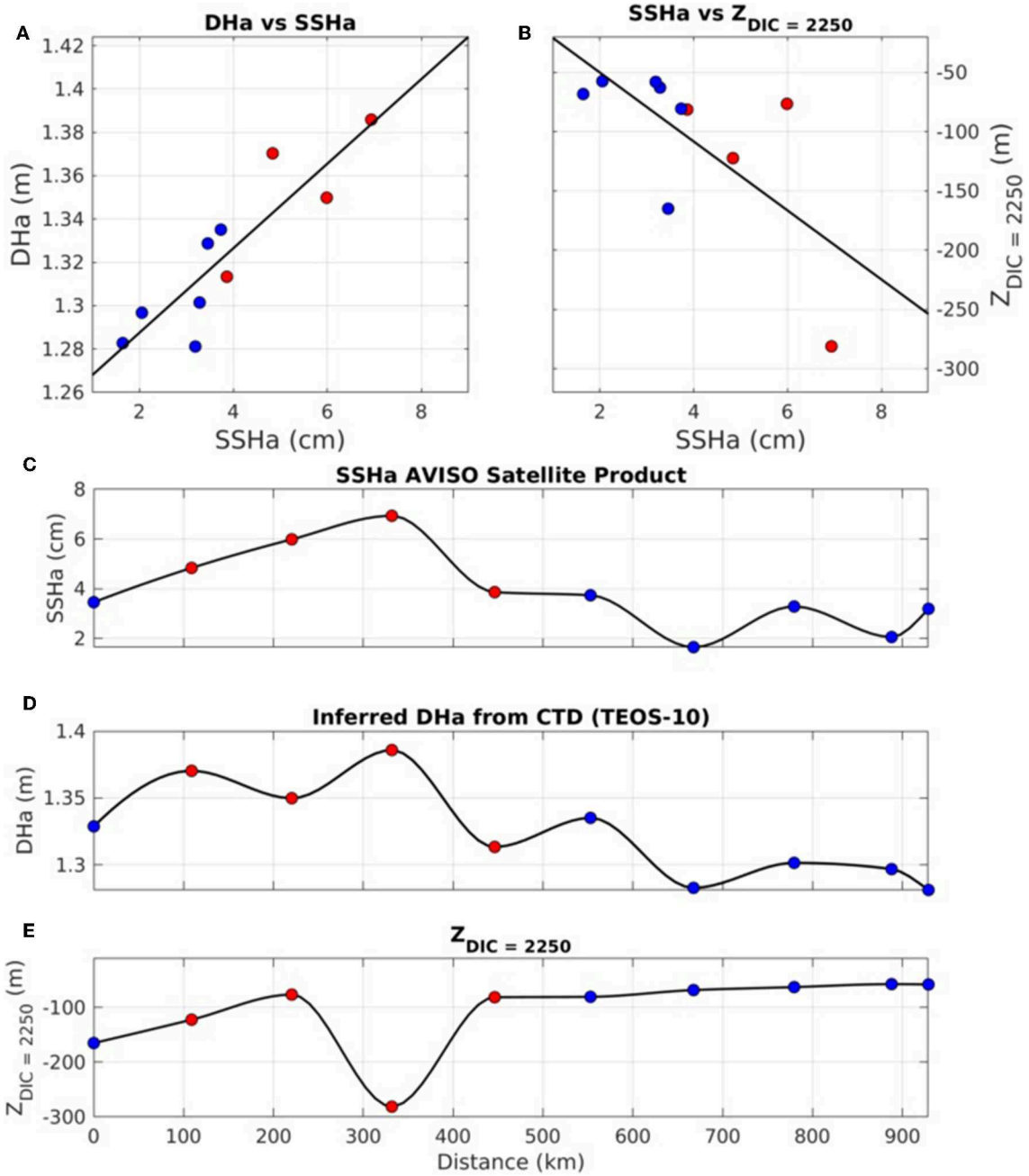

FIGURE 11 | (A) Association between DHa and SSHa for the deepest points of the main offshore transect (see **Figure 1**). The black straight line corresponds to the linear model obtained with $x_0 = 1.25$, $x_1 = 0.02$, $R^2 = 0.78$, and $r_p = 0.88$. **(B)** Association between $Z_{DIC = 2250}$ (depth at which DIC = 2,250 μmol/kg) and SSHa for the deepest points of the main offshore transect. The black straight line corresponds to the linear model obtained with $x_0 = -29.11$, $x_1 = 8.08$, $R^2 = 0.46$, and $r_p = -0.68$. From **(C–E)** we show the values of SSHa, DHa, and $Z_{DIC = 2250}$ from the deepest points of transect 1. The horizontal axis corresponds to distance (km), beginning from the North (0 km).

Water (CCW) water type is heavily influenced by upwelling (Ayón et al., 2008; Montes et al., 2011).

Based on the analysis of 1993–2014 SSHa data, we found that interannual variability plays the most important role (up to 60% of local SSHa variance) in determining the circulation of the coastal areas and in the southern region of our study area, followed by mesoscale variability. This result is different from what was observed by Godínez et al. (2010) for the OMZ located in the Eastern Tropical Pacific (ETP) off the coast of Mexico (15–24°N). In their study, seasonality was found to be the dominant signal, which was followed by the mesoscale signal. The mesoscale contribution to SSHa variability was four times larger

than what was observed for the ETP (10–20% of the local SSHa variance). In contrast with our study area, interannual variability was three times larger than mesoscale variability near the coast. The waters off Peru are intimately associated with the dynamics of the equatorial Pacific and are thus subject to large temporal variations. The ENSO cycle, with its warm El Niño phase and cold La Niña phase, is comprised of a natural interannual oscillation frequency of the ocean-atmosphere system in the tropical Pacific (Takahashi et al., 2011). Over several months, this cycle substantially alters the functioning of ecosystems associated with the coastal outcrop (Grados et al., 2018).

In our study, mesoscale variability was less important than interannual variability, but we also found that mesoscale eddy activity notably influenced carbon system variability within the inner and outer transects (**Figure 11**). We found that the large spatial variability observed in our study area was attributed to the influence of mesoscale eddies, which can modify the distribution of biochemical variables, such as the aragonite saturation horizon, in response to shallower (cyclonic eddies) or deeper (anticyclonic eddies) thermoclines. According to Willett et al. (2006), eddies are the main contributors of mesoscale variability in the ETP. Eddies affect the spatial distribution of dissolved chemicals by Ekman pumping and by exporting dissolved and particulate materials into the open ocean, fostering horizontal advection (Chen et al., 2007; Samuelsen and O'Brien, 2008; Gaube et al., 2014; Nagai et al., 2015). In the study area, mesoscale processes influenced the upper depth limit of ESSW, changing the depth of this water mass and affecting DIC, aragonite saturation, and the OMZ depth. Mesoscale eddies, whether they are driven by wind forcing or otherwise, can persist for weeks (cyclonic) or months (anticyclonic; Gonzalez-Silvera et al., 2004; Palacios and Bograd, 2005). Although mesoscale processes were not as important as interannual processes, they were still very important in the region during the cruise and affected the spatio-temporal variability of the biogeochemical patterns in the region and are thus key factors to consider when studying the carbonate system in the ocean offshore of Peru.

Variability of Dissolved Inorganic Carbon

The DIC concentrations detected in the study area were within the data ranges that have been reported for SSW in the ETP (Paulmier et al., 2011; Franco et al., 2014; Chapa-Balcorta et al., 2015). The DIC variability observed during sampling indicates that upwelling and mesoscale variability affect DIC values. The corresponding changes in pCO_2 and Ω_{arag} affected both regional biogeochemical conditions and habitat quality for calcifying or pH-sensitive species.

The impact of climate change on the dynamics of the Eastern Boundary upwelling system (EBUS) has been debated and a consensus has not been reached so far, mostly because of competing effects due to the increase in upwelling favorable winds induced by the expansion of the Hadley cell (Bakun et al., 2015; Rykaczewski et al., 2015) and the increase in surface warming that increases vertical stratification and tends to reduce upwelling (e.g., Echevin et al., 2012 for the coast of Peru). There is also uncertainty with regard to whether upwelling favorable winds will actually increase in the mid-latitudes (Goubanova et al., 2011) given that increasing trends in alongshore favorable winds are barely detected in existing data sets (e.g., Figure 1 of Belmadani et al., 2014). It has been postulated that along the Peruvian coast, global warming has increased the heat difference between the continent and the adjacent sea. This change has resulted in an intensification of the winds, which has resulted in the coastal outcrop. However, recent studies suggest a notable cooling of the marine-coastal strip between central Peru and northern Chile over the last 35 years, although records of coastal winds are scarce and the causes behind this trend remain unclear (Yáñez et al., 2018). The first simulations of climate change effects in the waters off Peru predicted a decrease of the coastal outcrop, an intensification of coastal retention processes, and a reduction in marine productivity, in which thermal stratification plays an important role (Gutiérrez et al., 2011). These changes in upwelling intensification will also be reflected in the carbon biogeochemistry of coastal areas.

Aragonite Saturation Horizon Maintenance

A lower oxygen concentration at the aragonite saturation depth was found in the southern stations near the coastline (**Figures 6**, **7**). The remineralization of organic matter produced at the surface may intensify the consumption of oxygen in the subsurface layer due to low ventilation driven by strong stratification in the area (Fiedler and Talley, 2006; Fiedler et al., 2013; Franco et al., 2014). The latter is consistent with what was reported by Fiedler and Talley (2006), who concluded that 90% of organic matter was remineralized in the first 200 m of the water column. In turn, Paulmier et al. (2006) showed that organic matter remineralization in the oxycline of the Humboldt system was 3-fold more intense than in the core of the OMZ, which favors the maintenance of these zones. In highly productive coastal zones, eutrophication due to runoff from terrestrial nutrient addition may have a greater effect on the decrease of aragonite saturation than on ocean acidification driven by anthropogenic CO_2 absorption (Borges and Gypens, 2010). Water with low oxygen and carbonate ion concentrations may have different biological responses, as this situation may lead to habitat increases or decreases for the species that reside in OMZs, particularly because these chemical environments affect their metabolic functions.

Like biological processes, physical drivers play a very important role in the vertical distribution of several CO_2 variables in the ocean. The results reported in this study clearly demonstrate that DIC concentrations, pCO_2, and Ω_{arag} depend not only on the upwelling season but also on the presence, absence, and intensity of mesoscale eddies. Therefore, proper evaluations of physical drivers should always include an analysis of the indicators of these eddies, such as dynamic height, geostrophic currents, or altimetry in models that are able predict which areas are likely to experience ocean acidification.

The upwelling system in Peru is a natural laboratory for the study of regional interactive processes between the land, ocean, and atmosphere while providing a unique opportunity to understand carbon variability in different scales. For example, the Peruvian anchovy *Engraulis ringens* lives and spawns in a region where pCO_2 values may be higher than 1,000 ppm (Friederich et al., 2008), and low survival rates have been attributed to these high values (Shen et al., 2017). These authors also highlight the

need to understand the effect of pCO_2 levels on spawning and mortality rates to predict the effects of ocean acidification on fisheries management. In response to future warming, changes in timing, intensity, and spatial heterogeneity are expected to occur in most EBUS (Wang et al., 2015).

CONCLUSIONS

During the upwelling events, the aragonite saturation depth was observed to be close 50 m, but values <1.2 were detected close to 20 m along with low pH (<7.5), high pCO_2 (>1,250 μatm), and high DIC (>2,250 μmol kg^{-1}) values. These chemical characteristics were associated with Equatorial Subsurface Water (ESSW). In addition, the aragonite saturation depth became gradually shallower from north to south, beginning at 140 m and decreasing to <40 m with pCO_2 values close to 1,250 μatm.

Large spatial variability in surface values was also observed. Part of this variability can be attributed to the influence of mesoscale eddies, which can modify the distribution of biogeochemical variables. The results reported here clearly demonstrate that DIC concentrations, pCO_2, and Ω_{arag} depend not only on upwelling but also on the presence, absence, and intensity of mesoscale eddies. Mesoscale eddies changed the upper depth limit of ESSW, changing the depth of this water mass and affecting DIC, aragonite saturation, and OMZ depth.

Our analysis of the decomposition of SSHa variability that was based on a 21-year data set, indicated that the interannual signal was the dominant coastal-oceanic signal. However, during our sampling period, mesoscale processes were key drivers of surface water dynamics. The 2014 cruise was characterized by weak Kelvin activity, and physical forcing was more associated with eddy activity. Large spatial variability at the surface was also found. Part of this variability was attributed to the influence of mesoscale eddies which modify biochemistry. For example, the aragonite saturation horizon was affected by shallower or deeper thermoclines, which were the result of cyclonic or anticyclonic eddies, respectively. Near the coast and south of 12°S, pH_T values from 8 to 7.6 were observed in upwelling zones but were also distributed in several shallow water types. Values <1.2 were detected close to 20 m along with low pH (minimum of 7.5), high pCO_2 (maximum of 1,250 μatm), and high DIC concentrations (maximum of 2,300 μmol kg^{-1}). Weighing the relative importance of each individual signal leads to a better understanding of the biogeochemical processes in the area.

AUTHOR CONTRIBUTIONS

The conceptualization and arrangement of the original manuscript was under the charge of JH-A, AP, and VG. The conceptual design and financial support of the oceanographic expeditions were under the direction of VG, AP, BD, and CM. All CTD data were facilitated through JS. Preprocessing of all data was carried out by CC-B, JS, IM, GD, and MB. Laboratory analyses were conducted by JH-A. All authors contributed equally to the original manuscript.

FUNDING

AMOP project was supported by IRD, CNRS/INSU, LEGOS.

ACKNOWLEDGMENTS

We wish to thank the crew of the French R/V Atalante during the cruise in the framework of the AMOP project (Activity of research dedicated to the Minimum of Oxygen in the eastern Pacific). We also thank Sergio Larios for his input in the data processing.

Sea surface level anomaly data were produced by Segment Sun Altimetrie et Orbitographie/Developing Use of Altimetry for Climate Studies (Ssalto/Duacs) and distributed by Archiving Validation. The interpretation of satellite Oceanographic Data (Warning) was carried out with the support of the Center National d'Etudes Spatiales (CNES).

REFERENCES

Ayón, P., Criales-Hernandez, M. I., Schwamborn, R., and Hirche, H.-J. (2008). Zooplankton research off Peru: a review. *Prog. Oceanogr.* 79, 238–255. doi: 10.1016/j.pocean.2008.10.020

Bakun, A., Black, B. A., Bograd, S. J., García-Reyes, M., Miller, A. J., Rykaczewski, R. R., et al. (2015). Anticipated effects of climate change on coastal upwelling. *Ecosystems* 1, 85–93. doi: 10.1007/s40641-015-0008-4

Bakun, A., and Nelson, C. S. (1991). The seasonal cycle of wind stress curl in subtropical eastern boundary current regions. *J. Phys. Oceanogr.* 21, 1815–1834. doi: 10.1175/1520-0485(1991)021<1815:TSCOWS>2.0.CO;2

Barnes, S. L. (1964). A technique for maximizing details in numerical weather map analysis. *J. Appl. Meteorol.* 3, 396–409. doi: 10.1175/1520-0450(1964)003<0396:ATFMDI>2.0.CO;2

Belmadani, A., Echevin, V., Codron, F., Takahashi, K., and Junquas, C. (2014). What dynamics drive future wind scenarios for coastal upwelling off Peru and Chile? *Clim. Dyn.* 43, 1893–1914. doi: 10.1007/s00382-013-2015-2

Bettencourt, J. H., López, C., Hernández-García, E., Montes, I., Sudre, J., Dewitte, B., et al. (2015). Boundaries of the peruvian oxygen minimum zone shaped by coherent mesoscale dynamics. *Nat. Geosci.* 8, 937–940. doi: 10.1038/ngeo2570

Borges, A. V., and Gypens, N. (2010). Carbonate chemistry in the coastal zone responds more strongly to eutrophication than to ocean acidification. *Limnol. Oceanogr.* 55, 346–353. doi: 10.4319/lo.2010.55.1.0346

Bretagnon, M., Paulmier, A., Garcon, V., Dewitte, B., Illig, S., Leblond, N., et al. (2018). Modulation of the vertical particles transfer efficiency in the Oxygen Minimum Zone off Peru. *Biogeosciences* 15, 5093–5111. doi: 10.5194/bg-15-5093-2018

Chapa-Balcorta, C., Hernandez-Ayon, J. M., Durazo, R., Beier, E., Alin, S. R., and López-Pérez, A. (2015). Influence of post-Tehuano oceanographic processes in the dynamics of the CO_2 system in the Gulf of Tehuantepec, Mexico. *J. Geophys. Res.* 120, 7752–7770. doi: 10.1002/2015JC011249

Chavez, F. P., Bertrand, A., Guevara-Carrasco, R., Soler, P., and Csirke, J. (2008). The northern Humboldt Current System: brief history, present

status and a view towards the future. *Prog. Oceanogr.* 79, 95–105. doi: 10.1016/j.pocean.2008.10.012

Chen, F., Cai, W.-J., Benitez-Nelson, C., and Wang, Y. (2007). Sea surface pCO_2-SST relationships across a cold-core cyclonic eddy: implications for understanding regional variability and air-sea gas exchange. *Geophys. Res. Lett.* 34:L10603. doi: 10.1029/2006GL028058

Croquette, M., Eldin, G., Grados, C., and Tamayo, M. (2007). On differences in satellitewind products and their effects in estimating coastal upwelling processes in the south-east Pacific. *Geophys. Res. Lett.* 34:L11608. doi: 10.1029/2006GL027538

Dewitte, B., Illig, S., Renault, L., Goubanova, K., Takahashi, K., Gushchina, D., et al. (2011). Modes of covariability between sea surface temperature and wind stress intraseasonal anomalies along the coast of Peru from satellite observations (2000-2008). *J. Geophys. Res.* 116:C04028. doi: 10.1029/2010JC006495

Dickson, A. G., Afghan, J. D., and Anderson, G. C. (2003). Reference materials for oceanic CO_2 analysis: a method for the certification of total alkalinity. *Mar. Chem.* 80, 185–197. doi: 10.1016/S0304-4203(02)00133-0

Echevin, V., Goubanova, K., Belmadani, A., and Dewitte, B. (2012). Sensitivity of the Humboldt Current system to global warming: a downscaling experiment of the IPSL-CM4 model. *Clim. Dyn.* 38, 761–774. doi: 10.1007/s00382-011-1085-2

Espinoza-Morriberon, D., Echevin, V., Colas, F., Tam, J., Ledesma, J., Vasquez, L., et al. (2017). Impacts of El Niño events on the Peruvian upwelling system productivity. *J.Geophys. Res. Oceans* 122, 5423–5444. doi: 10.1002/2016JC012439

Fabry, V. J., Seibel, B. A., Feely, R. A., and Orr, J. C. (2008). Impacts of ocean acidification on marine fauna and ecosystem processes. *ICES J. Mar. Sci.* 65, 414–432. doi: 10.1093/icesjms/fsn048

Feely, R. A., Sabine, C. L., Byrne, R. H., Millero, F. J., Dickson, A. G., Wanninkhof, R., et al. (2012). Decadal changes in the aragonite and calcite saturation state of the Pacific Ocean. *Glob. Biogeochem. Cycles* 26:GB3001. doi: 10.1029/2011GB004157

Feely, R. A., Sabine, C. L., Hernandez-Ayon, M., Ianson, D., and Hales, B. (2008). Evidence for upwelling of corrosive'acidified' water onto the Continental Shelf. *Science* 320, 1490–1492. doi: 10.1126/science.1155676

Fiedler, P. C., Mendelssohn, R., Palacios, D. M., and Bograd, S. J. (2013). Pycnocline variations in the Eastern Tropical and North Pacific, 1958 – 2008. *J. Clim.* 26, 583–599. doi: 10.1175/JCLI-D-11-00728.1

Fiedler, P. C., and Talley, L. D. (2006). Hydrography of the eastern tropical Pacific: a review. *Prog. Oceanogr.* 69, 143–180. doi: 10.1016/j.pocean.2006.03.008

Franco, A. C., Gruber, N., Frölicher, T. L., and Kropuenske Artman, L. (2018). Contrasting impact of future CO_2 emission scenarios on the extent of $CaCO_3$ mineral undersaturation in the Humboldt Current System. *J. Geophys. Res.* 123, 2018–2036. doi: 10.1002/2018JC013857

Franco, A. C., Hernández-Ayón, J. M., Beier, E., Garçon, V., Maske, H., Paulmier, A., et al. (2014). Air-sea CO_2 fluxes above the stratified oxygen minimum zone in the coastal region off Mexico. *J. Geophys. Res.* 119, 2923–2937. doi: 10.1002/2013JC009337

Friederich, G. E., Ledesma, J., Ulloa, O., and Chavez, F. P. (2008). Air-sea carbon dioxide fluxes in the coastal southeastern tropical Pacific. *Prog. Oceanogr.* 79, 156–166. doi: 10.1016/j.pocean.2008.10.001

Gaube, P., McGillicuddy, D. J., Chelton, D. B., Behrenfeld, M. J., and Strutton, P. G. (2014). Regional variations in the influence of mesoscale eddies on near-surface chlorophyll. *J. Geophys. Res.* 119, 8195–8220. doi: 10.1002/2014JC010111

Godínez, V. M., Beier, E., Lavín, M. F., and Kurczyn, J. A. (2010). Circulation at the entrance of the Gulf of California from satellite altimeter and hydrograhic observations. *J. Geophys. Res.* 115:C04007. doi: 10.1029/2009JC005705

Gonzalez-Silvera, A., Santamaria-del-Angel, E., Millán-Nuñez, R., and Manzo-Monroy, H. (2004). Satellite observations of mesoscale eddies in the Gulfs of Tehuantepec and Papagayo (Eastern Tropical Pacific). *Deep Sea Res. II* 51, 587–600. doi: 10.1016/j.dsr2.2004.05.019

Goubanova, K., Echevin, V., Dewitte, B., Codron, F., Takahashi, K., Terray, P., et al. (2011). Statistical downscaling of sea-surface wind over the Peru–Chile upwelling region: diagnosing the impact of climate change from the IPSL-CM4 model. *Clim. Dyn.* 36, 1365–1378. doi: 10.1007/s00382-010-0824-0

Graco, M.I., Ledesma, J., Flores, G., and Girón, M. (2007). Nutrientes, oxígeno y procesos biogeoquímicos en el sistema de surgencias de la corriente de Humboldt frente a Perú. *Rev. Biol. Peru* 14, 117–128. doi: 10.15381/rpb.v14i1.2165

Grados, C., Chaigneau, A., Echevin, V., and Dominguez, N. (2018). Upper ocean hydrology of the Northern Humboldt Current System at seasonal, interannual and interdecadal scales. *Prog. Oceanogr.* 165, 123–144. doi: 10.1016/j.pocean.2018.05.005

Guinotte, J. M., and Fabry, V. J. (2008). Ocean acidification and its potential effects on marine ecosystems. *Ann. N. Y. Acad. Sci.* 1134, 320–342. doi: 10.1196/annals.1439.013

Gutiérrez, D., Bertrand, A., Wosnitza-Mendo, C., Dewitte, B., Purca, S., Peña, C., et al. (2011). Sensibilidad del sistema de afloramiento costero del Perú al cambio climático e implicancias ecológicas. *Rev. Peru Geo Atmos.* 3, 1–26.

Hamersley, M. R., Lavik, G., Woebken, D., Ratray, J.E., Lam, P., Hopmans, E.C., et al. (2007). Anaerobic ammomium oxidation in the Peruvian oxygen minimum zone. *Limnol. Oceanogr.* 52, 923–933. doi: 10.4319/lo.2007.52.3.0923

Jiang, L.-Q., Feely, R. A., Carter, B. R., Greeley, D. J., Gledhill, D. K., and Arzayus, K. M. (2015). Climatological distribution of aragonite saturation state in the global oceans. *Glob. Biogeochem. Cycles* 29, 1656–1673. doi: 10.1002/2015GB005198

Köhn, E. E., Thomsen, S., Arévalo-Martínez, D. L., and Kanzow, T. (2018). Submesoscale CO_2 variability across an upwelling front off Peru. *Ocean Sci.* 13, 1017–1033. doi: 10.5194/os-13-1017-2017

León-Chávez, C. A., Beier, E., Sánchez-Velasco, L., Barton, E. D., and Godínez, V. M. (2015). Role of circulation scales and water mass distributions on larval fish habitats in the Eastern Tropical Pacific off Mexico. *J. Geophys. Res.* 120, 3987–4002. doi: 10.1002/2014JC010289

Lewis, E., and Wallace, D. W. R. (1998). *Program Developed for CO2 System Calculations*. ORNL/CDIAC-105. Carbon Dioxide Information Analysis Center; Oak Ridge National Laboratory; U. S. Department of Energy.

Macharé, J., and Ortlieb, L. (1993). Registros del fenómeno El Niño en el Perú. *Bull. Inst. Fr. Études Andin.* 22, 35–52.

Maes, C., Paulmier, A., Dewitte, B., and Garcon, V. (2014). AMOP cruise, RV L'Atalante.

Marchesiello, P., and Estrade, P. (2010). Upwelling limitation by onshore geostrophic flow. *J. Mar. Res.* 68, 37–62. doi: 10.1357/002224010793079004

McDougall, T. J., and Barker, P. M. (2011). *Getting Started with TEOS-10 and the Gibbs Seawater (GSW) Oceanographic Toolbox*. Available online at: www.TEOS-10.org

McNeil, B. I., and Sasse, T. P. (2016). Future ocean hipercapnia driven by anthropogenic amplification of the natural CO_2 cycle. *Nature* 529, 383–386. doi: 10.1038/nature16156

Mehrbach, C., Culberson, C. H., Hawley, J. E., and Pytkowicz, R. M. (1973). Measurement of the apparent dissociation constants of carbonic acid in seawater at atmospheric pressure. *Limnol. Oceanogr.* 18, 897–907. doi: 10.4319/lo.1973.18.6.0897

Montes, I., Schneider, W., Colas, F., Blanke, B., and Echevin, V. (2011). Subsurface connections in the eastern tropical Pacific during La Niña 1999–2001 and El Niño 2002–2003. *J. Geophys. Res.* 116:C12022. doi: 10.1029/2011JC007624

Mucci, A. (1983). The solubility of calcite and aragonite in seawater at various salinities, temperatures, and one atmosphere total pressure. *Am. J. Sci.* 283, 780–799. doi: 10.2475/ajs.283.7.780

Nagai, T., Gruber, N., Frenzel, H., Lachkar, Z., McWilliams, J. C., and Plattner, G.-K. (2015). Dominant role of eddies and filaments in the offshore transport of carbon and nutrients in the California Current System, *J. Geophys. Res.* 120, 5318–5341. doi: 10.1002/2015JC010889

Palacios, D. M., and Bograd, S. J. (2005). A census of Tehuantepec and Papagayo eddies in the northeastern tropical Pacific. *Geophys. Res. Lett.* 32:L23606. doi: 10.1029/2005GL024324

Paulmier, A., Ruiz-Pino, D., and Garçon, V. (2008). The Oxygen Minimum Zone (OMZ) off Chile as intense sources of CO_2 and N_2O. *Cont. Shelf Res.* 28, 2746–2756. doi: 10.1016/j.csr.2008.09.012

Paulmier, A., Ruiz-Pino, D., and Garçon, V. (2011). Carbon Maximum Zone (CMZ) formation associated with Oxygen Minimum Zone (OMZ). *Biogeoscience* 8, 239–252. doi: 10.5194/bg-8-239-2011

Paulmier, A., Ruiz-Pino, D., Garçon, V., and Farías, L. (2006). Maintaining of the eastern south Pacific oxygen minimum zone (OMZ) off Chile. *Geophys. Res. Lett.* 33:L20601. doi: 10.1029/2006GL026801

Penven, P., Echevin, V., Pasapera, J., Colas, F., and Tam, J. (2005). Average circulation, seasonal cycle, and mesoscale dynamics of the Peru Current System: a modelling approach. *J. Geophys. Res.* 110:C10021. doi: 10.1029/2005JC002945

Prentice, I. C., Farquhar, G. D., Fasham, M. J. R., Goulden, M. L., Heimann, M., Jaramillo, V. J., et al. (2001). "The Carbon Cycle and Atmospheric Carbondioxide," in *Climate Change 2001: the Scientific Basis. Contributions of Working Group I to the Third Assessment Report of the Intergovernmental Panel on Climate Change*, eds J. T. Houghton, Y. Ding, D. J. Griggs, M. Noguer, P. J. van der Linden, X. Dai, K. Maskell, and C. A. Johnson (Cambridge: Cambridge University Press), 185–237.

Revsbech, N. P., Larsen, L. H., Gundersen, J., Dalsgaard, T., Ulloa, O., and Thamdrup, B. (2009). Determination ofultra-low oxygen concentrations in oxygen minimum zones by the STOX sensor. *Limnol. Oceanogr. Methods* 7, 371–381. doi: 10.4319/lom.2009.7.371

Ripa, P. (2002). Least squares data fitting. *Cienc. Mar.* 28, 79–105. doi: 10.7773/cm.v28i1.204

Rykaczewski, R. R, Dunne, J. P., Sydeman, W. J., García-Reyes, M., Black, B. A., and Bograd, S. J. (2015). Poleward displacement of coastal upwelling-favorable winds in the ocean's eastern boundary currents through the 21st century. *Geophys. Res. Lett.* 42, 6424–6431. doi: 10.1002/2015GL064694

Samuelsen, A., and O'Brien, J. J. (2008). Wind-induced cross-shelf flux of water masses and organic matter at the Gulf of Tehuantepec. *Deep Sea Res.* 55, 221–246. doi: 10.1016/j.dsr.2007.11.007

Schwing, F. B., O'Farrell, M., Steger, J. M., and Baltz, K. (1996). *Coastal Upwelling Indices, West Coast of North America 1946-95 Report*. Pacific Grove, CA.

Shen, S. G., Thompson, A. R., Correa, J., Fietzek, P., Ayon, P., and Checkley, D. M. Jr. (2017). Spatial patterns of Anchoveta (*Engraulis ringens*) eggs and larvae in relation to pCO_2 in the Peruvian upwelling system. *Proc. R. Soc. B* 284:20170509. doi: 10.1098/rspb.2017.0509

Silva, N., and Neshyba, S. (1976). On the southernmost extension of the Peru-Chile undercurrent. *Deep Sea Res. A* 26, 1387–1393. doi: 10.1016/0198-0149(79)90006-2

Silva, N., Rojas, N., and Fedele, A. (2009). Watermasses in the Humboldt Current System:Properties, distribution, and the nitrate deficit as a chemical water mass tracer for Equatorial Subsurface Water off Chile. *Deep Sea Res. II* 56:10041020. doi: 10.1016/j.dsr2.2008.12.013

Simpson, J. H. (1981). The shelf-sea fronts: implications of their existence and behavior. *Philos. Trans. R. Soc. Lond. A* 302, 531–546. doi: 10.1098/rsta.1981.0181

Sobarzo, M., and Djurfeldt, L. (2004). Coastal upwelling process on a continental shelf limited by submarine canyons, Concepción, central Chile. *J. Geophys. Res.* 109:C12012. doi: 10.1029/2004JC002350

Stramma, L., Johnson, G. C., Sprintall, J., and Mohrholz, V. (2008).. Expanding oxygen-minimum zone in the tropical oceans. *Science* 320, 655–658. doi: 10.1126/science.1153847

Swartzman, G., Bertrand, A., Gutiérrez, M., Bertrand, S., and Vasquez, L. (2008). The relationship of anchovy and sardine to water masses in the Peruvian Humboldt Current System from 1983 to 2005. *Prog. Oceanogr.* 79, 228–237. doi: 10.1016/j.pocean.2008.10.021

Takahashi, K., Montecinos, A., Goubanova, K., and Dewitte, B. (2011). ENSO regimes: reinterpreting the canonical and Modoki El Niño. *Geophys. Res. Lett.* 38:L10704. doi: 10.1029/2011GL047364

Takahashi, T., Sutherland, S. C., Wanninkhof, R., Sweeney, C., Feely, R. A., Chipman D. W., et al. (2009). Climatological mean and decadal change in surface ocean pCO_2, and net sea-air CO_2 flux over the global oceans. *Deep Sea Res. II* 56, 554–577. doi: 10.1016/j.dsr2.2008.12.009

Trenberth, K., and National Center for Atmospheric Research Staff (eds). (2019). *The Climate Data Guide: Nino SST Indices (Nino 1+2, 3, 3.4, 4; ONI and TNI).* Available online at: https://climatedataguide.ucar.edu/climate-data/nino-sst-indices-nino-12-3-34-4-oni-and-tni (accessed January 11, 2019).

Wang, D., Gouhier, T. C., Menge, B. A., and Ganguly, A. R. (2015). Intensification and spatial homogenization of coastal upwelling under climate change. *Nature* 518:390. doi: 10.1038/nature14235

Willett, C. S., Leben, R. R., and Lavín, M. F. (2006). Eddies and tropical instability waves in the eastern tropical Pacific: a review. *Prog. Oceanogr.* 69, 218–238. doi: 10.1016/j.pocean.2006.03.010

Yáñez, E., Lagos, N. A., Norambuena, R., Silva, C., Letelier, J., Muck, K. P., et al. (2018). "Impacts of climate change on marine fisheries and aquaculture in Chile," in *Climate Change Impacts on Fisheries and Aquaculture*, eds B. F. Phillips and M. Pérez-Ramírez (Chichester: John Wiley & Sons), 239–332.

Zhang, H.-M., Bates, J. J., and Reynolds, R. W. (2006b). Assessment of composite global sampling: sea surface wind speed. *Geophys. Res. Lett.* 33:L17714. doi: 10.1029/2006GL027086

Zhang, H.-M., Reynolds, R. W., and Bates, J. J. (2006a). "Blended and gridded high resolution global sea surface wind speed and climatology from multiple satellites: 1987 - Present," in *American Meteorological Society 2006 Annual Meeting, Edited* (Atlanta, GA).

Conflict of Interest: The authors declare that the research was conducted in the absence of any commercial or financial relationships that could be construed as a potential conflict of interest.

Advantages of publishing in Frontiers

OPEN ACCESS
Articles are free to read for greatest visibility and readership

FAST PUBLICATION
Around 90 days from submission to decision

HIGH QUALITY PEER-REVIEW
Rigorous, collaborative, and constructive peer-review

TRANSPARENT PEER-REVIEW
Editors and reviewers acknowledged by name on published articles

Frontiers
Avenue du Tribunal-Fédéral 34
1005 Lausanne | Switzerland

Visit us: www.frontiersin.org
Contact us: info@frontiersin.org | +41 21 510 17 00

REPRODUCIBILITY OF RESEARCH
Support open data and methods to enhance research reproducibility

DIGITAL PUBLISHING
Articles designed for optimal readership across devices

FOLLOW US
@frontiersin

IMPACT METRICS
Advanced article metrics track visibility across digital media

EXTENSIVE PROMOTION
Marketing and promotion of impactful research

LOOP RESEARCH NETWORK
Our network increases your article's readership